STATE OF CALIFORNIA • DEPARTMENT OF TRANSPORTATION

TECHNICAL REPORT DOCUMENTATION PAGE

TR0003 (REV 10/98)

1. REPORT NUMBER	2. GOVERNMENT ASSOCIATION NUMBER	3. RECIPIENT'S CATALOG NUMBER
CA-11-0932		

4. TITLE AND SUBTITLE

Effects of Soil slope on The Lateral capacity of Piles in Cohesive and Cohesionless Soils

5. REPORT DATE

04/30/2012

6. PERFORMING ORGANIZATION CODE

7. AUTHOR

Nontapat Nimiyongskul, Paul barker, Scott A. Ashford

8. PERFORMING ORGANIZATION REPORT NO.

2012/01

9. PERFORMING ORGANIZATION NAME AND ADDRESS

School of Civil and Construction Engineering
101 Kearney Hall Oregon State University
Corvallis, OR 97331-3212

10. WORK UNIT NUMBER

11. CONTRACT OR GRANT NUMBER

59A0645

12. SPONSORING AGENCY AND ADDRESS

California Department of Transportation
Division of Engineering Services
Structure Policy and Innovation
1801 30th Street, MS #9-2/5I
Sacramento CA 95816

13. TYPE OF REPORT AND PERIOD COVERED

Final

14. SPONSORING AGENCY CODE

15. SUPPLEMENTARY NOTES

Prepared in cooperation with the State of California Department of Transportation.

16. ABSTRACT

A series of full-Scale lateral loading test for instrumented piles in cohesive and coheionless soils were carried out at Oregon State University to assess the lateral response of piles in free-field and near slop conditions. Instrumentation data from the free-field piles and the piles installed at different distances from the slop crest were used extensively to monitor lateral pile response and back-calculate p-y curves. For the cohesive soil test, it was found that for small pile head displacements (less than 1.0 inch), the proximity of slope has insignificant effects on piles 2D or further from the slope crest where D is the pile diameter. For the piles on the slope crest, the effects of the soil slope should always be considered. The presence of the slope has insignificant effects for piles installed at distances of 8D or greater from the crest. For the coheionless soil tests, the effects of slope on lateral pile capacity are insignificant at displacement of less than 2.0 inches for piles located 2D and further from the crest. For piles located at 4D or greater from the slope crest, the effects of slope on p-y curves are insignificant.

17. KEY WORDS	18. DISTRIBUTION STATEMENT
Piles, full-scale testing, soil slope, tateral loading, p-y curves, p-multipliers, soil-pile interaction	No restrictions. This document is available to the public through the National Technical Informations Service, Springfield, CA 22161

19. SECURITY CLASSIFICATION *(of this report)*	20. NUMBER OF PAGES	21. COST OF REPORT CHARGED
Unclassified	347	

DISCLAIMER STATEMENT

The Kiewit Center for Infrastructure and Transportation

Effects of Soil Slope on Lateral Capacity of Piles in Cohesive and Cohesionless Soils

by

Nontapat Nimityongskul
Paul Barker
Scott A. Ashford

Kiewit -2012/01

March 2012

Final Report of a Research Project Funded by Caltrans under Facilities Contract No. 59A0645

The Kiewit Center for Infrastructure and Transportation Oregon State University
111 Kearney Hall
Corvallis, OR 97331
cce.oregonstate.edu

Oregon State UNIVERSITY

Oregon State University
School of Civil and Construction Engineering

EFFECTS OF SOIL SLOPE ON LATERAL CAPACITY OF PILES IN COHESIVE AND COHESIONLESS SOILS

by

Nontapat Nimityongskul

Paul Barker

Graduate Student Researchers

and

Scott A. Ashford

Interim Dean, College of Engineering

Final Report on a Research Project Funded by

Caltrans under Facilities Contract No. 59A0645

The Kiewit Center for Infrastructure and Transportation

Oregon State University

111 Kearney Hall

Corvallis, Oregon 97331

March 2012

DISCLAIMER

This document is disseminated in the interest of information exchange. The contents of this report reflect the views of the authors who are responsible for the facts and accuracy of the data presented herein. The contents do not necessarily reflect the official views or policies of the State of California or the Federal Highway Administration. This publication does not constitute a standard, specification or regulation. This report does not constitute an endorsement by the Department of any product described herein.

For individuals with sensory disabilities, this document is available in Braille, large print, audiocassette, or compact disk. To obtain a copy of this document in one of these alternate formats, please contact: Division of Research and Innovation, MS-83, California Department of Transportation, P.O. Box 942873, Sacramento, CA 94273-0001.

ACKNOWLEDGEMENTS

This report presents the results and analysis of testing for the study entitled "Effects of Soil Slope on Lateral Capacity of Piles in Cohesive and Cohesionless Soils" under Caltrans Contract No. 59A0645 carried out at Oregon State University. Their support is greatly appreciated.

ABSTRACT

A series of full-scale lateral loading tests for instrumented piles in cohesive and cohesionless soils were carried out at Oregon State University to assess the lateral response of piles in free-field and near slope conditions. Instrumentation data from the free-field piles and the piles installed at different distances from the slope crest were used extensively to monitor lateral pile response and to back-calculate p-y curves. For the cohesive soil tests, it was found that for small pile head displacements (less than 1.0 inch), the proximity of slope has insignificant effects on piles 2D or further from the slope crest where D is the pile diameter. For the piles on the slope crest, the effects of the soil slope should always be considered. The presence of the slope has insignificant effects for piles installed at distances of 8D or greater from the crest. For the cohesionless soil tests, the effects of slope on lateral pile capacity are insignificant at displacements of less than 2.0 inches for piles located 2D and further from the crest. For piles located at 4D or greater from the slope crest, the effects of slope on p-y curves are insignificant.

TABLE OF CONTENTS

LIST OF FIGURES

LIST OF TABLES

1. INTRODUCTION

Driven piles are commonly used to support highway structures subjected to lateral forces. These structures include retaining walls, as well as bridge bents and abutments, and are often constructed near natural or man-made slopes. In some cases it is desirable to install a pile at an angle, or batter, relative to the horizontal surface to increase the foundation stiffness. Therefore, the understanding of the lateral response of pile near a slope and pile with a batter angle are of major interest in design of pile foundations for lateral loading. When properly designed, pile foundations can be economically adopted for foundations that need to support large lateral loads.

The design criteria of pile foundations subjected to lateral load is usually governed by the maximum allowable deflection of the foundation. For design of piles under Service Limit State Load (Caltrans BDS Article 4.5.6.5.1), the required lateral capacity of a pile is 5 kips for 1-ft diameter steel pipe piles and 13 kips for 16-inch diameter Cast-In-Drilled-Hole (CIDH) piles for pile deflection of 1/4 inch for a fully embedded pile. However, these requirements for lateral resistance of piles are independent of soil type (i.e. soil with standard penetration resistance value of 10 or greater). Therefore, in other soil conditions, full-scale lateral pile load tests and geotechnical analysis (i.e. soil-structure interaction) are required to verify that the lateral capacities of piles meet these requirements.

One of the most widely accepted methods for analysis and design of laterally loaded piles is the Winkler spring method in which the soil resistance along the pile is modeled using a series of nonlinear soil springs, commonly known as *p-y* curves. Most of the existing standard *p-y* curves (e.g., for sand, see Reese *et al*., 1974; for soft clay, see Matlock, 1970; for stiff clay above water table, see Reese and Welch, 1975 and for stiff clay below water table, see Reese *et al*., 1975) were developed based on results of full-scale lateral load tests on piles in level ground for a limited range of soil conditions and pile diameters. The degree of accuracy of the predicted lateral response of pile using available methods can be evaluated by comparing with measured lateral response of piles from full-scale test results.

Currently, some methods (e.g., Reese *et al*., 2006, Zhang *et al*., 1999, Reese and Van Impe, 2001, Mezazigh and Levacher, 1998) have been developed to account for the effect of batter angle and soil slope. These methods, for the most part, are based on results from analytical solutions, and in the case of cohesionless soils, some limited centrifuge test results. Some of these recommendations have been implemented in a current design practice (e.g., *LPILE*) but have yet to be validated with full-scale test results. The available recommendations accounting for cohesive soil slopes are based on analytical solutions and only account for the lateral capacity of short piles (Stewart, 1999). Based on field investigation results (EMI Report 2005), both cohesionless and cohesive soils have also been used as structural backfill in bridge abutments in California. Thus, there is a need to develop a design method that is based on results from full-scale test in both soil conditions.

In this light, two series of full scale lateral load tests were conducted in cohesive soils (Series-I) and cohesionless soils (Series-II). These tests included baseline pile tests as well as experiments on piles near slope, piles on the slope, and battered piles. A reliable and readily usable method to predict the lateral force capacity for piles with batter angle and soil slope effect is presented. This report includes site description, test set-up, observations, experimental test results as well as analyses results and recommendation for both test series.

2. LITERATURE REVIEW

Previous studies of laterally loaded pile yielded several analytical methods that attempt to model lateral pile response. These methods include elastic continuum (e.g., Spillers and Stoll 1964; Poulos 1971 and Banerjee and Davies 1978), finite element (e.g., Desai and Appel 1976; Kuhlmeyer 1979; Randolph 1981; Brown *et al*. 1989) and Winkler spring (e.g., Hetenyi 1946; McClelland and Focht 1958; Matlock 1970; Reese *et al*. 1974; Reese *et al*. 1975; Reese and Welch 1975; Georgiadis and Georgiadis 2010). In design, the most widely used method is the Winker spring method because of the ease of taking into account pile-soil nonlinearity and the ability to consider layered soil using commercially available computer code. Several mathematical expressions have been used to describe the non-linearity of *p-y* curves. More recently, hyperbolic equations have been adopted by researchers to represent *p-y* curves. The limitation of current available methods is that these methods have only been validated for piles in level ground. In practice, piles are often installed near natural or man-made slopes.

Several researchers investigated the effects of soil slope on lateral capacity of piles using small-scale model testing (e.g., Poulos 1976; Chae *et al*. 2004), centrifuge testing (e.g., Terashi 1991; Boufica and Bouguerra 1995; Mezazigh and Levacher 1998), Finite Element Method analysis (e.g., Brown and Shie 1991; Ogata and Gose 1995; Chae *et al*. 2004; Georgiadis and Georgiadis 2010). Other analytical studies include the upper bound plasticity method (e.g., Stewart 1999). Most researchers recommend using the Winkler spring method for design of piles near a slope. Main findings from these studies are: reduction factors to be applied to a pile in level ground (i.e., load ratio, *p*-multiplier); distance from the slope crest in which slope effects are insignificant t_{min}; and depth from the ground surface in which slope effect is negligible z_{max}.

In this chapter, the most commonly used *p-y* curves are summarized and discussed. The review is mainly focused on *p-y* curves developed from static, short-term, monotonic lateral pile loading tests. These *p-y* curves are readily available in *LPILE*, a 2-D finite difference computer code for analyzing laterally loaded piles, which is the current standard of practice. In addition, a review of other *p-y* curves not included in *LPILE* is presented. Furthermore, possible factors affecting *p-y* curves are briefly discussed. Finally, recommendations to account for laterally loaded piles with soil slope effects by previous studies are reviewed.

2.1 WINKLER SPRING METHOD AND CONCEPT OF P-Y CURVE

In this section, background of the Winkler Spring Method and the concept of *p-y* curves are presented. Other methods for the analysis of laterally loaded piles in level ground have been thoroughly summarized by Juirnarongrit (2002) and are not reviewed here in detail.

2.1.1 WINKLER SPRING METHOD

Winkler (1867) modeled the response of beam on an elastic subgrade by characterizing the soil as a series of independent linear-elastic soil springs. Since then, this method has been implemented to model laterally loaded piles by several researchers (e.g., Reese and Matlock 1956; and Davisson and Gill 1963). The concept is illustrated in **Figure 2-1**. In this method, the pile is modeled using a beam element and soil is replaced with a series of independent linear-elastic springs. The lateral pile response can be obtained by solving the fourth order differential equation:

$$E_p I_p \frac{d^4 y}{dz^4} + Ky = 0 \tag{2.1}$$

where E_p is the modulus of elasticity of the pile, I_p is the moment of inertia of the pile, z is depth, and K is the modulus of subgrade reaction that can be expressed as:

$$K = \frac{p}{y} \tag{2.2}$$

where p is the soil resistance per unit length of pile (F/L) and y is the pile deflection (L). The modulus of subgrade reaction K has the dimension of stress (F/L^2).

The solutions to the differential equation can be obtained analytically or numerically. Analytical solutions are available in the case of constant modulus of subgrade reaction with depth (e.g. Hetenyi 1946; Barber 1953) and also for several other variations of subgrade modulus with depth (Matlock and Reese 1960). Non-dimensional solutions to predict the response of laterally loaded piles in a two-layer soil system for both free- and fixed-head conditions are also available (Davission and Gill 1963). For very small soil resistance, the values of modulus of subgrade reaction *K* can be estimated from plate load testing (Terzaghi 1955) or the theory of elasticity (Vesic 1961). Methods for estimating *K* are discussed in the later section.

For larger values of pile deflections, the relationship between *p* and *y* is non-linear. Using finite difference method, numerical solutions to the governing differential equations can be obtained for a greater variation of *p-y* curves. For this purpose, several computer codes were developed (e.g., *COM624*, *LPILE*, *FLPIER*). The most commonly used *p-y* curves are discussed in the following sections.

2.1.2 CONCEPT OF P-Y CURVE

The majority of the solutions to predict the lateral pile response using Winkler spring method mentioned in the previous section are applicable only for a case of linear-elastic soil properties. Real soil behavior is highly inelastic and non-linear. Therefore, beyond the elastic range, the relationship between soil resistance *p* and pile deflection *y* is nonlinear. Taking into account the nonlinearity of soil, the linear soil springs are replaced with a series of nonlinear soil springs. The most widely used *p-y* curves have been developed based on back analysis of full-scale lateral pile loading test results. This concept was first developed by McClelland and Focht (1958).

The concept of *p-y* curves is illustrated in **Figure 2-2**. It was assumed that a pile was perfectly straight prior to pile installation and that it was installed without bending. The soil stresses around the pile at a given elevation can be reasonably assumed to be uniform. If the pile is loaded to a given deflection, the stresses acting on the side of the pile in the direction of pile movement have increased and those on the other side have decreased. Based on this stress diagram, a net soil reaction can be obtained by the integration of stresses along pile per unit pile length. The result of the integration is called soil resistance or soil reaction *p*. The soil resistance *p* is associated with the pile deflection *y*. This process needs to be repeated for a series of deflections to obtain the forces per unit length of pile which combine to form a *p-y* curve. A possible shape of the deflected pile subjected to a lateral load, and a moment is shown in **Figure 2-3** along with a set of *p-y* curves obtained as described above. Using *p-y* curves, the lateral response of a pile such as deflection, rotation, and bending moment can be obtained by solving the beam equation such as Equation 2.1.

The characteristics of *p-y* curves depend upon the soil type. For a given soil deposit, a series of *p-y* curves can be obtained experimentally by conducting full-scale lateral loading tests on instrumented piles. **Figure 2-4** presents the methodology in developing the *p-y* curves. The bending moment diagram along the pile can be computed by the product of pile curvature, which are computed from the measured strain along the pile, with the known pile bending stiffness. Double differentiation of the bending moment profile along the pile produces the soil reaction curve. The deflection along the pile can be obtained by the double integration of the curvature profile along the pile. Therefore, the soil reaction versus the deflection of the pile, *p-y* curve, at a given depth can be obtained. From **Figure 2-4,** it should be noted that the calculated pile deflection at several pile diameter below the ground surface are very small. Duncan *et al*. (2004) suggest that the soil within 8D below the ground surface is most important with regard to response to lateral load. Dustin (2004) performed a sensitivity analysis for laterally loaded piles and concluded that the lateral pile response depends significantly on the properties of soil approximately 10D from the ground surface.

Several researchers have proposed methods to construct *p-y* curves for various soil types based upon back-computation of full-scale test results. The methods to develop *p-y* curves commonly used in design have been well summarized by Juirnarongrit (2002). In general, the most widely used *p-y* curves for cohesionless soil is developed by Reese *et al.* (1974) and American Petroleum Institute (1987). For cohesive soils, the most widely used *p-y* curves are; for soft clay, Matlock (1970); for stiff clay below the water table, Reese *et al*. (1975); for stiff clay above the water table, Reese and Welch (1975). For cemented sand, the *p-y* curves were developed by Ismael (1990). The available *p-y* curves for silt were developed by Reese and Van Impe (2001). Most of these *p-y* curves have been incorporated in the commercial programs for analyzing behavior of laterally loaded pile, such as *COM624P* (Wang and Reese 1993), *LPILE* (Reese *et al*. 2000), and *FLPIER* (University of Florida 1996). Other *p-y* curves (e.g., Bushan *et al*. 1979, Georgiadis and Georgiadis 2010) which were developed analytically are also discussed in the later section.

2.2 CHARACTERISTICS OF P-Y CURVES FOR COHESIVE SOILS

In this section, characteristics of *p-y* curves for cohesive soils are discussed. The two key elements of *p-y* curves are modulus of subgrade reaction K and ultimate soil resistance p_u. Previous studies suggest that the modulus of subgrade reaction is mainly dependent on soil modulus E_s (e.g., Vesic 1961; Yegian and Wright 1973; Thompson 1977; Kooijman 1989; Brown *et al*. 1989). Following the development of *p-y* curves and current practice, E_s is typically represented with E_{50} which is the ratio between stress and strain at 50 percent of failure stress. For the determination of E_{50}, most researchers (e.g., Matlock 1970, Reese and Welch 1975) recommend Unconsolidated-Undrained (UU) triaxial tests, which is most representative of the loading condition for full-scale lateral pile loading tests in cohesive soils (i.e., undrained, short-term, static condition). The ultimate soil resistance is mainly dependent on the soil undrained shear strength S_u, pile dimension (e.g., pile diameter) and bearing capacity factor N_p.

The most commonly used *p-y* curves were derived from full-scale test results for vertical piles installed in level ground with lateral loading only. This pile condition is referred to as a free-field condition. For most full-scale lateral pile loading tests, short-term monotonic, or pseudo-static undrained loading was applied to a pile. The *p-y* curves obtained from this type of loading condition is commonly referred to as baseline, or static *p-y* curves. The baseline *p-y* curves are important because they can be used to investigate the effect of other loading condition, such as cyclic loading, sustained loading and dynamic loading. In this dissertation, only static monotonic, short-term, undrained *p-y* curves are discussed, and are referred to as *p-y* curves. In the following section, available *p-y* curves for cohesive soils (e.g., Matlock 1970; Reese and Welch 1975; Bushan *et al*. 1979; Georgiadis and Georgiadis 2010) are described briefly.

2.2.1 KEY ELEMENTS OF P-Y CURVES FOR COHESIVE SOILS

Since the terms used to describe *p-y* curves (e.g., K, k_s and k_{py}) are often confused in the literature, they are summarized in **Table 2-1** to make this dissertation easier to follow. An example of a typical *p-y* curve is shown in **Figure 2-5**. The straight line portion of the curve (initial slope of the *p-y* curve) is referred to as the modulus of subgrade reaction K. The modulus of subgrade reaction is critical in the design of a foundation for small soil displacement such as service loading or allowable deformation.. The values of K can be obtained using in-situ testing, such as a plate loading test. Reese *et al*. (2004) reported the values of K for different consistency of clay in **Table 2-2**, based on values of coefficient of subgrade reaction k_s (F/L^3) for stiff, very stiff, and hard clay based on results from plate load tests as recommended by Terzaghi (1955). For example, for very stiff clay, the range of K is 925-1850 lbs per square inch (psi).

Researchers have studied the relationship of K with depth (or confining pressure). Terzaghi (1955) suggests that the modulus of subgrade reaction for stiff clay is independent of depth, and that the linear relationship between the p and y was valid when values of p were smaller than about one-half of the undrained shear strength based on triaxial test results. Reese *et al*. (1975) found that for clay below the water table, the modulus of subgrade reaction increases with depth. The study recommends using initial modulus of subgrade reaction k_{py} to represent the change in initial slope of p-y curves with depth. The distinction between coefficient of subgrade modulus and initial modulus of subgrade reaction (both k with same dimension) is explained in more detail later.

Another method for estimating the modulus of subgrade reaction is proposed by Vesic (1961). The study provided a relationship between the modulus of subgrade reaction K for the Winkler spring problem, and the material properties in the elastic continuum problem as

$$K = \frac{0.65E_i}{(1-\mu_s^{\,2})}\left[\frac{E_i D^4}{E_p I_p}\right]^{1/12} \tag{2.3}$$

where E_i = initial soil modulus of elasticity, μ_s = Poisson's ratio of the soil, D = pile diameter, and E_pI_p = flexural rigidity of the pile. Using the soil modulus of elasticity from the laboratory or field testing, as well as the pile property, the modulus of subgrade reaction can be estimated. As mentioned earlier, K depends on E_s, which always depend on confining pressure and in the case of cohesive soil, the over-consolidation ratio (OCR) which is the ratio of the precosolidation stress σ'_p to the existing vertical effective overburden stress σ'_{vo}. For stiff cohesive soils, E_s appears constant with depth because the reduction in OCR with depth is balanced by an increase in confining pressure.

The horizontal portion of the *p-y* curve shown in **Figure 2-5** is referred to as the ultimate soil resistance p_u. Analytical methods to estimate the ultimate soil resistance of clay near the ground surface were developed based on a wedge type failure theory; whereas, that at some distance below the ground surface was derived based on the flow failure model (Reese *et al*. 2006) as presented in **Figure 2-6**. For undrained loading, the value of p_u at a depth (z) can be estimated using the following equation:

$$p_u = N_p S_u D \tag{2.4}$$

Earlier methods (i.e. Matlock 1970; Reese and Welch 1975) suggest that the value N_p depends on soil unit weight γ, depth z, soil undrained shear strength S_u and constant J. Stevens and Audibert (1980) summarized available methods to calculate N_p for piles in cohesive soils and reported that earlier methods, such as Matlock (1970), underestimate p_u. Other methods to calculate N_p (i.e., Randolph and Houlsby 1984; Murff and Hamilton 1993; Martin and Randolph 2006; Georgiadis and Georgiadis 2010) have taken into account pile roughness using the pile-soil adhesion factor α. Some of the methods to calculate N_p, and therefore p_u, are discussed later.

Several researchers have proposed methods to construct the *p-y* curves for cohesive soils that are based on soil properties and pile dimensions. Georgiadis and Georgiadis (2010) explained two different shapes of *p-y* curves are commonly used in design practice. The first shape of *p-y* curves, as shown in **Figure 2-7a**, (Matlock 1970; Reese *et al*. 1974; Reese and Welch 1975; Mokwa *et al*. 2004) is described by the following equation:

$$p = 0.5 p_u \left(\frac{y}{y_{50}} \right)^{\beta} \tag{2.5}$$

where y_{50} is the pile/soil displacement at half the ultimate soil resistance and β is an empirical coefficient that ranges from 0.25 to 0.5. One of the shortcomings of Equation 2.5 is that, in the case of small y_{50}, it gives a very large initial slope of the *p-y* curves (i.e., modulus of subgrade reaction), resulting in a very small lateral pile displacement at small loads. This may be unconservative for the estimation of the load-displacement curve for design. To overcome this shortcoming, a hyperbolic equation has been adopted by several researchers to represent a *p-y* curve (e.g., Georgiadis *et al*. 1991; Rajashree and Sitharam 2001; Kim *et al*. 2004; Liang *et al*. 2009; and Georgiadis and Georgiadis 2010) as shown in **Figure 2-7b**. This curve, which has an initial slope of K and ultimate value of p_u, is mathematically described by the following hyperbolic equation:

$$p = \frac{y}{\frac{1}{K} + \frac{y}{p_u}} \tag{2.6}$$

The advantage of using this equation is that the initial slope of the *p-y* curve can be calculated and specified using appropriate values for the modulus of subgrade reaction (e.g., Terzaghi 1955; Vesic 1961). In the following sections, some of the existing *p-y* curves for cohesive soils are discussed.

2.2.2 SOFT CLAY P-Y CURVES

Matlock (1970) conducted full-scale lateral loading tests on a 13 inch diameter, 42 ft long steel pipe embedded in a soft clay deposit at Lake Austin, Texas. **Figure 2-8** presents the characteristic shape of the proposed soft clay *p-y* curve for static loading which is described using Equation 2.5 where $\beta = ⅓$. To estimate y_{50}, the study proposed the following equation:

$$y_{50} = C\varepsilon_{50}D \tag{2.7}$$

where C is a constant (C = 2.5) and ε_{50} is the strain at one-half of the maximum principal stress difference from a triaxial compression test.

Procedure to develop the soft clay *p-y* curves for static loading is given in **Table 2-3**. For determining the shear strength of soil, Matlock (1970) recommended in-situ vane-shear tests or Unconsolidated-Undrained (UU) triaxial compression tests.

2.2.3 STIFF CLAY P-Y CURVES BELOW WATER TABLE

Reese *et al*. (1975) performed lateral loading tests on two 2-ft diameter steel pipe piles embedded in stiff clay under the water table at a site in Manor, Texas. The shape of a *p-y* curves for static loading is presented in **Figure 2-9**. The shape of the *p-y* curve shows a large loss of soil resistance, compared to the Matlock (1970) soft clay *p-y* curves. Juirnarongrit (2002) suggests that the loss of soil resistance is because the soil at this site was expansive and continued to imbibe water as the testing progressed. **Table 2-4** summarizes the methodology for developing the *p-y* curves for stiff clay below water table for static loading only.

It should be noted that, using the methodology in **Table 2-4** and **Figure 2-10**, the *p-y* curve at the ground surface is zero which is different from Matlock (1970) soft clay *p-y* curves. The observed slope of the back-calculated *p-y* curve increased with depth similar to sand *p-y* curves as discussed later. This depth dependency is different from the suggestion by Terzaghi (1955) for stiff clay as mentioned earlier. To account for this increase in initial slope of the *p-y* curve, Reese *et al*. (1975) introduced the use of the coefficient of change of modulus of subgrade reaction k_{py} (F/L^3) which increases linearly with depth as summarized in **Table 2-4**. The values of k_{py} were determined experimentally from back-calculated *p-y* curves using full-scale lateral loading test results to represent the change in slope of the *p-y* curves with depth. This value was not determined from plate load tests (coefficient of subgrade reaction, k_s) as recommended by Terzaghi (1955) even though both have identical unit (F/L^3). The distinction between coefficient of change of modulus of subgrade reaction k_{py} and coefficient of subgrade reaction k_s is also discussed in the cohesionless *p-y* curves section. Reese *et al*. (1975) recommended UU triaxial compression tests with confining pressure equal to in-situ pressures for determining the undrained shear strength of the soil.

2.2.4 STIFF CLAY P-Y CURVES ABOVE WATER TABLE

Welch and Reese (1972) conducted a lateral loading test for a 3-ft diameter bored pile at a test site in Houston, Texas. The characteristic shape of a *p-y* curve for static loading is presented in **Figure 2-11**. The shape and equation of the *p-y* curve is similar to the *p-y* curves for soft clay (Matlock, 1970). To fit the back-calculated *p-y* curves for their study, Reese and Welch (1975) recommend $\beta = 0.25$ and C = 2.5 for Equation 2.5. No loss of soil resistance was observed unlike the shape of the *p-y* curve for stiff clay below free water (Reese *et al*. 1975).

Table 2-5 summarizes a procedure for constructing the *p-y* curves as proposed by Reese and Welch (1975). UU triaxial compression tests with confining pressure equal to in-situ pressures are recommended for the determination of the undrained shear strength of the soil.

Bushan *et al*. (1979) conducted full-scale lateral loading tests on drilled piers in stiff clay. The study found that available *p-y* curves for stiff clay underestimate the lateral loading test results. As a result of parametric study, the study proposed using Equation 2.5 for the *p-y* curves, same as Matlock (1970) and Reese and Welch (1975), with $\beta = 0.5$, C = 2 and $J = 2$.

It should be pointed out that the *p-y* curves described above were developed based on a small number of lateral loading tests. Therefore, the use of these *p-y* curves for a wider range of soil conditions may be questionable.

2.2.5 HYPERBOLIC P-Y CURVES FOR UNDRAINED LOADING IN COHESIVE SOILS

As mentioned in the previous section, hyperbolic *p-y* curves (Equation 2.6) have been adopted by several researchers for the analysis of laterally load piles. The hyperbolic relationship has been widely used in modeling of non-linear stress-strain of soil (e.g., Konder 1963). For laterally load pile in sand, Kim *et al*. (2004) recommend hyperbolic *p-y* curves for the analysis. Liang *et al*. (2009) recommend hyperbolic *p-y* curves for analysis of laterally loaded drilled shafts in rock mass.

For cohesive soils, the most recent study was conducted by Georgiadis and Georgiadis (2010). A series of three-dimensional finite element analyses were performed to study the behavior of piles in sloping ground under undrained loading conditions. Most of the analyses were performed on soils with undrained shear strength of approximately 2400 psf. It was reported that current design methods (e.g., Matlock 1970; Reese and Welch 1975) underestimate the value of N_p in Equation 2.4, used to calculate the ultimate soil resistance p_u. The study proposed a new method for calculating the bearing capacity factor that takes into account the inclination of slope, θ, and the adhesion of the pile-slope interface, α, in estimating the bearing capacity factor. **Figure 2-12** presents available relationships for α and S_u. In general, rough pile-soil interface ($\alpha = 1$) gives larger bearing capacity factors than smooth pile-soil interface ($\alpha = 0$).

The initial slope of the *p-y* curve K is estimated using the following equation:

$$K = \frac{1.3E_i}{(1-\mu_s^{\,2})}\left[\frac{E_i D^4}{E_p I_p}\right]^{1/12} \tag{2.8}$$

It should be noted that Equation 2.8 is twice the value of K recommend by Vesic (1961). Rajashree and Sitharam (2001) was the first to propose Equation 2.8 for analysis of laterally loaded piles in cohesive soils. **Table 2-12** summarizes procedures to develop static *p-y* curves for cohesive soils under undrained loading based on the study by Georgiadis and Georgiadis (2010). Following the development of *p-y* curves and current practice, soil modulus E_s is typically represented with E_{50} which is the ratio between stress and strain at 50 percent of failure stress. The initial elasticity modulus E_i in Equation 2.8 can be related to E_{50} following an expression for triaxial compression (Kondner 1963; Robertson *et al*. 1989):

$$E_s = E_i\left(1 - \frac{R_f \sigma}{\sigma_f}\right) \tag{2.9}$$

where σ is the deviatoric stress, E_s is the elasticity modulus at deviatoric stress σ, σ_f is the deviatoric failure stress and R_f is the ratio of deviatoric stress over deviatoric ultimate stress. Setting $\mu_s = 0.5$ for theoretical undrained loading, $R_f = 0.8$ and $\sigma/\sigma_f = 0.5$, Equation 2.8 becomes

$$K = 3E_{50}\left[\frac{E_{50} D^4}{E_p I_p}\right]^{1/12} \tag{2.10}$$

It is noted that other values of μ_s gives a slightly different variation of Equation 2.10.

2.2.6 SUMMARY OF COHESIVE SOILS P-Y CURVES

The key elements of *p-y* curves are the modulus of subgrade reaction K and the ultimate soil resistance p_u. The conventional methods tend to give a large initial stiffness of *p-y* curves.

The use of hyperbolic equations allows the flexibility of specifying a value of K for *p-y* curves. For stiff cohesive soils, most studies suggest that the parameter K is independent of the initial confining pressure. For estimating the ultimate soil resistance, more recent studies suggest taking into account pile roughness using pile-adhesion factor α. In the next section, *p-y* curves for cohesionless soils are discussed.

2.3 CHARACTERISTICS OF P-Y CURVES FOR COHESIONLESS SOILS

In this section, characteristics of *p-y* curves for sand are discussed. The main difference from sand and clay *p-y* curve is that sand *p-y* curves are highly dependent on confining pressure. Like in clay, the commonly used sand *p-y* curves are derived from full-scale lateral pile load test results for free-field condition only. A brief summary of methods to construct *p-y* curves for sand is presented in this section.

2.3.1 KEY ELEMENTS OF P-Y CURVES FOR COHESIONLESS SOILS

Confining pressure is one of the most dominant factors affecting sand *p-y* curves. The *p-y* curve at the ground surface has zero values of p for all values of y and the slope of the *p-y* curve increases approximately linearly with depth (Terzaghi 1955; Reese *et al*. 1974). Terzaghi (1955) recommends a series of straight lines with slopes that increase linearly with depth as

$$K = k_s z \tag{2.11}$$

where: z = depth (L), k_s = coefficient of subgrade reaction from plate load tests (F/L^3), and K = modulus of subgrade reaction (F/L^2) which is zero at the ground surface (when z = 0) and linearly increasing with depth. Reese *et al*. (1974) suggests that the values of k_s recommended by Terzaghi (1955) for dry and submerged sand, as presented in **Table 2-6** give larger pile deflections than those measured in their pile load test results. Therefore, Reese *et al*. (1974) recommend values for k_{py}, referred to as the coefficient of change of modulus of subgrade reaction, for submerged and dry sand with different relative densities in **Table 2-7** based on experimental results. Several methods have been proposed to determine the ultimate soil resistance p_u for cohesionless soils (e.g., Brinch Hansen 1961; Broms 1964; Reese *et al*. 1974; Poulos and Davis 1980; Fleming *et al*. 1992; Zhang *et al*. 2005). For ultimate soil resistance near the ground surface, Reese *et al*. (1974) derived an expression based on a wedge type failure theory; whereas, that at some distance below the ground surface, was derived using the flow failure model as shown in **Figure 2-13**. A more recent study by Zhang *et al*. (2005) suggests that the ultimate soil resistance consists of frontal soil resistance and side shear resistance. Methods to construct the entire *p-y* curves for cohesionless soils are discussed in the next section.

2.3.2 REESE ET AL. (1974) SAND P-Y CURVES

Cox *et al*. (1974) performed static, short-term lateral loading on one 2-ft diameter steel pipe at a test site on Mustang Island. The soil at the site was uniform, fine sand with a friction angle of 39 degrees. The characteristic shape of *p-y* curves for static loading is presented in **Figure 2-14**.

Table 2-7 and **Figure 2-15** summarizes a procedure for constructing the *p-y* curves as proposed by Reese *et al*. (1974) based on the results of Cox *et al*. (1974). It was found that by using the equations for estimating the soil resistance based on the theoretical failure described earlier, the ultimate soil resistance was much smaller than the experimental one. Therefore, Reese *et al*. (1974) modified the ultimate soil resistance by introducing an empirical adjustment factor A as presented in **Figure 2-15** to bring the two quantities into agreement. Triaxial compression tests are recommended for obtaining the friction angle of sand which is a key component to obtain the theoretical ultimate soil resistance.

2.3.3 API SAND P-Y CURVES

The method in developing the *p-y* curve based on the procedure proposed by Reese *et al.* (1974) is cumbersome. As an alternative, the American Petroleum Institute (API 1987) presented methods to develop *p-y* curves for sand. Reese *et al*. (2004) stated that there is no difference for ultimate soil resistance (p_u) between the Reese *et al*. (1975) criteria and API criteria (1987). The main difference is the initial modulus of subgrade reaction and the characteristic shape of *p-y* curves. It is believed that the API (1987) method is easier to follow than the original method by Reese *et al*. (1974). In this method, the API sand *p-y* curves were prescribed with a hyperbolic tangent function as presented in **Table 2-8** and **Figure 2-16**. The equations for determining the ultimate soil resistance (Reese *et al.* 1974) were replaced by the use of three coefficients C1, C2 and C3 as a function of the friction angle, which can be obtained from the chart in **Figure 2-16a**. The chart for estimating the initial modulus of subgrade reaction is presented in **Figure 2-16b**. The API procedure for *p-y* curves in sand was validated by several field experiments. In the next section, *p-y* curves for other types of soils are discussed.

2.4 OTHER P-Y CURVES

Up to this point all of the *p-y* curves were developed for homogeneous sand and clay deposits. Most soil deposits consist of several soil layers and the soil properties within each layer are not always homogeneous. In the following sections, *p-y* curves for *c-ϕ* soils, partially saturated soil condition, and layered soil deposits are briefly discussed.

2.4.1 CHARACTERISTICS OF P-Y CURVES FOR c-ϕ SOILS

In design practice, cemented soils are often encountered. These types of soils possess both cohesion and friction and are often referred to as c-ϕ soils. Ismael (1990) proposed methods to develop *p-y* curves for cemented-sand based on two full-scale lateral pile loading tests. The test piles were 1-ft diameter reinforced concrete bored piles with lengths of 36 and 60 ft. The cemented sand had a friction angle of 35 degrees and cohesion of 420 psf based on drained triaxial test results. The study reported that Resse *et al*. (1974) sand *p-y* curves underestimated the experimental results because it ignored the cohesion component that contributed to soil resistance. The characteristic shape of *p-y* curves for cemented soil is shown in **Figure 2-17**. Procedures for developing cemented sand *p-y* curves are summarized in **Table 2-9**. The shape of the *p-y* curve is described with a polynomial function similar to soft clay *p-y* curves (Matlock 1970). Juirnarongrit (2002) suggests that this method can be used to reasonably predict the lateral response of Cast-In-Drilled-Hole (CIDH) piles in weakly cemented sand for a limited range of pile diameters. This method, however, has not been incorporated in *LPILE*.

Another method to develop *p-y* curves for cemented soil is proposed by Reese and Van Impe (2001). This method is available in *LPILE*, and is called silt *p-y* curves. The shape of a silt *p-y* curve, as presented in **Figure 2-18**, is different from that of cemented sand *p-y* curves (Ismael 1990) because it exhibits strain softening after reaching peak strength. A summary of procedure to develop silt *p-y* curves is given in **Table 2-10** and **Figure 2-19**. Juirnarongrit (2002) concluded that cemented sand *p-y* curves (Ismael 1990) gave better predictions of the lateral response of CIDH piles in weakly cemented sand than silt *p-y* curves (Reese and Van Impe 2001).

2.4.2 P-Y CURVES FOR PARTIALLY SATURATED SOILS

Some studies have been conducted for *p-y* curves in partially saturated soil conditions. Mokwa *et al*. (2004) performed twenty lateral loading tests on 8-inch diameter drilled shafts at several sites where the soils were partially saturated silts and clays with both cohesion and friction. The study adopted a variation of Equation 2.4 to represent *p-y* curves. To account for partially saturated soil condition, a reduction factor of 0.85 (Helmer *et al*. 1977) was adopted in estimating the ultimate soil resistance following Brinch-Hansen (1961) method.

2.4.3 DEVELOPMENT OF P-Y CURVES FOR LAYERED SOILS

All the methods to develop *p-y* curves mentioned above are applicable only for homogeneous soil deposit. For layered soil deposit, Georgiadis (1983) proposed an 'equivalent' depth concept to develop *p-y* curves. This concept is presented schematically in **Figure 2-20**. In this method, the *p-y* curves for the upper soil layer are determined using appropriate recommendation for a homogeneous soil deposit. The *p-y* curves for each successive layer are determined using equivalent depths. For the second layer, the equivalent depth can be computed by first solving for the equivalent force acting at the layer interface using the equation:

$$F_1 = \int_0^{H_1} p_{u1} dH \tag{2.12}$$

where F_1 is the force required to induce the soil failure of the pile segment embedded to the bottom of the upper layer, p_{u1} is the ultimate soil resistance of the upper layer, and H_1 is the thickness of the first layer. The equivalent depth of the second layer is determined by solving the following equation:

$$F_1 = \int_0^{h_2} p_{u2} dH \tag{2.13}$$

where h_2 is the equivalent depth of the first layer as if the entire soil profile consists of soil in the second layer, p_{u2} is the ultimate soil resistance of the second layer. Using the computed equivalent depth, the *p-y* curves of the second layer is determined using appropriate *p-y* recommendation. The equivalent depth h_3 and the *p-y* curves of the third layer are obtained by the same procedure.

The predicted lateral pile response using the equivalent depth approach for layered soil was in good agreement with the field test results. This procedure has been incorporated in *LPILE*.

2.5 AVAILABLE METHODS FOR PILES NEAR A SLOPE

Up to this point, the design methods and recommendations were developed for laterally loaded piles in level ground or free-field condition. In practice, piles are often installed near natural or man-made slopes. Several researchers investigated the effects of soil slope on lateral capacity of piles using small-scale model tests, centrifuge tests, Finite Element analysis and full-scale lateral pile loading tests. At present, results from full-scale tests are very limited. Some of the major findings are summarized in the following paragraphs.

In most of the previous studies, the effects of soil slope are typically evaluated by comparing the load-displacement relationship between free-field piles and piles near slope. As a result, the load ratios ψ which is only a function of distance from the pile to the slope crest were reported. The load ratio can be defined as:

$$\psi = \frac{V_{slope}}{V_{free-field}} \tag{2.14}$$

where V_{slope} is the measured lateral load, which is usually applied at the pile top, for pile near slope and $V_{free-field}$ is the lateral load at the pile top for free-field pile. The load ratio can be used as a simple measure of the effects of slope as well as to determine the smallest distance away from the slope crest in which slope effects become negligible ($\psi = 1$). It should be noted that the load ratio is not the same as *p*-multiplier, though both ratios describes the decrease in lateral resistance of piles near slope when compare to piles in level ground.

Following the *p-y* method, researchers recommend a scale factor to be applied to the *p*-component of the *p-y* curves. This scale factor is commonly known as *p*-multiplier. *P*-multipliers are derived from comparing back-calculated *p-y* curves between free-field piles and piles near a slope using the following equation:

$$p_{mult} = \frac{p_{slope}}{p_{free-field}} \tag{2.15}$$

The characteristic shape of the *p-y* curve using *p*-multiplier is presented in **Figure 2-21**. For design, Mezazigh and Lavecher (1998) proposed *p*-multipliers to account for slope effects as a function of the distance between the pile and the slope crest t and slope angle θ. Georgiadis and Georgiadis (2010) proposed new criteria for the initial slope of *p-y* curves and ultimate soil resistance for piles on a slope crest. **Table 2-11** summarizes a review of available literature regarding the lateral response of piles subjected to soil slope effects. The parameter t_{lim} represents the distance between the slope crest and the pile in which slope has negligible effects on the lateral pile response, typically reported in multiples of pile diameter D. The parameter z_{crit} is defined as the depth in which slope has insignificant effects on *p-y* curves reported in multiples of diameter. An expanded discussion of **Table 2-11** is provided in the following section.

2.5.1 SMALL-SCALE LABORATORY AND CENTRIFUGE TESTING

Some small-scale laboratory and centrifuge tests have been conducted to study the effects of slope on lateral capacity of piles. The main advantage of these tests is that various testing and soil conditions can be investigated in a controlled manner. The results from small scale tests offer insight into the effects of slope but uncertainties due to scaling effects may limit the use of these results in design practice. The majority of the studies are for piles in sand. Recommendations from these studies include both load ratio, ψ, and *p*-multiplier, p_{mult}.

Poulos (1976) conducted small-scale laboratory tests on piles in clay to study the effects of slope on lateral response of piles. The study suggests that t_{lim} is approximately 5D. Boufia and Bouguerra (1996) used a centrifuge to study the effects of the pile distance from slope crest on the lateral response of piles in sand. The study suggests that the range of t_{lim} is between 10D and 20D. Terashi (1991) performed centrifuge tests to investigate the behavior of laterally loaded piles in dense sand with different slope angles. The test results suggest that t_{lim} is approximately 2.5D. The same study also reported that p_{mult} for pile installed at the crest of the slope is 0.44, 0.63 and 0.64 for 33.7 (3 to 2), 26.5 (2 to 1) and 18.4 (3 to 1) degree slopes respectively indicating that slope effects appear to be a function of the slope angle.

Based on results from centrifuge testing for laterally loaded piles in sand, Mezazigh and Levacher (1998) reported that the lateral pile response is relatively insensitive to the soil relative density D_R. The following relationship for p_{mult} is proposed:

$$\begin{cases} p_{mult} = \dfrac{17-15\tan\theta}{100}\cdot\dfrac{t}{D}+\dfrac{1-\tan\theta}{2} & \quad if \quad t \le t_{\lim} \\ p_{mult} = 1 & \quad if \quad t \ge t_{\lim} \end{cases} \tag{2.16}$$

where t_{lim} = 4D (6tanθ - 1). The study suggests that t_{lim} is 8D and 12 D for slope angle of 26.5 (2 to 1) and 33.7 (3 to 2) degrees, respectively. It should be noted that Equation 2.16 is an empirical correlation of the test results. **Figure 2-22** presents load-displacement relationships and proposed p_{mult} by Mezazigh and Levacher (1998). It can be observed from **Figure 2-22a** that, for low pile head displacements (or low load levels), most of the load-displacement curves are similar to the baseline (reference) curve. This indicates that, in a small range of pile displacement, the slope may not have significant effects on the lateral pile response. **Figure 2-22b** shows that, at a given distance from the slope crest, the resulting p_{mult} contains considerable amount of scatter. This implies that there exists a range of p_{mult} for a pile at a given distance from the slope crest.

2.5.2 FINITE ELEMENT METHOD

Due to the availability of powerful computers, the Finite Element Method (FEM) has been used extensively to model soil-structure interaction problems. The main advantages of this method are that the continuity of soil can be taken into account and several other factors (e.g., loading height, pile-soil interface, and in-situ stress condition) can be investigated. In the future, this method is ideal for studying the response of laterally loaded piles because it can investigate several aspects of soil-structure interaction (e.g., stress-strain in the soil mass, influence of gapping, effect of construction sequence). Its accuracy depends on the ability to predict soil properties and select appropriate constitutive soil models to represent actual soil response-loading condition. One of the disadvantages of this method is the high computation time, especially in the case of 3-D analysis. Currently, FEM has been predominantly used in research for laterally loaded piles (e.g., Desai and Appel 1976; Randolph 1981; Kuhlemeyer 1979; Koojiman 1989; Brown *et al*. 1989; Chae *et al*. 2004; Georgiadis and Georgiadis 2010). For design, this method has rarely been used due to difficulties on defining the necessary parameters, requirement of engineering time in generating input and interpreting the results, as well as the limitation of current constitutive soil models.

Several researchers have conducted FEM analyses to study the effects of slope on lateral capacity of piles. Brown and Shie (1991) conducted 3-D elasto-plastic finite element analyses to study the effects of in-situ soil stresses, pile/soil interface friction, and sloping ground for laterally loaded piles in saturated clay. The study reported that the coefficient of earth pressure at rest K_o (varying ratio of horizontal to vertical stress from 0.5 to 1.5) was not a major factor affecting *p-y* curves. Pile/soil interface friction has significant effect on the lateral pile response. The effects of soil slope on the ultimate soil resistance, p_u, is maximum at the ground surface. The study suggests that z_{crit} is 4D. In addition, the study reported that the initial stiffness of the load-displacement curve, as well as *p-y* curve, is independent of ground slope. On the other hand, Ogata and Gose (1995) reported that the presence of a soil slope affected the spring stiffness (modulus of subgrade reaction, *K*), especially close to the ground surface.

Chae *et al*. (2004) performed a series of 3-D FEM analyses, as well as small model tests, to study the effects of soil slope on the lateral resistance of short single piles. The model piles had a diameter of 4 inch and a length of 20 inch. The test soil was a dense sand with relative density D_r of 90 percent, with a friction angle ϕ of 47.5 degrees. The slope angle for all the tests was 30 degrees. The load was applied at 4 inch (1D) from the ground surface. To account for the difference in the initial stress conditions between level ground and sloping ground, the study considered the variation of E_{50} as a function of mean confining pressure according to the following equation:

$$E_{50} = E_o(\sigma_m / \sigma_o)^n \tag{2.17}$$

where σ_m is the mean confining pressure, σ_o is the reference confining pressure, and E_o is the soil modulus at σ_o, and n is an exponent equal to 0.83. **Figure 2-23** shows the relationship between load ratio and displacement for each test case (i.e., 0D, 2D, 4D). The study concluded that the reduction of the lateral resistance due to slope effects is more significant for a small range of pile displacement and remain constant as the pile displacement increases. Based on the model test results, the load ratios at large pile displacements are approximately 0.4, 0.6 and 0.9 for piles located at 0D, 2D and 4D respectively. The load ratios at large pile displacements, from FEM analyses results, are 0.6, 0.8 and 0.9 for piles located at 0D, 2D and 4D respectively. The results from FEM analysis were generally stiffer than model test results.

In a more recent study, Georgiadis and Georgiadis (2010) performed 3-D Finite Element analyses to study the behavior of piles on the slope crest under undrained lateral loading conditions. Four slope angles considered were 0, 20, 30 and 40 degrees. The pile diameters were 1.6, 3.3, and 6.6 feet. Three different values of the adhesion factor α considered were 0.3, 0.5 and 1.0. For undrained static lateral loading of pile in level ground, the study proposed analytical methods for the ultimate soil resistance p_u and the initial stiffness of hyperbolic *p-y* curves K. The proposed *p-y* criteria take into account the inclination of soil slope θ and the adhesion of the pile-slope interface α. A summary of the procedure, given in **Table 2-12**, was discussed in the previous section. To account for slope effects on the initial slope of *p-y* curves, the study proposed the following relationship:

$$\mu = \frac{K_{i\theta}}{K_{io}} = \cos\theta + \frac{z}{6D}\left(1 - \cos\theta\right) \tag{2.18}$$

where $K_{i\theta}$ is the stiffness of *p-y* curve for piles on the slope crest, K_{io} is the stiffness of *p-y* curve for free-field piles. The study suggests that z_{crit} is 6D from the ground surface.

In summary, results from FEM analysis indicate that the lateral response of piles near a slope is dependent on the slope angle θ, the distance between the pile and the slope crest t, and pile-soil adhesion factor α. The depth in which slope effects become negligible ranges from 4D to 6D below the ground surface. In general, the results from FEM analysis are stiffer than model test results, even after accounting for the variation of E_{50} with confining pressure.

2.5.3 FULL-SCALE TESTS

At present, published full-scale test results for laterally loaded piles near a slope are limited. Bushan *et al*. (1979) conducted a lateral loading test on a drilled pier installed on clay slope crest. The study proposed other criteria for clay *p-y* curves as mentioned in the previous section. The test results were predicted with reasonable accuracy using the following recommendation for pile loaded downslope (Reese 1958 and also in Reese *et al*. 2006):

$$p_{slope} = \frac{p_{free-field}}{(1+\tan\theta)} \tag{2.19}$$

Reese (1958) developed the ratio $1/(1+\tan\theta)$ based on the approximate reduction of the volume of the soil in front of the pile. It should be noted that Equation 2.19 or any constant p_{mult} implies that the effects of slope are constant for any soil displacements or load levels. In addition, for design, Equation 2.19 has been used to modify the *p-y* curves at all depths along the pile. This assumption is reasonable for a flexible pile in a homogeneous soil deposit because pile displacements or soil displacements at several pile diameters below the ground surface are very small, and therefore the computed results are not affected.

Juirnarongrit and Ashford (2001) conducted a study to evaluate the effects of pile diameter on the initial modulus of subgrade reaction for Cast-In-Drilled-Hole (CIDH) piles in weakly cemented sand. Full-scale test results of two 3.9 ft diameter CIDH piles showed that a pile adjacent to a slope indicated significant reduced stiffness at larger displacements as compared to the pile without slope effects.

In a more recent study, Mirzoyan (2004) conducted a series of full-scale lateral loading tests to study the effects of soil slope on lateral capacity of piles in partially saturated cohesionless soils. The distances between piles and the slope crest considered were 0D (pile on crest) and 3D (3 pile diameter from slope crest). The study reported load ratio ψ for 0D pile and 3D pile as a function of pile head displacement as shown in **Figure 2-24**. Within 0.5 inch of pile head displacement, the load ratios for both the 0D pile and the 3D pile are not constant and appear to be decreasing as pile displacement increases. The load ratio is approximately 0.77 for the 0D pile when pile displacement is larger than 0.5 inch. Some of the observations include gapping that formed behind the pile as well as cracking in front of the piles. No back-calculated *p-y* curves were available from this study.

2.5.4 OTHER RECOMMENDATION FOR SOIL SLOPE EFFECT

Up to this point, the recommendations to account for slope effects were either based on FEM analyses or full-scale test results. Other methods include analytical solutions from the upper bound plasticity theory (i.e., Stewart 1999) and wedge failure theory (i.e., Reese *et al.* 2006). These methods have not been validated with full-scale test results.

Stewart (1999) used an upper bound plasticity method to estimate the undrained collapse load of laterally loaded short rigid piles near sloping ground. The study proposed the use of correction factors to reduce the ultimate lateral capacity of piles due to sloping ground in clay based on the method developed by Broms (1964). This reduction factor is the same as the load ratio which is defined as the ratio between the optimum collapse load for a given pile and slope geometry and the optimum collapse load for the pile in level ground. The reduction factors are presented in **Figure 2-25** for three different slope angles: 45 (1 to 1), 26.4 (2 to 1), and 14 (4 to 1) degrees; slope proximity ratio *B/D* (*t/D* in this study) from 0 to 4; and load eccentricity ratio *e/D* of 0 and 16 where *e* is the loading height above the ground surface.. For a long pile (*L/D* = 16) installed on the crest of the slope (*t/D* = 0) pile installed on the crest of a 2H: 1V slope, the slope correction factor was approximately 0.85. The influence of slope on the lateral capacity of piles was found to be minimal once the pile is located further than 4D from the slope crest. These charts are useful for predicting the collapse load of piles near sloping ground. However, this method gives only the ultimate lateral resistance of piles near slope, and does not allow for the prediction of the lateral displacement or the prediction the load ratio at lower load levels.

Reese *et al*. (2006) suggest modifications for the ultimate soil pressure of traditional *p-y* curves for sand and clay to account for piles in sloping ground. The proposed method includes modifying the analytical solutions for the ultimate soil resistance p_u near the ground surface for the case of horizontal surface to account for the presence of the slope assuming wedge-type failure. The equations for the ultimate soil resistance near the ground surface for a pile installed in a horizontal surface as derived by Reese *et al*. (1975) for sand and clay are summarized in **Table 2-13** and **Table 2-14** respectively.

2.5.5 SUMMARY OF STUDIES FOR PILES NEAR SLOPE

Based on the review of available literature, factors that affect lateral response of piles are the distance from the pile to the slope crest *t* and slope angle θ. The values for t_{lim} range between 4D and 20D depending on soil properties, pile type and slope angle. The range of values for z_{crit} is between 4D and 6D based on FEM analysis. In the next section, other factors affecting *p-y* curves are discussed.

2.6 FACTORS AFFECTING P-Y CURVES

In addition to slope effects, there are several factors affecting the lateral response of the soil-pile system and therefore the characteristics of *p-y* curves. The effects of these factors, such as loading type, pile diameter, and near field condition, have been investigated, to some extent, by several researchers and are summarized in the following paragraphs.

2.6.1 EFFECTS OF LOADING

In design of laterally loaded piles, there are four classes of lateral loading (Reese *et al*. 2004): short-term static, repeated cyclic, sustained, and dynamic. The *p-y* curves developed for short-term static loading are used to investigate the influence of other loading types.

The influence of cyclic loading has been studied by few researchers (e.g., Matlock 1970; Reese *et al*. 1975; Reese and Welch 1975). In general, cyclic loading results in the loss of soil resistance. For clay below water table, Reese *et al*. (2006) summarized the results from Wang (1982) and Long (1984) who studied the influence of cyclic loading on the *p-y* curves. The studies concluded that the loss of soil resistance for clay is a result of repeated strains of large magnitude and scour from the flow of water in the vicinity of the pile. For cohesionless soils, the loss of soil resistance is not as significant as in cohesive soils. Reese *et al*. (2006) suggested that the relative density of cohesionless soil is the key factor governing the lateral response of piles under cyclic loading.

Reese *et al*. (2004) discussed the effects of sustained loading on *p-y* curves. For soft and saturated clay, creep or stress relaxation was observed as a resulted of soil consolidation during sustained loading. For soft clay, Matlock (1970) observed creep at higher load levels and concluded that the change in bending moment due to creep was not significant. For overconsolidated clay, the effects of sustained loading are generally believed to be negligible. Bushan *et al*. (1979) reported that the increment of deflections (due to creep) under sustained loading is less than 20 percent of short-term (static-undrained) deflections for loads within one-half of the ultimate load. No studies on stress relaxation for lateral pile loading tests are available.

The rate of loading also affects the lateral response of piles and the characteristics of *p-y* curves. For dynamic loading, such as earthquake loading, the rate of loading is much larger than for static loading. Therefore, the static *p-y* curves should be adjusted with correlation factors to account for dynamic loading. The effects of loading rate on the lateral response of piles have been investigated by some researchers (for clay; Bea 1980, 1984; for sand; see Kong and Zhang 2007). Bea (1984) reported that high strain rate increases the soil shear strength and stiffness. Kong and Zhang (2007) suggested that the relationship between the lateral resistance and the loading rate can be expressed as

$$T_{s=k}(\dot{s}) = T_{s=k}(\dot{s}_{ref})\left[1+\alpha_a \log\left(\frac{\dot{s}}{\dot{s}_{ref}}\right)\right] \tag{2.20}$$

where $T_{s=k}(\dot{s})$ and $T_{s=k}(\dot{s}_{ref})$ are the lateral resistance at a specified horizontal displacement at loading rates $\dot{s}$ and $\dot{s}_{ref}$, respectively; α_a is a coefficient that represents an increase in lateral resistance at specified loading rate normalized by the lateral resistance at the reference loading rate, for one logarithmic cycle of loading rate. The lateral loading tests were conducted in a centrifuge using a robotic manipulator to control the rate of loading. The reference loading rates were 0.030 inch/sec and 0.028 inch/sec for loose and dense sands, respectively. For the range of horizontal displacements considered in the study, the values of α_a is 0.035-0.04 for loose sand and 0.04-0.15 for dense sand. It was concluded that loading rate has minor effect on the lateral pile resistance, but has significant effects on the bending moment distribution. At a high rate of loading, the location of maximum bending moment shifted upwards and an increased in soil reaction *p* was observed at shallow depths.

2.6.2 EFFECT OF PILE DIAMETER

As presented in the review of various types of *p-y* curves, most of the *p-y* curves were developed based on the results of full-scale tests on a limited number of pile sizes. The theory was then developed based on available information and then empirically extrapolated to use for other diameters. Juirnarongrit (2002) conducted a thorough literature review on the effects of pile diameter on *p-y* curves and carried out several lateral loading tests on CIDH piles with different diameter in cemented sand. It was concluded that pile diameter has insignificant effects at the displacement level below the ultimate soil resistance. Beyond this range, the ultimate soil resistance increases as pile diameter increases. For large diameter piles in cemented sand, the study also concluded that standard *p-y* curves may be appropriate. The existing *p-y* curves tend to underestimate soil resistance for smaller diameter piles.

2.6.3 PILE GROUP EFFECTS

When piles are installed close to each other, as in pile groups, interactions between piles, known as pile group effects, shadow effects or near-field effects, reduces the lateral capacity of each individual pile. Several studies have been conducted to investigate pile group effects on lateral load behavior of piles (e.g., Bogard and Matlock 1983; Brown *et al*. 1987; Rollins *et al*. 2003a,b; Rollins *et al*. 2005). Walsh (2004) and Snyder (2004) discussed pile group effects and summarized available design recommendations for pile groups subjected to lateral loads. The studies suggest that the overlapping of passive wedges or shear zones, generated as each pile is laterally loaded, adversely affects the lateral response of piles. **Figure 2-26** illustrates the interaction of piles group under lateral load.

In design of a pile group, researchers also propose *p*-multipliers (similar to Equation 2.15) which were derived from comparing back-calculated *p-y* curves using the following equation:

$$p_{mult,g} = \frac{p_{group}}{p_{free-field}} \tag{2.21}$$

where p_{group} is the soil resistance for pile in a pile group and $p_{free\text{-}field}$ is the soil resistance for a single pile or pile in free-field condition. It is believed that Brown *et al*. (1987) was the first to propose this concept. The characteristic shape of a *p-y* curve using *p*-multiplier is presented in **Figure 2-21**. The use of a single multiplier implies that the initial slope of the *p-y* curve is also affected and that group effects are constant for all soil displacements or load levels.

For design of a pile group, *p*-multipliers are dependent on soil type, distance between piles and location of piles in the group. Most studies found that piles in the front row (Row 1 in **Figure 2-26**) carry significantly higher loads than the subsequent rows (i.e., Row 2 and 3 in **Figure 2-26**). In general, the proposed *p*-multiplier to account for group effects shows considerable amount of scatter. Most studies agreed that the effects of pile group is negligible when group spacing is 8 pile diameter (8D) or larger. As mentioned earlier, this concept of *p*-multiplier has also been adopted for the use of other design condition such as laterally loaded piles with soil slope effects (e.g. Mezazigh and Levacher 1998; Reese *et al*. 2006).

2.7 SUMMARY OF LITERATURE REVIEW

The main findings from previous studies for laterally loaded piles in level ground are:

1. Key elements of the *p-y* curves are: the modulus of subgrade reaction, *K,* which is critical at small displacements, and the ultimate soil resistance, p_u, which is a function of the soil bearing capacity;
2. For stiff cohesive soils, *K* appears to be independent of confining pressure;
3. For cohesionless soils, *K* is highly dependent on confining pressure;
4. For cohesive soils, conventional equations for *p-y* curves (Matlock 1970; Reese and Welch 1975) give a very large initial stiffness;

5. The hyperbolic equation has been adopted to represent *p-y* curves for piles in level ground which allows for the specification of the initial stiffness of *p-y* curves; and

6. Pile-soil adhesion has significant effects on the estimation of bearing capacity factor N_p, and consequently the ultimate soil resistance p_u for piles in cohesive soils.

The findings for laterally loaded piles near a slope are:

7. The lateral response of a pile near a slope depends on the distance between the pile and the slope crest *D*, where D is the pile diameter and for the case of cohesionless soils, slope angle (θ)

8. Slope effects are more significant in cohesionless soils than in cohesive soils

9. The distance between the pile and the slope crest in which slope effects become negligible, t_{lim}, ranges between 4D and 20D depending on soil properties, pile type and slope angle.

10. The depth in which slope effects become insignificant, z_{crit}, ranges between 4D and 6D based on FEM analyses.

11. Two typical recommendations to account for slope effects are the load ratio (ψ) and p_{mult}.

12. FEM analyses generally predict stiffer lateral pile response compare to model test results.

Based on review of literature above, available full-scale test results for laterally loaded piles with slope effects are limited. Some methods have been developed to account for the effects of soil slope on the lateral response of piles. These methods, for the most part, are developed based on results from analytical solutions and some limited centrifuge tests. Some of these recommendations have been implemented in current design practice, but have yet to be validated with full-scale test results. For these reasons, the development of a better understanding of the full-scale lateral response of pile with slope effects is of major interest. To address the gap in literature, a series of full scale lateral loading tests were conducted in cohesive and cohesionless soils that included baseline pile tests as well as experiments on piles near slope.

The main objective was to gain a better understanding of the effects of soil slope on the lateral response of piles.

Table 2-1 Summary of Definition and Dimension of Terms Used in Analysis of Laterally Loaded Piles

Description	Symbol	Dimension	Comment
Soil resistance per unit length	p	F/ L	
Pile deflection	y	L	
Pile diameter	D	L	
Modulus of subgrade reaction	K	F/ L^2	
Coefficient of subgrade reaction[a]	k_s	F/ L^3	Plate Load Test
Initial modulus of subgrade reaction[b]	k_{py}	F/ L^3	Change in slope of experimental *p-y* curves

Notes

[a] Terzaghi (1955)
[b] Reese *et al*. (2006)

Table 2-2 Terzaghi (1955) Recommendations for Modulus of Subgrade Reaction *K* for Laterally Loaded Piles in Stiff Clay (after Reese *et. al.* 2004)

Consistency of Clay	Stiff	Very Stiff	Hard
Undrained Shear Strength, S_u (lb/ft^2)	2000-4000	4000-8000	>8000
Modulus of Subgrade Reaction, k_s (lb/in^2)	460-925	925-1850	>1850

Table 2-3 Summary of Procedure in Developing Soft Clay *p-y* Curves (Matlock 1970)

1. Compute Ultimate Soil Resistance, p_u (Using the smaller value)	$p_u = \left[3 + \frac{\gamma'}{S_u} z + \frac{J}{D} z\right] S_u D$ $p_u = 9 S_u D$
2. Compute Deflection at One-Half the Ultimate Soil Resistance, y_{50}	$y_{50} = 2.5 \varepsilon_{50} D$
3. Develop *p-y* Curves using the following Expression	$\frac{p}{p_{ult}} = 0.5 \left(\frac{y}{y_{50}}\right)^{1/3}$

where:

S_u	=	Undrained Shear Strength
D	=	Pile Diameter
J	=	Constant (0.5 for Soft Clay and 0.25 for Medium Clay)
p_u	=	Ultimate Soil Resistance
y_{50}	=	Deflection at One-Haft the Ultimate Soil Resistance
z	=	Depth
γ'	=	Effective Soil Unit Weight
ε_{50}	=	Strain at One-Half the Maximum Principal Stress Difference 0.020 for soft clay, 0.010 for medium clay, and 0.005 for stiff clay

Table 2-4 Summary of Procedure in Developing Stiff Clay with Free Water *p-y* Curves (Reese *et al*. 1975)

1. Compute Ultimate Soil Resistance, p_u (Using the smaller values)	$p_{ut} = 2c_a D + \gamma' Dz + 2.83c_a z$ (Wedge Failure) $p_{ud} = 11S_u D$ (Flow Failure)
2. Establish Initial Straight Line Portion	$p = (k_{py}z)y$ for Static Loading
3. Develop *p-y* Curves using the following Expression	$p = 0.5p_u\left(\frac{y}{y_{50}}\right)^{0.5}$, $y_{50} = \varepsilon_{50}D$
4. Develop the Second Parabolic Portion of the p-y Curves (from $A_s y_{50}$ to $6A_s y_{50}$)	$p = 0.5p_u\left(\frac{y}{y_{50}}\right)^{0.5} - 0.055p_u\left(\frac{y - A_s y_{50}}{A_s y_{50}}\right)^{1.25}$
5. Establish Straight-Line Portion (from $6A_s y_{50}$ to $18A_s y_{50}$)	$p = 0.5p_u(6A_s)^{0.5} - 0.411p_u - \frac{0.0625}{y_{50}}p_u(y - 6A_s y_{50})$
6. Establish Final Straight-Line Portion (beyond $18A_s y_{50}$)	$p = 0.5p_u(6A_s)^{0.5} - 0.411p_u - 0.75p_u A_s$

where: A_s = Constants (from **Figure 2-10**)

c_a = Average Undrained Shear Strength over Depth z

S_u = Undrained Shear Strength

D = Pile Diameter

k_{py} = Coefficient of Change Subgrade Reaction Constant (lb/in^3), for static loading,
For Clay with Avg. S_u between 7-15 psi, k_{py} = 500
For Clay with Avg. S_u between 15-30 psi, k_{py} = 1000
For Clay with Avg. S_u between 40-60 psi k_{py} = 2000

y_{50} = Deflection at One-Half the Ultimate Soil Resistance

z = Depth

ε_{50} = Strain at One-Half the Maximum Principal Stress Difference (0.004- 0.007)

γ' = Effective Soil Unit Weight

Table 2-5 Summary of Procedure in Developing Stiff Clay with No Free Water *p-y* Curves (Welch and Reese 1972; and Reese and Welch 1975)

1. Compute Ultimate Soil Resistance, p_u (use the smaller value)	$p_u = \left[3 + \frac{\gamma'}{S_u} z + \frac{J}{D} z\right] S_u D$ $p_u = 9 S_u D$
2. Compute Deflection at One-Half the Ultimate Soil Resistance, y_{50}	$y_{50} = 2.5 \varepsilon_{50} D$
3. Develop *p-y* Curves using the following Expression	$\frac{p}{p_u} = 0.5 \left(\frac{y}{y_{50}}\right)^{1/4}$ for $y \le 16 y_{50}$ $p = p_u$ for $y > 16 y_{50}$

where: S_u = Undrained Shear Strength
D = Pile Diameter
J = Constant = 0.5
p_u = Ultimate Soil Resistance
y_{50} = Deflection at One-Half the Ultimate Soil Resistance
y_s = Deflection under Short-Term Static
z = Depth
ε_{50} = Strain at One-Half the Ultimate Soil Resistance
0.020 for soft clay, 0.010 for medium clay, and 0.005 for stiff clay
γ' = Effective Soil Unit Weight

Table 2-6 Terzaghi (1955) Recommendations for Coefficient of Subgrade Reaction Constant for Laterally Loaded Piles in Dry and Submerged Sand (after Reese *et al*. 2004)

Relative Density of Sand	Loose	Medium	Dense
Dry or moist sand, k_s (lb/in^3)	3.5-10.4	13.0-40.0	51.0-102.0
Submerged sand, k_s (lb/in^3)	2.1-6.4	8.0-27.0	32.0-64.0

Table 2-7 Summary of Procedure in Developing Sand *p-y* Curves (Reese *et al*. 1974)

1. Preliminary Computation	$\alpha = \frac{\phi}{2}$, $\beta = 45 + \frac{\phi}{2}$, $K_0 = 0.4$, $K_a = \tan^2\left(45 - \frac{\phi}{2}\right)$
2. Compute Ultimate Soil Resistance from Wedge Failure, p_{st}	$p_{st} = \gamma' z \left[\begin{array}{l} \frac{K_0 z \tan\phi \sin\beta}{\tan(\beta - \phi)\cos\alpha} + \frac{\tan\beta}{\tan(\beta-\phi)}(D + z\tan\beta\tan\alpha) \\ + K_0 z \tan\beta(\tan\phi\sin\beta - \tan\alpha) - K_a D \end{array} \right]$
3. Compute Ultimate Soil Resistance from Flow Failure, p_{sd}	$p_{sd} = K_a D\gamma' z(\tan^8\beta - 1) + K_0 D\gamma' z\tan\phi\tan^4\beta$
4. Select Governing Ult. Soil Resistance, p_s	p_s = the smaller of the values given from step 2 and 3
5. Ultimate Soil Resistance, p_u	$p_u = \overline{A}_s p_s$ for static loading
6. Soil Pressure at D/60	$p_m = B_s p_s$ for static loading
7. Establish Initial Straight Line Portion	$p = (k_{py} z) y$
8. Establish Parabolic Section of *p-y* Curves	$p = \overline{C} y^{1/n}$, $m = \frac{p_u - p_m}{y_u - y_m}$, $n = \frac{p_m}{m y_m}$, $\overline{C} = \frac{p_m}{y_m^{1/n}}$, $y_k = \left(\frac{\overline{C}}{k_{py} z}\right)^{n/(n-1)}$

where:

$\overline{A}_s$	=	Adjustment Coefficient for Static p-y Curves from **Figure 2-15a**
B_s	=	Nondimensional Coefficient for Static p-y Curves from **Figure 2-15b**
D	=	Pile Diameter
k_{py}	=	Coefficient of Change of Modulus of Subgrade Reaction (lb/in^3) Loose Sand 20 (submerged) 25 (above water) Medium Dense Sand 60 (submerged) 90 (above water) Dense Sand 125 (submerged) 225 (above water)
p_{sd}	=	Theoretical Ultimate Soil Resistance due to Flow Failure
p_{st}	=	Theoretical Ultimate Soil Resistance due to Wedge Failure
p_s	=	Govern Ultimate Soil Resistance
p_u	=	Ultimate Soil Resistance
z	=	Depth
ϕ	=	Friction Angle
γ'	=	Effective Soil Unit Weight for Soil under Water

Table 2-8 Summary of Procedure in Developing API Sand *p-y* Curves (API 1987)

1. Compute Ultimate Soil Resistance from Wedge Failure, p_{st}	$p_{st} = (C_1 z + C_2 D)\gamma' z$
2. Compute Ultimate Soil Resistance from Flow Failure, p_{sd}	$p_{sd} = C_3 D\gamma' z$
3. Select Governing Ultimate Soil Resistance, p_s	p_s = the smaller of the values given from step 2 and 3
4. Determine Adjustment Coefficient for Static Loading	$\overline{A}_s = \left(3.0 - 0.8\frac{z}{D}\right) \geq 0.9$ for static lading
5. Develop Characteristic Shape of p-y Curves	$p = \overline{A} p_s \tanh\left(\frac{kz}{\overline{A} p_u} y\right)$

where: $\overline{A}_s$, $\overline{A}_c$ = Adjustment Coefficient for Static and Cyclic p-y Curves

C_1, C_2, C_3 = Coefficients from **Figure 2-16**a

D = Pile Diameter

k = Coefficient of Change of Modulus of Subgrade Reaction (lb/in^3) from **Figure 2-16**b

p_{sd} = Theoretical Ultimate Soil Resistance due to Flow Failure

p_{st} = Theoretical Ultimate Soil Resistance due to Wedge Failure

p_s = Govern Ultimate Soil Resistance

p_u = Ultimate Soil Resistance

z = Depth

ϕ = Friction Angle

γ' = Effective Soil Unit Weight for Soil under Water

Table 2-9 Summary of Procedure in Developing Cemented Sand *p-y* Curves (Ismael 1990)

1. Ultimate Soil Resistance, p_u	$p_u = C_p \sigma_p D$
2. Correction Factor, C_p	$C_p = 1.5$ for $\phi \leq 15^o$ $C_p = \dfrac{\phi}{10}$ for $\phi > 15^o$
3. Passive Earth Pressure, σ_p	$\sigma_p = 2c \tan\left(45 + \dfrac{\phi}{2}\right) + \sigma_v \tan^2\left(45 + \dfrac{\phi}{2}\right)$
4. Characteristic Shape of p-y Curves	$\dfrac{p}{p_u} = 0.5\left(\dfrac{y}{y_{50}}\right)^{1/3}$
5. Pile Deflection at which $p = 0.5p_u$, y_{50}	$y_{50} = 2.5\varepsilon_c D$

where: c = Soil Cohesion

C_p = Correction Factor for Small Width of Pile

D = Pile Diameter

p_u = Ultimate Soil Resistance

y_{50} = Pile Deflection at $p = 0.5p_u$

ϕ = Soil Friction Angle

σ_p = Passive Earth Pressure

σ_v = Effective Vertical Stress

ε_c = Strain at $(\sigma_1\text{-}\sigma_3) = 0.5(\sigma_1\text{-}\sigma_3)_u$

$(\sigma_1\text{-}\sigma_3)_u$ = Ultimate Principal Stress Difference in Triaxial Test

σ_1 = Major Principal Stress

σ_3 = Minor Principal Stress

Table 2-10 Summary of Procedure in Developing Silt *p-y* Curves (Reese and Van Impe 2001)

1. Preliminary Computation	$\alpha = \frac{\phi}{2}$, $\beta = 45 + \frac{\phi}{2}$, $K_0 = 0.4$, $K_a = \tan^2\left(45 - \frac{\phi}{2}\right)$
2. Ultimate Soil Resistance, p_u	$p_u = \overline{A_s} p_{u\phi} + p_{uc}$ for Static Loading
2. Friction Component, $p_{u\phi}$ (The smaller values from these 2 Eqs.)	$p_{u\phi} = \gamma' z\left[\frac{K_o \tan\phi \sin\beta}{\tan(\beta-\phi)\cos\alpha} + \frac{\tan\beta}{\tan(\beta-\phi)}(D + z\tan\beta\tan\alpha)\right] + \gamma z\left[K_o z \tan\beta(\tan\phi\sin\beta - \tan\alpha) - K_a D\right]$ $p_{u\phi} = K_a D\gamma' z(\tan^8\beta - 1) + K_o D\gamma' z \tan\phi \tan^4\beta$
3. Cohesion Component, p_{uc} (The smaller values from these 2 Eqs.)	$p_{uc} = \left(3 + \frac{\gamma'}{c}z + \frac{J}{D}z\right)cD$ $p_{uc} = 9cD$
4. Soil Pressure at D/60	$p_m = B_s p_{u\phi} + p_{uc}$ for Static Loading
5. Establish Initial Straight Line Portion	$p = (k_{py} z)y$, $k_{py} = k_c + k_\phi$ k_c and k_ϕ from **Figure 2-19**
6. Establish Parabolic Section of *p-y* Curves	$p = \overline{C} y^{1/n}$, $m = \frac{p_u - p_m}{y_u - y_m}$, $n = \frac{p_m}{m y_m}$, $\overline{C} = \frac{p_m}{y_m^{1/n}}$, $y_k = \left(\frac{\overline{C}}{k_{py} z}\right)^{n/n-1}$

where: c = Soil Cohesion
- D = Pile Diameter
- J = Constant
- B_s = Nondimensional Coefficient for Static *p-y* Curves from **Figure 2-15**b
- k_c, k_ϕ = Initial Subgrade Reaction Constant from Cohesion and Friction Components, Respectively (from **Figure 2-19**)
- k_{py} = Initial Subgrade Reaction Constant
- p_u = Ultimate Soil Resistance
- p_ϕ = Ultimate Soil Resistance from Friction Component
- p_c = Ultimate Soil Resistance from Cohesion Component
- z = Depth
- ϕ = Friction Angle
- γ' = Effective Soil Unit Weight

Reference	Soil Type		Test Type			# of test	Load Height	Analysis Type	Pile Properties			θ (°)	Pile at crest		t_{lim}	z_{crit}
	Sand	Clay	F	C	M				Type	Dia.	Length		ψ	p_{mult}		
Poulos (1976)		x			x	5	2 in.	Elastic Cont.		.25-.5 in	4.5 in.	90	n/a	n/a	5D	n/a
Bhushan *et al*. (1979)		x	x			4	G.S.	p-y criteria	conc.	2-4 ft	9-22 ft	20-50	n/a	n/a	n/a	-
Uto *et al*. (1985)	x	(Rock)	x			n/a	n/a	Sub. Reaction	n/a	10-11 ft	32 ft	20-30	n/a	n/a	-	-
Gabr and Borden (1990)	x		x				n/a	Pass.Wedge		11 in.	15 ft	30	0.5	n/a	n/a	n/a
Brown and Shie (1991)		x		n/a		n/a	n/a	3-D FEM	steel	n/a	n/a	15, 30	n/a	.68, .5	n/a	4D
Terashi *et al*. (1991)	x			x		26	20 in.	Modified p-y		30 in.	52 ft	18,27,34	n/a	.64,.63,.44	n/a	n/a
Boufia and Bouguerra (1995)	x			x		n/a	n/a	n/a	n/a	n/a	n/a	27	0.62	n/a	10-20D	n/a
Ogata and Gose (1995)	Rock			n/a		n/a	n/a	3-D FEM	n/a	n/a	n/a	n/a	n/a	n/a	n/a	n/a
Mezazign and Levacher (1998)	x			x		59	1.6 in.	Modified p-y	alum.	28 in.	40 ft	27,34	.62,.42	.47,.33	8D,12D	n/a
Stewart (1999)		x		n/a		n/a	n/a	UB Plasticity	n/a	n/a	n/a	14,27,34	.75,.85,.9	n/a	n/a	n/a
Chen and Martin (2001)	c-ϕ soil			n/a		n/a	n/a	3-D FD	conc.	3 ft	n/a	15,30,45	n/a	.44,.6,.64	6D	
Ng and Zhang (2001)	Granite					n/a	25 ft	3-D FEM	conc.	7 ft	100 ft	32	n/a	n/a	n/a	n/a
Juirnarongrit and Ashford (2001)	Cemented Sand		x			2	3 ft	n/a	CIDH	4 ft	39 ft	n/a	n/a	n/a	n/a	n/a
Chae *et al*. (2004)	x				x	4	4 in.	3-D FEM	alum.	4 in.	20 in.	30	0.4	n/a	>4D	n/a
Mirzoyan (2004)	x		x			3	19.5 in.	Modified p-y		1 ft	44 ft	30	0.77	n/a	>3D	n/a
Reese et al. (2006)	x	x				n/a	n/a	p-y criteria	n/a	n/a	n/a	27	x	0.67	n/a	n/a
Gerogiadis and Georgiadis (2010)		x		n/a		n/a	G.S.	p-y criteria	steel	3 ft	40 ft	0-40	n/a	Table	n/a	6D

Table 2-11 Summary of Available Literature for Laterally Loaded Piles with Soil Slope Effect

Table 2-12 Summary of Procedure in Developing Clay *p-y* Curves for Static Undrained Lateral Loading for Horizontal Ground with Adjustments for Slope Angle and Adhesion Factor (Georgiadis and Georgiadis 2010)

1. Compute Ultimate Soil Resistance, p_u	$p_u = N_p S_u D$
2. Compute Lateral Bearing Capacity Factor, N_p	$N_p = N_{pu} - \left(N_{pu} - N_{po}\cos\theta\right)e^{-\lambda(z/D)/(1+\tan\theta)}$
3. Compute Ultimate Lateral Bearing Capacity Factor, N_{pu}	$N_{pu} = \pi + 2\Delta + 2\cos\Delta + 4\left(\cos\frac{\Delta}{2} + \sin\frac{\Delta}{2}\right)$; $\Delta = \sin^{-1}\alpha$
4. Compute Lateral Bearing Capacity Factor at Surface, N_{po}	$N_{po} = 2 + 1.5\alpha$
5. Compute Non-Dimensional Factor, λ	$\lambda = 0.55 - 0.15\alpha$
6. Compute the Initial Stiffness of *p-y* Curves	$K_i = \frac{1.3E_i}{1-v^2}\left(\frac{E_i D^4}{E_p D_p}\right)^{1/12}$
7. Compute E_i from E_{50} using E_s expression (Konder, 1963; Robertson et al., 1989)	$E_s = E_i\left(1 - \frac{R_f\sigma}{\sigma_f}\right)$; $R_f = 0.8$; $\frac{\sigma}{\sigma_f} = 0.5$; $E_i = 1.67E_{50}$
8. Develop p-y Curves using the following Hyperbolic Expression	$p = \frac{y}{\frac{1}{K_i} + \frac{y}{p_u}}$
9. For Pile on the Slope Crest	$\mu = \frac{K_{i\theta}}{K_{io}} = \cos\theta + \frac{z}{6D}\left(1-\cos\theta\right)$

where: S_u = Undrained Shear Strength
θ = Slope Angle
D = Pile Diameter
N_p = Lateral Bearing Capacity Factor
Np_u = Ultimate Lateral Bearing Capacity Factor
Np_o = Lateral Bearing Capacity Factor at the Surface for Horizontal Ground
α = Pile-Soil Adhesion Factor (**Figure 2-12**)
λ = Non-Dimensional Factor
K_i, K_{io} = Initial Stiffness of *p-y* Curves
R_f = Ratio of Deviatoric Failure Stress over Deviatoric Ultimate Stress, commonly taken equal to 0.8

Table 2-12 - Continued

E_s = Elasticity Modulus at Deviatoric Stress σ
σ_f = Deviatoric Failure Stress
E_{50} = Elasticity Modulus at 50 Percent of the Failure Stress from Triaxial Compression Test
$K_{i\theta}$ = Initial Stiffness of *p-y* Curves for Pile on the Slope Crest

Table 2-13 Summary of Ultimate Soil Resistance for Piles in Sand Slopes (Reese *et al*. 1975)

1. Compute Ultimate Soil Resistance for Level Ground (**Table 2-10**)	min.of: $p_{st} = \gamma z\left[\begin{array}{l}\dfrac{K_o z\tan\phi\sin\beta}{\tan(\beta-\phi)\cos\alpha}+\dfrac{\tan\beta}{\tan(\beta-\phi)}(D+z\tan\beta\tan\alpha)\\ +K_o z\tan\beta(\tan\varphi\sin\beta-\tan\alpha)-K_A D\end{array}\right]$ and $p_{st} = K_A D\gamma z(\tan^8\beta-1)+K_o D\gamma z\tan\phi\tan^4\beta$
2. Ultimate Soil Resistance for Pile Load Upslope	$p_{usa} = \gamma z\left[\begin{array}{l}\dfrac{K_o z\tan\phi\sin\beta}{\tan(\beta-\phi)\cos\alpha}(4D_1^3-3D_1^2+1)\\ +\dfrac{\tan\beta}{\tan(\beta-\phi)}(DD_2+z\tan\beta\tan\alpha D_2^2)\\ +K_o z\tan\beta(\tan\phi\sin\beta-\tan\alpha)\\ (4D_1^3+3D_1^2+1)-K_A D\end{array}\right]$
3. Ultimate Soil Resistance for Pile Loaded Downslope	$p_{usa} = \gamma z\left[\begin{array}{l}\dfrac{K_o z\tan\phi\sin\beta}{\tan(\beta-\phi)\cos\alpha}(4D_3^3-3D_3^2+1)\\ +\dfrac{\tan\beta}{\tan(\beta-\phi)}(DD_4+z\tan\beta\tan\alpha D_4^2)\\ +K_o z\tan\beta(\tan\phi\sin\beta-\tan\alpha)\\ (4D_3^3+3D_3^2+1)-K_A D\end{array}\right]$

where : D = Pile Diameter

ϕ = Friction Angle

K_o = Coefficient of Earth Pressure at Rest

= 0.4 for loose sand and 0.6 for dense sand (Sowers and Sowers 1970)

K_A = Minimum Coefficient of Active Earth Pressure

β = $45+\varphi/2$

α = $\varphi/2$

D_1 = $\dfrac{\tan\beta\tan\theta}{\tan\beta\tan\theta+1}$

D_2 = $1-D_1$

D_3 = $\dfrac{\tan\beta\tan\theta}{1-\tan\beta\tan\theta}$

D_4 = $1+D_3$

Table 2-13 - Continued

$$K_{A_s} = \cos\theta \frac{\cos\theta - (\cos^2\theta - \cos^2\phi)^{0.5}}{\cos\theta + (\cos^2\theta - \cos^2\phi)^{0.5}}$$

$$K_{A_s} = \cos\theta \frac{\cos\theta - (\cos^2\theta - \cos^2\phi)^{0.5}}{\cos\theta + (\cos^2\theta - \cos^2\phi)^{0.5}}$$

Table 2-14 Summary of Ultimate Soil Resistance for Piles in Clay Slopes (Reese *et al*. 1975)

Piles in level ground	$p_{uca} = 2c_a B + \gamma bz + 2.83 c_a z$
Piles in positive slopes	$p_{uca} = (2c_a B + \gamma bz + 2.83 c_a z)\left(\frac{1}{1+\tan\theta}\right)$
Piles in negative slopes	$p_{uca} = (2c_a B + \gamma bz + 2.83 c_a z)\left(\frac{\cos\theta}{\sqrt{2}\cos(45+\theta)}\right)$

where: c_a = Average Undrained Shear Strength over the Depth z
b = Diameter (width) of Pile
γ = Unit Weight of Soil
z = Depth from the Ground Surface to the Desired *p-y* Curve
θ = Angle of Slope as Measured from Horizontal
p_u = Ultimate Soil Resistance per Unit Length

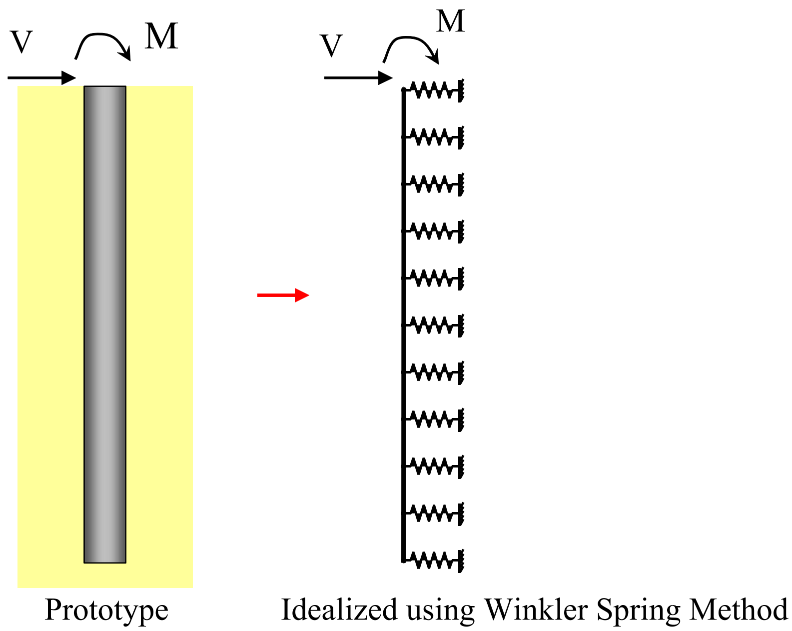

Figure 2-1 Implementation of Winkler Spring Concept for Laterally Loaded Piles (after Juirnarongrit 2002)

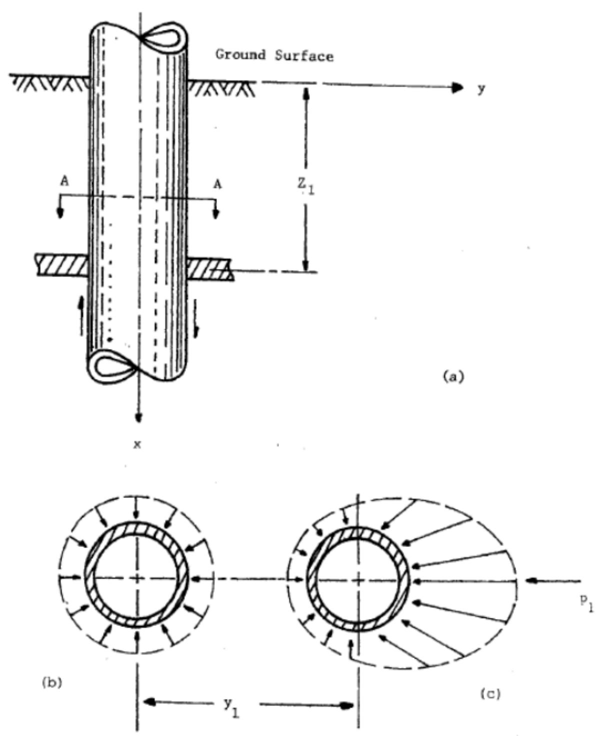

Figure 2-2 Distribution of Soil Pressure against the Pile before and after Lateral Loading: a) Elevation View of Pile; b) Soil Pressure at Rest; c) Soil Pressure after Lateral Loading (after Reese *et al*. 2006)

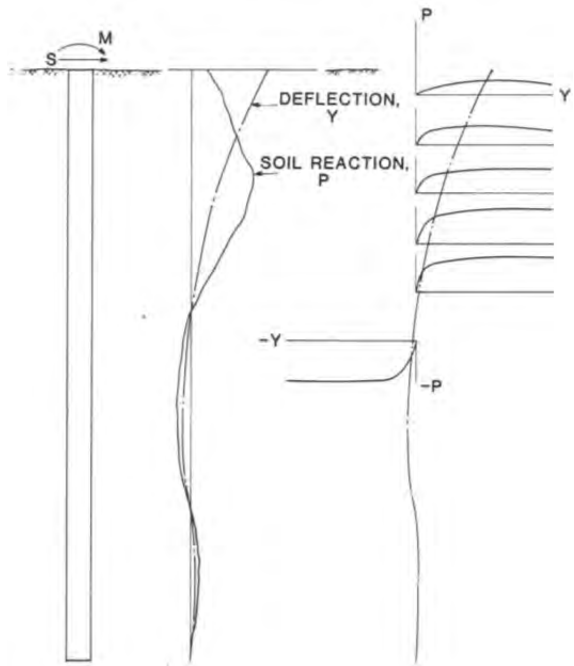

Figure 2-3 Typical Family of *p-y* Curves Response to Lateral Loading (after Dunnavant 1986)

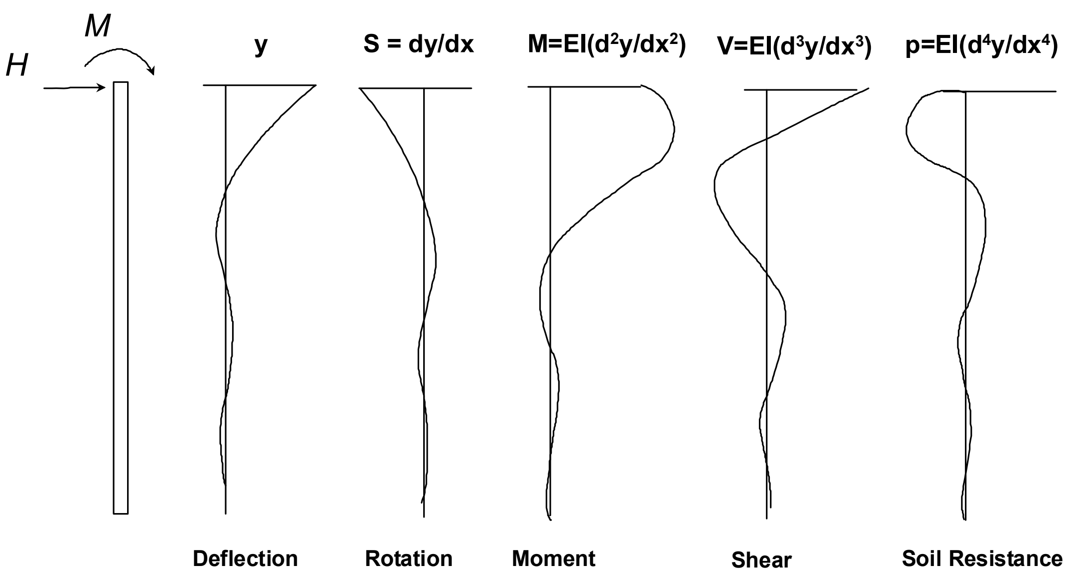

Figure 2-4 Methodology in Developing *p-y* Curves (after Reese and Van Impe 2001)

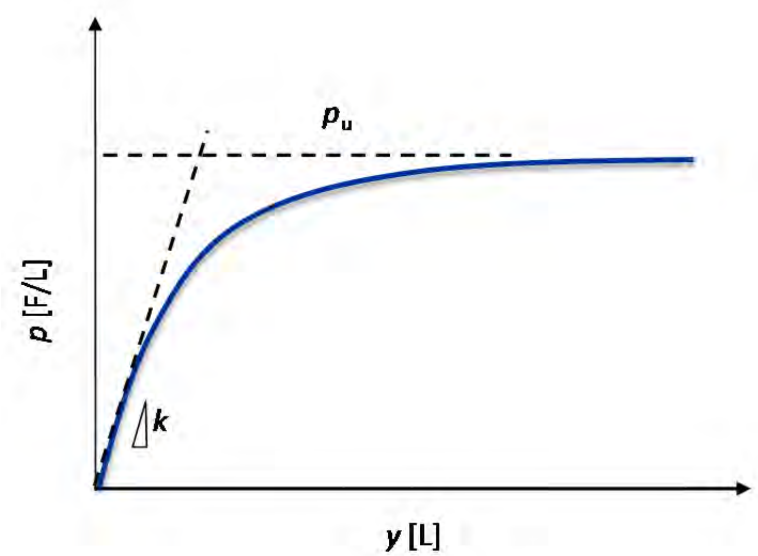

Figure 2-5 Conceptual *p-y* Curve for Static Loading

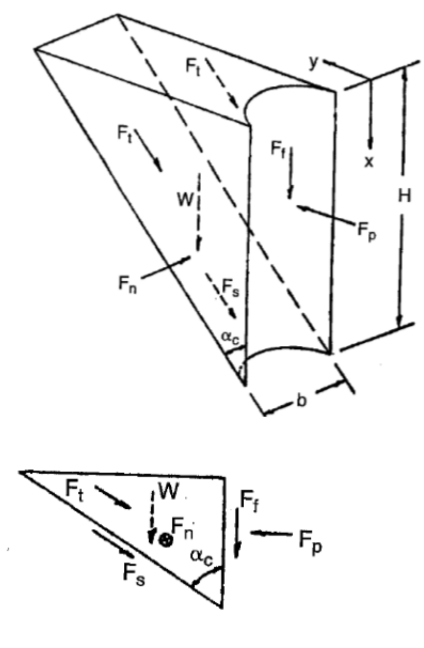

a) Assumed Passive Wedge Failure

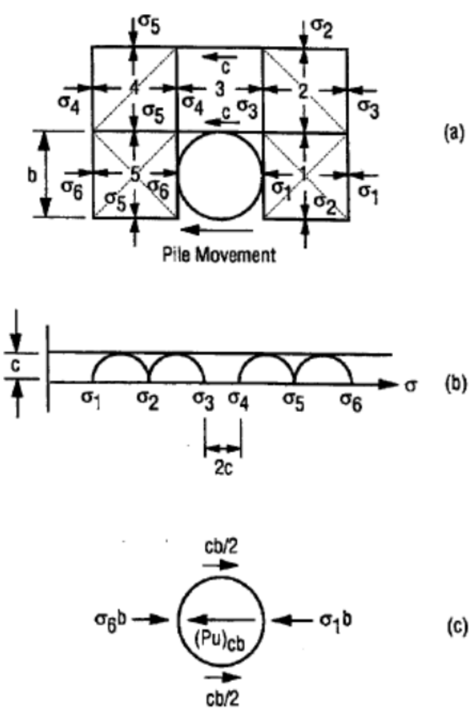

b) Assumed Lateral Flow Failure

Figure 2-6 Clay Failure Modes in Laterally Loaded Pile Problem a) Assumed Passive Wedge Failure; b) Assumed Lateral Flow Failure (after Reese *et al*. 2006)

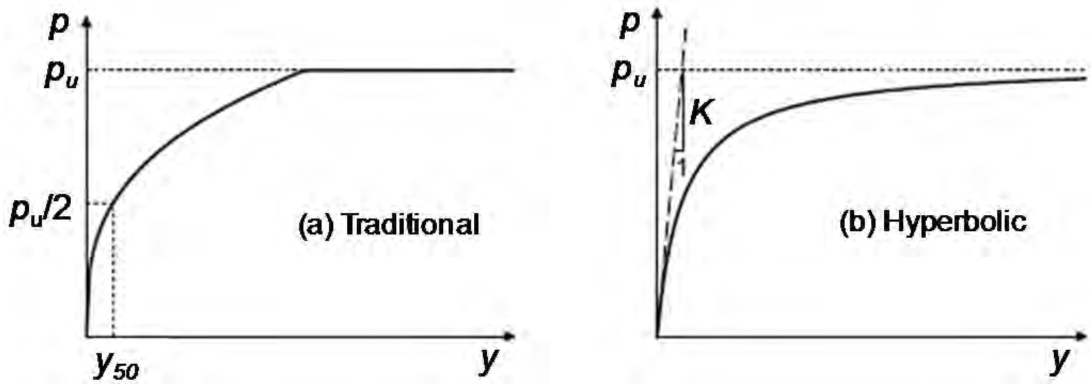

Figure 2-7 Typical Shapes of *p-y* Curves (after Georgiadis and Georgiadis 2010)

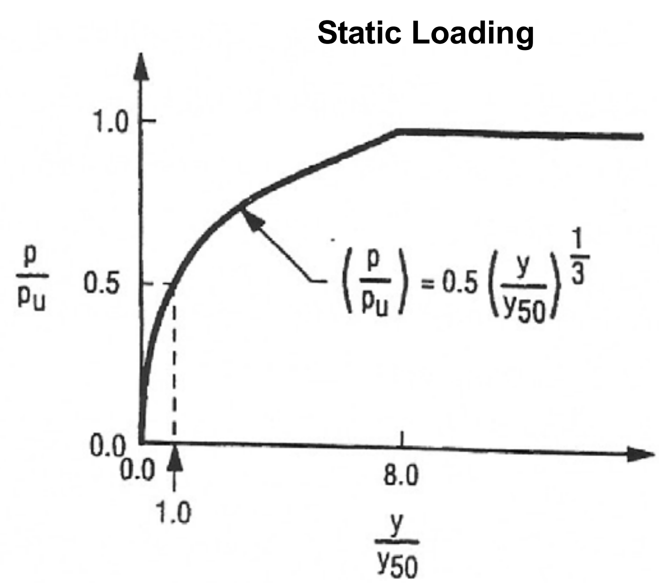

Figure 2-8 Characteristic Shape of *p-y* Curve for Soft Clay for Static Loading (after Matlock 1970)

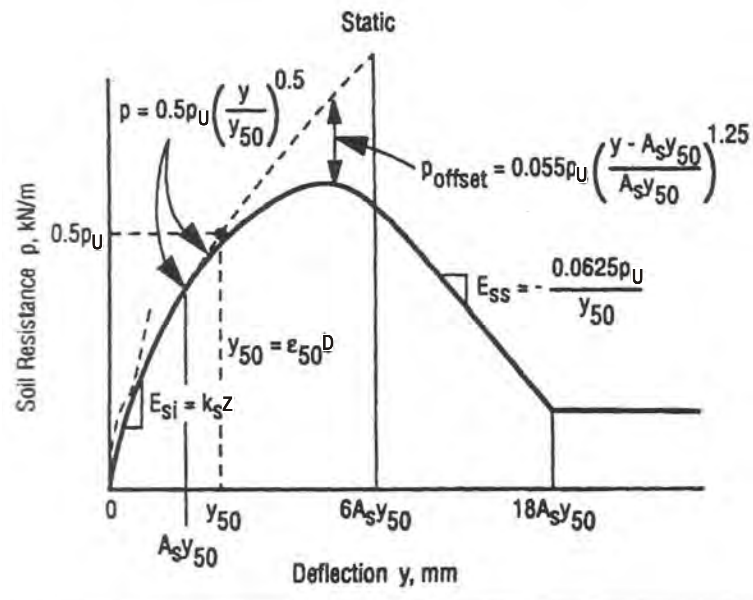

Figure 2-9 Characteristic Shape of *p-y* Curve for Stiff Clay below Water Table for Static Loading (after Reese *et al*. 1975)

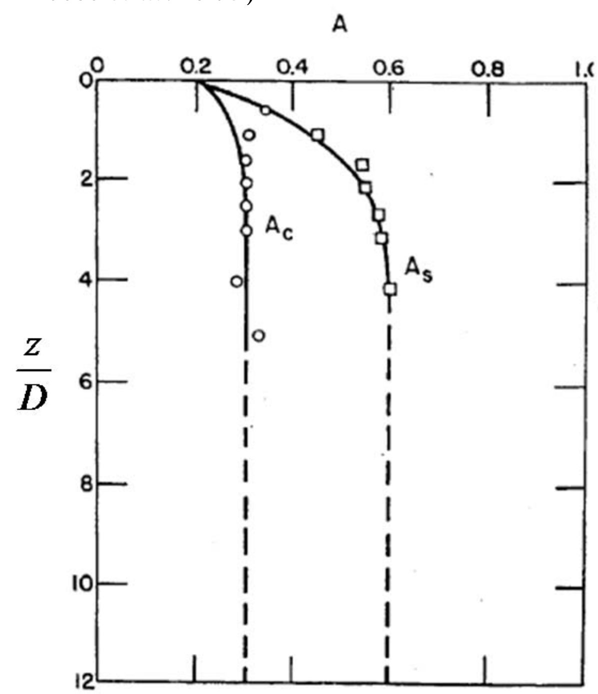

Figure 2-10 Value of Constant A for *p-y* Curves for Stiff Clay Below Water Table (after Reese *et al*. 1975)

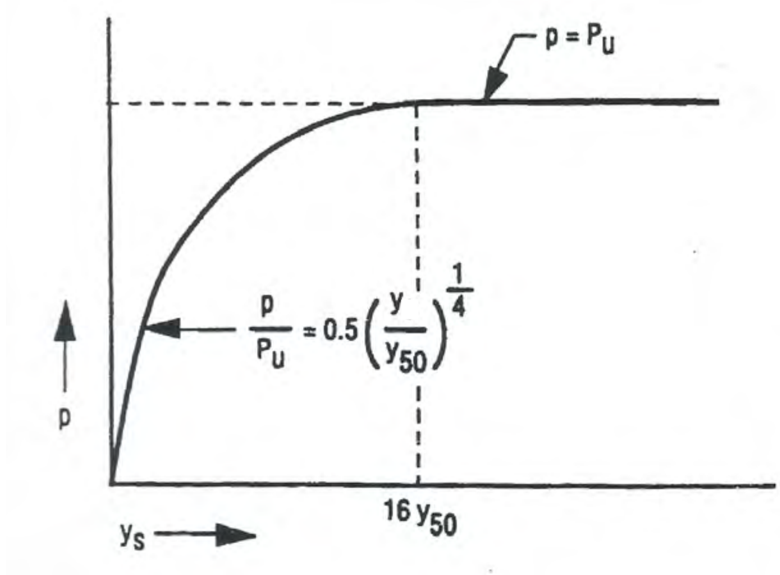

Figure 2-11 Characteristic Shape of *p-y* Curve for Stiff Clay above Water Table for Static Loading (after Welch and Reese 1972; Reese and Welch 1975)

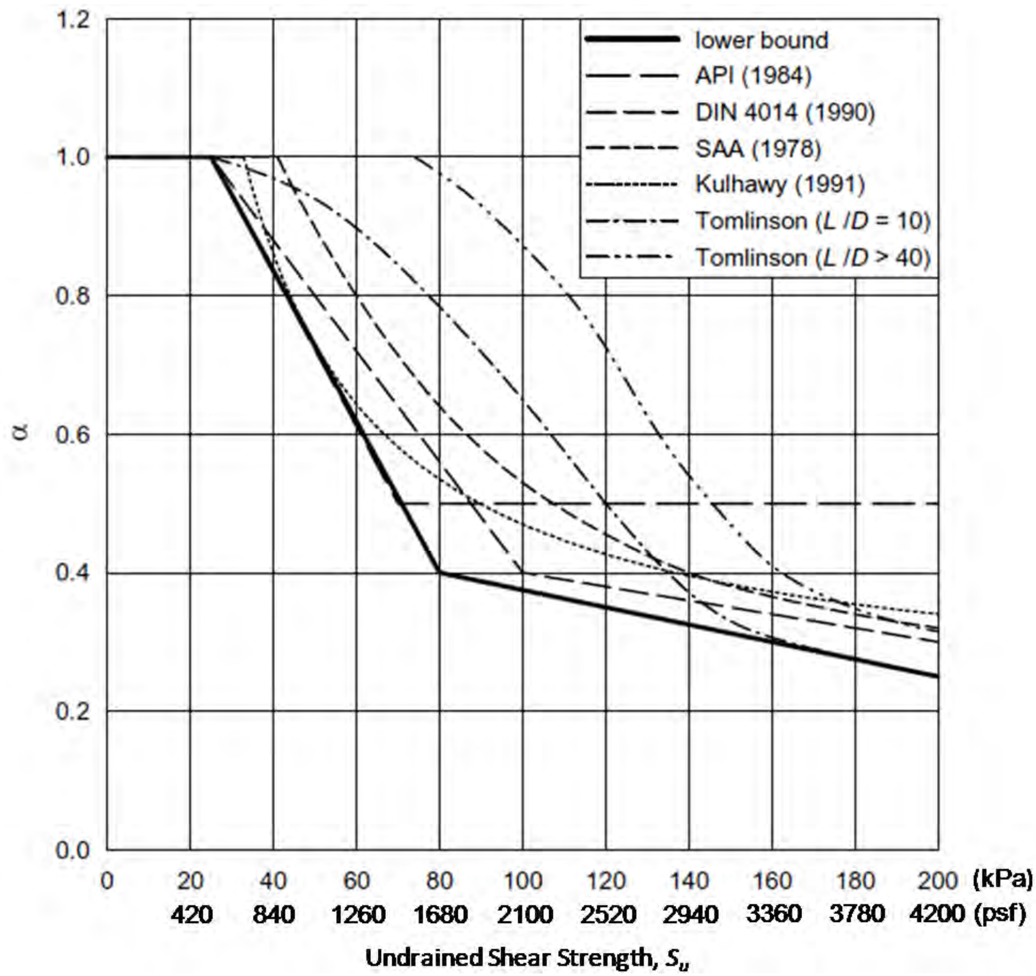

Figure 2-12 Summary of Adhesion factor (α) versus Undrained Shear Strength (S_u) Relationships for Piles and Drilled Shafts (after Georgiadis and Georgiadis 2010)

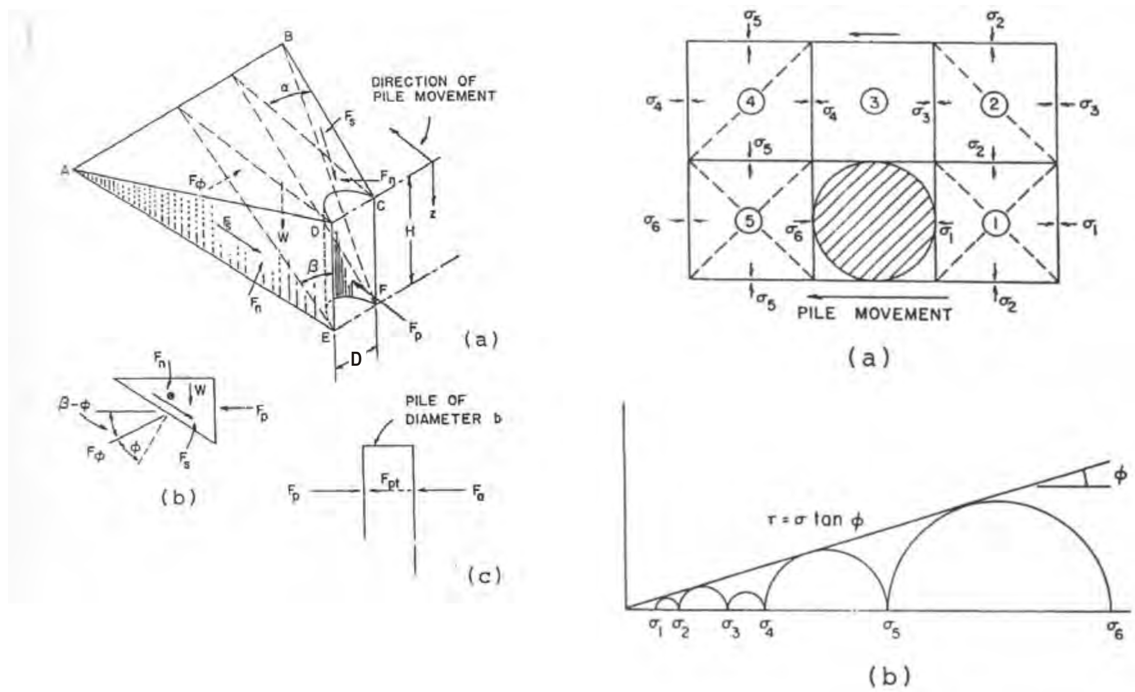

a) Assumed Passive Wedge Failure
b) Assumed Lateral Flow Failure

Figure 2-13 Sand Failure Modes in Laterally Loaded Pile Problem a) Assumed Passive Wedge Failure; b) Assumed Lateral Flow Failure (after Reese *et al*. 1974)

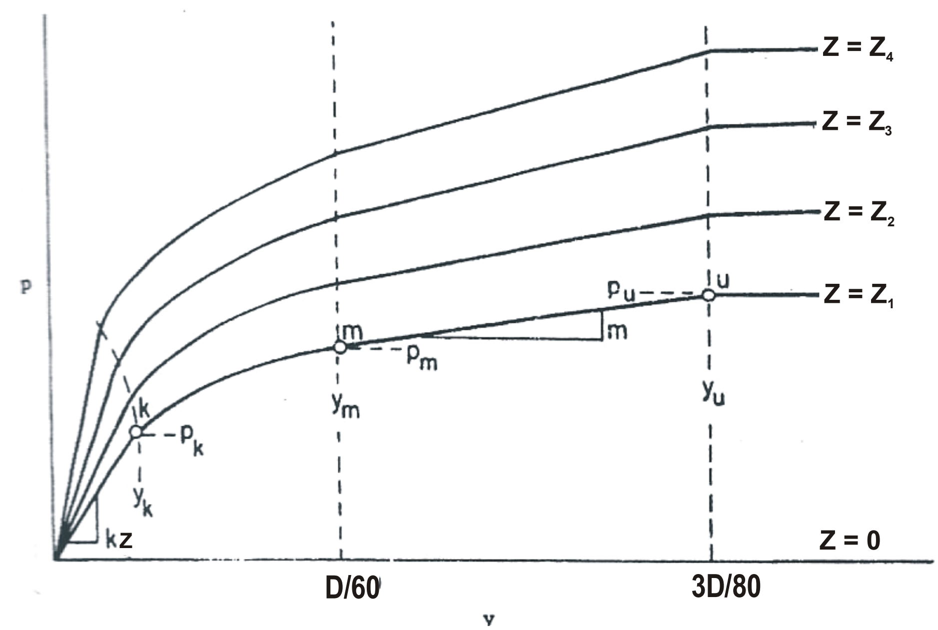

Figure 2-14 Characteristic Shapes of *p-y* Curves for Sand (Reese *et al*. 1974)

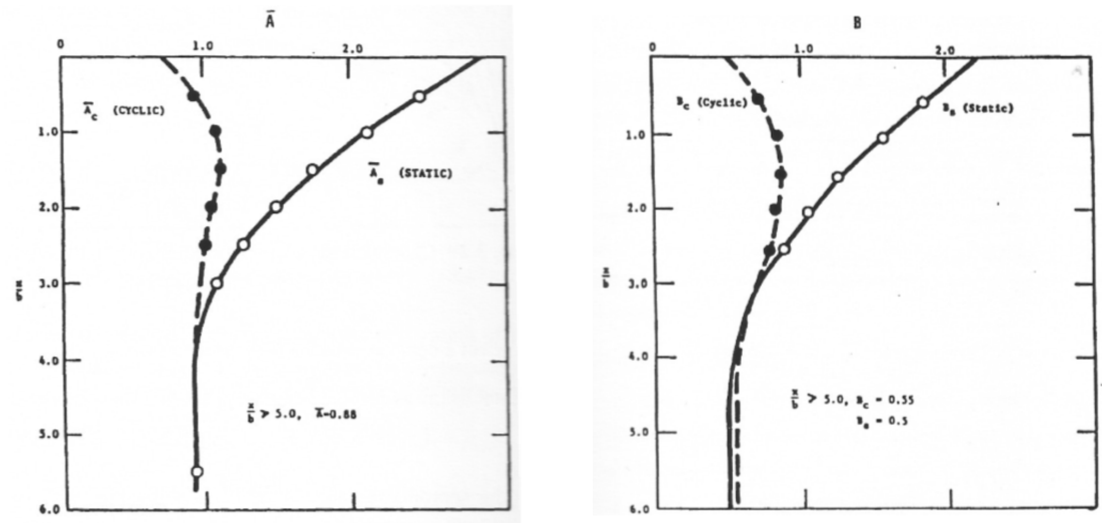

a) Coefficient A

b) Coefficient B

Figure 2-15 Values of Coefficients Used for Developing *p-y* Curves for Sand a) Coefficient A; b) Coefficient B (after Reese *et al.* 1974)

`

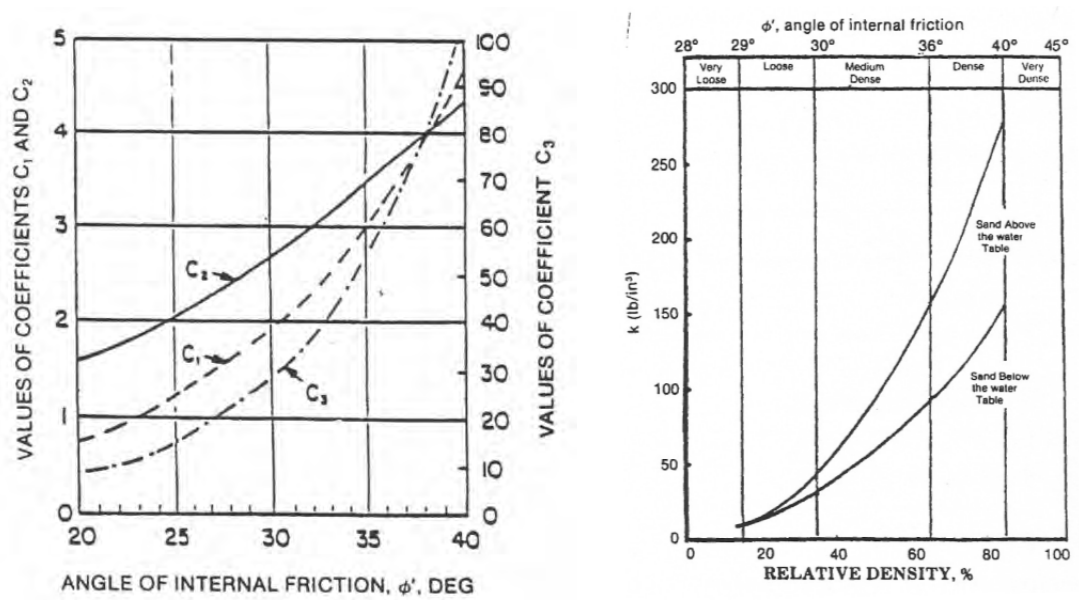

a) Coefficients as Function of ϕ for API Sand

b) Initial Modulus of Subgrade Reaction for API Sand

Figure 2-16 Charts for Developing API Sand *p-y* Curves (API 1987)

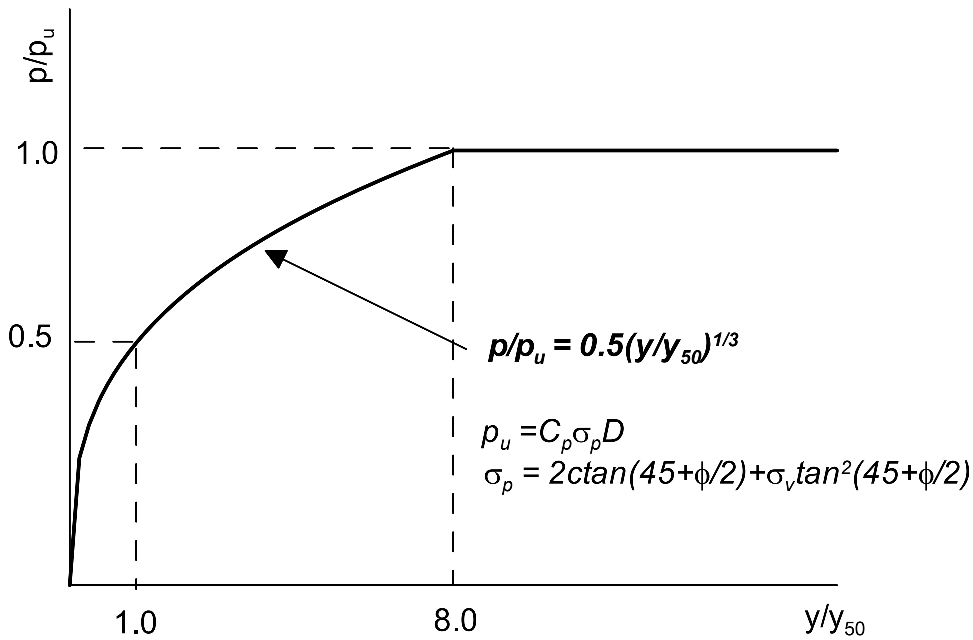

Figure 2-17 Characteristic Shape of *p*-y Curve for Cemented Sand (after Ismael 1990)

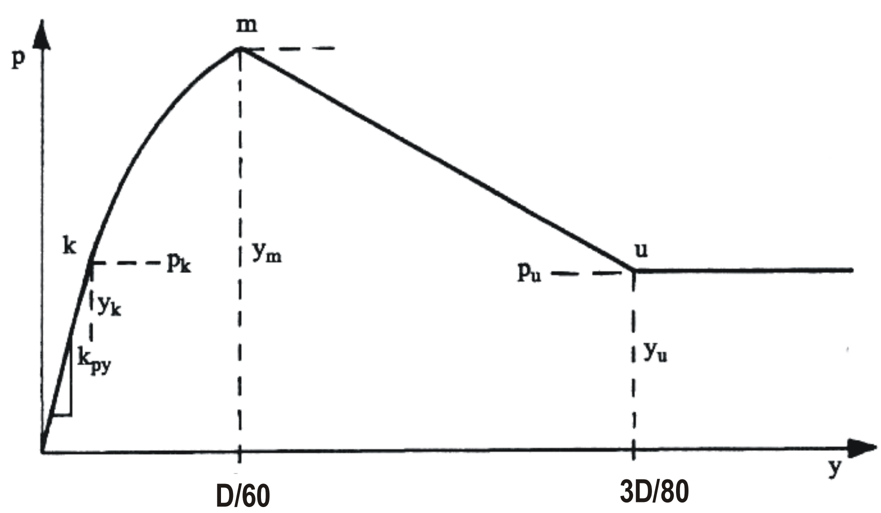

Figure 2-18 Characteristic Shape of *p*-y Curve for *c*-*ϕ* Soil (Reese and Van Impe 2001)

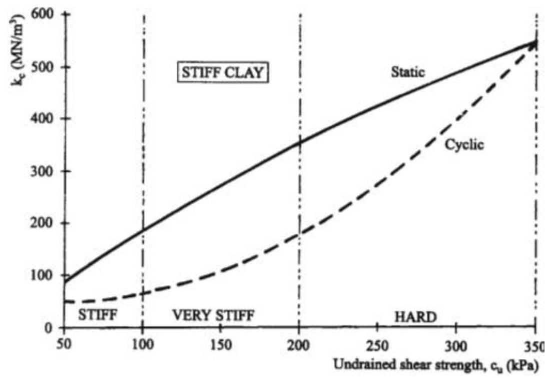

a) Values of k_c

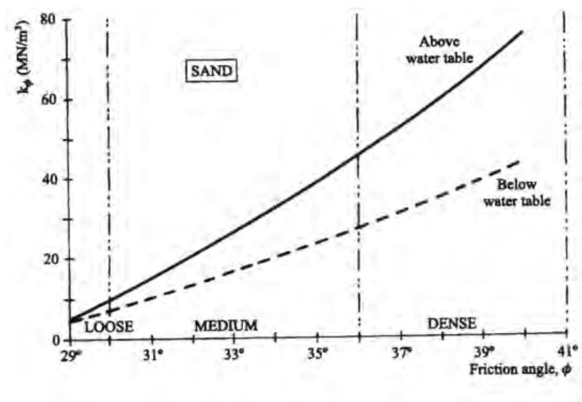

b) Values of k_ϕ

Figure 2-19 Initial Subgrade Reaction Constant (Reese and Van Impe 2001) a) Values of k_c; b) Values of k_ϕ

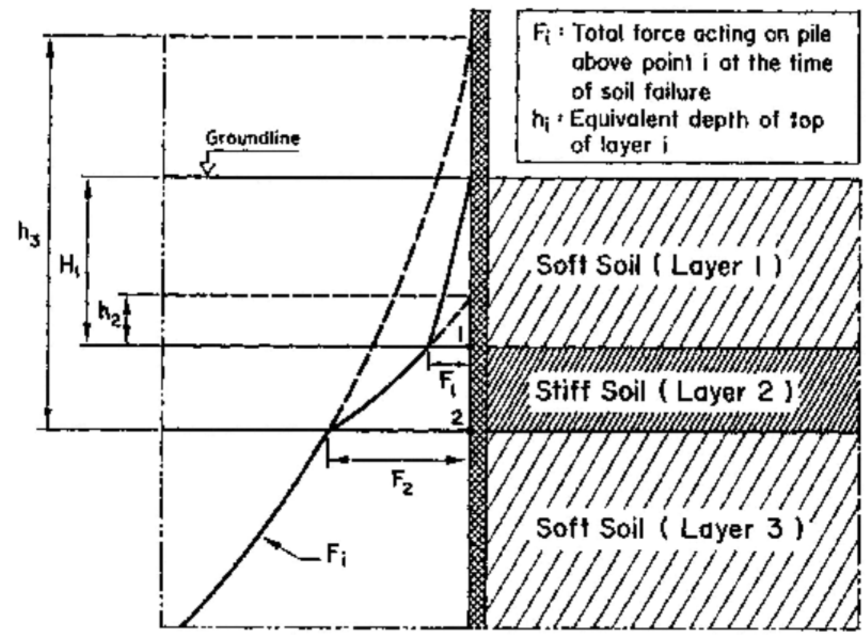

Figure 2-20 Typical Determination of Equivalent Depths in a Layered Soil Profile (Georgiadis 1983)

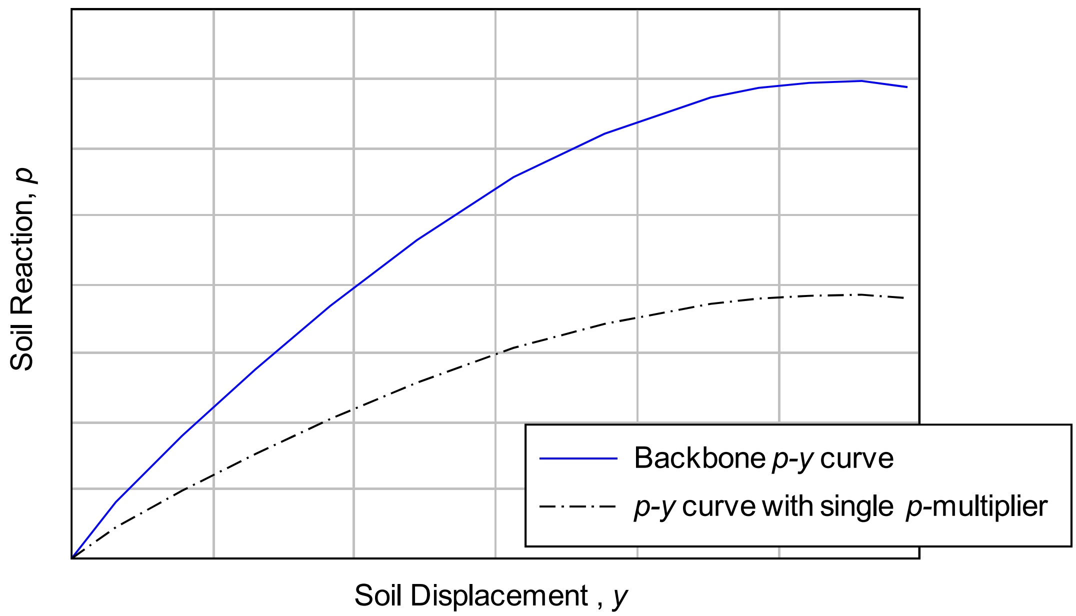

Figure 2-21 Concept of *p*-Multiplier

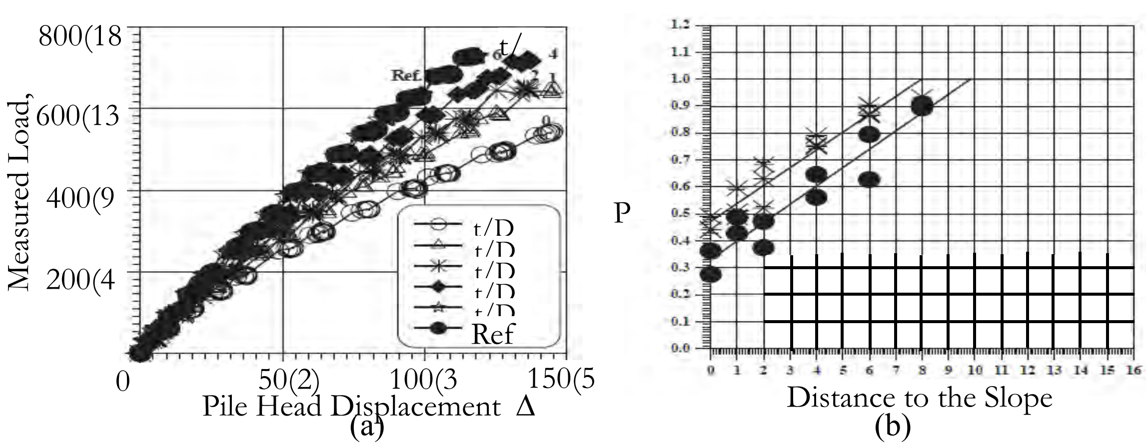

Figure 2-22 Load Displacement Curves (a) and Recommended p_{mult} (b) for Centrifuge Tests (after Mezazigh and Levacher 1998)

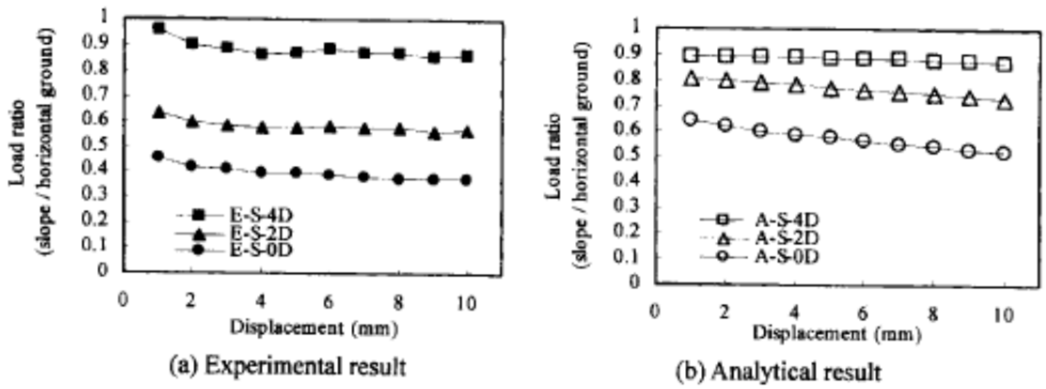

Figure 2-23 Load Ratio from Single Pile Tests a) Experimental Results; b) Analytical Results (from Chae *et al*. 2004)

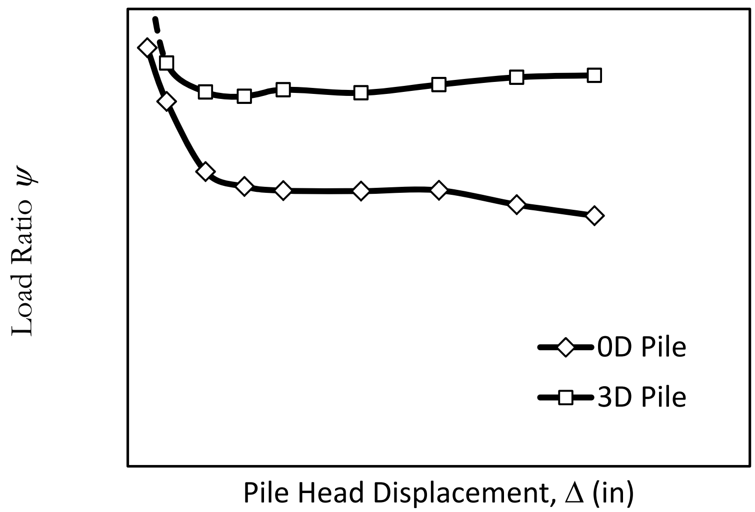

Figure 2-24 Load Ratio for Piles Near Sand Slope (after Mirzoyan 2004)

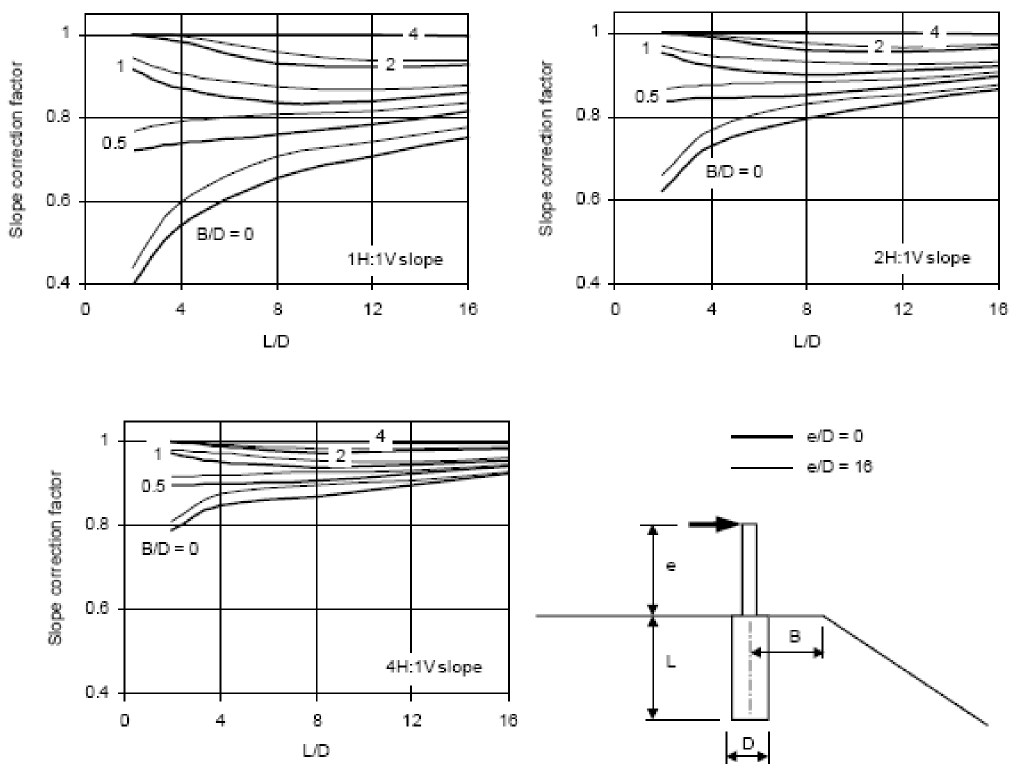

Figure 2-25 Reduction Factors to Account for the Effect of a Slope on Pile Capacity: Frictionless pile, Weightless soil (from Stewart 1999)

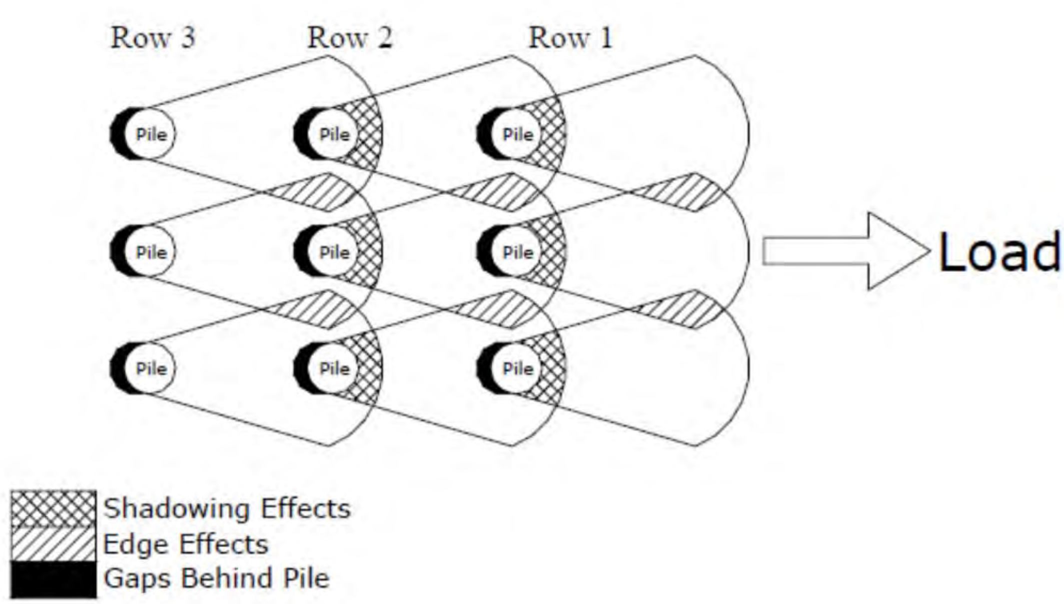

Figure 2-26 Illustration of Shadowing and Edge Effects for Pile Groups under Lateral Load (from Walsh 2005)

3. SITE DESCRIPTION AND SOIL PROPERTIES

The testing location is near the western edge of the Oregon State University (OSU) campus, near SW 35th St and Jefferson St in Corvallis, Oregon. It is located within the Geotechnical Engineering Field Research Site (GEFRS) at OSU where several site explorations have been conducted since 1972. The Caltrans test area is located directly west of the O. H. Hinsdale Wave Research Lab. The test site is relatively flat with some gentle slope on the western half. The location map of the test site is shown in **Figure 3-1**. An aerial photo of the site is shown in **Figure 3-2**. Both test series were carried out at this location. Series-I was conducted in the native cohesive soils and Series-II in an engineered cohesionless backfill material delivered to the testing site.

3.1 GENERAL SITE AND SOIL INFORMATION

Several soil types are present around the OSU campus as the area is influenced by the proximity of the Willamette River and Oak Creek. According to the Benton County Survey, the test site is mapped as Quaternary higher terrace deposits consisting of mixtures of gravel, sand, silt, and clay (Knezevich, 1975). The topsoil in this area was mapped by the United States Department of Agriculture as the Dayton-Amity Association which was interpreted to have been deposited during the Late Pleistocene epoch (Knezevich, 1975). Several site explorations have been conducted around the site and all available soil information is summarized in the GERFS Report (Dickenson, 2006). The location of the borings and their projected cross-sections are shown in Appendix A. A summary of available geotechnical information extracted from GEFRS report is presented in **Table 3-1**.

Based on the GEFRS Report, the soil layers are generally uniform across the site. Stiff to very stiff cohesive soil is encountered from the ground surface to a depth of approximately 10 ft. This layer is referred to as upper cohesive layer throughout this report. A relatively wide range of liquid limits and plasticity indices were reported. The cohesive material varies from low plasticity silt (ML) to highly plastic clay (CH) across the entire site, but data from site specific borings show it to be MH and CH. This layer is underlain by a layer of dense, poorly graded sand with silt and gravel which extends to a depth of approximately 13 ft. This layer is referred to as upper sand layer. Below this sand layer is a stratum of medium stiff, high plasticity sandy silt that is approximately 5 ft thick. This layer is referred to as the lower cohesive layer. This is underlain by a layer of medium dense to dense, well-graded sand with silt and gravel which extends to a depth of approximately 23 ft. This layer is referred to as the lower sand layer. A layer of stiff to very stiff, blue-gray, high plasticity silty clay then extends to a depth of approximately 70 ft. This layer is referred to as the blue-gray clay layer. The water table varies from 3 ft to 7 ft during the year. Results from Atterberg limit tests, Standard Penetration Tests (SPT) and Triaxial tests from GEFRS report are included in **Table A-2**, **Table A-4**, **Table A-6** and **Table A-7** respectively in Appendix A.

3.2 COHESIVE SOIL TESTING INVESTIGATION (SERIES-I)

Apart from the available literature, two additional site specific subsurface explorations were conducted to obtain more geotechnical information of the test site, especially near the testing area. The testing area is referred to as the Caltrans site throughout this report. The explorations were completed on October 2, 2008 (before test) and October 14, 2009 (during test) respectively. The explorations include four exploratory boreholes, three Cone Penetration Test (CPT) boreholes, 2 Dilatometer (DMT) boreholes. The locations of boreholes are shown along with pile locations in **Figure 3-3**. The two boreholes from 2008 site explorations were drilled to a depth of 10 ft and 52 ft by means of hollow stem auger and rotary mud drilling methods, respectively. The subsurface conditions were generally consistent with GEFRS report. The soil boring logs from the first site explorations are shown in **Figure A-3** and **Figure A-4** in Appendix A. Two boreholes from 2009 site explorations were drilled during the pile load testing period to assess the soil conditions at the time of the pile load tests. Soil sampling was conducted with emphasis on the top 10 ft of the upper cohesive layer. Several undisturbed Shelby tube samples and split spoon samples were collected for laboratory testing. In addition, several soil samples from within the upper cohesive layer were collected during slope excavation for the determination of initial soil condition (i.e., water content) prior to lateral load testing. A comparison between measured water content from bag samples and Shelby tube samples indicates that the soil condition did not change significantly throughout the testing period. A laboratory program was carried out on the soil samples that include index tests and strength tests.

Based on site specific geotechnical investigation results, a typical soil profile within the area of the pile load tests is shown in **Figure 3-4**, together with in-situ test results (i.e. CPT and SPT), index test results and laboratory strength parameters. Based on cone tip resistances, the first layer encountered is a very stiff silt crust that extends to a depth of approximately 2.5 ft. According to the unified soil classification system (ASTM D2487), this crust is classified as ML. Below the crust to a depth of approximately10 ft is a stiff silt and clay layer that is classified as MH and CH with a range of liquid limits from 60 to 70 and a range of plastic limits from 30 to 35. A summary of index test results is presented in **Table 3-3**. A series of Unconsolidated Undrained (UU) triaxial test was carried out to determine the undrained shear strength profile of the upper cohesive layer. It was determined that UU triaxial tests with confining pressure equal to the overburden pressure were appropriate for this type of soil because it is an unsaturated soil. Another type of test (e.g. Consolidated Undrained Triaxial Test) that includes saturating the soils prior to shearing is not appropriate for this purpose. The results from UU triaxial tests for the top 10 ft of the soil layer are summarized in **Table 3-4**. Due to the nature of cohesive soil in this area, significant sample disturbance may be induced during sample preparation as well as sampling process resulting in a wide range of undrained shear strength values. Test results from samples with significant sample disturbance are reported, but not considered for comparisons. In general, for the top 2.5 ft of soil, undrained shear strength from UU triaxial tests ranges from 900 to 2200 psf. Below 2.5 ft, the undrained shear strength ranges from 1200 to 2400 psf. UU test results indicated that there is no significant difference in shear strength within the layer despite the observed difference in cone tip resistances. In subsequent analysis, this layer is represented as a single layer with uniform average and upper bound shear strength of 1600 psf and 2400 psf, respectively.

The second layer encountered and identified by cone tip resistances corresponds to the upper sand layer described above. The thickness of this layer is approximately 3ft. The upper sand layer had an average corrected blow counts, N_1, of 33. Below this sand is a layer of stiff, high plasticity silt with an approximate thickness of 5ft. This layer is classified as MH. The undrained shear strength from DMT results ranges from 800-1700 psf. The lower sand layer had an average N_1 of greater than 50. A layer of dark brown, high plasticity blue-grey clay was found from depth of 23 ft. Results from index tests, SPT, and UU triaxial tests from Caltrans borings including bag samples are presented in **Table A-3**, **Table A-5**, and **Table A-8** in Appendix A respectively.

In summary, the upper cohesive layer has an average undrained shear strength of 1600 psf with an upper bound strength of 2400 psf. An average unit weight of approximately 115 pcf appears to be reasonable based on laboratory results. The upper sand layer is a dense sand with estimated friction angle of 40 based on correlations of the SPT and CPT results (Meyerhof, 1956). The unit weight of 130 pcf is assumed to be reasonable for this sand layer. The lower cohesive layer is assumed to have the same characteristic as the upper layer. SPT and CPT results indicate that the lower sand layer is a very dense sand. Using correlations proposed by Meyerhof (1956), the friction angle for this layer was estimated to be 45 degree. Average undrained shear strength of 3500 psf is suggested for the blue-gray clay layer with an average unit weight of 110 pcf. An idealized soil profile for analysis is shown in **Figure 7-1**.

Lateral load test Series-I was carried out in original soils at the Caltrans test site which, for the first 10 ft, consists of cohesive soils with properties similar to a common cohesive soil in the Western part of Oregon known as the Willamette Silt (Dickenson, 2006). The properties of upper cohesive layer had a reasonable agreement with the 'lean clay' category which is one of three soil categories used as backfill material in bridge abutments in the state of California (Bozorgzadeh, 2007 and EMI, 2005). **Table 3-4** defines these three categories. The cohesive soil at this site can be classified as 'competent soil' (undrained shear strength, S_u > 1500 psf) according to Caltrans Seismic Design Criteria (SDC, 2006) which would be the majority of cohesive soil used to support foundation.

3.3 COHESIONLESS SOIL PROPERTIES (SERIES-II)

The Lateral load tests for Series-II were conducted in a cohesionless backfill material on the Caltrans Test site about 200 ft west of the Series-I testing location. **Figure 3-5** shows the Series-II testing location on site in relation to the Series-I tests. As described in the previous section, the native surface soils consist of clays to silty clays at the Caltrans test site. Series-II required testing in a cohesionless material therefore; this material type would need to be transported to the site to conduct lateral load testing.

The material supplied by a local aggregate company was processed and delivered to match the Caltrans structural backfill gradation specification (19-3.06 Caltrans 2006 Standard Specifications). **Table 3-5** summarizes the gradation requirements from the Caltrans specifications with an added fines content constraint. The material obtained was required to have less than 12% fines passing the number 200 sieve to ensure the material was cohesionless for this series of tests. **Figure 3-6** presents the final gradation curve for the material used during testing.

On site, an embankment was constructed to a height of 10 ft above the original ground surface with the cohesionless material. Through this embankment all ten of the Series-II test piles were driven at specific locations for lateral testing. **Figure 3-5** shows the layout of the embankment on the Caltrans test site. The embankment was constructed to a final height of 10 ft above the native surface. This elevation was chosen because the majority of lateral pile resistance is developed in the top 5-10 piles diameters (Reese & Van Impe, 2001), where the test piles for this project had a diameter of 12 inches. The footprint of the embankment was 117 ft by 90 ft with a total volume of 2550 cubic yards with a 2H: 1V test slope.

The embankment was constructed in 8 inch compacted lifts to a relative compaction of not less than 95% according to Caltrans Test 216 (Method of Test for Relative Compaction of Untreated and Treated Soils and Aggregates). The maximum adjusted wet density for the embankment material was 2.12 g/cc or 132 pcf according to Test 216. The test results can be found in Appendix C **Figure C-** . During construction and compaction, nuclear density gauge testing (Caltrans Test 231) was conducted to confirm the 95% relative compaction specification was achieved. Four nuclear density readings meeting or exceeding the relative compaction requirement were achieved for each lift and the results can be found in Appendix C, **Figure C-** through **Figure C-**. From the nuclear density results the in-situ embankment material had an average unit weight of 127 pcf (96% of relative compaction of Test 216) with a water content between six and nine percent. A modified proctor test was also conducted on the embankment material and found a maximum dry density of 135 pcf at a water content of 9%.

An in-situ soil investigation was conducted on September 14, 2011. Three mud rotary borings were conducted to a depth of 30 ft through the embankment and into native soils. Split spoon samples and standard penetration tests (SPT) were conducted at 2.5 ft intervals in the top 10ft (through the embankment). Alternating split spoon/SPT and Shelby tube samples were conducted for the remainder of each boring at 5 ft sampling intervals. **Table 3-6** shows the SPT blow counts for each test in the cohesionless embankment. The uncorrected averaged blow counts ranged between 30 and 35. Using correlation factors (Peck et al. (1974) and Schmertmann (1975)) from the SPT data, an internal friction angle of 43 degrees is assumed for the cohesionless embankment material. The boring logs for the bottom 20 ft of each boring, in native soils, are consistent with the boring logs from the soil investigation presented for Series-I and are considered to have the same soil properties and depths in this analysis. Therefore, the soil profile consists of 10 ft of cohesionless embankment material underlain by the stratification described in the previous section for Series-I.

Table 3-1. Summary of Geotechnical Soils Properties around GEFRS Site

Soil Layer	Thickness (ft)	Atterberg Limits			Soil Classification	N_1 (Blows per foot)	Undrained Shear Strength (TXICU), S_u (psf)	
		LL	w_n	PL			GEFRS	Other Sites
Upper Cohesive	10	37-75	28-46	21-37	MH/CH	4-24	900-1700	900-1500
Upper Sand	3	-	-	-	SP-SM/SP	75	-	-
Lower Cohesive	5	39	30	22	ML/MH	21-25	1600-1900	2000
Lower Sand	5	-			SW-SM/SM	45	-	-
Blue Gray Clay	to bedrock	81-90	37-85	46-57	MH/CH	15-26	2000	-

Table 3-2. Summary of UU Test Results on Samples from Site Specific Borings

Depth (ft)	Sample No.	Cell Pressure (psi)	Strain rate (%/min)	S_u (psf)	ε_{50} (%)
0-0.5	SH-1-1	-	1	2200	0.7
1-1.5	SH-1-1a	-	1	900	1
3.5-4	SH-1-3*	3.0	1	700	0.55
6.5-7	SH-2-5	6.2	1	2400	1.9
7.5-8	SH-1-5*	6.8	1	250	0.11
8-8.5	SH-1-5a	7.2	1	1100	0.5
8.5-9	SH-2-6	7.1	1	1200	1.4
26-26.5	SH-1-15	14.6	1	5000	2.3

Note: * = large amount of sample disturbance

Table 3-3. Summary of Index Test Results on Samples from Site Specific Borings

Depth (ft)	Sample No.	USCS[a]	Grain Size Distribution[b] (Percentage Passing, %)			Atterberg Limits[a]		
			75mm	4.75 mm	74mm	LL	Wn	PI
0-0.5	SH-1-1	ML	100	100	98	44	13	18
3.5-4	SH-1-3	MH	100	100	92	TBD	25	TBD
6.5-7	SH-2-5	MH	100	100	82	62	34	14
7.5-8	SH-1-5	MH	100	100	90	81	43	36
8.5-9	SH-2-6	MH	100	100	66	53	37	21

Note: [a]ASTM D2487, [b]ASTM D422

Table 3-4. Soil Type for Abutment Structural Backfill (from Bozorgzadeh, 2007; after EMI, 2005)

Soil Type	Grain Size Distribution (Percentage Passing, %)			SE	PI
	75mm	4.75 mm	74mm		
Sands	100	>75	5-12	40+	<5
Silty Clayey Sands	100	>80	20-40	20-30	5-15
Lean Clay	100	100	60-80	<10	>15

Table 3-5. Caltrans 2006 Standard Specs for Granular Backfill Material with added Fines Constraint

Sieve Size	Percent Passing
3 "	100
No. 4	35-100
No. 30	20-100
No. 200	0-12

Table 3-6. Uncorrected SPT Blow Counts for the Boring in the Cohesionless Embankment

	SPT N-Value			
Depth (ft)	Boring 1	Boring 2	Boring 3	Average
2.5	26	30	32	30
5	36	36	29	34
7.5	35	37	32	35

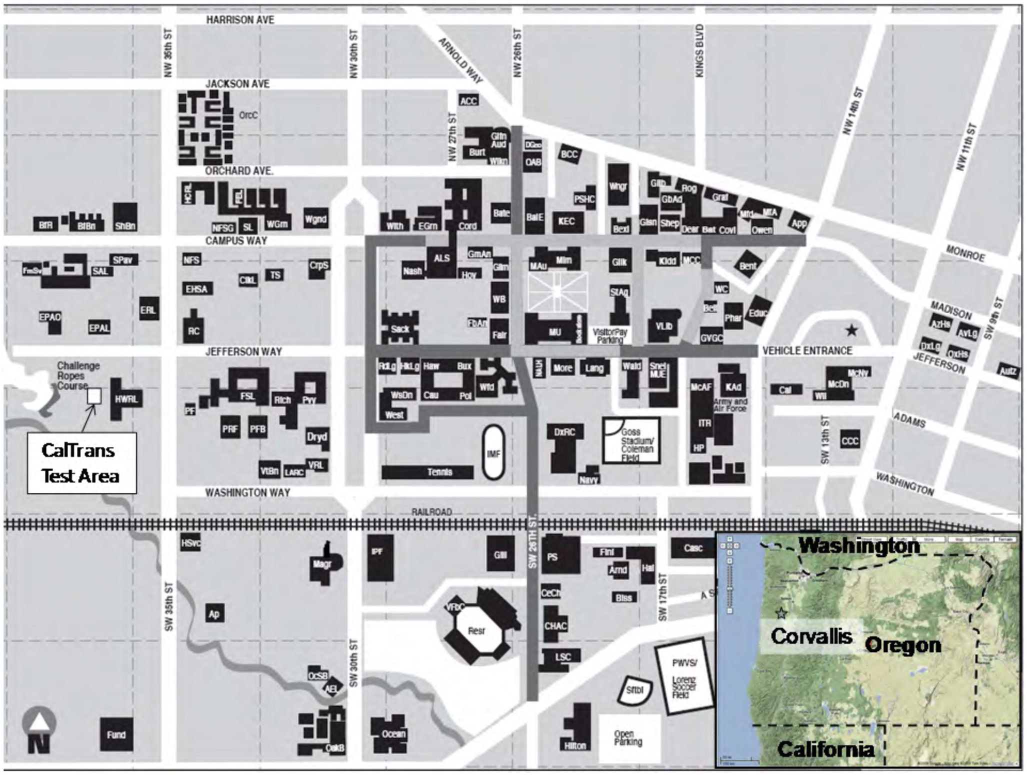

Figure 3-1. General Site Location in Corvallis, Oregon (OSU website 2008, Google Map, 2008)

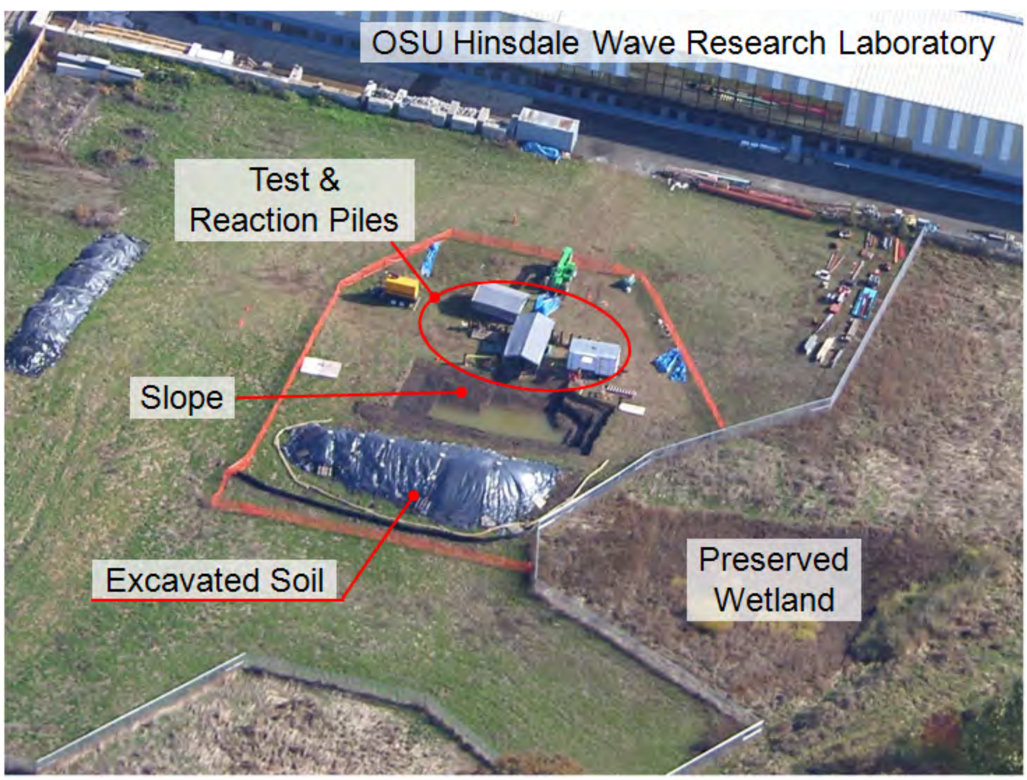

Figure 3-2. Aerial View of the Cohesive Test Site Relative to Hinsdale Wave Research Lab

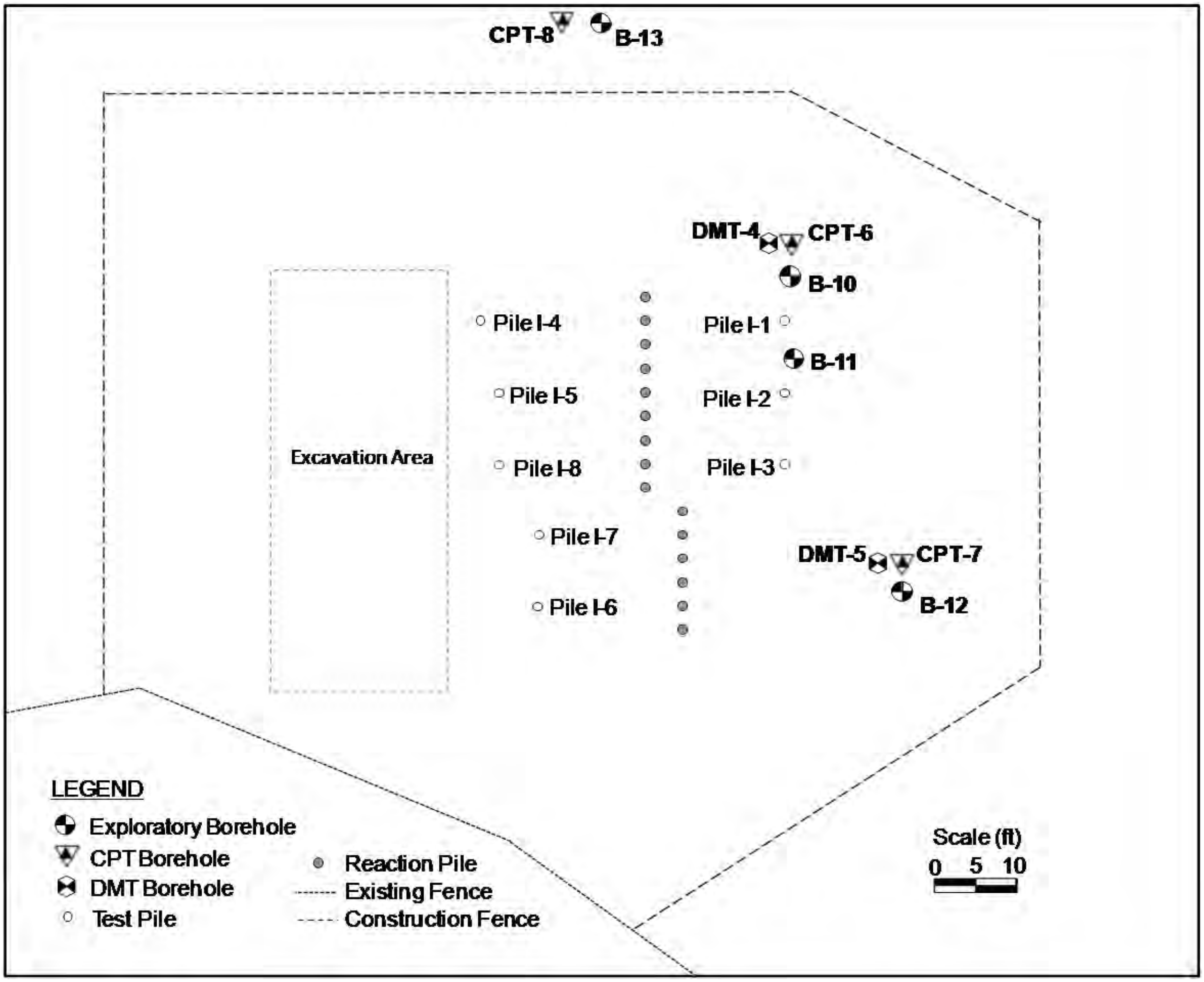

Figure 3-3. Locations of Borings and Test Piles locations at the Caltrans Test Site.

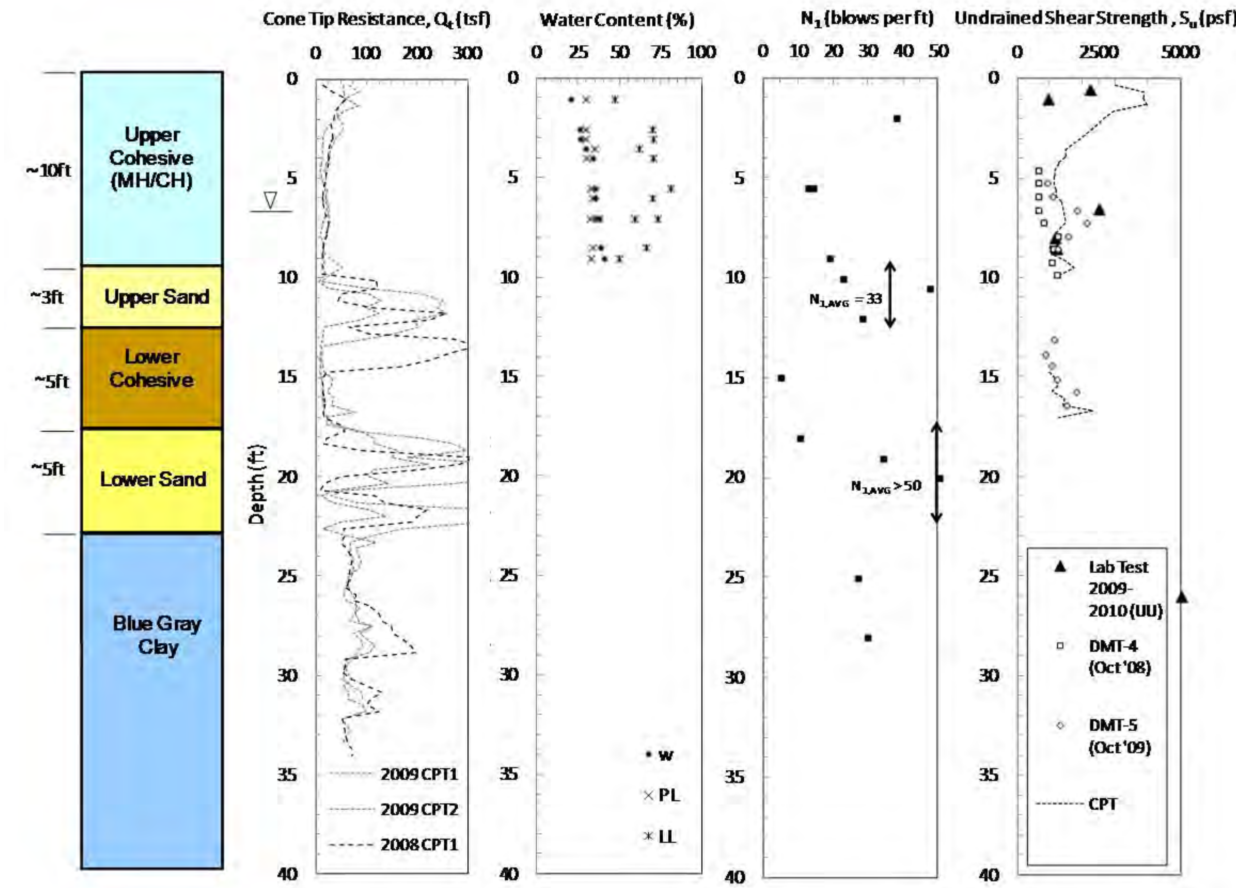

Figure 3-4. Summary of Site Specific Explorations for Caltrans Pile Load Study (as of March 31, 2010)

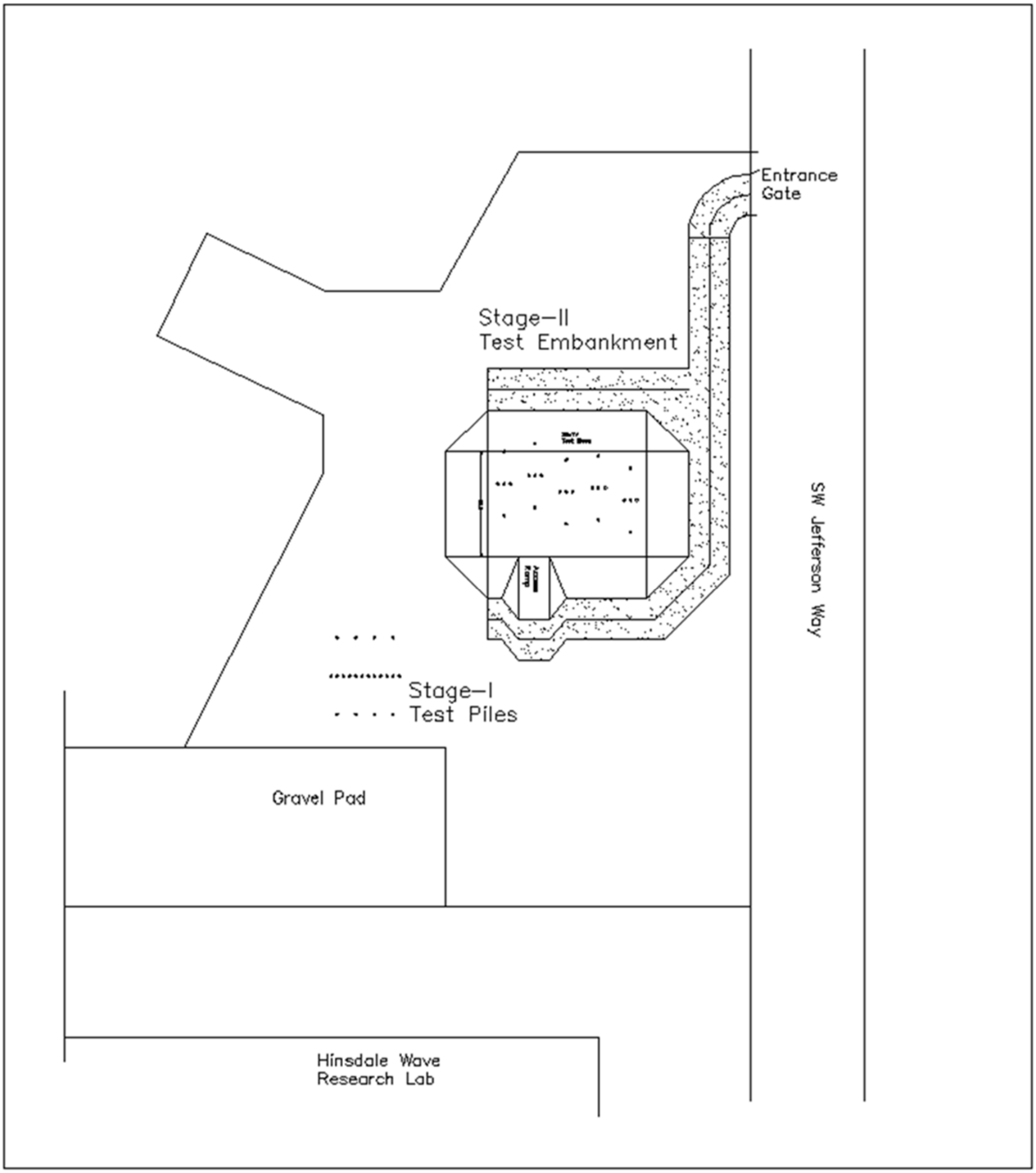

Figure 3-5. Series-II Lateral Load Testing Layout on the Caltrans Test Site

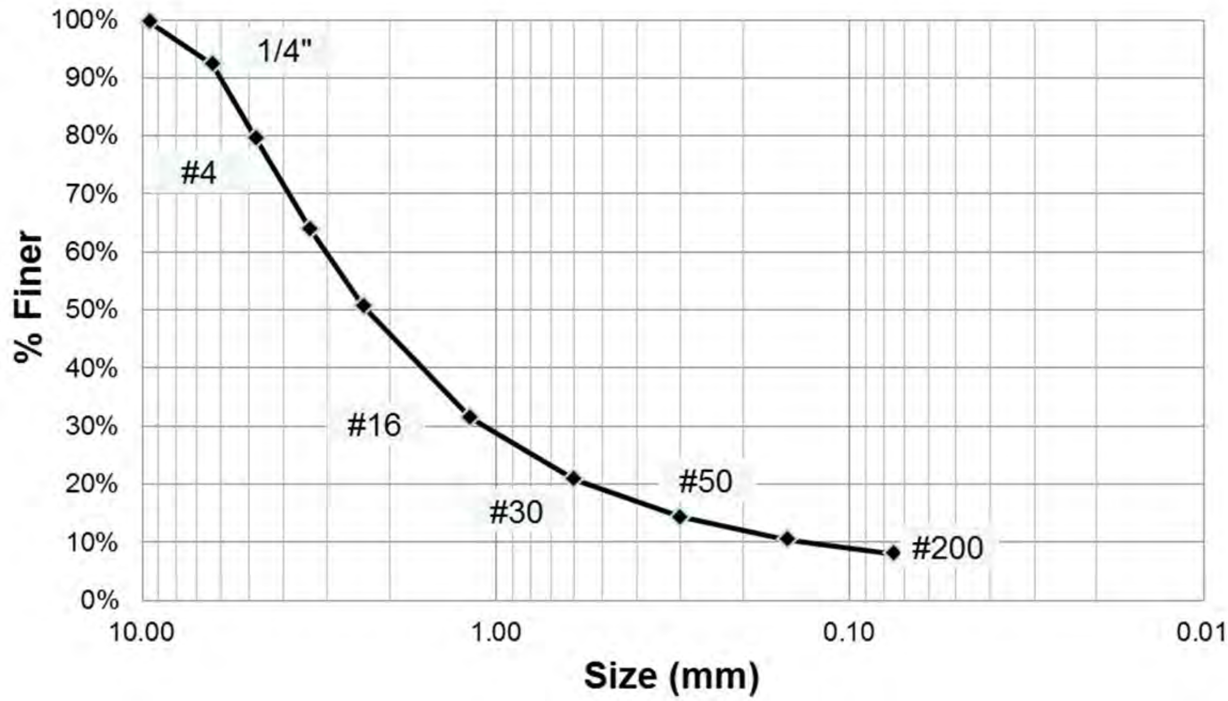

Figure 3-6. Gradation Curve of the Cohesionless Material used in Series-II

4. TEST SET-UP

In design of the full-scale testing program to study the effects of soil slope, several factors (e.g., pile properties, testing method, soil properties) must be controlled for consistency of the test results. The majorities of these factors can be controlled within the limits of the experimental planning and design. These are called internal factors. **Table 4-1** summarizes the internal factors and their impact on the test results. Some of the internal factors cannot be controlled (e.g., pile yield strength, equipment operator) but it is believed that the variability of these factors have low to moderate impact on the test results. Other factors that are beyond the limits of the experimental planning can be more difficult to control (e.g., seasonal weather, human factor). These factors are called external factors. **Table 4-2** summarizes the external factors and their impact on the test results. Some of the external factors, such as soil properties, have a significant impact on the test results. Therefore, the experimental program was carefully planned and carried out such that the variability of external factors between tests was held to a minimum. The assessment ratings of low, medium, and high for internal and external testing factors were qualitatively determined by the research group. The research group based these ratings on previous testing experiences and observations made during full-scale testing throughout this project.

For this project a total of eighteen lateral load tests in cohesive and cohesionless soils were conducted. The testing program for the project is summarized in **Table 4-3**. The purpose of the two baseline tests (I-1, I-2, P-1, and P-2) is to evaluate available methods for predicting the lateral response of free-field piles to use as baseline results for comparisons. The objectives of the lateral loading tests for piles near a slope (I-4, I-5, I-6, I-7 P-6, P-7, P-8, P-9) is to obtain a better understanding of the effects of soil slope on lateral capacity of piles. The battered pile tests (I-3, P-3, P-4, P-5) and the piles on slope test (I-8, P-10) were conducted to complement the existing database. **Figure 4-1** shows a transversal view of the planned testing set-up for the baseline pile and the piles near the constructed slope. In this section, the pile geometry, material properties of test specimen, method of pile installation, and load protocol are presented for both series of tests. Furthermore, a brief description on the instrumentation and the lateral loading test arrangement is provided.

4.1 PILE GEOMETRY AND CALIBRATION TEST RESULTS

The geometry of all test piles was that of a standard 1-ft nominal diameter steel pipe with an outer diameter of 12 ¾ inch, 0.375 inch wall thickness, and a length of approximately 30 ft. All steel pipe piles conform to ASTM specification A252 Gr 3 with average yield strength of 74.7 ksi. The material properties of all steel piles used for lateral load testing are included in Appendix C. Additionally, two steel channels, C 3x4.1, were attached on opposite sides of the piles to protect the strain gauges from being damaged during pile driving. The geometry of a typical test pile used during all full-scale experiments is shown in **Figure 4-2** used during both testing series.

A three point loading calibration test was conducted to validate strain gauge performance and verify theoretical moment-curvature relationship. Strain gauges were instrumented at 11 levels along the pile to measure the strain along the cross section of the pile. **Figure 4-3** shows test setup for calibration of instrumented piles. The yield strength of the calibration pile was reported as 51.6 ksi. A comparison between measured and theoretical moment-curvature relationship is shown in **Figure 4-4**. The measured results compared well with theoretical results. Based on the theoretical and measured results, an elastic bending stiffness (EI) of 84,450 k-ft^2 seems to be reasonable for the pile cross section. From this calibration test it was determined a pile with a higher yielding moment was required for full-scale lateral load tests. The pile sections used during all full-scale lateral loading tests had an average effective yielding moment of approximately 416 kips-ft; this is based on an average yield strength of 74.7 ksi. A post yielding bending stiffness of approximately 5% of the elastic stiffness was selected for analyses. It should be noted that due to the nonlinear behavior of steel past the effective yielding moment the analyzed results obtained from the strain gauges beyond the elastic range may contain significant uncertainties and should be used with judgment as will be discussed later.

4.2 INSTRUMENTATION OF TEST SPECIMENS

Several types of instrumentation (i.e., strain gauges, tiltmeters, load cells, and linear potentiometers) were installed on each test pile to measure pile responses during lateral loading. All test piles were carefully instrumented with 15 to 16 levels of strain gauges at 1-ft, 2-ft and 4-

ft spacing. Each level contained four strain gauges, two on each side of the pile. Steel channels, C3x4.1, were welded to the steel pipe piles to protect the strain gauges installed along the piles from damage during pile installation. A series of tiltmeters were installed along the pile to monitor pile rotation. Tiltmeters are sensitive to strong vibrations and were installed after pile driving. Each tiltmeter was fixed on a linear actuator that was fitted against the inner wall of the test pile. A cross-section view of the test pile and tiltmeters is shown in **Figure 4-13**. The load acting on the piles was measured by load cells in the hydraulic actuator. String-activated linear potentiometers were attached to the piles to monitor pile displacements during the lateral load tests. Typical locations of all sensors are summarized in **Figure 4-14**. Similar instrumentation was used for both testing series.

The elevations presented in the report represent locations along the length of the test pile in relation to the point of lateral loading. The top set of strain gauges was located at the ground surface and was three feet below the location of lateral loading for all pile tests. The following fifteen levels of gauges were located at intervals of 1ft, 2ft, and 4ft intervals along each test pile. During lateral loading of the vertical test piles the change in elevation of the strain gauges is considered to be minimal and does not significantly change the findings or results presented in the report. The strain gauges were located along the length of the battered piles in a similar arrangement to the vertical piles where the locations are based on the length along the pile. All battered pile figures presented in this report are based on load-displacement curves where the load was applied at an elevation near 3 ft above the ground surface. This elevation was measured vertically, not along the battered pile length. The difference in vertical depth below ground surface and the corresponding gauges locations due to batter angle does not affect the presented information because only pile head load-displacement curves are presented.

4.3 LOAD PROTOCOL

Static load tests were performed to obtain the load-displacement information as to develop the *p-y* curves. Each test pile was loaded monotonically until a target displacement was reached. Then, in general, the displacement was maintained for 5-10 minutes depending on the displacement level to allow the pile displacement to stabilize. Afterward, the next displacement increment was applied and the same procedure was repeated. Within elastic range, the specimen were loaded to 10%, 20%, 30%, 40%, 50%, 60%, 70%, 80%, 90% and 100% of the predicted yield displacement. The estimation of yielding displacement was based on available geotechnical parameters obtained from site investigation and available *p-y* curves in LPILE.

In general, relatively large pile displacement is required for cohesive soil to develop ultimate soil resistance. Therefore, each pile was loaded to 120%, 140%, 160%, 180% and 200% of the predicted yield displacement. Based on the predicted yield displacement of 5 inches, target displacements were 0.5, 1, 1.5, 2, 2.5, 3, 3.5, 4, 4.5, 5, 6, 7, 8, 9 and 10 inch. The load protocol for pseudo static lateral load tests is shown in **Figure 4-15**. The loading was stopped once it was determined that the maximum load carrying capacity of each test pile was reached.

The prediction analysis of yielding displacement for Series-II was also based on geotechnical parameters and LPILE *p-y* curves. Based on the predicted yield displacement of 2.5 inches, target displacements of 0.1, 0.25, 0.5, 0.75, 1, 1.25, 1.5, 1.75, 2, 2.25, 2.5, 3, 3.5, 4, 4.5, 5, 6, 7, 8, 9, 10 inches were used during lateral load testing in the cohesionless soils.

A ramp rate of the actuator was approximately 0.1 inch/min for all lateral load tests. This ramp rate results in the pile head loading rate of approximately 0.05-0.08 inch/min because the reaction piles were also displacing during testing. This rate was selected because it is comparable to that of Caltrans abutment testing at UCSD (Bozorgzadeh, 2007) in which the load was applied monotonically, using a displacement increment of 0.001 inch/sec (0.06 inch/min). It was believed that this rate is slow enough for pseudo static tests and fast enough such that each load test could be completed in a single day.

It should be noted that the rate of loading in the field can affect the undrained shear strength of soil and, therefore, pile response during lateral loading. Previous studies showed that the undrained shear strength increased about 10% per log cycle of time increase in speed of shear (Taylor, 1943 and Bjerrum, 1972). Bea (1984) studied the effect of loading rate on laterally loaded piles in cohesive soils and reported that high strain rate increases the soil shear strength and stiffness.

The strain rate of loading for a soil specimen as recommended by ASTM D2850 for a Unconsolidated Undrained Triaxial test is 1% per minute (for a 5 inch height specimen, it is 0.05 inch/min). For this study, the pile head loading rate is in reasonable agreement with the recommended loading rate (strain rate) of a standard UU triaxial test. This load rate is also considered slow enough for pore water pressure dissipation during testing in the cohesionless materials.

4.4 PILE INSTALLATION FOR SERIES-I (COHESIVE TEST)

On May 21, 2009, test pile I-1 was driven closed-ended using an impact diesel hammer, Delmag D19-32. The installation of pile I-1 is shown in **Figure 4-11**. Three additional steel pipe piles were driven open-ended to serve as reaction piles. On August 12, 2009, seven remaining test piles were driven closed-ended using an impact diesel hammer, APE D19-42. All test piles were driven to a depth of 26 ft to obtain a degree of fixity at the pile tips. Pile I-8 (pile on the slope located at -4D from slope crest) was driven to a depth of 28 ft to maintain the loading elevation at 3 ft above the ground surface after the slope excavation was completed during Series-I. The driving of pile I-2 was stopped when it was only driven to 22.5 ft because a steel channel on one side of the pile sheared off during pile driving. Twelve additional steel pipe piles were driven open-ended to serve as reaction piles. Pile driving logs for pile I-1 and three reaction piles are presented in **Figure 4-12**. The driving logs were consistent with the soil profile at the site. Test piles were driven close-ended to facilitate the installation of the tiltmeters along the piles.

4.5 LATERAL LOAD TEST ARRANGEMENT FOR SERIES-I (COHESIVE)

Eight lateral pile load tests were carefully planned and carried out at the Caltrans test site at OSU such that all tests were conducted in similar soil and loading conditions. Plan view for all pile tests is shown in **Figure 4-5**. A total of fifteen 1-ft diameter steel pipe piles with a length of 40 ft were driven 36 ft into the ground to provide reaction for the test piles. Pseudo static load tests were performed on each test pile using a 500-kip hydraulic actuator. Photographs of the actual test setup for the baseline pile (I-1) and the pile located two diameters from the slope crest (I-4) are presented in **Figure 4-6**. Each test pile was pushed against a transfer beam that was connected to three 1-ft dia. steel pipe piles arrangement, as shown in **Figure 4-7**. Lateral loads were applied at 3 ft from the ground surface by controlling input displacement. The test setup for the battered pile was slightly different from other tests and will be discussed in the next section.

After completion of lateral load test for piles in level ground (piles I-1, I-2 and I-3), the test area was excavated along the slope crest line shown in **Figure 4-5** to a 2H:1V slope for remaining load tests for piles near sloping ground (Stage 1: piles I-4, I-5 and I-6). The completed slope excavation for Stage 1 is shown in **Figure 4-8**.

After completion of test piles I-4, I-5 and I-6, the test area was excavated along slope crest line as shown in **Figure 4-9**. Stage 2 includes load tests of piles I-7 and I-8 which were located at the slope crest (0D) and on the slope (-4D) respectively. The completed slope excavation for Stage 2 is shown in **Figure 4-10**

4.6 PILE INSTALLATION FOR SERIES-II (COHESIONLESS)

Between June 6-7, 2011, test piles P-1 through P-10 were installed closed-ended. The driving process was completed using an APE 19-42 diesel impact hammer. Each test pile was 30 ft in length and driven to a depth of 26 ft below the embankment surface to ensure the piles acted as long piles with fixed ends during testing. Pile P-10 was driven into the slope at an elevation 2 ft below the embankment surface. Additionally, fifteen open-ended steel pipe piles were driven into the embankment to serve as reaction piles. Pile driving logs for a selection of the piles are shown in **Figure 4-16**. During driving, piles P-3, P-4, and P-10 were driven with a slight rotation where the strain gauges were slightly off from perpendicular with the testing slope. This error is taken into account during data analysis. Each test pile was tied to three reaction piles for lateral support. **Figure 4-18** shows a view of the completed embankment.

4.7 LOAD TEST ARRANGEMENT FOR SERIES-II (COHESIONLESS)

Ten lateral pile load tests were conducted on the cohesionless embankment during the summer of 2011. These ten tests included two baseline tests, three battered tests, and five on or near slope tests. A plan and cross sectional view for the pile testing and embankment arrangement is shown in **Figure 4-17**. Similar to Series-I, pseudo static load tests were performed on the test piles using a 500-kip hydraulic actuator to apply the lateral loading. **Figure 4-18** shows pictures of the testing set up, reaction piles, and hydraulic actuator for Pile P-1. Generally, lateral loads were applied by the hydraulic actuator at 3 ft from the ground surface by controlling input displacement. Five piles were tested near on the 2:1 test slope. The other five tests were conducted on the opposite side of the embankment with enough distance as not be influenced by the back slope. These tests were representing the baseline piles and battered piles in free field conditions. The test setup for the battered piles (P-3, P-4, P-5) was slightly different from other tests and will be discussed more in depth in a later chapter.

4.8 SUMMARY

A total of eighteen fully instrumented steel pipe piles were driven at a test site at Oregon State University. In most cases, the lateral pile load tests with similar pile properties were conducted in similar soil condition and loading condition. Two baseline pile tests were conducted for each series (total of four). Four piles were installed at -4D, 0D, 2D, 4D and 8D from the slope crest to investigate the effect of slope on lateral capacity of piles in cohesive and cohesionless soils. In these tests, a 2:1 slope of 9 to 10 ft in height was present in each series of tests. A total of four piles were battered at varying angles from vertical and tested during this project. The observations made during these tests are presented in the following sections.

Table 4-1. Internal Factors and Their Impact on Test Results

Factors		Controllable ?	Variability between tests	Impact on test results
Loading Type	Lateral load	Yes	Low	High
	Axial load	Yes	Low	Moderate
	Rate of loading	Yes	Low	High
Pile Properties	*EI*	Yes	Low	High
	Pile dia.	Yes	Low	Moderate
	f_y	No	Moderate	Moderate
	L/D ratio	Yes	Low	High
	Material	Yes	Low	Moderate
Instrumentation (e.g. strain gauges, tiltmeters)	Type	Yes	Low	Low
	Spacing	Yes	Low	Moderate
	Installation	Yes	Low	Low
	Orientation	Yes	Moderate	Moderate
	Data collection	Yes	Low	Low to None
Boundary Condition	Head condition	Yes	Low	Moderate
	Toe condition	No	Low	Moderate
Testing Method	Test set-up	Yes	Low	Moderate
	Equipment operator	No	Moderate	Moderate
	Load protocol	Yes	Low	Moderate
	Time between test	No	Moderate	Moderate
	Spacing between piles	Yes	Low	Moderate

Table 4-2. External Factors and Their Impact on Test Results

Factors		Controllable ?	Variability between tests	Impact on test results
Construction of Slope	Equipment operator	No	Moderate	Low
	Dimension of slope	No	Low	Moderate
	Excavation equipment	No	Moderate	Low
Soil properties (seasonal weather)	Moisture content	No	Low	High
	S_u	No	Low	High
	E_{50}	No	Low	High
Pile Installation	Equipment	Yes	Low	Moderate
	Equipment operator	No	Moderate	Moderate

Table 4-3. Summary of Testing Program (D = pile diameter)

Series	Test Pile	Soil Type	Slope (θ)	Batter Angle (θ)	Distance from Slope Crest	Comment
	I-1			n/a		Baseline
	I-2		n/a	n/a	n/a	Baseline
	I-3			26.5°		1
I	I-4	Cohesive			2D	2
	I-5		2:1, 26.5°		4D	2
	I-6			n/a	8D	2
	I-7				0D	2
	I-8				-4D	3
	P-1			n/a		Baseline
	P-2			n/a		Baseline
	P-3		n/a	14°	n/a	1
	P-4			-14°		1
	P-5			26.5°		1
II	P-6	Cohesionless		n/a	2D	2
	P-7			n/a	4D	2
	P-8		2:1, 26.5°	n/a	8D	2
	P-9			n/a	0D	2
	P-10			n/a	-4D	3

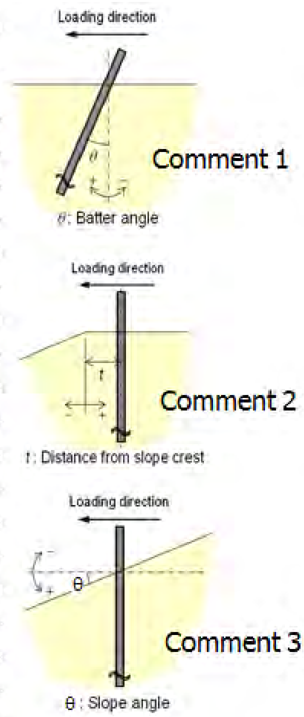

* Note : D = Pile diameter

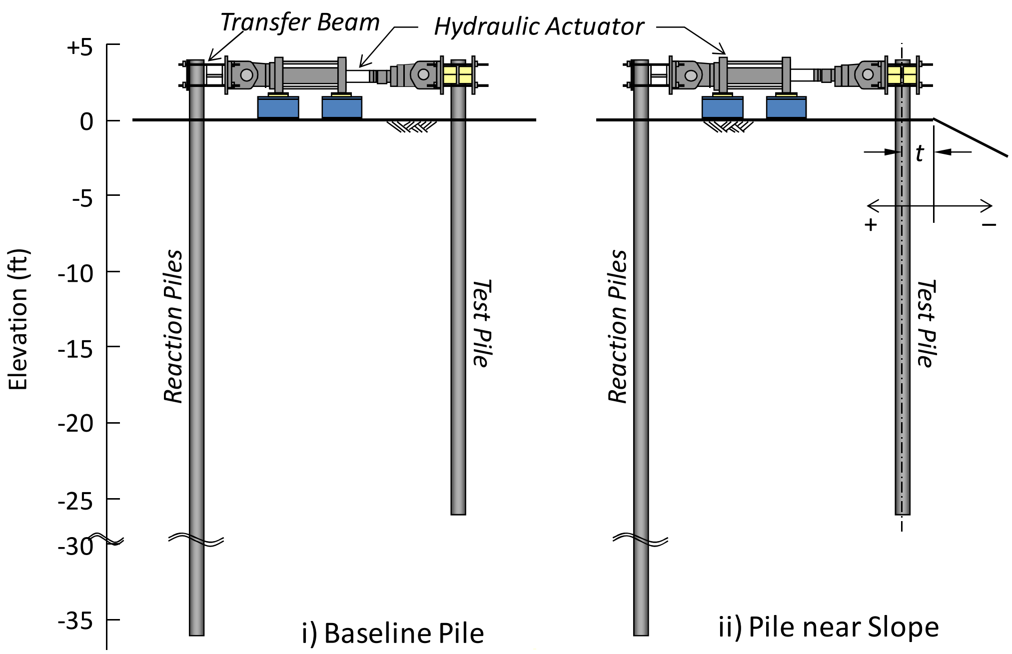

Figure 4-1. Transversal View of Test Set-Ups

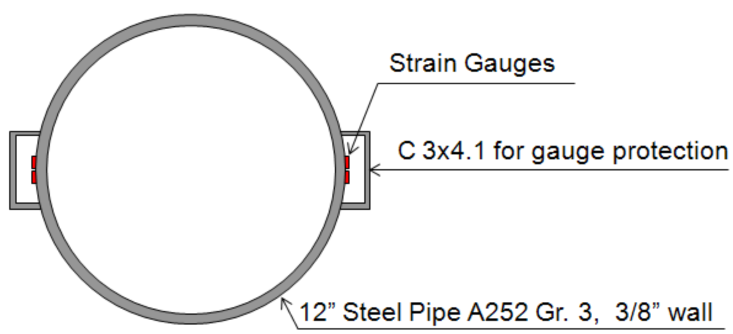

Figure 4-2. Geometry of Experimental Test Piles used in all Full-Scale Lateral LoadTests

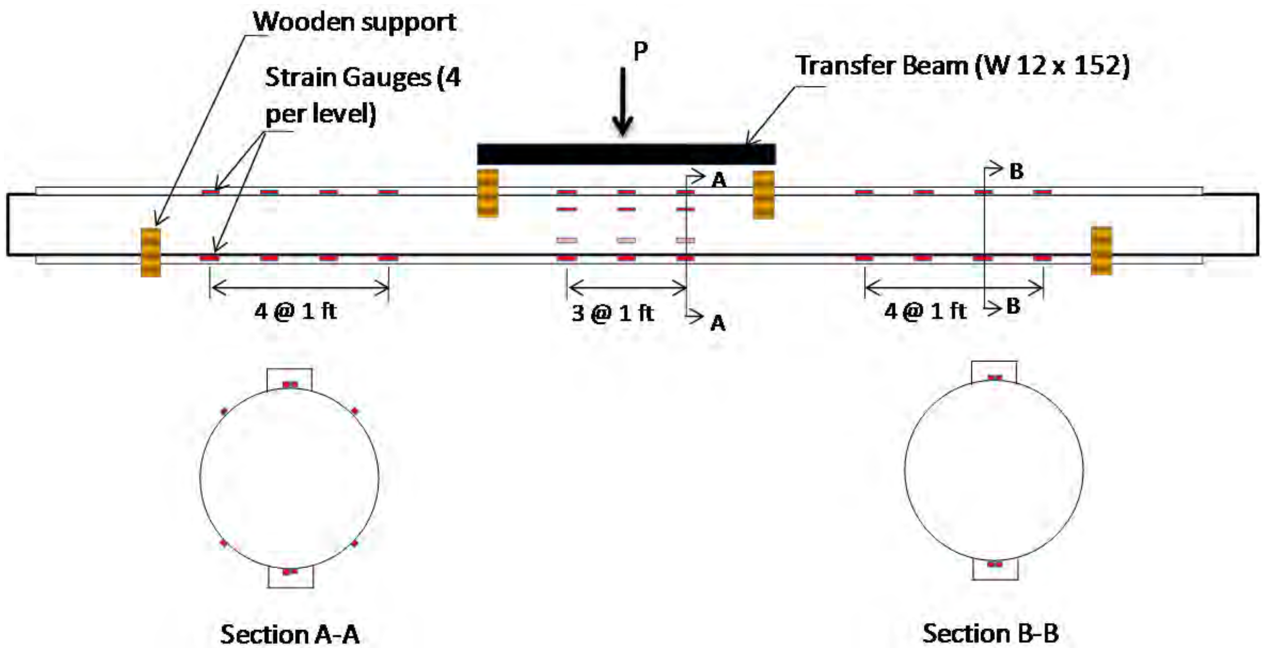

Figure 4-3. Test Set-Up for Calibration Pile

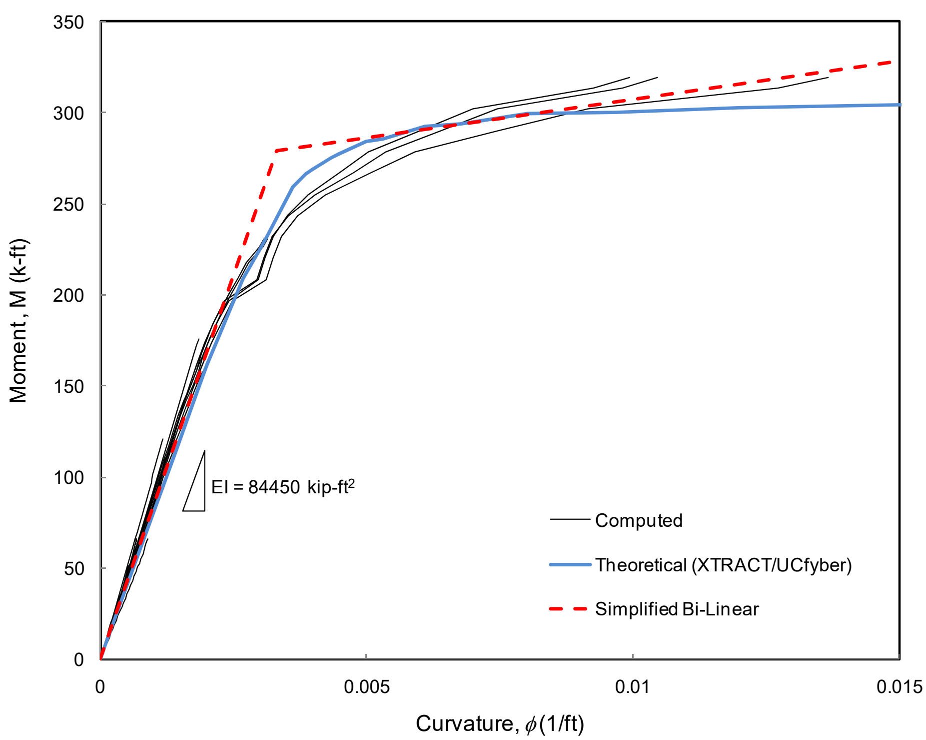

Figure 4-4. Comparison of Computed and Theoretical Moment-Curvature Relationship

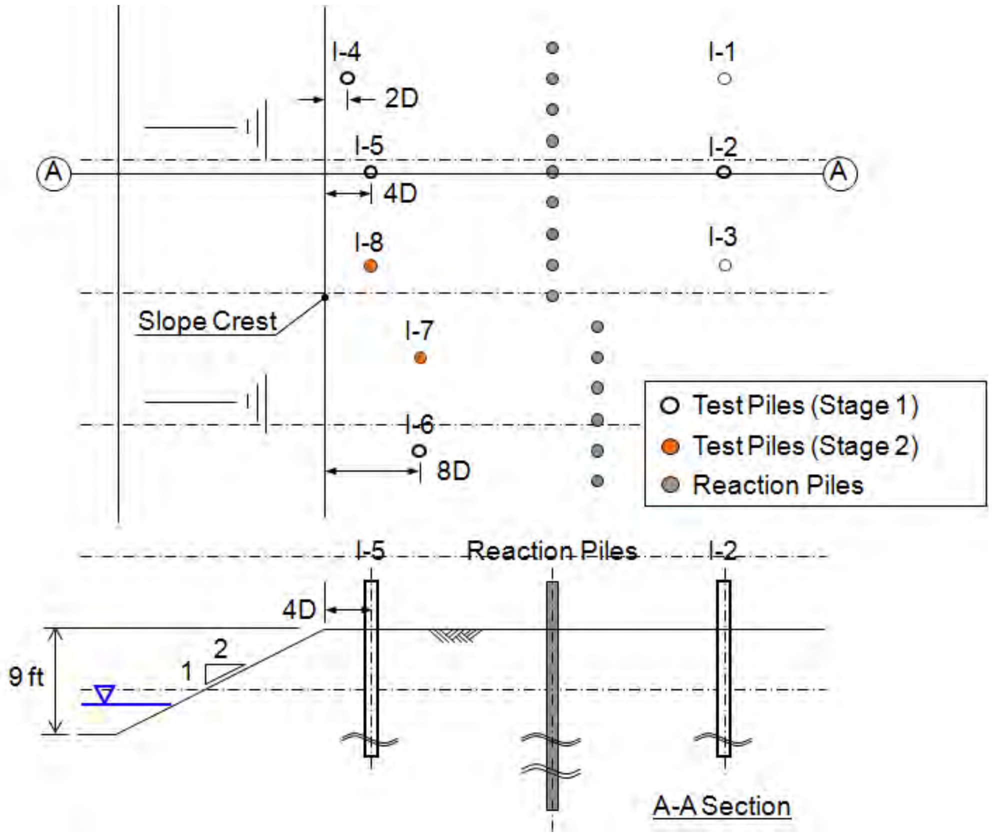

Figure 4-5. Plan View for Test Stage I with location of Test Piles, Reaction Piles and Slope 1

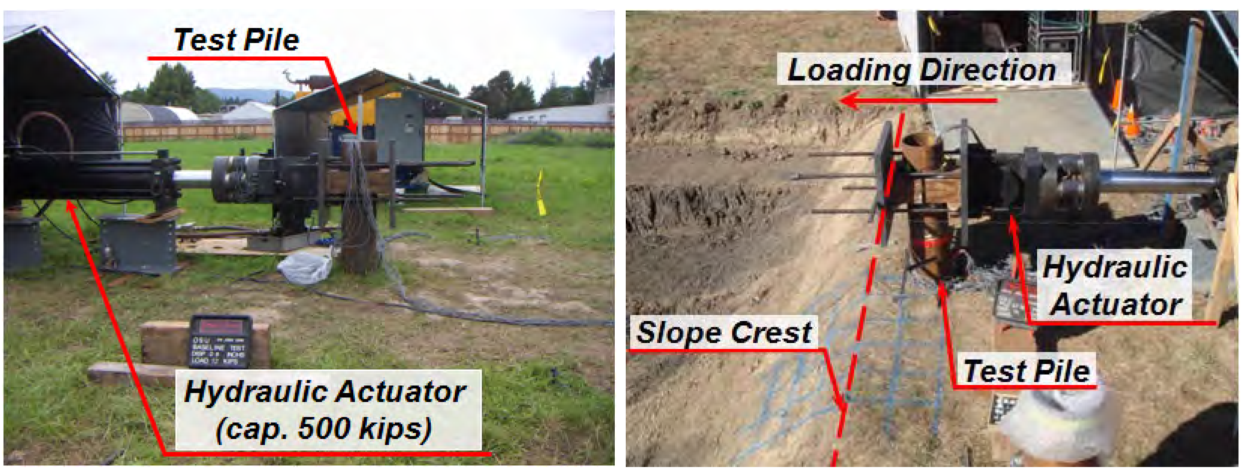

Figure 4-6. Actual test setup – Baseline Pile Test (left) and Pile Located at 2D from the Slope Crest (right)

Figure 4-7. Actual test setup – Three-in-a-row Reaction Pile Arrangement

Figure 4-8. Overall view of the completed slope excavation (Stage 1)

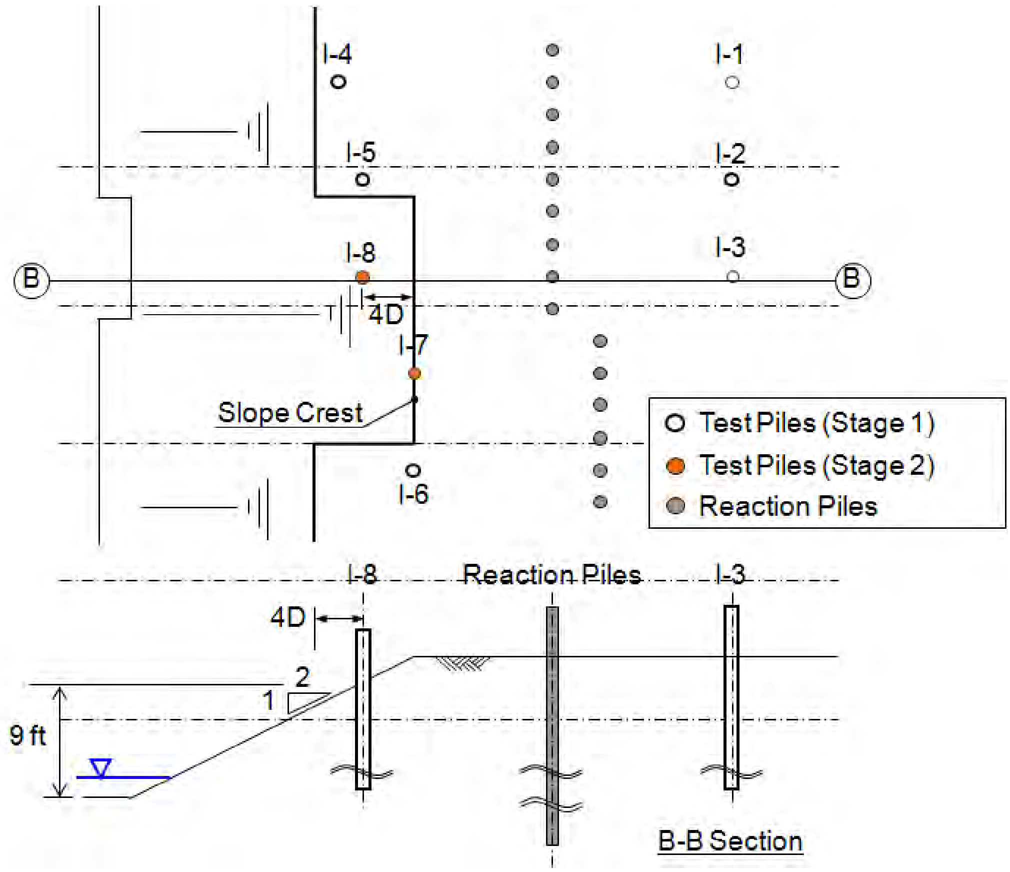

Figure 4-9. Plan View for Test Stage I with Location of Slope 2

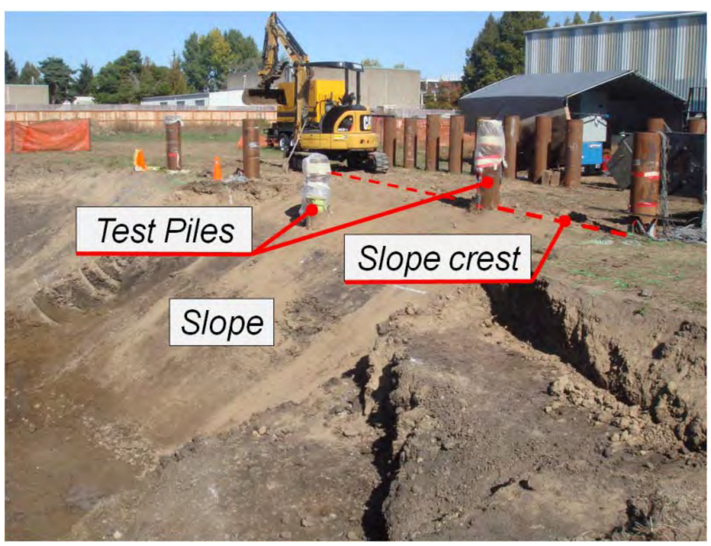

Figure 4-10. Overall View of the completed slope excavation in Stage 2 of Series-I

Figure 4-11. Installation of Baseline Pile (I-1)

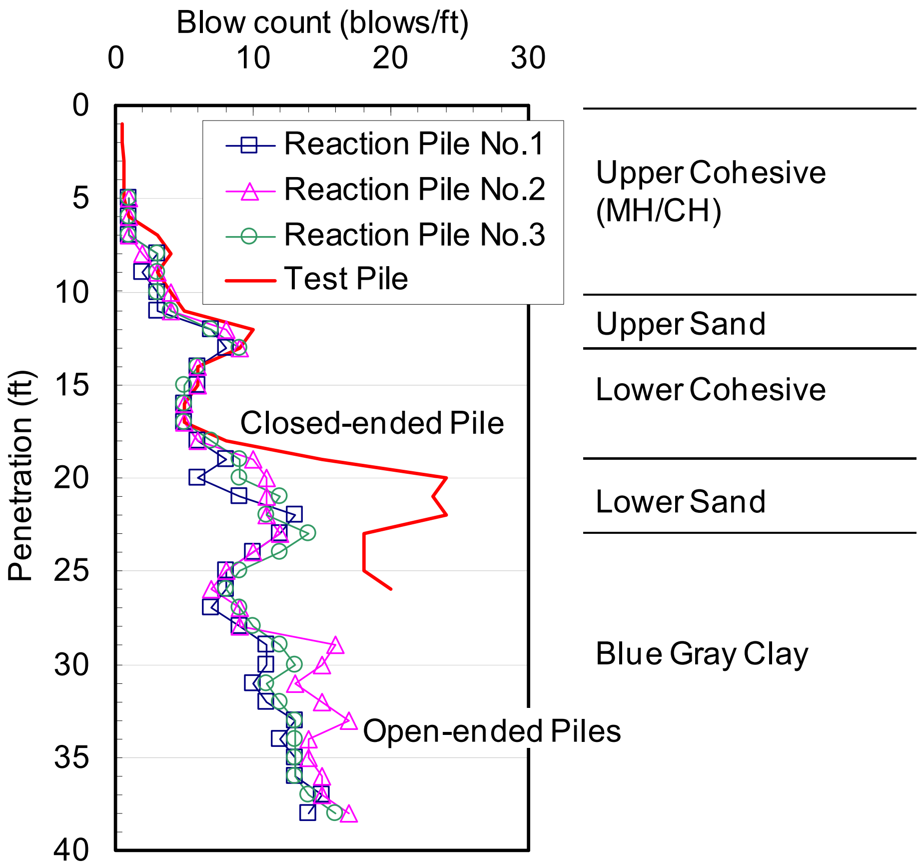

Figure 4-12. Pile Driving Logs for Baseline Pile (I-1) and Reaction Piles for Series-I

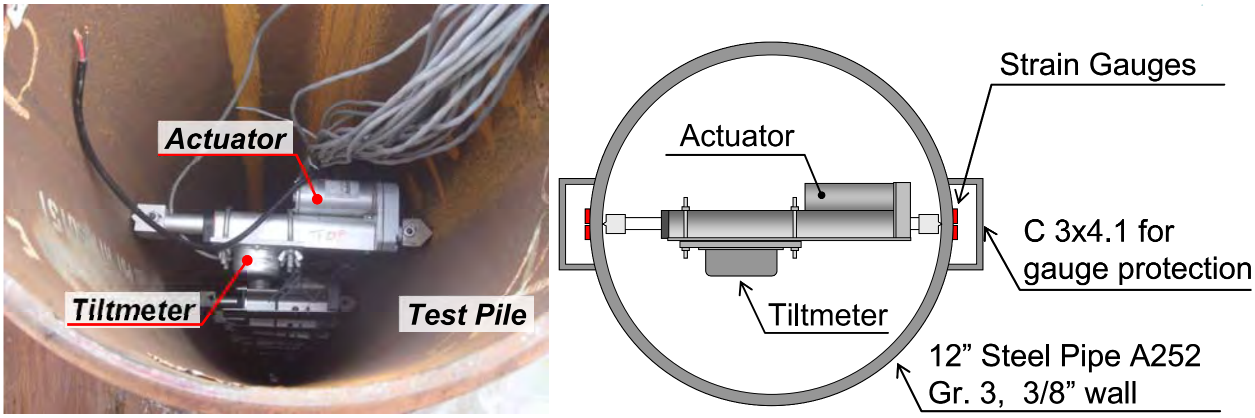

Figure 4-13. Cross-section view of test pile showing tiltmeter arrangement

Elevation (ft)	Instrumentation		
	Strain gauge	Tiltmeter	Potentiometer
0		●	●
2		●	●
3	●	●	
4	●	●	
5	●	●	
6	●	●	
7	●	●	
8	●	●	
9	●	●	
10	●	●	
11	●	●	
12	●	●	
14	●		
16	●	●	
18	●		
22	●		
26	●		

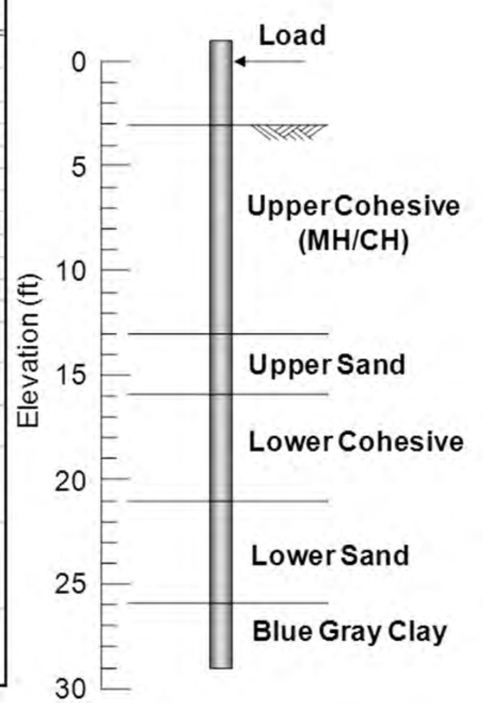

Figure 4-14. Summary of Sensor Locations

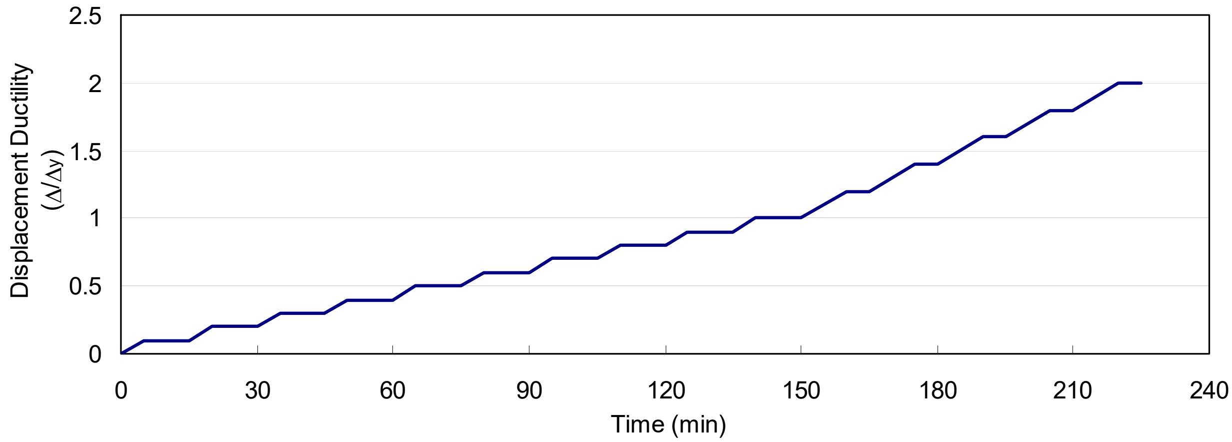

Figure 4-15. Load Protocol for Pseudo Static Lateral Load Tests

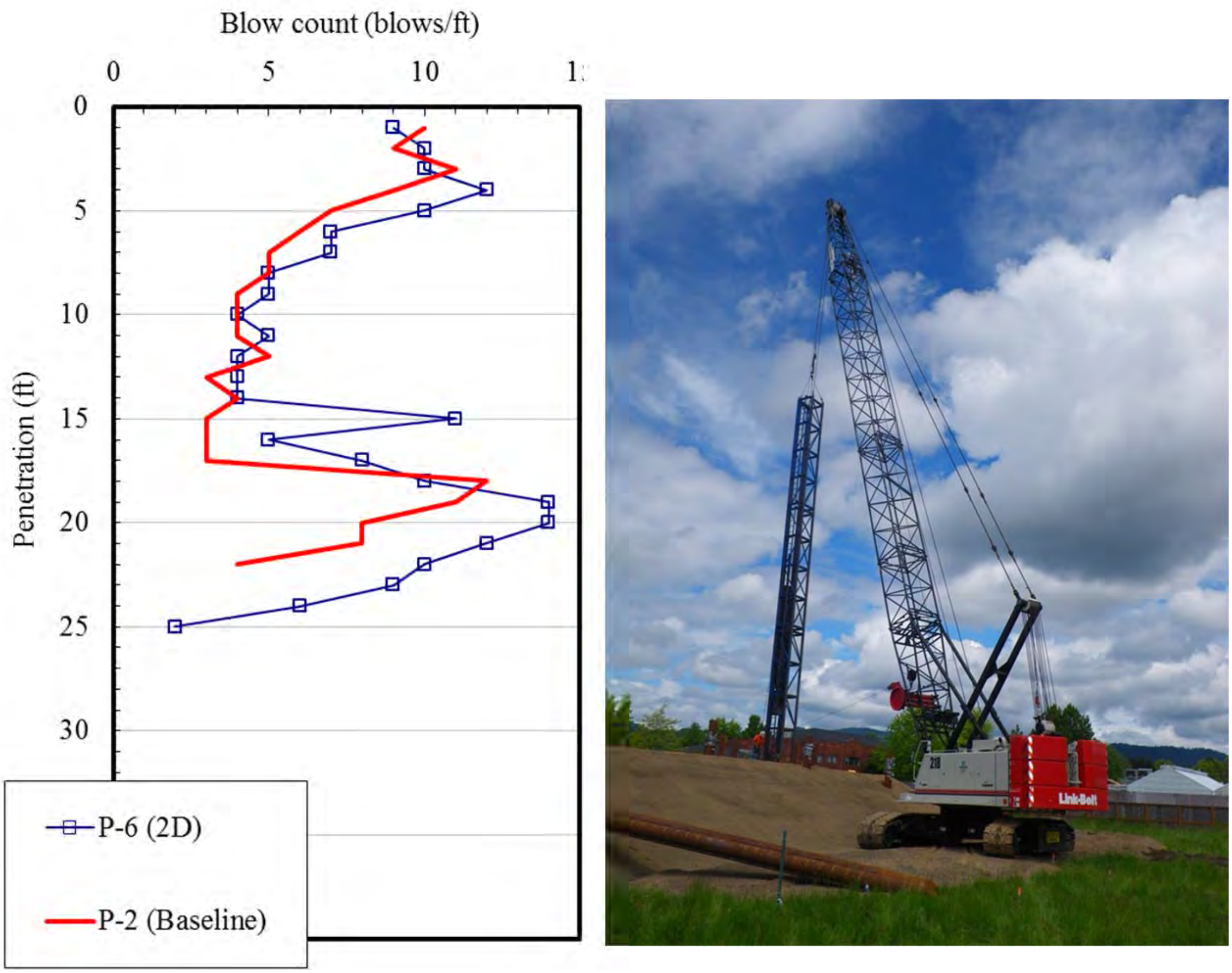

Figure 4-16. Pile Driving Logs for Baseline Piles for Series-II

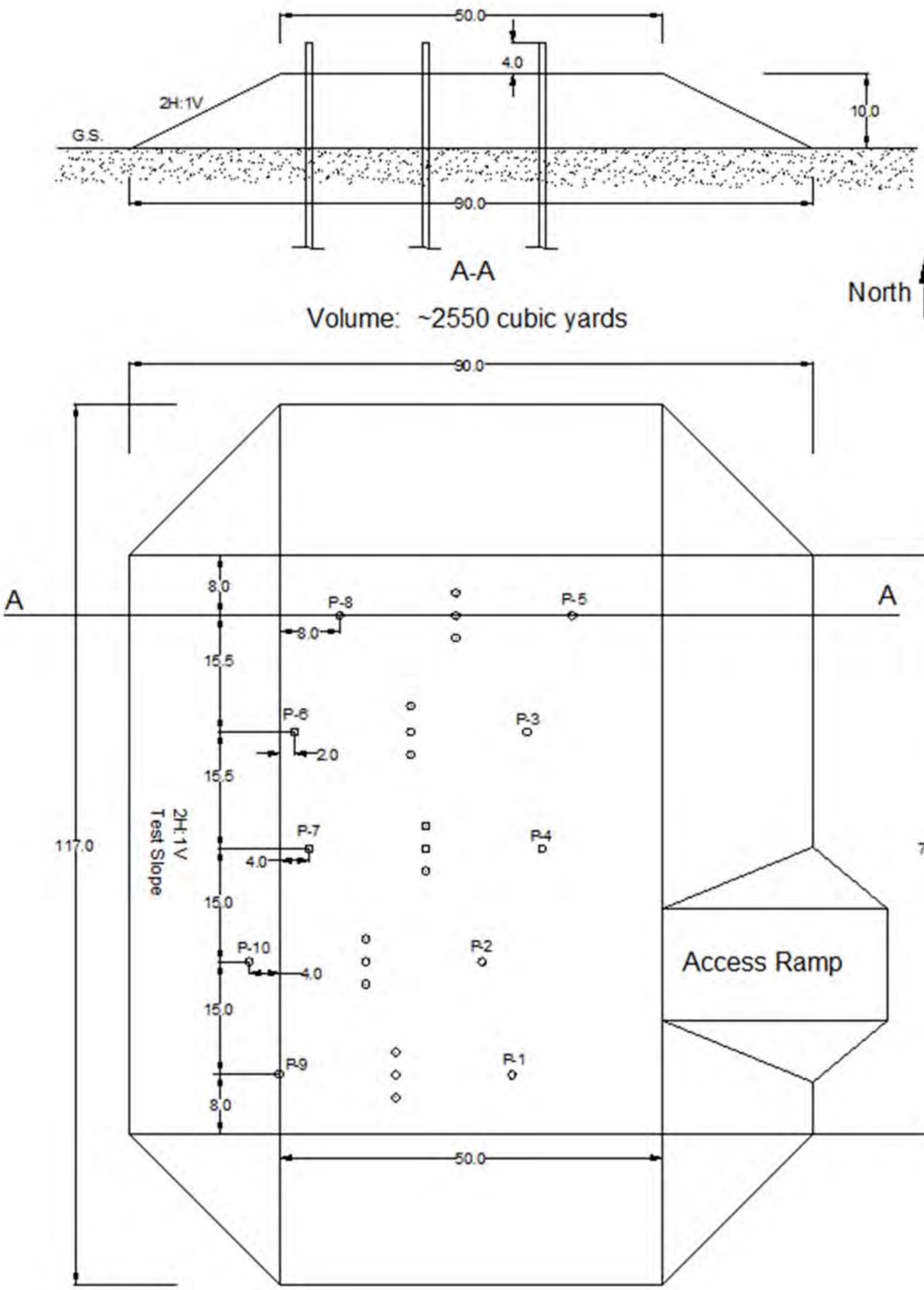

Figure 4-17. Plan and Cross-Sectional Views of the Series-II Cohesionless Embankment

Figure 4-18. Top: Constructed Embankment and Test slope Bottom: Test Pile, Reaction Piles, and Hydraulic Actuator Set up

5. LATERAL LOAD TESTING IN COHESIVE SOIL (SERIES-I)

Eight lateral load tests were performed in order to study the effect of soil slope and batter angle on the performance of piles and battered pile. A brief description of the observations during the load tests and photographs are provided.

5.1 BASELINE LOAD TESTS

The 1st baseline load test, pile I-1, was carried out at the test site on June 9, 2009. The load test results compared well with the preliminary analysis using stiff clay *p-y* curves above water table (Reese and Welch, 1975). Therefore, it was determined that the in-situ soil condition is suitable for the remaining full-scale lateral load tests in cohesive soils. The 2nd baseline load test, pile I-2, was carried out at the test site on August 27, 2009. The same load protocol was used for pile I-2. **Figure 5-1** shows observations made during lateral load testing of baseline piles. Large gap formed behind both baseline pile tests indicating that the soil is cohesive. Ground heaving in front of pile was observed in both tests. Gridlines were used to monitor soil movement around the pile during the test. The deformed gridlines after each target displacement indicate that the soil movement occurs along a line slightly less than 45 degrees measured from the pile axis in the direction perpendicular to loading. Similar soil movement was observed during pile near slope tests.

5.2 PILE NEAR SLOPING GROUND LOAD TESTS

Piles near slope tests include piles I-4, I-5, I-6 and I-7 which were located at 2D, 4D, 8D, and 0D from the slope crest respectively. For convenience, these piles are referred to as 2D pile (I-4), 4D pile (I-5), 8D pile (I-6) and 0D pile (I-7). The purpose of the tests was to investigate the effect of soil slope on lateral capacity of piles installed at different distances from the slope crest.

The lateral load test for 2D pile (I-4) was conducted on September 17, 2009. **Figure 5-2** shows observations made during lateral load test of the 2D pile. The first major crack observed during the test occurred on the slope face directly in front the test pile. Following this were cracks that formed along a line with an angle of approximately 45 degrees from the pile axis perpendicular to loading direction. Gridlines were used on only one side of the pile to monitor soil movement during the load test assuming identical crack patterns would form on the other side. However, the crack patterns on the side without gridlines are slightly different from the side with gridlines indicating that actual failure wedges may be different from theories (i.e., Broms, 1964, Reese *et al*., 1974). At large displacements, crack with an approximately size of a coin formed next to the pile along the line perpendicular to the loading direction. At an input displacement of 9 in., the observed cracks on the slope had propagated in the direction of 4D pile. Therefore, the load test was stopped to prevent the cracks from influencing the test results of 4D pile

The lateral load test for the 4D pile (I-5) was conducted on September 28, 2009. The photographs of the observations made during this test are presented in **Figure 5-3**. To fully monitor the soil movement and cracking pattern around the test pile, gridlines were installed on both sides of the pile. The observed cracking patterns in this test were similar to those observed in the 2D pile test. At pile head displacement of 3.5 inch, the first major crack was observed directly in front of the pile followed by the cracks forming perpendicular to the loading directing. Following these cracks were a cracks that formed along at line with an angle slightly less than 45 degrees from the pile axis perpendicular to the loading direction. The cracking pattern on both side of the gridlines were similar. The test was ceased once the ultimate load carrying capacity of 4D pile was reached.

Lateral Load test for the 8D pile (I-6) was carried out on October 7, 2009. **Figure 5-4** shows observations made during lateral load test of the 8D pile. No major crack on the slope was observed throughout the load test. Several minor cracks formed around the test pile. Ground heaving in front of the pile was observed similar that observed in the two baseline pile load tests.

Lateral load test for the 0D pile (I-7) was conducted on October 13, 2009. **Figure 5-5** shows observations made during lateral load test of the 0D pile. Like in 2D pile and 4D pile, several cracks on the slope were observed during the load test. The first major cracked was observed next to the pile at pile head displacement of 1.5 inch. At 4.5 inch of pile head displacement, large crack on the slope directly in front of the pile was observed. Several cracks around the pile with different patterns were observed throughout the test.

5.3 PILE ON SLOPE TEST

Lateral load test for -4D pile (I-8) was conducted on October 20, 2009. **Figure 5-6** shows photographs of the observations during lateral load test of -4D pile. As mentioned earlier, this pile was driven 2 ft lower than all the other piles in order to keep the loading height above the ground constant at 3 ft. Ground cracking next to the pile was observed at very low displacement. A very large crack formed on one side of the pile along the line perpendicular to loading direction was observed at pile head displacement of 3 inch. Several cracks around the pile were observed to form along several lines with different angles from the pile axis. Significantly more severe cracking of the slope was observed at the end of the load test compared to observations made at the end of 0D pile test. **Table 5-1** presents the test pile loading rates between target displacements at 3ft above the ground surface. The actuator extension rate was 0.1 in/min and this translated into an average pile head loading rate of 0.90 in/min due to lateral movement of the reaction pile system. A slight increase in pile head loading rate (maximum increase of 0.015 inch/min) occurred with increasing pile head displacements and this is likely due to near slope effects on lateral resistance.

5.4 BATTERED PILE LOAD TEST

Lateral load test on battered pile (I-3) was conducted on September 8, 2009. The purpose of battered pile test was to compare the performance of battered piles to piles on slope because in practice (i.e. Reese *et al*., 2004), battered piles are treated as if equivalent to pile on the slope. The test setup for the battered pile was significantly more complicated than other piles tests. Two types of setups are attempted in this study.

The test pile was driven with a batter angle of 2:1 from vertical. The 1st setup attempt was designed such that the actuator will be pushed against the test pile as to apply lateral load at 3 ft from the ground surface as shown in **Figure 5-7**. During the load test, it was observed that the load stub was moving down along the pile. The test was stopped once slip occurred. After the test, it was believed that the friction between the load stub and the pile was underestimated. Therefore, as the lateral load increased, slip occurred as the axial force component became large enough to overcome friction in the load stub.

The second attempt on battered pile test was made on November 4, 2009. This latter setup was designed such that the load was applied laterally and axially to the test pile such the resultant force is equivalent to a lateral load that was applied at 3 ft from the ground surface. This test setup was believed to provide more friction between the load stub and the pile than in previous setup. **Figure 5-7** shows test set-ups for the 2nd attempt for battered pile test. **Figure 5-8** shows photographs of the observations made for both lateral load tests for battered pile (I-3). Ground heaving was present at the start of the 1st attempt for battered pile test as a result from driving the pile at an angle relative to the horizontal surface. At a target displacement of 1 inch, it was observed that the swivel head in the actuator was beginning to rotate and the loading plate was moving down with respect to the loading blocks. This was due to the moment generated in the swivel head which causes the actuator to move downwards. An additional loading block was inserted to prevent the rotation of the loading plate and the test was continued. At the end of the test, it was observed that the loading blocks were cracked and local deformations occurred at the loading points.

5.5 SUMMARY

Eight full scale lateral load tests were conducted at Oregon State University that included two baseline pile tests, four piles near sloping ground tests, one pile on slope test and one battered pile test. Major observations are heaving of the ground in front of the pile during the baseline pile tests, gap forming behind all test piles and cracking of the ground around the pile and on the slope. The test results of each test are presented in the next section. **Table 5-2** presents the testing dates for all Series-I lateral load tests.

Table 5-1 Average Loading Rates from Pile I-8 between Target Displacements

Displacement Range (in)	Average Loading Rate (in/min)
1.0-1.5	0.082
1.5-2.0	0.084
2.5-3.0	0.086
3.0-3.5	0.087
3.5-4.0	0.088
4.0-4.5	0.092
4.5-5.0	0.093
5.0-6.0	0.094
6.0-7.0	0.093
7.0-8.0	0.095
8.0-9.0	0.095
Average Loading Rate (in/min)	0.090
Maximum Loading Rate	0.095
Minimum Loading Rate	0.082

Table 5-2 Testing Dates for Series-I Lateral Load Tests

Pile	Orientation	Testing Date
I-1	Baseline	6/9/2009
I-2	Baseline	8/27/2009
I-3	26° Batter	9/8/2009
I-4	2D	9/17/2009
I-5	4D	9/28/2009
I-6	8D	10/7/2009
I-7	0D	10/13/2009
I-8	-4D	10/20/2009

(a) Gap behind pile

(b) Heaving in front of pile

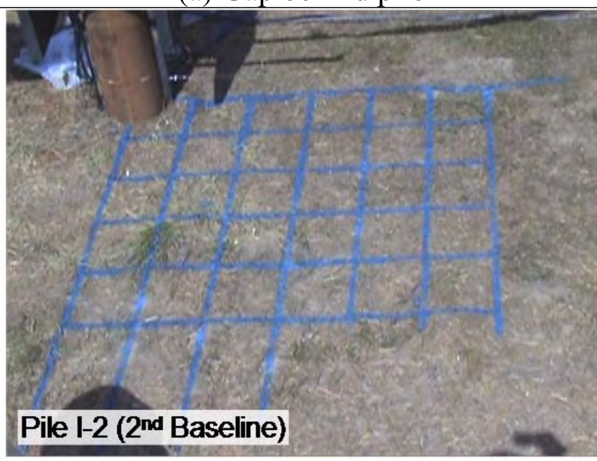

(c) Initial gridlines

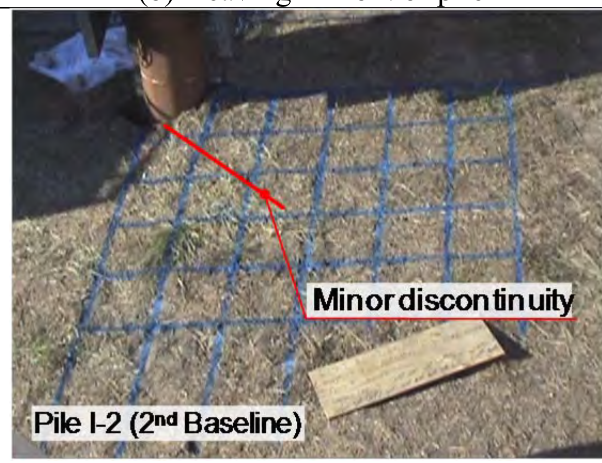

(d) After loading

Figure 5-1. Observations during Load Test of 1st and 2nd Baseline Piles (Free Field)

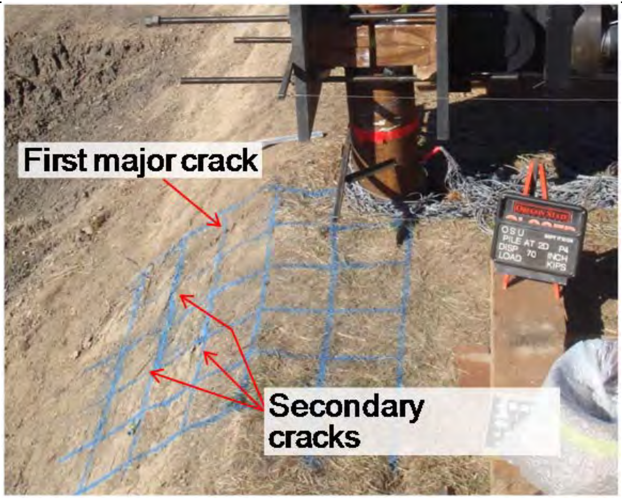

a) Cracks on slope at 7” pile-top displacement


b) Slope collapse at 9” pile-top displacement


c) Cracks on side without gridlines


d) Cracks in front of the test pile


e) Crack perpendicular to loading direction

Figure 5-2. Observations from Lateral Load Test for 2D Pile (I-4)

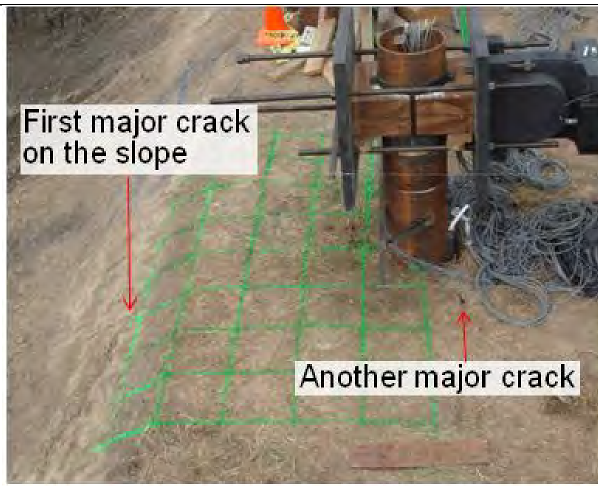

a) Crack pattern at 3.5” pile-top displacement

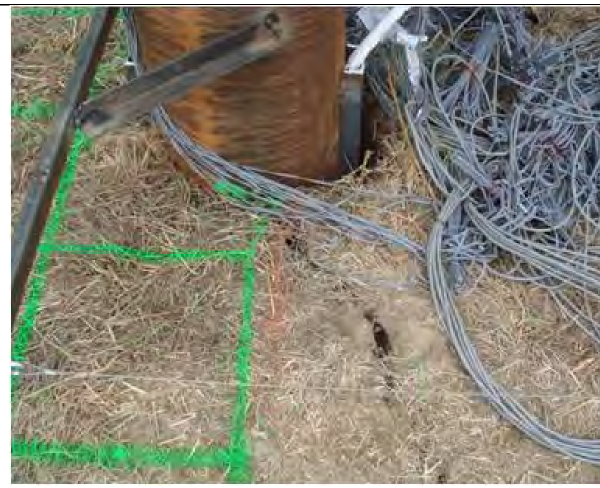

b) Crack around the pile

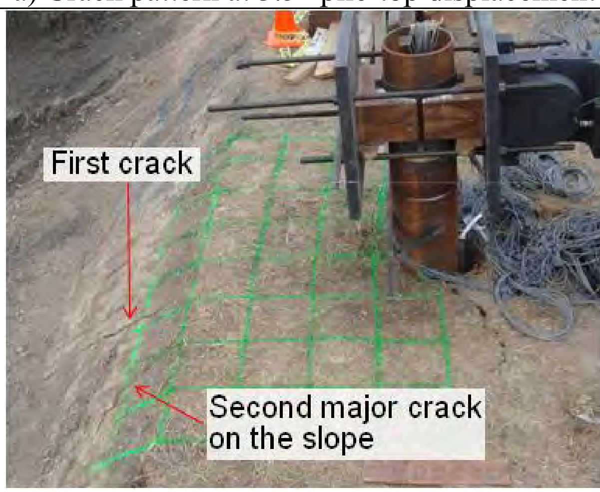

c) Crack pattern at 6” pile-top displacement

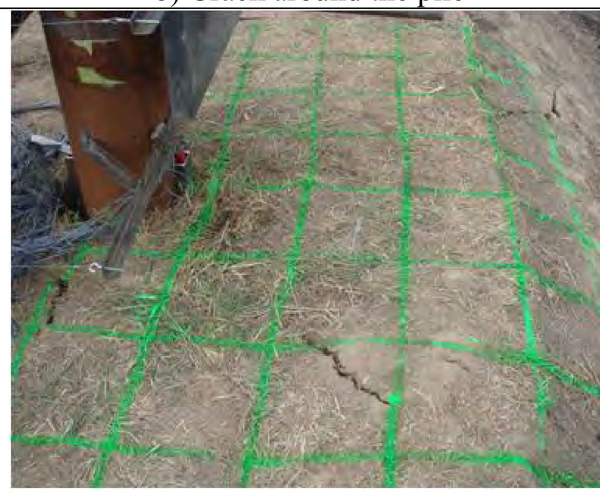

d) Similar crack pattern on the other side

Figure 5-3. Observations from Lateral Load Test for 4D Pile (I-5)

a) Minor crack around the test pile

b) Minor crack around the test pile

c) Ground heaving in front of the test pile

d) No major crack observed

Figure 5-4. Observations from Lateral Load Test for 8D Pile (I-6)

a) Crack developed at 1.5” disp.

b) Crack on the slope at 4.5” disp.

c) Multi-cracks around the pile

d) Crack pattern at 9” disp.

Figure 5-5. Observations from Lateral Load Test for 0D Pile (I-7)

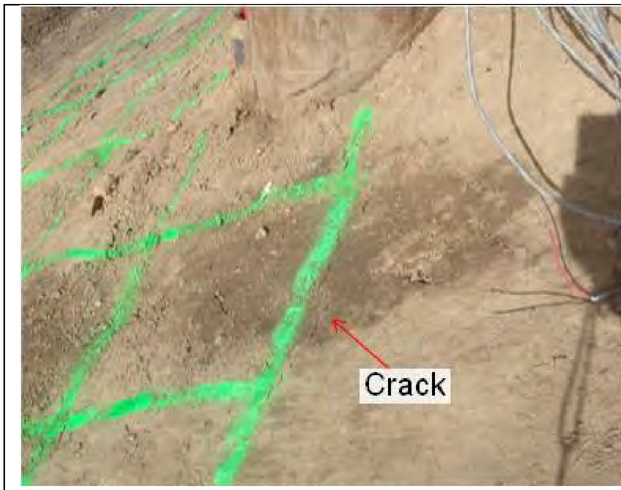

a) Crack developed even at 1” displacement

b) Large crack at 3” displacement

c) Crack propagation at 4” disp.

d) Severe cracking at the end of loading

Figure 5-6. Observations from Lateral Load Test for -4D Pile (I-8)

Figure 5-7. First Attempt (left) and Second Attempt (right) for Battered Pile Test (I-3)

a) Initial condition before 1st battered pile test

b) Slippage of load stub in the 1st test

c) Initial condition for 2nd battered pile test

d) Crack pattern at 5" displacement

e) Bent actuator rod due to section deformation

f) Significant cracks on timber spacer blocks

Figure 5-8. Observations from Both Lateral Load Tests for Battered Pile (I-3)

6. TEST RESULTS FROM SERIES-I (COHESIVE SOILS)

In this section, the test results from all lateral load testing are presented. A comparison of the results of piles which were installed at different distances from the slope crest (2D, 4D, 8D and 0D respectively) that were tested under similar soil loading conditions, offers insight into the effect of slope of lateral load response of piles.

In general, stress-relaxation was observed during the 5-10 minutes wait after each target displacement similar to creep observed at high loads in full-scale lateral pile load tests in soft clay (i.e., Matlock, 1970). The study by Matlock (1970) found that the change in moment due to creep was minor and had a constant rate. Therefore, it was assumed that stress-relaxation observed after each target displacement did not have significant effect on the lateral response of piles in this study.

6.1 BASELINE LOAD TESTS AND PILE LOCATED AT 8D FROM SLOPE

In this section, test results for two baseline piles (I-1 and I-2) and the pile located at 8D from the slope crest (I-6) are presented. A comparison between measured responses for pile I-2 and 8D pile are discussed.

6.1.1 LOAD DISPLACEMENT CURVE

Load-displacement curves under static loading for two baseline piles and the 8D pile are presented in **Figure 6-1**. The load carrying capacity of pile I-1 (1^{st} baseline) was 7.9 kips and 13.4 kips at target pile head displacements of 0.5 and 1.0 inch respectively. The measured load of pile I-2 (2^{nd} baseline) was 11.6 and 18.6 kips at target pile head displacements of 0.5 and 1.0 inch respectively. For 8D pile, the load-displacement curve was similar to pile I-2. The measured load of 8D pile was 11.1 and 20.0 kips at target pile head displacements of 0.5 and 1.0 inch respectively. The results for pile I-1 were different from pile I-2 and 8D pile due to different time of testing resulting in different soil condition due to seasonal changes. As mentioned in the previous section, the lateral load testing of pile I-1 (1^{st} baseline) was conducted on June 9, 2009. The lateral load testing of pile I-2 (2^{nd} baseline) and 8D pile were conducted on August 27, 2009 and October 7, 2009 respectively. Pile I-1 was tested after the rainy season while the other tests were conducted in the middle of summer. The evaporation of surface water during the summer months reduced the water content of top soil and therefore increased cohesion (Terzaghi and Peck, 1967). Therefore, results from pile I-2 and 8D pile were considered as baseline results. A comparison of the calculated curvature and rotation shown in **Figure 6-2** indicate that pile I-2 and 8D pile have similar lateral response. Therefore, the results from 8D pile was analyzed and use as baseline results for subsequent analyses.

6.1.2 CURVATURE AND ROTATION PROFILES

The calculated curvature and measured rotation at different depths for 8D pile are presented in **Figure 6-3** and **Figure 6-4**. The calculated curvature from strain gauge data indicates that the location of maximum moment occurs at a depth of 4 ft below the ground surface corresponding to a depth of 4D. At all target pile head displacements, no significant strain was observed at a depth of 25 ft. No significant rotation was measured from the tiltmeter below a depth of 16 ft. These results indicate that the locations of instrumentations are sufficient to measure pile responses under lateral loading and that the test piles are long enough to behave as flexible piles under lateral loading.

6.2 LATERAL LOAD TEST FOR 2D PILE (I-4)

In this section, the load displacement curves along with calculated curvature and measured rotation for 2D pile (I-4) are presented. The load-displacement characteristics and location of maximum moment for 2D pile and 8D pile are compared and discussed.

6.2.1 LOAD DISPLACEMENT CURVE

Load-displacement curve for 2D pile are presented in **Figure 6-5**. The measured load was 11.6 and 18.6 kips at target pile head displacements of 0.5 and 1.0 inch respectively. The load-displacement characteristic of 2D pile was similar to 8D pile at target pile head displacement of 0.5 inch indicating that the slope has insignificant effect on the lateral load carrying capacity. Beyond this displacement, the measured load of 2D pile was smaller than 8D pile indicating that the presence of slope has significant effect on the lateral capacity of pile. For this lateral loading test, there was a power supply problem when the target displacement was increased from 0.5 to 1.0 inch that resulted in the resetting of the data collection system and the hydraulic actuator. The process of reloading affected the pile response, therefore some assumptions were needed in the interpretation of the test results. The power supply problem was corrected for the remainder of the tests.

6.2.2 CURVATURE AND ROTATION PROFILES

The calculated curvature and measured rotation at different depths for the 2D pile are presented in **Figure 6-6** and **Figure 6-7**. The calculated curvature from strain gauge data shows that the location of maximum bending moment occurs at a depth between 4 ft at pile head displacement of 0.5 inch and increases to a depth of 6 ft at a displacement of larger than 3 inch. This observation indicates that, at a displacement larger than 0.5 inch, 2D pile is more flexible under lateral load than 8D pile which is consistent with the observed load-displacement relationship.

6.3 LATERAL LOAD TEST FOR 4D PILE (I-5)

In this section, the load displacement curve along with calculated curvature and measured rotation for 4D pile are presented. The load-displacement characteristics and location of maximum moment for 4D pile and 8D pile are compared and discussed.

6.3.1 LOAD DISPLACEMENT CURVE

Load-displacement curve for 4D pile is presented in **Figure 6-8**. The measured load was 11.5 and 19.8 kips at target pile head displacements of 0.5 and 1.0 inch respectively. The load-displacement characteristic of the 4D pile was similar to the 8D pile for pile displacement of 1.0 inch indicating that the slope has minor effect on the lateral load carrying capacity. Beyond this displacement, the measured load of 4D pile was smaller than 8D pile indicating that slope has significant effect on the lateral capacity of pile at higher displacements.

6.3.2 CURVATURE AND ROTATION PROFILES

The calculated curvature and measured rotation at different depths for 4D pile are presented in **Figure 6-9** and **Figure 6-10**. The calculated curvature from strain gauge data shows that the location of maximum bending moment occurs at a depth between 4 ft at pile head displacement of 0.5 to 2.0 inch and increases to a depth of 5 ft at a displacement of larger 3 inch. This observation indicates that, beyond target pile head displacement of 1.0 inch, 4D pile is more flexible under lateral load than 8D pile but stiffer than 2D pile which is consistent with the observed load-displacement relationship.

6.4 LATERAL LOAD TEST FOR 0D PILE (PILE ON SLOPE CREST, I-7)

In this section, the load displacement curve along with calculated curvature and measured rotation for 0D pile (pile on the slope crest, I-7) are presented. The load-displacement characteristics and location of maximum moment for 0D pile and 8D pile are compared and discussed.

6.4.1 LOAD DISPLACEMENT CURVE

Load-displacement curve for 0D pile are presented in **Figure 6-11**. The measured load was 8.5 and 14.8 kips at target pile head displacements of 0.5 and 1.0 inch respectively. The load-displacement characteristic of 0D pile is more flexible than 2D pile, 4D pile and 8D pile at all target displacement range. This result is expected because 0D pile was installed on the slope crest.

6.4.2 CURVATURE AND ROTATION PROFILES

The calculated curvature and measured rotation at different depths for 0D pile are presented in **Figure 6-12** and **Figure 6-13**. The calculated curvature from strain gauge data indicates that the location of maximum moment occurs at a depth of 5 ft below the ground surface corresponding to 5D. This observation indicates that 0D pile is more flexible under lateral load than 2D pile, 4D pile and 8D pile.

6.4.3 SUMMARY OF PILE NEAR SLOPE TESTS

A comparison of the measured lateral load-pile head displacement curves of 2D pile (I-4), 4D pile (I-5), 8D pile (I-6) and 0D pile (I-7) are shown in **Figure 6-14**. At low displacement, the load-displacement characteristics of 2D pile, 4D pile, 8D pile were similar. After approximately 0.5 inch of displacement, the load carrying capacity for 2D pile was lower than that of 8D pile. For 4D pile, the load carrying capacity was lower than that of 8D pile after approximately 1.5 inch of displacement. The ultimate lateral load of 2D pile was lower than 4D pile. The measured load at 9 inch of pile head displacements of 2D pile and 4D pile were 53.0 kips and 63.1 kips respectively. The measured load at 9 inches of displacement for 0D pile was 52.5 kips similar to that of 2D pile. Based on these observations, it can be concluded that at small displacement range, the slope has insignificant effect on the lateral capacity of piles. At larger displacement range, the presence of the soil slope adversely affected the ultimate load carrying capacity of pile when the piles were installed within 4D from the slope crest. For pile on the slope crest, the load carrying capacity of the pile was adversely affected at all displacement range. The ultimate load carrying capacity of piles was independent of the distance from the slope crest when piles were located within 2D from the slope crest.

6.5 LATERAL LOAD TEST FOR -4D PILE (PILE ON THE SLOPE, I-8)

Load-displacement curve for -4D pile (I-8) are presented in **Figure 6-15**. The measured load was 13.7 and 21.5 kips at target pile head displacements of 0.5 and 1.0 inch respectively. This indicates that pile I-8 is stiffer than 8D pile in small displacement range. Beyond this displacement, the measured load of pile I-8 was lower than 8D pile. However, the ultimate load of pile I-8 was 48.0 kips at a target displacement of 9 inch which was lower than that of 0D pile. This might be due to different soil condition because -4D pile was installed 2 ft lower than all other test piles. It was also believed that the presence of soil upslope might have affected the initial stiffness. Due to uncertainties in the test set-up and the difference in soil conditions, the pile on the slope test (I-8) was not considered for this study.

6.6 LATERAL LOAD TEST FOR PILE I-3 (BATTERED PILE)

Load-displacement curve for battered pile (I-3) is presented in **Figure 6-16**. The measured load was 9.4 and 18.0 kips at target pile head displacements of 0.5 and 1.0 inch respectively. For pile I-3, the maximum target displacement was 7.5 inch and the measured load was 61.6 kips. Due to uncertainties in the test set-up the battered pile test was not fully analyzed for this study.

6.7 COMPARISON OF TEST RESULTS WITH CALTRANS RECOMMENDATION

For a steel pile with a 12-inch diameter, Caltrans BDS (2003) requires lateral capacity of piles under Service Limit State Load, with maximum horizontal deflection of 1/4 inch, (BDS Article 4.5.6.5.1) of 5 kips for piles fully embedded in soil. To compare with the Caltrans requirement (i.e., piles fully embedded in soil), the tiltmeter data was utilized to estimate the soil-pile deflection at the ground surface for 0D pile (I-7), 2D pile (I-4), 4D pile (I-5) and 8D pile (I-6). A comparison between the measured load and soil displacement at the ground surface is presented in **Figure 6-17**. The results indicate that the tested piles meet the required capacity of 5 kips at 1/4 inch of pile deflection at the ground surface.

6.8 SUMMARY

Results from pile near slope tests (0D, 2D, 4D, and 8D) indicate that slope has significant impact on lateral capacity of piles at target pile head displacement of great than 0.5 inch for 2D pile and 1.0 inch for 4D pile. For 0D pile, slope adversely affected the lateral capacity of the pile at all target pile head displacements.

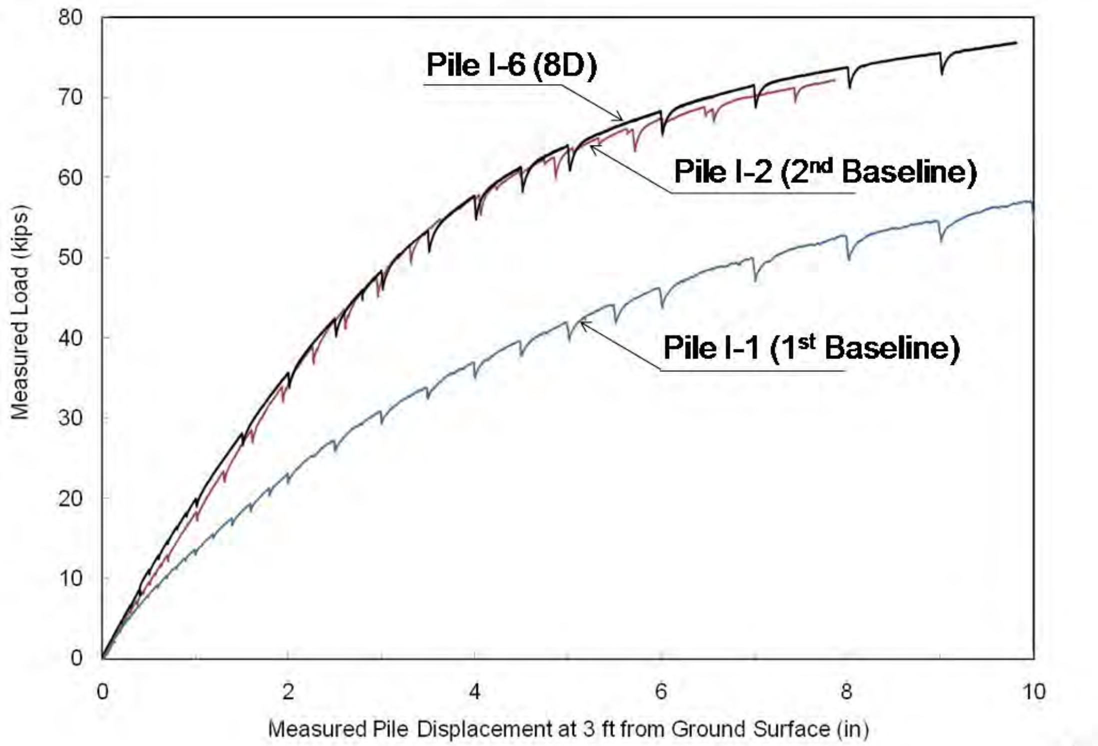

Figure 6-1. Comparison of Load-Displacement Curves between Baseline Piles (I-1 and I-2) and Pile at 8D from the Slope Crest (I-6)

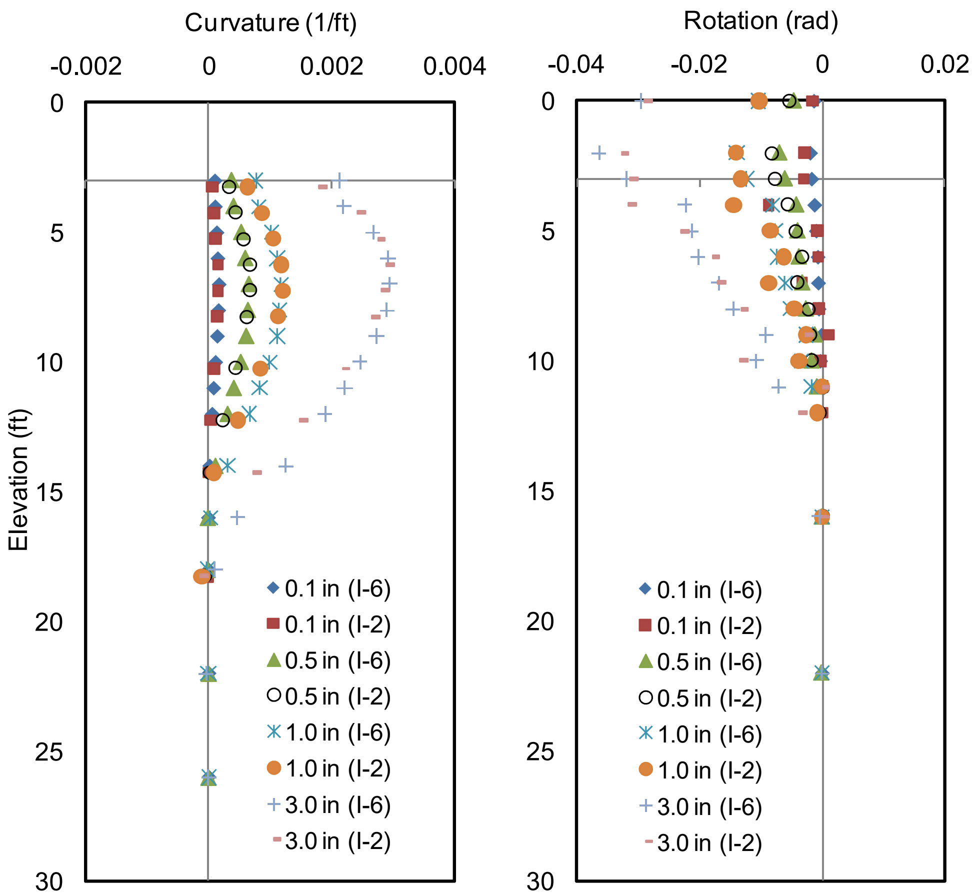

Figure 6-2. A Comparison of Calculated Curvature and Measured Rotation for 2nd Baseline Pile (I-2) and 8D pile (I-6)

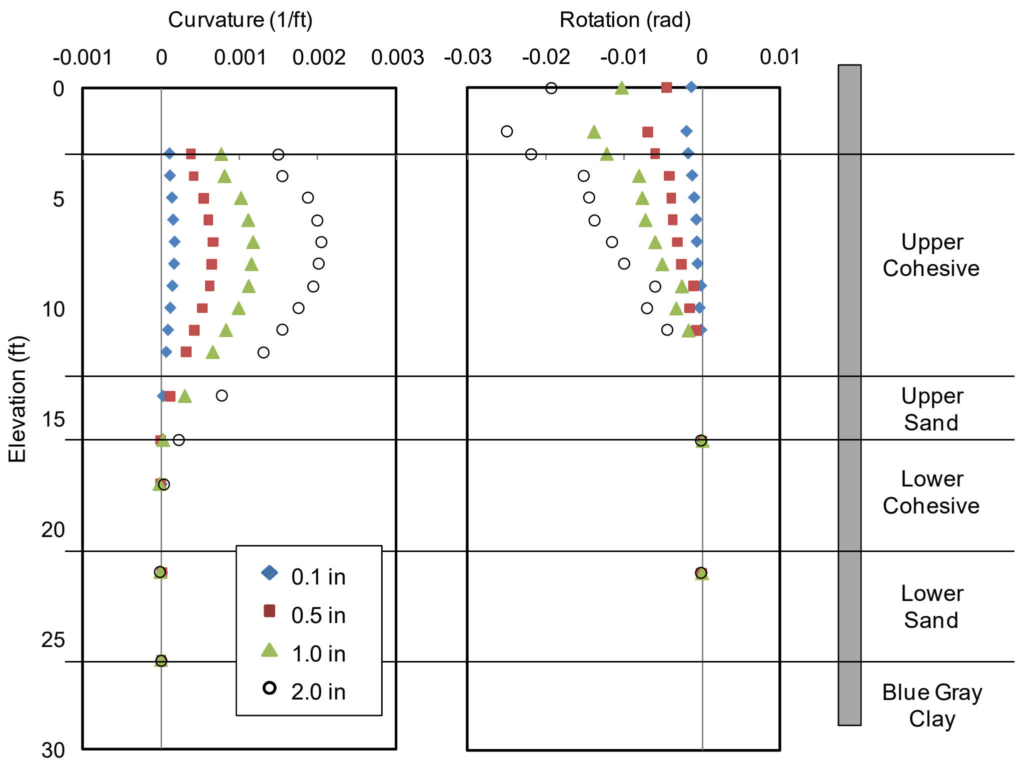

Figure 6-3. Test Results of 8D pile (I-6) for Pile Head Displacement of 0.1, 0.5, 1.0 and 2.0 in

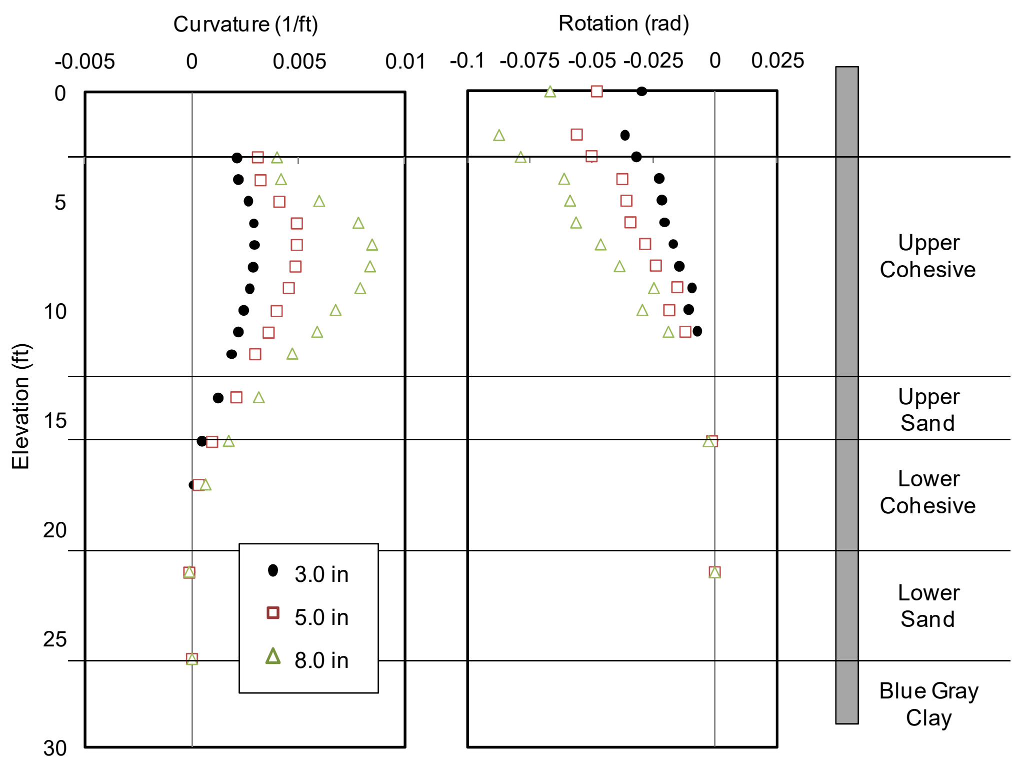

Figure 6-4. Test Results of 8D pile (I-6) for Pile Head Displacement of 3.0, 5.0 and 8.0 in

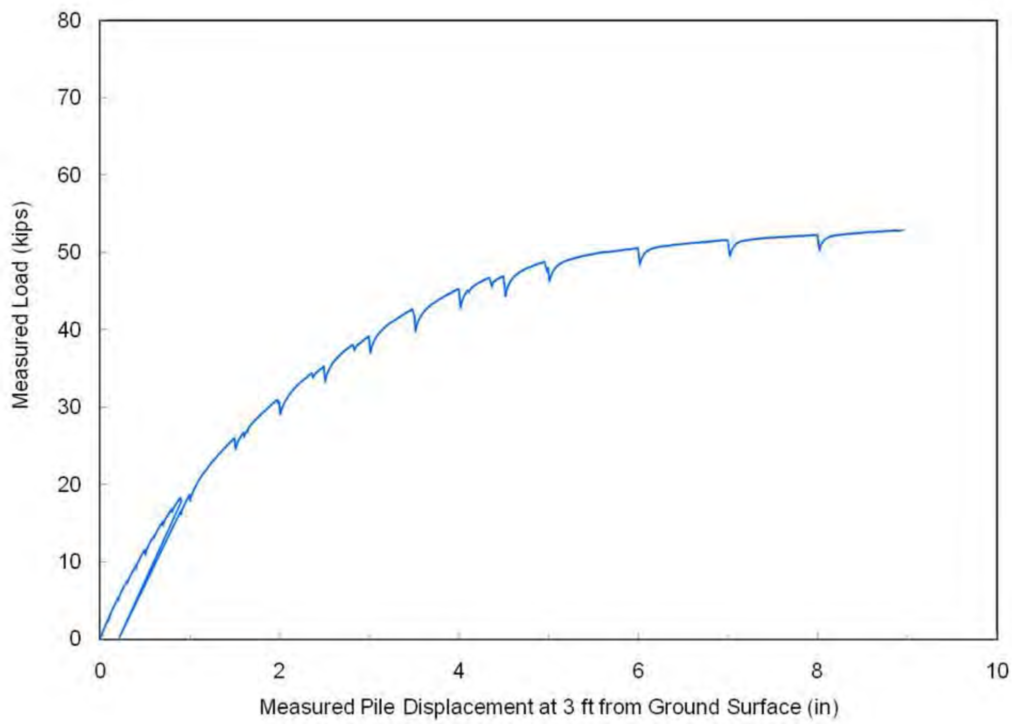

Figure 6-5. Load Displacement Curve for 2D pile (I-4)

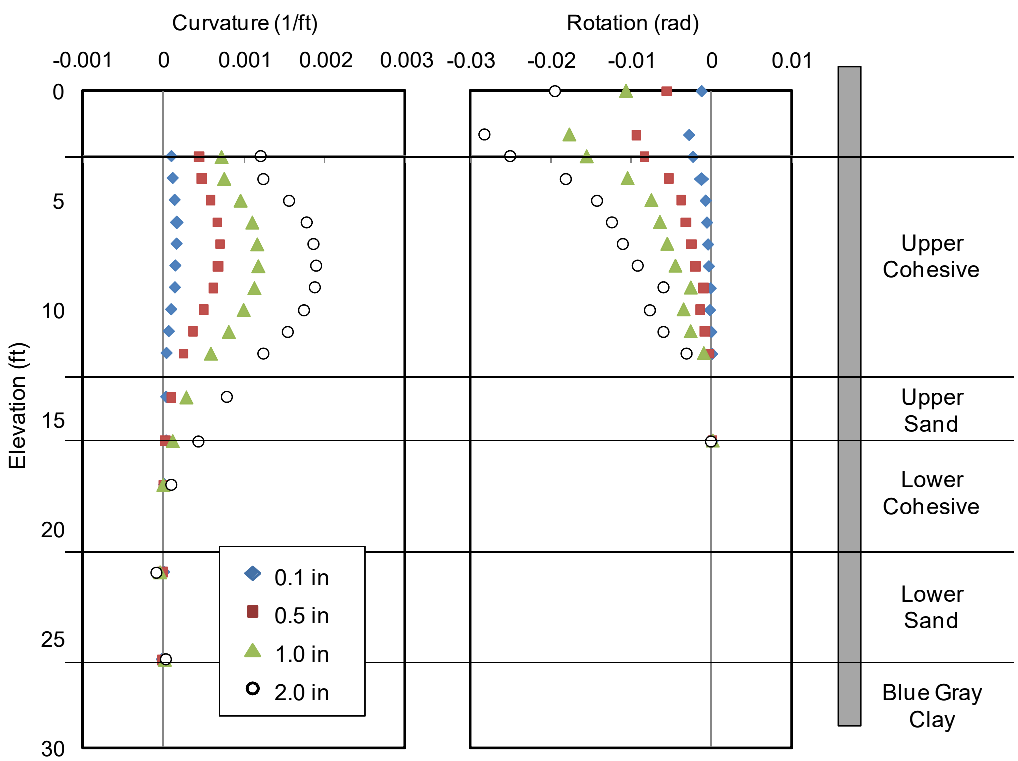

Figure 6-6. Test Results of 2D pile (I-4) for Pile Head Displacement of 0.1, 0.5, 1.0 and 2.0 in

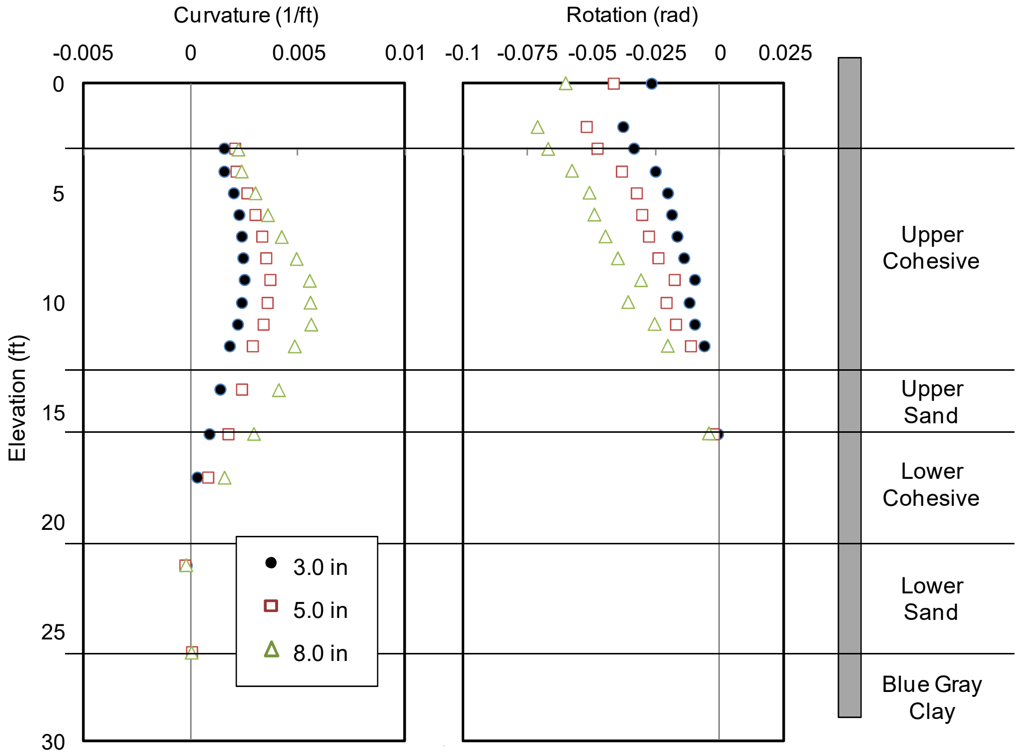

Figure 6-7. Test Results of 2D pile (I-4) for Pile Head Displacement of 3.0, 5.0 and 8.0 in

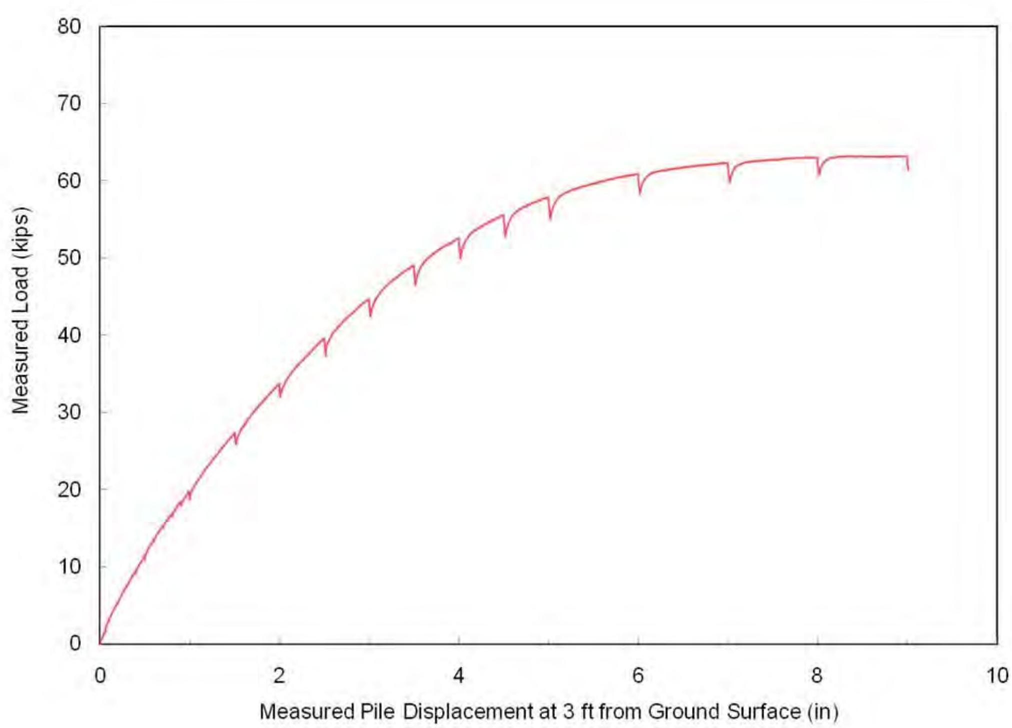

Figure 6-8. Load Displacement Curve for 4D pile (I-5)

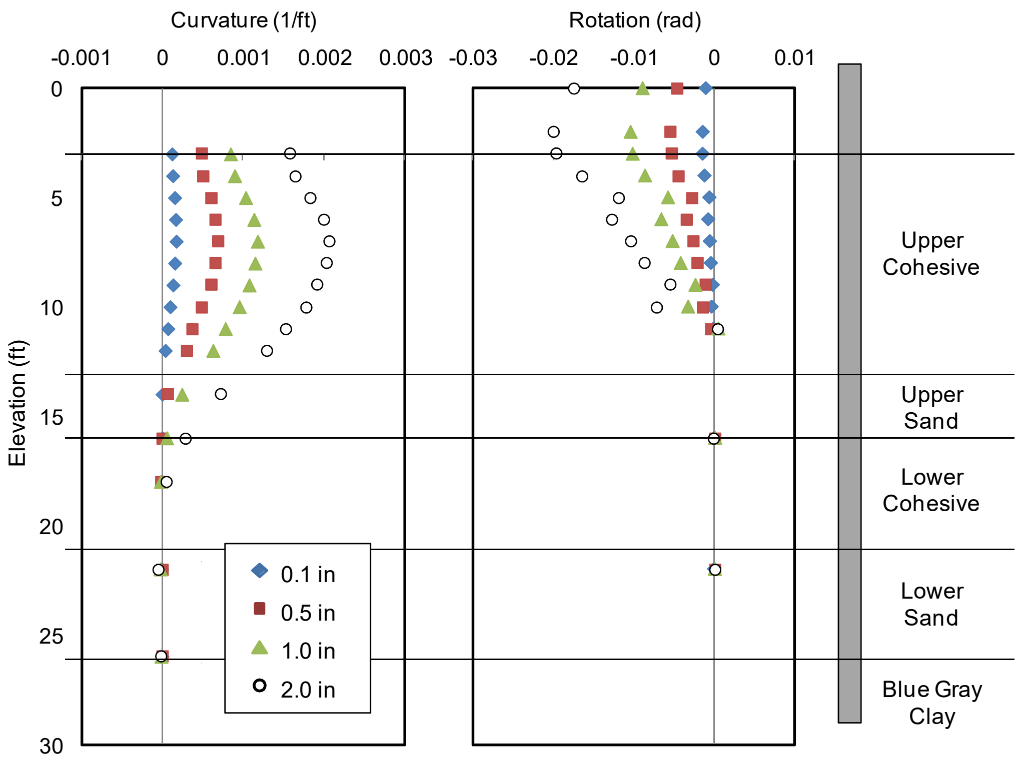

Figure 6-9. Test Results of 4D pile (I-5) for Pile Head Displacement of 0.1, 0.5, 1.0 and 2.0 in

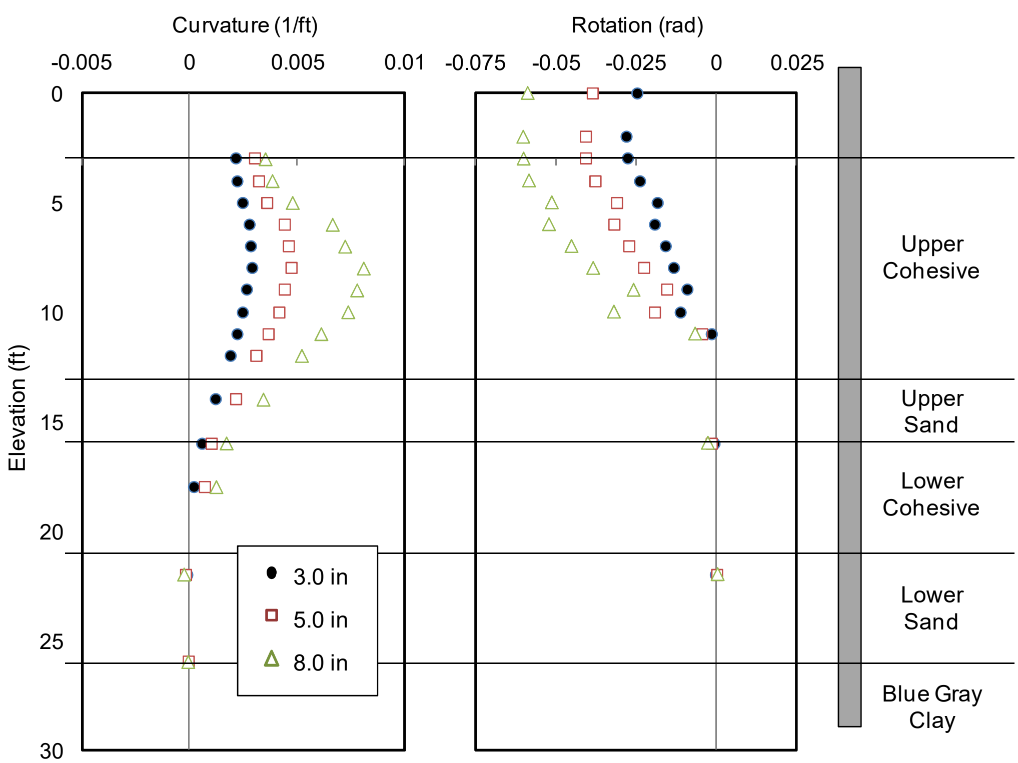

Figure 6-10. Test Results of 4D pile (I-5) for Pile Head Displacement of 3.0, 5.0 and 8.0 in

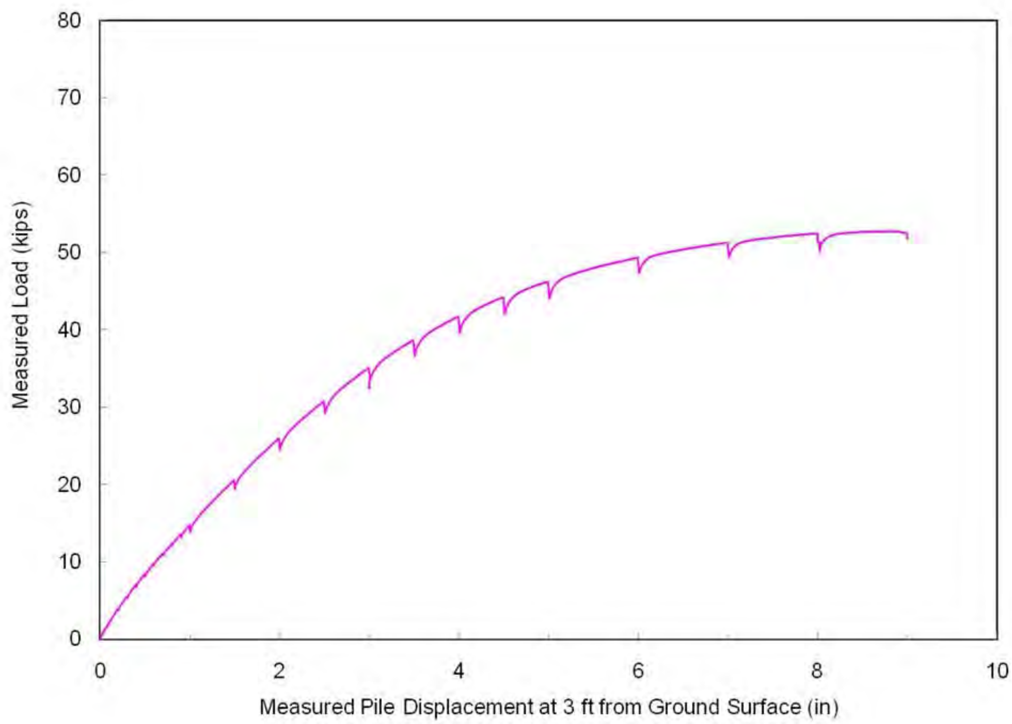

Figure 6-11. Load Displacement Curves for 0D pile (I-7)

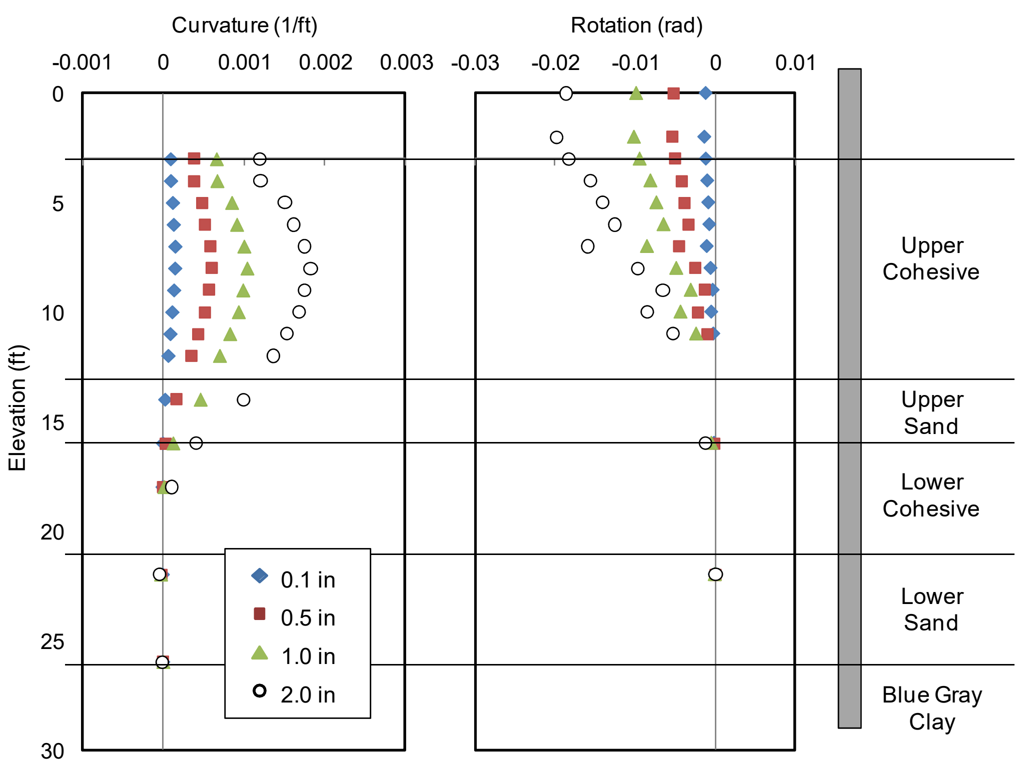

Figure 6-12. Test Results of 0D pile (I-7) for Pile Head Displacement of 0.1, 0.5, 1.0 and 2.0 in

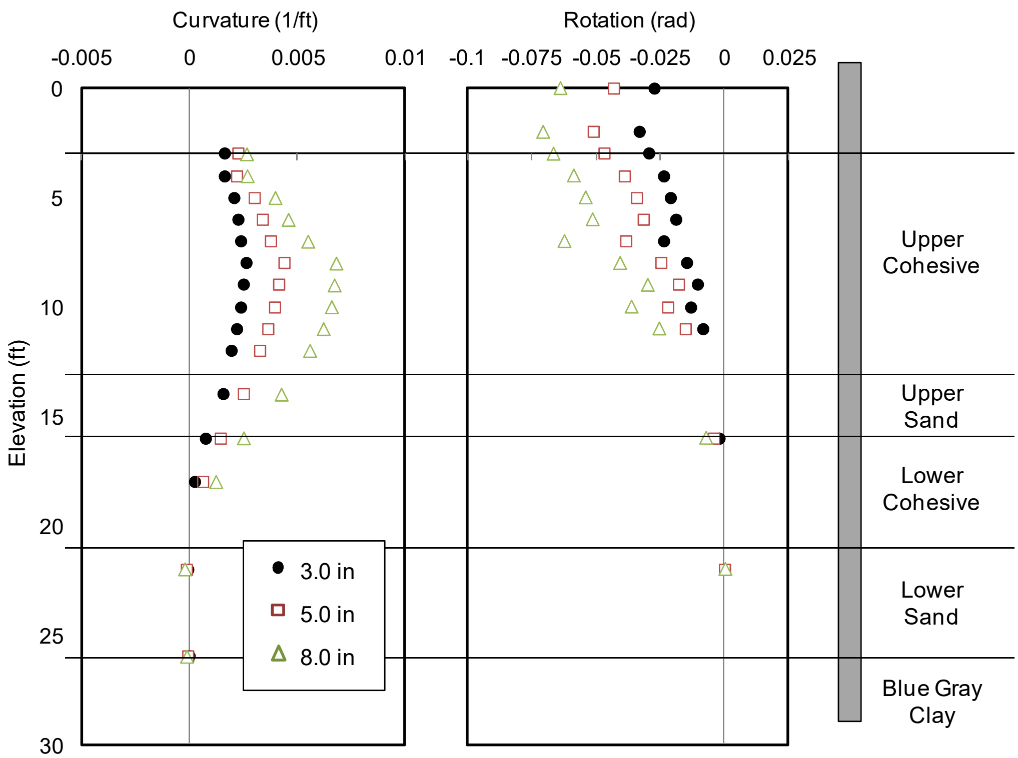

Figure 6-13. Test Results of 0D Pile (I-7) for Pile Head Displacement of 3.0, 5.0 and 8.0 in

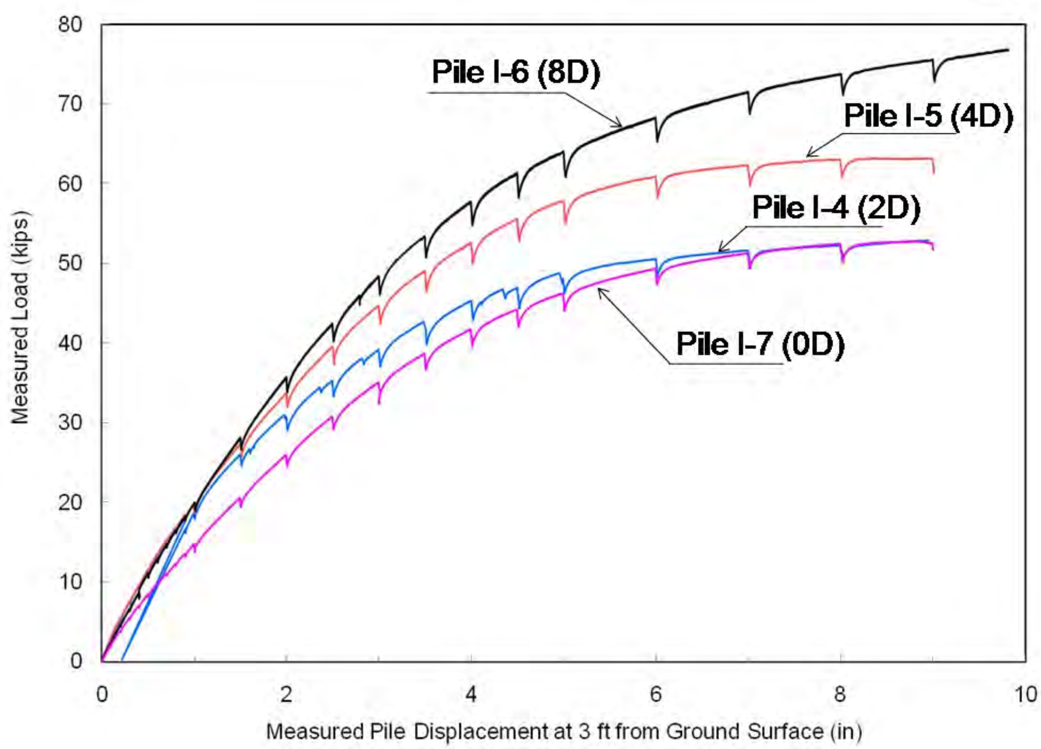

Figure 6-14. A Comparison of Load-Displacement Curves for 2D, 4D, 8D and 0D Pile

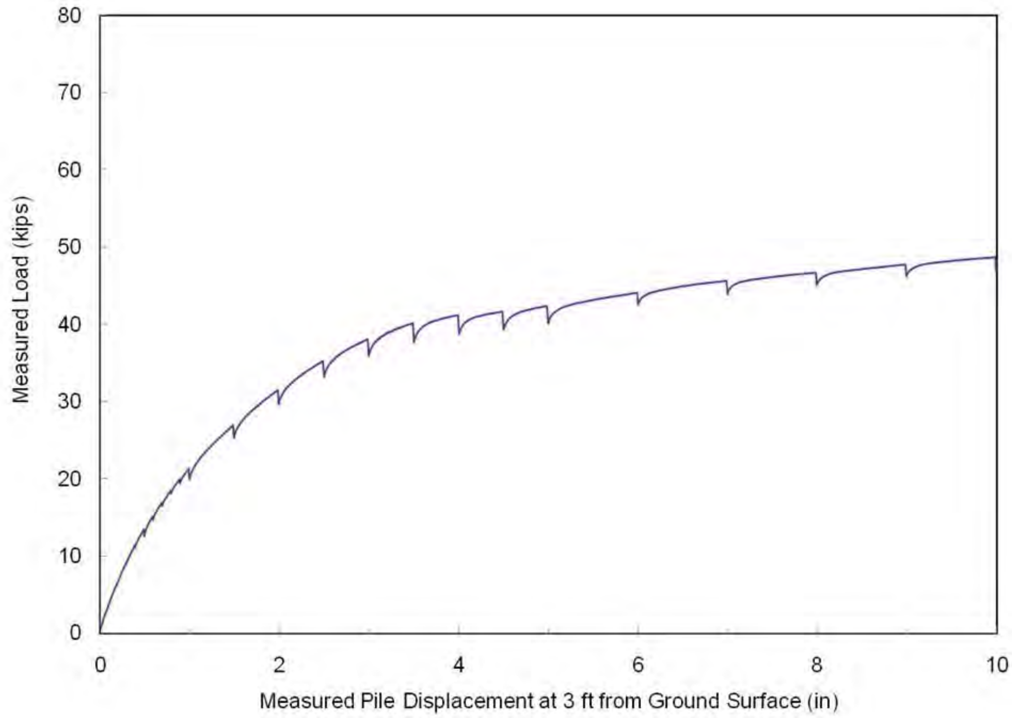

Figure 6-15. Load-Displacement Curve for -4D Pile (I-8)

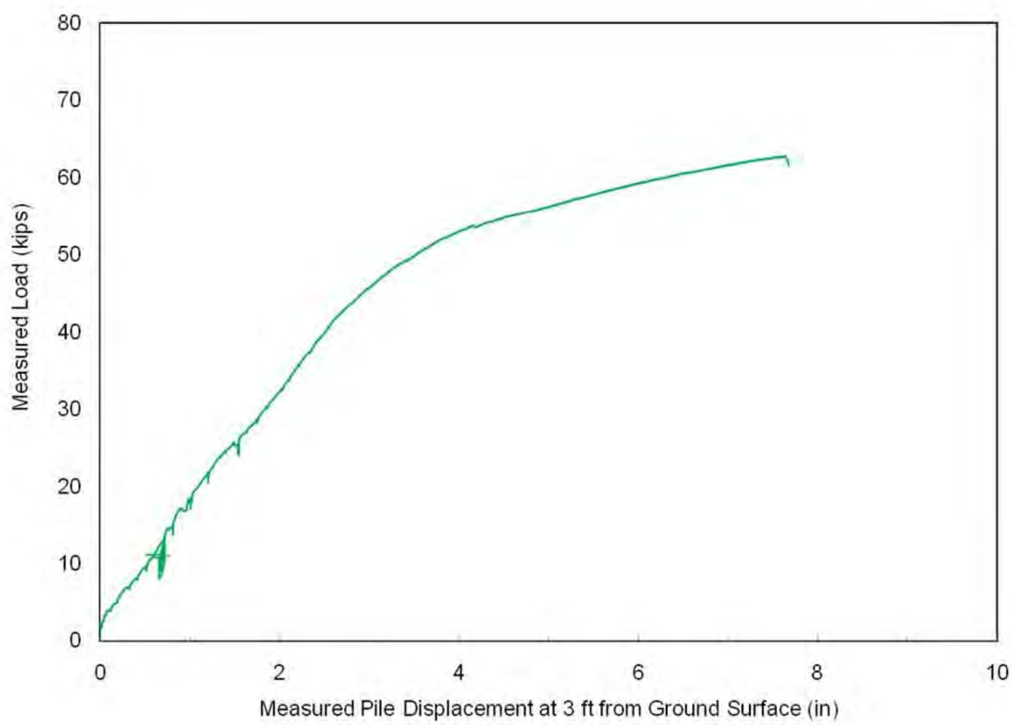

Figure 6-16. Load-Displacement Curve for Battered Pile (I-3)

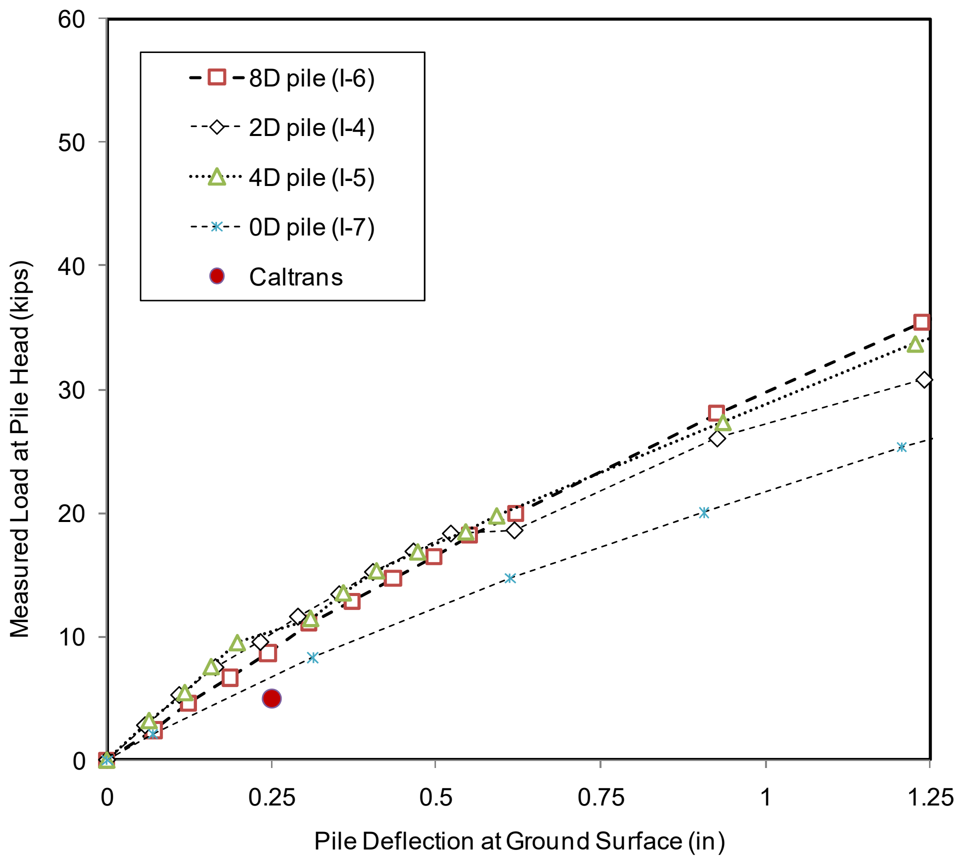

Figure 6-17. Comparison of Caltrans Method and Measured Results for 0D Pile, 2D Pile, 4D Pile and 8D Pile

7. LATERAL LOAD ANALYSES FOR SERIES-I (COHESIVE)

In this chapter, the evaluation of slope effect on lateral capacity of piles using the results from full-scale experiments is presented. The effect of distance from slope crest on the soil reaction, *p*, was evaluated using the back-calculated *p-y* curves based on the results from lateral load testing. Furthermore, based on the back-calculated *p-y* curves, design recommendation to account for slope effect for cohesive soil was proposed and validated with the results from full-scale test loading.

7.1 SLOPE EFFECT ON P-Y CURVES

In this section, full-scale test results were utilized in the back-computation of the *p-y* curves. This concept was first developed by McClelland and Focht (1958). A comparison of back-calculated *p-y* curves at different depth show the effect of slope on *p-y* curves. Lateral load analyses were conducted using the computer program *LPILE Plus version 5.0* (Reese et al., 2000), distributed by ENSOFT, Inc. An idealized soil profile for analysis is shown in **Figure 7-1**.

7.1.1 METHOD FOR BACK-CALCULATING P-Y CURVES

The lateral soil resistances per unit pile length developed along the test piles, p, as well as associated soil-pile displacement, y, were back-calculated using the basic beam theory. The strain gauge data, along with tiltmeter, load cell and string potentiometer data, were utilized extensively in the back-computation of the *p-y* curves. The methodology used to calculate *p-y* curves is described as the following:

To determine the lateral soil resistance as well as associated soil displacements, the curvature of the pile, ϕ, at each depth was determined using the strain gauge data. The neutral axis of the pile was assumed to remain at the center throughout the test. In this study, four strain gauges were installed at each depth. Assuming a linear distribution of strain along the pile cross section, the curvature of the pile can be determined.

The 6th order polynomial function was chosen to fit the discrete curvature obtained in the series of experiments. Then the rotation of the pile, θ, was computed by an integration of the curvature polynomial function along the pile length using the following equation:

$$\theta = \int \phi(z)dz$$

where: θ is the pile rotation, $\phi(z)$ is the polynomial curvature function, and z is depth.

The computed rotation along the pile was compared to the measured rotation from the tiltmeters to confirm that the fitted polynomial function was reasonable. Subsequently, the soil displacements, y, were determined by integrating the polynomial function of the pile rotation along the pile length using the following expression:

$$y = \int \theta(z)dz$$

where: y is the pile displacement, $\theta(z)$ is the polynomial rotation function, and z is depth.

In order to determine the soil resistance along the pile, the moment of the pile was computed using the following expression:

$$M = EI * \phi$$

where: M is the moment, EI is the flexural rigidity or flexural stiffness of the pile, and ϕ is the pile curvature.

Based on the results of the pile calibration test and results from UCFyber/XTRACT, a finite element program for section analysis, the measured EI of the test pile in the elastic range compared well with the theoretical results. A simplified moment-curvature relationship for the entire curve with post-yielding stiffness of approximately 5% of the elastic flexural stiffness was chosen for subsequent analysis. It is noted that once the pile yielded, the computed moment are less reliable resulting in poor estimation of the lateral soil resistance which will be discussed in the subsequent section.

The 6th order polynomial function was chosen to fit the discrete moment data along the length of the pile. The shear forces along the length of the pile were calculated by differentiating the moment data with respect to depth using the following relationship:

$$S = \frac{dM(z)}{dz}$$

where: S is shear force, M is moment, and z is depth.

At this step, the calculated shear force at ground surface was compared with the measured shear force from the load cells in the actuator. This step was to confirm that the polynomial function chosen to fit the moment data was reasonable. Then the lateral soil resistance was determined by the following equation:

$$p = \frac{dS(z)}{dz}$$

where: p is soil resistance per unit pile length, z is depth and S is shear force. With the lateral soil resistance and associated soil-pile displacement computed from the above equations, the *p-y* curves at each depth can be obtained.

The results of the double differentiation of the moment along the pile depend on the estimation of moment profile along the pile (Yang and Liang, 2007). Since this process can lead to a significant error in estimating the soil resistance, a verification of the *p-y* curves was required at the end of the process as will be discussed in the next section.

7.1.2 BACK-CALCULATED P-Y CURVES FOR 8D PILE (I-6)

The back-calculated *p-y* curves of 8D pile at various depths based on the methodology mentioned in the previous section are presented in **Figure 7-2**. It can be observed that the soil resistance increases with depth. Furthermore, the soil resistance at the ground surface is not zero which is consistent for *p-y* curves in cohesive soil (e.g., stiff clay *p-y* curve, Reese and Welch, 1975).

The back-calculated *p-y* curves were used as input in a numerical model (i.e., *LPILE*) shown in **Figure 7-1** to simulate the lateral responses of the piles and then to compare with the experimental results. The upper cohesive layers were modeled with back-calculated p-y curves. The sand layers were modeled with sand *p-y* curves (Reese *et al*., 1974). The lower cohesive and blue-gray clay layers were modeled with stiff-clay-above-water *p-y* curves (Reese and Welch, 1975). Good agreement of the measured and computed load-displacement curve was observed for a pile head deflection of less than 4 inch as shown in **Figure 7-3**, indicating that the back-calculated *p-y* curves for 8D pile was reasonable. **Figure 7-4** and **Figure 7-5** also show good agreement of the measured and computed bending moment, deflection and rotation at different pile head displacement for 8D pile. It is noted that due to error in estimating the soil resistance from the double differentiation of the moment along the pile, the *p-y* curves computed from pile head deflection larger than 4 in. will be neglected in subsequent analysis.

7.1.3 BACK-CALCULATED P-Y CURVES FOR 2D PILE (I-4)

Figure 7-6 shows the back-calculated *p-y* curves of 2D pile at various depths. It can be observed that the soil resistance increases with depth. After the *p-y* curves were back-calculated, the analysis was performed to verify that the back-calculated *p-y* curves provide a reasonable estimate of the pile responses. **Figure 7-7** through **Figure 7-8** show the pile responses from the analysis using back-calculated *p-y* curves compared with measured test results.

7.1.4 BACK-CALCULATED P-Y CURVES FOR 4D PILE (I-5)

The back-calculated *p-y* curves of 4D pile are shown in **Figure 7-10**. Similar characteristics of the *p-y* curves as observed in 8D pile were observed in the 4D pile. **Figure 7-11** through **Figure 7-13** show the results from the analysis using back-calculated *p-y* curves compared to the measured test results. Good agreement between measured and computed responses is observed for a pile head deflection of less than 4 inch. The results indicated that the back-calculated *p-y* curves for 4D pile are reasonable up to pile deflection of 4 inch.

7.1.5 BACK-CALCULATED P-Y CURVES 0D PILE (I-7)

The back-calculated *p-y* curves of 0D pile (I-7) are presented in **Figure 7-14**. **Figure 7-15** through **Figure 7-17** shows the results of the analysis using back-calculated *p-y* curves compared to the measured test results. Good agreement between measured and computed responses is observed for pile head deflections smaller than 4 inch. The results indicated that the back-calculated *p-y* curves for 0D pile are reasonable up to pile head deflection of 4 inch.

7.1.6 COMPARISON OF P-Y CURVES FOR PILE NEAR SLOPE TESTS

A comparison of the *p-y* curves from the results of full-scale lateral load tests on piles located at different distance (0D, 2D, 4D and 8D) from the slope crest provides insight into the effect of slope of the *p-y* curves. **Figure 7-18** presents a comparison of the *p-y* curves of pile near slope tests at different depth. The *p-y* curves for 8D pile are considered as backbone *p-y* curves. It is observed that the back-calculated *p-y* curves for 2D pile (I-4), 4D pile (I-5) and 8D pile (I-6) are generally similar at small soil displacement range, indicating that the presence of slope has insignificant effect on *p-y* curves. The *p-y* curves of 0D pile are different from 8D pile especially near the ground surface. The initial stiffness of the *p-y* curves of 0D pile is lower than all other piles because it is located on the slope crest. The *p-y* curves for all piles at a depth of 7 ft below the ground surface are similar indicating that within pile head displacement range of 4 inch the slope has negligible effect on the *p-y* curves at deeper depths.

7.2 DEVELOPMENT OF METHOD TO ACCOUNT FOR SLOPE EFFECT

In this section, the ratio of soil resistance, commonly known as *p*-multipliers, was calculated by comparing the soil resistance at each soil displacement for each pile tests (0D pile, 2D pile and 4D pile) and depths with backbone *p-y* curves using the *p-y* curves in the previous section.

7.2.1 EXISTING METHOD FOR SLOPE EFFECT

Available recommendation to account for slope effect is to use a single *p*-multiplier to be applied to backbone *p-y* curves (e.g., Mezazigh and Levacher, 1998). The p-multiplier is a function of distance from the slope crest. The use of this single *p*-multiplier changes the initial stiffness of *p-y* curves, as shown in **Figure 7-19**, and does not fully describe the effect of slope on *p-y* curves. Based on the comparison of *p-y* curves, the initial portion of *p-y* curves for 2D, 4D and backbone indicate that p-multiplier is 1.0 for small soil displacement range. Beyond a certain soil displacement, the effect of slope gradually becomes more significant as soil displacement increases. The effect of slope appears to reach a certain factor at larger soil displacement. Therefore, p-multiplier that varies with soil displacement is more appropriate as illustrated in **Figure 7-19**.

7.2.2 P-MULTIPLIER FOR SLOPE EFFECT FROM THIS STUDY

The *p*-multiplier for each soil displacement for 4D pile were computed by normalizing the back-calculated *p-y* curves for 4D pile with the backbone *p-y* curves for each depth. **Figure 7-20** presents the resulting *p*-multiplier for 4D pile. P-multiplier appears to be a function of soil displacement. There appears to be some depth dependency but no obvious trend was found. Recall that the initial stiffness of backbone *p-y* curves is almost identical to *p-y* curves for 4D pile. As expected, the resulting *p*-multiplier is 1.0 up until soil displacement of 0.4 to 1.1 inch. Beyond these soil displacement, p-multiplier decreases as soil displacement increases. To simplify, a p-multiplier that is a function of soil displacement and independent of depth is derived using a trial and error method. Recommendation of *p*-multiplier for 4D pile is presented in **Figure 7-20**.

Similar to 4D pile, the *p*-multiplier for each soil displacement for 2D pile were computed by normalizing the back-calculated *p-y* curves for 4D pile with the backbone *p-y* curves. **Figure 7-21** presents the resulting *p*-multiplier for 2D pile. P-multiplier for 2D also appears to be a function of soil displacement. The resulting *p*-multiplier did not show an obvious dependency on depth. The resulting *p*-multiplier is 1 up until soil displacement of approximately 0.3 to 0.5 inch because the initial stiffness of backbone p-y curves and *p-y* curves for 2D pile are almost identical. Beyond these displacement, *p*-multiplier decreases as soil displacement increases. Similar to 4D pile, a simplified *p*-multiplier for 2D pile that is a function of soil displacement and independent of depth was derived. A recommendation of *p*-multiplier for 2D pile is presented in **Figure 7-21**.

Similar to 4D and 2D pile, the *p*-multiplier for each soil displacement for 0D pile were computed by normalizing the back-calculated *p-y* curves for 0D pile with the backbone *p-y* curves. **Figure 7-22** presents the resulting *p*-multiplier for each soil displacement for 0D pile. P-multiplier appears to be a function of soil displacement with some degree of depth dependency. As mentioned earlier that the characteristics of *p-y* curves for 0D pile is different from all other piles, especially the initial slope of the *p-y* curves. The resulting *p*-multiplier is less than 1, even at small displacement range, indicating that the presence of slope affected the initial stiffness of *p-y* curves. In theory, *p*-multiplier should be 1 for soil displacements very close to zero but this was not observed from the test results. Using trial and error method, a simplified *p*-multiplier that is a function of soil displacement and independent of depth was derived. Recommendations of *p*-multipliers for the 0D pile are presented in **Figure 7-22**.

The proposed recommendation were verified by implementing them to the back-bone *p-y* curves to predict the test results for all tested piles with different distance from slope crest. **Figure 7-24** through **Figure 7-29** show that the recommendation can well predict the response of piles under lateral loading for all tested piles at different distances from the slope crest. A comparison of recommendation is presented in **Figure 7-23**. Based on the comparison, for a small displacement, such as ¼ inch, slope effect on lateral capacity is insignificant for piles located at 2D or greater from the slope crest. For pile located on the slope crest, the effect of slope is significant for all ranges of soil displacements.

7.3 SUMMARY OF RECOMMENDATIONS

A comparison of the recommendation is presented in **Figure 7-23**. Based on the comparison, for a small displacement, such as ¼ inch, slope effect on lateral capacity is insignificant for piles located at 2D or greater from the slope crest. For pile located on the slope crest, the effect of slope is significant for all ranges of soil displacements. Generalized design recommendations to account for soil slope (*p*-multipliers) in cohesive soils are presented in Section 11.2.1.

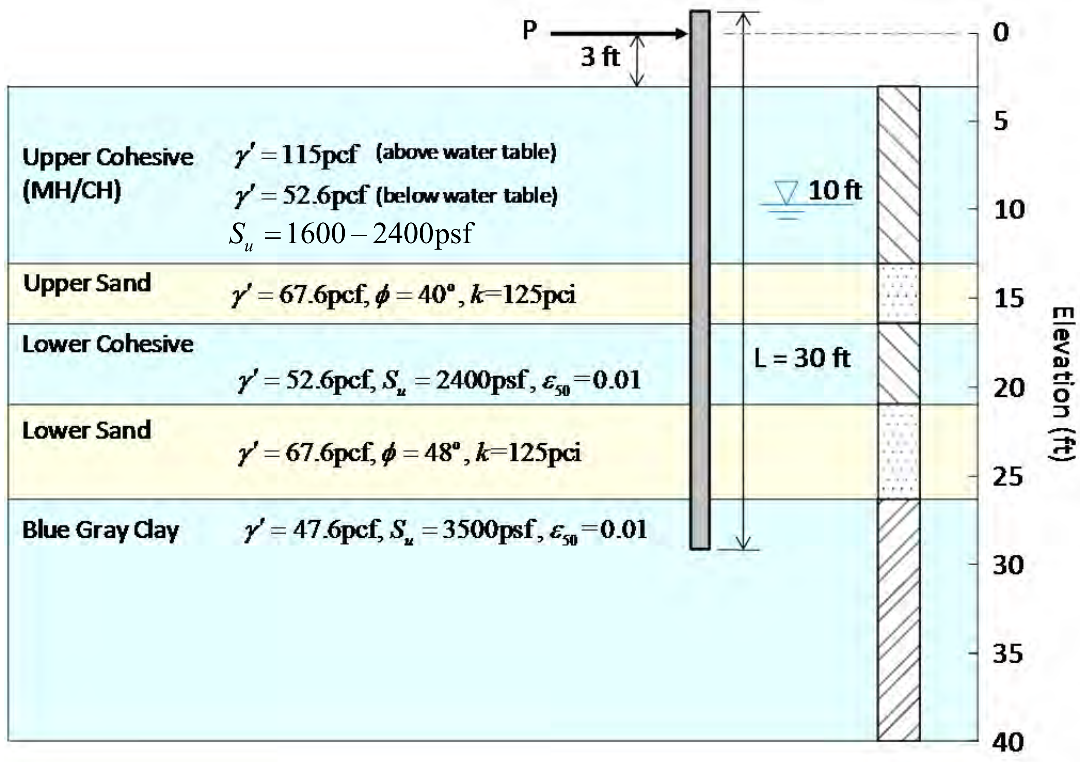

Figure 7-1. Idealized Soil Profile for Lateral Load Analyses

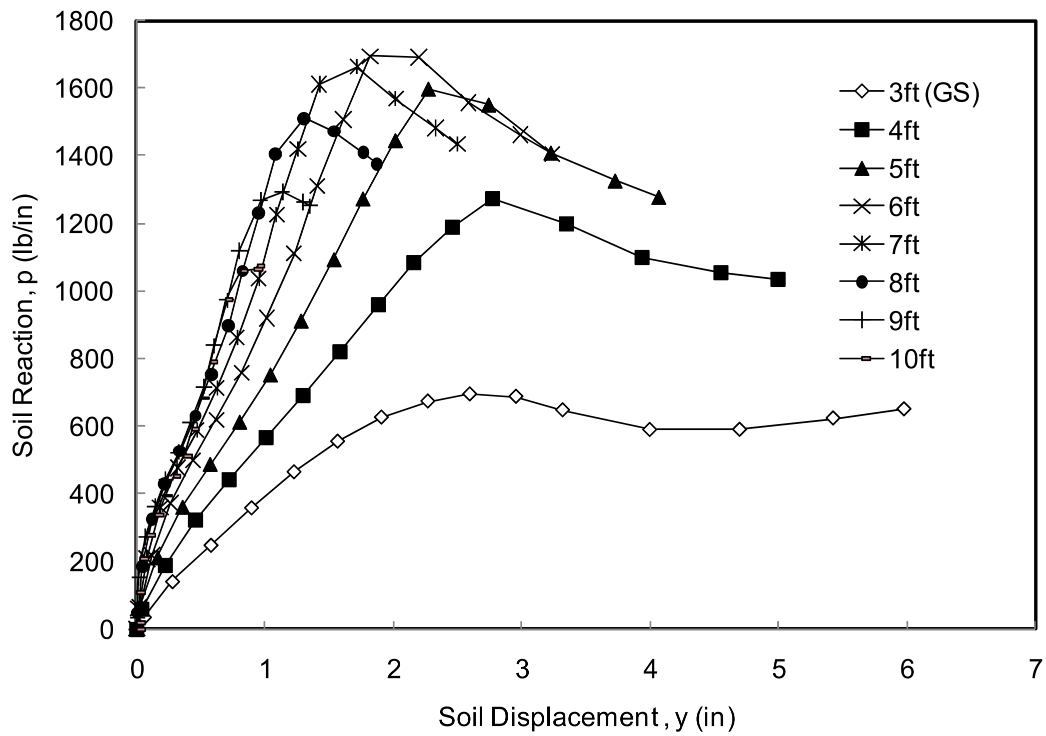

Figure 7-2. Back-Calculated *p-y* Curves for 8D Pile (I-6) (8D from crest)

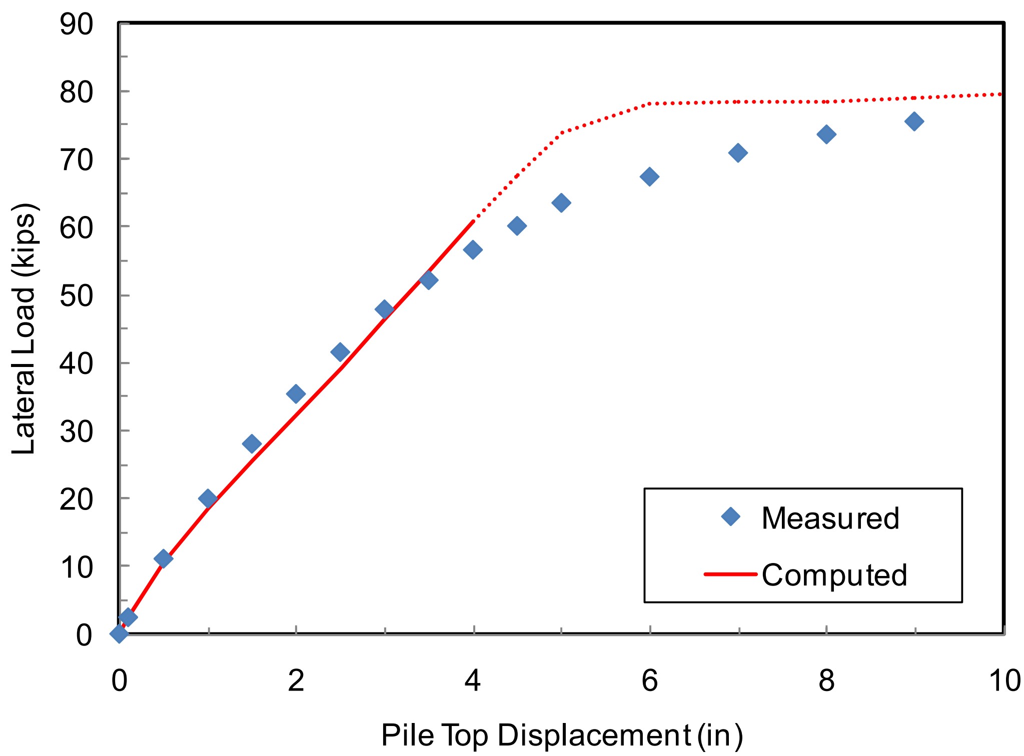

Figure 7-3. Comparison of Load-Displacement Curves from Test Results and Analysis Using Back-Calculated *p-y* Curves for 8D Pile (I-6)

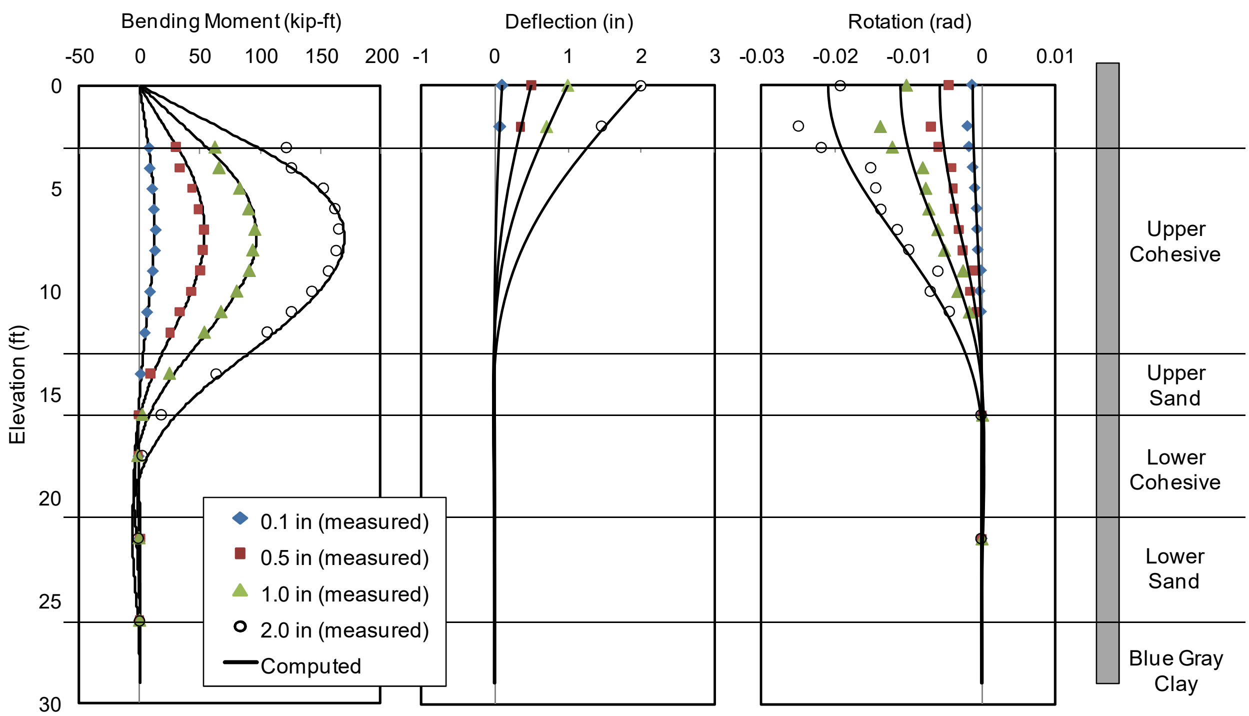

Figure 7-4. Comparison of Test Results and Analysis Using Back-Calculated *p-y* Curves for 8D Pile (I-6) for Pile Head Displacement of 0.1, 0.5, 1.0 and 2.0 in.

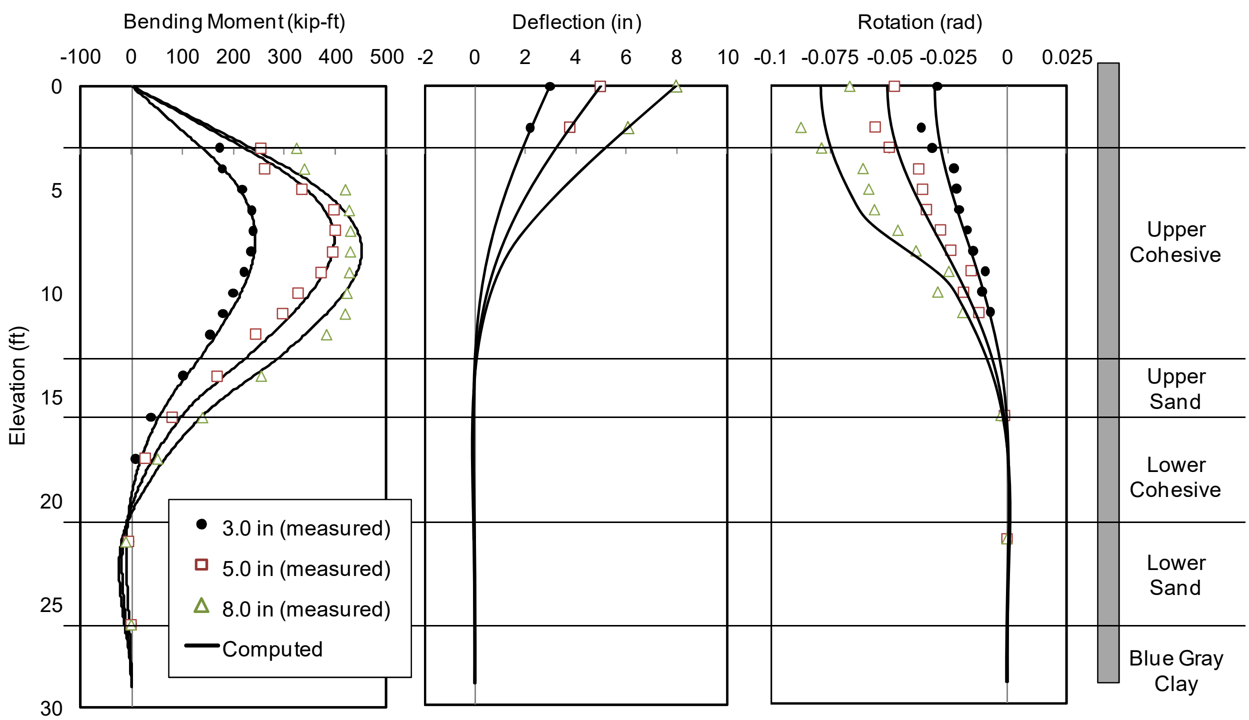

Figure 7-5. Comparison of Test Results and Analysis Using Back-Calculated *p-y* Curves for 8D Pile (I-6) for Pile Head Displacement of 3.0, 5.0 and 8.0 in.

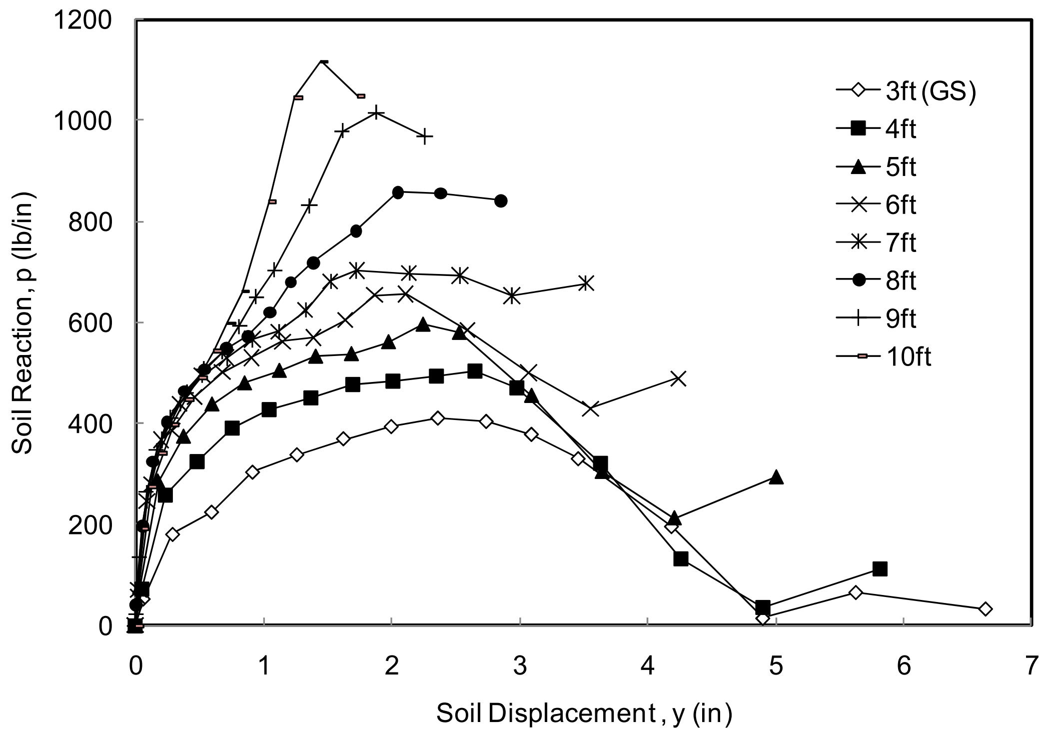

Figure 7-6. Back-Calculated *p-y* Curves for 2D Pile (I-4) (2D from crest)

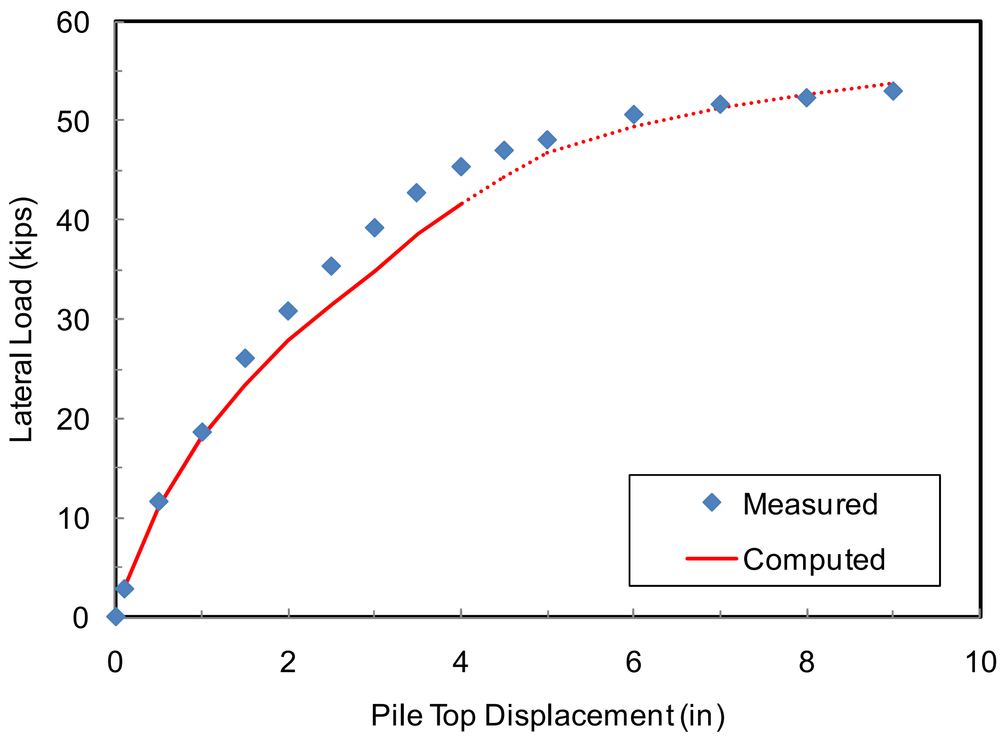

Figure 7-7. Comparison of Load-Displacement Curves from Test Results and Analysis Using Back-Calculated *p-y* Curves for 2D Pile (I-4)

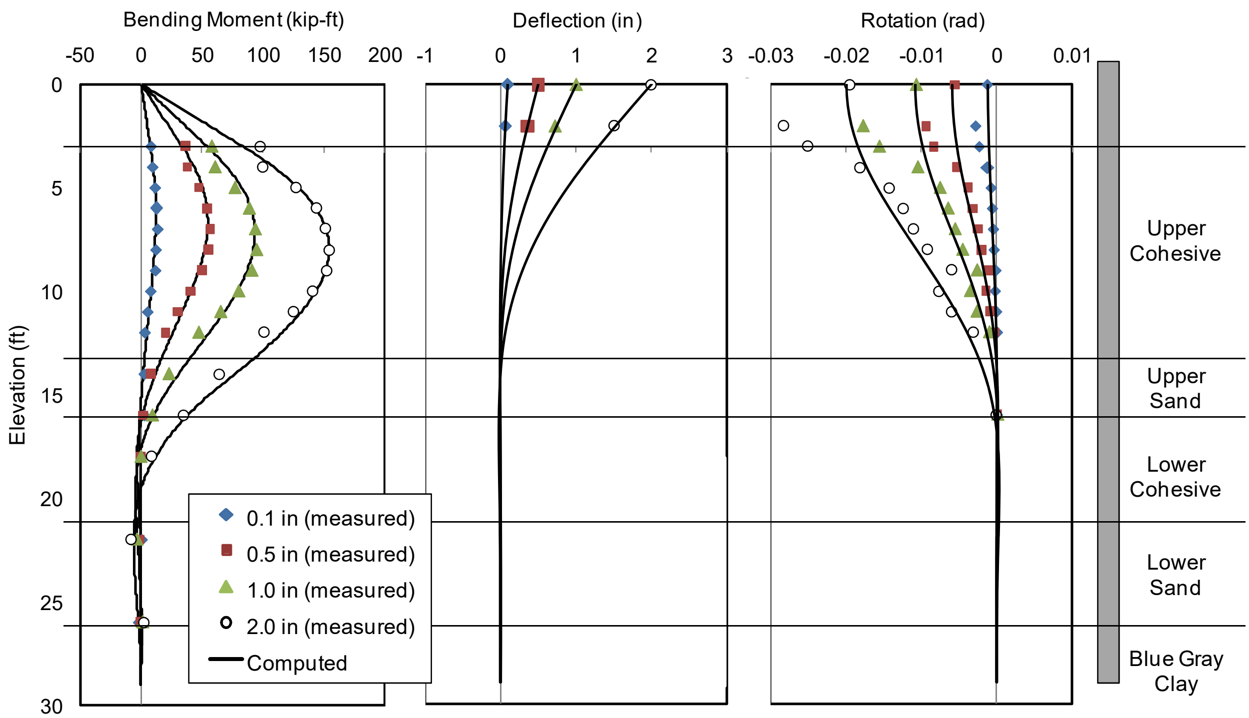

Figure 7-8. Comparison of Test Results and Analysis Using Back-Calculated *p-y* Curves for 2D Pile (I-4) for Pile Head Displacement of 0.1, 0.5, 1.0 and 2.0 in.

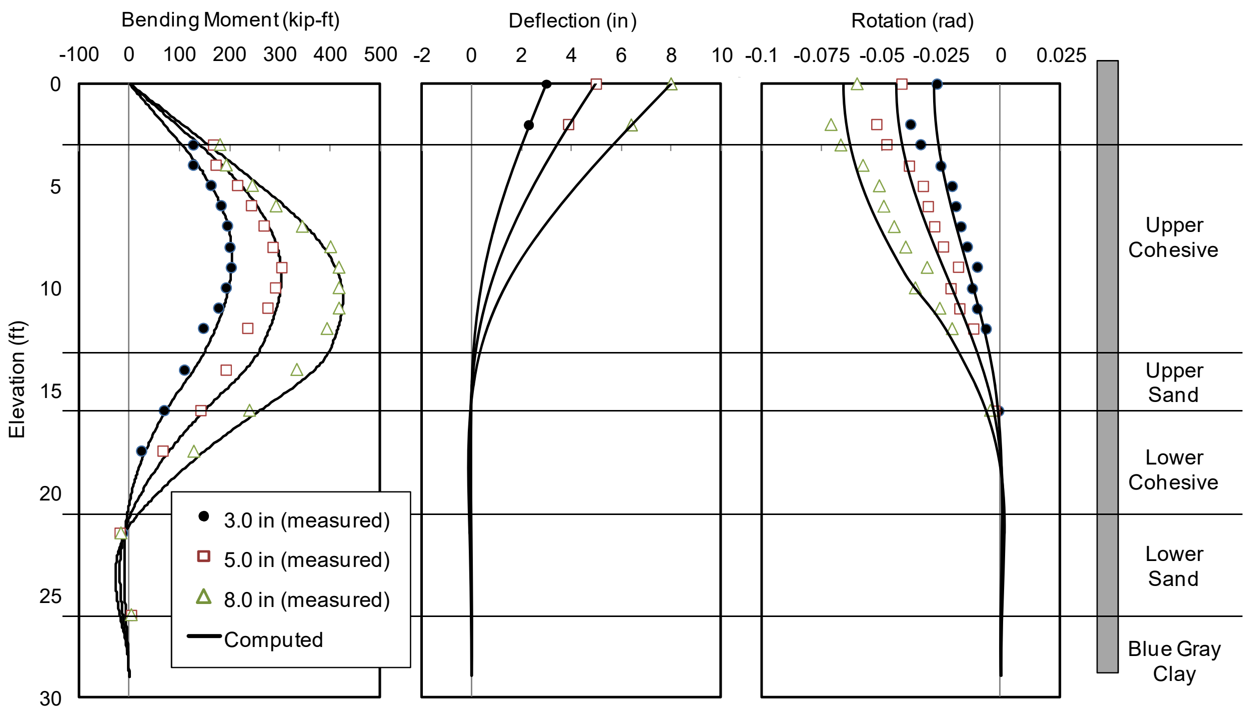

Figure 7-9. Comparison of Test Results and Analysis Using Back-Calculated *p-y* Curves for 2D Pile (I-4) for Pile Head Displacement of 3.0, 5.0 and 8.0 in.

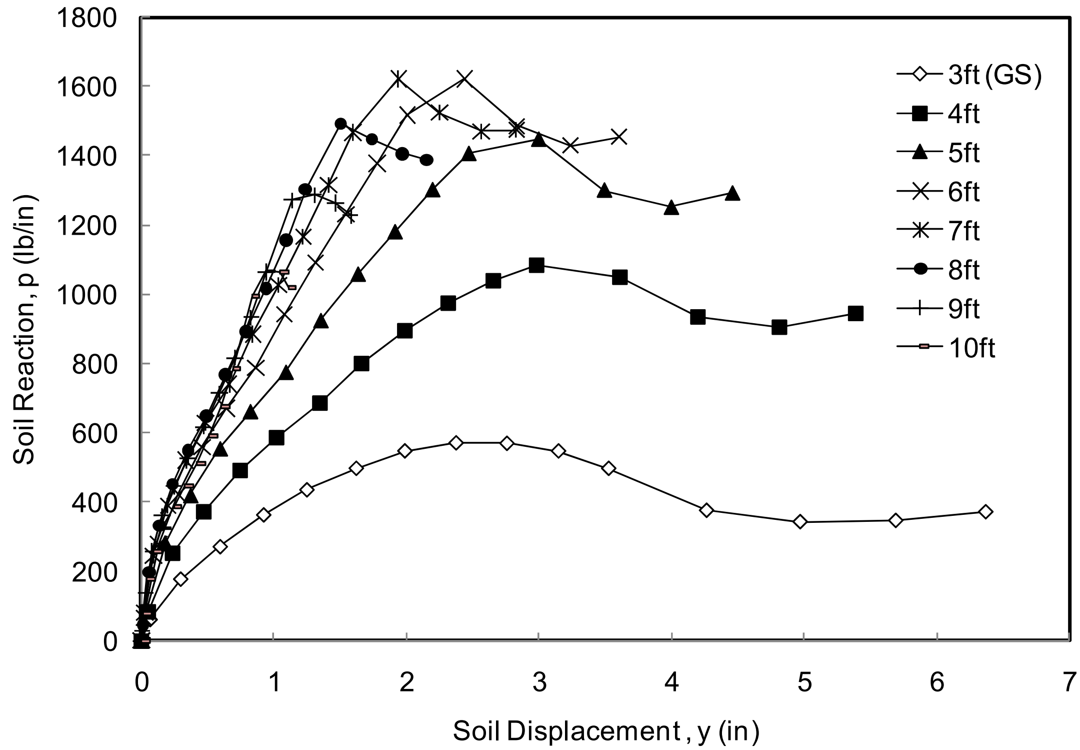

Figure 7-10. Back-Calculated *p-y* Curves for 4D Pile (I-5)

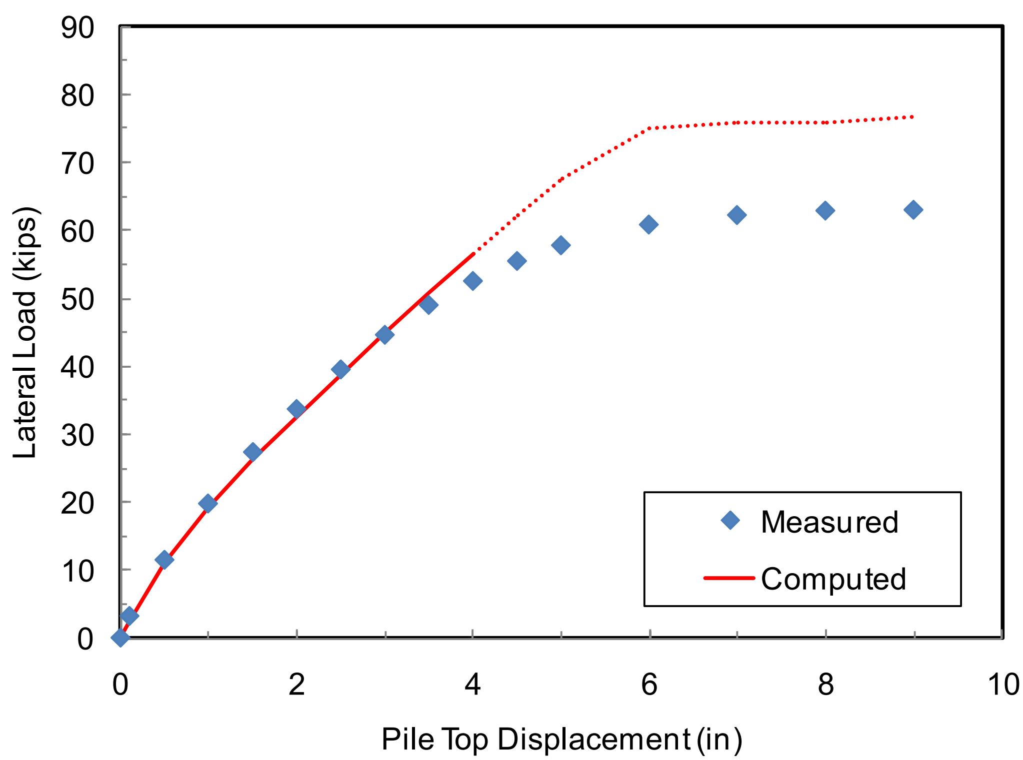

Figure 7-11. Comparison of Load-Displacement Curves from Test Results and Analysis Using Back-Calculated *p-y* Curves for 4D pile (I-5)

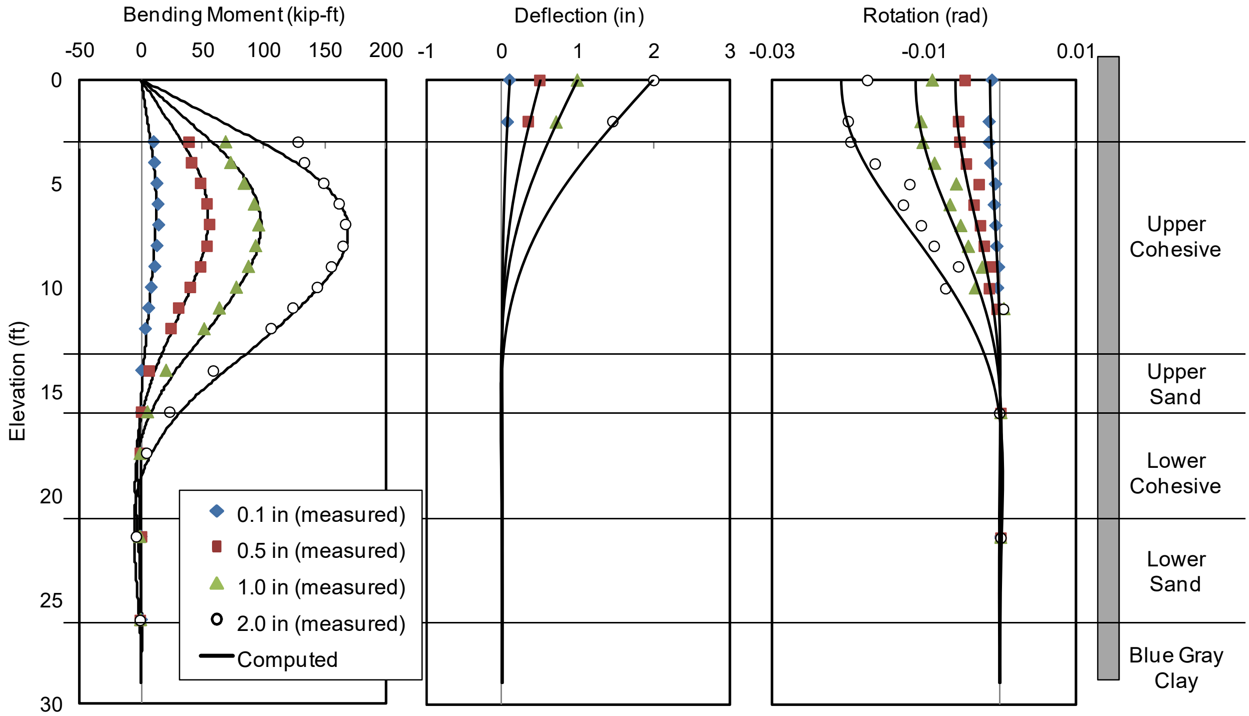

Figure 7-12. Comparison of Test Results and Analysis Using Back-Calculated *p-y* Curves for 4D Pile (I-5) for Pile Head Displacement of 0.1, 0.5, 1.0 and 2.0 in.

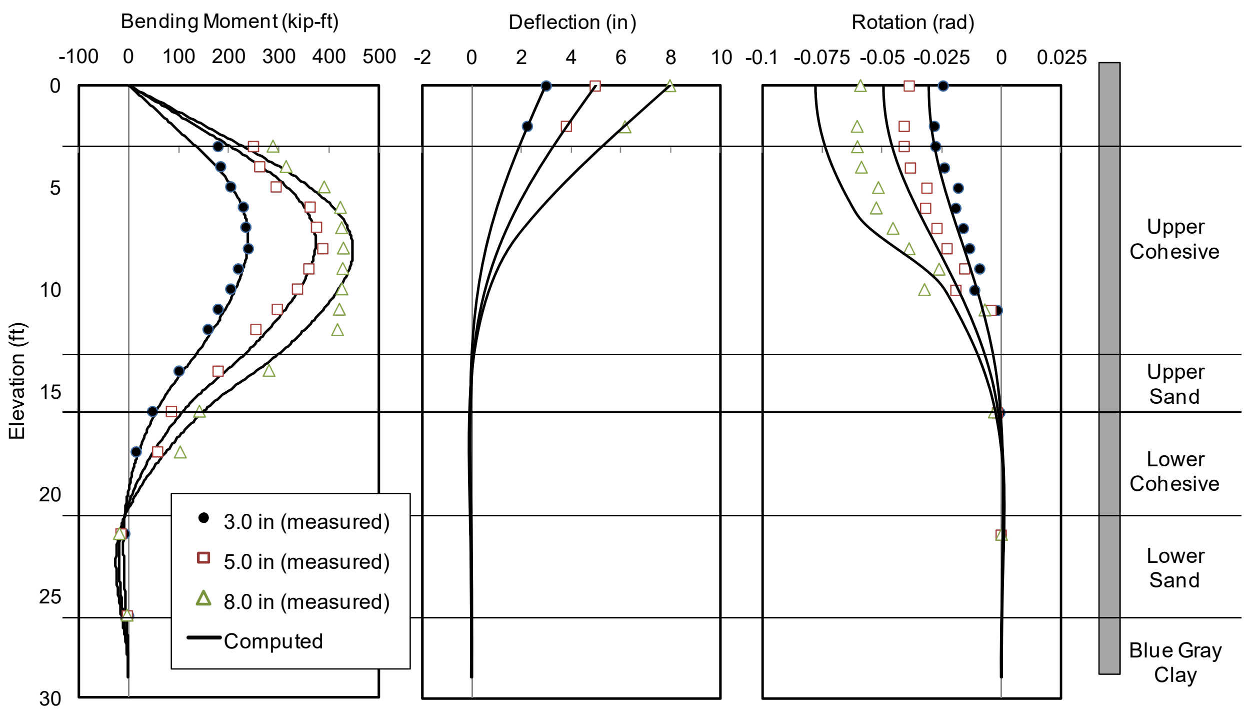

Figure 7-13. Comparison of Test Results and Analysis Using Back-Calculated *p-y* Curves for 4D Pile (I-5) for Pile Head Displacement of 3.0, 5.0 and 8.0 in.

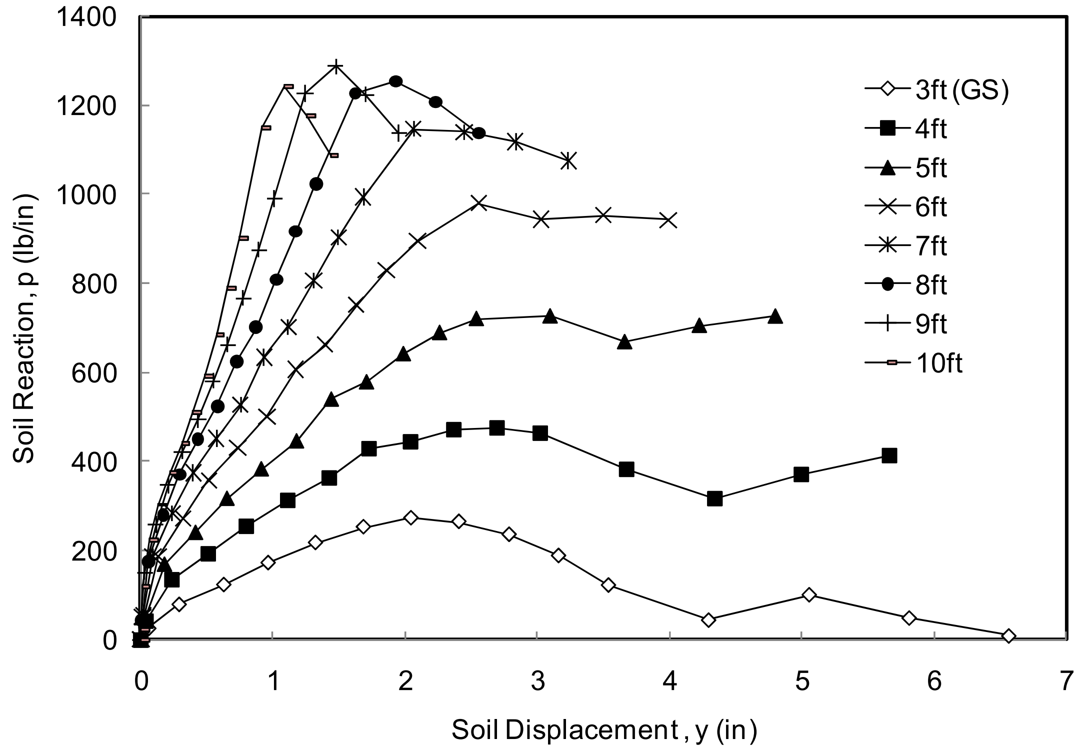

Figure 7-14. Back-Calculated *p-y* Curves for 0D Pile (on the crest)

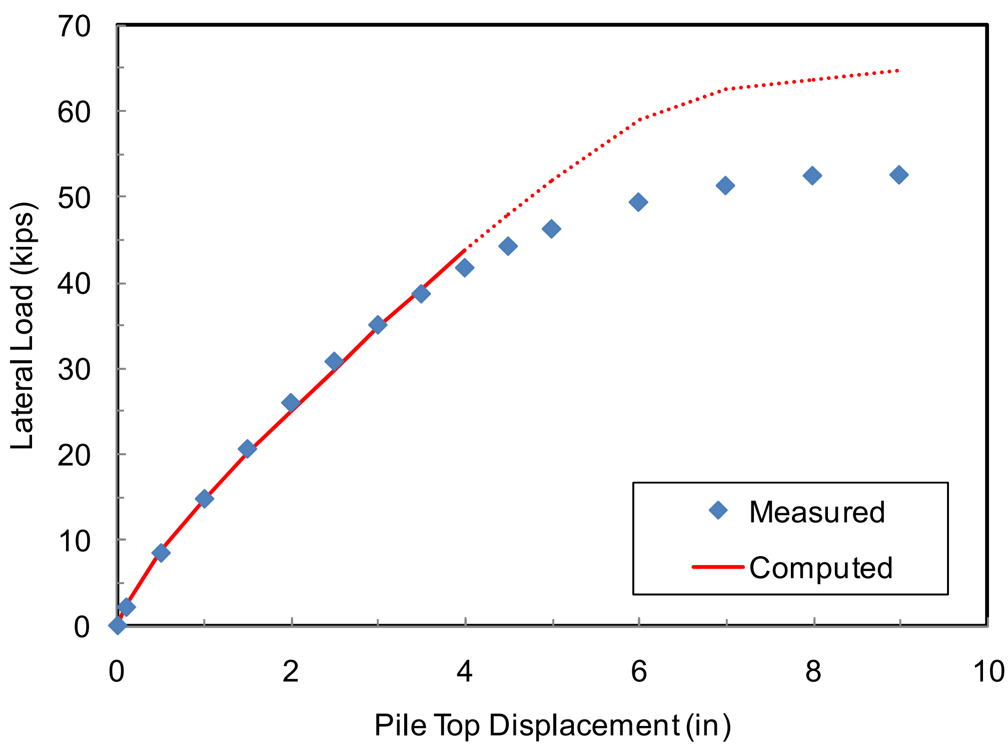

Figure 7-15. Comparison of Load-Displacement Curves from Test Results and Analysis Using Back-Calculated *p-y* Curves for 0D Pile (I-7)

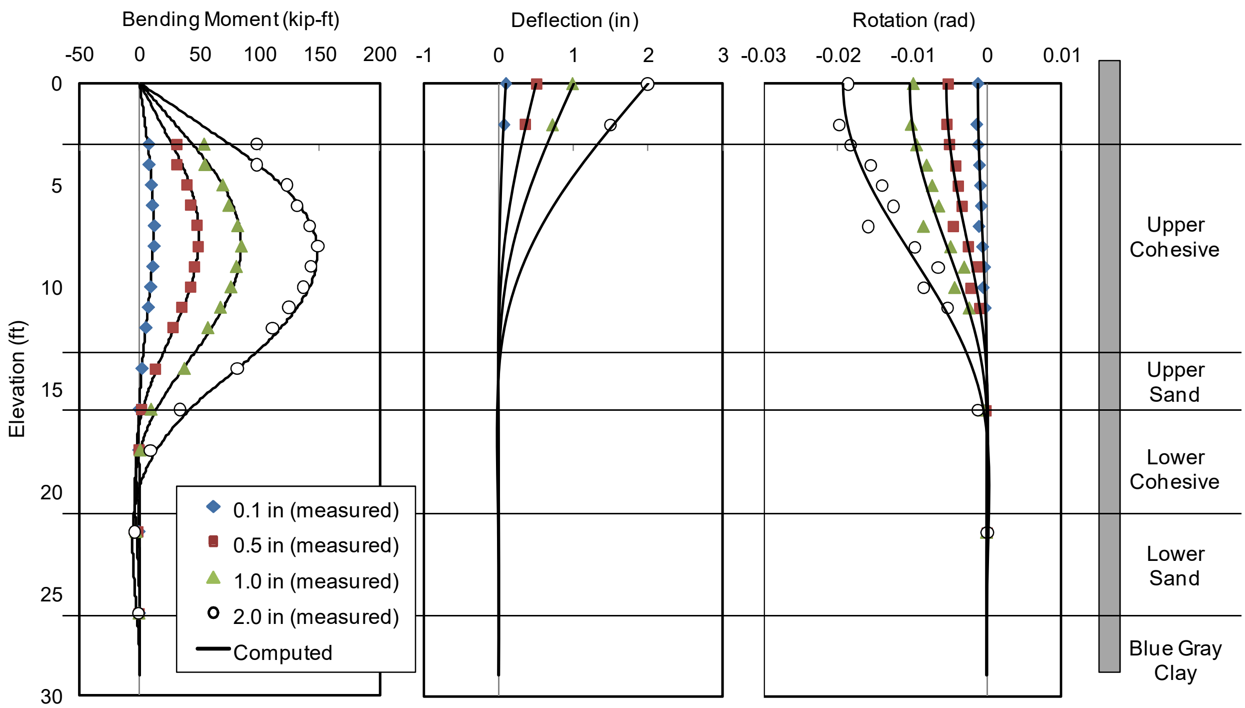

Figure 7-16. Comparison of Test Results and Analysis Using Back-Calculated *p-y* Curves for 0D Pile (I-7) for Pile Head Displacement of 0.1, 0.5, 1.0 and 2.0 in.

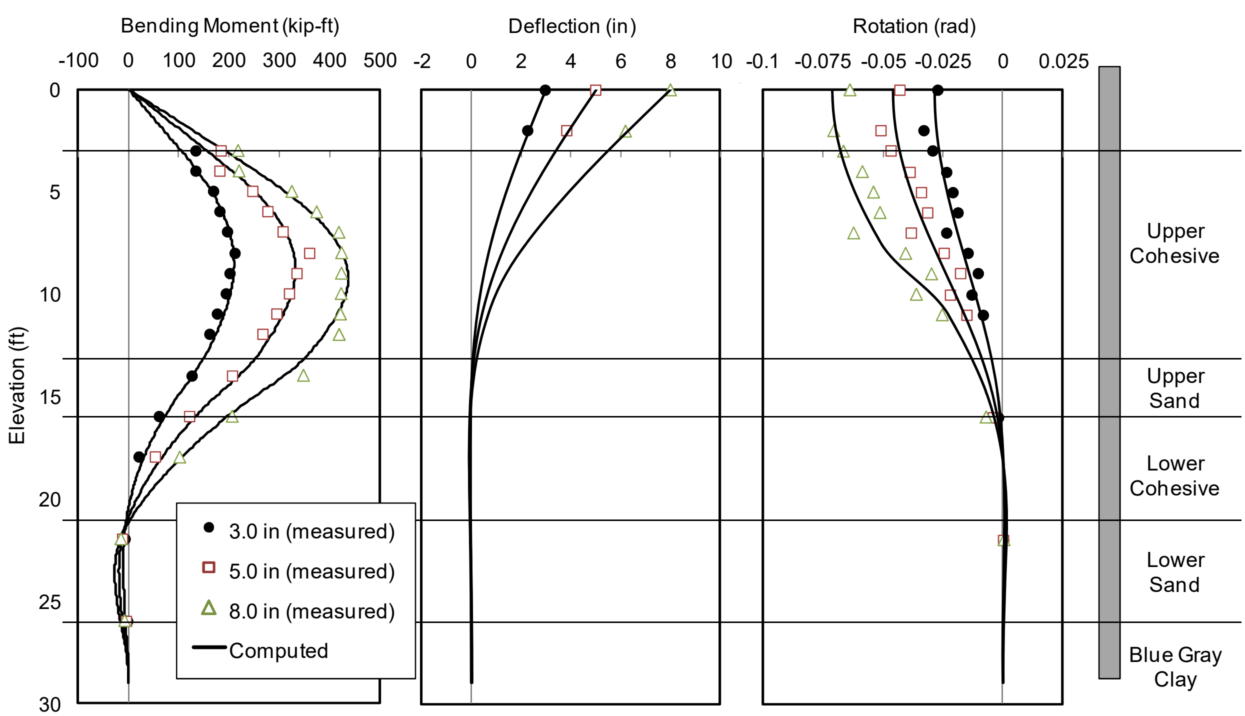

Figure 7-17. Comparison of Test Results and Analysis Using Back-Calculated *p-y* Curves for 0D Pile (I-7) for Pile Head Displacement of 3.0, 5.0 and 8.0 in.

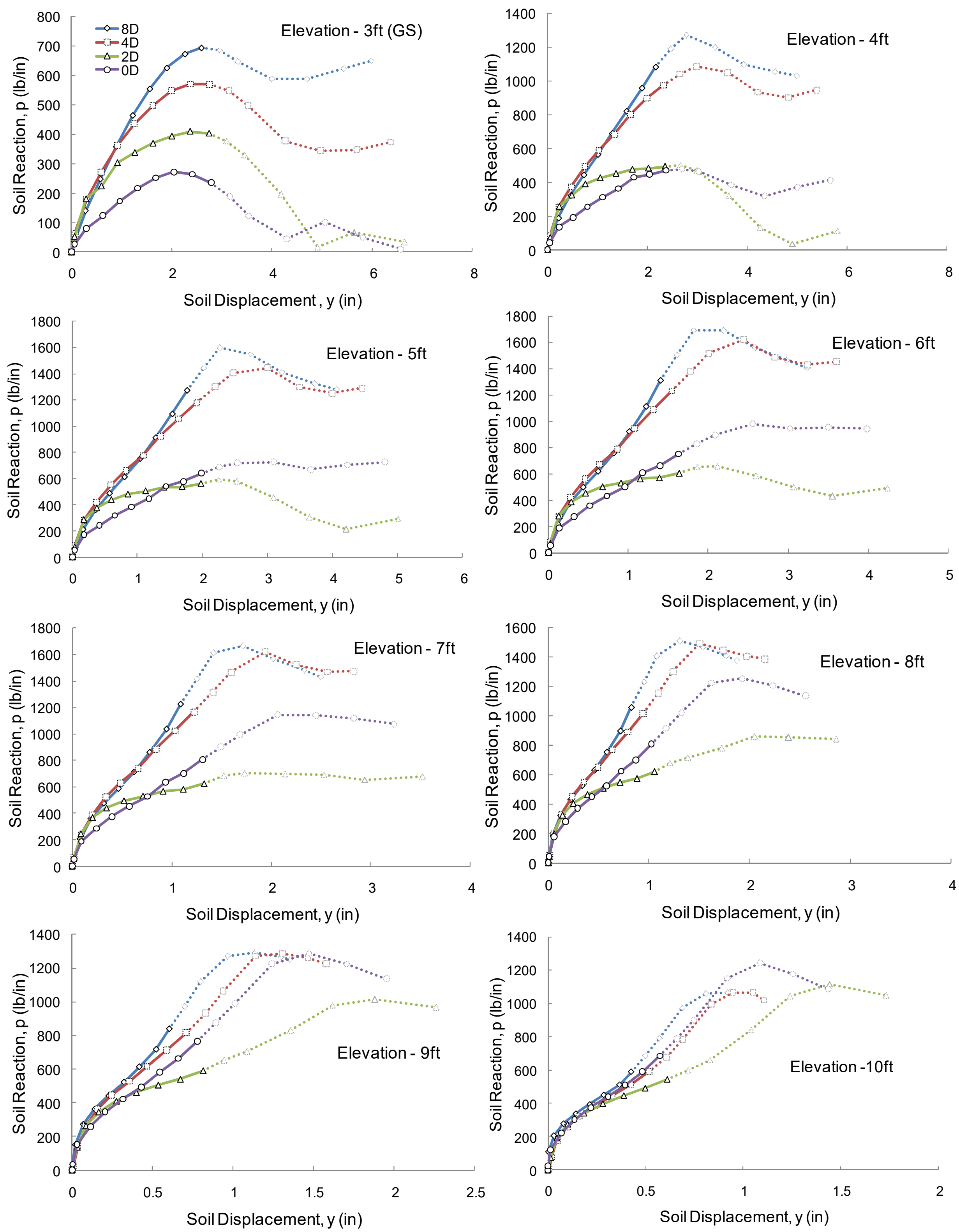

Figure 7-18. Comparison of *p-y* Curves for Piles at Different Distance from Slope Crest at Various Depths

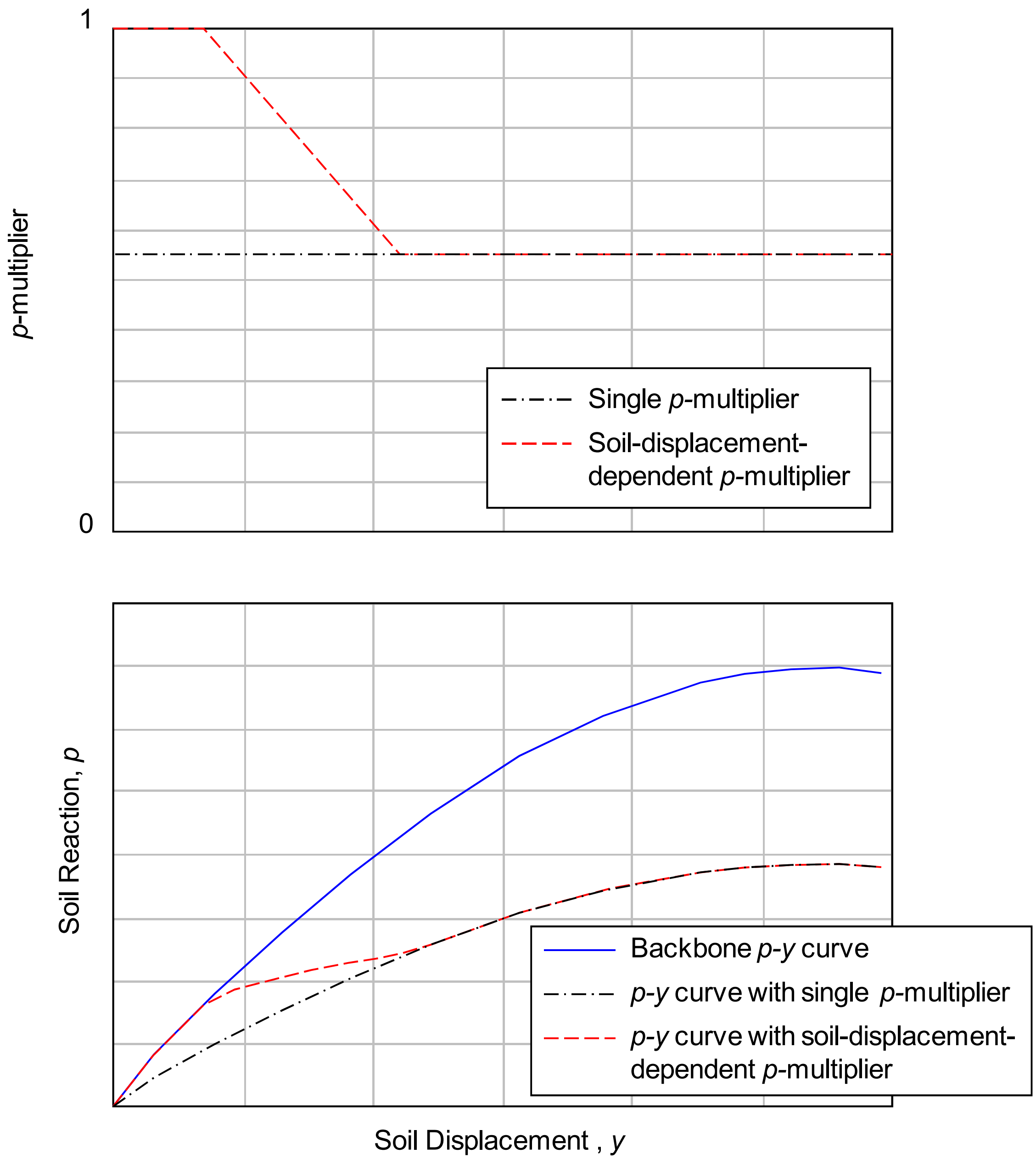

Figure 7-19. Concept of Single p-Multiplier and Soil Displacement Dependent p-Multiplier

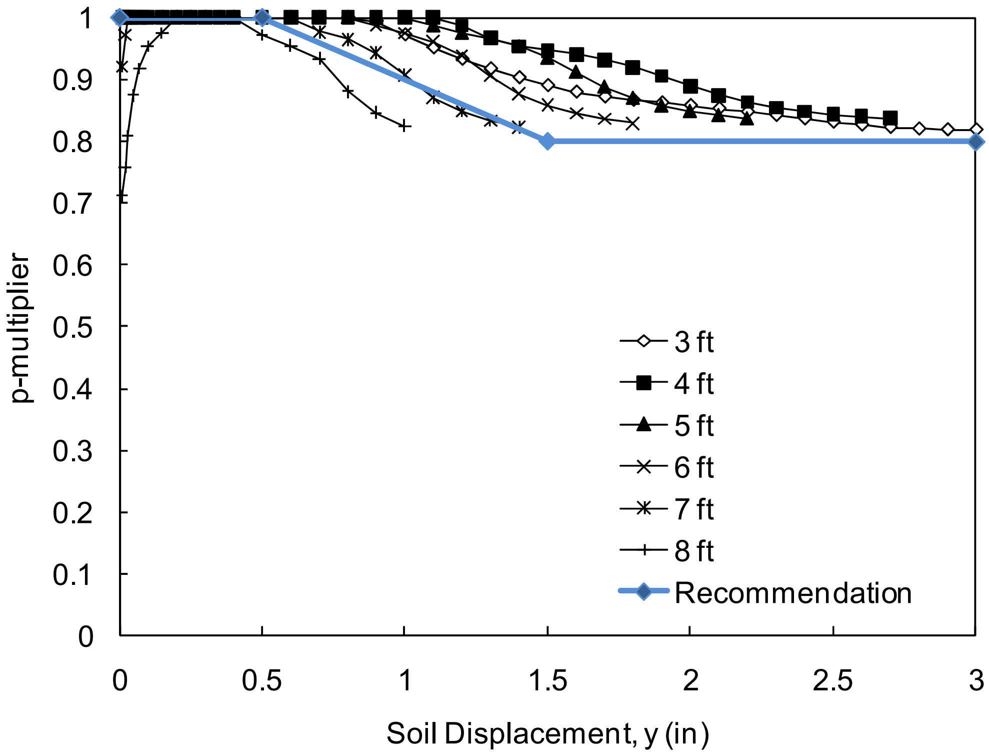

Figure 7-20. Direct Comparison of p-multiplier at Different Depths for 4D Pile (I-5)

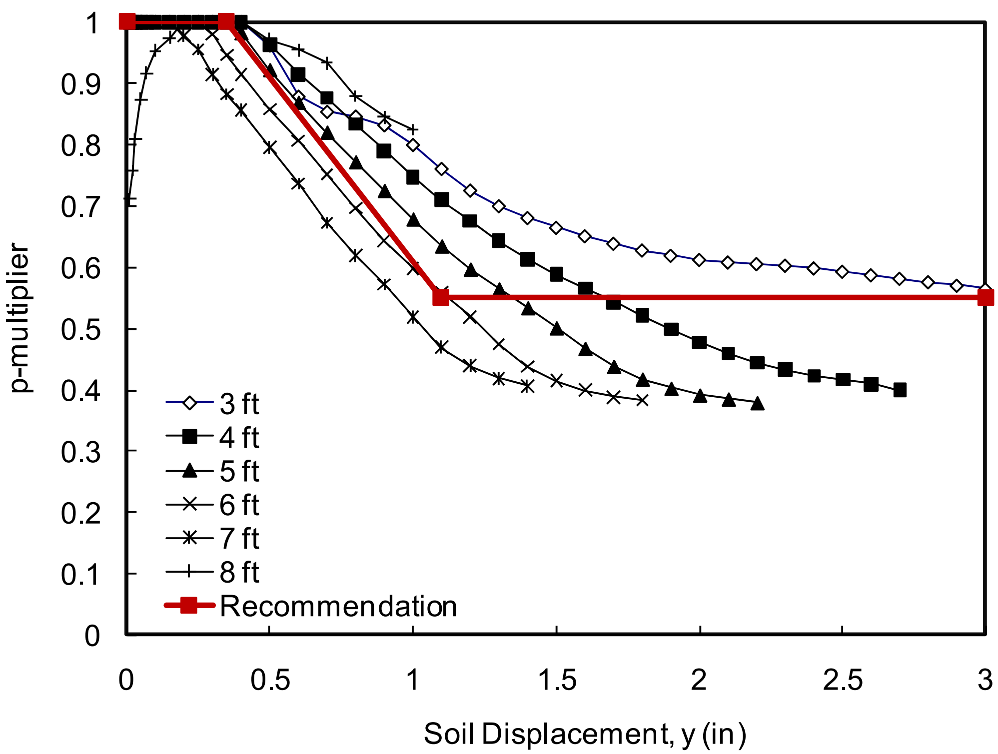

Figure 7-21. Direct Comparison of p-Multiplier at Different Depths for 2D Pile (I-4)

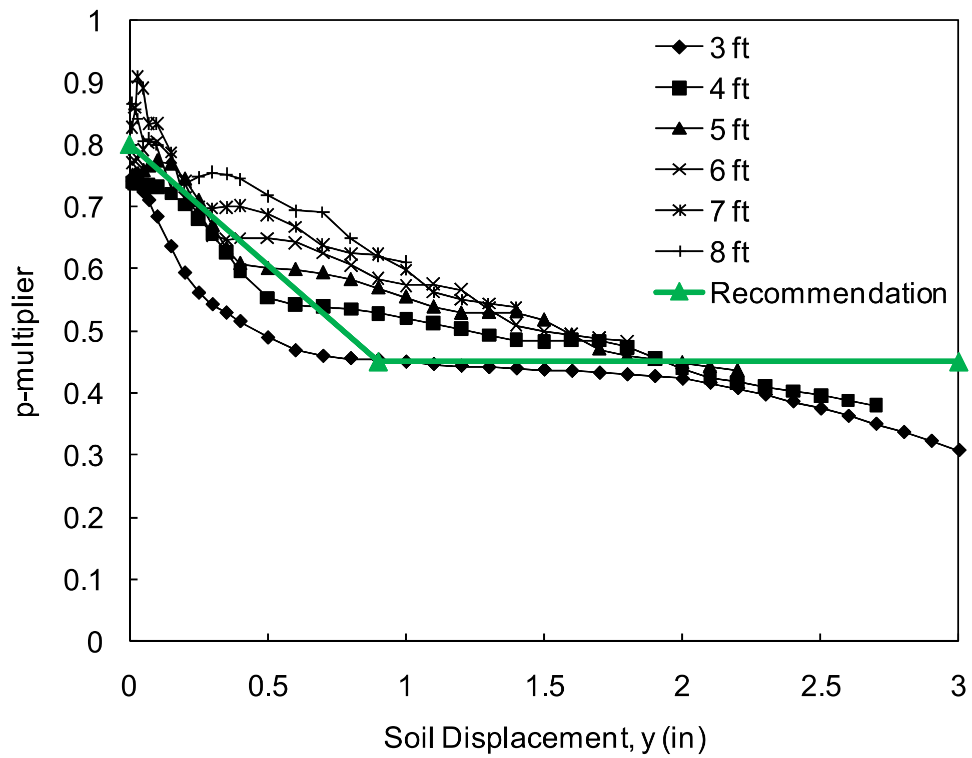

Figure 7-22. Direct Comparison of p-Multiplier at Different Depths for 0D Pile (I-7)

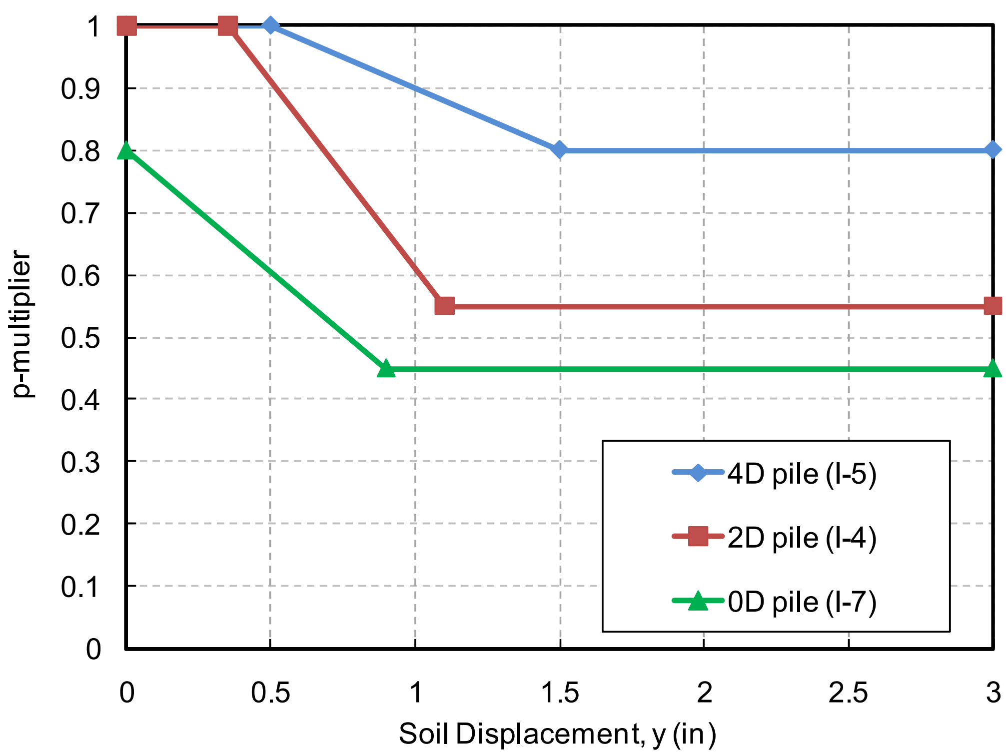

Figure 7-23. Proposed p-multiplier for Piles at Different Distances from the Slope Crest

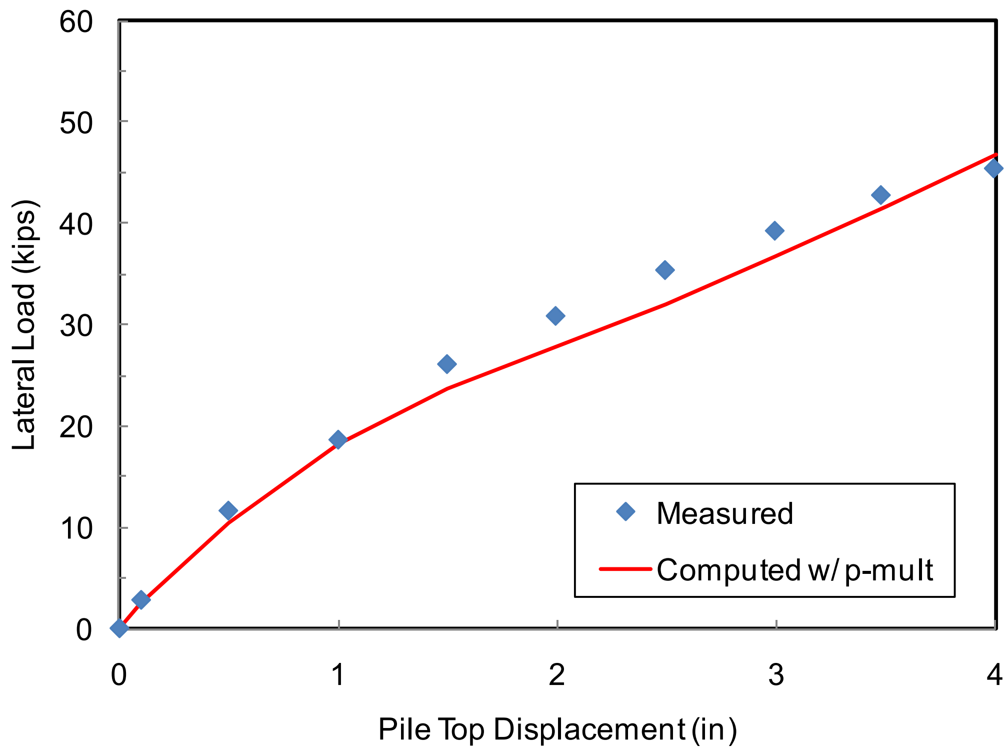

Figure 7-24. Comparison of Load-Displacement Curves from Test Results and Analysis Using Proposed Recommendation for 2D Pile (I-4)

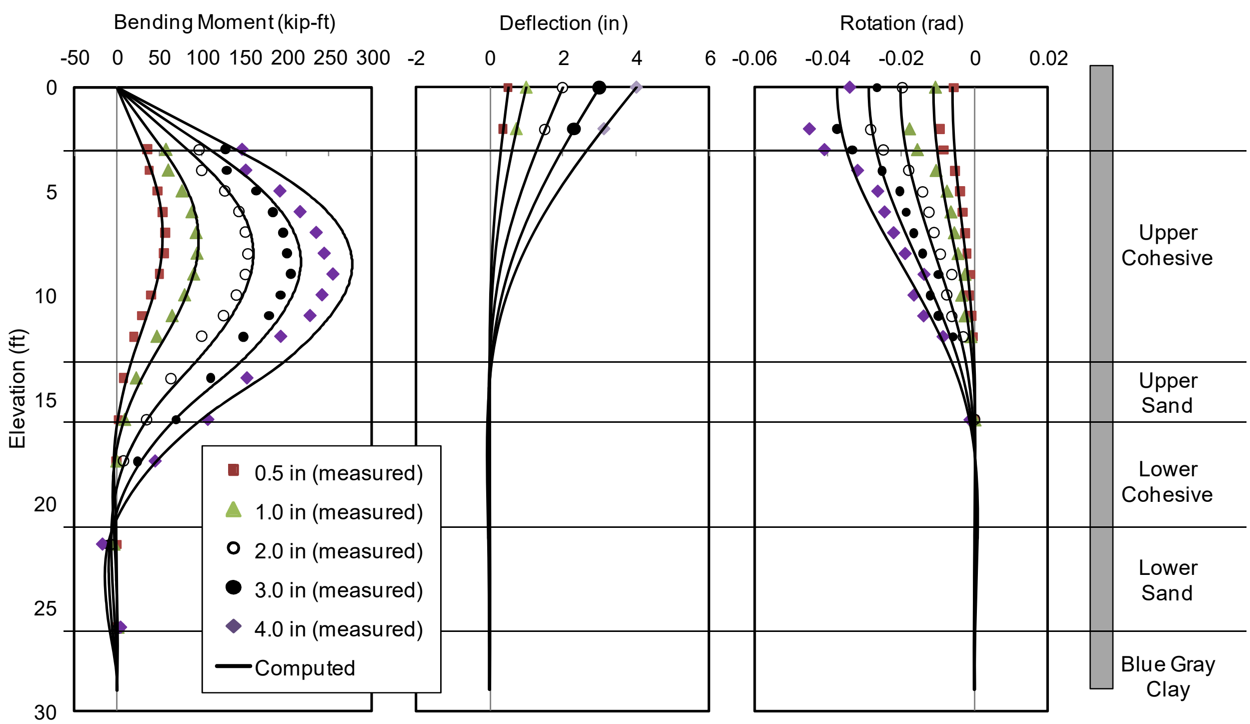

Figure 7-25. Comparison of Test Results and Analysis Using Proposed Recommendation for 2D Pile (I-4)

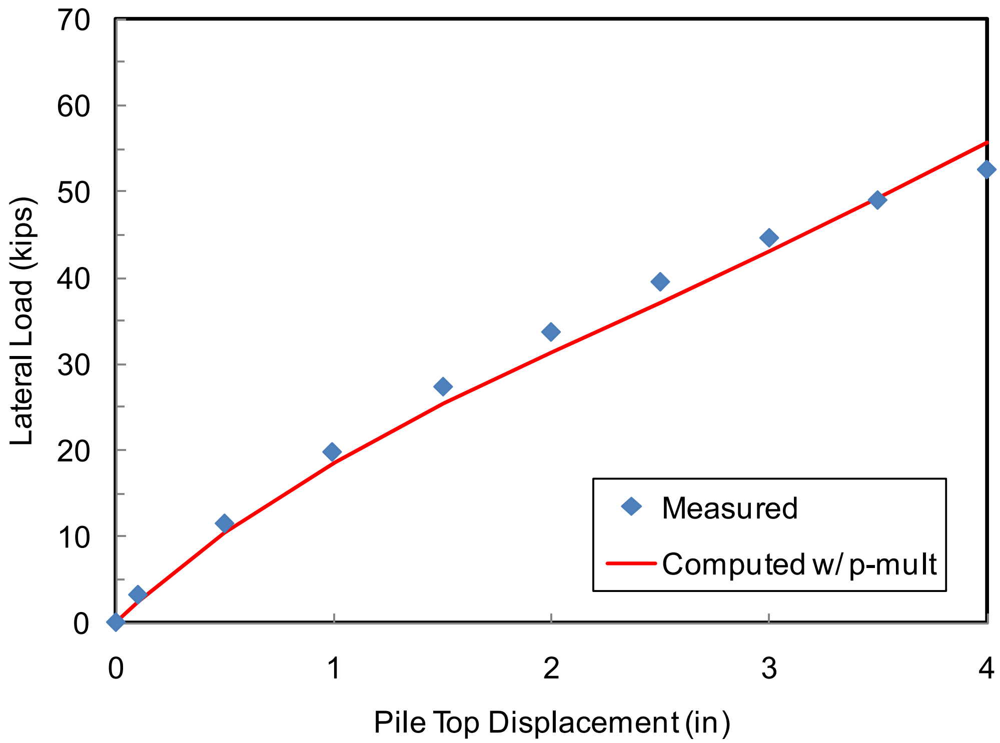

Figure 7-26. Comparison of Load-Displacement Curves from Test Results and Analysis Using Proposed Recommendation for 4D Pile (I-5)

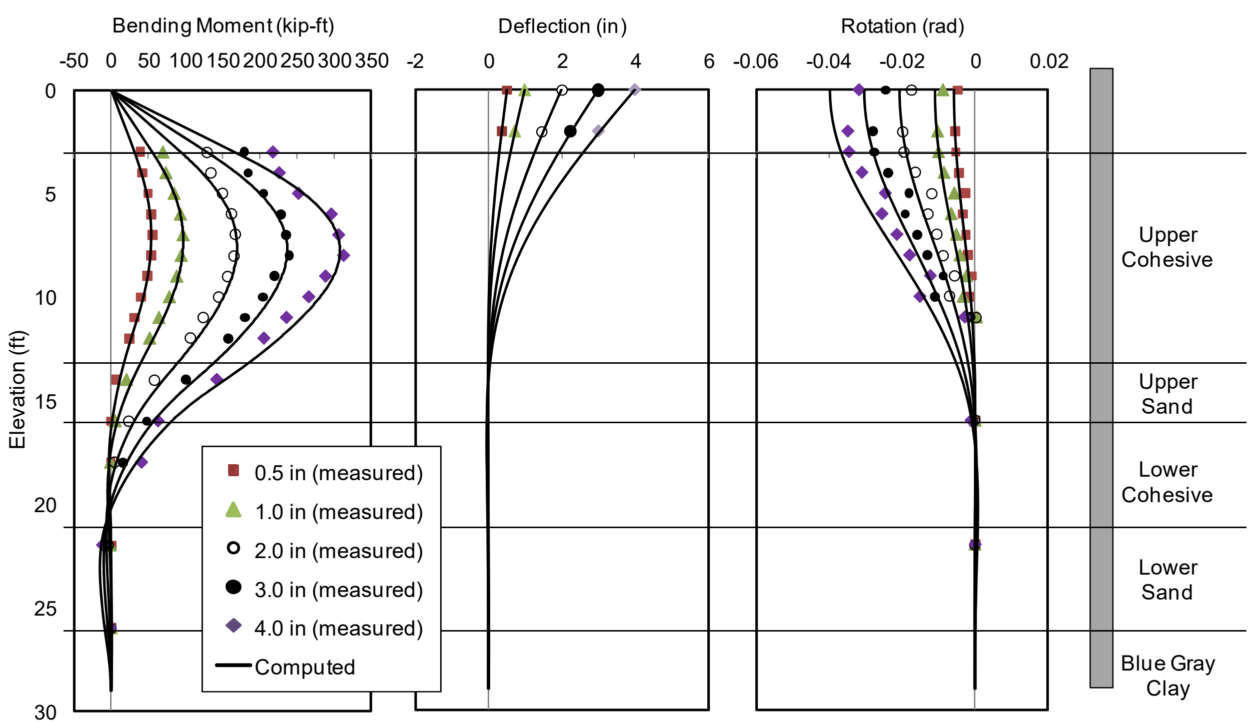

Figure 7-27. Comparison of Test Results and Analysis Using Recommendation for 4D Pile (I-5)

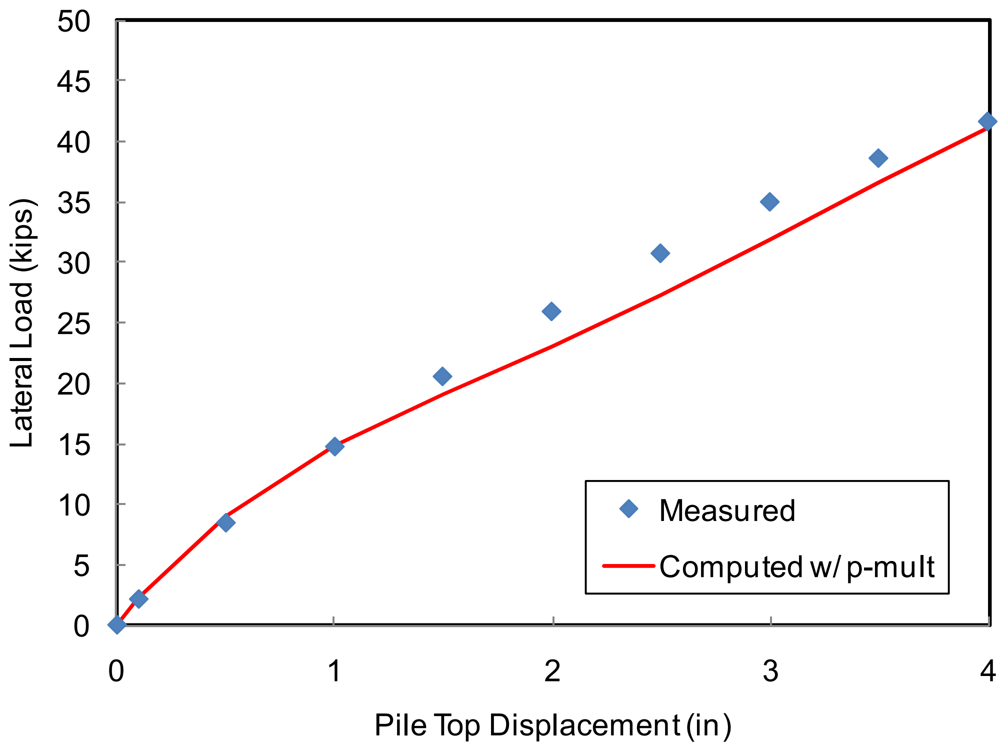

Figure 7-28. Comparison of Load-Displacement Curves from Test Results and Analysis Using Proposed Recommendation for 0D Pile (I-7)

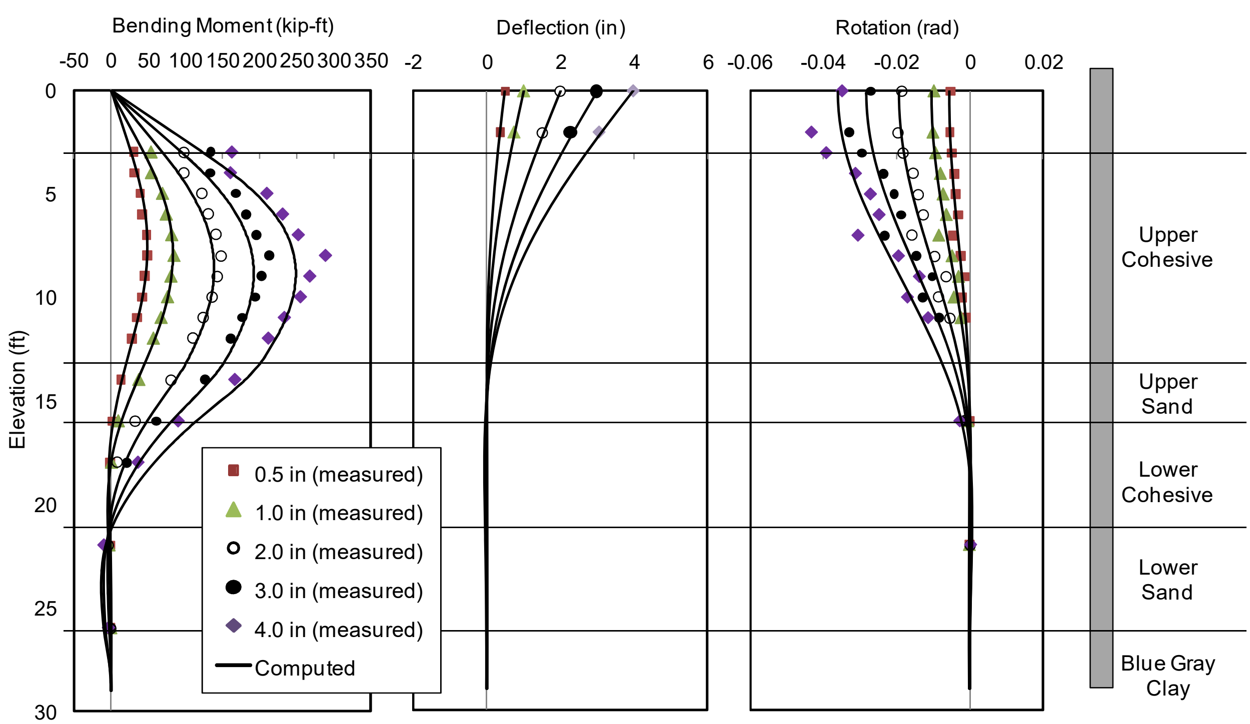

Figure 7-29. Comparison of Test Results and Analysis Using Recommendation for 0D Pile (I-7)

8. IMPLEMENTATION OF EXISTING P-Y CURVES FOR COHESIVE SOIL AND VALIDATION OF PROPOSED RECOMMENDATIONS

In this section, the capability of existing *p-y* curves in predicting the lateral pile response in cohesive soil is evaluated. The proposed recommendations from this study were used to assess the stiff clay *p-y* curve recommendations from previous models used to predict the lateral response of the 4D pile, 2D pile, and 0D pile.

In design practice, three different types of *p-y* curves for cohesive soils are available; soft clay curves (Matlock, 1970), stiff clay below water table (Reese *et al.*, 1975), stiff clay above water table (Reese and Welch, 1975). Based on geotechnical investigation results, stiff clay above water table *p-y* curves were considered to be most appropriate for the soil in this test site. Stiff clay above water table *p-y* curves proposed by Reese and Welch (1975) were developed based on results of full-scale lateral pile load test in Houston, Texas. The test pile used was a bored pile with 36-inch diameter with an embedment length of 42 ft. The average undrained shear strength of the clay was approximately 2200 psf in the upper 20 ft. **Figure 8-1** present a comparison of the back-calculated *p-y* curves for cohesive soil in this study with the stiff clay above the water table *p-y* curves. The numerical model with soil parameters shown in **Figure 7-1** were used for the analysis. The soil properties for the upper cohesive layer used in the model were based on results from UU triaxial tests. Average and upper bound undrained shear strength were considered. A comparison between the predicted load-displacement curves using stiff clay *p-y* curves and measured load-displacement curve for 8D pile are shown in **Figure 8-2**.

In general, the back-calculated *p-y* curves for 8D pile are in better agreement with the stiff clay *p-y* curves using upper bound value. In all cases, the initial stiffness of the stiff clay *p-y* curves are larger than back-calculated *p-y* curves at a soil displacement of less than 1 inch for *p-y* curves at the ground surface and approximately 0.5 inch for *p-y* curves at deeper depth. Beyond this range, the stiff clay *p-y* curves provide less soil resistance although the difference between the two becomes smaller at deeper depths. This difference can be accounted to the variation in soil condition and pile properties used in this study and the study by Reese and Welch (1975). In subsequent analysis, only the upper bound *p-y* curves were considered.

As mentioned earlier, currently recommendation to account for soil slope effect in cohesive soils are based on analytical solutions and applicable for estimating ultimate lateral capacity of short piles. Therefore, the recommendation to account for slope effect from this study were implemented to predict the response of 2D pile, 4D pile and 0D pile using stiff clay *p-y* curves proposed by Reese and Welch (1975) as backbone *p-y* curves. **Figure 8-3** shows the predicted load-displacement curve using stiff clay *p-y* curves and proposed recommendation from this study. The ratio of predicted to measured responses of 2D pile, 4D pile, 8D pile and 0D pile (pile head load, maximum moment, and depth to maximum moment) are presented in **Figure 8-4**. In general, for pile head displacement greater than 0.5 inch, the error in estimating the pile head load, maximum moment, and depth to maximum moment is less than approximately 30%. For displacement less than 0.5 inch, the ratio of predicted to measured responses is not considered for comparison. This is because of low absolute error for low measured responses can result in very high ratio. It should be noted that the accuracy of the prediction for 2D pile, 4D pile and 0D pile depends significantly on the accuracy of the prediction of 8D pile. For 8D pile, the accuracy in predicting the load ratio is reasonable with error ranging between 5 to 30%. The predicted moment ratio is with an error between 10-30%. The predicted depth of maximum moment ratio is with an error between 10-25%. For 2D pile and 4D pile, the accuracy in predicting the load and maximum moment ratios is slightly higher than for 8D pile with error within 20%. The predicted depth to maximum moment ratio for 2D pile and 4D pile is with an error less than 15%. For 0D pile, the accuracy in predicting the ratios is similar to 8D pile.

In summary, stiff clay p-y curve developed by Reese and Welch (1975) can be used to reasonably predict the response of pile (i.e., load, maximum moment, and depth to maximum moment) in cohesive soil. The characteristics of stiff clay *p-y* curves are different from back-calculated p-y curves at shallower depths but the difference becomes smaller at deeper depths. The proposed recommendation to account for slope effect can be used to modify stiff clay *p-y* curve to predict lateral responses of 2D pile, 4D pile and 0D pile with reasonable accuracy.

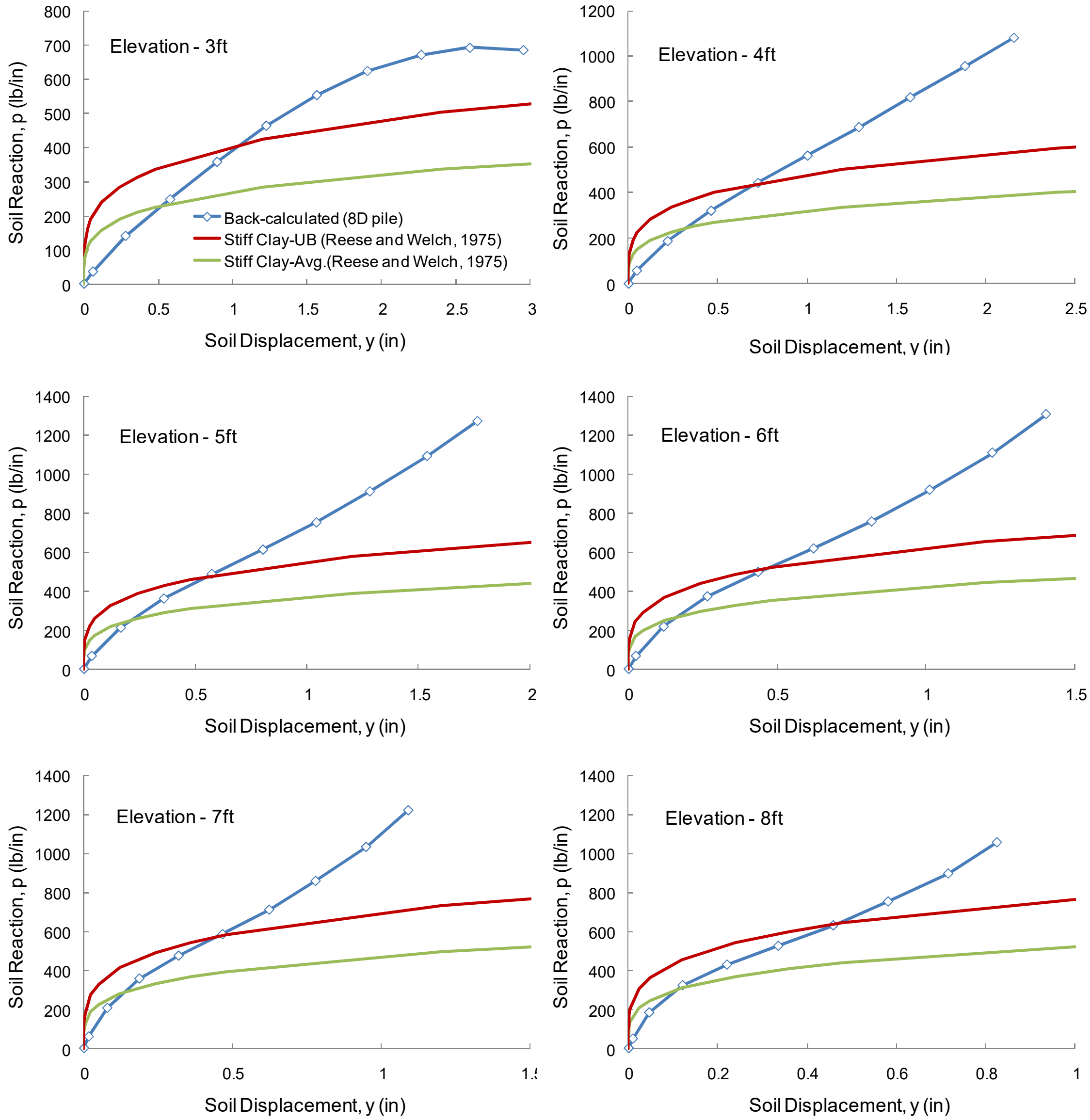

Figure 8-1. Comparison of Back-Calculated *p-y* Curves for 8D Pile (I-6) to Stiff Clay *p-y* Curves (Reese and Welch, 1975) for Elevation 3ft (GS) to 8ft

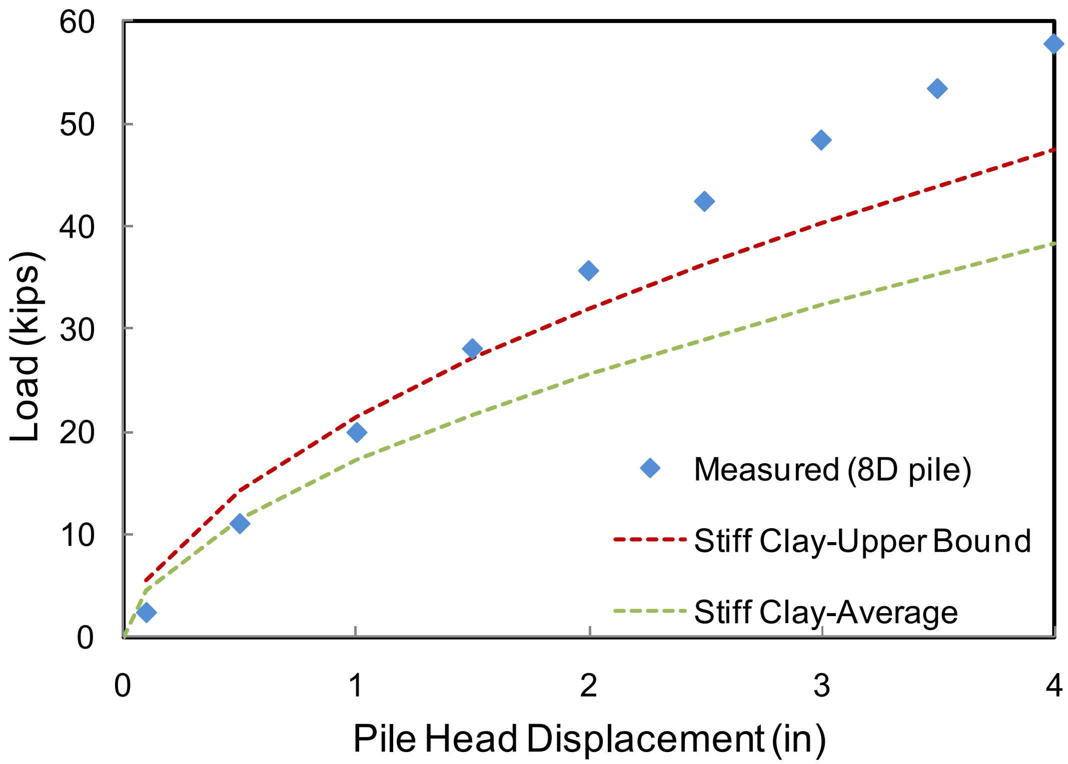

Figure 8-2. Comparison of Load-Displacement Curve Using Stiff Clay p-y Curves and Measured Results from 8D pile

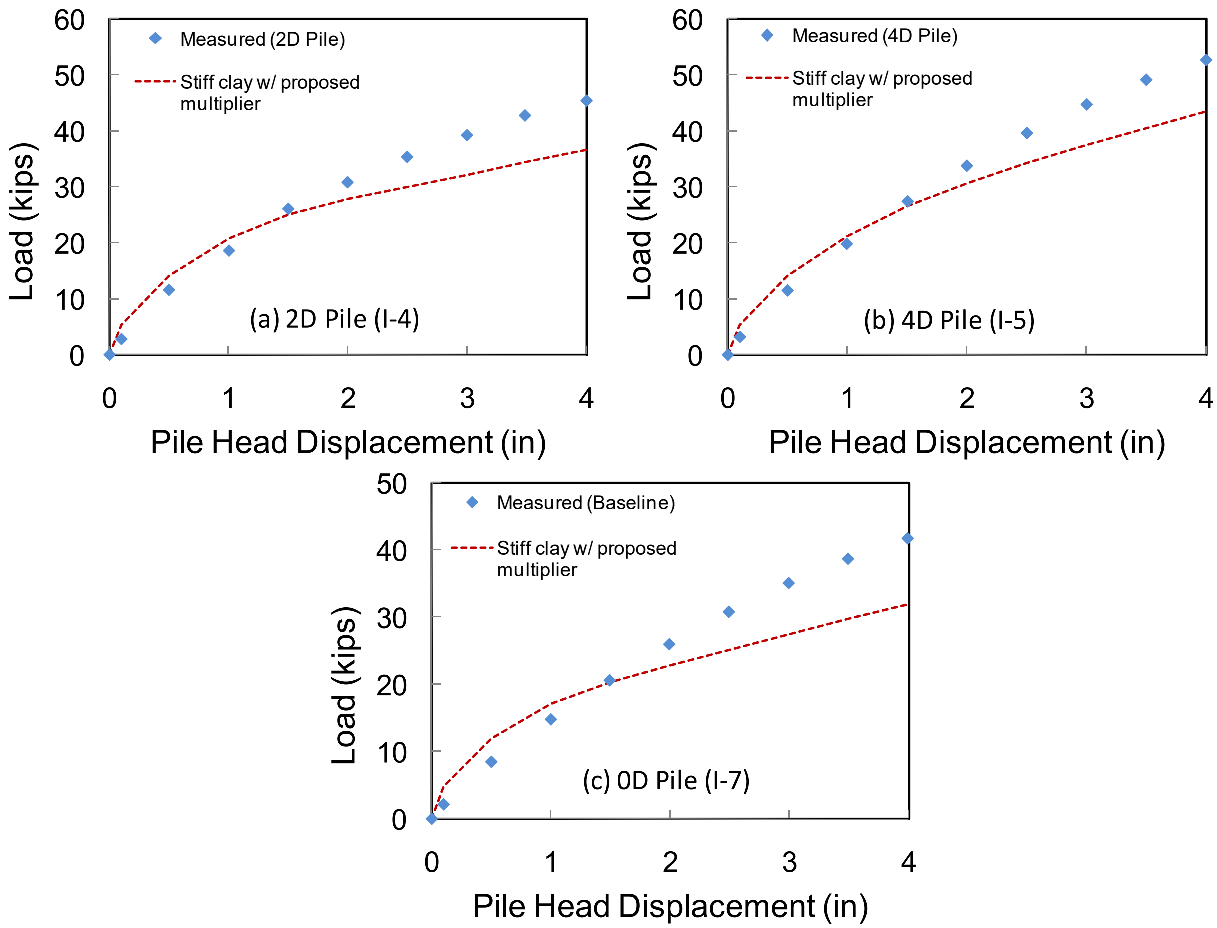

Figure 8-3. Computed Load Displacement Curves using Stiff Clay *p-y* Curve (Reese and Welch, 1975) and Proposed Recommendation Compared to Measured Response (a) 2D Pile (I-4), (b) 4D Pile (I-5) and 0D Pile (I-7)

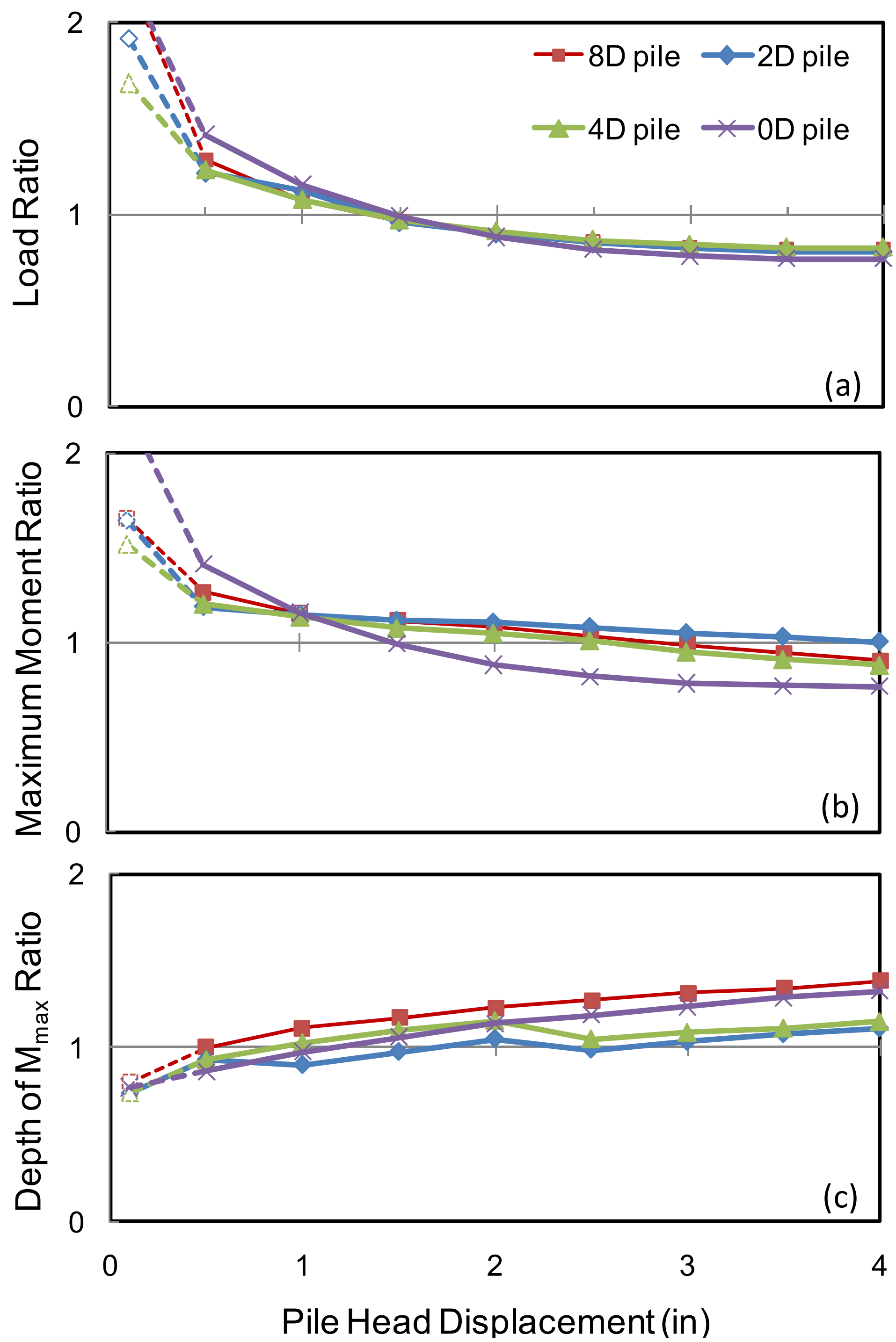

Figure 8-4. Predicted Pile Head Load, Maximum Moment and Depth to Maximum Moment using Stiff Clay curve (Reese and Welch, 1975) and Proposed Design Recommendation Compared to Measured Response for (a) Pile Head Load, (b) Maximum Moment, and (c) Depth to Maximum Moment

9. SERIES-I FINITE ELEMENT SIMULATION OF TEST RESULTS

In this chapter, the procedure for estimating the lateral capacity of piles using the finite element computer program *Plaxis 3D Foundation – V2.2* (Brinkgreve and Swolfs 2007) is presented. For highway structures such as abutments, plane strain 2-dimensional Finite Element Method simulation was adequate to simulate the lateral response of bridge abutment (Bozorgzadeh 2007). For laterally loaded piles, 3-dimensional FEM simulation is necessary to simulate the lateral response of pile.

On this basis, a 3-dimensional finite element analysis was performed in attempt to simulate the lateral loading test results of the baseline piles and the piles installed near slope. The purpose of the analysis was to obtain more understanding of the effect of soil slope on stiffness and lateral capacity of piles using FEM. The procedure was validated by comparing the computed results with the measured test results. In addition, a parametric analysis was conducted for the 0D pile.

As of this writing, several soils models (e.g., Mohr-Coulomb, Duncan-Chang, Hardening Soil, hyperelastic, hypoelastic, viscoelastic and viscoplastic) have been developed for various types of geotechnical problems. The advantages and limitations of each model are summarized by Ti *el al*. (2009). To model the behavior of cohesive soils during undrained static loading for a laterally loaded pile problem, linear elastic-perfectly plastic soil models, such as the Mohr-Coulomb model, have been recommended by several investigators (e.g., Brown and Shie 1991; Georgiadis and Georgiadis 2010). For this reason, the MC model was selected for simulating the soil behavior during undrained lateral pile loading in this research study.

9.1 GENERAL DEFORMATION MODELING

Plaxis is a finite element computer program with advanced constitutive models for the simulation of non-linear behavior of soils. The program allows modeling of structures and the interaction between the structure and surrounding soil which are necessary to simulate many geotechnical problems.

In *Plaxis*, 3D modeling consists of creating soil layers, structures, boundary conditions, and loading using boreholes and horizontal work planes. One or multiple boreholes are used to define the soil stratigraphy at the site. Structures and loads are defined in horizontal work planes. A 3D finite element mesh is generated, taking into account the soil layers and structure levels as defined in the boreholes and work planes. The program allows for the addition or removal of elements (i.e., structure, load, and soils) above, below and within a horizontal work plane to simulate construction sequence. Since all work planes are horizontal, it is out of limits of functionality of the program to generate an inclined excavation once the model geometry is defined. However, the program can generate an inclined mesh (slope), but the stress conditions of the soil after the slope excavation must be manually accounted for. To account for this limitation, it is possible to specify a reasonable initial stress condition of the model to simulate the change in stresses as a result of the slope excavation. In *Plaxis*, one method to generate initial stresses is the K_o procedure. The value K_o, the coefficient of lateral earth pressure, represents the relationship between vertical stress σ_{vo} and horizontal stress ($\sigma_{ho} = K_o\ \sigma_{vo}$). It is believed that K_o is a major factor affecting the lateral response of pile. However, using the FEM method, a variation of K_o does not significantly affect the computed pile response (Brown and Shie 1991). A reasonable value for K_o was selected for the analysis as discussed later.

9.2 MATERIAL MODELING

The accuracy of the FEM simulations depends significantly on the selection of appropriate material models to represent the soil, structure and soil-structure interaction. In the following section, the soil models, pile models and their interactions through interface elements are described.

9.2.1 SOIL MODEL

For laterally loaded pile under static condition, several researchers have adopted the Mohr-Coulomb (MC) soil model to represent the undrained behavior of cohesive soils. Even though this model is considered as a first order approximation of the soil behavior, the formulation of the model is robust and has been proven to be stable for a variation of soil parameters unlike other advanced soil model. For example, the Hardening-Soil (HS) is an advanced model for simulating soil behavior (Schanz 1998; Brinkgreve and Swolfs 2007). One of the improvements of this soil model is that the stress-strain relationship can be approximated by a hyperbola instead of a bi-linear curve in the MC soil model. In addition, the formulation of the HS soil model automatically accounted for stress-dependency of the soil stiffness modulus as well as the ultimate deviatoric stress based on drained triaxial tests. In the initial analysis, both the MC soil model and HS model were considered. It was found that the HS model appears to be unstable when used for simulating undrained behavior of cohesive soils ($\phi = 0$). For this reason, only the MC soil model was considered.

The Mohr-Coulomb model is a linear-elastic perfectly-plastic model with a fixed yield surface. The yield surface is defined by model parameters and is not affected by plastic straining. In this model, plasticity is associated with the development of irreversible strains (Brinkgreve and Swolfs 2007). **Figure 9-1** shows the stress-strain and the deviatoric stress-mean pressure relationship in elastic-perfectly plastic model. The full Mohr-Coulomb yield condition consists of six yield functions defined as (Smith and Griffith 1983; Brinkgreve and Swolfs 2007):

$$f_{1a} = \frac{1}{2}(\sigma'_2 - \sigma'_3) + \frac{1}{2}(\sigma'_2 + \sigma'_3)\sin\phi - c\cos\phi \le 0 \tag{9.1}$$

$$f_{1b} = \frac{1}{2}(\sigma'_3 - \sigma'_2) + \frac{1}{2}(\sigma'_2 + \sigma'_3)\sin\phi - c\cos\phi \le 0 \tag{9.2}$$

$$f_{2a} = \frac{1}{2}(\sigma'_3 - \sigma'_1) + \frac{1}{2}(\sigma'_1 + \sigma'_3)\sin\phi - c\cos\phi \le 0 \tag{9.3}$$

$$f_{2b} = \frac{1}{2}(\sigma'_1 - \sigma'_3) + \frac{1}{2}(\sigma'_1 + \sigma'_3)\sin\phi - c\cos\phi \le 0 \tag{9.4}$$

$$f_{3a} = \frac{1}{2}(\sigma'_1 - \sigma'_2) + \frac{1}{2}(\sigma'_1 + \sigma'_2)\sin\phi - c\cos\phi \le 0 \tag{9.5}$$

$$f_{3b} = \frac{1}{2}(\sigma'_2 - \sigma'_1) + \frac{1}{2}(\sigma'_1 + \sigma'_2)\sin\phi - c\cos\phi \le 0 \tag{9.6}$$

where f_i represents each individual yield function, ϕ is the friction angle, c is the cohesion and σ_1, σ_2 , σ_3 are principle stresses. In addition, six plastic potential functions are defined as (Brinkgreve and Swolfs 2007):

$$f_{1a} = \frac{1}{2}(\sigma'_2 - \sigma'_3) + \frac{1}{2}(\sigma'_2 + \sigma'_3)\sin\phi - c\cos\phi \le 0 \tag{9.7}$$

$$f_{1b} = \frac{1}{2}(\sigma'_3 - \sigma'_2) + \frac{1}{2}(\sigma'_2 + \sigma'_3)\sin\phi - c\cos\phi \le 0 \tag{9.8}$$

$$f_{2a} = \frac{1}{2}(\sigma'_3 - \sigma'_1) + \frac{1}{2}(\sigma'_1 + \sigma'_3)\sin\phi - c\cos\phi \le 0 \tag{9.9}$$

$$f_{2b} = \frac{1}{2}(\sigma'_1 - \sigma'_3) + \frac{1}{2}(\sigma'_1 + \sigma'_3)\sin\phi - c\cos\phi \le 0 \tag{9.10}$$

$$f_{3a} = \frac{1}{2}(\sigma'_1 - \sigma'_2) + \frac{1}{2}(\sigma'_1 + \sigma'_2)\sin\phi - c\cos\phi \le 0 \tag{9.11}$$

$$f_{3b} = \frac{1}{2}(\sigma'_2 - \sigma'_1) + \frac{1}{2}(\sigma'_1 + \sigma'_2)\sin\phi - c\cos\phi \le 0 \tag{9.12}$$

where ψ represents each dilatency angle which is required to model positive plastic volumetric strain for dense soils.

The Mohr-Coulomb model requires five parameters that are well known in most practical situations. The other two parameters, in addition to c, ϕ and ψ, are Young's modulus E and Poisson's ratio v, based on Hooke's law for isotropic elastic material behavior. In this research study, the main soil parameters were determined from the UU triaxial test results (Appendix A). For the lateral pile loading tests in this study, the soil-loading condition is considered undrained. Therefore, undrained soil parameters (i.e., $c = S_u$, $\phi = 0$) were selected for the analysis. To be consistent with the previous analysis using *LPILE*, only the upper bound soil parameters were considered. The MC model, which is an elastic-perfectly plastic model, was adopted for the calibration of the soil response in the numerical model to represent the upper bound stress-strain curve from UU triaxial tests which show a softening behavior. Therefore, softening behavior of soils was not considered. The Poisson ratio μ_s of 0.495 was selected for cohesive soils under undrained loading instead of 0.5 to avoid numerical difficulties. The Poisson ratio of 0.35 was assumed to be appropriate for the cohesionless layers (Bozorgzadeh 2007). The dilatency angle ψ was set to zero for undrained loading condition. **Table 9-1** summarizes the material properties for the MC model.

It was found in Chapter 6 that, for a uniform cohesive soil layer in this study, using constant values of soil properties (i.e., E_{50} and S_u) give a good prediction of the pile response.

Therefore, to be consistent with the previous analysis, the upper cohesive layer was modeled with constant soil properties for the baseline model.

Modeling the stress conditions in the field as a result of the slope excavation and consequently selecting the appropriate soil parameters are complicated. As a result of the removal of overburden stress, the resulting stress conditions and the associated soil properties may not be uniform. To determine the appropriate soil parameters for the FEM model, assumptions were made based of the functionality of *Plaxis* (i.e., only horizontal work planes with uniform soil properties). Based on the similarities of the initial stiffness of back-calculated *p-y* curves for the baseline pile (8D pile), the 4D pile and the 2D pile, it was judged that the change in in-situ stress conditions as a result from slope excavation did not significantly affect the 'medium' strain soil properties, such as E_{50}, especially near the pile. Therefore, for modeling of the initial stress conditions of the 2D pile and the 4D pile, the use of a constant E_{50} for the upper cohesive layers appears to be reasonable. For similar reasons, a constant value for the undrained shear strength was assumed for the upper cohesive layer.

For the pile on the slope crest, the slope excavation significantly affected the soil properties especially near the pile and consequently the lateral pile response even at small soil/pile displacement range. However, to validate the numerical results of Georgiadis and Georgiadis (2010) for the pile installed on the slope crest, constant soil properties were also used for the upper cohesive layer.

9.2.2 PILE MODEL

The pile cross section is modeled with shell elements consisting of wall elements and interfaces. In *Plaxis*, walls are composed of plate elements. The basic wall geometry included thickness *d*, the unit weight of the wall material γ_{wall}, Young's modulus of steel E_{steel}, and Poisson's ratio ν_{wall}. The pile was modeled as an elastic material. The material properties for the steel piles are listed in **Table 9-2**. Interfaces are automatically generated at both sides of the wall to allow for proper soil-structure interaction.

It should be noted that pile installation effects are not taken into account. Pestana *et al*. (2002) stated that the effects of pile installation (driven pile) in cohesive soils are significant within 1D from the pile. Reese *et al*. (2004) stated that lateral deflection of a pile will cause strain and stress to develop from the pile wall to several diameters away. Therefore, it was assumed that pile installation effects are not significant for laterally loaded piles in this research study, especially at large pile head displacements ($\Delta > 1$ inch).

9.2.3 INTERFACE PROPERTIES

Interface elements are automatically generated along wall elements to model the soil-wall interaction (smooth to rough). Pile roughness is modeled by choosing a strength reduction factor for the interface (R_{inter}). This reduction factor relates the interface strength (wall friction and adhesion) to the soil strength (friction angle and cohesion). For undrained behavior of cohesive soils, this factor is related to the undrained shear strength S_u and is similar to the factor α (see **Figure 2-12**) which was discussed in the earlier section. For this analysis, the value for R_{inter} of 0.7 appears to be reasonable following Tomlinson (1994) and previous FEM analysis (Bozorgzadeh 2007).

In *Plaxis*, an elastic-perfectly plastic Mohr-Coulomb model is used to describe the behavior of interfaces. The elastic range is related to the small displacement within the interface. The plastic range is related to permanent slip that may occur. The basic property of an interface element is related to basic soil properties (friction angle and cohesion). The strength properties of interfaces are calculated by applying the R_{inter} to the associated soil properties. The values of R_{inter} for the pile-soil interaction are listed in **Table 9-1**.

9.3 BOUNDARY CONDITION

A set of general fixities to the boundaries of the geometry model are imposed automatically by *Plaxis*. A full fixity ($u_x = u_y = u_z = 0$) at the bottom of the model geometry considered. For the vertical boundaries of the sides of the model geometry, a fixity is imposed only in the direction normal to the axis (e.g., for x-axis, $u_x = 0$), and the other two directions are free ($u_y = u_z =$ free). For ground surface, the model boundary is considered free in all directions.

A horizontal point load was applied at the top of the pile (3ft from the ground surface) to simulate the lateral load applied to the pile by the hydraulic actuator similar to the testing condition. The applied point loads are equivalent to the maximum measured lateral load at each target displacement from each test.

9.4 MODEL GEOMETRY AND INITIAL STRESS CONDITIONS

In this section, the effects of model boundary and mesh sizes are discussed. In addition, the generation of initial stress conditions for the finite element models to represent actual field conditions is also discussed.

9.4.1 MESH GENERATION

In *Plaxis*, the soils are modeled with 15-node wedge elements. As shown in **Figure 9-2**, the 15-node wedge element is composed of 6-node triangular elements and 8-node quadrilateral elements (Brinkgreve and Swolfs 2007). At present, higher order elements (e.g., 15-node triangular elements in *Plaxis* 2D) are not available in *Plaxis* 3D due to large memory consumption and calculation times.

Regarding the model geometry, two main factors that affect the computed results are mesh size and model boundaries. For general meshing consideration, fine meshes are required near loads and structures. Larger meshes may be used near the model boundary. For model boundary consideration, Karthigeyan *et al*. (2007) suggest that boundary effects on the computed results (displacement and stresses around the pile) are not significant when the width of the soil mass is greater than 40D and the height of the soil mass is greater than L+20D where L is the pile length and D is the pile diameter. In the generation of finite element mesh for each numerical model, the dimensions of the soil mass are chosen arbitrarily to be large enough that the effects of model boundary are insignificant. In addition, finer mesh size were chosen to model the soils near the pile while larger mesh size were used near the model boundary. The 3D finite element mesh for the baseline (free-field) pile is shown in **Figure 9-3**.

Next the baseline model was modified to represent the geometry of the piles near slope. The geometry of the excavated slope in the model was the same as that in the field. In attempt to minimize boundary effects, the length of the model was adjusted to account for the pile distance from the slope crest while keeping the width and length of the model constant. For example, the dimensions of the model geometry for the 0D pile are the same as those for the baseline pile.

The length of the model for the 2D pile and the 4D pile are larger than that for the baseline pile by 2D and 4D respectively. The 3D finite element mesh for the 0D pile, the 2D pile and the 4D pile are presented in **Figure 9-4**, **Figure 9-5** and **Figure 9-6** respectively.

9.4.2 INITIAL STRESS CONDITIONS

In order to simulate the field conditions in the numerical modeling, the initial stresses were calculated before loading. Stress conditions for each soil layers are accounted for manually by specifying appropriate K_0 values. Based on soil investigation results, the K_0 value of 1.6 appears to be appropriate for the upper cohesive layer. For the analysis of the piles near slope, the same K_0 value was assumed because a variation of K_0 did not significantly affected the computed results.

9.5 ANALYSIS RESULTS

In this section, the numerical model for the baseline pile was validated by comparing the computed results with the measured results. The FEM analysis for the pile on the slope crest (0D pile) was validated by comparing the computed results with Georgiadis and Georgiadis (2010) predictions. Then a comparison between the results of the FEM analysis and the measured results for the 0D pile is discussed. In addition, comparisons between computed and measured results for the 2D pile and the 4D pile are also discussed.

9.5.1 THE BASELINE PILE

Figure 9-7 and **Figure 9-8** show the results of the FEM analysis compared to the measured test results. Good agreement between the measured and the computed pile response indicates that the numerical model for the baseline pile is reasonable. From **Figure 9-8**, the computed curvatures along the pile appear to be negative at the top and bottom of the pile. This may be a result from the double differentiation of the computed deflection profiles.

Based on the comparison results, it can be concluded that FEM analysis can simulate the lateral pile response of the baseline pile with reasonable accuracy while the pile remained elastic (i.e., pile head displacement less than 4 inch). Because non-linear pile properties were not considered, a comparison of the results for larger pile head displacements is not provided. The predicted load-displacement curve appears to be stiffer than the measured for pile head displacement larger than 2 inch. This can be attributed to the use of an elastic-perfectly plastic model (e.g., MC model) that does not account for strain softening. The use of a soil model that accounts for strain softening should be considered for future research. Despite some limitations of the material model, the results of the validation process suggest that, for a uniform cohesive layer, the use of constant soil parameters (E_{50}, S_u) gives a reasonable prediction of the lateral load response of the baseline pile which is consistent with the observation from the previous chapter.

9.5.2 THE PILE ON THE SLOPE CREST (0D PILE)

Comparisons between the computed and the measured load-displacement curve and the pile response for the 0D pile are shown in **Figure 9-9** and **Figure 9-10**. For comparison, Georgiadis and Georgiadis (2010) predictions using *p-y* criteria for the pile installed on the slope crest (0D pile) based on their FEM study as presented in the previous chapter are plotted on the same figure. Good agreement between the computed load-displacement curve from the FEM analysis and Georgiadis and Georgiadis (2010) method indicates that the numerical model for the pile on the slope crest is reasonable for the case of constant soil properties and the use of an elastic-perfectly plastic soil model. The reason that the load-displacement curve from Georgiadis and Georgiadis (2010) method appears to be in better agreement with the measured results may be credited to the approximation of *p-y* curves using a hyperbolic equation.

From **Figure 9-9**, it can be observed that the computed load-displacement curve from the FEM analysis is stiffer than the measured results. A comparison between the computed and the measured curvature profiles indicates that the computed lateral pile-soil response appears to be stiffer than the measured pile response as shown in **Figure 9-10**. For example, the locations of maximum moment from the FEM analysis occur closer to the ground surface than those measured. For possible reasons mentioned in the earlier chapter, the lateral load behavior of the soil-pile system of the 0D pile is more flexible than that of baseline pile. This implies that the FEM analysis does not automatically capture the entire physical phenomenon that affects the lateral behavior of the soil-pile system when a pile is installed on a slope crest. This is consistent with Bozorgzadeh (2007) conclusions that the FEM analysis could not capture the post-peak degradation behavior observed from the full-scale testing of bridge abutments because the material models do not account for softening due to soil dilatancy and de-bonding. To improve the computed results, it is believed that a soil constitutive model that account for the softening behavior is required. In addition to the soil constitutive model, appropriate soil parameters should also be selected to model the different soil failure mechanisms observed in full scale testing, especially at larger soil displacements (e.g., cracking).

9.5.3 THE 2D PILE

Figure 9-11 and **Figure 9-12** present comparisons between the computed and the measured load-displacement curves and pile response for the 2D pile. For low lateral loads, the computed load-displacement curve from the FEM analysis is similar to the measured results. This is similar to the observations that, for a small soil displacement range, the lateral pile stiffness is not affected by the presence of slope. However, due to reasons mentioned previously for the case of the 0D pile, the computed load-displacement curve is stiffer than the measured results for larger loads (or pile head displacements).

9.5.4 THE 4D PILE

Figure 9-13 and **Figure 9-14** present comparisons between the computed and the measured load-displacement curves and pile response for the 4D pile. Good agreement between the computed and measured load displacement curve were observed for small pile head displacements. However, the computed load-displacement curve is stiffer than the measured results for larger loads (or pile head displacement) due to reasons mentioned previously for the case of the 0D pile.

9.5.5 SUMMARY OF ANALYSIS RESULTS

Results from the validation process for the baseline pile indicate the numerical model, along with selected soil parameters, are reasonable. For the pile on the slope crest, the results from FEM analysis appears to predict stiffer lateral pile response when compared to the corresponding test results. Possible reasons are that the material models do not account for softening due to soil dilatancy and de-bonding (Bozorgzadeh 2007). In addition, it is difficult select appropriate soil models and soil parameters to model the different soil failure mechanisms observed in full-scale tests using FEM. In the next section, an attempt was made to extrapolate the recommendation from this study (*p*-multiplier) to improve the FEM results for the pile installed on the slope crest.

9.6 QUALITATIVE PARAMETRIC ANALYSIS FOR THE PILE ON THE SLOPE CREST

In this section, qualitative parametric analysis was conducted in attempt to improve the FEM results of the 0D pile. As mentioned previously, many factors contributed to the reduction of the lateral capacity of the pile when it is installed on the slope crest. At the time of writing, it is difficult to select appropriate constitutive model to represent non-linearity of soils (e.g., softening). In addition, it is also difficult to select appropriate soil parameters to model cracking. Therefore, for the first sensitivity analysis, it was assumed that the reduction of the undrained shear strength for the upper cohesive layer is equivalent to the *p*-multiplier for the 0D pile (**Figure 7-22**). For this analysis, a factor of 0.45 was applied to the undrained shear strength of the upper cohesive layer. A comparison between the computed and the measured load-displacement curves are shown in **Figure 9-15**. It was observed that the computed load-displacement curve is in better agreement with the measured results than for the case without any reduction of the undrained shear strength.

It was also observed from the previous analysis that, in addition to the reduction of the undrained shear strength, other factors also affected the lateral response of pile on the slope crest. As observed from the comparison of the 0D *p-y* curves and baseline *p-y* curves, the excavation of slope adversely affected the 'medium' strain soil property (soil modulus E_{50}) especially near the slope crest (also near the pile for this testing condition). For this next analysis, it was assumed that the reduction of the soil modulus E_{50} is equivalent to the initial value of the *p*-multiplier for the 0D pile (**Figure 7-22**). Because the initial portion of the *p*-multiplier for the 0D pile varies from 0.8 to 0.45, a value of 0.6 appears to be reasonable to represent the reduction of E_{50}. The computed load-displacement for this analysis was plotted in **Figure 9-15** for comparison. It can be observed that the computed load-displacement curve is in good agreement with the measured results. It can be concluded that the reduction of the soil modulus is also one of the main factors contributing to the reduction of lateral capacity of pile installed on the slope crest.

It should be noted, while the results of the sensitivity analysis appear to be in good agreement with the measure results, several assumptions have been made to simplified real soil behavior which is highly non-linear into uniform soil properties for the FEM analysis. In summary, the two major factors affecting the computed lateral response of a pile installed on a slope crest are the soil modulus and the soil undrained shear strength. At the time of writing, it is difficult to use FEM to study the effects of soil slope as observed in full-scale tests due to the difficulties in selecting an appropriate constitutive soil model and soil parameters.

9.7 SUMMARY AND CONCLUSION

A 3-dimensional finite element analysis was performed in attempt to simulate the lateral loading test results of the baseline piles and the piles installed near slope in this study. The FEM analysis was aimed at providing information on the effects of soil slope on the lateral capacity of piles. In addition, a parametric study of the soil properties was conducted for the 0D pile. The procedure was validated by comparing the computed results with the corresponding test results.

For the case of constant soil properties in each analysis, the computed load-displacement relationship was in good agreement with the measure test results only for the baseline pile. For the 0D pile, the 2D pile and the 4D pile, the FEM analysis give stiffer lateral pile response than the corresponding test results. Possible explanations are that the material models do not consider softening due to soil dilatancy and de-bonding (Bozorgzadeh 2007).

In addition, a preliminary parametric study was conducted in attempt to improve the computed results. It was found that the soil modulus and the undrained shear strength significantly affected the computed lateral response of pile and that both should be manually adjusted for the case of a laterally loaded pile on the slope crest.

Table 9-1 Material properties for the MC-Soil Model

Soil Layer	Soil Unit Weight		Cohesion	Young's Modulus	Poisson's Ratio	Friction Angle	Dilatency Angle	Interface Reduction Factor
	γ_{unsat}	γ_{sat}	c_{ref}	E_{ref}	ν	ϕ	ψ	R_{inter}
	pcf	pcf	psf	ksf	–	degrees	degrees	-
Upper Cohesive	115	115	2400	158	0.495	-	0	0.7
Upper Sand	130	130	-	600	0.35	40	0	0.7
Lower Cohesive	115	115	2400	158	0.495	-	0	0.7
Lower Sand	130	130	-	600	0.35	45	0	0.7
Blue Gray Clay	110	110	3500	158	0.495	-	0	0.7

Table 9-2 Material Properties for the Steel Pipe Pile

Material Parameter	Type of Behavior	Element type	Density	Thickness	Young's Modulus	Poisson's Ratio
			γ_{steel}	d	E	v
			lb/in^3	in.	ksf	-
Steel Pipe Pile	Elastic	plate (wall)	0.289	0.375	4.1x10^7	0.1
Bottom Cap	Elastic	plate (floor)	0.289	1.5	2.9x10^7	0.15

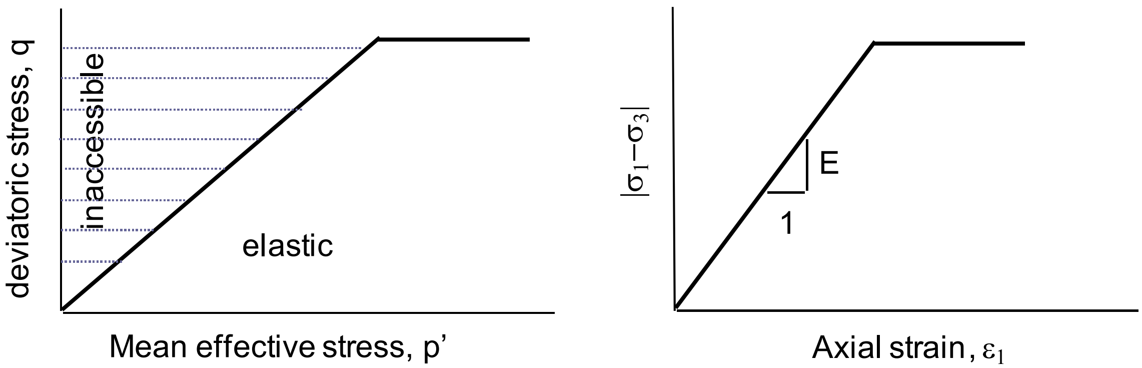

Figure 9-1 Deviatoric Stress-Mean Effective Stress Relationship and Stress-Strain Relationship in Elastic-Perfectly Plastic Model (after Brinkgreve and Swolfs 2007)

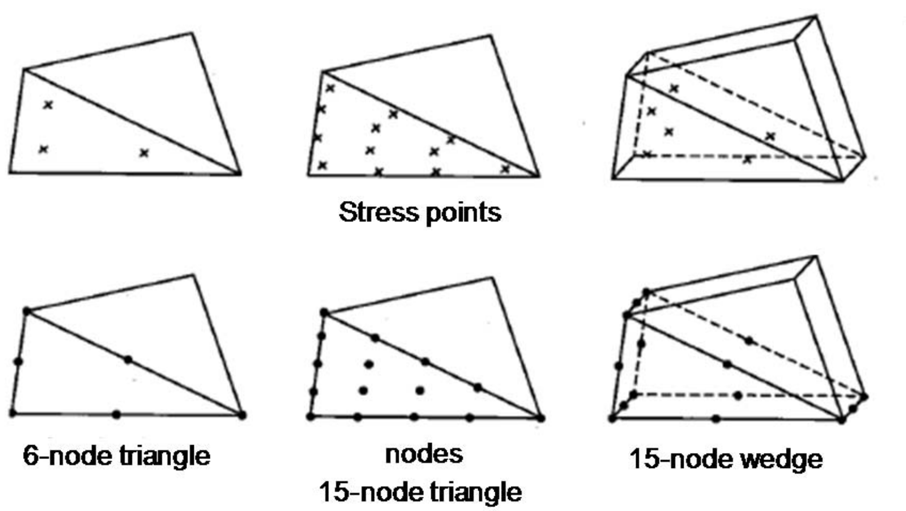

Figure 9-2 Distribution of Nodes and Stress Points in a 15-Node Wedge Element (after Brinkgreve and Swolfs 2007)

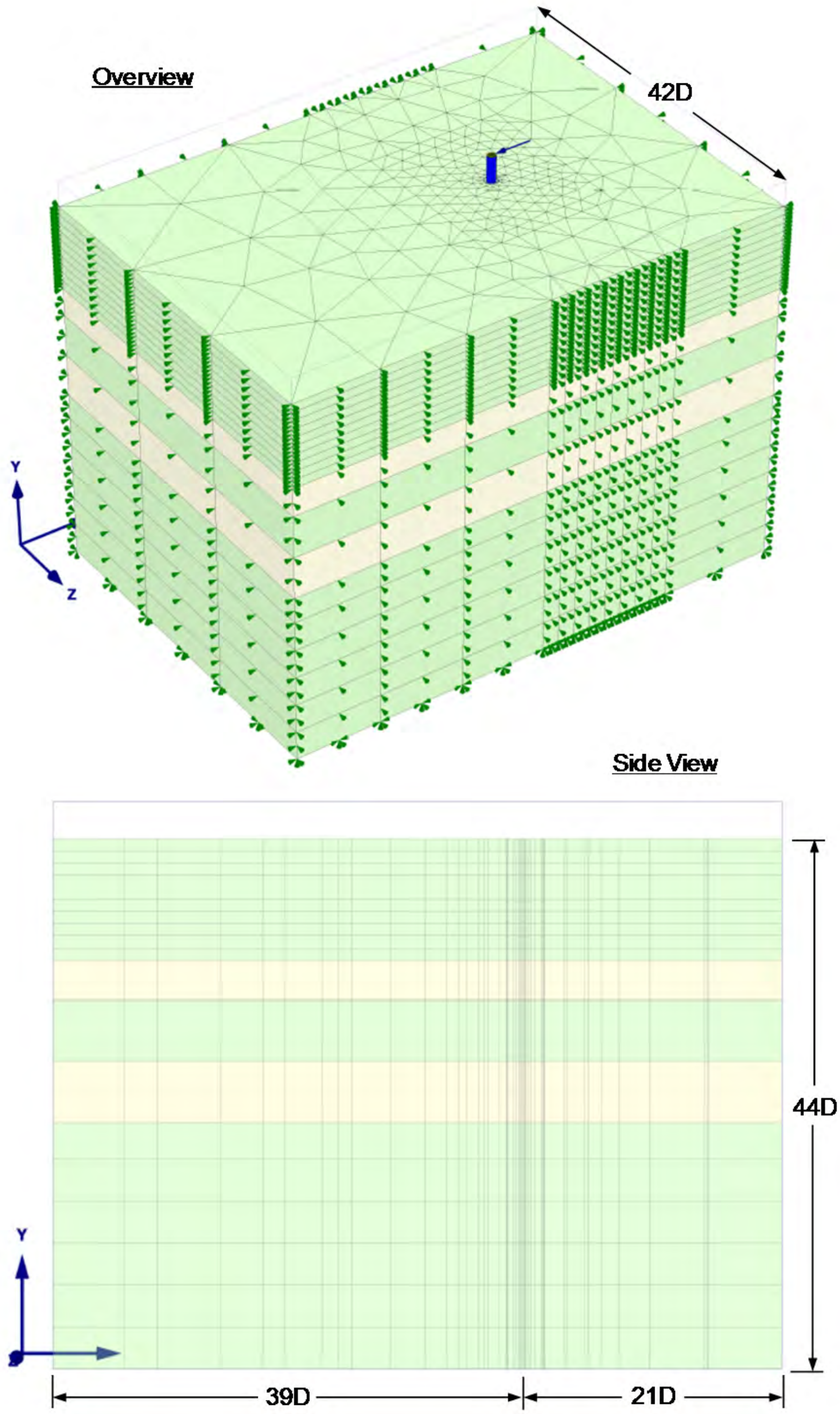

Figure 9-3 Finite Element Mesh for the Baseline Pile

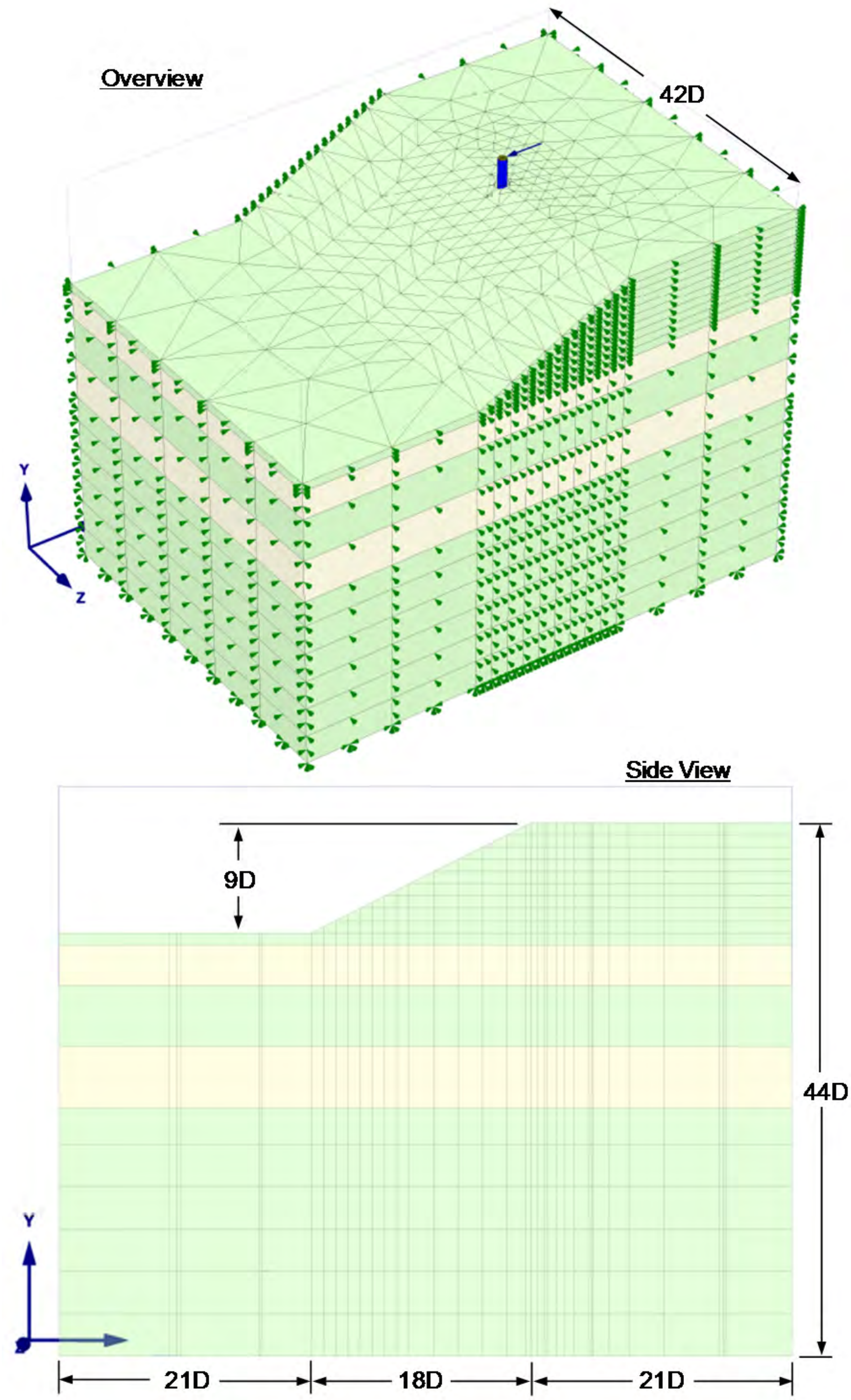

Figure 9-4 Finite Element Mesh for the 0D Pile

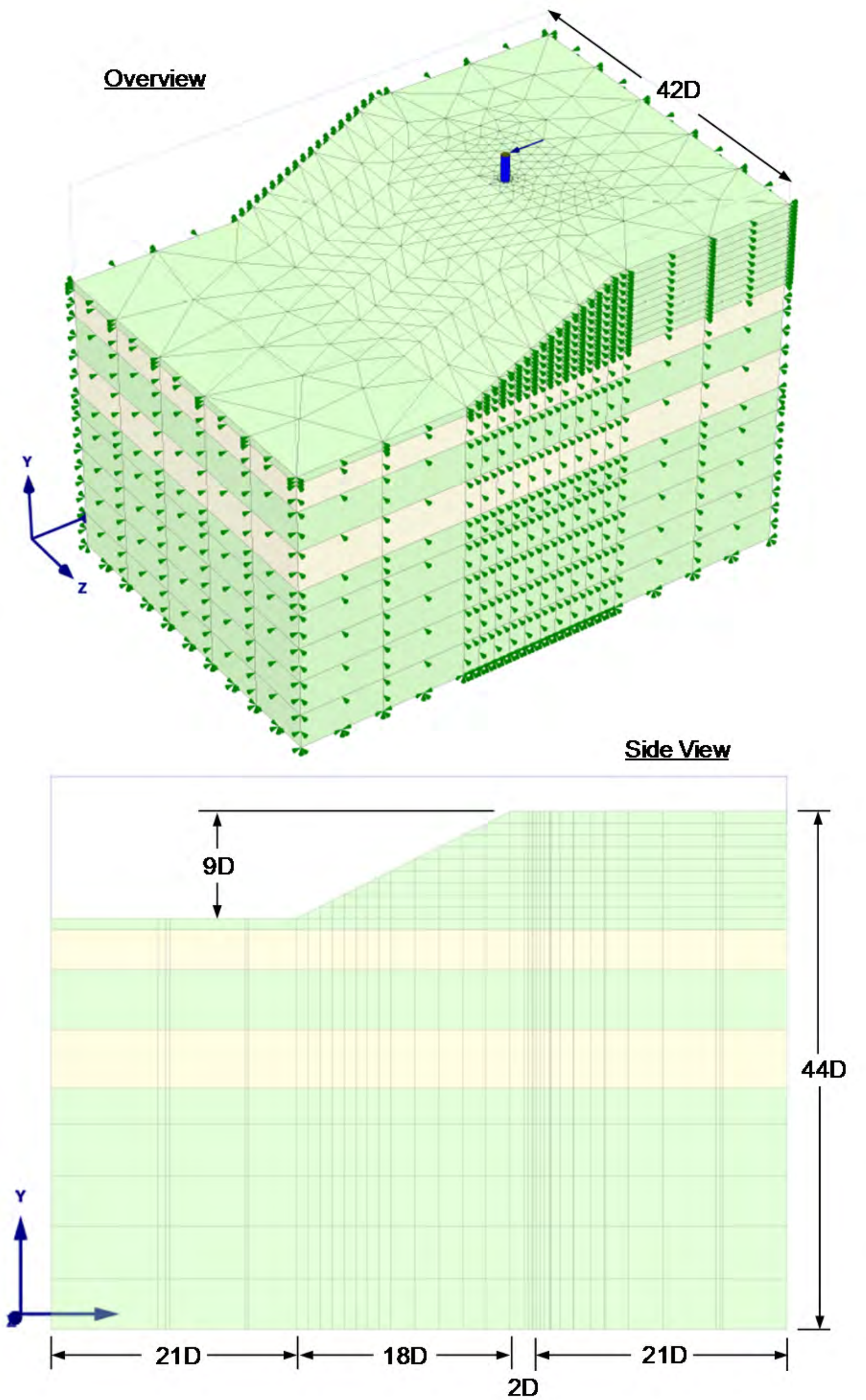

Figure 9-5 Finite Element Mesh for the 2D Pile

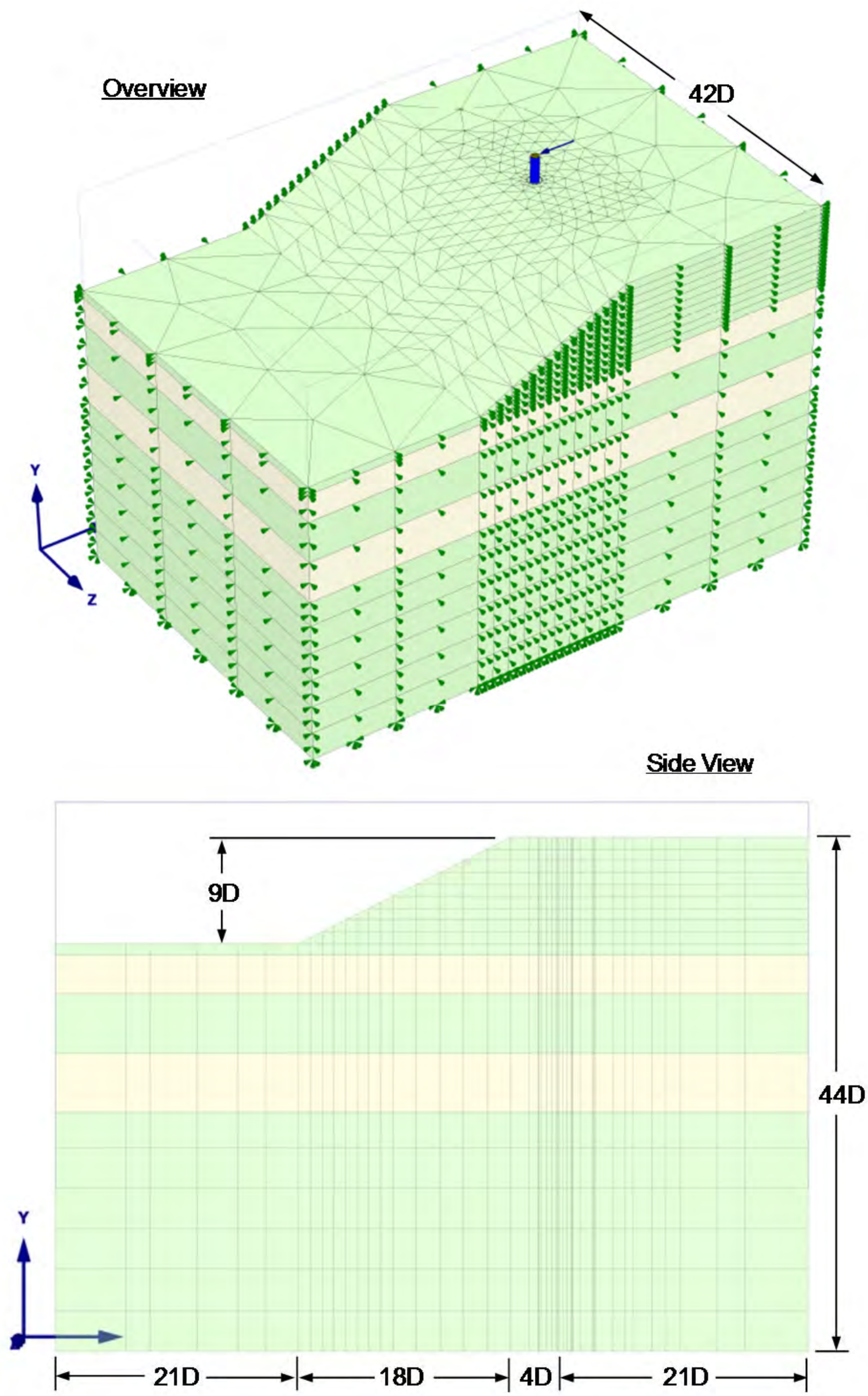

Figure 9-6 Finite Element Mesh for the 4D Pile

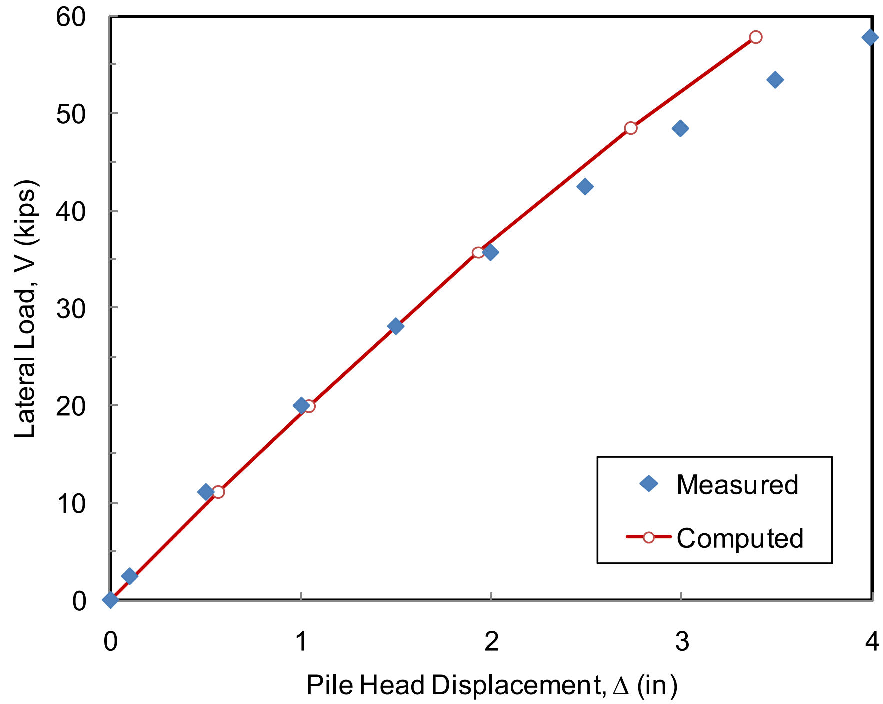

Figure 9-7 Comparison of Load-Displacement Curve from Test Results and FEM Analysis for the Baseline Pile

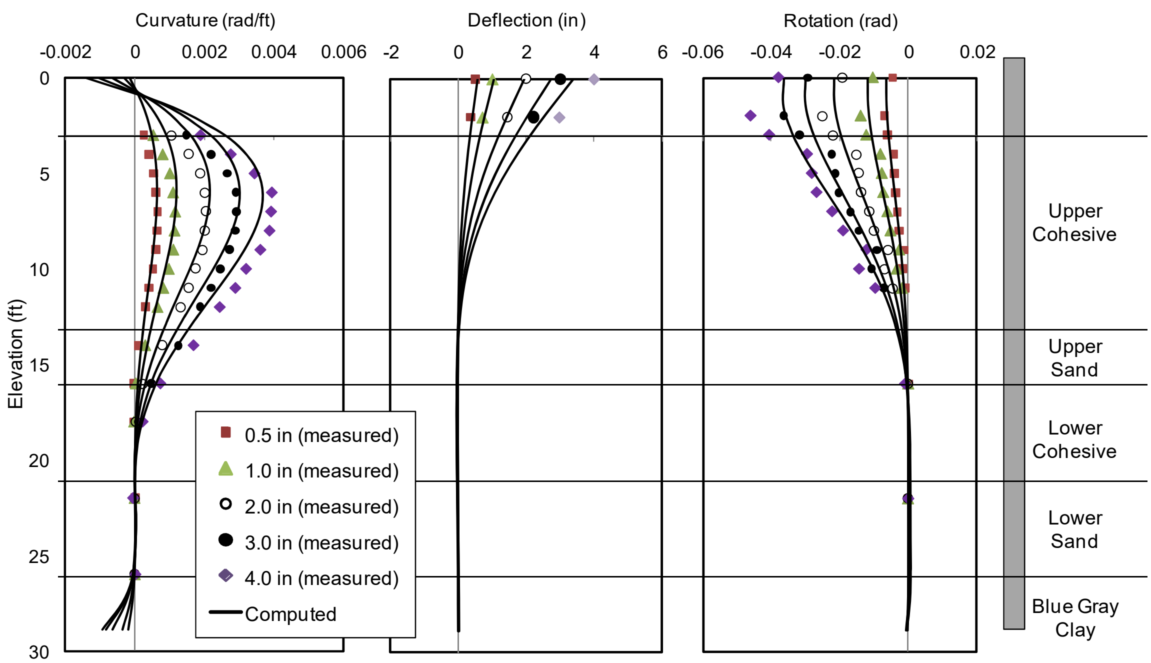

Figure 9-8 Comparison of Test Results and FEM Analysis for the Baseline Pile

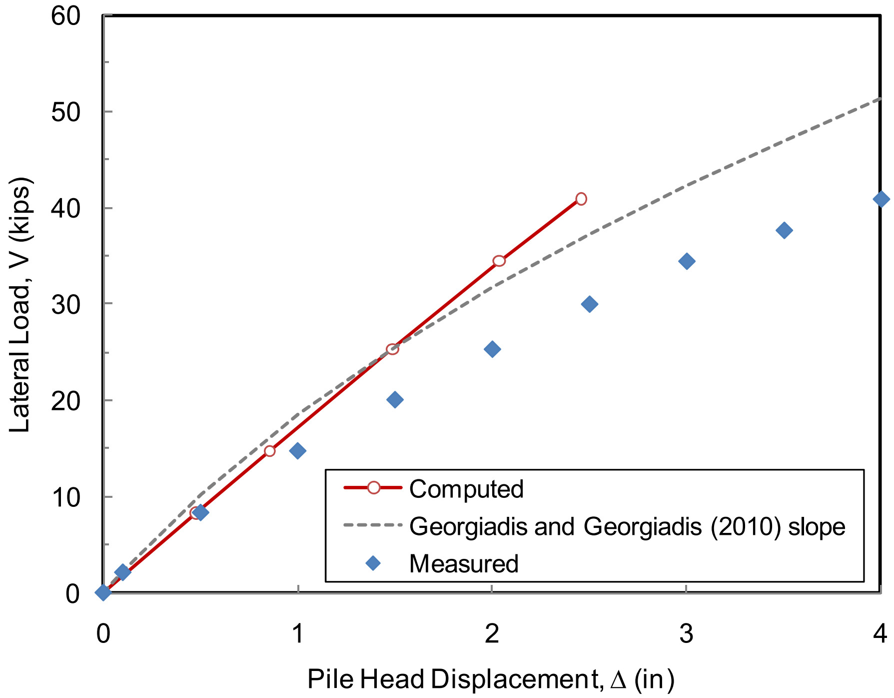

Figure 9-9 Comparison of Load-Displacement Curve from Test Results and FEM Analysis for the 0D Pile

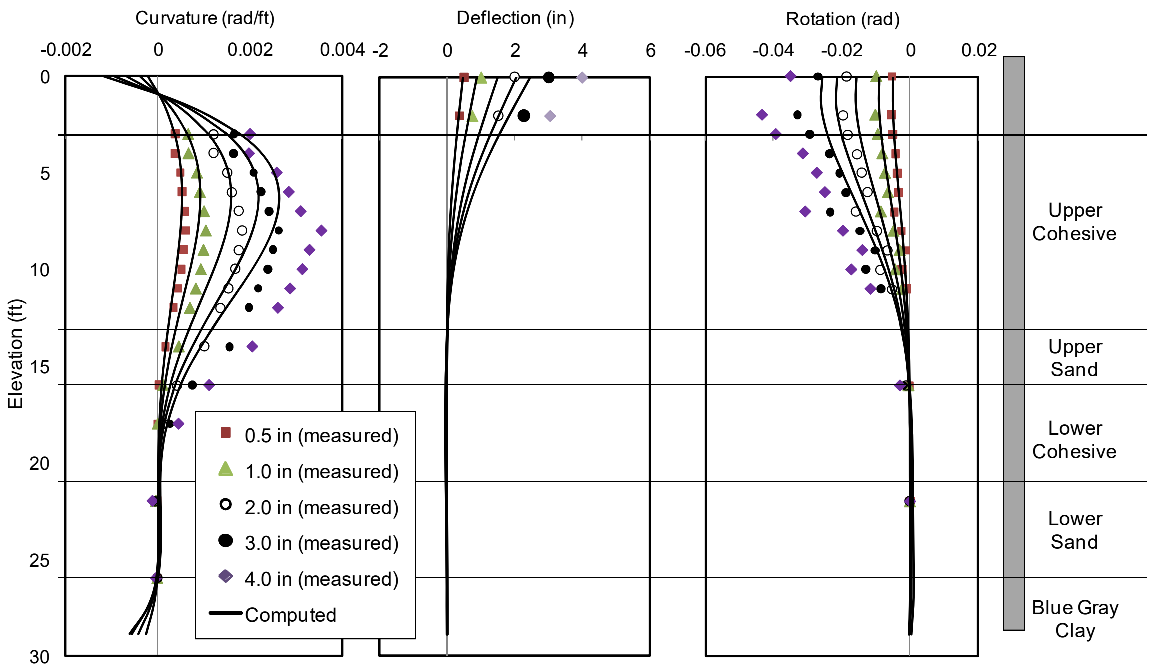

Figure 9-10 Comparison of Test Results and FEM Analysis for the 0D Pile

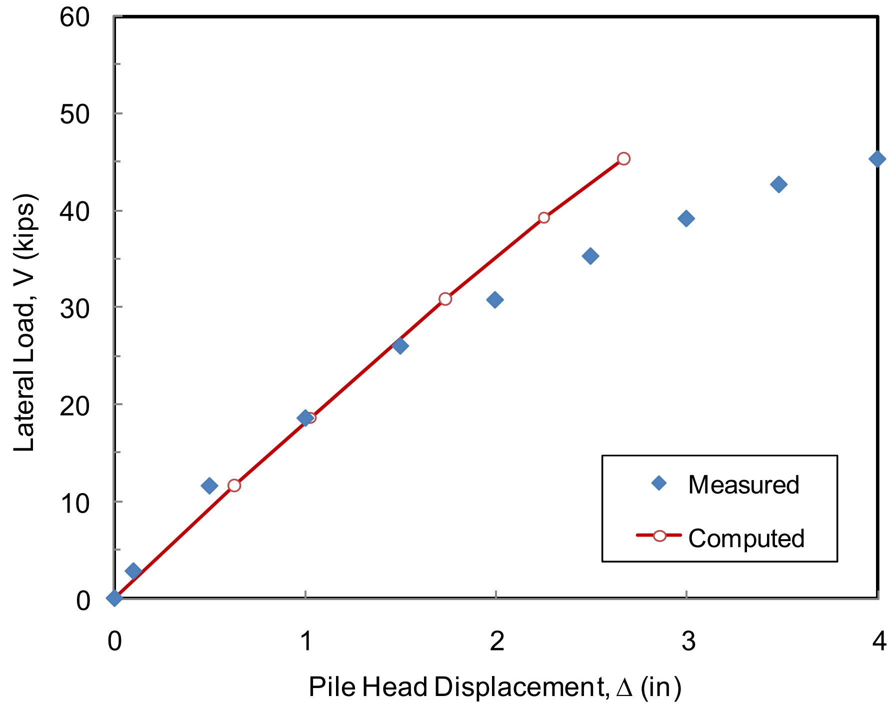

Figure 9-11 Comparison of Load-Displacement Curve from Test Results and FEM Analysis for the 2D Pile

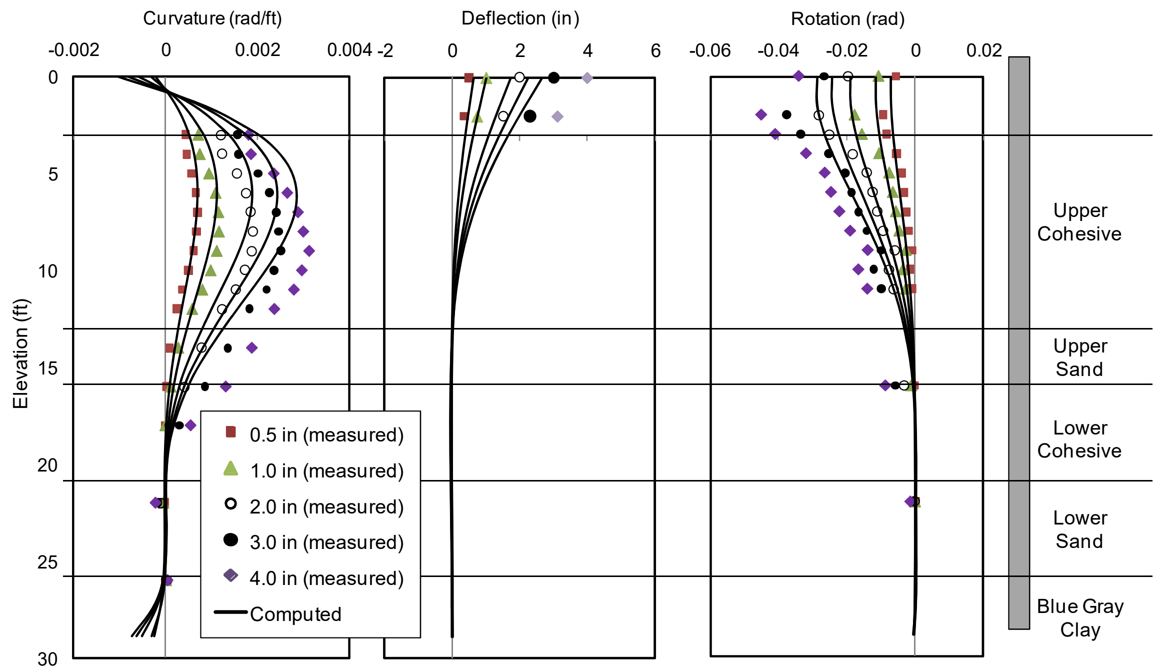

Figure 9-12 Comparison of Test Results and FEM Analysis for the 2D Pile

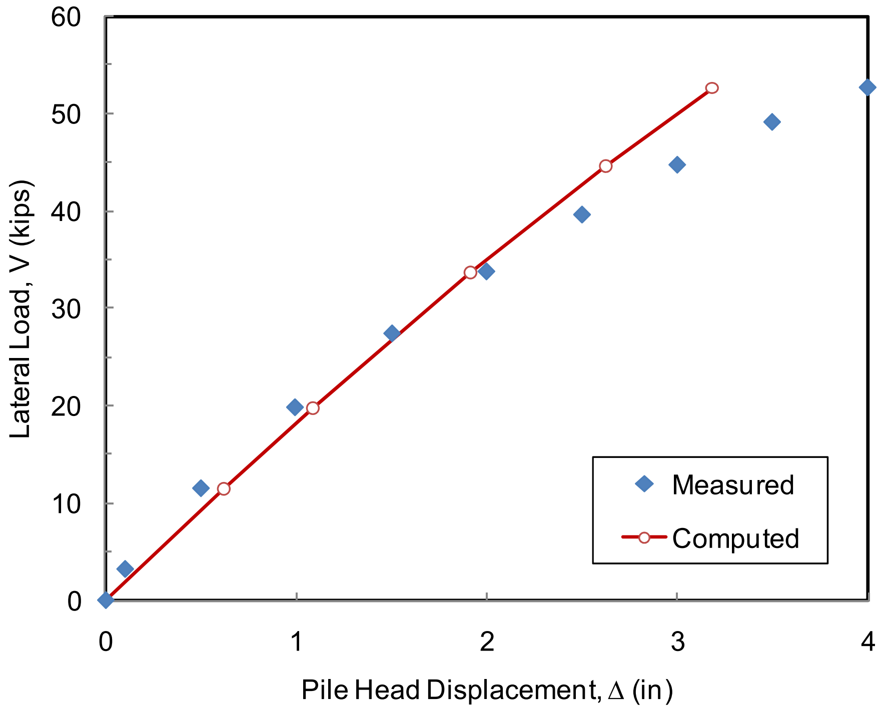

Figure 9-13 Comparison of Load-Displacement Curve from Test Results and FEM Analysis for the 4D Pile

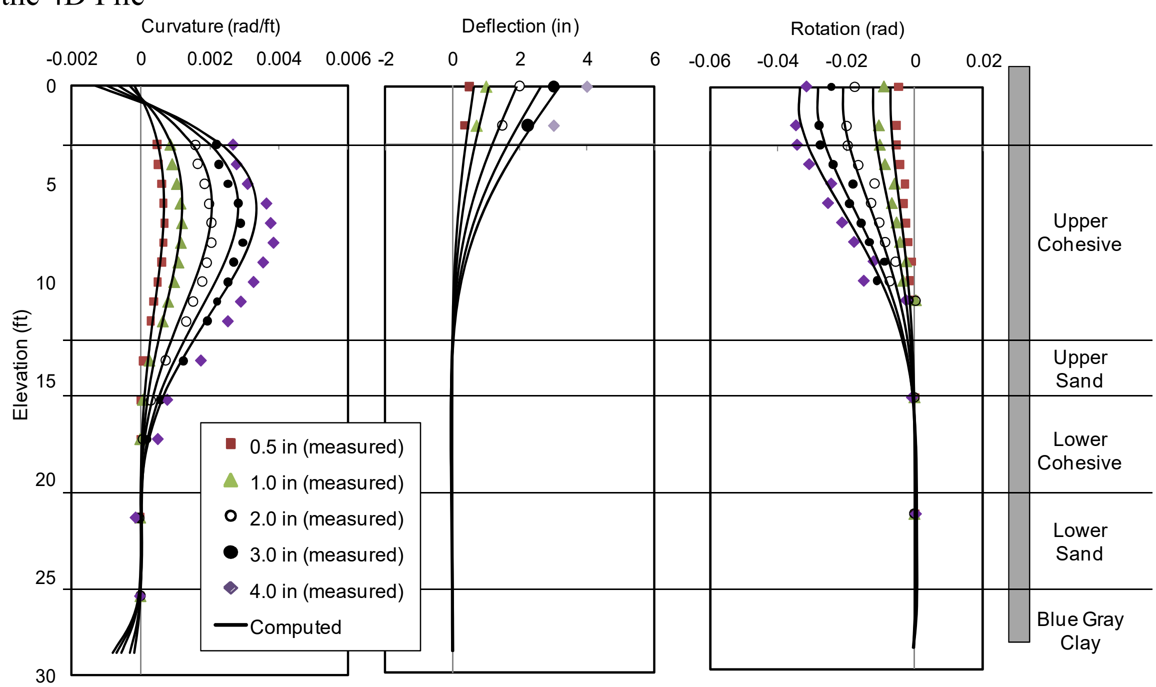

Figure 9-14 Comparison of Test Results and FEM Analysis for the 4D Pile

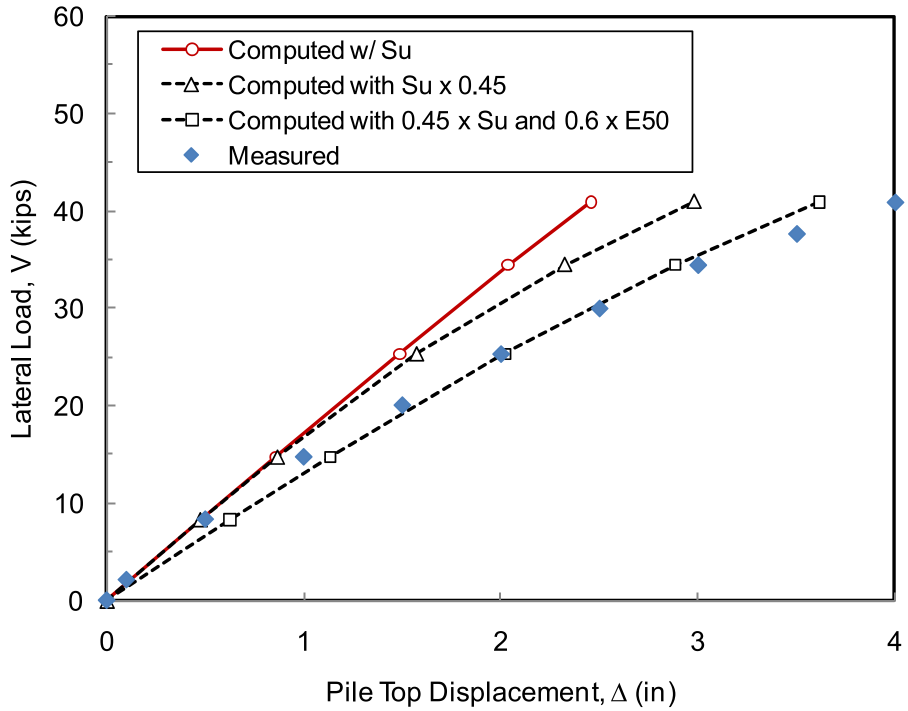

Figure 9-15 Comparison of Load-Displacement Curves from Sensitivity Analysis and the Measured Results for the 0D Pile

10. LATERAL LOAD TESTING -II (COHESIONLESS SOILS)

Ten lateral load tests were performed in order to study the effect of soil slope and batter angle on the performance of piles. A brief description of the observations during the load tests and photographs are provided for the cohesionless testing series.

10.1 BASELINE LOAD TESTS

The 2nd baseline load test, pile P-2, was carried out on August 10, 2011. The same load protocol was used for pile P-2. One foot square gridlines were painted in front of each pile to analyze the ground deformations during lateral pile movement**. Figure 10-1** shows observations made during the 2nd baseline pile test. Some slumping of the soil occurred behind the pile, but a large gap also formed in the cohesionless soil. This is most likely due to apparent cohesion from capillarity effect between soil particles. The embankment, at the time of construction, had a water content between six and nine percent. Ground heaving in front of the pile was observed and increased with increased displacement. Gridlines demonstrate the cracking that occurred in front of the test pile. Large cracks formed in front of the pile and propagated straight out about 4ft. Smaller crackers also formed on both sides of the pile and increased in size and width with an increase in displacement.

The 1st baseline load test, pile P-1, was conducted on July 1, 2011. This load test encountered a problem midway through lateral loading. At a displacement of 3.5 inches the connecting frame between the hydraulic actuator and the test pile slipped and rotated downward. This induced an axial load into the pile during testing. The test was immediately stopped and the pile was unloaded. The connection frame was realigned and the test was completed to a final pile head displacement of 8.0 inches. During testing there was also a slight loading oscillation from the actuator leading a small amount of data scatter. Due to these two factors and a successful 2nd Baseline (Pile P-2) test the results and analyses from the 1st Baseline (P-1) are not included in this report. The connecting frame and actuator oscillation were resolved and were not an issue for the remainder of the tests.

10.2 TESTING OF PILES NEAR AND ON SLOPE

A series of lateral loading tests for piles near the slope crest were carried out, including piles which were located at 8D, 4D, 2D, and 0D from the slope crest. For convenience, these piles are referred to as the 8D pile (P-8), the 4D pile (P-7), the 2D pile (P-6) and the 0D pile (P-9). The main purpose of this series of tests was to investigate the effects of soil slope on lateral capacity of piles installed at different distances from the slope crest.

The lateral load test for 2D pile was conducted on July 19, 2011. **Figure 10-2** shows observations made during lateral load test of the 2D pile. The first major crack observed during the test occurred on the side of the pile propagating out perpendicular to the pile. The following cracks formed along a line with an angle of approximately 35 degrees from the pile axis perpendicular to loading direction on both sides of the pile. These cracks appeared to be the initial movement of a passive soil wedge. At the end of the tests large cracks had formed and the crack patterns are slightly off from symmetrical. At a final pile head displacement of 10 inches a large passive soil wedge movement was apparent out into the slope. This wedge propagated at around a 45 degree angle out from the pile on either side. The wedge formed six pile diameters long and propagated three feet (vertically) down the slope as seen in **Figure 10-2**. Offset was seen between gridlines where the soil wedge had moved outward up to three inches from the original position. Less heave occurred in this test compared to the baseline, but significantly more cracking was seen. A large gap also formed behind the pile.

The lateral load test for the 4D pile (P-7) was conducted on July 22, 2011. The photographs of the observations made during this test are presented in **Figure 10-3.** The observed cracking patterns in this test were similar to those observed in the 2D pile test. At pile head displacement of 1.0 inch, the first minor crack was observed moving outward at a 45 degree angle from the pile and appeared to be the initial formation of a passive wedge. Also, large cracks formed perpendicular to the loading directing at the pile base. The cracking pattern on both side of the gridlines were similar. The test was ceased at a final pile head displacement of 10 inches. Passive wedge cracking on slope occurred at larger displacement than the 2D pile, occurring at pile head displacements larger than 7 inches. A gap also formed behind the pile during testing.

The lateral load test for the 8D pile (P-8) was carried out on July 28, 2011. **Figure 10-4** shows observations made during lateral load test of the 8D pile. No major crack on the slope was observed throughout the duration of the load test, with a final pile head displacement of more than 9 inches. Several minor cracks formed around the 8D pile. Ground heaving in front of the pile was observed similar that observed in the baseline pile load tests.

The lateral load test for the 0D pile (P-9) was conducted on July 12, 2011. **Figure 10-5** shows observations made during lateral load testing of the 8D pile. The first major cracked was observed next to the pile at pile head displacement of 1.25 inch propagating out at a near 45 degree angle. At 3.0 inches of pile head displacement, these cracks moved out 4 ft onto the slope on either side of the pile to show initial signs of a passive wedge movement. Several cracks around and perpendicular to the pile with different patterns were observed during testing. At higher displacement, greater than 4.5 inches, it was apparent that the soil wedge was moving outward with increased load, because the grid lines started to move downslope relative the lines outside of the passive wedge. By the end of the test a large passive wedge had formed on the slope and the majority of the cracking occurred within this area.

The lateral load test for the -4D pile (p-10) was conducted on August 19, 2011. **Figure 10-6** presents observations made during lateral load test of -4D pile. Ground cracking next to the pile was observed at small displacements similar to the 0D and 2D tests. At higher displacement, great than 4.5 inches, it was apparent that the soil wedge was moving outward with increased load, because the grid lines started to move downslope relative the lines outside of the passive wedge. By the end of the test a large passive wedge had formed on the slope and the majority of the cracking was similar to the 0D and 2D.

10.3 BATTERED PILE LOAD TESTS

As presented earlier, the purpose of battered pile test was to compare the performance of battered piles to piles on slope because in practice (i.e. Reese et al., 2004), battered piles are treated as if it was equivalent to piles on the slope. For Series-II, three battered piles were tested in free-field (level ground) conditions, batted at -14, +14, and +26 degrees. A negative batter angle corresponds with a pile battered in the loading direction and, inversely, a positive angle is battered against the loading. The test setup for the three battered pile tests in Series-II was improved to ensure slipping would not occur between pile and the transfer frame. The new loading frame set up consisted of a steel loading plate welded vertically to the battered pile to ensure a lateral load was applied by the actuator as shown in **Figure 10-7A**. These welded plates for the battered piles were designed to ensure connection slipping and local buckling from the large lateral loads would not occur during testing. The free head or zero moment requirements were still met during lateral testing of the Series-II battered piles. The swivel joint in the actuator head provided this free head condition and this was not affected by the different connection set-up (welded plate instead of wooden blocks).

The lateral Load test for the -14 degree battered pile (P-4) was conducted on September 8, 2011. **Figure 10-7** shows observations made during lateral load test of pile P-4 and the new load transfer set up. A relatively small amount of heave occurred during the testing directly in front of the pile. A small gap formed behind the pile during testing. The majority of the cracking was small and fanned out around the front of the pile in the region of heaving. This area was within a 2-ft diameter around the pile.

The lateral Load test for the +14 degree battered pile (P-3) was conducted on September 1, 2011. **Figure 10-8** shows observations made during this lateral load test of pile P-3. During this test, heaving occurred over a broader area when compared to pile P-4. The heave was apparent at five pile diameters directly in front of the pile at the end of testing. Larger cracking also occurred during this battered pile test. Cracking occurred around the front of the pile with the largest cracks propagating directly out and perpendicular with the load direction.

The lateral Load test for the +26 degree battered pile (P-5) was conducted on August 26, 2011. **Figure 10-9** shows observations made during this lateral load test of pile P-5. Heaving was significant during this test, the largest amount of heave out of the ten piles tested in Series-II. Heaving was apparent 7 ft directly in front of the pile by end of testing. A very large crack formed directly in front of the pile in the area of most heave. Slumping of the material was seen in front of and behind the pile. Smaller cracking was also observed at a distance further out during this test.

10.4 CRACKING AND SHEAR FAILURE ANGLE

According to Reese et al. (2006) the shear failure angle of a passive soil wedge in cohesionless soils ranges between ϕ and $\phi/2$ and states that angle is dependent on the soil density.

Higher density leads to a higher friction angle, ϕ, and therefore a larger shear failure angle, Ω. **Figure 10-10** shows the passive wedges from the full-scale tests ranged between 24° and 39°. This angle increased with greater distances from the slope crest. A recommendation of 70% of ϕ was found for the shear failure angle in dense cohesionless material. The cracking patterns observed for all tests were drawn with 1 ft square gridlines. These are shown in **Figure 10-11** through **Figure 10-15**.

10.5 FACTORS EFFECTING TESTING RESULTS

Special care was taken throughout testing to ensure testing conditions were as consistent as possible between each load test. With full-scale testing many outside factors can influence the results. For this research experiment these factors include: weather, construction details, soil conditions, equipment compliance and malfunction, and human error.

Changing weather conditions may have had an influence on the overall results. These factors include temperature and moisture. The total amount of rainfall throughout the period of testing was 1.26 inches. The greatest amount of rain occurred between the 0D and 2D load test where almost 1.0 inches of rain fell. There was a day of dry weather before testing of the 2D pile. The number of days with precipitation was 5 days during the course of testing and the average high was between 66 and 89 degrees Fahrenheit. The weather most likely had limited effects on testing results. The rain before the 2D test likely had the largest weather related effects on testing. During testing, the depth to moisture in the embankment was typically between 2”-5” below the surface.

Care was taken to restrict movement of testing equipment in front of testing piles when possible. The weight of the testing equipment may have slightly densified the soil around the level ground piles resulting in a slight increase in soil stiffness. This is not considered to have a major effect on the test results because the embankment was constructed at a relatively high compaction to begin with. Testing equipment was not taken in front of the near slope piles.

The cohesive soils below the testing embankment likely experience consolidation after placement of the embankment resulting in added axial load on the test pile but likely had little effect on the lateral loading results. Even though nuclear density gauge testing was conducted to verify the density of the cohesionless embankment during construction, it is likely the density in the embankment may have varied slightly resulting in variations in soil stiffness.

10.6 SUMMARY

Ten full scale lateral load tests were conducted during Series-II, including two baseline pile tests, four piles near sloping ground tests, one pile on slope test and three battered pile tests. Major observations are heaving of the ground in front of the pile for the baseline pile tests, 8D test and the three battered tests. A gap formed behind all test piles as well as cracking of the ground around the pile. The test results of each test are presented in the next section. **Table 10-1** presents the testing dates for all piles tested during Series-II.

The laterally loaded piles in proximity to a slope (i.e., the 4D, 2D, 0D, -4D piles) formed visible passive soil wedges as displacements increased. It is believed that this type of soil failure occurred because of the removal of soil volume in front of the pile allowing for the wedge to overcome resistance and move out laterally. The closer the proximity to the slope the sooner (at lower loads and displacements) the passive wedge cracking formed on the ground surface. Heaving was more evident in the baseline, battered, and 8D tests as pile head displacements increased. For the majority of the tests, cracks formed near the pile along the line perpendicular to the loading direction. The presence of asymmetrical cracks can be attributed to inherent soil variability imperfection of the loading direction and lateral movement of the soil within passive wedges

Table 10-1 Testing Dates for Series-II Lateral Load Tests

Pile	Orientation	Testing Date
P-1	Baseline	7/1/2011
P-2	Baseline	8/10/2011
P-3	14° Batter	9/1/2011
P-4	-14° Batter	9/8/2011
P-5	26° Batter	8/26/2011
P-6	2D	7/19/2011
P-7	4D	7/22/2011
P-8	8D	7/28/2011
P-9	0D	7/12/2011
P-10	-4D	8/19/2011

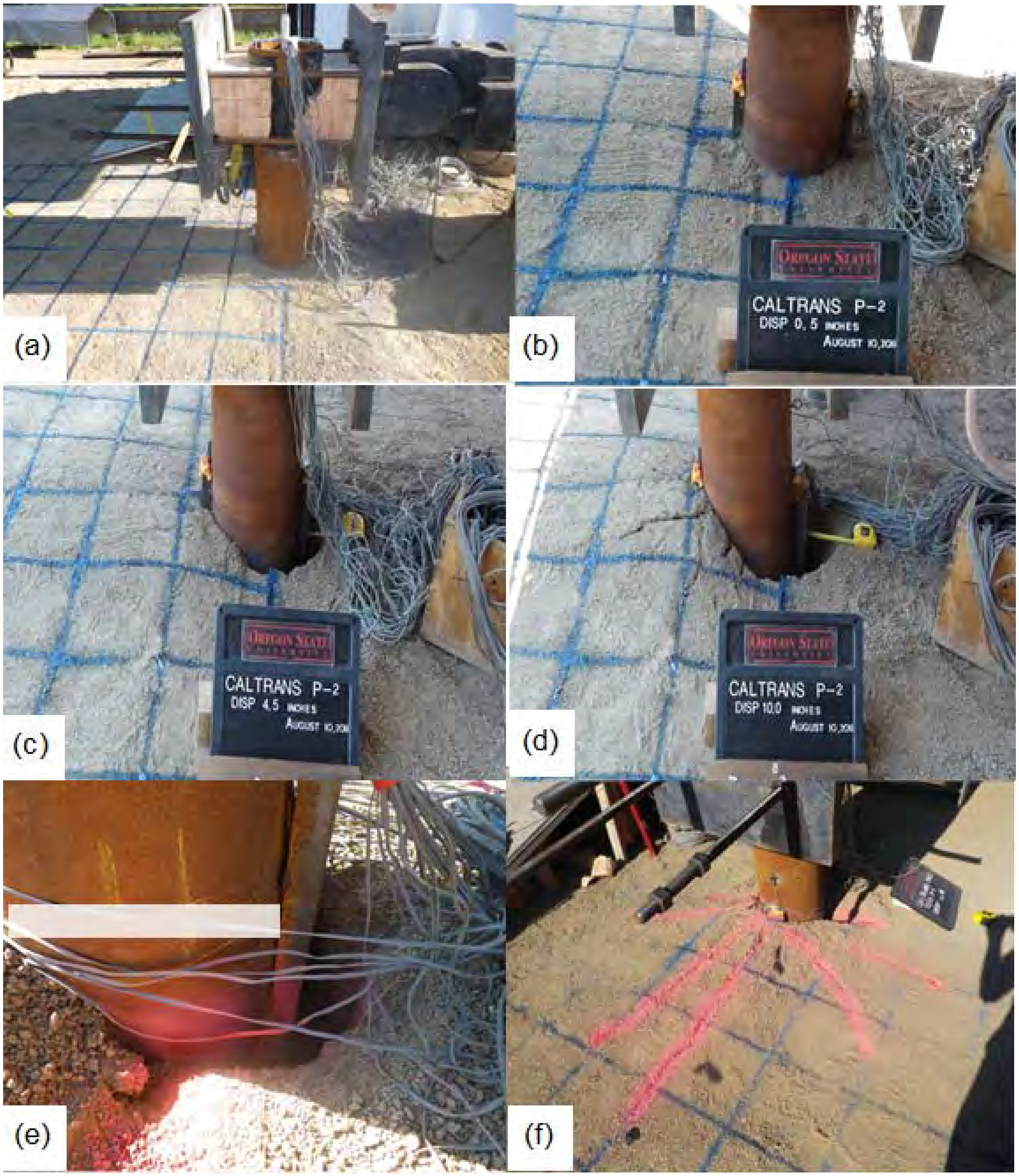

Figure 10-1 Observations during load test of first and second baseline piles
a) Pile before loading b) Pile at 0.5” of displacement c) Pile at 4.5” of displacement d) Pile at end of testing e) Gap formation behind pile f) Heave and cracking in front of pile

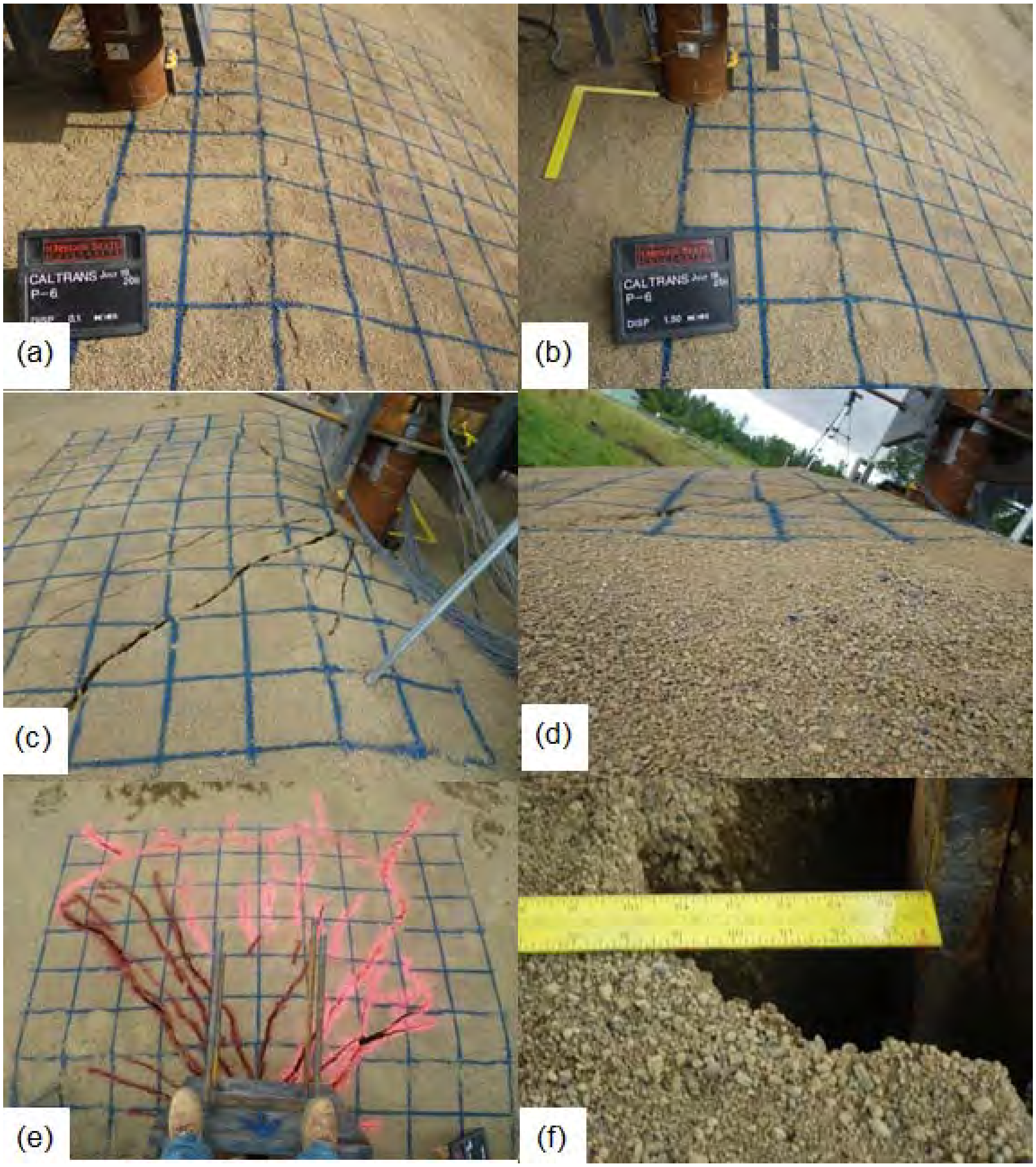

Figure 10-2 Observations during lateral loading testing of pile P-5 (2D)
a) Pile before loading b) Pile at 1.5” of displacement with cracks forming c) Pile at 8.0” of displacement with passive wedge cracking d) Passive wedge movement on slope e) Passive wedge movement in front of pile at end of testing f) Gap formation behind pile

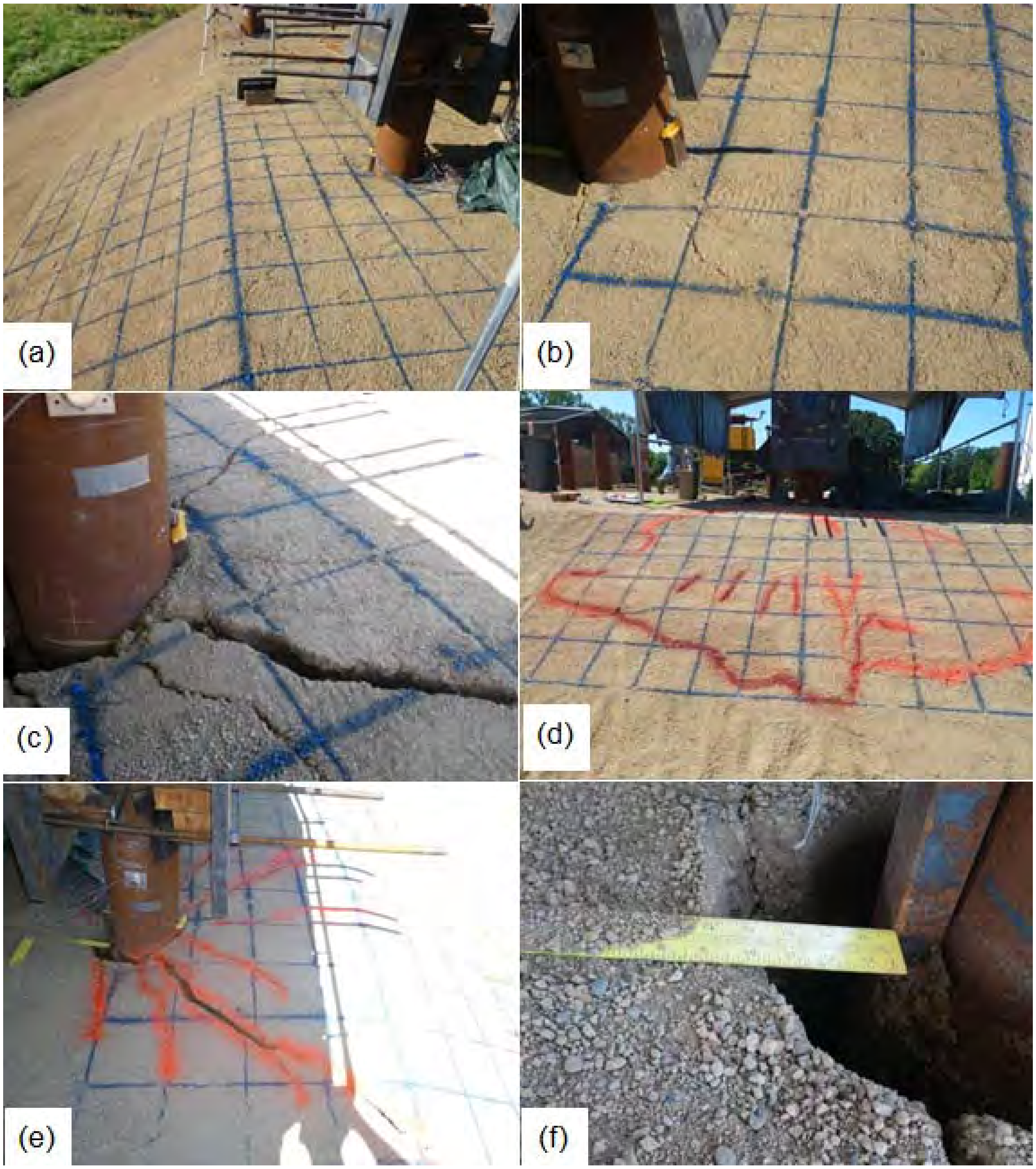

Figure 10-3 Observations during lateral loading testing of pile P-6 (4D)
a) Pile before loading b) Pile at 3.5" of displacement with large cracking c) Pile at 8.0" of displacement with passive wedge cracking d) Passive wedge cracking on slope e) Passive wedge movement in front of pile f) Gap formation behind pile

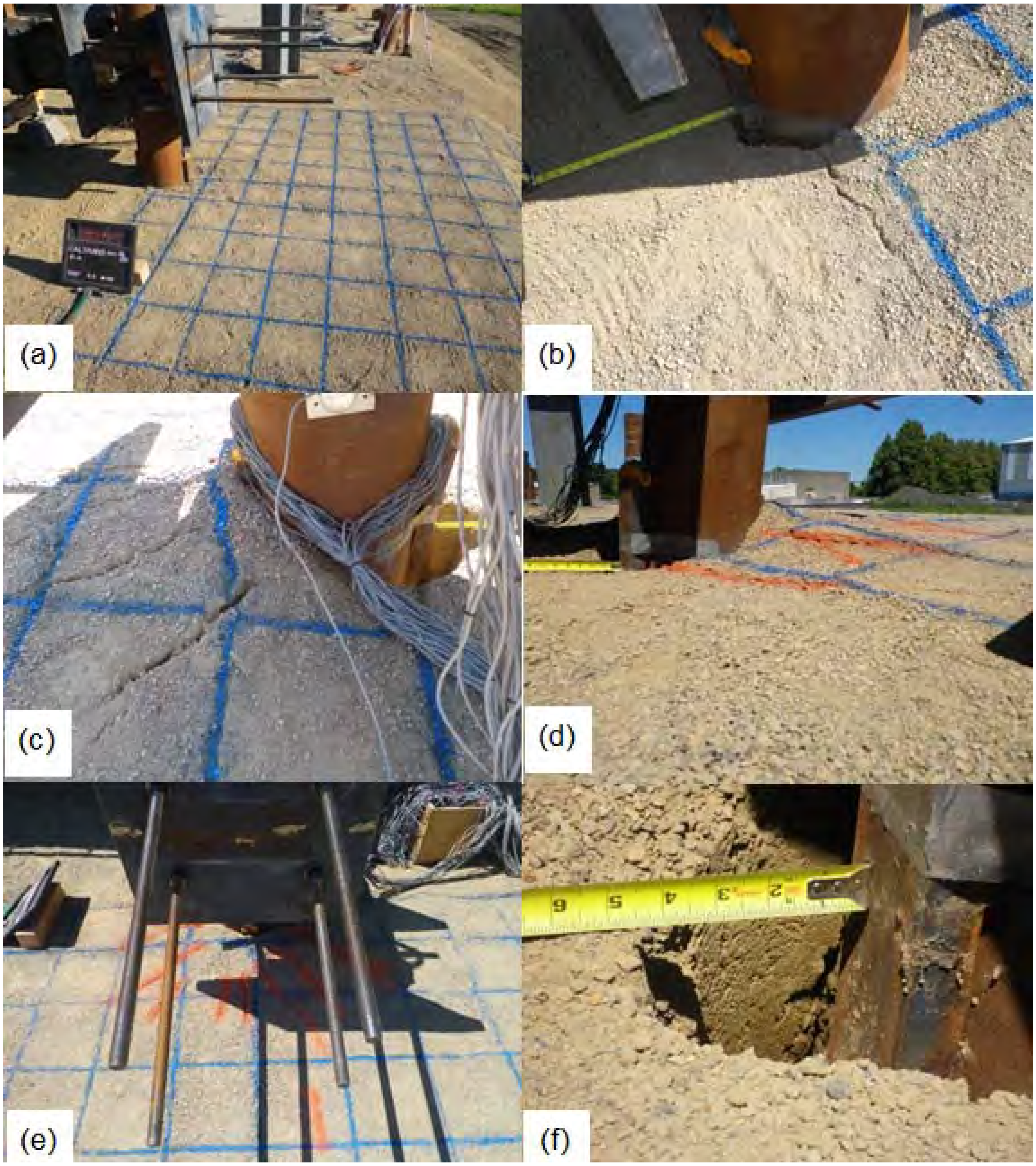

Figure 10-4 Observations during lateral loading testing of pile P-8 (8D) a) Pile before loading b) Pile at 0.5” of displacement c) Pile at 5.0” of displacement with cracking d) Soil heave at end of testing e) Soil cracking at end of testing f) Gap formation behind pile

Figure 10-5 Observations during lateral loading testing of pile P-9 (0D)
a) Pile before loading b) Pile at 5.0” of displacement with cracks forming c) Pile at 10.0” of displacement with passive wedge cracking d) Passive wedge movement on slope at end of testing e) Passive wedge movement at end of testing f) Gap formation behind pile

Figure 10-6 Observations during lateral loading testing of pile P-10 (-4D)
a) Pile eat 0.5" of displacement b) Pile at 5.0" of displacement c) Pile at 10.0" of displacement with passive wedge cracking d) Passive wedge movement on slope

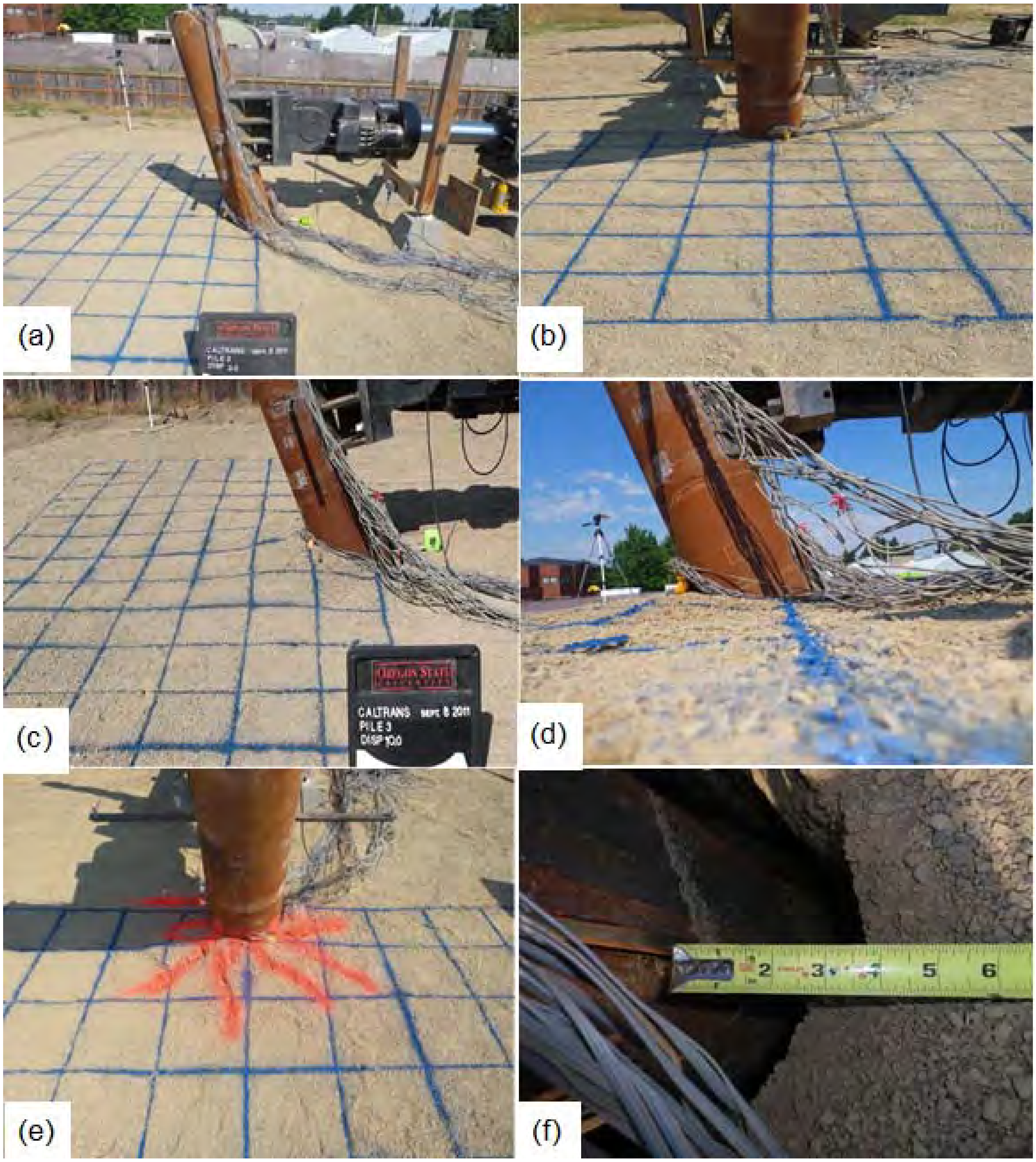

Figure 10-7 Observations during Lateral Loading Testing of Pile P-4 (-14 Batter) a) Pile before loading b) Front of pile before loading c) Pile at 10.0” of displacement d) Soil heave at end of testing e) Soil cracking at end of testing f) Gap formation behind pile

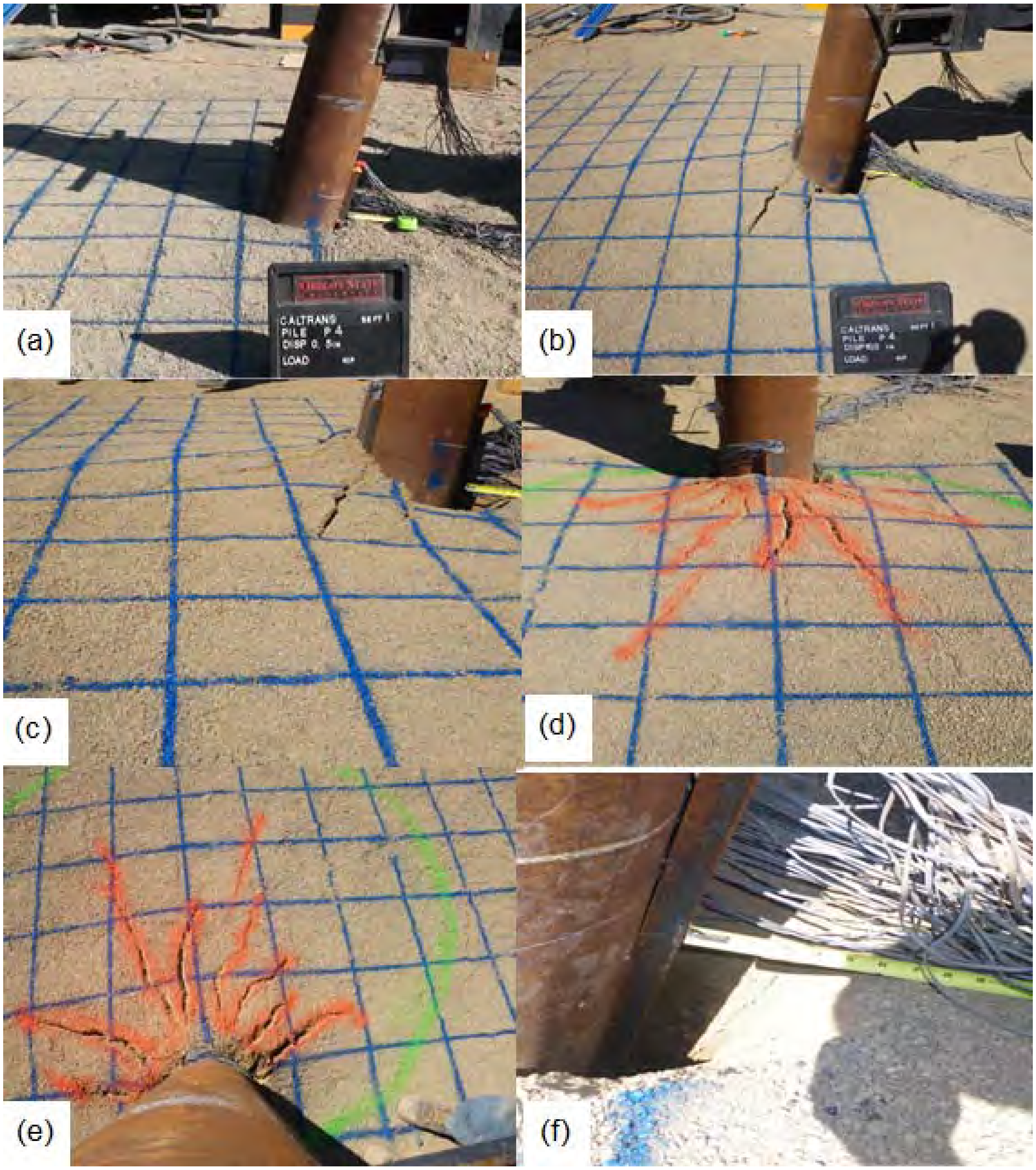

Figure 10-8 Observations during Lateral Loading Testing of Pile P-3 (+14 Batter) a) Pile before loading b) Pile at end of testing c) Soil heave at end of testing d) Soil heave at end of testing e) Extensive cracking and heave f) Gap formation behind pile

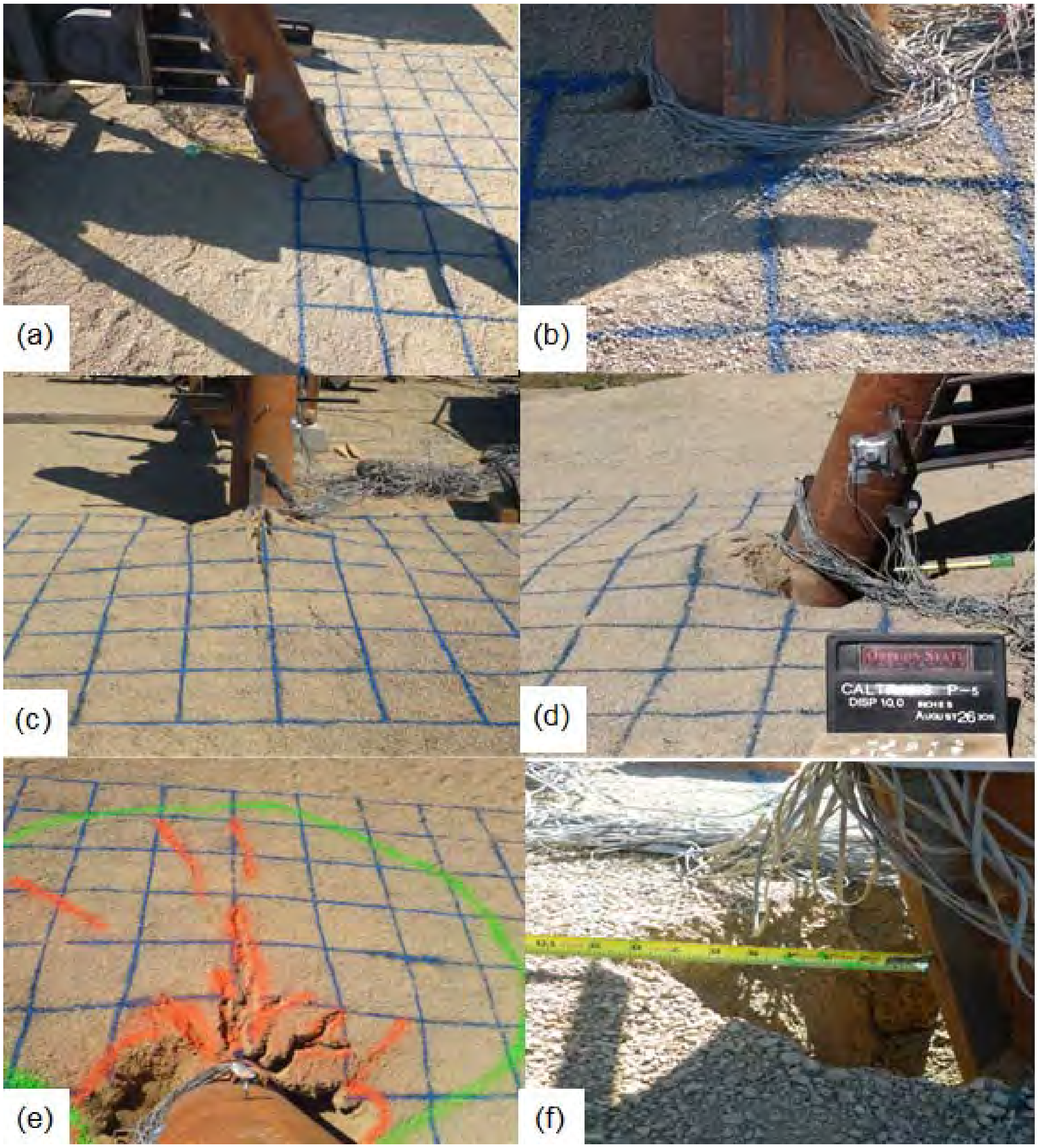

Figure 10-9 Observations during Lateral Loading Testing of Pile P-5 (+26 Batter) a) Pile before loading b) Front of pile before testing c) Soil heave and cracking at end of testing d) Soil heave at end of testing e) Extensive cracking f) Gap formation behind pile

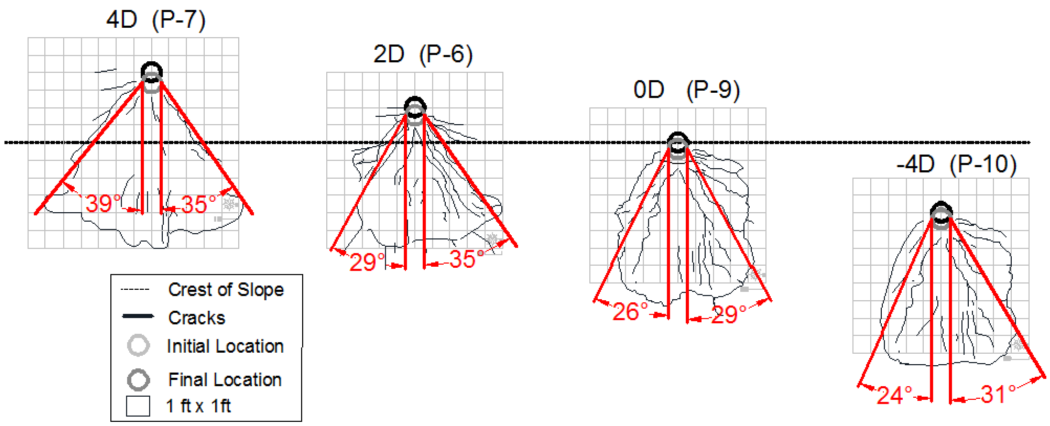

Figure 10-10 The Shear Failure Angle, Ω, for the Near Slope Tests

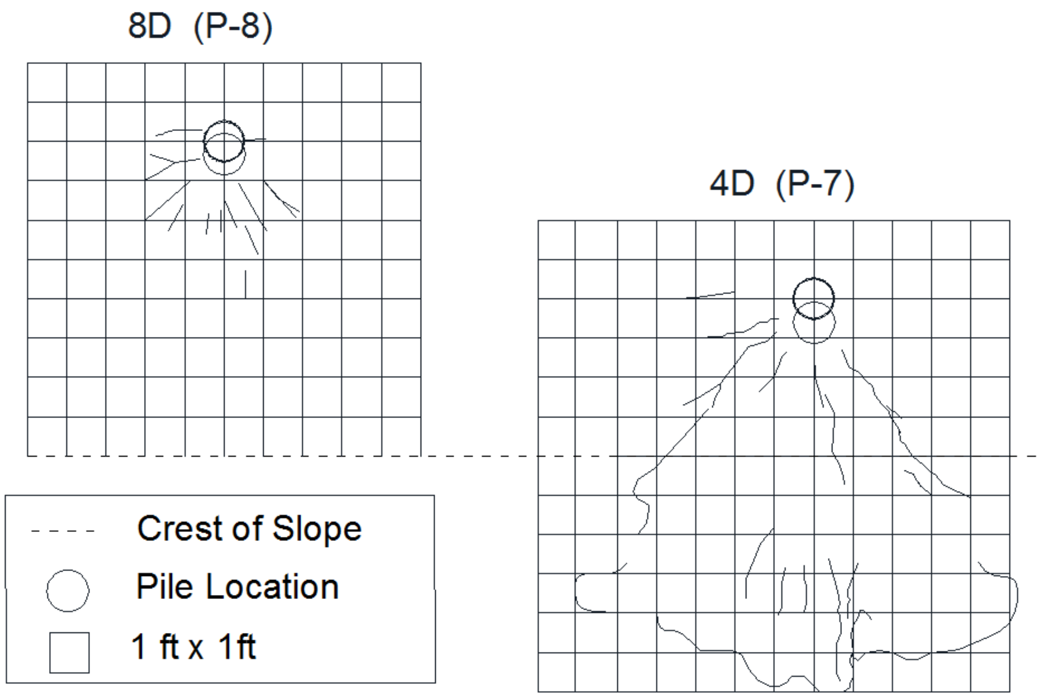

Figure 10-11 Cracking Patterns for the 8D And 4D Test Piles

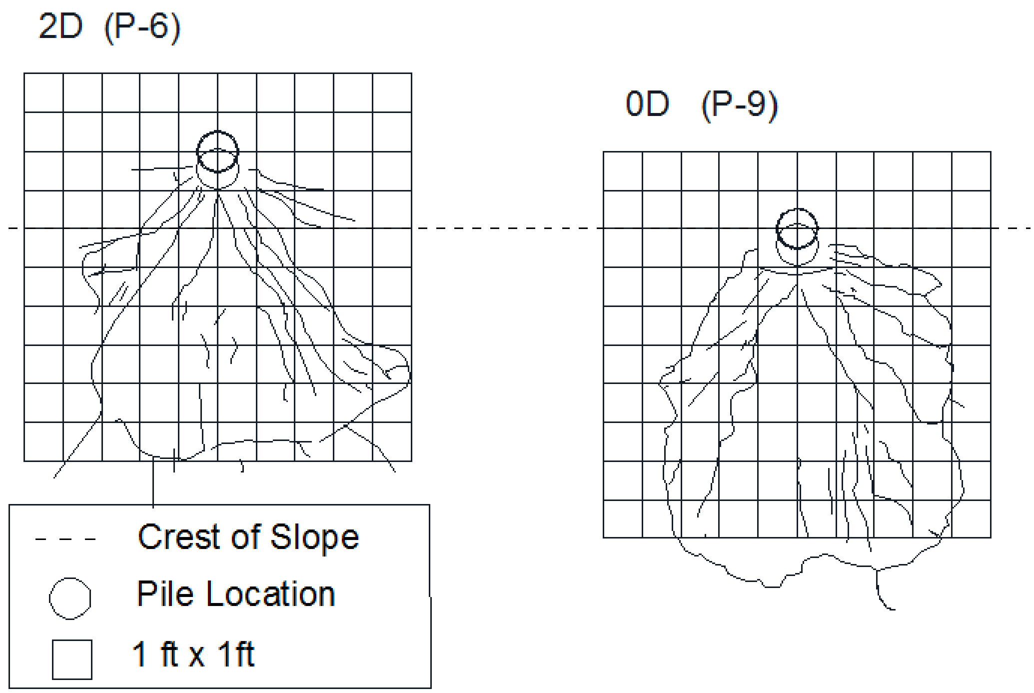

Figure 10-12 Cracking Patterns for the 2D and 0D Test Piles

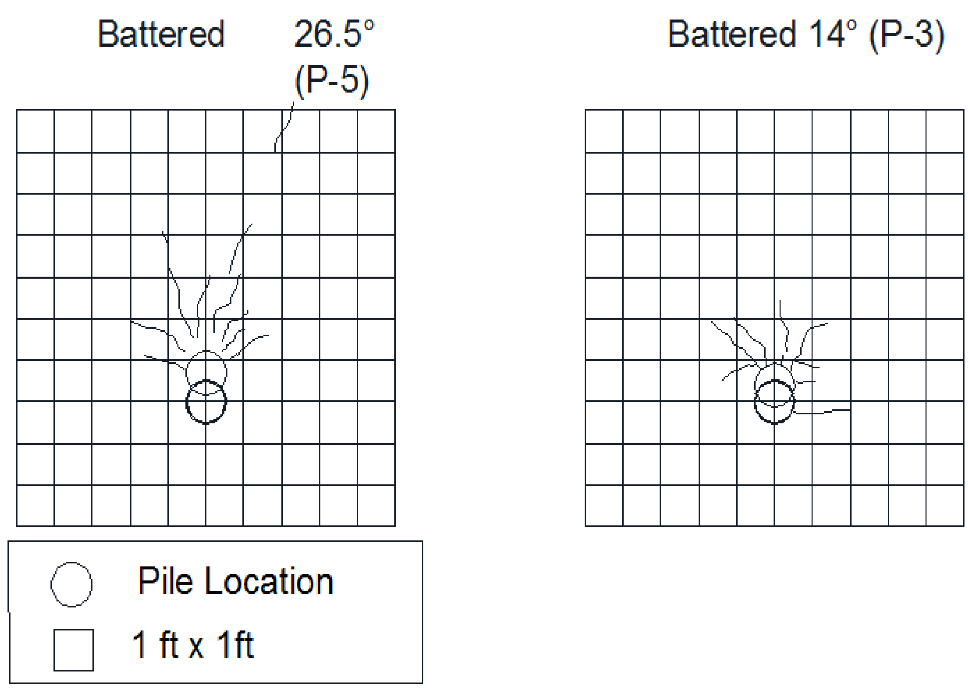

Figure 10-13 Cracking Patterns for the +26° and +14° battered test piles

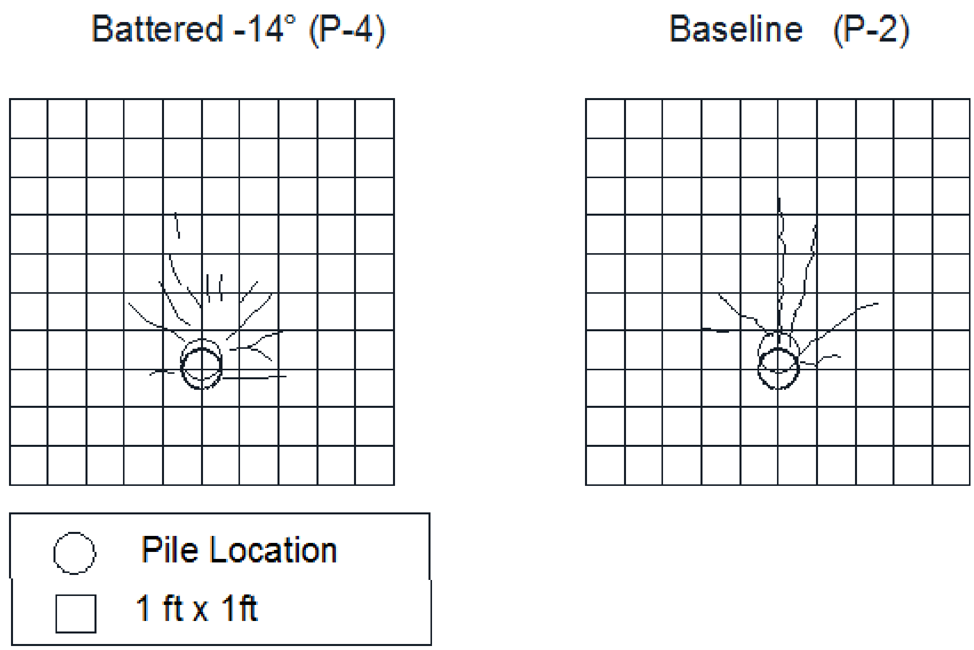

Figure 10-14 Cracking Patterns for the Baseline and -14° Battered Piles

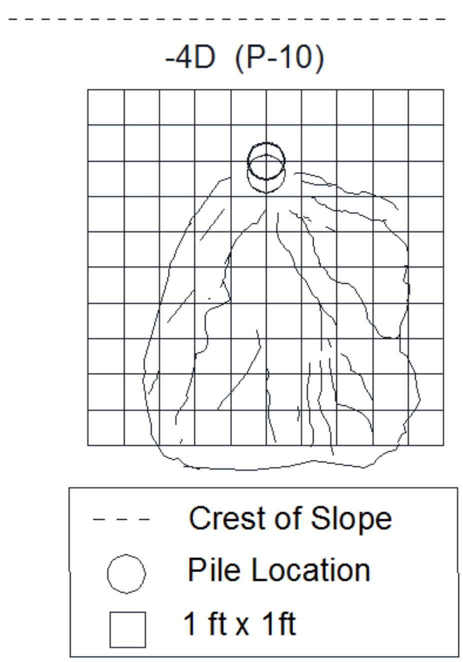

Figure 10-15 Cracking Patterns for the -4D (on slope) Pile

11. TEST RESULTS FROM SERIES-II (COHESIONLESS SOILS)

This section presents the test results from all lateral load tests conducted during Series-II. A comparison of the results of piles installed at different distances from the slope crest that were tested under similar soil loading conditions, offers insight into the effect of slope on the lateral load response of piles. This chapter presents the load displacement curves, curvature, and rotation for each test. During each targeted displacement hold of 5 to 10 minutes, stress relaxation was seen in the load displacement curves. This relaxation tended to level off and stay constant within a 2 to 5 minute period. Note: the rotation figures in this chapter have zero elevation located at the ground surface and the curvature plots have zero elevation located at the point of loading (3ft above ground surface).

11.1 BASELINE LOAD TESTS PILE 8D FROM SLOPE

In this section, test results for the baseline pile (P-2) and the pile located at 8D from the slope crest (P-8) are presented. A comparison between measured responses for baseline and 8D piles are discussed.

11.1.1 LOAD DISPLACEMENT CURVES AND TESTS

Load-displacement curves under short term static loading for the baseline and 8D piles are presented in **Figure 11-1**. The load carrying capacity of the baseline pile (P-2) was 8.8 kips and 29.5 kips at target pile head displacements of 0.25 and 1.0 inch, respectively. For the 8D pile, the load-displacement curve was similar to the baseline pile. The 8D curve was slightly stiffer between 1 inch and 4 inches of displacement, but still considered to be similar curves. The difference is most likely caused by discontinuities in the embankment. The measured load of the 8D pile was 9.0 and 29.7 kips at target pile head displacements of 0.25 and 1.0 inch respectively. Both piles had a maximum lateral capacity of approximately 87 kip.

11.1.2 CURVATURE AND ROTATION PROFILES

In addition to the load-displacement comparison, a comparison of the calculated curvature and rotation profiles for the second baseline pile and the 8D pile are presented in **Figure 11-2**. The measured response between these piles was similar in shape and load. Based on comparisons of the load-displacement curves, and the curvature and rotation profiles, it was concluded that the effects of slope on the lateral capacity of piles is insignificant when piles are installed at 8D or greater from the slope crest. The results from the 2nd baseline pile and the 8D pile were considered as baseline results for subsequent analyses. The results from the lateral loading test for the Baseline pile were analyzed and referenced as the 8D results. Thus, the second baseline test (P-2) data was analyzed for the comparison of both the 8D and baseline information.

The calculated curvature and measured rotation at different depths for the baseline pile are presented in **Figure 11-3** and **Figure 11-4**, respectively. The calculated curvature from the strain gauge data indicates that the location of the maximum moment occurred at a depth of 3 ft below the ground surface corresponding to a depth of 3D. At all target pile head displacements, no significant strain was observed at a depth of 25 ft. No significant rotation was measured from the tiltmeter below depths of 10 ft below ground surface. These results indicate that; the spacing of sensors at deeper elevations was reasonable, additional sensors at deeper elevations were not necessary, and that the test piles were long enough to behave as flexible long piles under lateral loading.

11.2 LATERAL LOAD TEST FOR PILE P-7 (4D)

Presented in the following sections are the load displacement curves along with the curvature and rotation profiles for the lateral load test conducted on Pile P-7. This pile was tested four pile diameters (4ft) from the slope crest. The results from this lateral load test are presented beside the baseline test results for comparison and discussion.

11.2.1 LOAD DISPLACEMENT CURVE

Figure 11-5 presents the load-displacement curve for Pile P-7 (4D). The initial stiffness, up to a pile head displacement of 2.5 inches is similar to the baseline curve. Thereafter, the stiffness and load are lower to a final displacement of ten inches. At displacements of 0.25, 0.5 and 1.0 inch the lateral load was 9.4 kip, 16.5 kip and 30.0 kip, respectively. For these lower displacements, the load was similar to the baseline pile test. These loads, when compared to the baseline, demonstrate that the proximity of the slope had no effect on the lateral capacity at 4D from the crest at small displacements. The peak capacity saturated at a load of 78 kip around a pile head displacement of 5.5 inches through the end of the load test. This capacity was less than the baseline demonstrating a noticeable effect from the presence of the 2:1 test slope at high displacements, above 2.5 inches at the point of loading. **Figure 11-6** and **Figure 11-7** present the curvature and rotation profiles, respectively with depth along the 4D pile. The curvature profile is obtained and calculated from the strain gauge data for selected pile head displacement. The rotation profile from the 4D was obtained from the tilt sensor data.

11.3 LATERAL LOAD TEST FOR PILE P-6 (2D)

Presented in the following sections are the load displacement curves along with the curvature and rotation profiles for the lateral load test conducted on Pile P-6. This pile was tested two pile diameters (2ft) from the slope crest. The results from this lateral load test are presented beside the baseline test results for comparison and discussion.

11.3.1 LOAD DISPLACEMENT CURVES

Figure 11-8 presents the load-displacement curve for Pile P-6 (2D). The initial stiffness, up to a pile head displacement of 2.5 inches is similar to the baseline curve. Thereafter, the stiffness and load are lower to a final displacement of ten inches. At displacements of 0.25, 0.5 and 1.0 inch the lateral load was 7.9 kip, 14.7 kip and 29.1 kip, respectively. For these lower displacements, the load was similar to the baseline pile test. These loads, when compared to the baseline, demonstrate that the proximity of the slope had little to no effect on the lateral capacity at low displacements. The peak capacity saturated at a load of 78.0 kip around a pile head displacement of 6.5 inches through the end of the load test. This load displacement curve is similar in ultimate capacity and shape to the 4D pile throughout the entire test. This magnitude was less than the baseline demonstrating an effect from the presence of the test slope at high displacements, above 2.5 inches at the point of loading. **Figure 11-9** and **Figure 11-10** present the curvature and rotation profiles, respectively with depth along the 2D pile. The curvature profile is obtained and calculated from the strain gauge data for selected pile head displacement. The rotation profile from the 2D was obtained from the tilt sensor data.

11.4 LATERAL LOAD TEST FOR PILE P-9 (0D)

Presented in the following sections are the load displacement curves along with the curvature and rotation profiles for the lateral load test conducted on Pile P-9. This pile was tested on the slope crest. The results from this lateral load test are presented beside the baseline test results for comparison and discussion.

11.4.1 LOAD DISPLACEMENT CURVES

Figure 11-11 presents the load-displacement curve for Pile P-9 (0D). The initial stiffness was lower than the baseline at smaller pile head displacements. The stiffness remained lower throughout the duration of the test. At displacements of 0.25, 0.5 and 1.0 inch the lateral load was 5.5 kip, 10.5 kip and 21.8 kip, respectively. For these lower displacements, the load was less at all data points compared to the baseline pile test. These loads, when compared to the baseline, demonstrate that the proximity of the slope had a significant effect on the lateral capacity. The peak capacity saturated at a load of 65 kip around a pile head displacement of 7.0 inches through the end of the load test. This resistance was about 20 kip less than the baseline peak, demonstrating there is also a significant effect at higher lateral displacements. **Figure 11-12** and **Figure 11-13** present the curvature and rotation profiles, respectively with depth along the 0D pile. The curvature profile is obtained and calculated from the strain gauge data for selected pile head displacements.

11.5 LATERAL LOAD TEST FOR PILE P-10 (-4D)

Presented in the following sections are the load displacement curves along with the curvature and rotation profiles for the lateral load test conducted on Pile P-10. This pile was tested four pile diameters (4 ft) horizontally behind the crest onto the slope. The results from this lateral load test are presented beside the baseline test results for comparison and discussion.

11.5.1 LOAD DISPLACEMENT CURVES

Figure 11-14 presents the load-displacement curve for Pile P-10 (-4D). The initial stiffness was lower than the baseline at smaller pile head displacements. The stiffness remained lower throughout the duration of the test. At displacements of 0.25, 0.5 and 1.0 inch the lateral load was 4.8 kip, 9.2 kip and 16.5 kip, respectively. For these lower displacements, the load was significantly less than when compared to the baseline pile test and the 0D. These loads, when compared to the baseline, demonstrate that the proximity of the slope had significant effect on the lateral capacity. The peak capacity saturated at a load of 51 kip around a pile head displacement of 7.0 inches through the end of the load test. This demonstrates that the -4D pile was affected by the slope a substantial amount throughout the entire lateral load range. **Figure 11-15** and **Figure 11-16** present the curvature and rotation profiles, respectively with depth along the -4D pile. The rotation profile from the -4D was obtained from the tilt sensor data.

11.6 COMPARISON OF TEST RESULTS WITH CALTRANS

For a steel pile with a 12-inch diameter, Caltrans BDS (2003) requires the lateral capacity of piles under Service Limit State Load, with maximum horizontal deflection of 1/4 inch, (BDS Article 4.5.6.5.1) of 5 kips for piles fully embedded in soil. To compare with the Caltrans requirement (i.e., piles fully embedded in soil), the tiltmeter data was utilized to estimate the soil-pile deflection at the ground surface for each pile. A comparison between the measured load and soil displacement at the ground surface is presented in **Figure 11-17.** The top graph in this figure represents the load displacement curves at the ground surface for each non-battered test pile with a dot representing the Caltrans 5 kip specification. The bottom is the same load displacement curve shown with ground surface displacements of less than 1.0 inch. The results indicate that all tested piles meet the required capacity of 5 kips at 1/4 inch of pile deflection at the ground surface. The load was significantly higher (10-15 kips) than 5 kips for all tests, except the -4D pile where the load was just above this threshold.

11.7 LOAD DISPLACEMENT CURVES FOR BATTERED PILES

The load-displacement curves for the three battered pile tests (P-3, P-4, and P-5) are presented in **Figure11-18** along with the baseline and -4D curve for comparison. Pile P-4 with a -14° batter angle (battered in same direction as the load) had the highest stiffness of all piles tested in this study. The ultimate capacity was also significantly higher with a peak load measured at the pile of head of 113 kip compared to 87 kip for the baseline pile. The higher load and stiffness of pile P-4 was similar to predictions for this testing case. The greater load and stiffness is likely due to the direction of the soil failure mechanism. This negative battered pile, when loaded laterally, forces the passive soil wedge to move laterally and in a downward direction. This downward movement of the wedge interacts with deeper, and presumably stiffer, soils results in the increased resistance. Pile P-3 (14° positive batter) had the lowest stiffness of the tested battered piles and was also lower than the baseline pile. The maximum capacity of pile P-3 was 78 kip.

Pile P-5 with a positive batter angle of 26° (battered in the opposite direction of loading) was initially stiffer (up to a displacement of 2.5 in) than the baseline pile. At higher displacements the stiffness and load quickly decreased with a final capacity of 81 kips, 6 kips less than the baseline. This reduction is likely due to the upward movement of the passive soil wedge. According to Reese *et al*. (2004), battered piles are treated as if it was equivalent to a pile on a slope with a similar angle. Therefore, predictions suggest that the load displacement curves of pile P-5 would be similar to pile P-10, which was tested on a 26° or 2H:1V slope. Comparing the curves on **Figure11-18**, the battered pile had a significantly higher capacity and the stiffness was greater throughout the entire range of displacements. The trend does not fit the suggestions that a batter angle and slope of similar angle act in the same mechanism.

Figure 11-19 presents the LPILE predictions for all battered piles and the baseline pile load displacement curves. The predicted load displacements for pile P-3 (+14°) and P-4 (-14°) follow the same trend as the full-scale results (**Figure11-18**), with Pile P-4 reaching higher loads than the baseline and Pile P-3 with lower loads than baseline. Overall, LPILE predictions of stiffness and loads are conservative, but accurately predict the trends observed in full-scale results. **Figure 11-20** compares the load ratio model used for LPILE battered pile predictions with the +14° and -14° battered pile results. This figure demonstrates that the full-scale ratios match well with the ratios used in LPILE predictions.

Pile P-5 (+26°) has a much higher than predicted stiffness and load where it was predicted to have to lowest of all battered tests. A conclusion was made from analyzing the load displacement data from this battered pile that the testing equipment was near its limitations to laterally load a pile with this steep batter angle. According to the United States Army Corps of Engineers (USACE, 2005) a pile should rarely be battered at an angle greater than 20° and never greater than 26°. The results from the full-scale test are likely inaccurate, due to testing a pile at this upper batter angle limit. The unexpectedly high stiffness and load are likely due to unintended axial loading

11.8 SUMMARY OF LATERAL LOAD TEST RESULTS

Results from pile near slope tests (-4D, 0D, 2D and 4D) indicate that slope has an impact on the lateral capacity of piles at target pile head displacements. **Figure 11-21** displays all non-battered load displacement curves. For the 0D and -4D piles the slope had a significant effect for all ranges of pile head displacements. For the 2D and 4D piles the slope had little to no effect for displacements less than 2.0 inches. Piles eight pile diameters or greater from the crest show no impact from the presence of a soil slope. Battered pile P-5 (26°) is significantly different than the load displacement curve of the pile on slope (-4D), it is stiffer and has a higher overall load. Pile P-3(+14°) and P-4 (-14°) followed the trends observed in the LPILE, where LPILE was conservative in the overall load-displacement curves for Series-II battered piles.

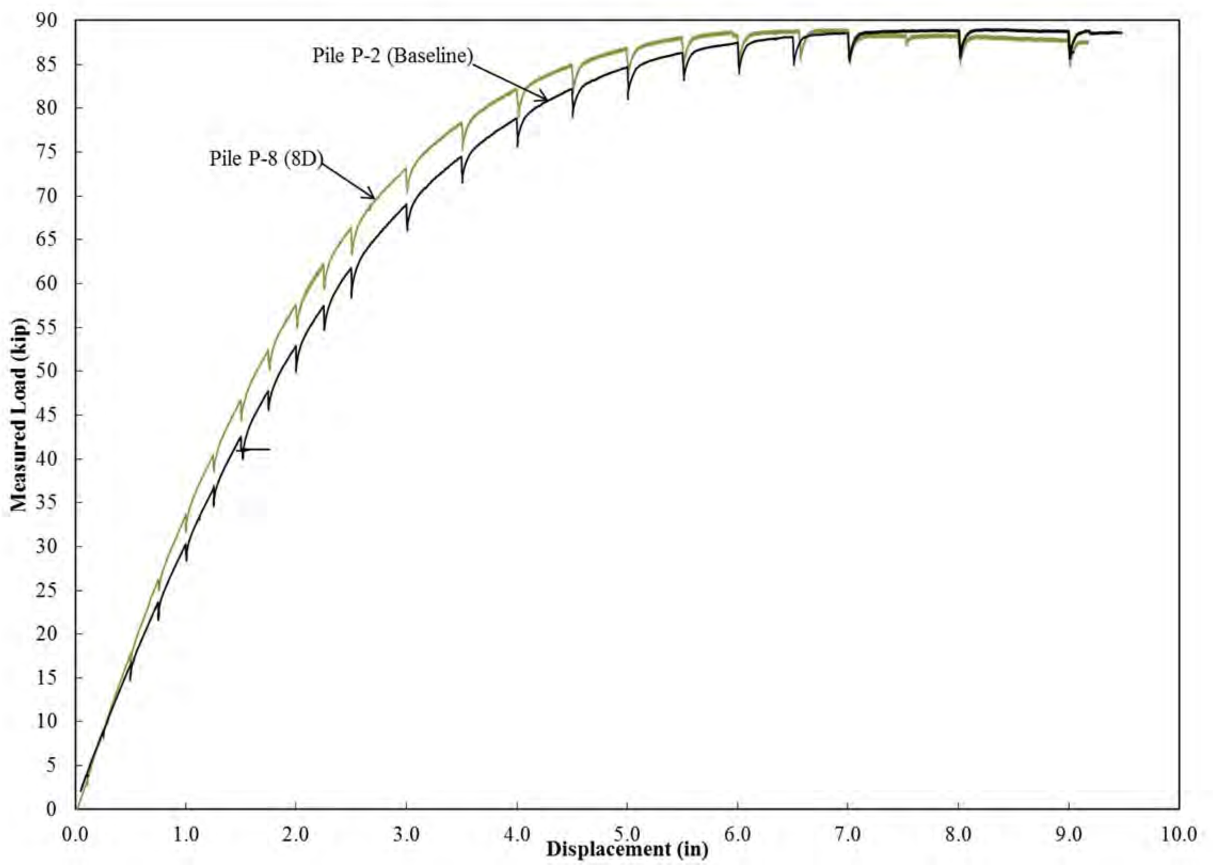

Figure 11-1 Comparison of Load-Displacement Curves between the Baseline Pile (P-2) and the 8D Pile (P-6)

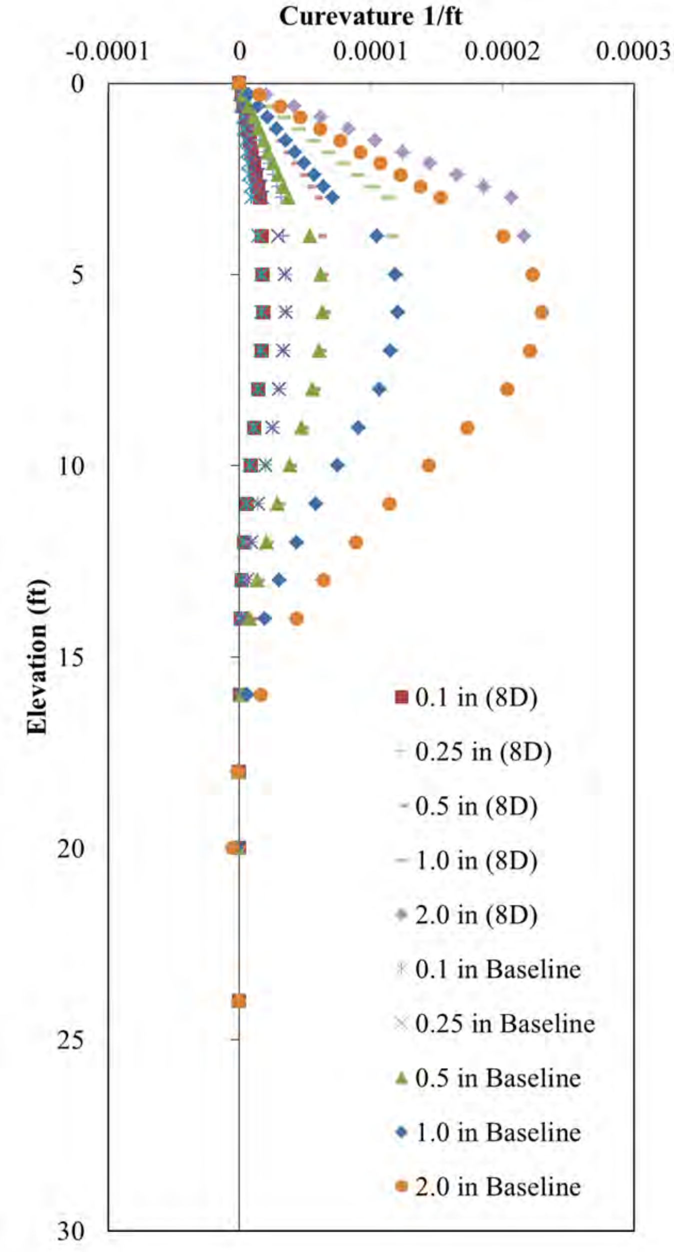

Figure 11-2 Comparison of Calculated Curvature for 2nd Baseline Pile (P-2) and 8D pile (P-8)

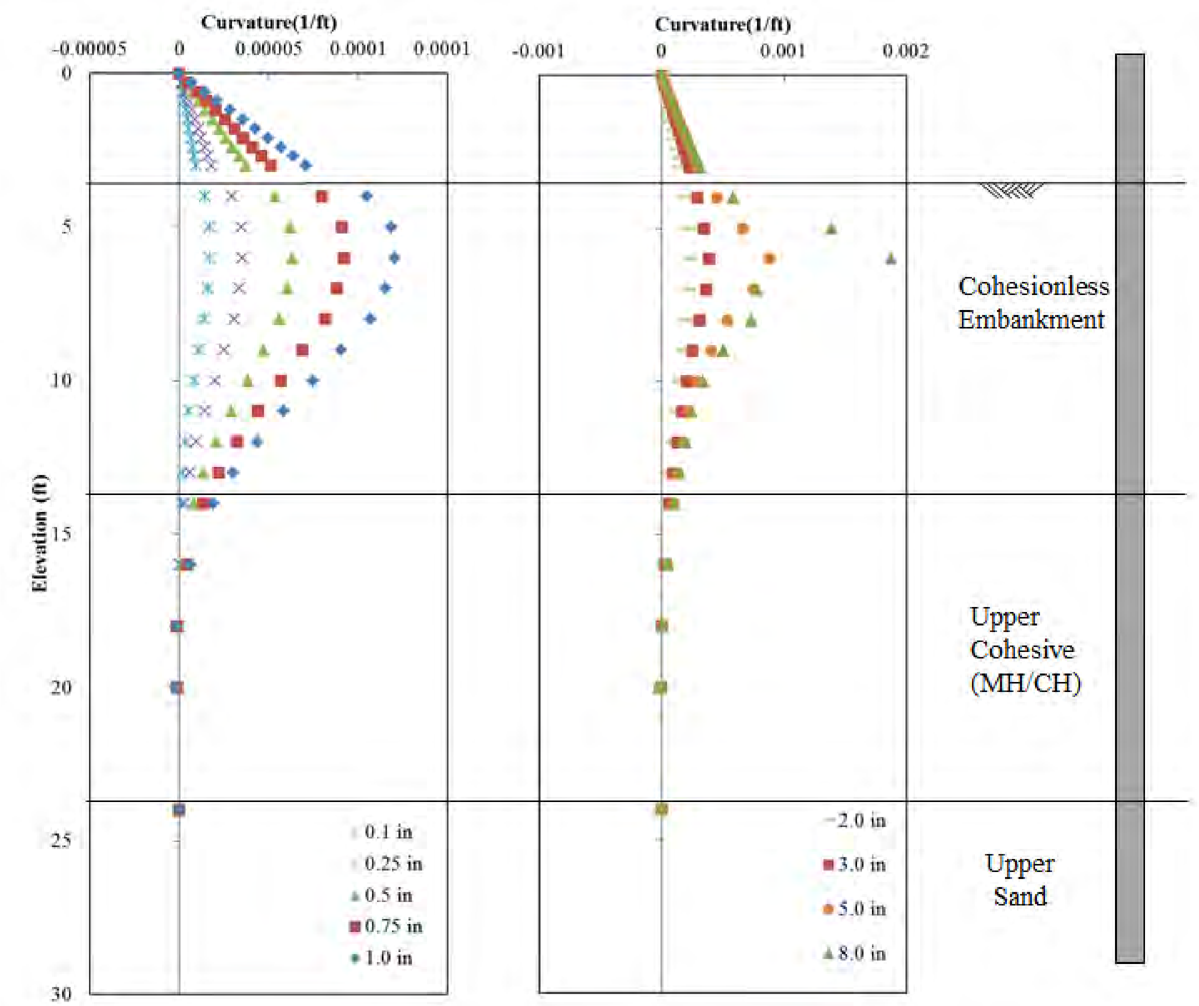

Figure 11-3 Curvature Results for Baseline Pile (P-2) at varying Displacements

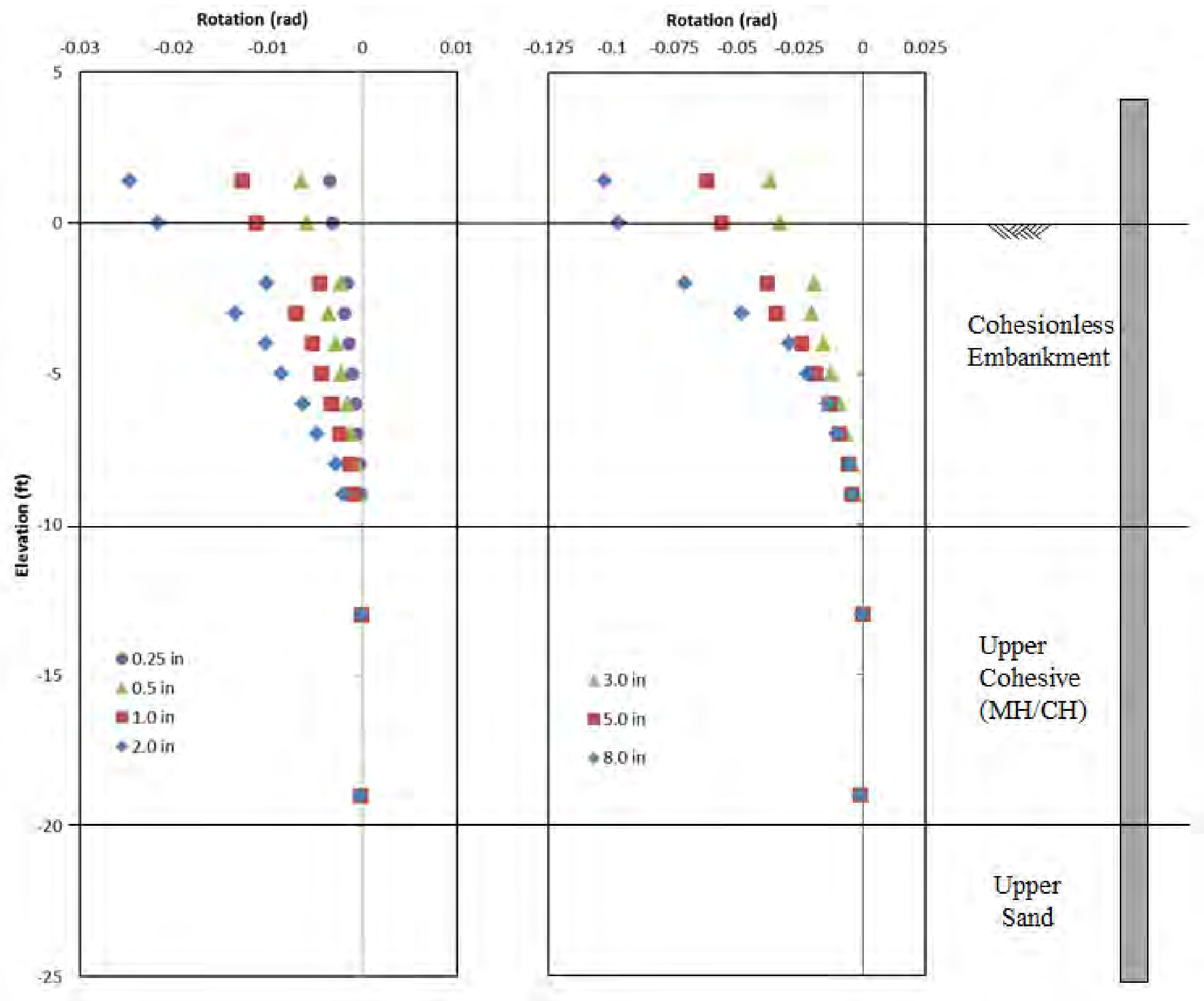

Figure 11-4 Rotation Results for Baseline Pile (P-2) at varying Displacements

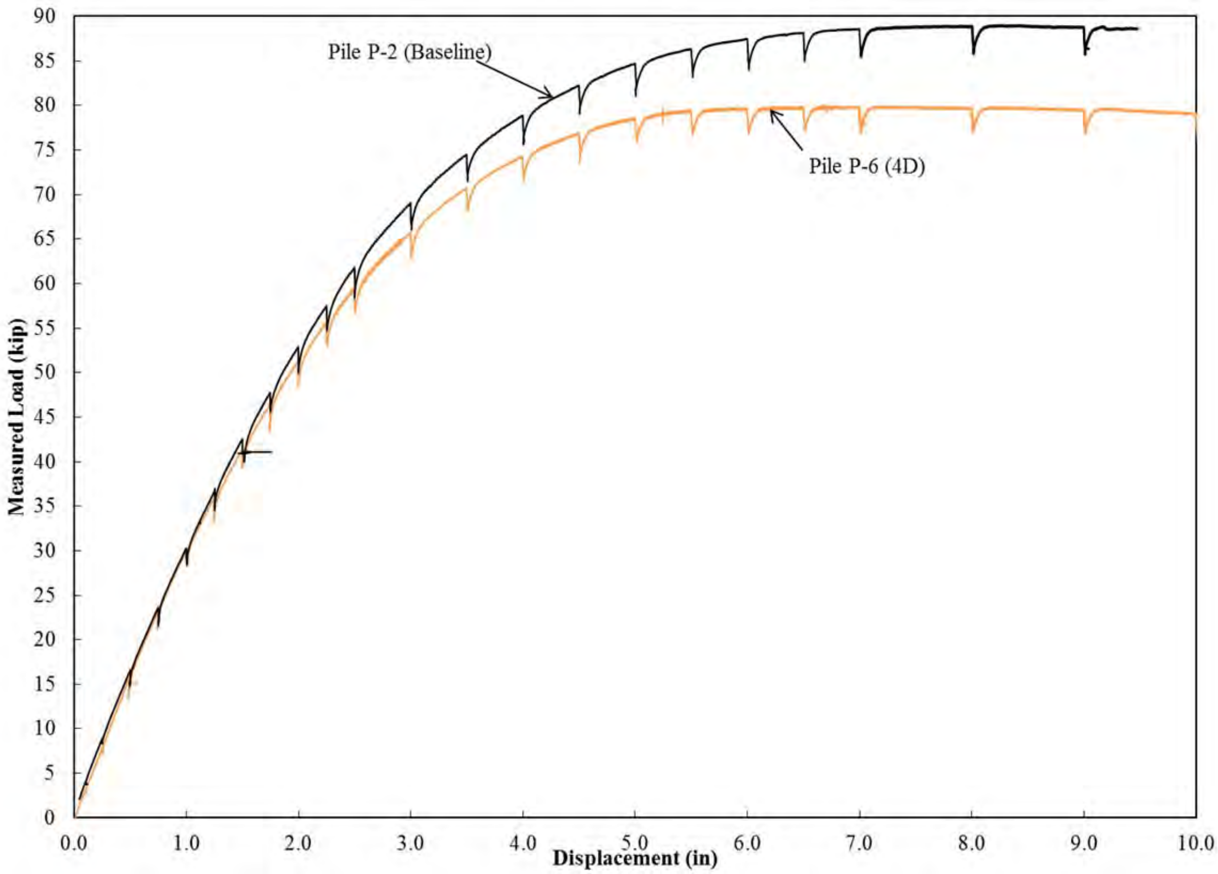

Figure 11-5 Comparison of Load-Displacement Curves between the Baseline Pile (P-2) and the 4D Pile (P-7)

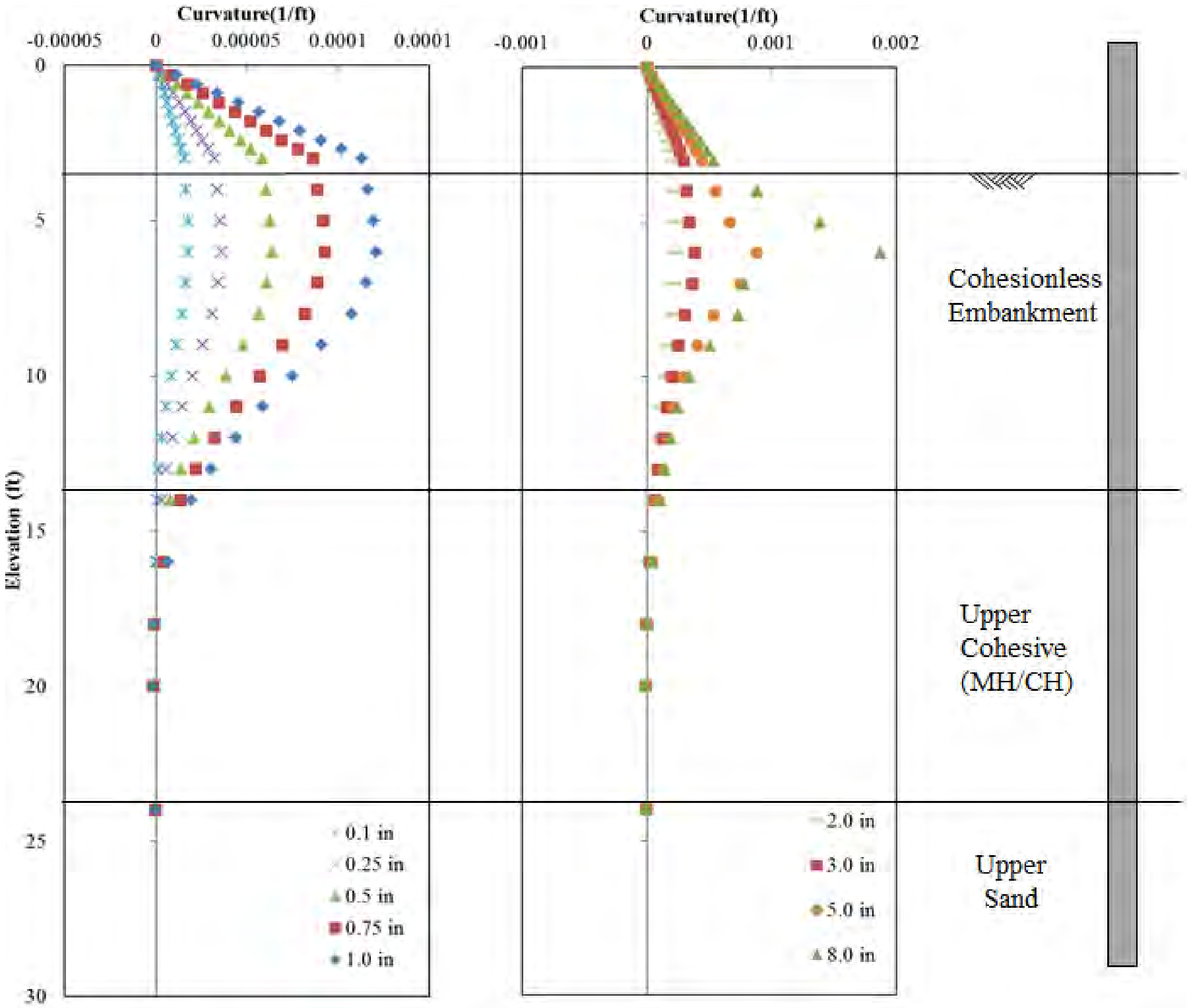

Figure 11-6 Curvature Results for the 4D Pile (P-7) at varying Displacements

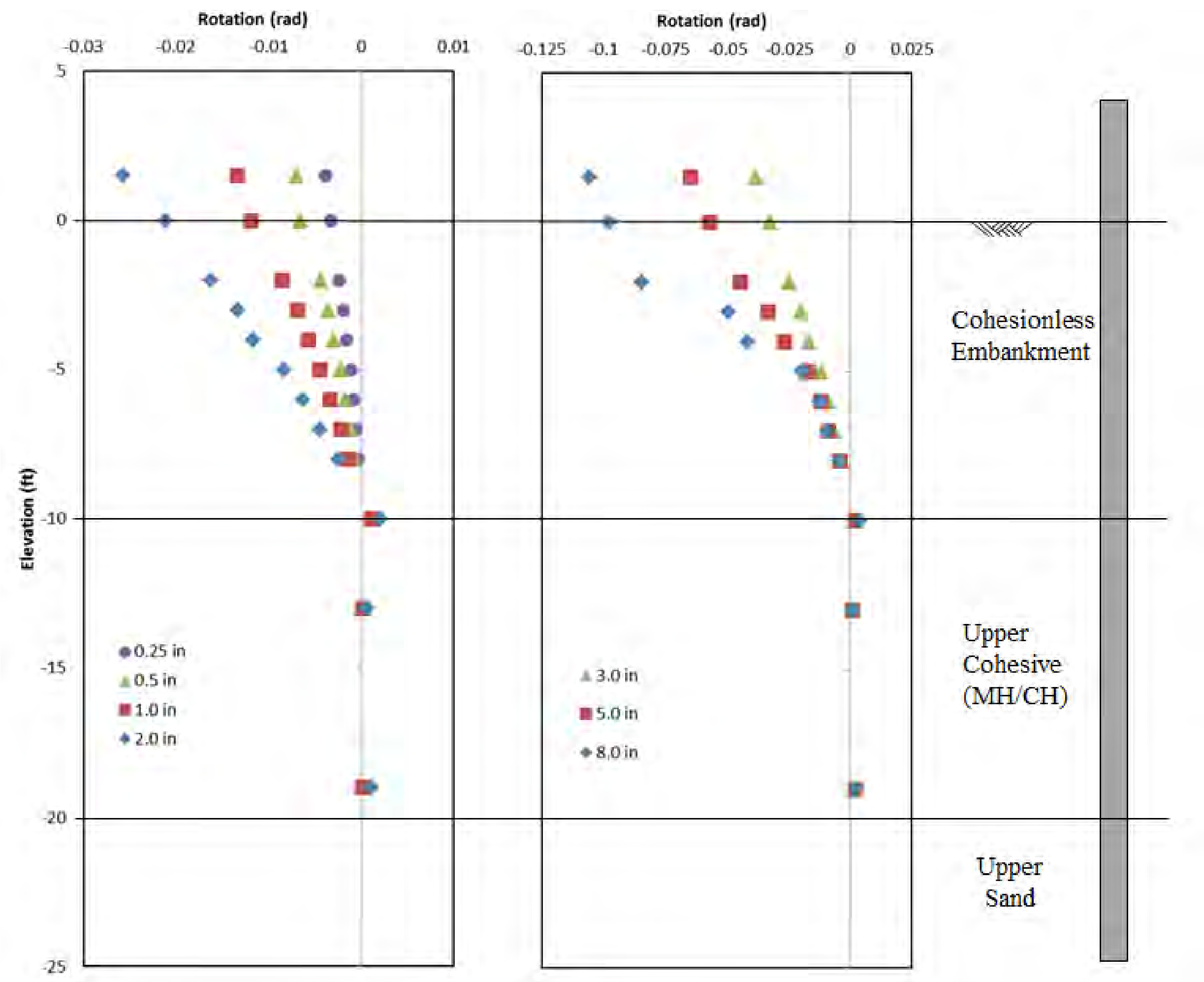

Figure 11-7 Rotation Results for the 4D Pile (P-7) at varying Displacements

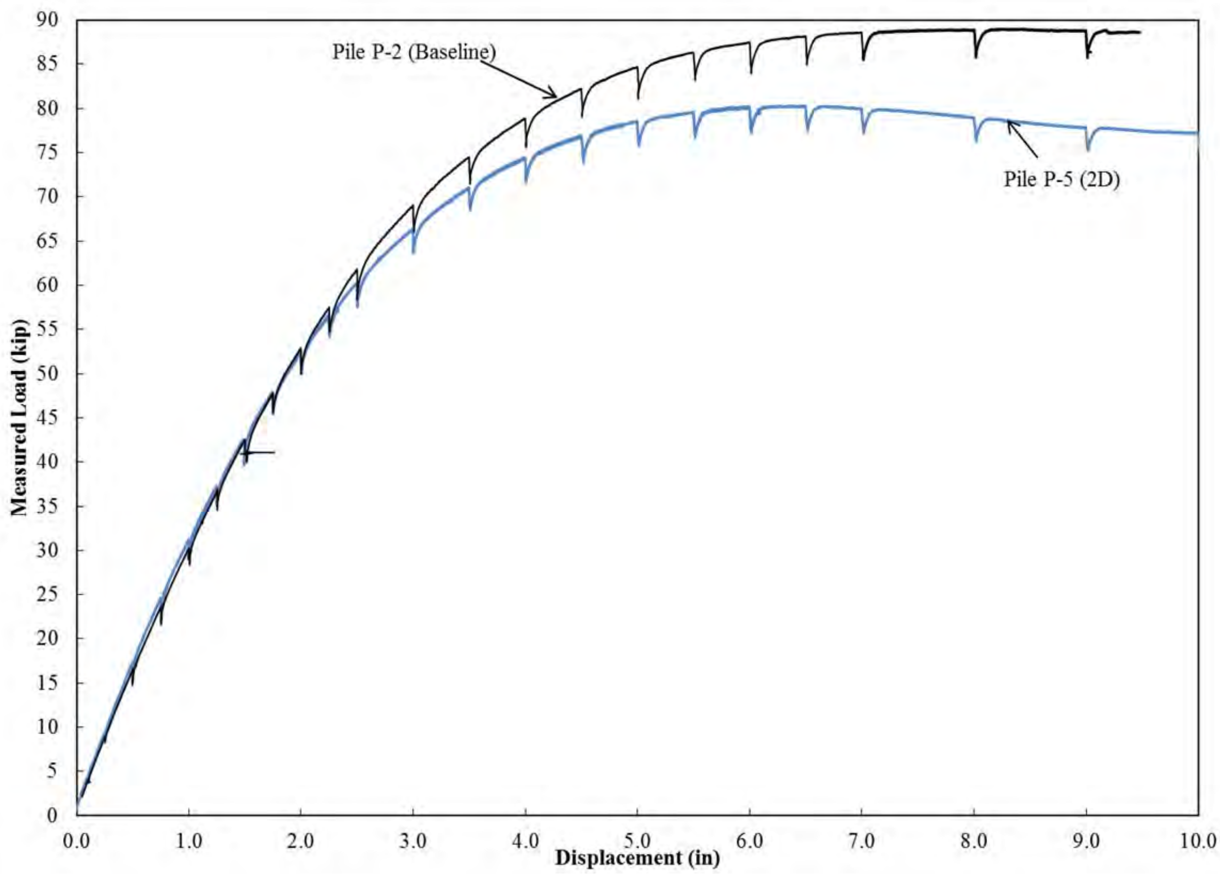

Figure 11-8 Comparison of Load-Displacement Curves between the Baseline Pile (P-2) and the 2D Pile (P-6)

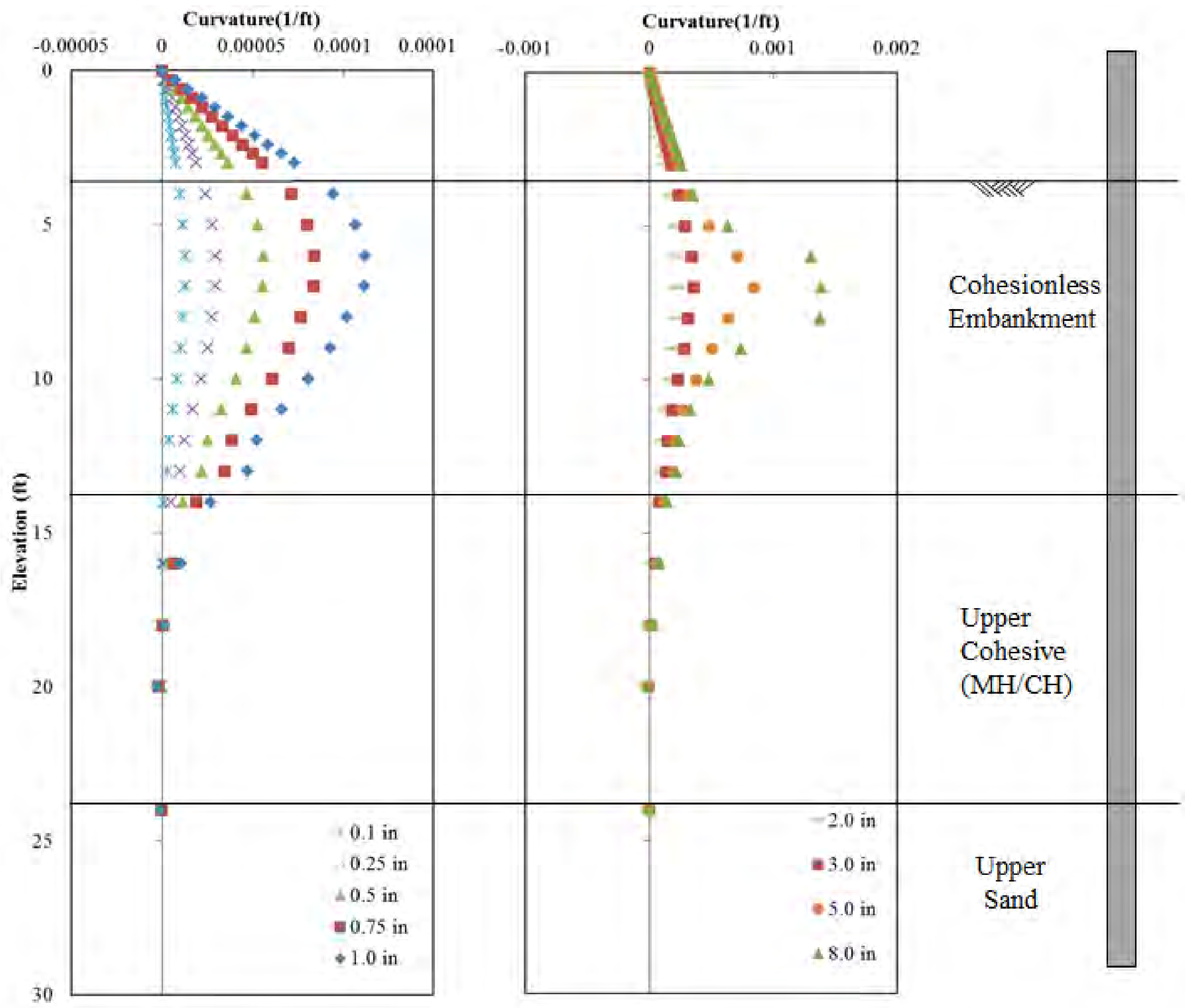

Figure 11-9 Curvature Results for the 2D Pile (P-6) at varying Displacements

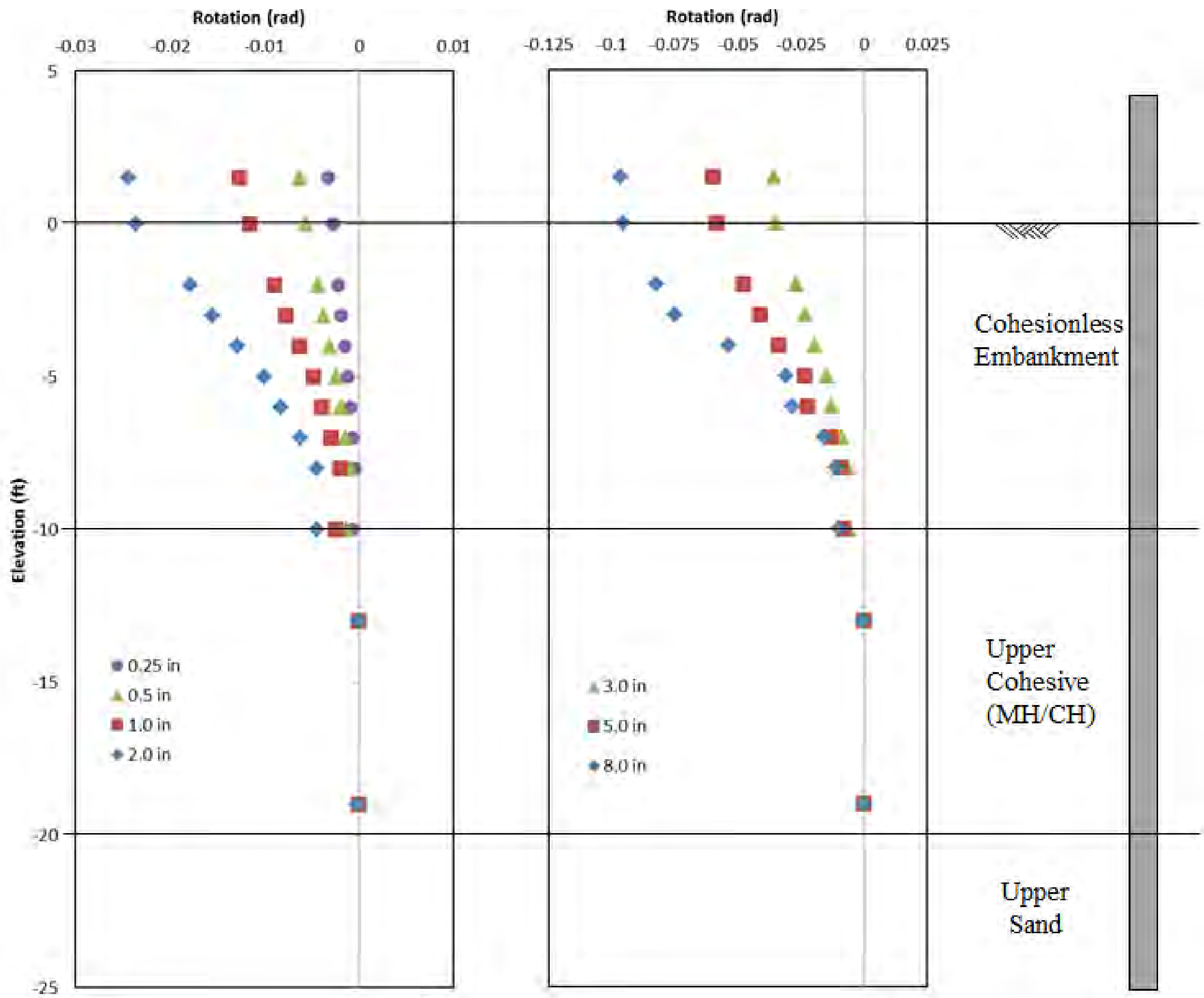

Figure 11-10 Rotation Results for the 2D Pile (P-6) at varying Displacements

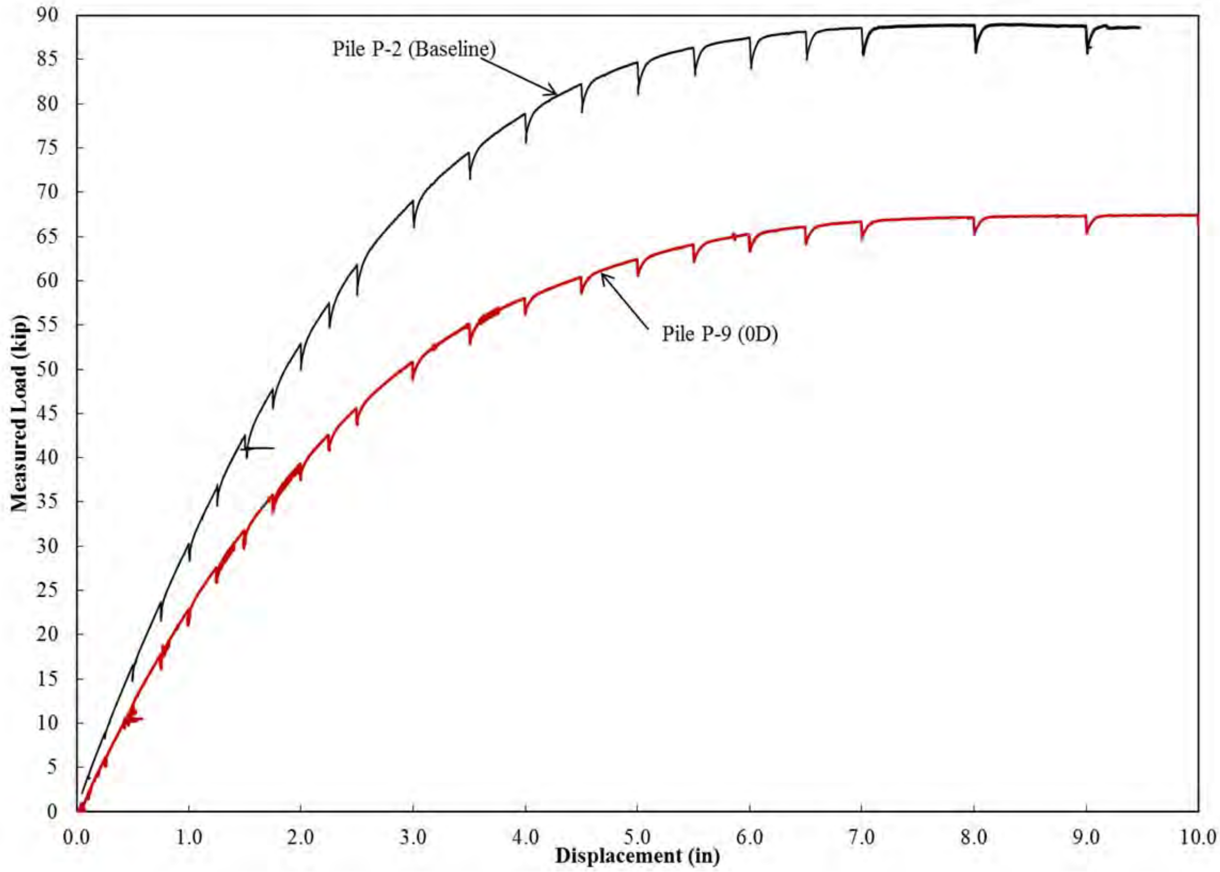

Figure 11-11 Comparison of Load-Displacement Curves between the Baseline Pile (P-2) and the 0D Pile (P-9)

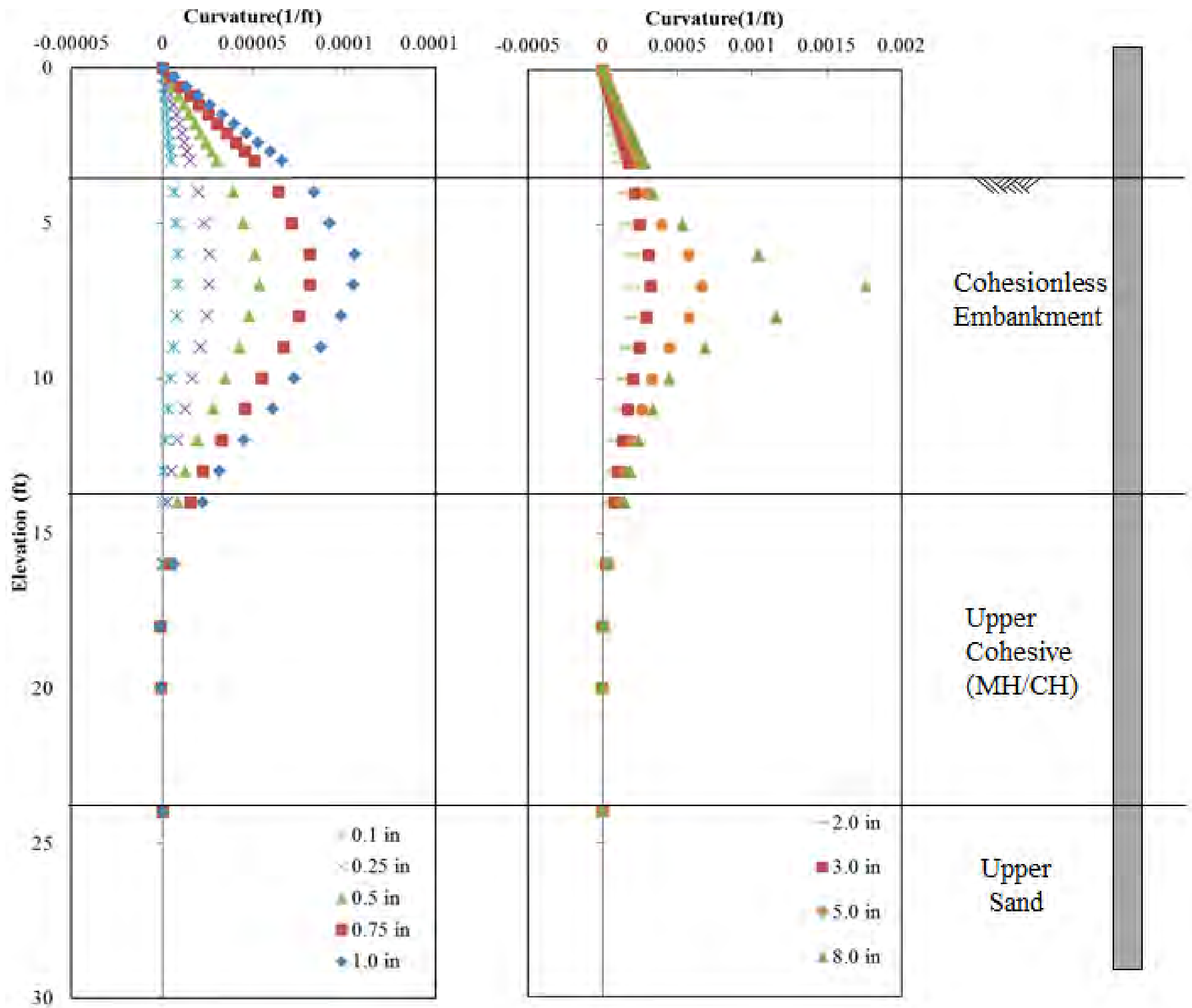

Figure 11-12 Curvature Results for the 0D Pile (P-9) at varying Displacements

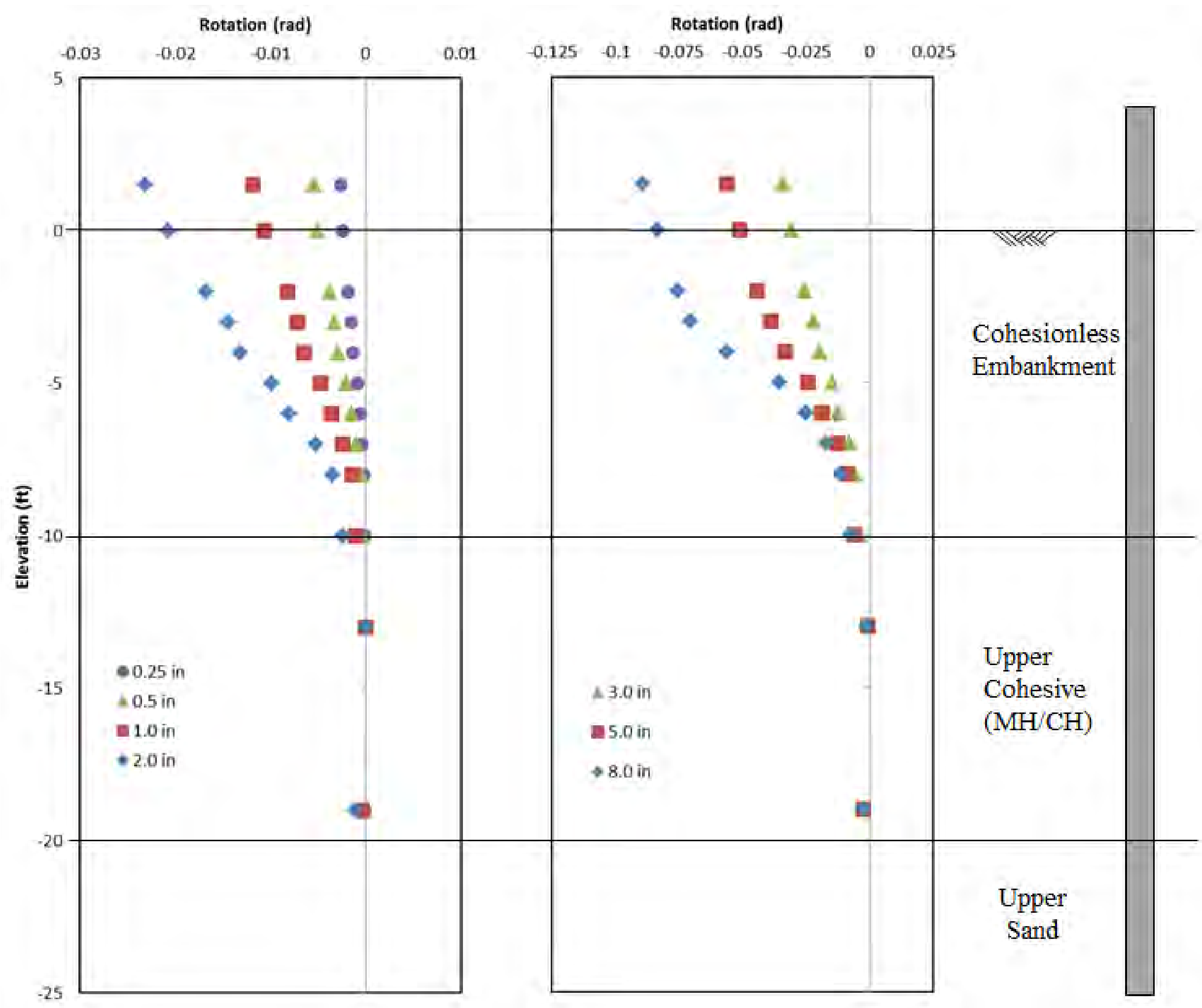

Figure 11-13 Rotation Results for the 0D Pile (P-9) at varying Displacements

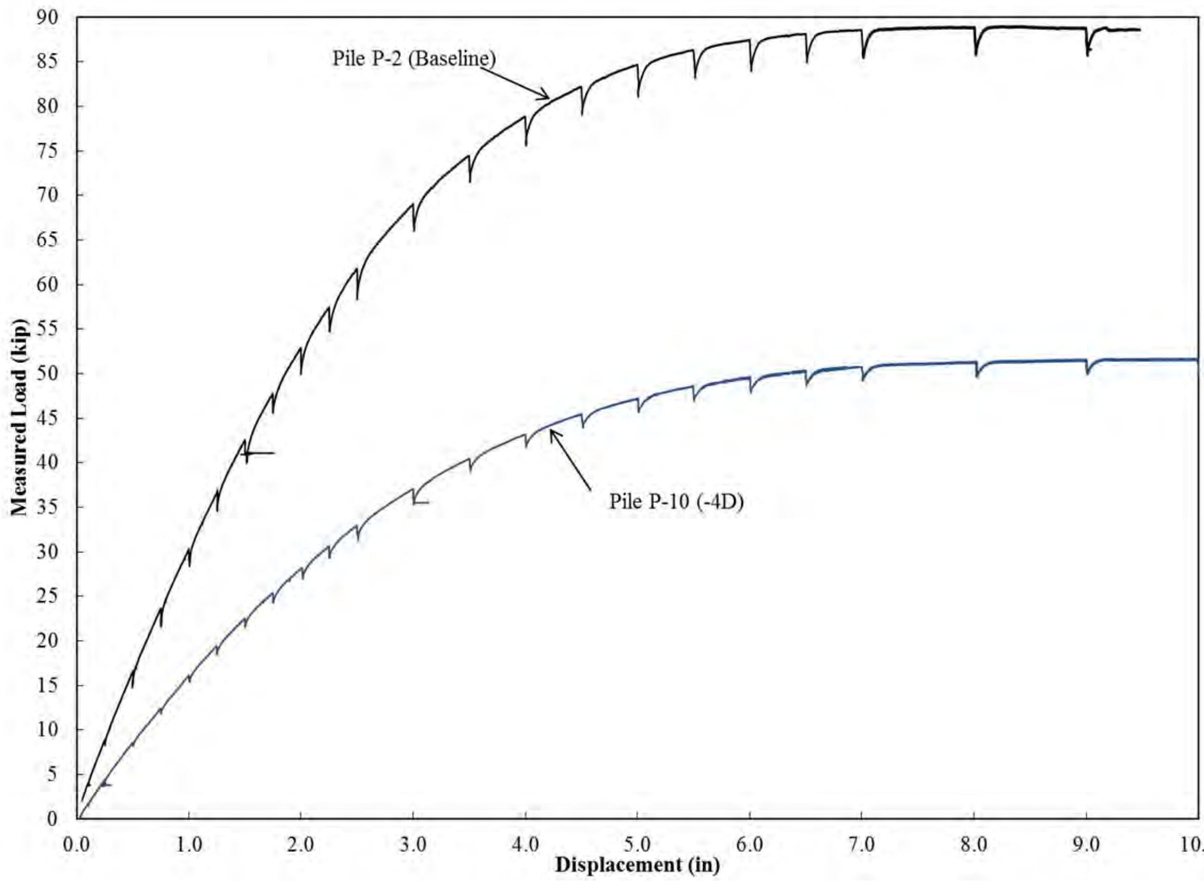

Figure 11-14 Comparison of Load-Displacement Curves between the Baseline Pile (P-2) and the -4D Pile (P-10)

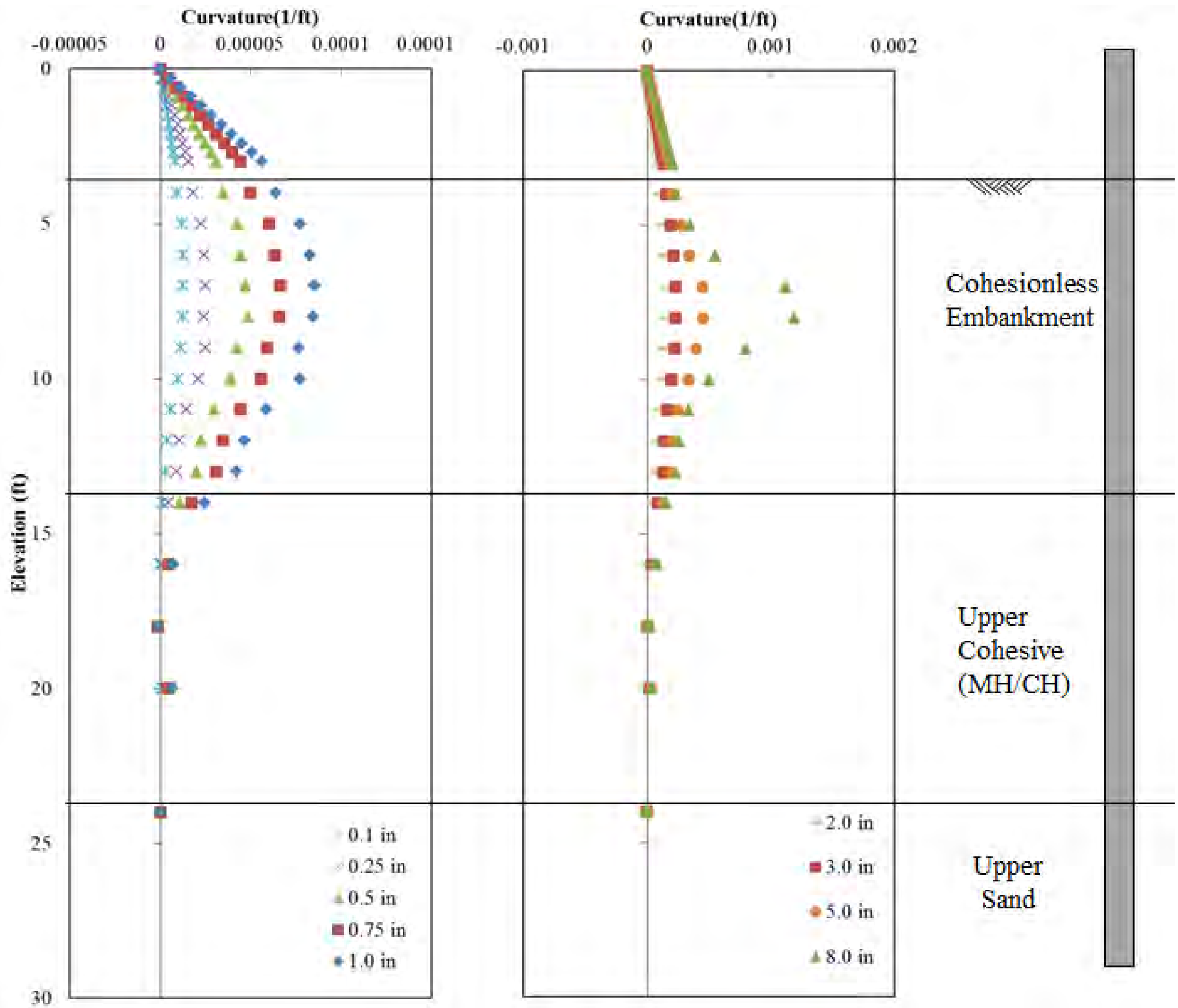

Figure 11-15 Curvature Results for the -4D Pile (P-10) at varying Displacements

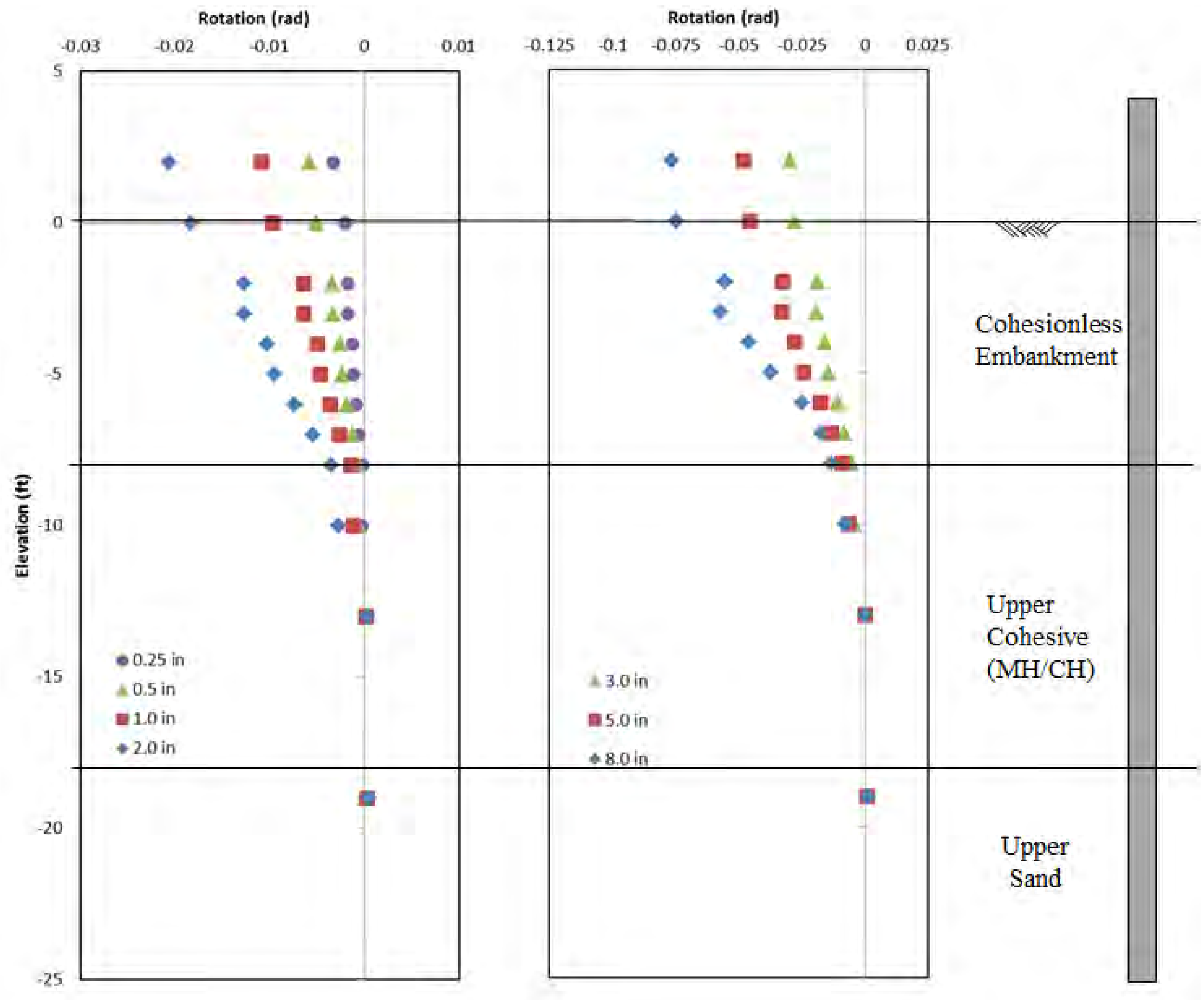

Figure 11-16 Rotation Results for the -4D Pile (P-10) at varying Displacements

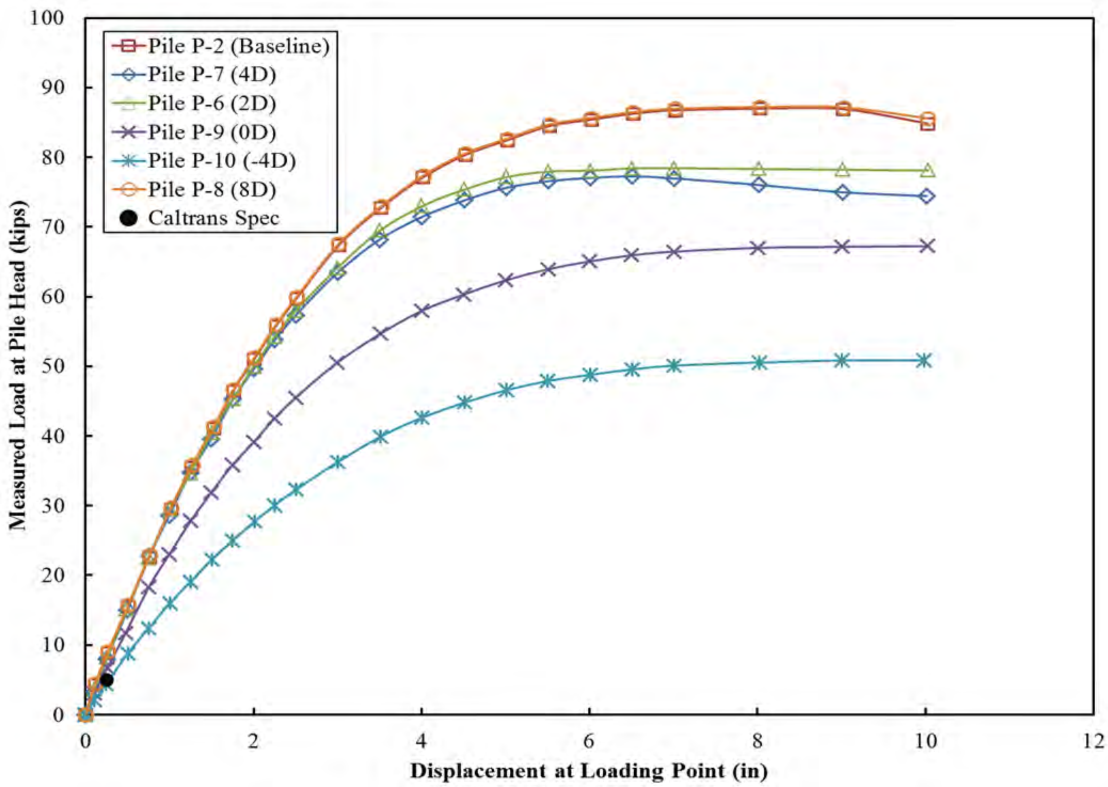

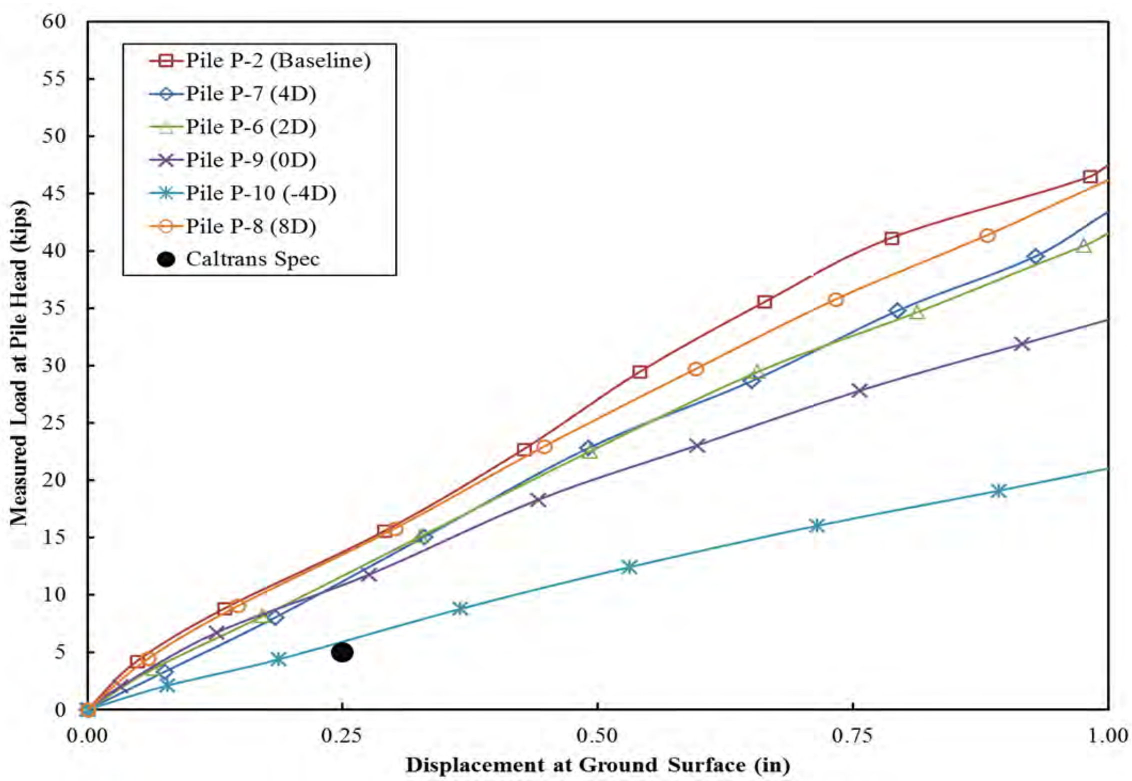

Figure 11-17 Top: Load Displacement Curve at Ground Surface with Caltrans Spec
Bottom: Load-Disp with Caltrans Spec up to 1 in. of Displacement

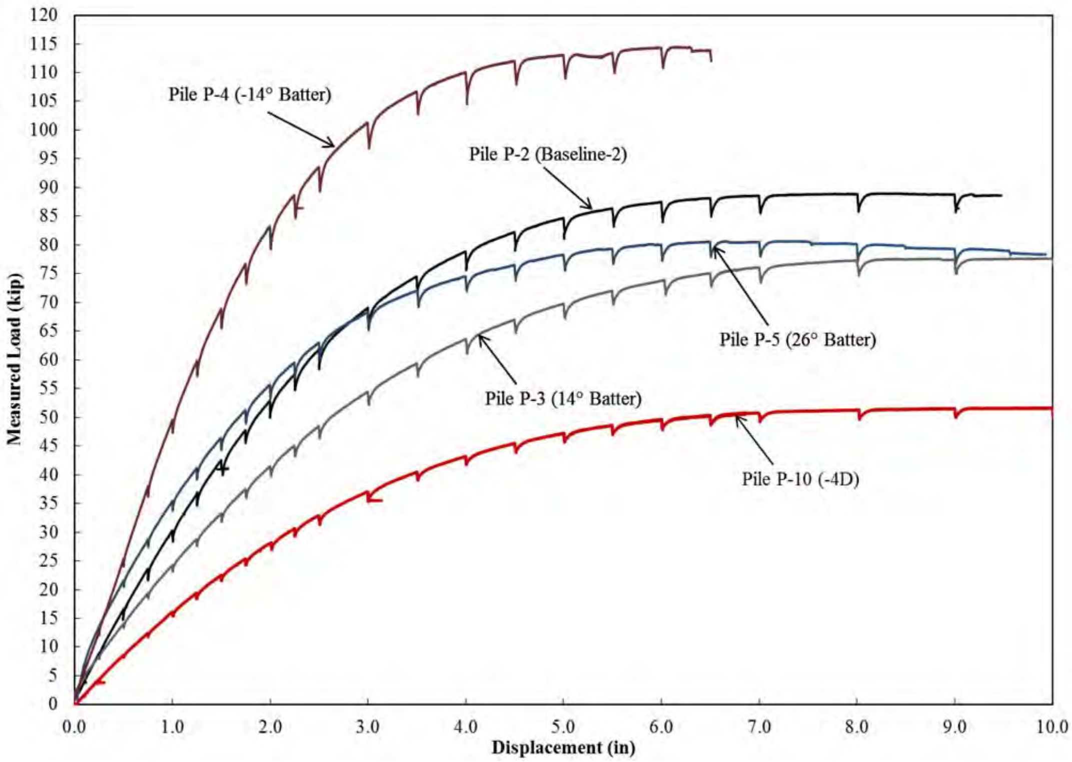

Figure11-18 Comparison of Load-Displacement Curves between the Baseline Pile (P-2), Pile P-10 (-4D) and Battered Piles

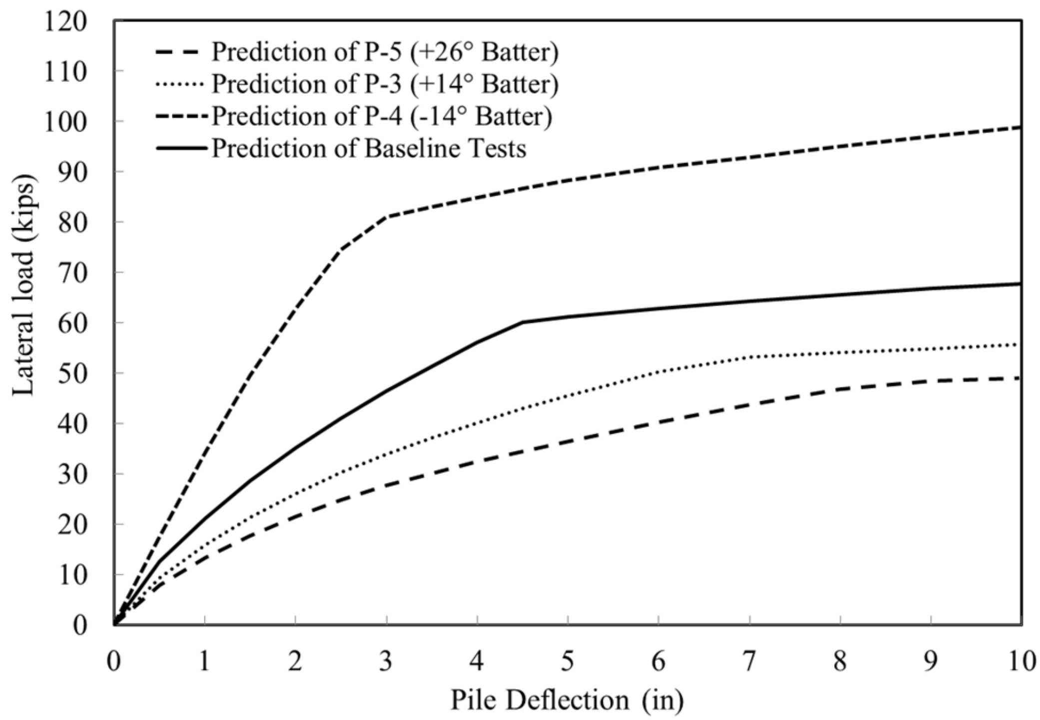

Figure 11-19 Predicted Load-Displacement Curves for the Battered Pile and Baseline Piles from LPILE

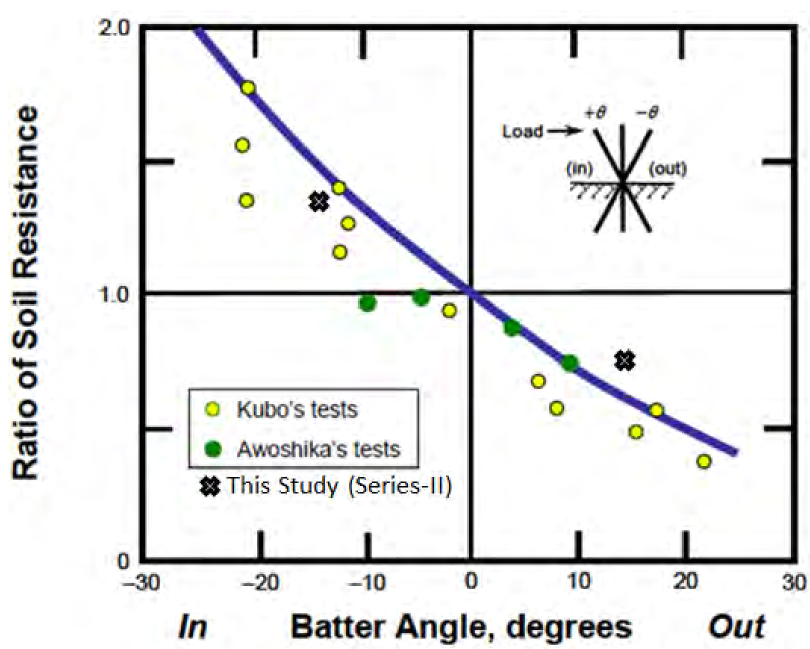

Figure 11-20 Model used for LPILE Battered Pile Predictions with the +14° and -14° Battered Pile Results from this Study (Series-II) (after Reese et al., 2004)

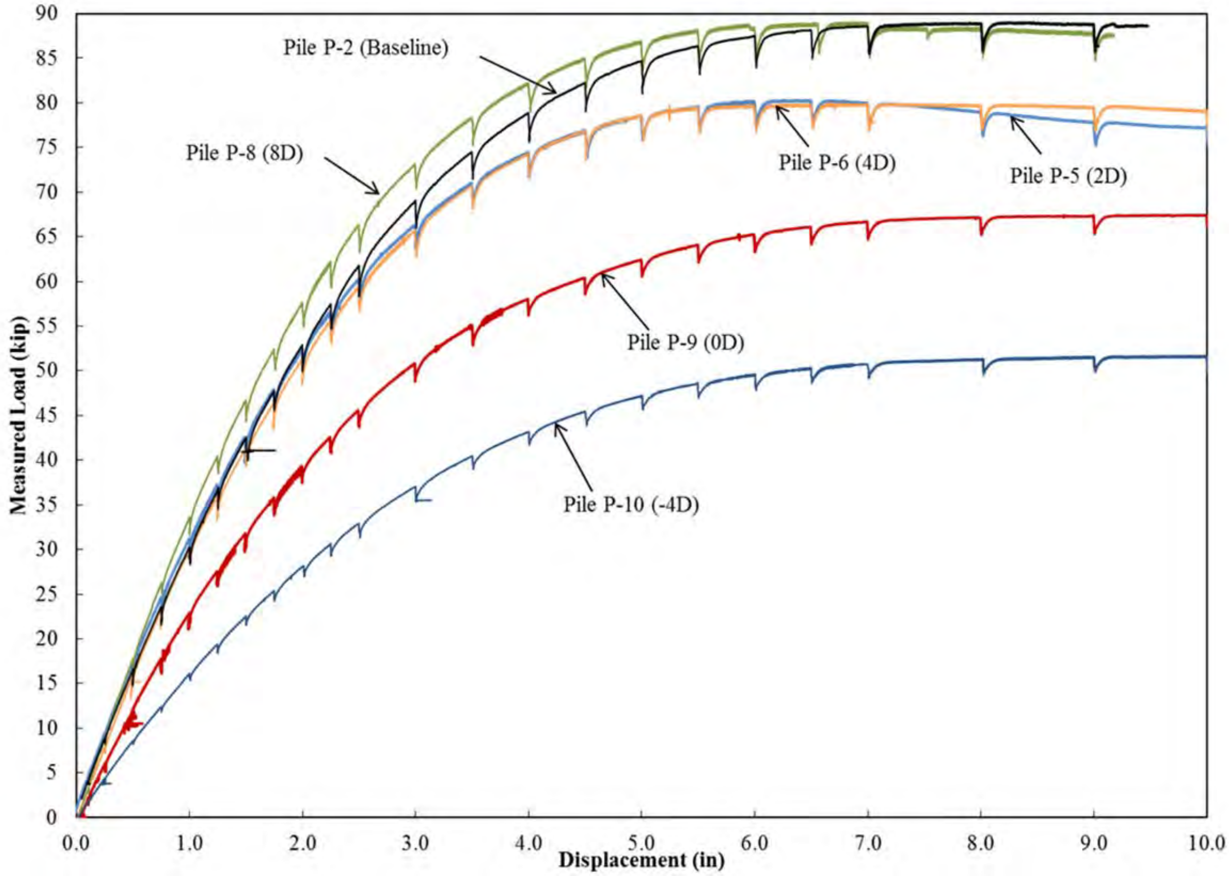

Figure 11-21 Comparison of all Non-Battered Load-Displacement Curves

12. LATERAL LOAD ANALYSES FOR SERIES-II (COHESIONLESS)

In this chapter, the evaluation of slope effect on lateral capacity of piles in cohesionless soils using the results from full-scale experiments is presented. The effect of distance from slope crest on the soil reaction, *p*, was evaluated using the back-calculated *p-y* curves based on the strain gauge data obtained during testing conducted in the summer of 2011. Similar to the methods used for back-calculating *p-y* curves with the cohesive soil data, as presented and explained in section 6.1.1, were used for analysis of the cohesionless testing data. Note: All figures containing *p-y* curves in this chapter present the *p-y* curves as a function of depth from the ground surface and not from the point of loading (i.e., *p-y* curves at 1 ft below ground surface are labeled as 1 ft compared to the *p-y* curves presented in Chapter 7 where the same curve is labeled as -4ft or 4 ft below the point of lateral loading.)

12.1 EARLY PILE YIELDING

During the design phase of this project, initial predictions and calculations were conducted to estimate the load-displacement, moment, curvature, and *p-y* curves. This analysis was conducted using predicted soil properties. These predictions were a unit weight of 125 pcf, friction angle of 42°, and an initial coefficient of subgrade reaction of 225 pci. The soil properties from the native soil conditions below the embankment were input in this prediction. Based on these properties, an idealized soil profile was created in LPILE Plus version 5.0 (Reese et al., 2004). The analysis was conducted using available standard sand p-y curves (Reese et al., 1974 and API, 1987) in LPILE 5.0.

The design of the required pile section was selected for the lateral load testing with this output data. As discussed previously, the geometry of the test pile was that of a standard 1-ft inner diameter steel pipe with a wall thickness of 0.375 inch and a length of approximately 30 ft. This pile section was also selected, in part, because it is a standard size presented in the Caltrans Bridge Design Specifications for lateral pile resistance.

During back-calculation of the p-y curves for the lateral load tests conducted in the cohesionless soil, it was discovered that the selected pile section began to yield plastically at pile displacements lower than that predicted. Pile yielding occurred at a pile head displacement of

1.5 inches in the baseline pile and at displacements up to 5.0 inches for piles closer to the crest of the slope. The point of plastic yielding was determined by examining the strain and moment profiles for each pile. The point of yielding for the test piles occurred at 3 ft to 6 ft below ground surface.

Back-calculated p-y curves are shown as solid lines at locations where the strain data used in analysis was within the elastic range for the pile section. The dashed lines (with shown calculated data points in this chapter) are the computed p-y curves past the point of plastic yielding. This portion of the p-y curves should not be considered accurate as the methods used for back-calculations of these p-y curves is not developed for analyses outside of the elastic range based on the method used. There was an adequate amount data obtained in this series of tests to investigate the effects of slope on lateral pile capacities at small piles displacements, in the range where Caltrans is most interested.

12.2 BACK-CALCULATED P-Y CURVES FOR SERIES-II

The following section presents the back-calculated p-y curves for the second baseline (considered similar to 8D for this test), 4D, 2D, 0D, and -4D. Discussions of the p-y curves are presented along with the calculated bending moment, deflection, and rotation profiles for each test at varying pile head displacements. As stated previously, the dashed portions of the presented p-y curves represent data calculated after plastic yielding began in the piles.

12.2.1 BACK-CALCULATED P-Y CURVES FOR 2ND BASELINE (P-2)

The back-calculated *p-y* curves of the baseline pile are shown in **Figure 12-1** for the full range of displacements to a depth of 6ft. **Figure 12-2** presents the same *p-y* curves for displacements up to 1 inch to emphasize the reaction at lower pile movements. The *p-y* curves for the baseline test have reliable data up to a displacement of 0.8 inches. As would be expected, with increased depth the soil reaction (*p*) increased for a given displacement (*y*). The ultimate soil reaction was not obtained for this test, but a comparison of the baseline at low displacements (less than 0.8 inches) with near slope piles is possible.

Figure 12-3 and **Figure 12-4** present the results from the analysis for the bending moment, deflection and rotation profiles for varying pile head displacements. The plots for the lower displacements present expected curves. The higher displacement plots present errors due to pile yielding. The bending moment in the latter figure (displacements of 2 in and greater) saturates around a moment of 430 kip-ft for a pile head displacement of 5.0 inches or greater. This bending moment is similar to the stated maximum determined in the calibration test. An inaccuracy is observed in the deflection plots at the higher displacements as a result of inaccuracies in strain data resulting from pile yielding. The rotation profile shows movement at the base of the pile (i.e. not a fixed end) but this is not shown in the rotation data from the tilt sensors. The displacements do not match with the measured pile head movement. These results are likely due to carrying through the post-yield strain data during integration steps.

12.2.2 BACK-CALCULATED P-Y CURVES FOR 4D PILE (P-7)

The back-calculated *p-y* curves for the 4D pile are shown in **Figure 12-5** for the full range of displacements to a depth of 6ft. **Figure 12-6** presents the same *p-y* curves for displacements up to 1 inch to emphasize the reaction at lower pile movements. The *p-y* curves for the 4D pile have reliable data up to a displacement of 0.8 inches, similar to the baseline test. The ultimate soil reaction was not obtained for this test, but a comparison to the baseline at lower displacements (less than 0.8 inches) with near slope piles is possible. When compared to the baseline, the soil reaction (*p*) is slightly less at similar displacements near the ground surface and almost the same at lower depths. This demonstrates that the proximity of the slope had little to no effect on the *p-y* curves at 4D from the slope.

Figure 12-7 and **Figure 12-8** present the results from the analysis for the bending moment, deflection and rotation profiles for varying pile head displacements. The plots for the lower displacements present expected curves. The higher displacement plots present errors due to pile yielding. The bending moment in the latter figure saturates around a moment of 430 kip-ft for a pile head displacement of 5 inches or greater. This bending moment is similar to the stated maximum determined in the calibration test. An inaccuracy is observed in the deflection plots at the higher displacements as a result of inaccuracies in strain data resulting from pile yielding. The rotation profile shows movement at the base of the pile (i.e. not a fixed end) but this is not shown in the tilt sensor results and is likely due to carrying through the post-yield strain data during integration.

12.2.3 BACK-CALCULATED P-Y CURVES FOR 2D PILE (P-6)

The back-calculated *p-y* curves for the 2D pile are shown in **Figure 12-9** for the full range of displacements at 1 ft intervals to a depth of 6ft. Error! Reference source not found. presents the same *p-y* curves for displacements up to 1 inch to emphasize the reaction at lower pile movements. The *p-y* curves for the 2D pile have reliable data up to a displacement of 1.5 inches. The ultimate soil reaction was not obtained for this test, but a comparison of the baseline at low displacements (less than 1.5 inches) with near slope piles is possible. The shape of the *p-y* curves are similar to what would be expected with a higher stiffness that flattens when ultimate resistance is reached. For the back-calculated p-y curves the apparent ultimate soil capacity is past the elastic range of the pile. Therefore, these results (dashed segments on *p-y* curves) are not considered to be reliable. When compared to the baseline, the soil reaction (*p*) is considerably less at similar displacements at all depths. This demonstrates that the proximity of the slope has a significant effect on the *p-y* curves at 2D from the slope.

Figure 12-11 and **Figure 12-12** present the results from the analysis for the bending moment, deflection and rotation profiles for varying pile head displacements. The plots for the lower displacements present expected curves. The higher displacement plots present errors due to pile yielding. The bending moment in the latter figure saturates around a moment of 430 kip-ft. An inaccuracy is observed in the deflection plots at the higher displacements as a result of inaccuracies in strain data resulting from pile yielding.

12.2.4 BACK-CALCULATED P-Y CURVES FOR 0D PILE (P-9)

The back-calculated *p-y* curves for the 0D piles are shown in **Figure 12-13** for the full range of displacements to depth of 6ft. **Figure 12-14** presents the same *p-y* curves for displacements up to 1 inch to emphasize the reaction at lower pile movements. The *p-y* curves for the 0D pile have reliable data up to a displacement of 1.75 inches. The ultimate soil reaction was not obtained for this test, but a comparison at low displacements (less than 1.75 inches) with near slope piles is possible. The shape of the *p-y* curves are similar to what would be expected with an initial higher stiffness that flattens when ultimate resistance is reached. For the back-calculated p-y curves the apparent ultimate soil capacity is past the elastic range of the pile.

Therefore, these results (dashed segments on *p-y* curves) are not considered to be reliable. When compared to the baseline, the soil reaction (*p*) is considerably less at similar displacements at all depths and slightly less than the 2D. This demonstrates that the proximity of the slope a significant effect on the *p-y* curves at slope crest.

Figure 12-15 and **Figure 12-16** present the results from the analysis for the bending moment, deflection and rotation profiles for varying pile head displacements. The plots for the lower displacements present expected curves. The higher displacement plots present errors due to pile yielding. The bending moment in the latter figure saturates around a moment of 430 kip-ft.

12.2.5 BACK-CALCULATED P-Y CURVES FOR -4D PILE (P-10)

The back-calculated *p-y* curves for the -4D are shown in **Figure 12-17** for the full range of displacements to depth of 6ft. **Figure 12-18** presents the same *p-y* curves for displacements up to 1 inch to emphasize the reaction at lower pile movements. The *p-y* curves for the -4D pile have reliable data up to a displacement of 2.25 inches. The ultimate soil reaction was not obtained for this test, but a comparison at low displacements (less than 2.25 inches) with near slope piles is possible. The shape of the *p-y* curves are similar to what would be expected with an initial higher stiffness that flattens when ultimate resistance is reached. For the back-calculated p-y curves the apparent ultimate soil capacity is past the elastic range of the pile. Therefore, these results (dashed segments on *p-y* curves) are not considered to be reliable. When compared to the baseline, the soil reaction (*p*) is significantly less at similar displacements at all depths and considerably than the 0D. This demonstrates that the slope a significant effect on the *p-y* curves. **Figure 12-19** and **Figure 12-20** present the results from the analysis for the bending moment, deflection and rotation profiles for varying pile head displacements. The figures for the lower and higher displacements look similar to predictions.

12.2.6 COMPARISON OF P-Y CURVES FOR PILE NEAR SLOPE TEST

A comparison of the *p-y* curves from the results of full-scale lateral load tests on piles located at different distance (-4D, 0D, 2D, 4D) from the slope crest provides insight into the effect of slope on the *p-y* curves. The *p-y* curves for baseline pile are considered as backbone *p-y* curves for comparison. **Figure 12-21** and **Figure 12-22** present a comparison of the *p-y* curves of each test pile at varying depths within the cohesionless profile. Examination of these plots reveals almost identical *p-y* curves for the second baseline and 4D piles from the ground surface to a depth of 5 ft. The baseline tended to be just slightly higher for all depths except for the ground surface curve. The soil resistance of the *p-y* curves for the -4D, 0D, and 2D pile are significantly less than the baseline pile in the range of available data. The curves for the baseline and 4D piles are similar in shape and ultimate capacities showing that the effect of the slope was relatively small at four pile diameters from the slope. This data was used to develop methods to account for soil slope.

A full range of *p*-multipliers that vary with pile displacement and depth were calculated but are not presented for Series-II due to the early pile yielding. Rather, generalized *p*-multiplier figures were constructed by analyzing the available soil reaction-displacement data for each test pile. These figures were constructed with a higher degree of conservatism, and they are viable for design at all range pile displacements.

During data reduction for Series-II, comparisons between rotation data and pile head displacement from the string potentiometers was conducted during the strain gauge data reduction to ensure the accuracy of the information used to obtain the p-y curves. Similar moment, deflection and rotation profile figures were not produced for Series-II (compare **Figure 7-4** from Series-I with **Figure 12-3** From Series-II) because the team saw it was redundant and not necessary to compare the measured data with the back-calculated profiles again. The p-y data was not input into LPILE to produce the profiles because the output would produce almost identical results.

It is important to note that the 2D and 4D load-displacement curves are almost identical at all displacements, but this is not seen in the p-y curves for the 2D and 4D results. The p-y curves for the 4D pile are similar to the baseline curves and the 2D results are similar to the 0D p-y curves. This was not expected after observing the similarities in the load-displacement curves. These trends suggest that the 2D p-y curve would be steeper than the 0D p-y curves, and more closely follow the 4D results. This may be a result of the 1.0 of rainfall that occurred over a five day period before the testing of the 2D pile. One day of dry weather separated the rainfall events and the testing of the 2D pile. This rainfall may have an effect on the resulting p-y curves by reducing the near surface stiffness. During pile installation of the 2D pile there was soil disturbance in front of the pile that extended out onto the slope. This disturbance consisted of a wedge of soil moving outward onto the slope during pile driving. The disturbance was about 3 ft in width and moved about 2 inches laterally onto the slope. This near slope disturbance and the rain event may have caused a decrease in near surface soil stiffness for the 2D p-y curves but may not have affected overall load-displacement of the entire 2D test pile. This may explain the discrepancies between the 2D and 4D load-displacement curves with the near surface 2D and 4D p-y curves.

12.3 SUMMARY

A sixth order polynomial function was fit to the strain gauge data along the depth of each pile to compute the soil reaction and pile deflection profiles. The moment, shear, and rotation profiles were also calculated. Based on the comparison of p-y curves, for all displacements, the slope effect on lateral resistance is significant for piles located at 2D or closer from the slope crest. For a pile located at 4D or greater from the slope crest, the effect of slope is insignificant for the analyzed ranges of p-y curves. The soil resistance at a given displacements for the -4D, 0D, and 2D pile p-y curves are significantly less than the baseline pile in the range of pre-plastic yielding p-y curve data. The curves for the baseline and 4D piles are similar in shape and ultimate capacities showing that the effect of the slope was relatively small at four pile diameters from the slope crest. Final design recommendations are presented in Chapter 14.

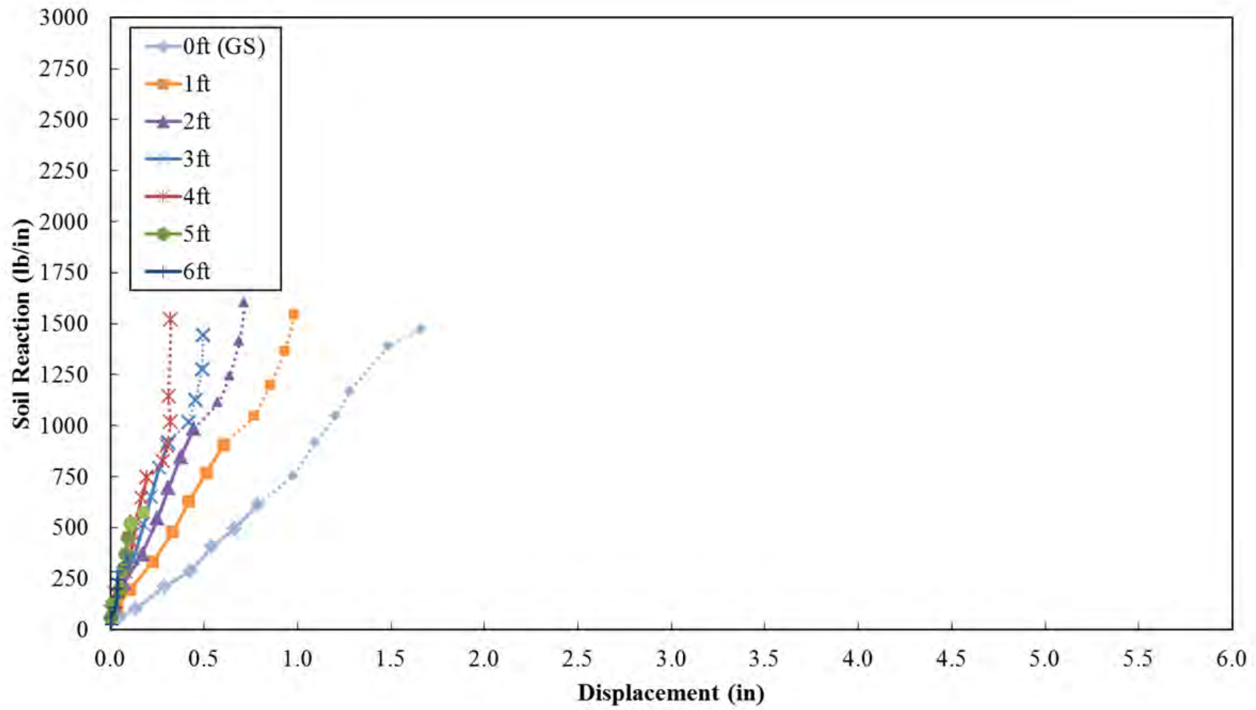

Figure 12-1 Back-Calculated *p-y* Curves for the 2nd Baseline Pile (P-2)
Note: Dotted Lines Present Data after Initial Pile Yielding

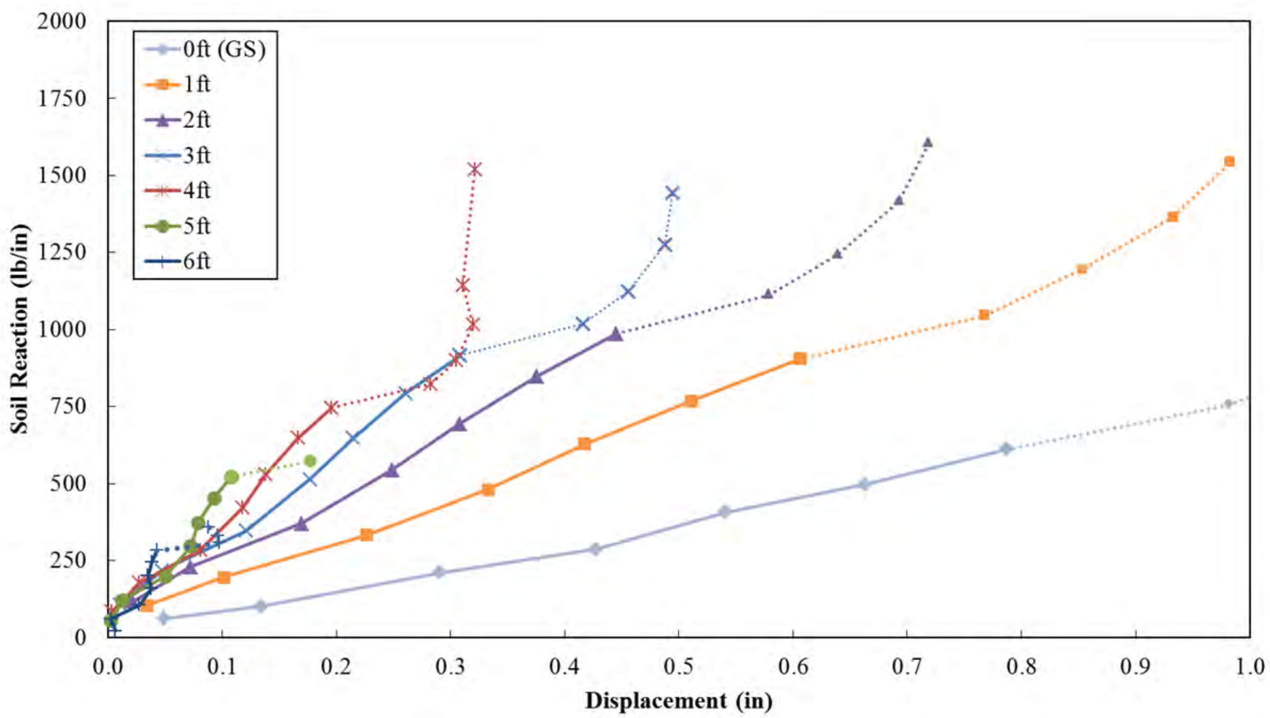

Figure 12-2 Back-Calculated *p-y* Curves for the -Baseline Pile (P-2) with Lower Displacements
Note: Dotted Lines Present Data after Initial Pile Yielding

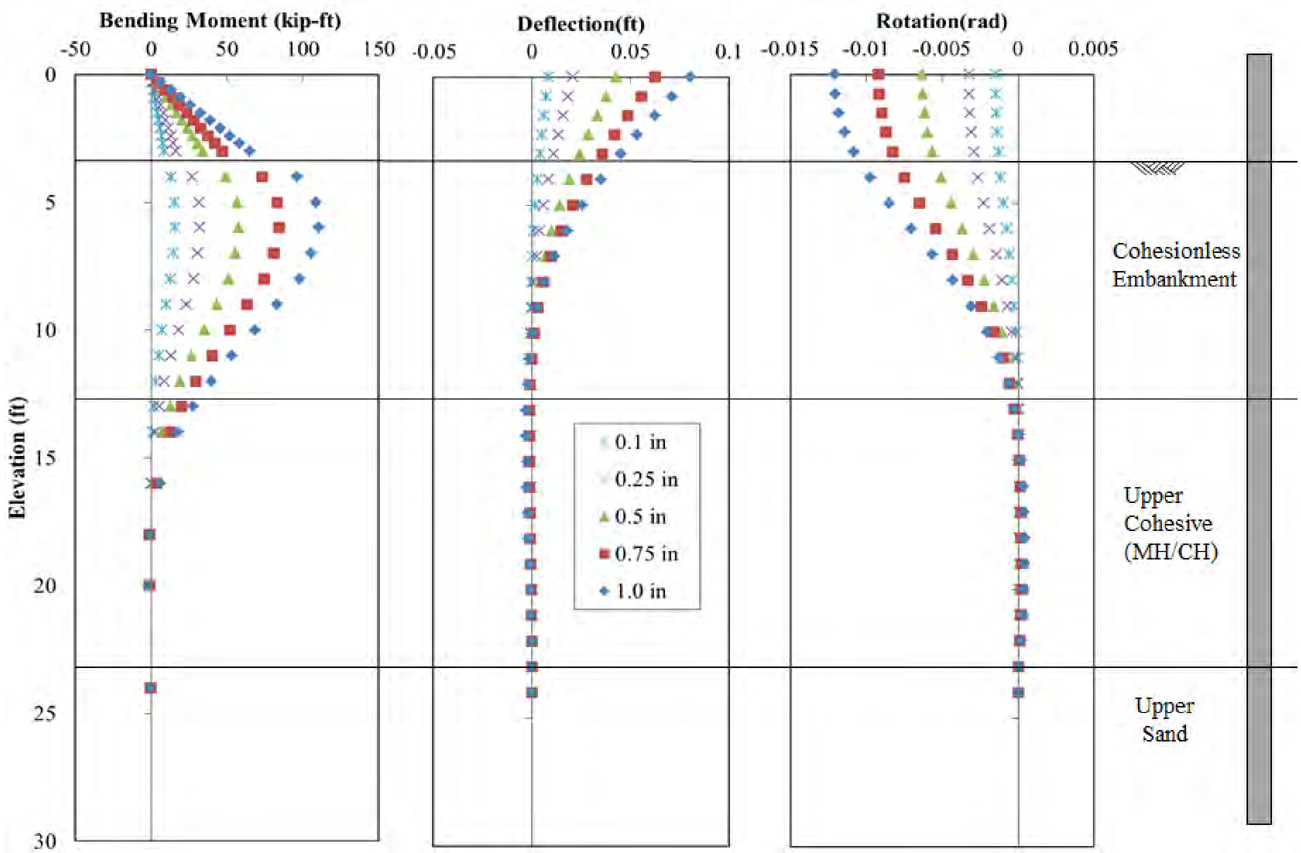

Figure 12-3 Comparison of Test Results and Analysis Using Back-Calculated *p-y* Curves for the 2nd Baseline Pile (P-2) for Pile Head Displacement of 0.1, 0.25, 0.5 and 1.0 in.

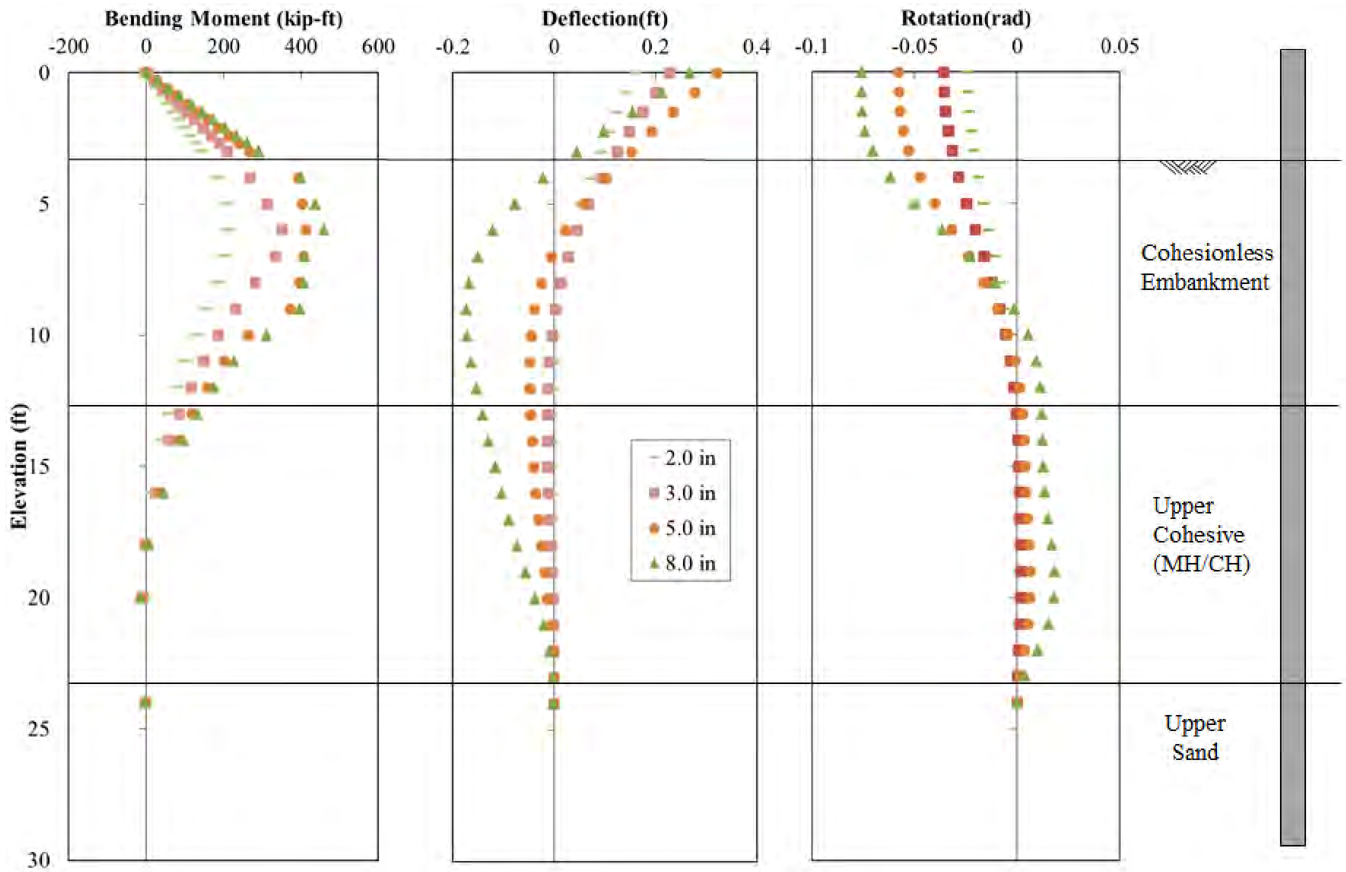

Figure 12-4 Comparison of Test Results and Analysis Using Back-Calculated *p-y* Curves for the 2nd Baseline Pile (P-2) for Pile Head Displacement of 2.0, 3.0, 5.0 and 8.0 in.

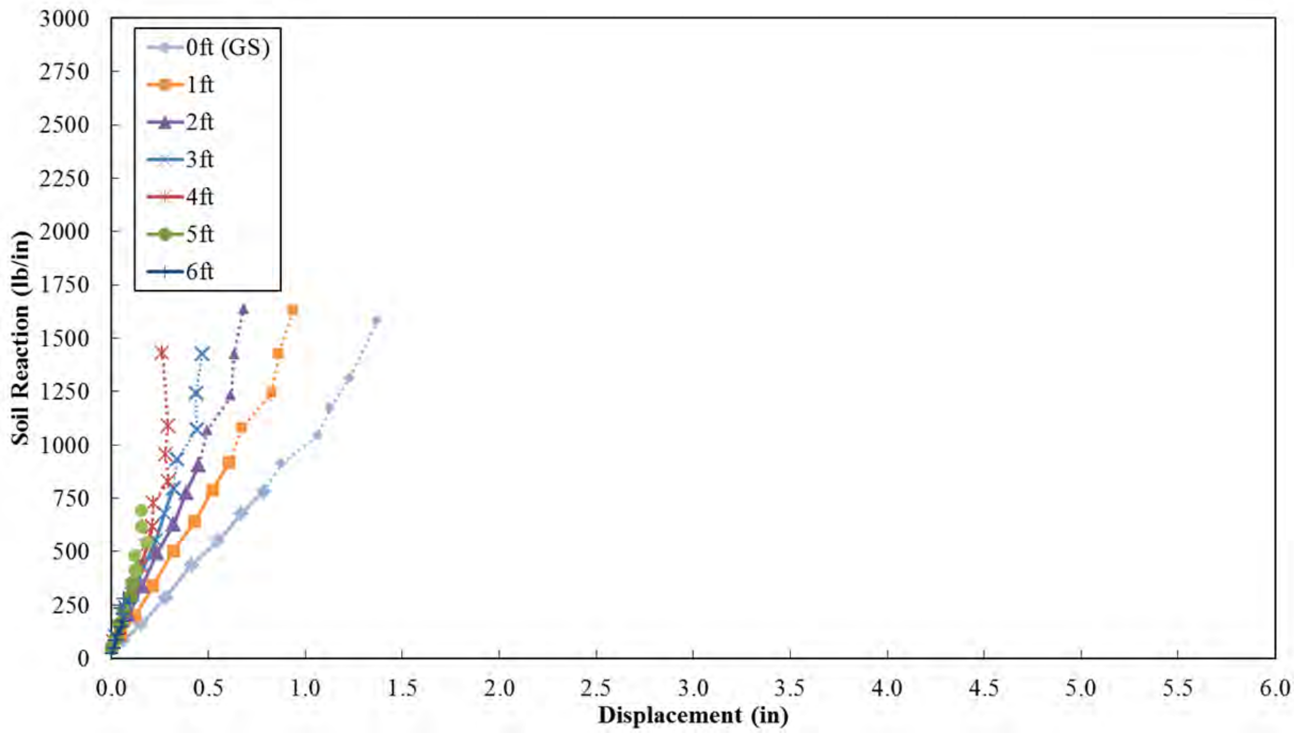

Figure 12-5 Back-Calculated *p-y* Curves for the 4D Pile (P-7)
Note: Dotted Lines Present Data after Initial Pile Yielding

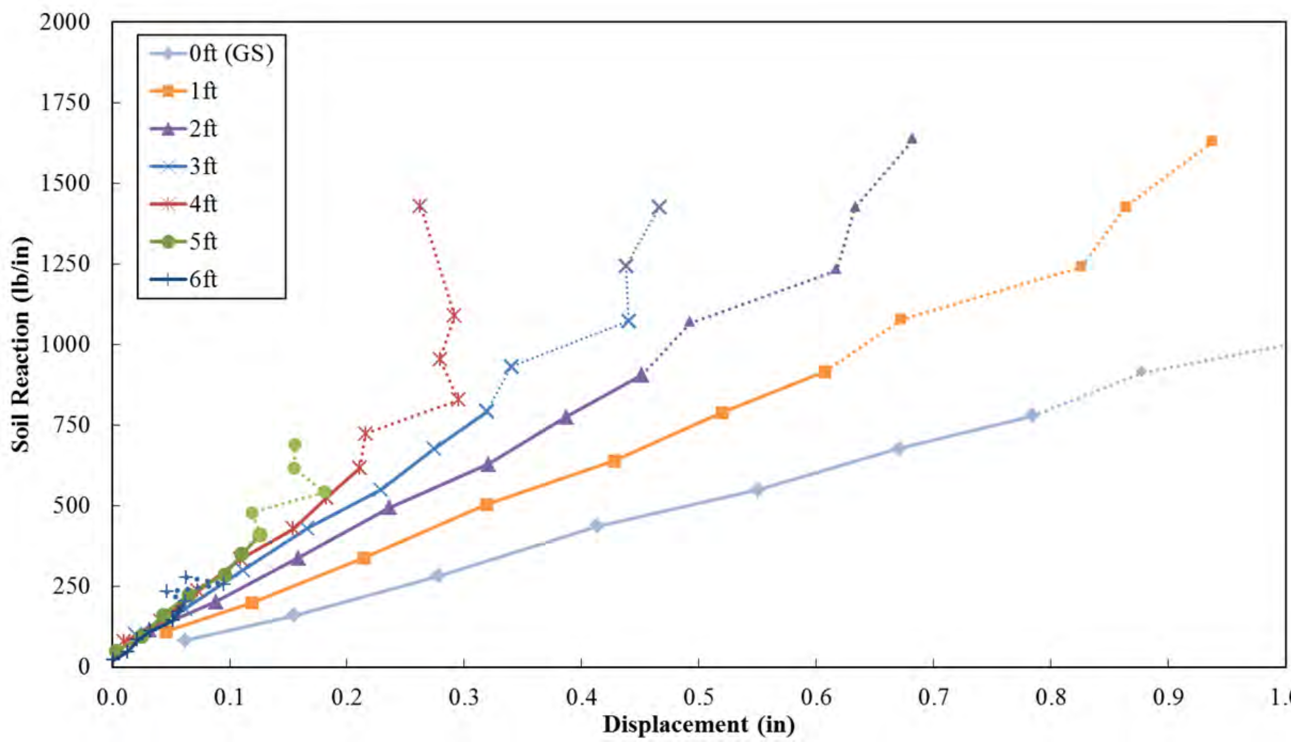

Figure 12-6 Back-Calculated *p-y* Curves for the 4D Pile (P-7) Showing Lower Displacements
Note: Dotted Lines Present Data after Initial Pile Yielding

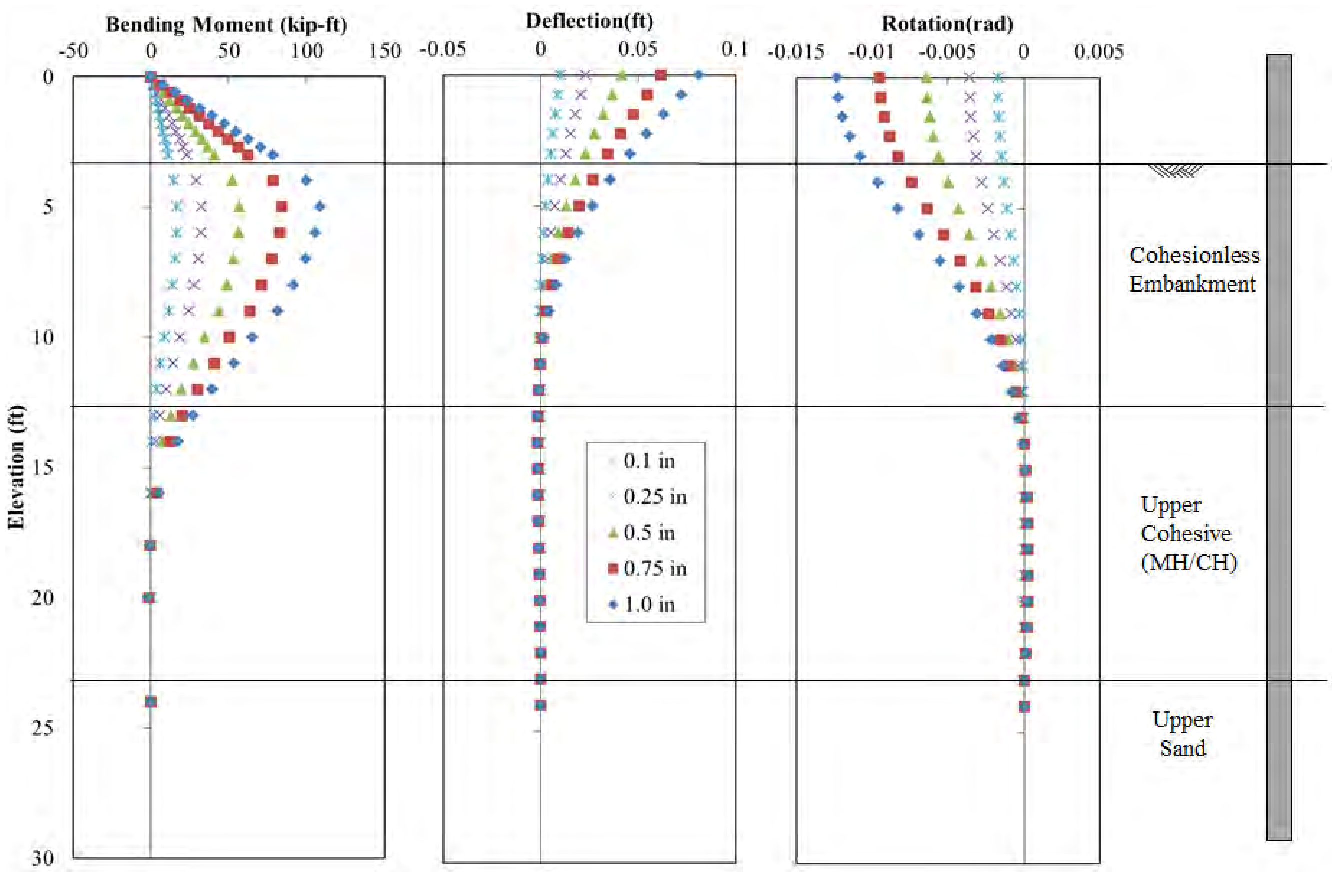

Figure 12-7 Comparison of Test Results and Analysis Using Back-Calculated *p-y* Curves for the 4D Pile (P-7) for Pile Head Displacement of 0.1, 0.25, 0.5 and 1.0 in.

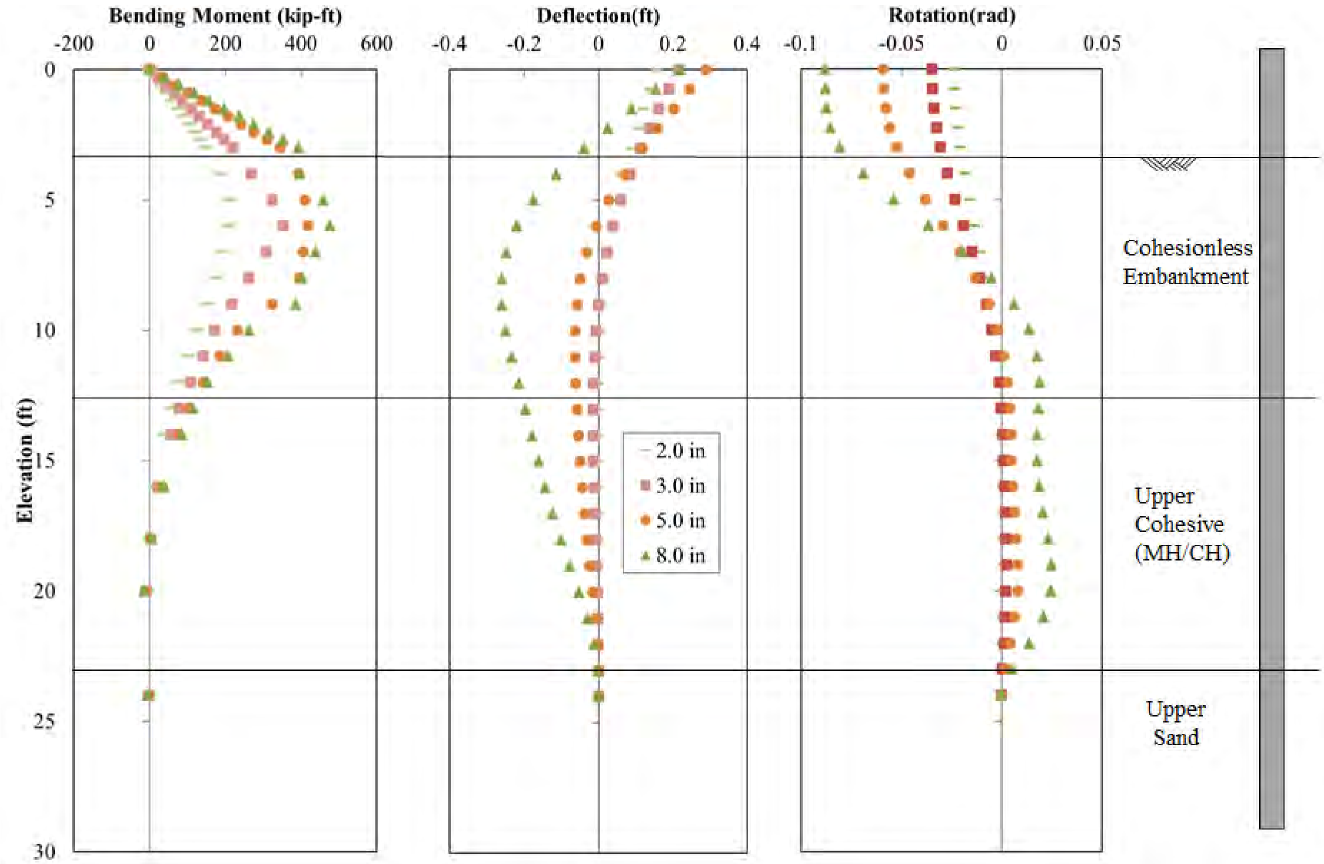

Figure 12-8 Comparison of Test Results and Analysis Using Back-Calculated *p-y* Curves for the 4D Pile (P-7) for Pile Head Displacement of 2.0, 3.0, 5.0 and 8.0 in.

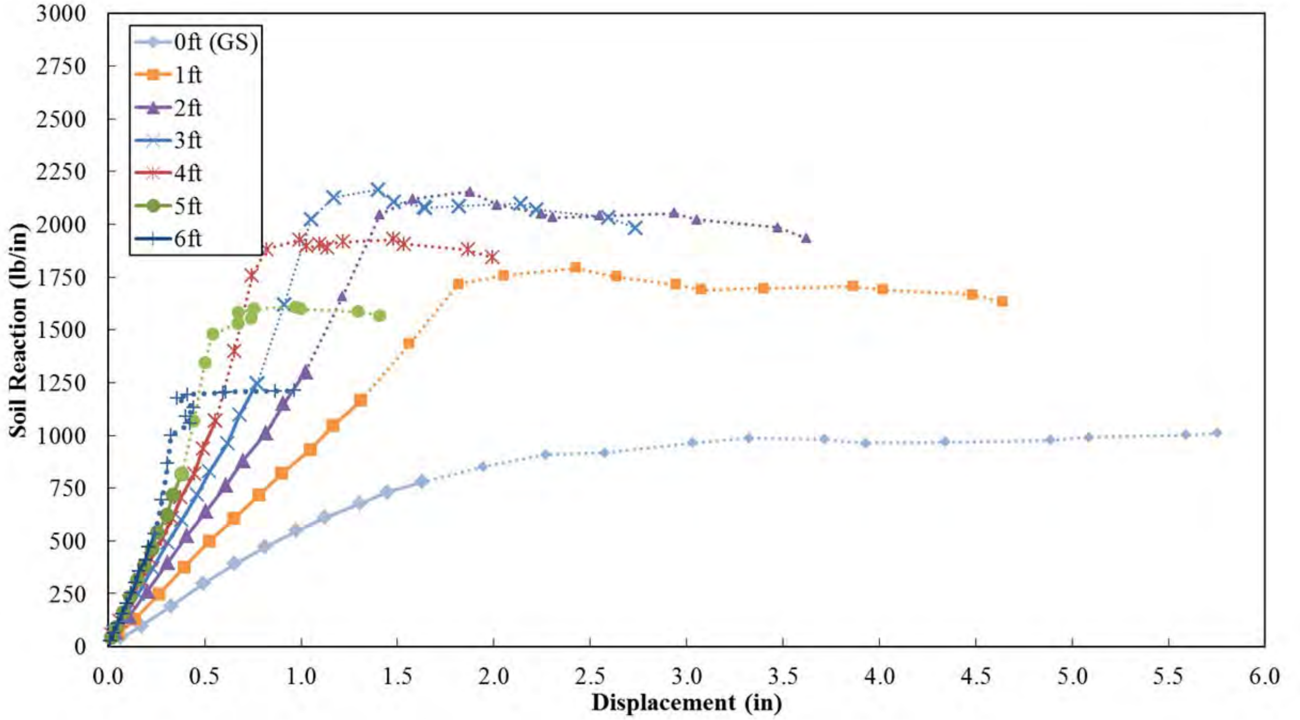

Figure 12-9 Back-Calculated *p-y* Curves for the 2D Pile (P-6)
Note: Dotted Lines Present Data after Initial Pile Yielding

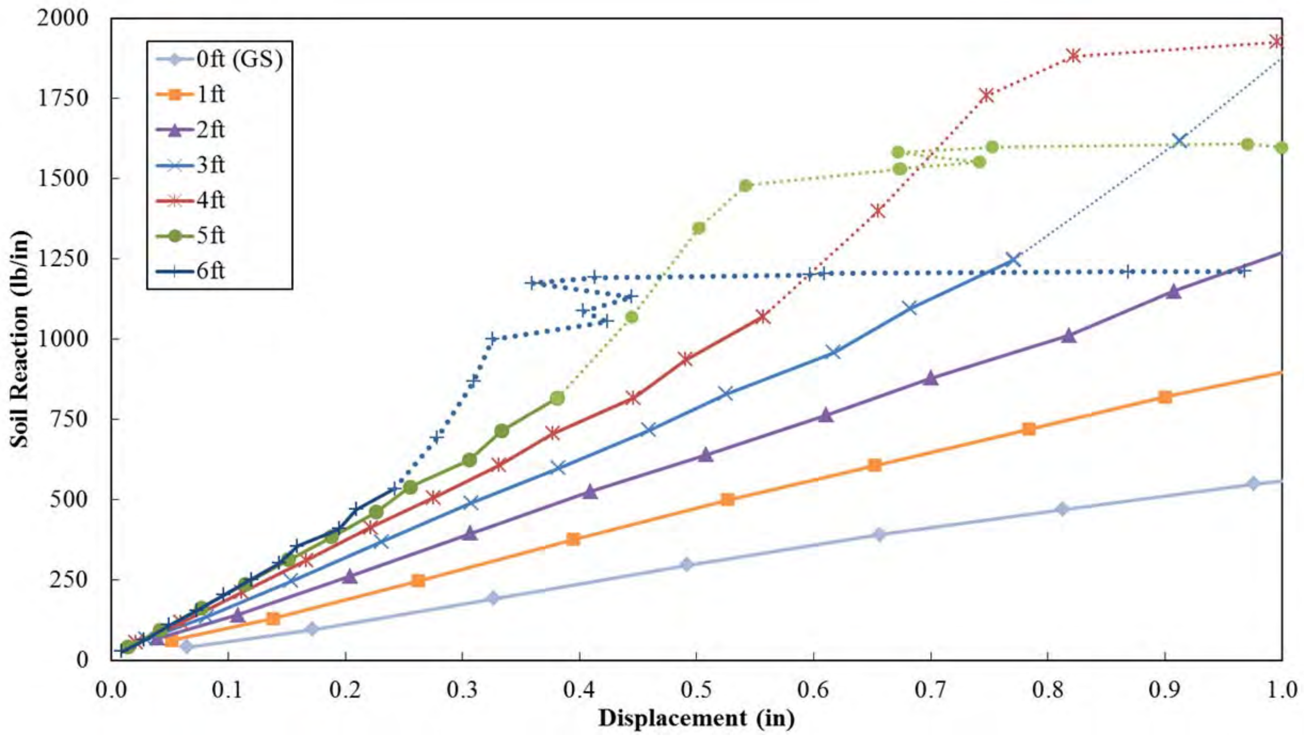

Figure 12-10 Back-Calculated *p-y* Curves for the 2D Pile (P-6) Showing Lower Displacements
Note: Dotted Lines Present Data after Initial Pile Yielding

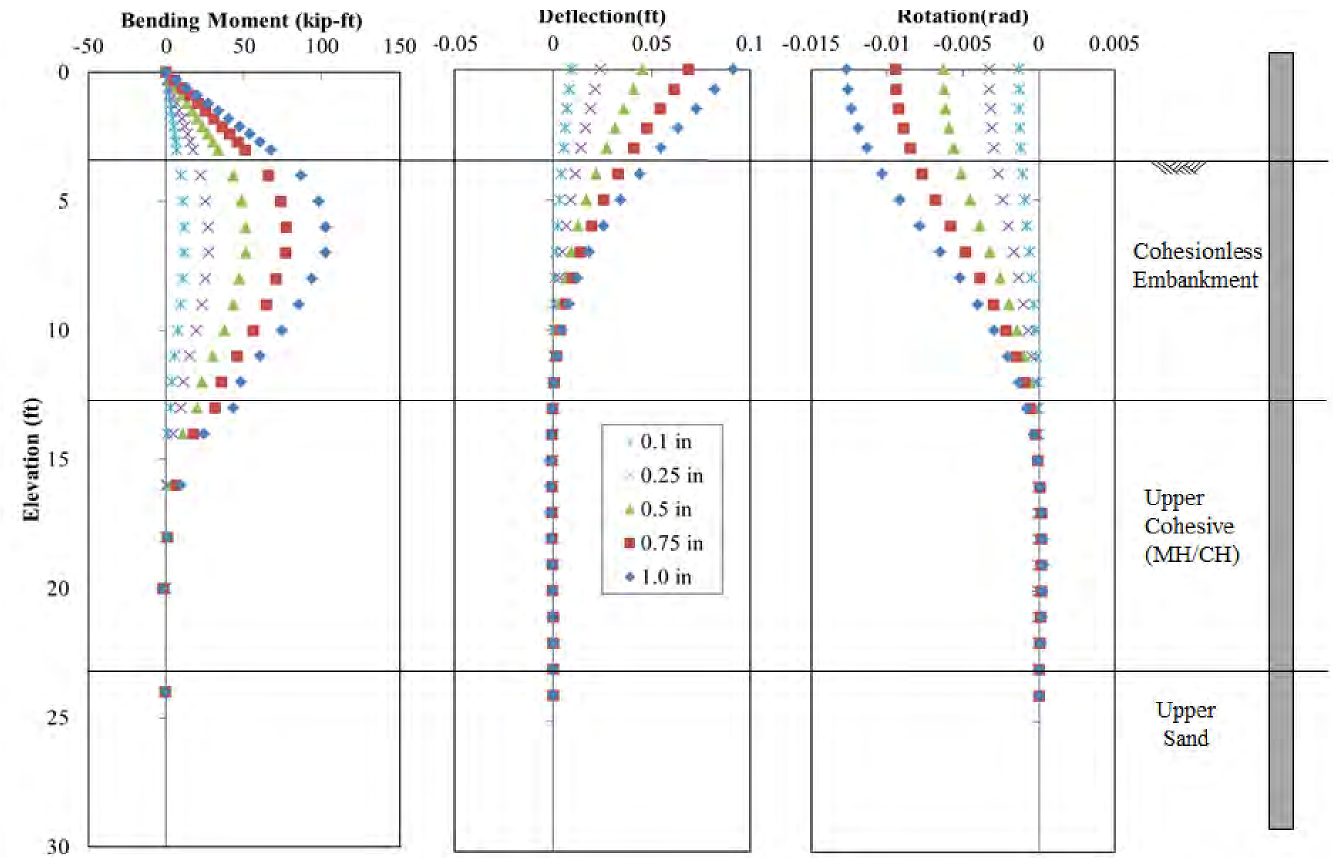

Figure 12-11 Comparison of Test Results and Analysis Using Back-Calculated *p-y* Curves for the 2D (P-6) for Pile Head Displacement of 0.1, 0.25, 0.5 and 1.0 in.

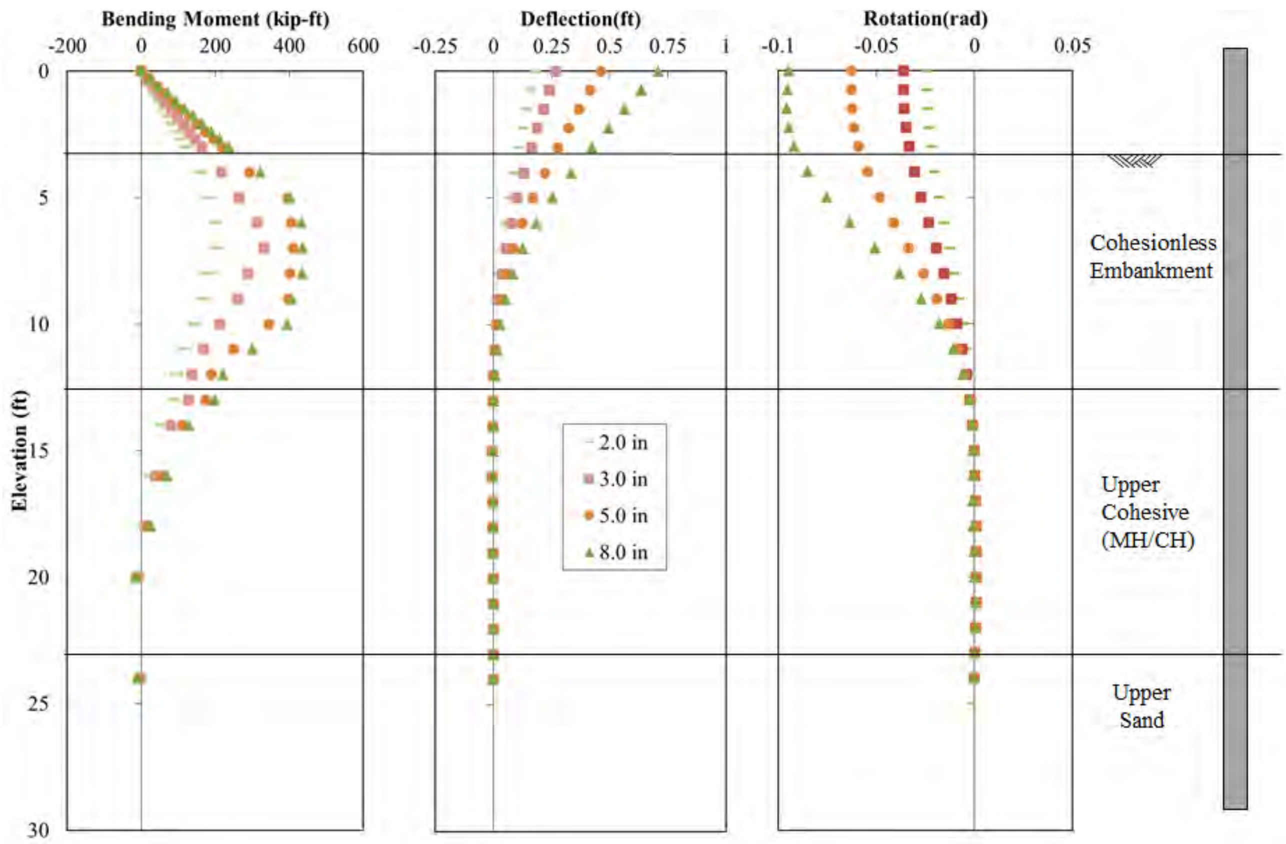

Figure 12-12 Comparison of Test Results and Analysis Using Back-Calculated *p-y* Curves for the 2D Pile (P-6) for Pile Head Displacement of 2.0, 3.0, 5.0 and 8.0 in.

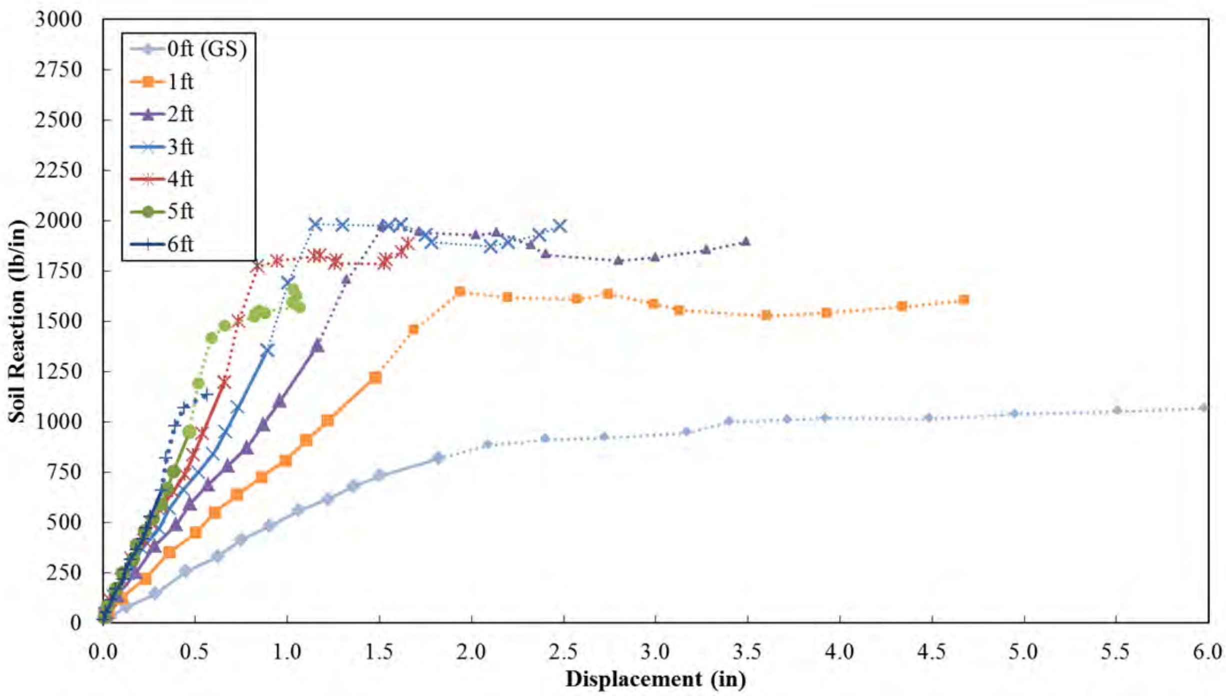

Figure 12-13 Back-Calculated *p-y* Curves for the 0D Pile (P-9) (On Crest)
Note: Dotted Lines Present Data after Initial Pile Yielding

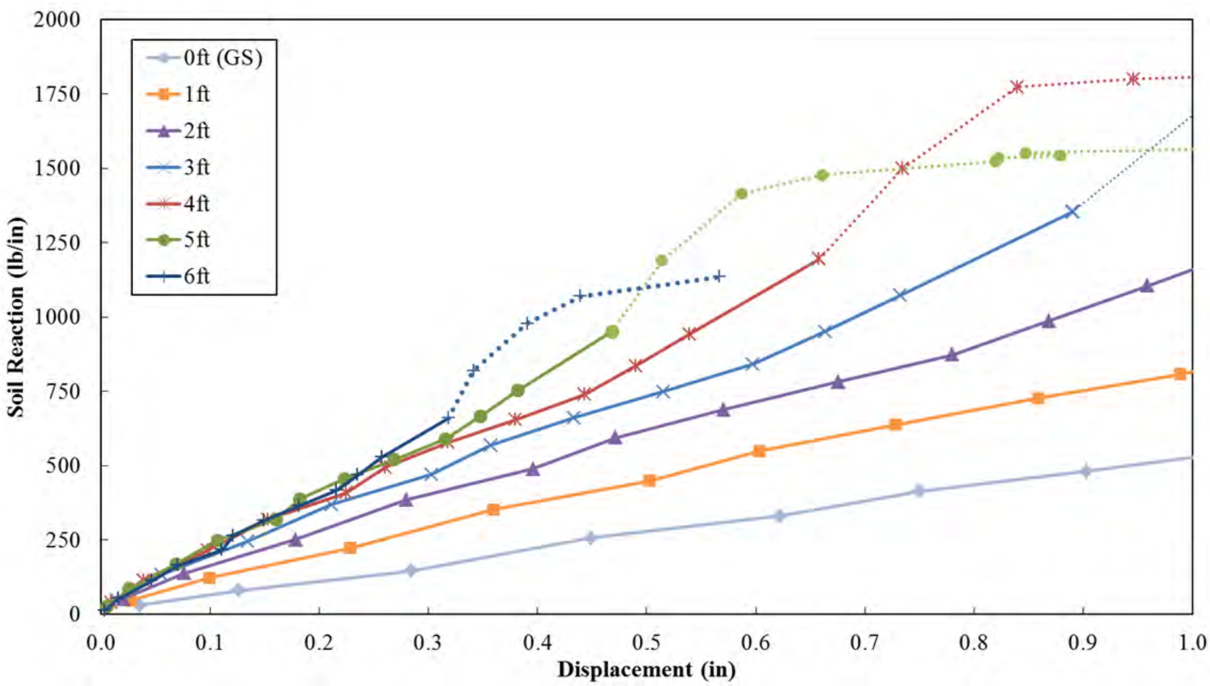

Figure 12-14 Back-Calculated *p-y* Curves for the 0D Pile (P-9) Showing Lower Displacements
Note: Dotted Lines Present Data after Initial Pile Yielding

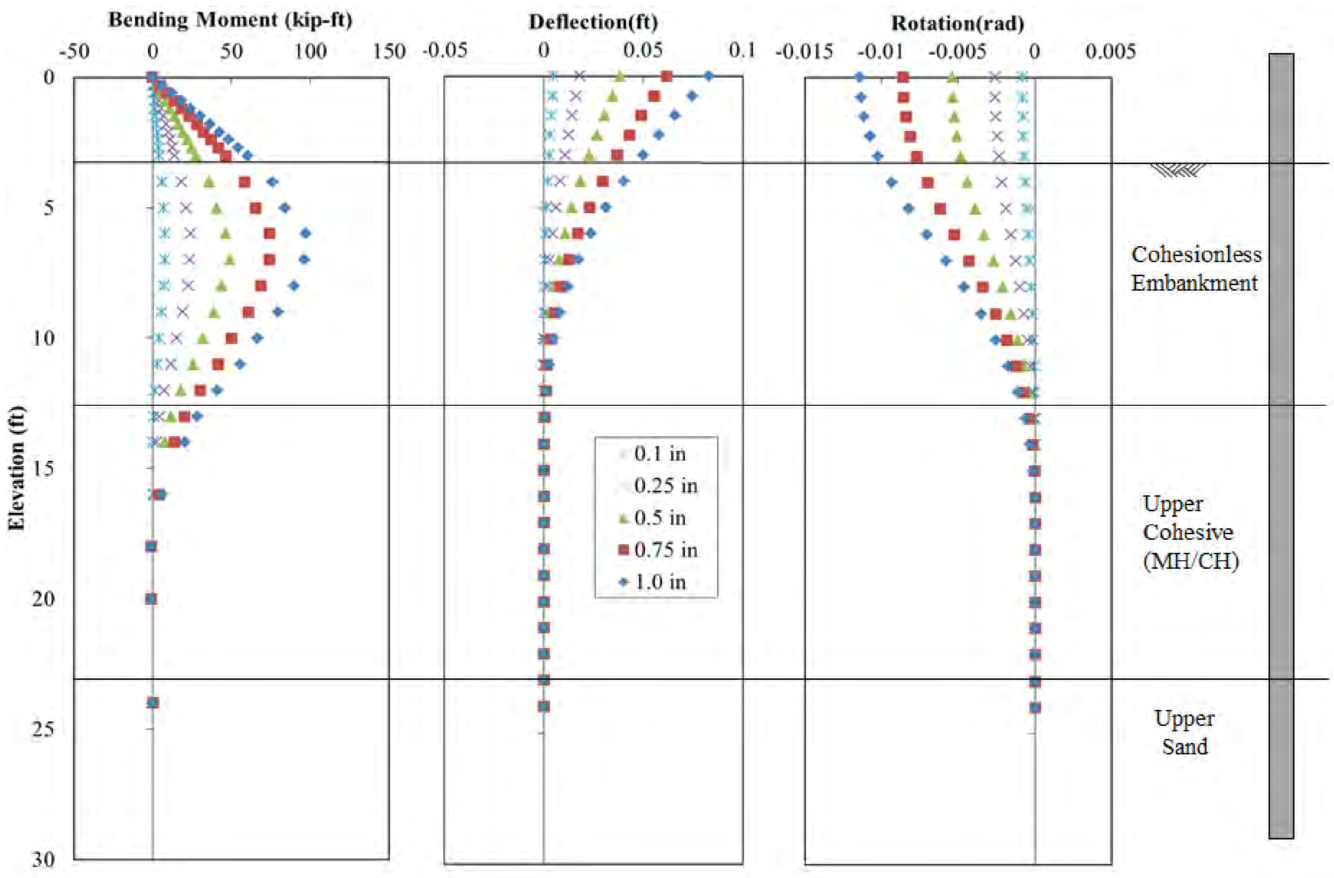

Figure 12-15 Comparison of Test Results and Analysis Using Back-Calculated *p-y* Curves for the 0 (P-9) for Pile Head Displacement of 0.1, 0.25, 0.5 and 1.0 in.

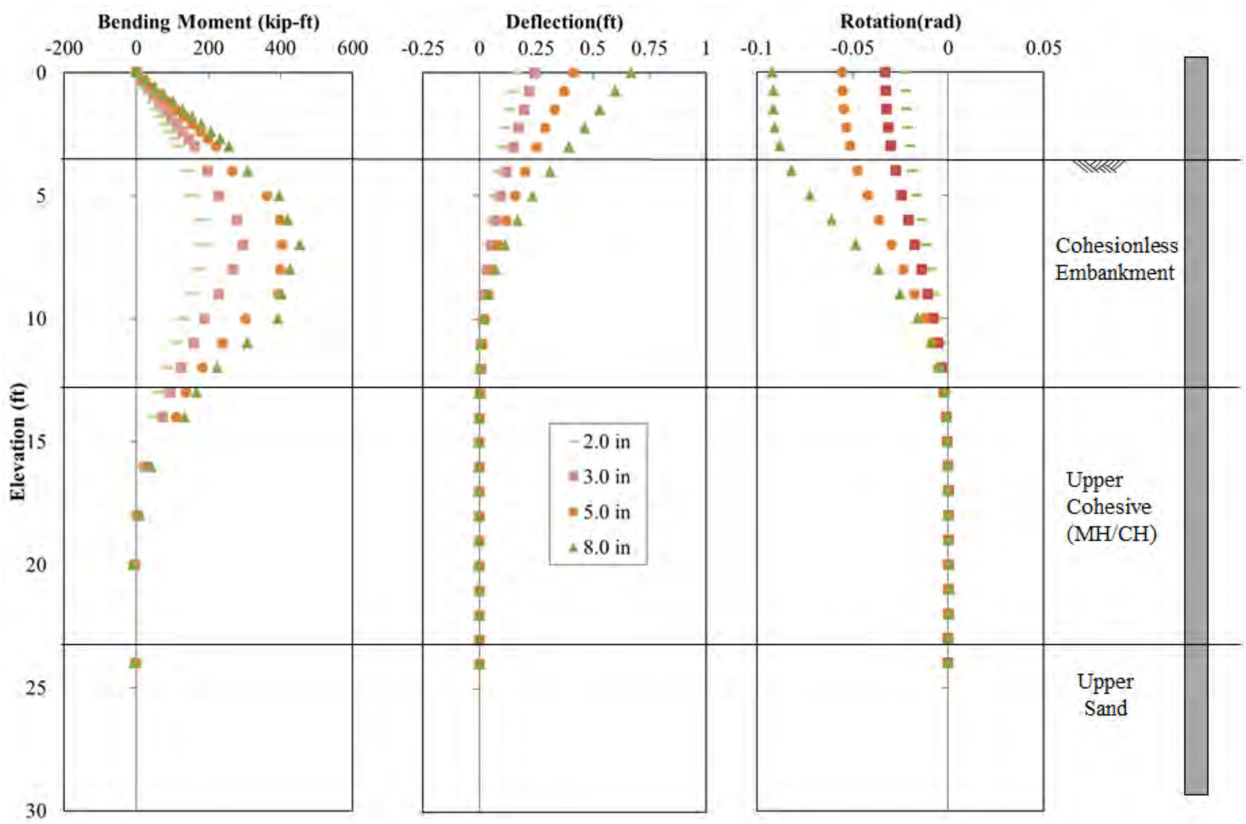

Figure 12-16 Comparison of Test Results and Analysis Using Back-Calculated *p-y* Curves for the 0D Pile (P-9) for Pile Head Displacement of 2.0, 3.0, 5.0 and 8.0 in.

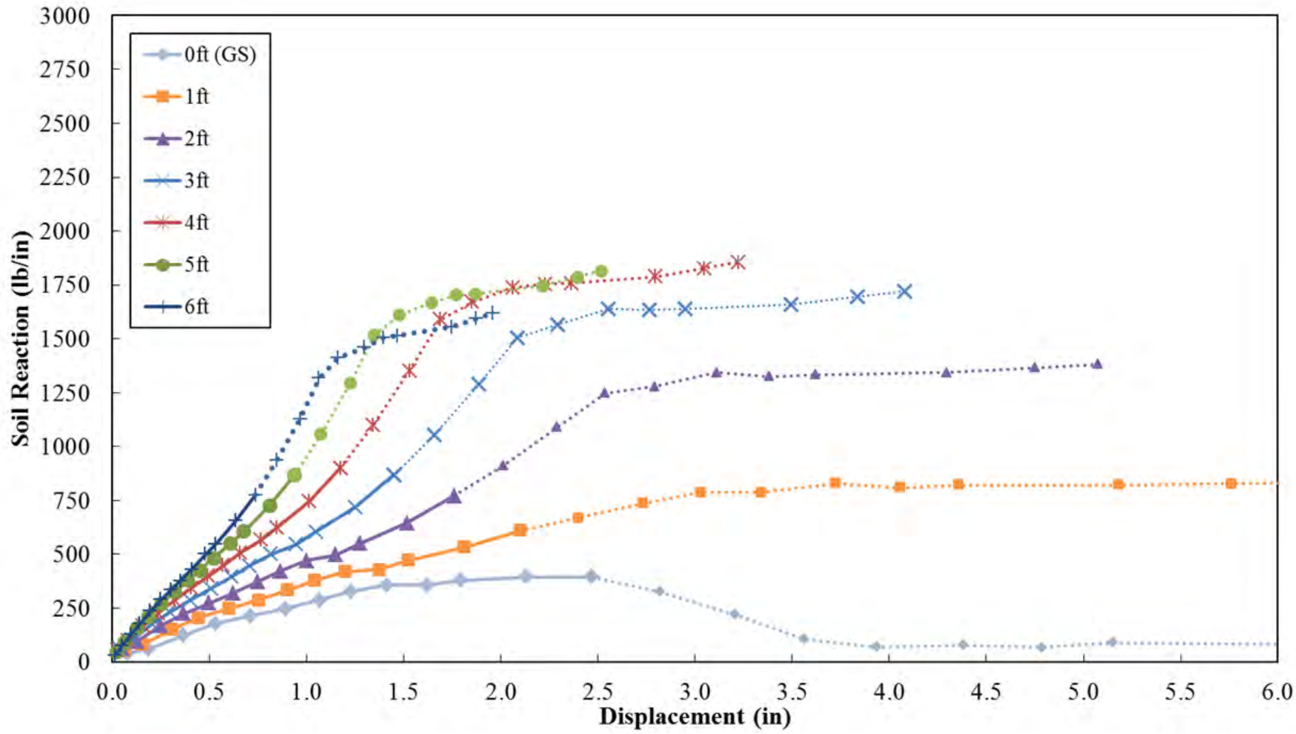

Figure 12-17 Back-Calculated *p-y* Curves for the -4D Pile (P-10) (On Slope)
Note: Dotted Lines Present Data after Initial Pile Yielding

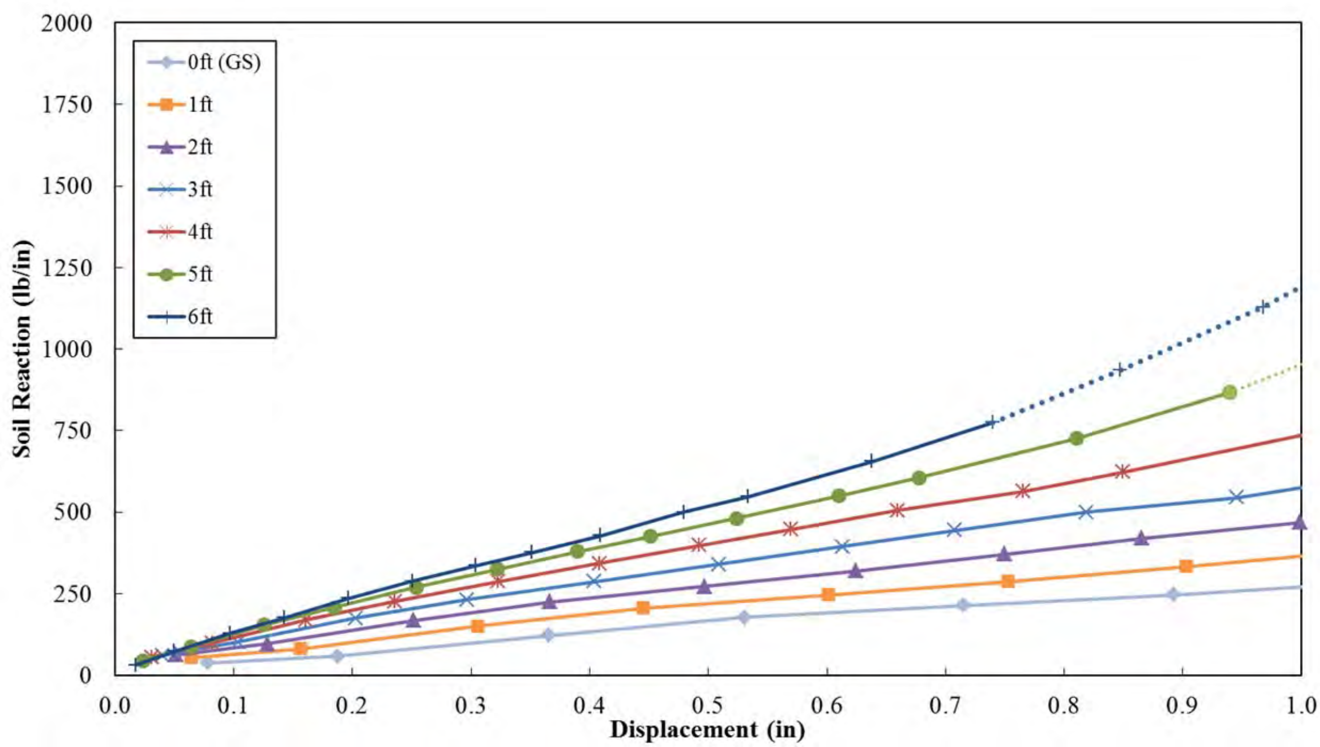

Figure 12-18 Back-Calculated *p-y* Curves for the -4D Pile (P-10) With Lower Displacements
Note: Dotted Lines Present Data after Initial Pile Yielding

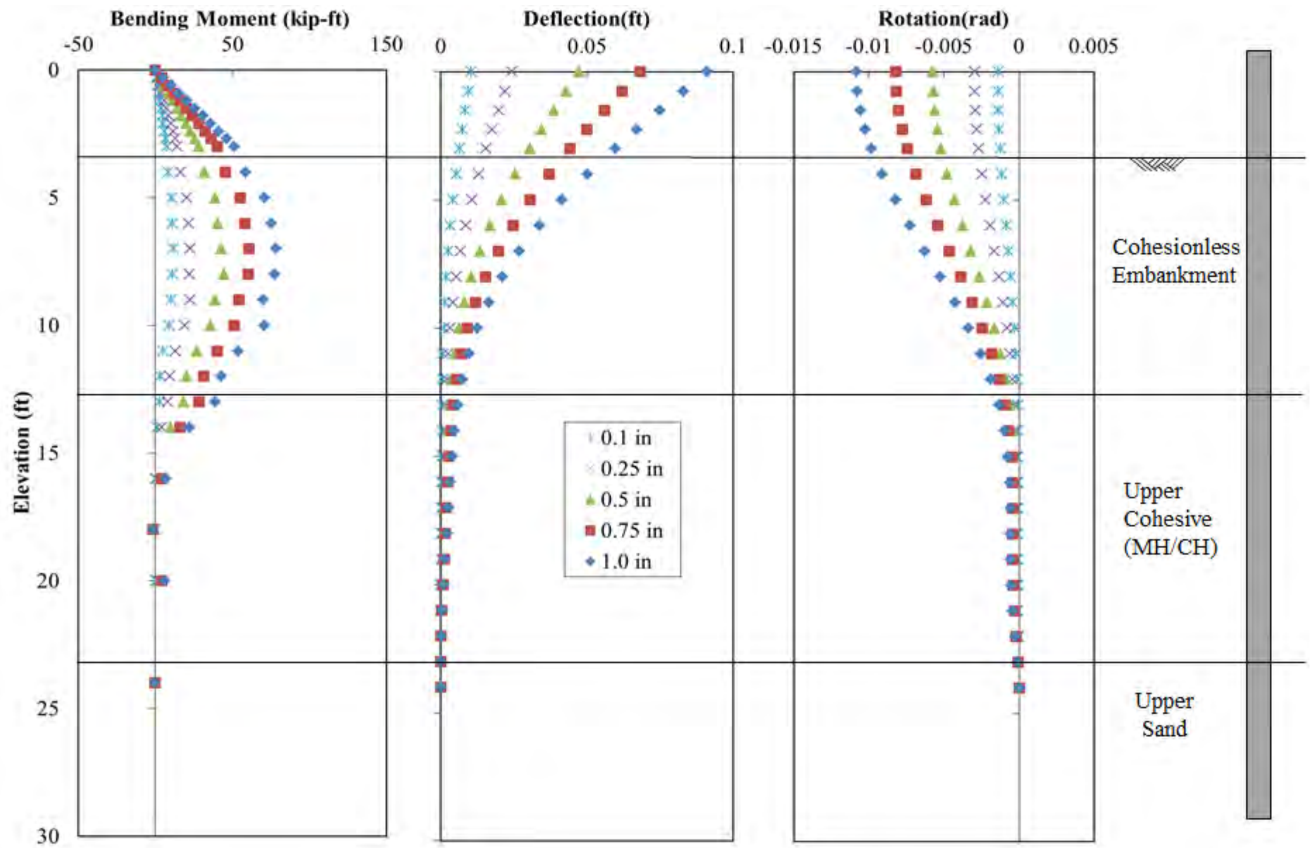

Figure 12-19 Comparison of Test Results and Analysis Using Back-Calculated *p-y* Curves for the -4D (P-10) for Pile Head Displacement of 0.1, 0.25, 0.5 and 1.0 in.

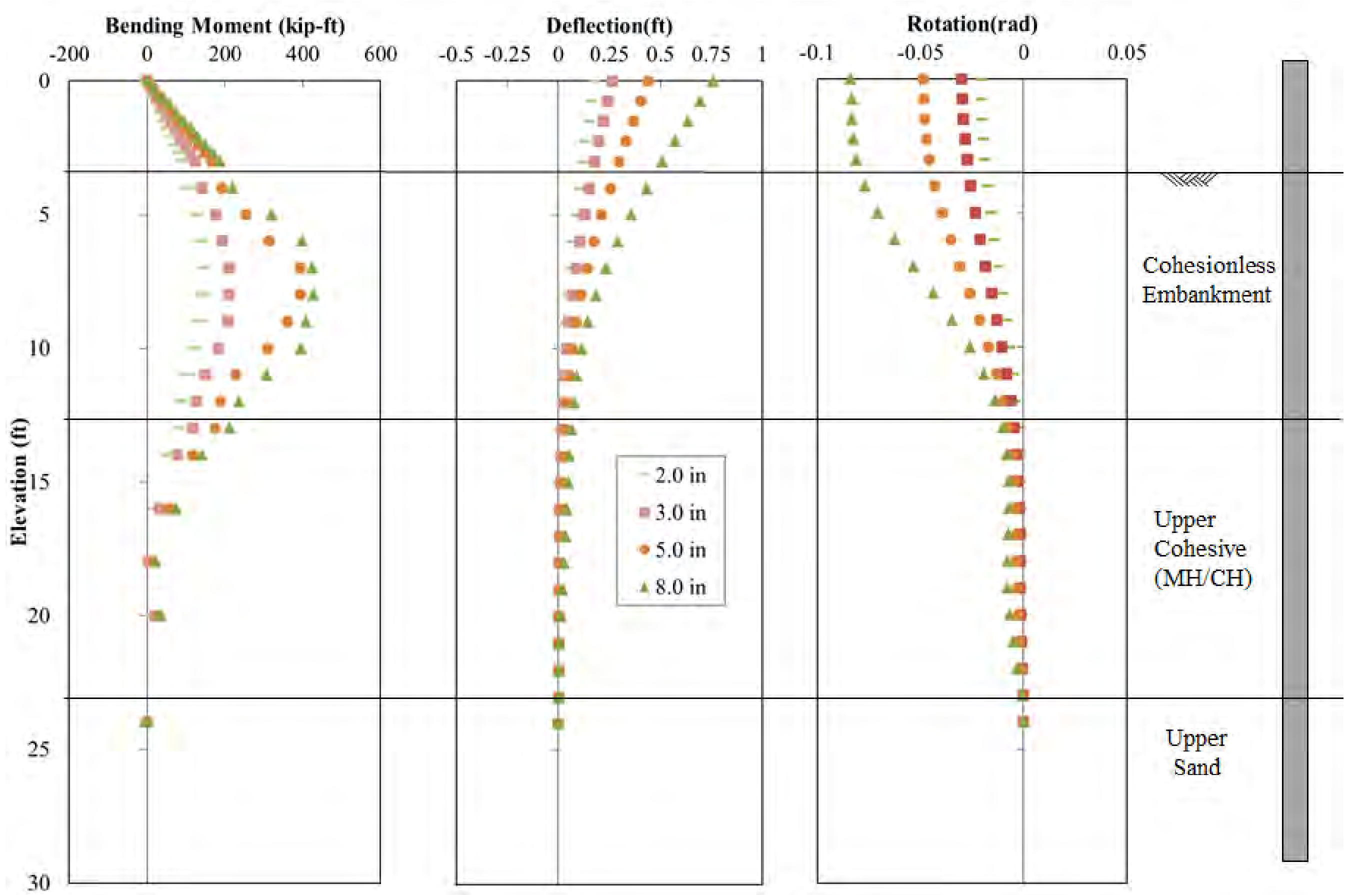

Figure 12-20 Comparison of Test Results and Analysis Using Back-Calculated *p-y* Curves for the -4D Pile (P-10) for Pile Head Displacement of 2.0, 3.0, 5.0 and 8.0 in.

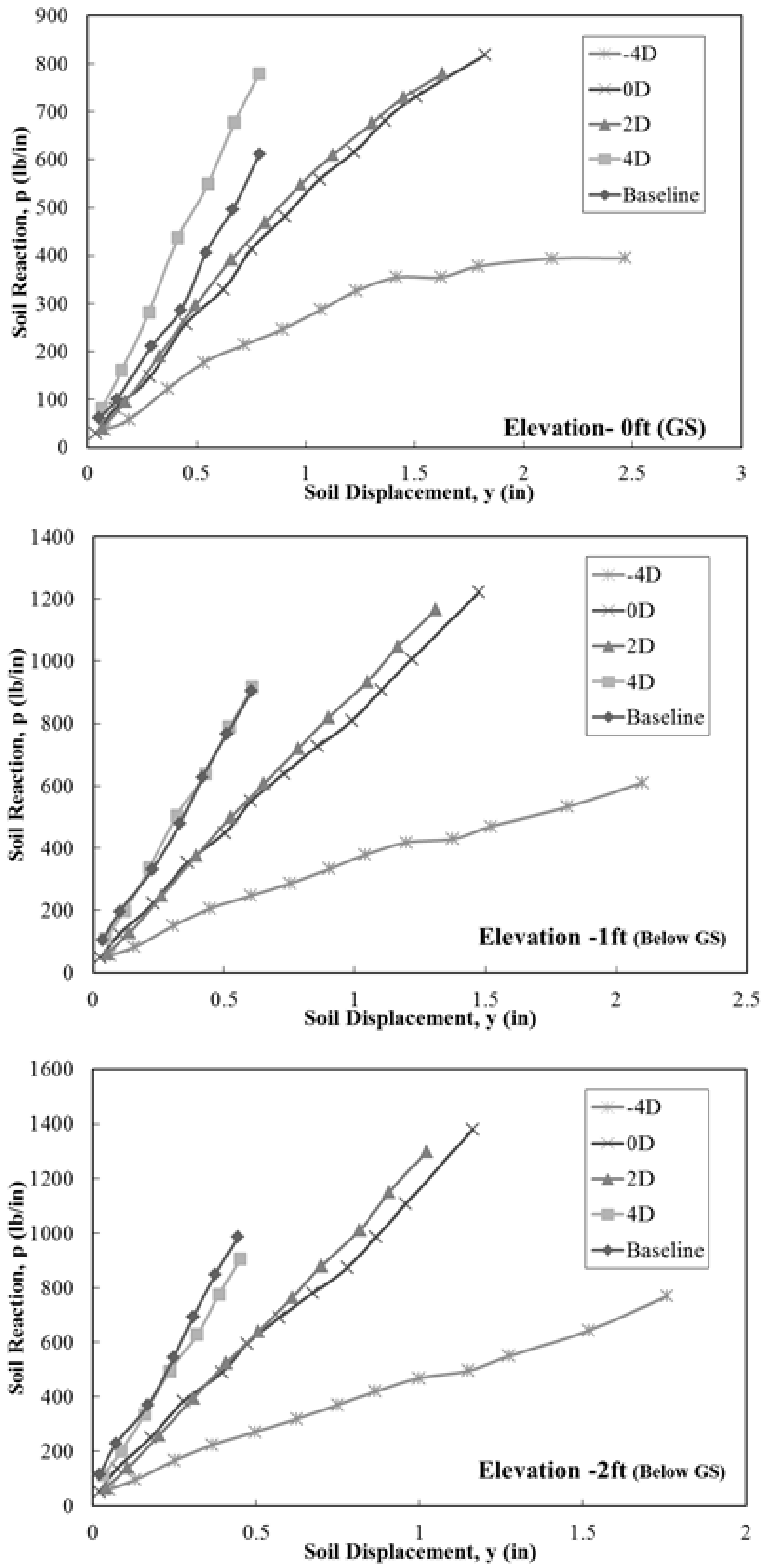

Figure 12-21 Comparison of *p-y* Curves for Each Pile at the Same Depth (GS to -2ft)

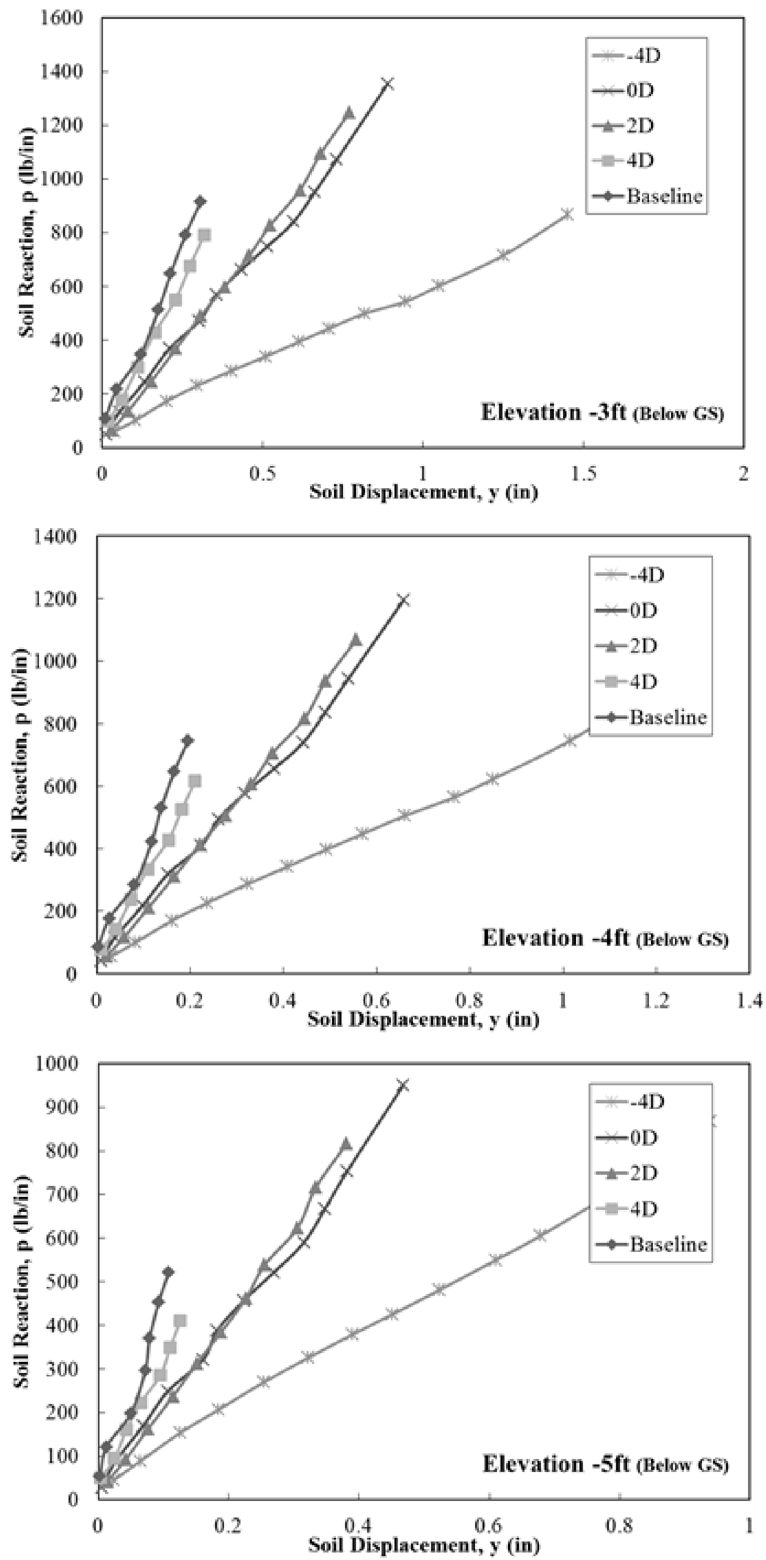

Figure 12-22 Comparison of *p-y* Curves for Each Pile at the Same Depth (-2ft to-5ft)

13. COMPARISON OF CURRENT METHODS & MODELS

13.1 INTRODUCTION

Several researchers have proposed methods to account for lateral pile capacities in level ground cohesionless soils and near slopes. With the results obtained from this study a comparison of existing methods was conducted. Comparisons were made between back-calculated and predicted p-y curves, load-displacement curves, reduction factors, and load resistance ratios. A simplified design procedure to account for the effects of soil slope is proposed from the results. Note: All figures containing *p-y* curves in this chapter present the *p-y* curves as a function of depth from the ground surface and not from the point of loading (i.e., *p-y* curves at 1 ft below ground surface are labeled as 1 ft compared to the *p-y* curves presented in Chapter 7 where the same curve is labeled as -4ft or 4 ft below the point of lateral loading.)

13.2 PROPOSED P-MULTIPLIERS

p-multipliers, or reduction factors, were constructed for piles located near or in a cohesionless slopes by analyzing the available back-calculated p-y curves. The near slope soil resistances, *p*, (-4D, 0D, 2D, and 4D) were normalized with the baseline soil resistance to obtain reduction factors. Linear interpolation was used to obtain the reduction in soil resistance at locations between each near slope pile. The recommended p-multipliers range between 0.3 to 0.6 and are based on the distance from the slope crest and depth below the ground surface measured in pile diameters, D. These recommendations are created to account for a large range of pile displacements (i.e. more conservative, higher reduction in load). The conservatism built into the p-multipliers ranges from 5% to 25%. Final design recommendations are presented in Chapter 14.

13.3 COMPARISON OF HORIZONTAL GROUND MODELS

Two commonly used methods to predict lateral load capacity and p-y curves in level ground are the Reese et al. (1994) and API (1987) methods. The soil properties from the testing site were input in these models to compare the predictions with the back-calculated results.

13.4 REESE ET AL. 1794 (LPILE 6.0)

The pile properties obtained from the pile calibration test were input into the computer program LPILE Plus 6.0 (Reese et al., 2004). The average yield strength of the piles is 74.7 ksi and the effective yielding moment of the test piles was 416 kip-ft. A post yielding bending stiffness of 5% of the elastic stiffness was chosen for the LPILE analysis. The recommended coefficient of subgrade reaction, K, of 225 pci was used with a soil unit weight of 127pcf.

Figure 13-1 shows the LPILE predicted load-displacement curve with the full-scale test results for the baseline pile. LPILE underestimates the lateral capacity for all pile head displacements. The ultimate resistance was underestimated by almost 20% and the initial stiffness was also lower.

Figure 13-2 presents the predicted baseline p-y curves calculated using the same soil parameters with the Reese et al. (1974) cohesionless soil procedures. These curves are shown at 1ft intervals to a depth of 4 ft with displacements up to 0.6 inches. These values were chosen for comparison with the available back-calculated p-y curves. This model is based on an initial linear soil modulus and then a hyperbolic function before reaching the ultimate soil reaction. The ultimate soil reaction is reached in this model at just under 0.5 inches. A further comparison of these curves, API (1987) predictions, and the back-calculated results are presented in section 13.5.

The LPILE predicted load displacement curve for the Series-II baseline pile is conservative and under predicts the stiffness and ultimate load found in full-scale results. Application of the proposed cohesionless p-multipliers to the LPILE predictions will not results in "similar" near slope results because the starting points or curves (baseline load-displacement curves) are not similar. The application of the proposed p-multipliers to the baseline predictions would result in over conservative estimations for near slope results. To make a better prediction, LPILE was "tweaked" to predict the greater magnitude baseline load displacement curve obtained in the full scale results. Then the application of the p-multipliers were applied this new baseline prediction to provide a better estimation of results from the proposed cohesionless p-multipliers. The effects of applying the p-multipliers to this "tweaked" baseline curve with the near slope full-scale results are shown in **Figure 13-3** through **Figure 13-5**. The results show that the LPILE predictions with the p-multipliers is conservative for the 2D and 0D load displacement curves and slightly over predicts the on slope (-4D) load displacement curve.

13.5 AMERICAN PETROLEUM INSTITUTE (1987)

The cohesionless embankment soil parameters were input into the API (1987) model to predict the baseline p-y curves. **Figure 13-6** presents the predicted baseline p-y curves with this procedure. A coefficient of subgrade reaction, K, of 225 pci was estimated in this model for sand above the water table using the API (1987) correlations with the friction angle as presented in Chapter 2.0. The p-y curves are shown at 1ft intervals to depth of 4 ft with displacements up to 0.6 inches. This model is based on hyperbolic functions before reaching the ultimate soil reaction. The ultimate soil reaction is reached in this model at a displacement of less than 0.2 inches.

Figure 13-7 and **Figure 13-8** show the predicted baseline API (1987) and Reese et al. (1974) p-y curves with the back-calculated p-y curves from this study. Only p-y curves to depth of 4 ft are compared. Deeper comparisons are not made because the pile displacements back-calculated at these depths are less than 0.2 inches. Both models over predict the initial stiffness at displacements of less than 0.2 inches at depths below 1ft. The API model has the greatest subgrade modulus at these displacements and reaches ultimate resistance before the Reese et al. (1974) model. The soil stiffness of the full-scale results is more representative of Reese et al. (1974) prediction model. At higher displacements, more than 0.2 inches, the soil reaction is significantly under predicted by both models at depths above 4ft. The available data from the back-calculated p-y curve at a depth of 4 ft is similar in stiffness to the Reese et al. (1974) p-y curve.

In **Figure 13-7** and **Figure 13-8** only the pre-plastic yielding p-y curves are presented for comparison. No apparent ultimate soil resistance is reached from the available back-calculated data. The ultimate soil resistance is about 200 lb/in for both models at a depth of 1ft, and the back-calculated resistance is close to 700 lb/in at a displacement of 0.45 inches without an obvious ultimate resistance reached. At depths of 2 ft and 3 ft the ultimate soil reaction is significantly under predicted by both models. The magnitudes of the Reese et al. (1974) model more closely predicted the resistances obtained in the full-scale test results.

Table 13-1 presents the mean bias and coefficient of variation (COV) values between the back-calculated and predictive model p-y curves at increasing pile displacements. A total of

110 data points were used in this statistical analysis. The mean bias was calculated by the observed divided by the predicted.

13.6 COMPARISON OF SLOPING GROUND MODELS

13.6.1 REESE ET AL. 2006 (LPILE 6.0)

The embankment soil properties were input into LPILE 6.0 to predict to lateral response of a pile located on a crest slope. The Reese et al. (1974) soil model was used with a coefficient of subgrade modulus of 225pci. **Figure 13-9** shows the LPILE predicted load-displacement curve with the full-scale test results for the 0D test pile. LPILE slightly underestimates the lateral capacity for pile head displacements over 0.5 in. The ultimate resistance was underestimated by about 10% and the predicted initial stiffness was lower between pile head displacements of 0.5 in. and 3.0 in. **Table 13-2** shows the mean bias and COV between the full-scale load-displacement curves with LPILE predictions for the 0D and baseline pile tests. These results show that COV and mean bias are greater for both piles at low displacements (less than 3 inches), again concluding this method underestimates the ultimate resistance.

13.6.2 MEZAZIGH AND LEVACHER (1998)

From the results obtained from centrifuge tests in sands, Mezazigh and Levacher (1998) presented reduction coefficients, $r_{(D)}$ that can be applied to p-y curves for piles in level ground. This reduction coefficient, also known as a p-multiplier, is then applied to the resistance pressure, p. The slope angle, pile diameter, and distance from slope crest all effect the value of this reduction factor. Using the parameters from this research project the proposed reductions factors from Mezazigh and Levacher (1998) are 0.25, 0.44, 0.62, and 1.0 for piles located at 0D, 2D, 4D, and 8D respectively. **Figure 13-10** through **Figure 13-12** show the results of applying the corresponding reduction factors to the back-calculated baseline p-y curves with the 0D, 2D, and 4D test results.

The Mezazigh and Levacher (1998) reduction coefficients are considered conservative from this analysis. The baseline soil resistance was reduced to levels significantly below the 0D results for all depths investigated. At distances of 2D and 4D from the slope crest the reduced baseline curves better represent the p-y curves at these locations while still being conservative.

The mean bias and coefficient of variation between the reduced baseline and the 0D, 2D, and 4D piles are shown in **Table 13-3** through **Table 13-5**. Each of these tables compare the baseline p-y curves reduced with Mezazigh and Levacher (1998) reduction coefficients with result from the 0D, 2D, and 4D pile. The mean bias and COV was computed for targeted displacements along all p-y curves and between all p-y curves at target depths. The results from the calculated bias and COV for each pile locations demonstrates that the Mezazigh and Levacher (1998) reduction coefficients are more accurate for the 2D and 4D piles and for the deeper p-y curves. This model over predicts the reduction required from a slope crest and is conservative in all cases examined.

13.7 LATERAL RESISTANCE RATIOS

In addition to reduction factors, many researchers use lateral load resistance ratios to compare baseline load-displacement curves with near slope curves. The data obtained at target pile head displacements for near slope tests were normalized with the baseline load-displacement data. **Figure 13-13** presents the lateral resistance ratios from this study.

The 8D pile, as previously discussed, has no reduction in lateral capacity and had a load ratio, Ψ, of 1.0. Single value averages of the load ratios (**Figure 13-13**) for the -4D, 0D, 2D and 4D piles are 0.55, 0.70, 0.90, and 0.95, respectively. The ratio of the 4D pile does not drop below 1.0 until 2.5 inches of pile head displacement. For the -4D, 0D, 2D piles, the load ratio increased from a minimum value during the first 0.75 inches of movement and stayed relatively consistent for the remainder of the pile displacement. This may be caused by the reduced initial subgrade modulus observed in the p-y curves from the reduction of overburden pressure caused by the presence of the test slope.

Figure 13-14 compares the load resistance ratios obtained from these full-scale tests with the finding from other researchers. The results from this project are near the upper bound of the recommendations and are very similar to the full-scale results of Mirzoyan (2007). The predictions from FEM, analytical equations, and scaled tests tend to overestimate the effects of soil slope.

13.8 SUMMARY

Multiple observations and conclusions were made from comparisons between the back-calculated full-scale results and models proposed by other researchers. The significant points include:

1. The Computer program LPILE 6.0 underestimates the initial stiffness and the lateral pile capacity in level ground conditions by as much as 20%. The predicted lateral capacity for the 0D pile was relatively accurate and only underestimated the lateral capacity by less than 10%.
2. The predicted baseline API (1987) and Reese et al. (1974) p-y curves over predict the initial stiffness at low displacements, less than 0.2 inches.
3. The API model has the greatest subgrade modulus at low displacements and reaches ultimate resistance at low displacements.
4. Reese et al. (1974) model more accurately predicted the back-calculated p-y curves but significantly underestimates soil resistance at displacements greater than 0.25 inches.
5. Mezazigh and Levacher (1998) reduction coefficients are conservative and significantly reduced the baseline p-y curve below the near slope back-calculated curves.

The load resistance ratio from this study were 0.55, 0.70, 0.90, and 0.95 for piles located at -4D, 0D, 2D, and 4D respectively. These results are on the upper bound of the ratios presented by other researchers, demonstrating that many models tend to overestimate the effects of a slope. A simplified design procedure was presented to account for the effects of soil slope on lateral pile capacities.

Table 13-1 Mean bias and COV between the back-calculated and predictive model p-y curves at various pile displacements

Displacement (in)	Mean Bias	COV (%)
0.1	0.7	29.8
0.2	0.8	35.0
0.3	1.3	30.3
0.4	1.9	29.5
0.5	2.6	33.3

Table 13-2 Mean bias and COV between the full-scale and LPILE load displacement curves

Pile	Pile Displacements < 3 inch		Pile Displacements > 3 inch	
	Mean Bias	COV (%)	Mean Bias	COV (%)
Baseline	1.41	5.5	1.34	3.2
0D	1.25	8.1	1.16	4.6

Table 13-3 Mean bias and COV between the reduced baseline and 0D p-y curves with the Mezazigh and Levacher (1998) reduction coefficients

Displacement (in)	Mean Bias	COV (%)
0.05	2.22	3.9
0.1	2.52	2.1
0.15	2.51	8.0
0.2	2.47	10.1
0.25	2.50	9.4
0.3	2.43	9.7
0.4	2.41	7.0
Mean	2.44	7.2

Depth (ft)	Mean Bias	COV (%)
1.0	2.42	11.5
2.0	2.27	11.8
3.0	2.18	13.6
4.0	2.14	16.7
Mean	2.25	13.4

Table 13-4 Mean Bias and COV between the reduced Baseline and 2D P-Y Curves with the Mezazigh and Levacher (1998) Reduction Coefficients

Displacement (in)	Mean Bias	COV (%)
0.05	1.00	4.1
0.1	1.20	2.7
0.15	1.25	7.0
0.2	1.29	8.6
0.25	1.33	9.1
0.3	1.33	9.0
0.4	1.37	6.9
Mean	1.25	6.8

Depth (ft)	Mean Bias	COV (%)
1.0	1.25	20.5
2.0	1.14	18.0
3.0	1.06	17.7
4.0	1.02	19.1
Mean	1.12	18.8

Table 13-5 Mean Bias and COV between the reduced Baseline and 4D P-Y Curves with the Mezazigh and Levacher (1998) Reduction Coefficients

Displacement (in)	Mean Bias	COV (%)
0.05	1.26	7.3
0.1	1.39	3.1
0.15	1.41	10.2
0.2	1.44	11.4
0.25	1.49	12.1
0.3	1.48	11.5
0.4	1.52	8.7
Mean	1.43	9.2

Depth (ft)	Mean Bias	COV (%)
1.0	1.58	6.1
2.0	1.39	6.5
3.0	1.26	7.8
4.0	1.18	12.3
Mean	1.35	8.2

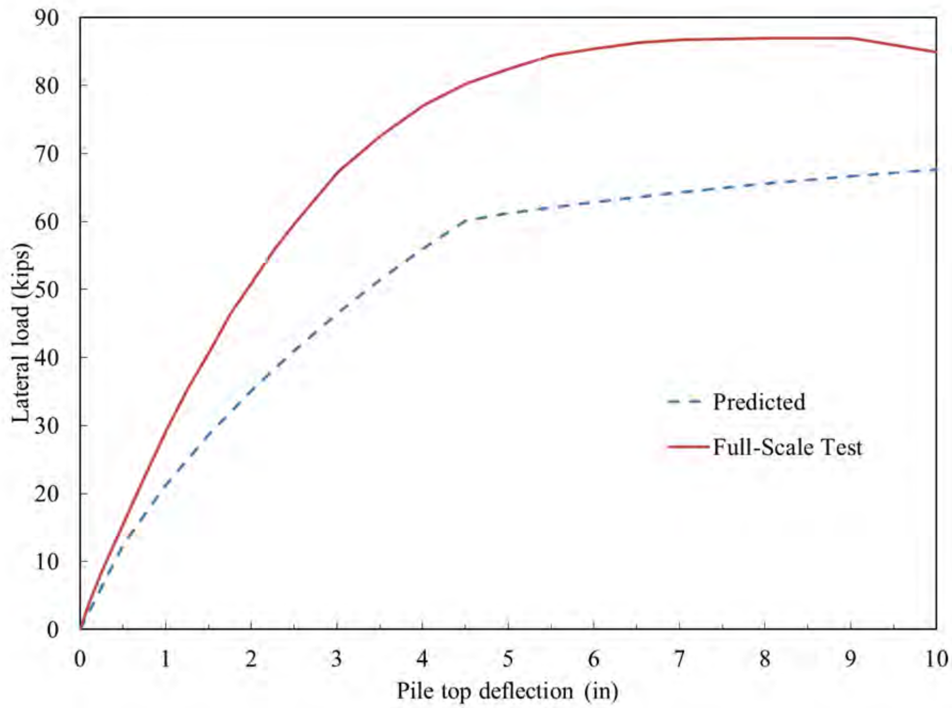

Figure 13-1 LPILE predicted baseline load-displacement curve with the full-scale test results

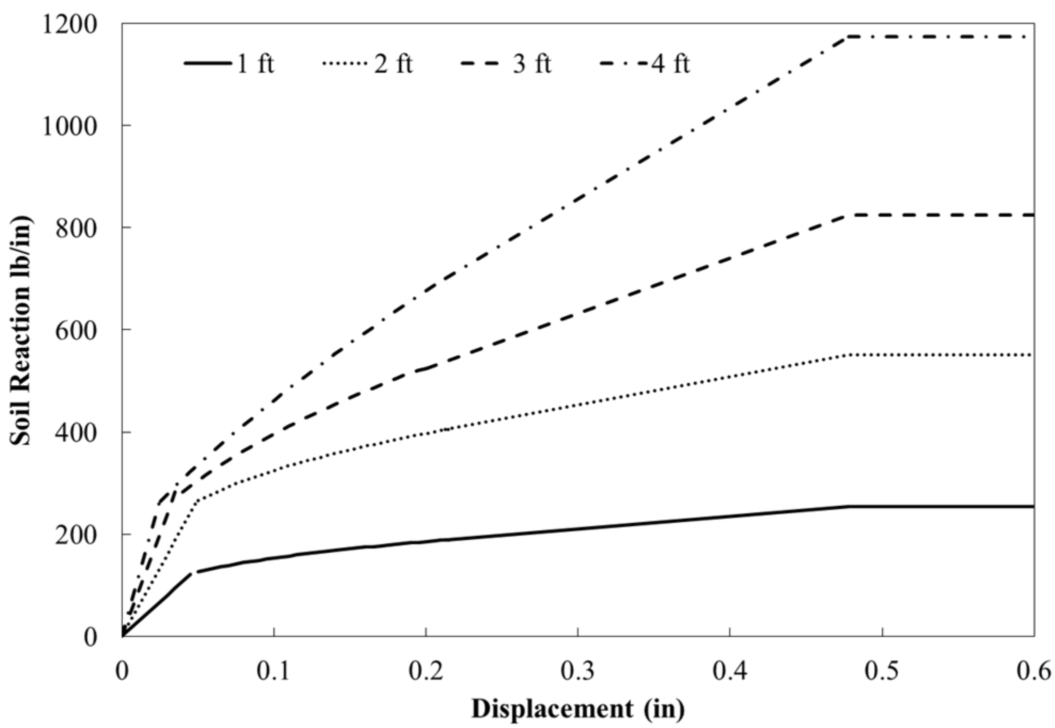

Figure 13-2 Reese et al. (1974) predicted baseline p-y curves with input soil properties matching the full-scale tests

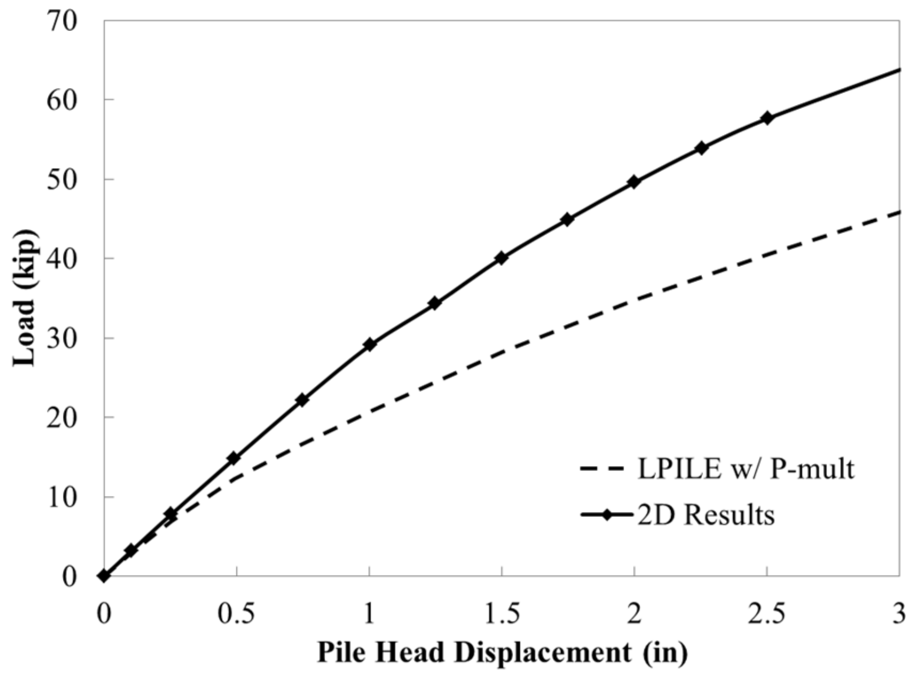

Figure 13-3 Comparison of the 2D full-scale results with the LPILE prediction using the proposed p-multipliers for a pile 2D from a slope crest

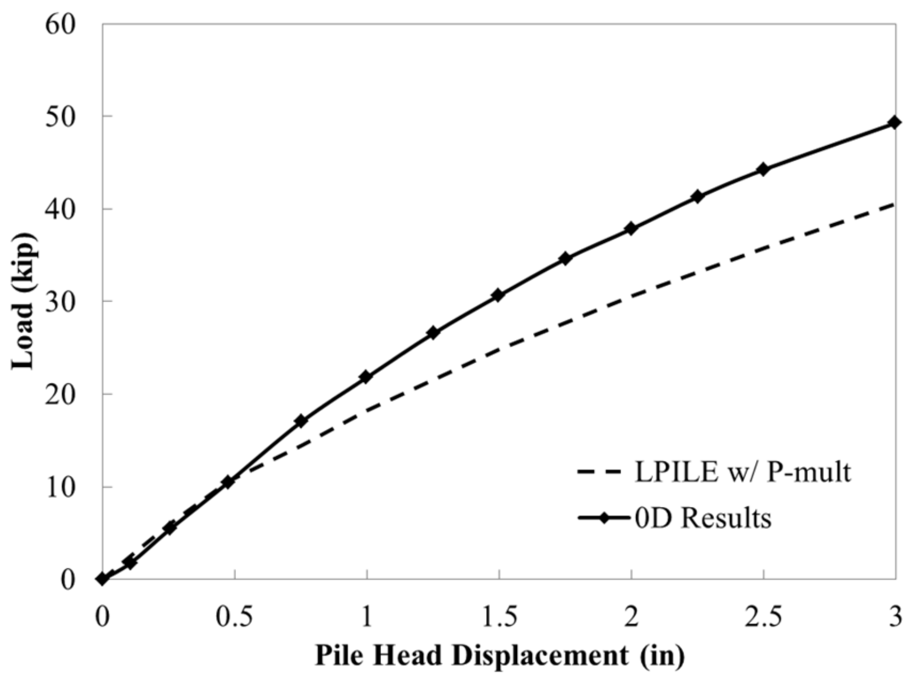

Figure 13-4 Comparison of the 0D full-scale results with the LPILE prediction using the proposed p-multipliers for a pile on a slope crest

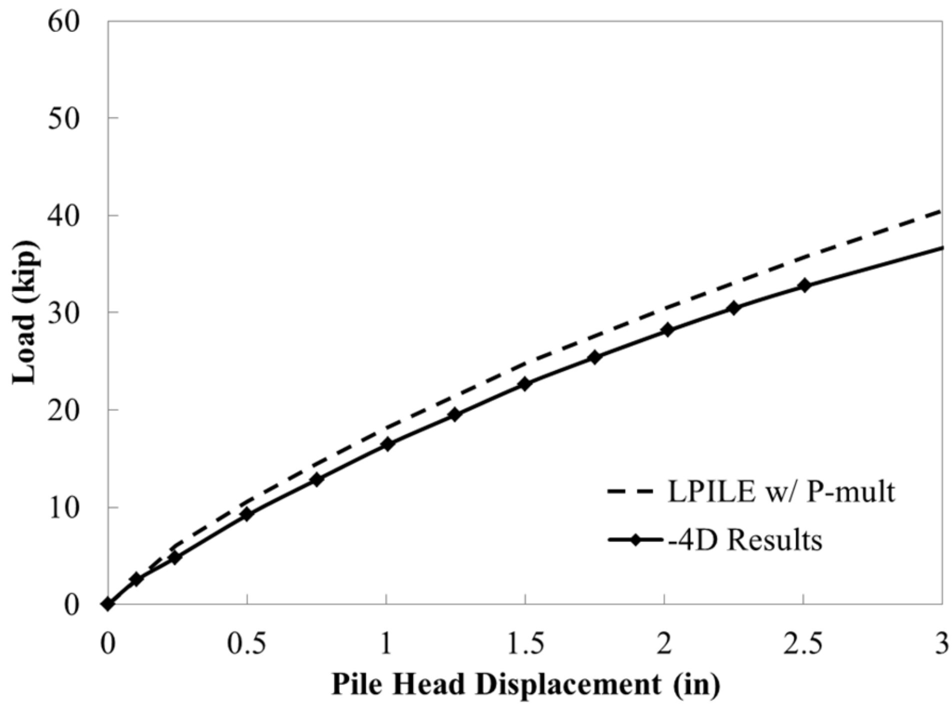

Figure 13-5 Comparison of the -4D (on slope) full-scale results with the LPILE prediction using the proposed p-multipliers for a pile on a slope

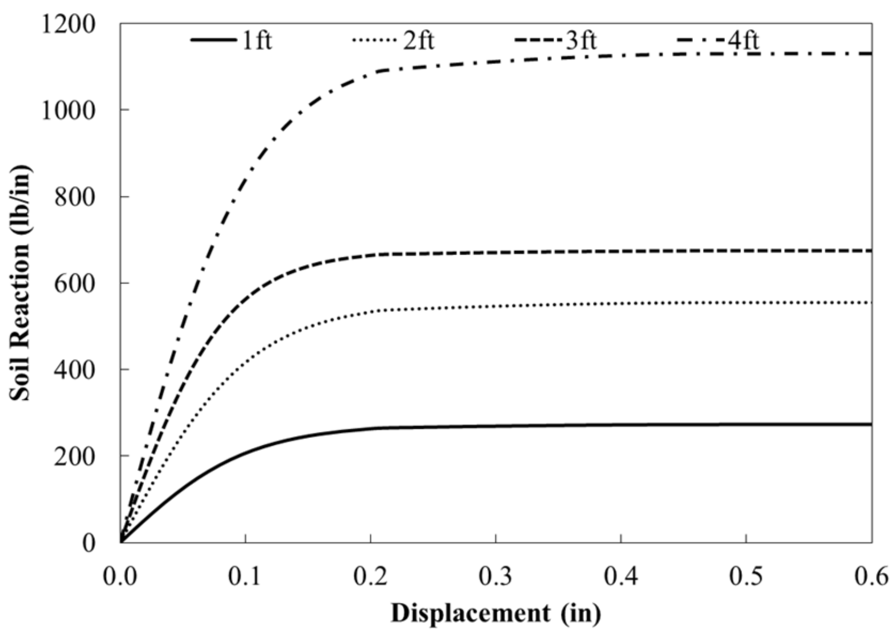

Figure 13-6 API (1987) predicted baseline p-y curves with input soil properties matching the full-scale tests

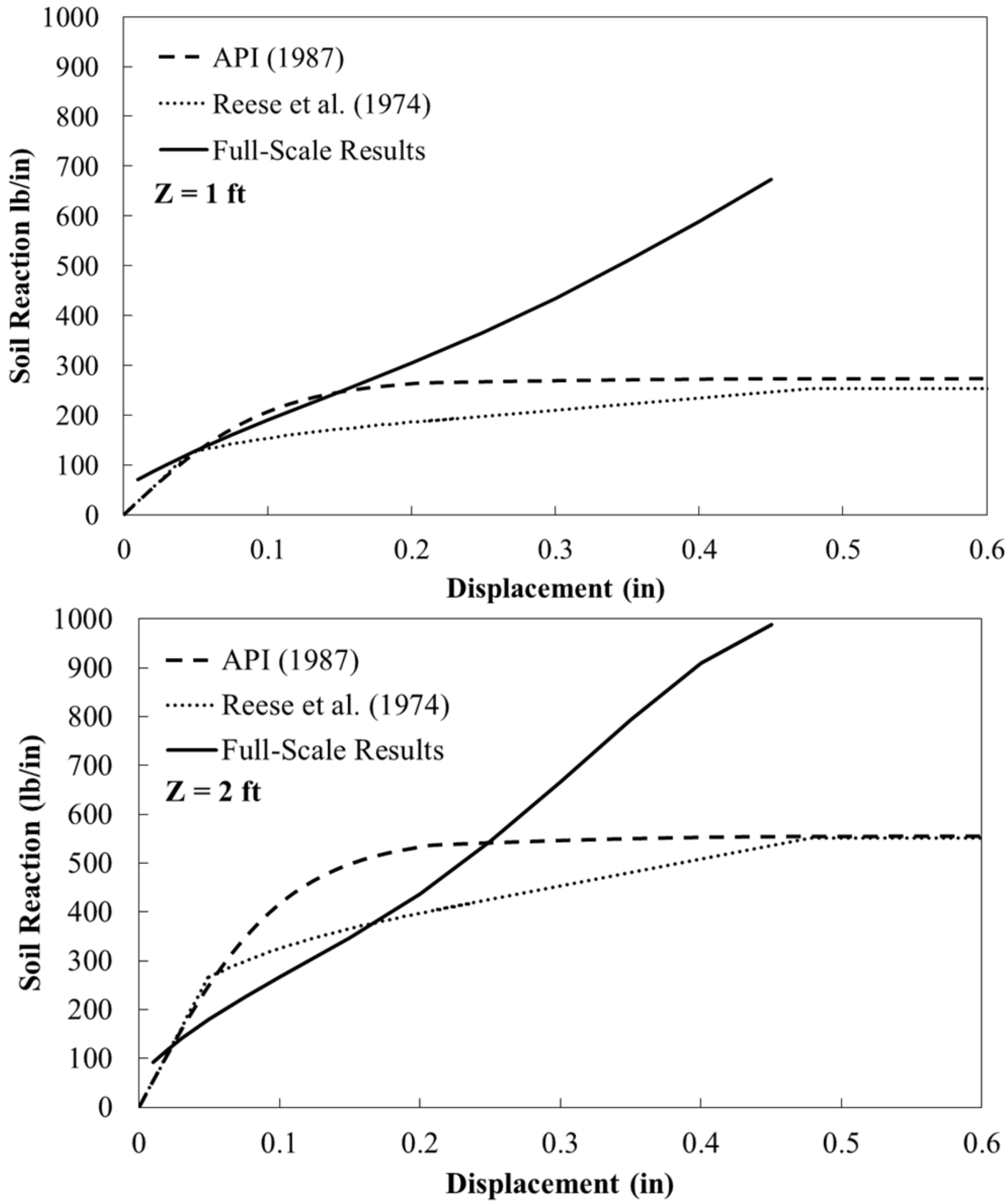

Figure 13-7 Comparison of the API (1987), Reese et al. (1974) predicted baseline p-y curves with full-scale results at depths of 1 ft (top) and 2 ft (bottom)

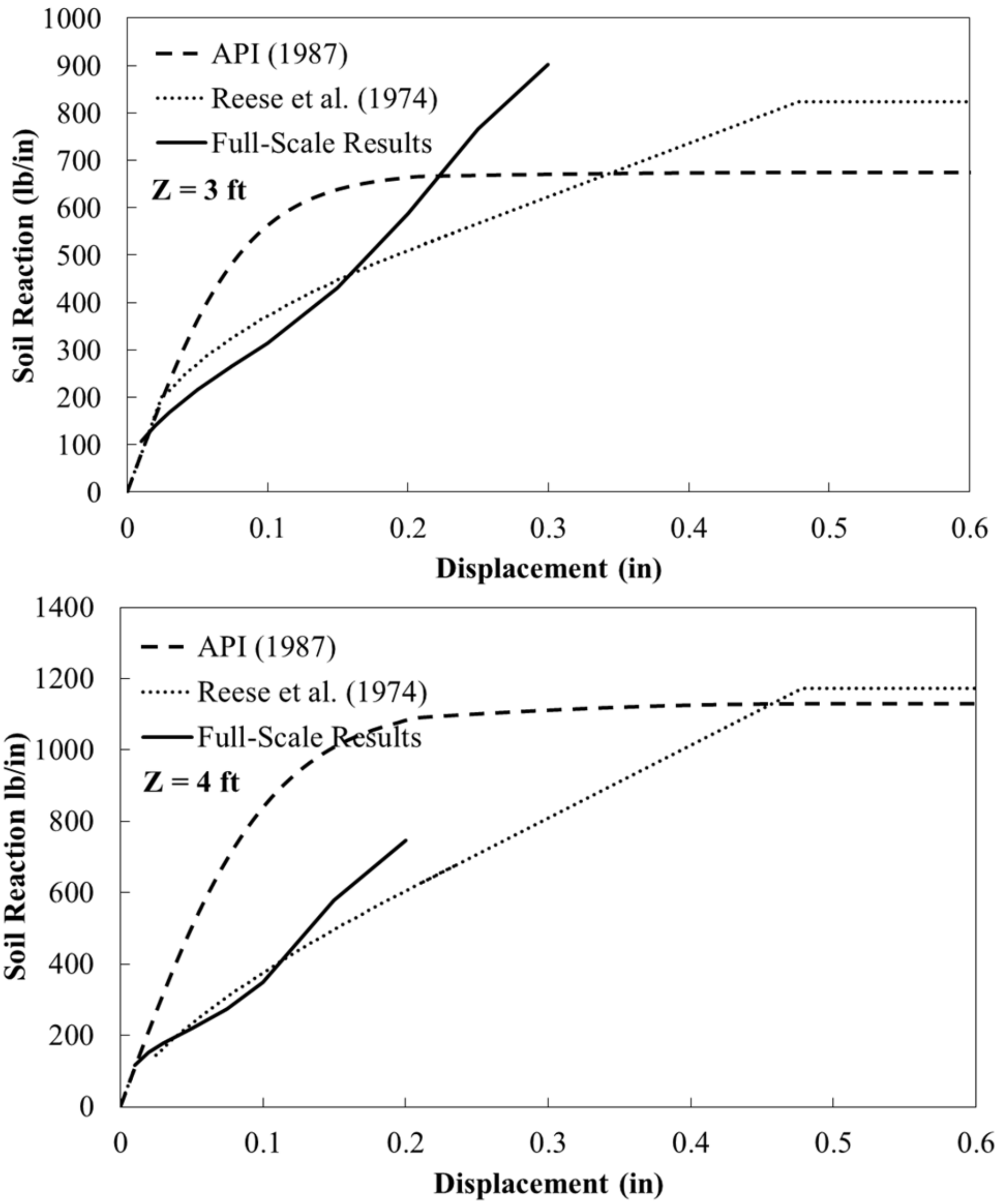

Figure 13-8 Comparison of the API (1987), Reese et al. (1974) predicted baseline p-y curves with full-scale results at depths of 3 ft (top) and 4 ft (bottom)

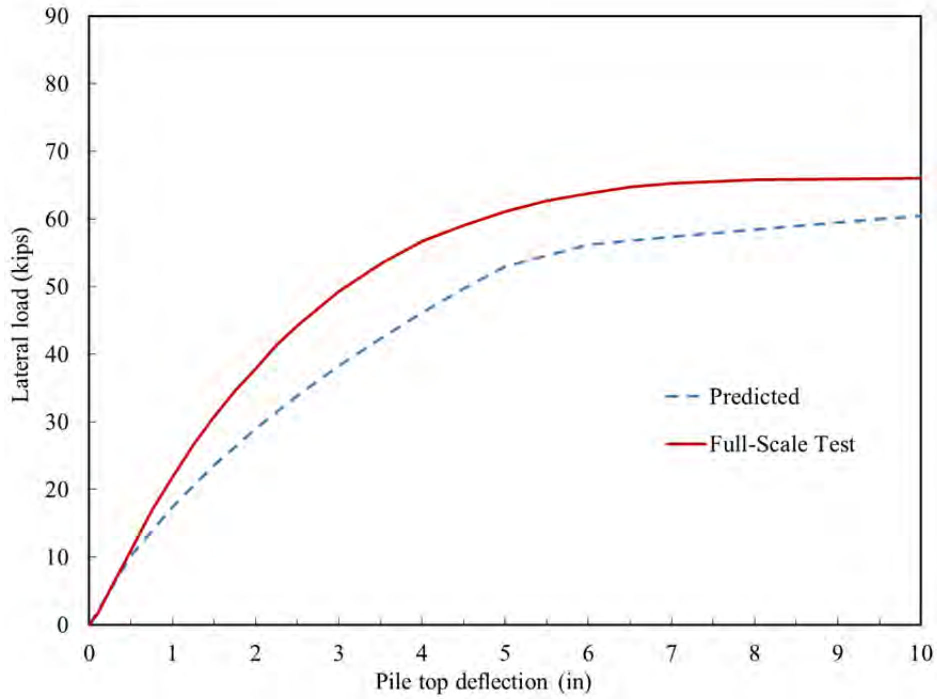

Figure 13-9 LPILE predicted 0D (slope crest) load-displacement curve with the full-scale test results

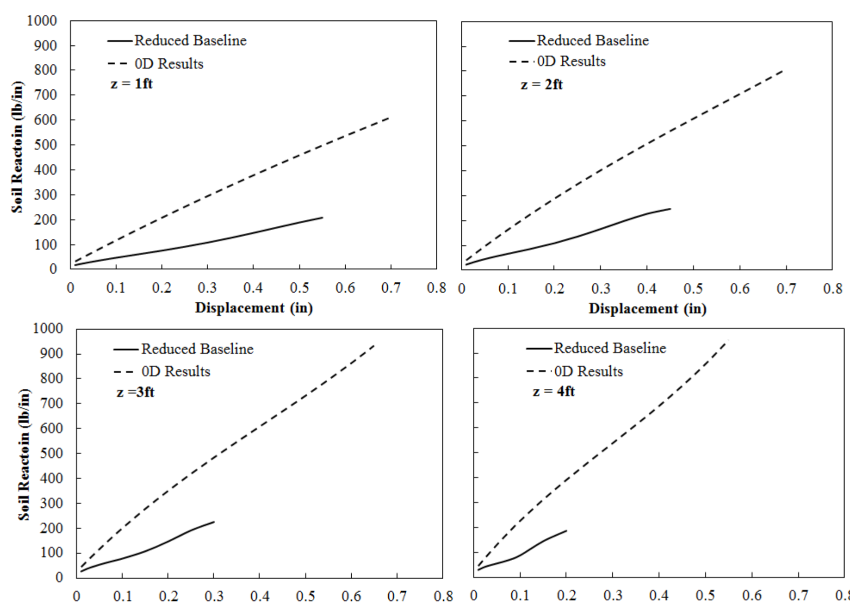

Figure 13-10 Reduced baseline (with Mezazigh and Levacher (1998) reduction coefficients**)** and 0D p-y curve comparison

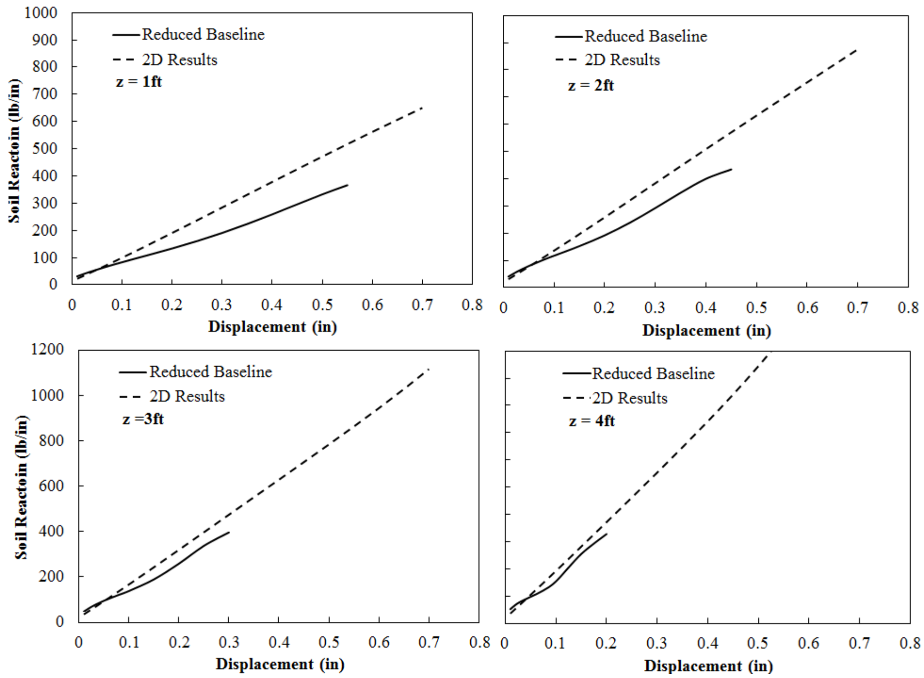

Figure 13-11 Reduced baseline (with Mezazigh and Levacher (1998) reduction coefficients**)** and 2D p-y curve comparison

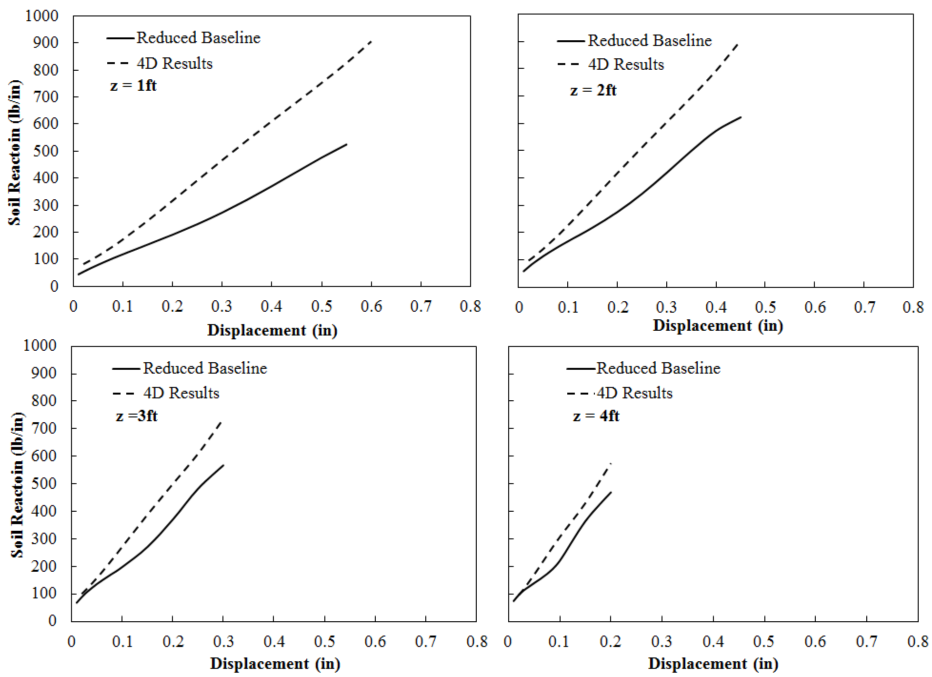

Figure 13-12 Reduced baseline (with Mezazigh and Levacher (1998) reduction coefficients**)** and 4D p-y curve comparison

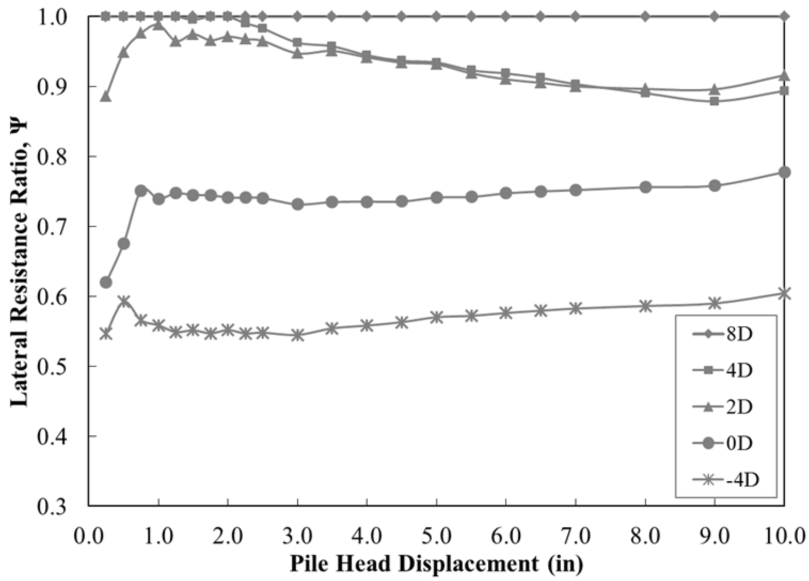

Figure 13-13 Lateral resistance ratios as a function of displacement

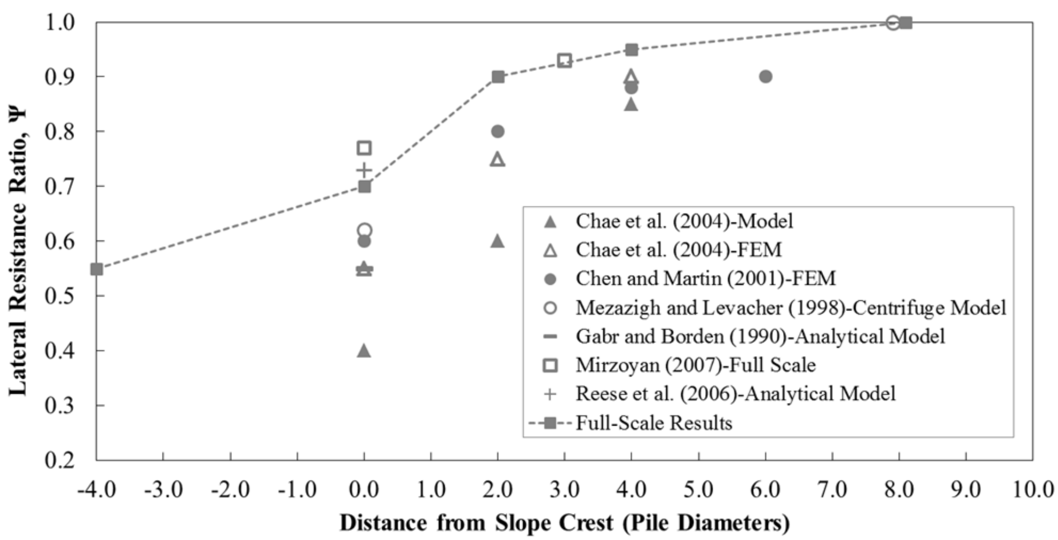

Figure 13-14 Comparison of resistance ratios presented by researchers as a function of distance from a slope crest with the findings from this study

14. CONCLUSIONS AND DESIGN RECOMMENDATIONS

The effect of soil slope on the lateral capacity of piles in cohesive and cohesionless soils was investigated in this study. This experimental study includes a series of full-scale lateral loading tests under static loading for two baseline piles, piles installed at 0D (on the crest), 2D, 4D, and 8D from the slope crest, and one pile installed on the slope for each testing series. Four battered piles were also tested, one in cohesive soils and three in cohesionless soils. A total of 18 full scale tests were conducted for this project. For consistency of the test results and to accurately evaluate the effects of soil slope, variations of other factors (e.g., pile properties, soil properties) were maintained at a minimum throughout the lateral loading tests for the piles installed near the slope so that their impacts on the test results were small to insignificant.

The slope effects were evaluated using strain gauge and tilt sensor data collected from the full-scale tests. Recommendations to account for slope effect were developed from the comparisons of back-calculated *p-y* curves for the baseline piles with the piles near the test slope. This chapter compares p-y curves between Series-I and Series-II, presents conclusions for each series, simplified design recommendations, and recommendations for future research.

14.1 CONCLUSIONS FOR SERIES-I (COHESIVE SOILS)

The effects of the proximity of slope and pile on the soil reaction, *p*, was evaluated using the back-calculated *p-y* curves based on the results from the lateral loading tests. Consistent with the comparison of load-displacement curves, it is found that, for small soil displacements (e.g., *y* less than ¼ inch), the presence of slope has insignificant effects on *p-y* curves for piles installed at 2D or greater from the slope crest (i.e., 2D and 4D from this study). The *p-y* curves for the 0D pile are different from the 8D pile for all soil displacement ranges, especially near the ground surface, indicating that slope effect is always significant for piles installed on the slope crest. For *p-y* curves at the ground surface, the ultimate soil resistance p_u is largest for the baseline pile and smallest for the 0D pile. Possible factors contributed to the reduction of the ultimate soil resistance are cracking, lateral movement of the passive wedge and reduction of the volume of soil in front of the pile. It was also found that the presence of soil slope has negligible effects on the *p-y* curves 9D below the ground surface.

The *p*-multipliers for the 4D pile, the 2D pile and the 0D pile for each soil displacement were computed by normalizing the back-calculated *p-y* curves with the baseline (8D pile) *p-y* curves for each depth. Based on this comparison, it can be said that the effects of slope on *p-y* curves are non-linear. For small soil displacements (i.e., initial stiffness of *p-y* curves), the effects of slope are small for the pile installed on the slope crest, and for the case of piles installed at 2D or greater from the slope crest, insignificant. For example, for a 2D pile, p_{mult} is 1 until soil displacements of 0.3 to 0.5 inch and decreases beyond those displacements. The effects of slope become more significant as soil displacement increases and appear to remain constant for larger soil displacements. The effects of slope are most significant for piles installed on the slope crest. Polynomial regression analysis was performed to determine the best fit lines that describe the difference between the baseline *p-y* curves and the *p-y* curves for the 4D, 2D and 0D piles for any depths.

Based on the comparison of the computed *p*-multipliers as a function of pile distance to the slope, two trends were observed: 1) the maximum observed reduction of soil resistance appears to be a function of the pile distance to the slope (i.e., increasing as the piles are installed closer to the slope), and 2) a soil displacement in which slope effects are insignificant (i.e., *p*-multiplier equals to 1) appears to be a function of the pile distance to the slope crest (i.e., smaller as the piles are installed closer to the slope). The proposed recommendations were validated by applying *p*-multipliers to the baseline *p-y* curves to predict the lateral response of the 4D pile, the 2D pile and the 0D pile. A simplified and conservative procedure to obtain p-multipliers is recommended in the following section for pile located in or near cohesive soil slopes. The *p*-multipliers from the simplified procedure and are a function of distance and depth from the slope crest and are independent of pile displacement.

14.2 DESIGN RECOMMENDATIONS FOR SERIES-I (COHESIVE SOILS)

14.2.1 SIMPLIFIED DESIGN PROCEDURE

For this study, a full range of p-y curves and p-multipliers that vary with pile displacement and depth were calculated for each load test. These analyses are pivotal in determining the true effects of the soil slope on lateral pile capacity. After completion of this investigation, a generalized procedure and slope profile was constructed to simplify design procedures to account for a reduction in capacity.

Figure 14-1 presents a generalized soil slope profile created for cohesive soils to obtain recommended p-multipliers (or reduction factors). These recommended p-multipliers are created to account for larger pile displacements (more conservative, higher reduction in load) and do not need to be modified for increasing pile displacements during design. These reduction factors are based on the distance from the slope crest and depth below the ground surface measured in pile diameters, D.

Recommended simplified design procedure to account for soil slope in cohesive soils:

- Determine the designed pile size (diameter) being installed within proximity of the slope
- Identify cohesive soil properties and determine the corresponding free-field (level ground) *p-y* curves for the site
- Define the location and distance (in number of pile diameters) the pile will be located from the slope crest
- Using **Figure 14-1**, determine where the design pile will be located on the generalized slope shown in this figure
- Apply the corresponding *p*-multipliers from the figure to the free-field p-y curves to account for the presence of the slope
    - For piles located on the slope or within four diameters behind the crest apply a reduction factor of 0.5 for the top three pile diameters, 0.6 for the following three pile diameters, and 0.7 for the subsequent three pile diameters
    - No reduction factor (*p*-multiplier of 1.0) is required below 9D
    - For piles located outside of this range no reduction factors are required

These recommendations are conservative due to the simplifications of this design procedure, but present an efficient way to account for the reduction in lateral capacity due to proximity of a slope in cohesive soils.

14.2.2 GENERALIZED RECOMMENDATIONS AND OBSERVATIONS FOR SERIES-I

Based on the results of full-scale experiments and lateral load analyses, the main findings of this research study on the effect of soil slope on lateral capacity of piles in cohesive soils are provided as the following:

- For small soil displacements (i.e., less than 0.5 inch), the proximity of slope has small to insignificant effect on the lateral pile response. At larger soil displacements, the proximity of slope adversely affected the lateral capacity of piles and consequently the back-calculated *p-y* curves.

- For maximum allowable pile deflection of ¼-inch under Service Limit State Load (Caltrans BDS Article 4.5.6.5.1), the slope appears to have insignificant effect for piles located at 2D or further from the slope crest. In all cases, even for the pile on the slope crest, the lateral capacity was significantly higher than the 5 kips noted in the Caltrans BDS for 12-inch steel pipe piles.

- For piles installed on the slope crest, the effect of slope should always be considered at all displacement levels.

- The effect of slope on the lateral capacity was insignificant for piles installed at distances of 8D or greater from the slope crest.

- Based on comparison of the back-calculated *p-y* curves from these experiments, *p*-multipliers that are a function of soil displacement are proposed to account for slope effects.

- Slope effects are insignificant for *p-y* curves below 9D from the ground surface

- For the ultimate soil resistance, the method considering pile-adhesion factor provide better estimation than conventional method (Matlock 1970; Reese and Welch 1975)

- The lateral load analysis of the baseline piles using constant soil modulus and undrained shear strength give good prediction of the measured pile response for a uniform cohesive soil layer in this study

- Reese *et al*. (2006) methodology to account for piles on a slope crest in cohesive soils give a reasonable prediction of the lateral response of the pile on the slope crest.

The limitations of these recommendations should always be considered when extrapolating for other design conditions that differ from the testing conditions in this study including slope angle, pile diameter, soil conditions and loading conditions.

14.3 CONCLUSIONS FOR SERIES-II (COHESIONLESS SOILS)

The effects of a soil slope on the lateral capacity of a pile in cohesionless soils and the soil reaction, *p*, was evaluated using the back-calculated *p-y* curves based on the results from full scale lateral load tests. When comparing the load-displacement curves it appears that the slope has an insignificant effect on piles 2D or greater from the slope for small pile head displacements (less than 2.0 inches). In contrast, when examining the back-calculated p-y curves it is found that, for all displacements the presence of slope has a significant effects on *p-y* curves for piles installed closer than 4D from the slope crest. The *p-y* curves for the test piles closer than 4D showed a significant reduction in stiffness for all measured pile displacements. Possible factors contributed to the reduction of the ultimate soil resistance are the reduction of overburden pressure and lateral movement of well-defined passive wedges on the slope crest for piles installed near the slope. It was also found that the presence of soil slope has negligible effects on the *p-y* curves 10D below the ground surface.

14.4 DESIGN RECOMMENDATIONS FOR SERIES-II (COHESIONLESS SOILS)

14.4.1 SIMPLIFIED DESIGN PROCEDURE

Figure 14-2 presents a generalized soil slope profile created for cohesionless soils to obtain recommended p-multipliers (or reduction factors). These recommended p-multipliers are created to account for larger pile displacements (more conservative, higher reduction in load) and do not need to be modified for increasing pile displacements during design. These reduction factors are based on the distance from the slope crest and depth below the ground surface measured in pile diameters, D.

Recommended simplified design procedure to account for soil slope in cohesionless soils:

- Determine the designed pile size (diameter) being installed within proximity of the slope
- Identify cohesionless soil properties and corresponding free-field (level ground) *p-y* curves for the site
- Define the location and distance (in number of pile diameters) the pile will be located from the slope crest
- Using **Figure 14-2**, determine where the design pile will be located on the generalized slope shown in this figure
- Apply the corresponding *p*-multipliers from the figure to the free-field p-y curves to account for the presence of the slope
    - For piles located on the slope, apply a reduction factor of 0.3 for the top four pile diameters and 0.4 for the following six pile diameters
    - For piles located from the slope crest to four pile diameters back from the crest, apply a reduction factor of 0.5 for the top 4 pile diameters and 0.6 for the following 6 pile diameters
    - No reduction factor (*p*-multiplier of 1.0) is required below 10D
    - For piles located outside of this range no reduction factors are required

These recommendations are conservative due to the simplifications of this design procedure but present an efficient way to account for the reduction in lateral capacity due to proximity of a slope in cohesionless soils.

14.4.2 GENERALIZED CONCLUSIONS FOR SERIES-II

Based on the results of full-scale experiments and lateral load analyses, the main findings of this research study on the effect of soil slope on lateral capacity of piles in cohesionless soils are provided as the following:

- The effects of slope on lateral pile capacity are insignificant at displacements of less than 2.0 inches for piles located 2D and further from the crest.
- For pile located at 4D or greater from the slope crest, the effect of slope is insignificant for the analyzed ranges of soil displacements on p-y curves.
- Analytical, small scale, and computer models typically overestimate the effects of slope on lateral pile capacities and conservatively predict the ultimate resistance and initial soil stiffness.
- For all testing cases in the cohesionless material the lateral capacity was significantly higher than the 5 kips noted in the Caltrans BDS for 12-inch steel pipe piles for maximum allowable pile deflection of ¼-inch under Service Limit State Load according to Caltrans BDS Article 4.5.6.5.1.

The limitations of these conclusions and recommendations should always be considered when extrapolating for other design parameters that differ from the testing conditions in this study including slope angle, pile diameter, loading type, and pile type.

14.4.3 OTHER OBSERVATIONS FROM SERIES-II TESTING

The following sections present observations made during full-scale lateral load testing:

- Piles installed on a slope should not be considered to have similar lateral capacities as piles installed on the slope crest. In this study, the capacities and reduction factors were significantly different between these two cases.

- Ultimate capacity for load-displacement curves is reduced for piles closer than 8D
- The effects of reduced overburden pressure due to presence of soil slope has a larger impact on the reduction of lateral capacity in cohesionless soils
- The shear failure angle, Ω, of the passive wedge ranged between 24° and 39°. This angle increased with greater distances from the slope crest. A recommendation of 70% of ϕ is proposed for the shear failure angle in dense cohesionless material.
- LPILE 6.0 underestimates the initial stiffness and the lateral pile capacity in level ground conditions. The full-scale test results had an ultimate resistance of 20% more than predicted by LPILE 6.0. The lateral capacity for the 0D pile was relatively close and only underestimated the lateral capacity by about 10%.
- The predicted baseline API (1987) and Reese et al. (1974) p-y curves over predict the initial soil stiffness at displacements of less than 0.2 inches
- API (1987) and Reese et al. (1974) models significantly under predicted the back-calculated ultimate soil reaction at displacements greater than 0.25 inches.
- Mezazigh and Levacher (1998) reduction coefficients are considered conservative when applied to the baseline p-y curve and then compared to the near slope results.

14.5 COMPARISON BETWEEN COHESIVE & COHESIONLESS RESULTS

During this study seven non-battered piles were tested in each soil type, cohesive and cohesionless. The cohesionless load-displacement curves had higher ultimate capacities for all load tests (baseline through 0D) when compared to the cohesive results. The initial stiffness at lower displacements was also greater for the cohesionless piles. These curves show a larger effect from slope (when compared to baseline) on the 2D and 4D piles capacities in cohesive soils. A greater effect on capacities was seen for the 0D and -4D piles in the cohesionless soils.

The shapes and the effects of slope on the *p-y* curves differed between Series-I and Series-II. For displacements less than 0.25 inches, the slope a small to insignificant effect on the lateral pile response in cohesive soils. The effect also increased with increased soil displacement (i.e. a larger reduction in capacity with displacement) for cohesive soils. This was not the case for Series-II, as the lateral capacities were affected at all soil displacements. When compared to respective baseline tests, the results from the cohesionless series had a larger reduction in lateral capacities. The recommended *p*-multipliers for the cohesionless ranged from 0.3 to 0.6, while the cohesive recommended *p*-multipliers ranged from 0.5 to 0.7. The presence of a slope, and consequently a reduction in overburden pressure for the soil resisting lateral movement has a greater impact on cohesionless soils. This is, most likely, due to the absence of cohesion, wherein Series-I the presence of the test slope has less of an effect on the resistance due to apparent cohesion between soil grains.

14.6 BATTERED PILE TEST CONCLUSIONS (SERIES-II)

Pile P-4 with a -14° batter angle had the highest stiffness and capacity of all piles tested in this study. Pile P-3 (+14° positive batter) had the lowest capacity of the tested battered piles. The load displacement results from pile P-5 (+26°) do not fit the predicted trend. The LPILE predicted load-displacement curves from pile P-3 (+14°) and P-4 (-14°) follow the trend of the full-scale results, but LPILE is conservative in estimating the initial stiffness and ultimate lateral resistances. The full-scale results from Pile P-5 (+26°) had a significantly greater stiffness and capacity than the LPILE prediction, where it was predicted to have the lowest overall load. An analysis of the load displacement data from the +26° battered pile showed that the testing equipment was likely near its limitations to laterally load a pile with this high batter angle. The unexpected stiffness and load from the full-scale test are likely due to unintended axial loading. Overall, LPILE is a conservative method to predicted lateral capacity of battered piles in cohesionless soils. The load ratio model used in LPILE battered pile predictions compares well with the ratios obtained for full-scale lateral load tests.

14.7 RECOMMENDATIONS FOR FUTURE RESEARCH

- Soil slope effects for different pile diameter can be considered in a controlled environment, such as using physical model testing. The soil properties and slope geometry can therefore be controlled. The stiffness of the pile should remain constant for different pile diameters in order to achieve the same level of soil displacement for a proper comparison of *p-y* curves. The constant pile stiffness with varying pile diameter can be achieved by selecting different pile thickness or using different materials.

- Three-dimensional finite element modeling, which can model construction sequences and some aspects observed during the testing, such as gapping and cracking, as well as accounting for softening due to soil dilatency should be conducted to understand if these aspects have significant contribution to the effects of slope on the pile response. Results from full-scale lateral loading tests can be used to calibrate the 3-D model, and therefore the analysis for slope effects can be reasonably extrapolated to use for different slope geometry, soil type, pile type and different distance between pile-slope crest.

- The effects of slope for pile groups may be different than that for a single pile and should be investigated.

- Though *p-y* curves have been developed based on the results of the full-scale lateral pile loading tests for a case of long, flexible piles, they have been used in design to predict the lateral response for rigid pile as well. However, the implementation of *p-y* curves for short, rigid piles has not been verified with the results from full-scale tests. Research on the effects of pile length on the pile response using full-scale testing should be conducted to verify if they existing *p-y* curves are appropriate for the case of rigid pile.

- The effects of loading type such as cyclic loading, sustained loading and dynamic loading should be investigated. In addition, the effects of axial loads on the lateral pile response also require further study. The effects of varying slope angle on should also be examined.

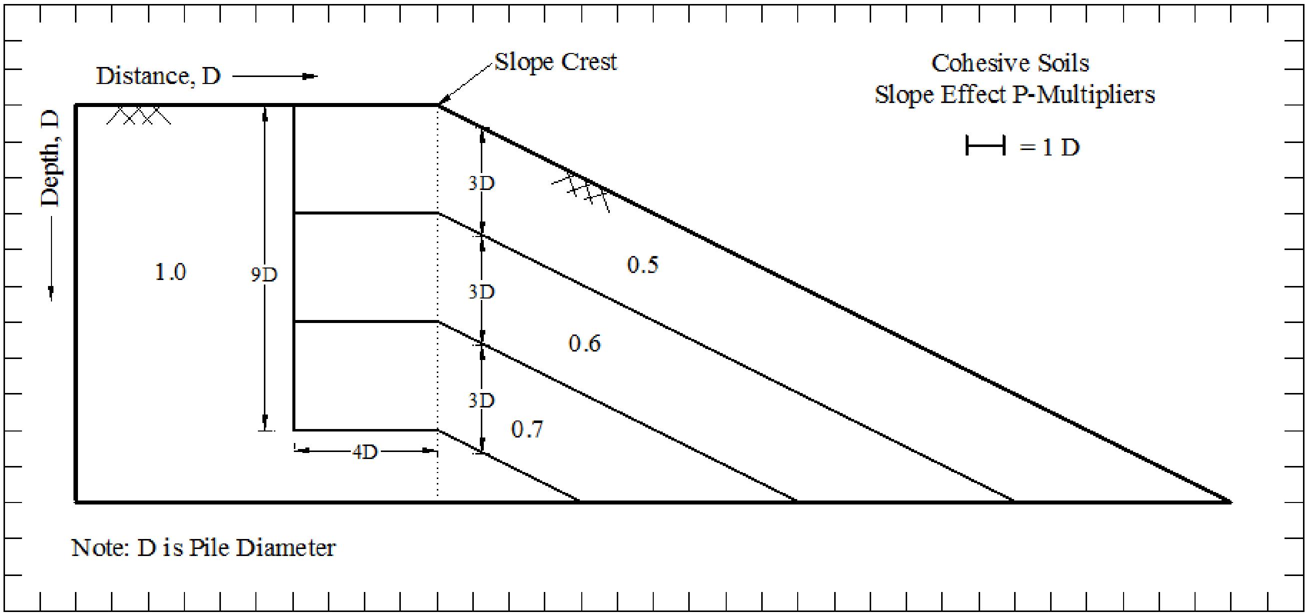

Figure 14-1 Recommended p-Multipliers for a Generalized Cohesive Slope

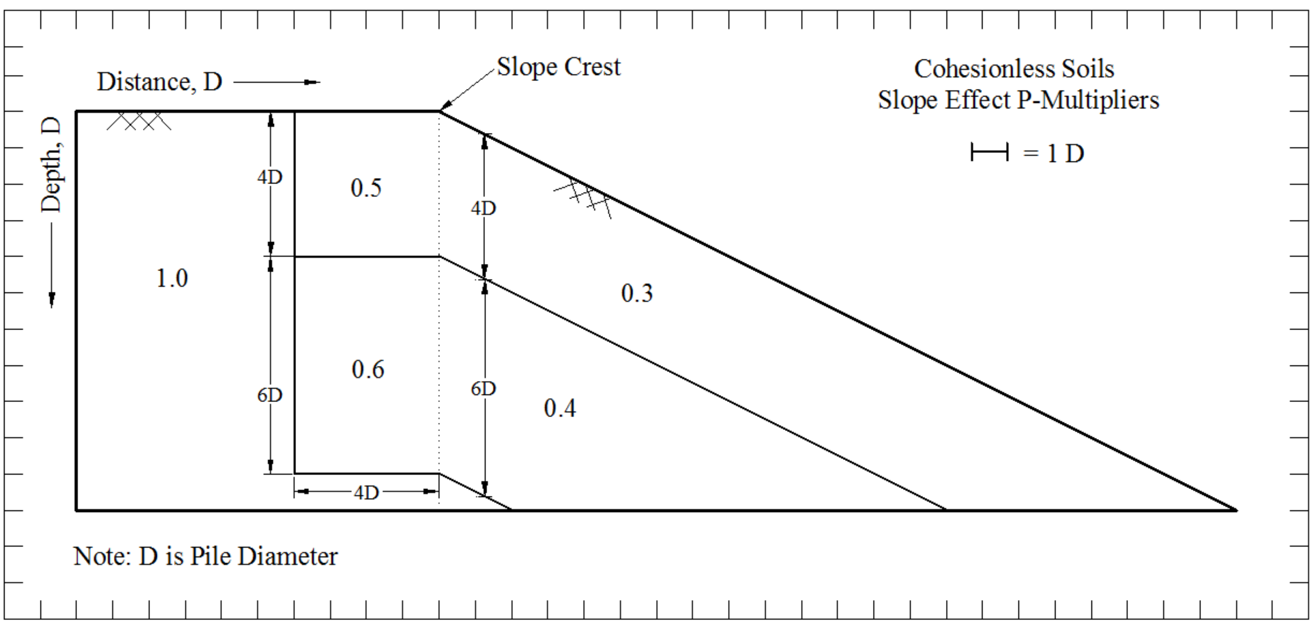

Figure 14-2 Recommended p-Multipliers for a Generalized Cohesionless Slope

15. REFERENCES

American Association of State Highway and Transportation Officials (AASHTO). (2007). LRFD bridge design specifications, 4th Ed., Washington, D.C.

American Petroleum Institute (API) (1984). "API Recommended Practice for Planning, Designing, and Constructing Fixed Offshore Platforms." Washington, D.C., 15th edn.

American Petroleum Institute (API) (1987). "Recommended practice for planning, designing, and constructing fixed offshore platforms." *API Recommended Practice* 2A (RP-2A), 17th edn.

Ashford, S. A., Juirnarongrit, T., Sugano, T., and Hamada, M. (2006). "Soil-pile response to blast-induced lateral spreading." *Journal of Geotechnical and Geoenvironmental Engineering*, 132(2), 152-162

*A*STM, D 2487, "Standard Classification of Soils for Engineering Purposes (Unified Soil Classification System)", American Society for Testing and Materials, West Conshohocken, Pennsylvania, USA.

ASTM, D 422, "Standard Test Method for Particle-Size Analysis of Soils", American Society for Testing and Materials, West Conshohocken, Pennsylvania, USA.

Banerjee, P. K., and Davies, T. G. (1978). ''The behavior of axially and laterally loaded single pile embedded in non-homogeneous soils.'' *Geotechnique,* Vol. 21(3), pp. 309–326.

Barber, E. S. (1953). "Discussion to paper by S. M. Gleser." *ASTM, STP* 154, 94-101.

BDS Caltrans (2003). *Caltrans Bridge Design Specifications.*

Bea, R. G. (1980). "Dynamic response of piles in offshore platforms," *Proc. of the Specialty Conference on Dynamic Response of Pile Foundations – Analytical Aspects*, ASCE, Geotechnical Engineering Division

Bea, R. G. (1984). "Dynamic response of marine foundations." *Proc. of Ocean Structural Dynamics Symposium*, Oregon State University, Corvallis, OR, pp. 1-78.

Bjerrum, L. (1972). "Embankments on soft ground." Proc., Specialty Conference on Performance of Earth and Earth Supported Structures, Vol. 2, ASCE, pp. 1-54.

Bogard, D., and Matlock, H. M. (1983). "Procedures for analysis of laterally loaded pile groups in soft clay." *Proc., Geotechnical Practice in Offshore Engineering*, ASCE, pp. 499-535.

Bouafia A., and Bouguerra A. (1996). "Centrifuge testing of the behavior of a horizontally loaded flexible pile near to a slope." *International Journal of Rock Mechanics and Mining Sciences and Geomechanics*, Vol. 33(3)

Bozorgzadeh, A. (2007). “Effect of structural backfill on stiffness and capacity of bridge abutments.” Ph.D. thesis, Dept. of Structural Engineering, University of California, San Diego.

Brinkgreve, R. B. J., and Swolfs, W. M. (2007). *Plaxis 3D foundation version 2 user’s manual*, Plaxis B.V., Netherlands.

Brinch J. H. (1961). “The ultimate resistance of rigid piles against transversal forces.” *Bulletin No. 12*, Danish Geotechnical Institute, Copenhagen, Denmark, pp. 5–9.

Broms, B. B. (1964). “Lateral resistance of piles in cohesive soils.” *Journal of Soil Mechanics and Foundation Division*, 90(2), pp. 27-64.

Brown, D. A., Reese, L. C., and O’ Neill, M. W. (1987). “Cyclic lateral loading of a large scale pile group.” *Journal of Geotechnical Engineering*, ASCE, Vol. 113(11), pp. 1326-1343.

Brown, D. A., Shie, C. F., and Kumar, M. (1989). “*p-y* curves for laterally loaded piles derived from three dimensional finite element model.” *Proc., 2nd Int. Symp., Numerical Models in Geomechanics, Niagara Falls, Canada*, New York, Elsevier Applied Sciences, 683-690.

Brown, D. A., and Shie, C. F. (1991). “Some numerical experiments with a three-dimensional finite element model of a laterally loaded pile,” *Computers and Geotechnics*, 12, 149-162.

Bushan, K., Haley, S. C., and Fong, P. T. (1979). “Lateral load tests on drilled piers in stiff clays.” *Journal of Geotechnical Engineering Division*, ASCE, 105(8), 969-985.

Chae K.S., Ugai K., and Wakai A. (2004). “Lateral resistance of short single piles and pile groups located near slopes.” *International Journal of Geomechanics*, 4(2), 93-103.

Chen, B.S.Y. and Mayne, P.W. (1996). "Statistical relationships between piezocone measurements and stress history of clays." *Canadian Geotechnical Journal*, Vol. 33(3), pp. 488-498.

Cox, W. R., L. C. Reese, and B. R. Grubbs (1974). “Field Testing of Laterally Loaded Piles in Sand,” *Proceedings, Offshore Technology Conference*, Houston, Texas, Vol. II, Paper No. 2079, pp. 459-472.

Davisson, M. T., and Gill, H. L. (1963). “Laterally loaded piles in a layered soil.” *J. Soil Mech. and Found. Div.*, ASCE, 89(3), 63-94.

Desai, C. S., and Appel, G. C. (1976). ‘‘3-D analysis of laterally loaded structures.’’ *Proc., 2nd Int. Conf. on Numerical Methods in Geomechanics*, ASCE, Blackburg, Vol. 1, 405–418.

Dickenson, S. (2006). *Characterization of the geotechnical engineering field research site at Oregon State University*. 3rd Edition.

DIN 4014 (1990). “Bored cast-in-place piles. Formation, design and bearing capacity”. Deutsche Norm.

Duncan, J. M., Evans, L. T., and Ooi, P. S. (1994). “Lateral load analysis of single piles and drilled shafts.” *ASCE Journal of Geotechnical Engineering*, 120(6), 1018-1033.

Dunnavant, T. W. (1986). “Experimental and analytical investigation of the behavior of single piles in overconsolidated clay subjected to cyclic lateral loads.” *Ph.D. Dissertation*, University of Houston, Houston, Texas.

Dustin, S. C. (2006). “Full-scale static lateral load test of a 9 pile group in sand.” M.S. thesis, Brigham Young University, Department of Civil and Environmental Engineering. Utah.

Earth Mechanics, Inc. (2005). *Field investigation report for abutment backfill characterization*, January 2005.

Fleming, W. G. K., Weltman, A. J., Randolph, M. F., and Elson, W. K. (1992). *Piling engineering*, Surrey University Press, London.

Georgiadis, M., Anagonostopoulos, C., and Saflekou, S. (1991). “Interaction of laterally loaded piles.” *Proc. Foundations Profondes*, Ponts et Chaussees, Parus, 177-184.

Georgiadis and Georgiadis (2010). “Undrained lateral pile response in sloping ground.” *Journal of Geotechnical and Geoenvironmental Engineering*, ASCE.

Helmers, M. J., Duncan, J. M., and Filz, G. M. (1997). “Use of ultimate load theories for design of drilled shaft sound wall foundations.” The Charles E. Via, Jr. Department of Civil Engineering, Virginia Tech, Blacksburg, VA.

Hetenyi, M. (1946). *Beams on elastic foundations*. University of Michigan Press, Ann Arbor, Michigan.

Holtz, R. D. and Kovacs, W. D. (1981). *An Introduction to Geotechnical Engineering*, Prentice-Hall, Inc., Englewood Cliffs, N. J., 733 p

Ismael, N. F. (1990). “Behavior of laterally loaded bored piles in cemented sands.” *J. Geotech. Engrg.*, ASCE, 116(11), 1678-1699.

Juirnarongrit, T. (2002). “Effect of diameter on the behavior of laterally loaded piles in weakly cemented sand.” Ph.D. thesis, Dept. of Structural Engineering, University of California San Diego, CA.

Karthigeyan, S., Ramakrishna, V. V. G. S. T., and Rajagopal, K. (2007). “Numerical investigation of the effect of vertical load on the lateral response of piles.” *Journal of Geotechnical and Geoenvironmental Engineering*, Vol. 133(5), pp. 512-521.

Kim, B. T., Kim, N. K., Lee, W. J., and Kim, Y. S. (2004). "Experimental load-transfer curves of laterally loaded piles in Nak-Dong river sand." *Journal of Geotechnical and Geoenvironmental Engineering*, ASCE, 130(4), 416-425.

Knezevich, C. A. (1975). *United States Department of Agriculture Soil Conservation Service*. Soil Survey of Benton County Area, Oregon. Washington, D.C.

Kondner, R. L. (1963). "Hyperbolic stress-straain response: Cohesive soils." *Journal of Soil Mechanics and Foundation Division*., Vol. 89(1), pp. 115-144.

Kong, L. G. and Zhang, L. M. (2007). "Rate-controlled lateral-load pile tests using a robotic manipulator in centrifuge." *Geotechnical Testing Journal* Vol. 30(3).

Kooijman, A. P. (1989). "Comparison of an elastoplastic quasi three-dimensional model for laterally loaded piled with field tests." *Proc. of the III International Symposium, Numerical Models in Geomechanics (NUMOG III)*, Niagara Falls, Canada, Elsevier Applied Science, New York, 675-682.

Kuhlemeyer, R. L. (1979). ''Static and dynamic laterally loaded floating piles.'' *Journal of Geotechnical Engineering Division, ASCE,* Vol. 105(2), pp. 289–304.

Kulhawy, F. H. (1991). "Drilled shaft foundations." *Foundation Engineering Handbook*, H. Y. Fang, ed., Chapman and Hill, New York.

Kulhawy, F.H. and Mayne, P.W. (1990). "Manual on estimating soil properties for foundation design", Report No. EL-6800, Electric Power Research Institute, Palo Alto, CA, August 1990, 306 pages.

Liang, R., Yang, K., and Nusairat, J. (2009). "*p-y* criteria for rock mass." *Journal of Geotechnical and Geoenvironmental Engineering*, ASCE, Vol.135(1), pp. 26-36.

Long, J. H. (1984). "The behavior of vertical piles in cohesive soil subjected to repeated horizontal loading." Ph.D. thesis, University of Texas at Austin, TX.

Matlock, H. (1970). "Correlations for design of laterally loaded piles in soft clay." *Proc., 2nd Annual Offshore Technology Conference.*, *Paper No. OTC 1204*, Houston, Texas, pp. 577-594.

Matlock, H. and Reese, L. C. (1960). "Generalized solutions for laterally loaded piles." *Journal of Soil Mechanics and Foundation Division.*, ASCE, Vol. 86(5), pp. 63-91.

McClelland, B., and Focht, J. A. Jr. (1958). "Soil modulus for laterally loaded piles." *Transactions*, ASCE, Vol. 123, pp. 1049-1086.

Meyerhof, G. G. (1956). "Penetration tests and bearing capacity of cohesionless soils." *Journal of Soil Mechanics and Foundation Division.*, ASCE, Vol. 82(1), pp. 1-19.

Mezazigh, S., and Levacher, D. (1998). “Laterally loaded piles in sand: Slope effect on *p-y* reaction curves.” *Canadian Geotechnical Journal,* 35, 433-441.

Mirzoyan, A. D. (2007). “Lateral resistance of piles at the crest of slope in sand.” M.S. thesis, Brigham Young University, Department of Civil and Environmental Engineering, Utah.

Mokwa R. L., Duncan, J. M., and Helmers M. J. (2004). “Development of *p-y* curves for partially saturated silts and clays.” *Proc. of the new technological and design developments in deep foundation,* GSP 100, pp. 224-239.

Murff, J. D., and Hamilton, J. M. (1993). “P-Ultimate for undrained analysis of laterally loaded piles.” *Journal of Geotechnical Engineering*, ASCE, 119(1), 91-107.

Ogata, N., and Gose, S. (1995). “Sloping rock layer foundation of bridge structure.” *Proc. Rock Foundation*, Tokyo, Yoshinaka R. and Kikuchi R., eds., Balkema, Rotterdam, 285-292.

Poulos, H. G. (1971). ‘‘Behavior of laterally loaded piles. I: Single piles.’’ *Journal of Soil Mechanics and Foundation Division., ASC.,* Vol. 97(5), pp 771–731.

Poulos, H. G. (1976). “Behavior of laterally loaded piles near a cut or slope.” *Australian Geomechanics Journal,* Vol. 6(1), pp.6-12.

Poulos, H. G., and Davis, E. H. (1980). *Pile foundation analysis and design*. John Wiley, New York.

Rajashree, S. S., and Sitharam, T. G. (2001). “Nonlinear finite element modeling of batter piles under lateral load.” *Journal of Geotechnical and Geoenvironmental Engineering*, ASCE, Vol. 127(7), pp. 604-612.

Randolph, M. F. (1981). ‘‘The response of flexible piles to lateral loading.’’ *Geotechnique,* Vol. 31(2), pp. 247–259.

Randolph, M. F., and Houlsby, G. T. (1984). “The limiting pressure on a circular pile loaded laterally in cohesive soil.” *Geotechnique*, Vol. 34(4), pp. 613-623.

Reese, L. C., and Matlock, H. (1956). “Nondimensional solutions for laterally loaded piles with soil modulus assumed proportional to depth.” *Proc. of the VIII Texas Conference on Soil Mechanics and Foundation Engineering*, University of Texas, Austin.

Reese, L. C., Isenhower, W. M., Wang, S. T. (2006). *Analysis of design of shallow and deep foundations*. John Wiley & Sons, Inc.

Reese, L. C., Cox, W. R., and Koop, F. D. (1974). “Analysis of laterally loaded piles in sand,” Proc*. 6th Offshore Technology Conference, Paper 2080*, Houston, Texas, pp. 473-483.

Reese, L. C., Cox, W. R. and Koop, F. D. (1975). "Field testing and analysis of laterally loaded piles in stiff clay." *Proc., 7th Offshore Technology Conf., Paper No. OTC 2321*, Houston, Texas, pp. 671-690.

Reese, L. C. and Welch, R. C. (1975), "Lateral loading of deep foundations in stiff clay," *Journal of Geotechnical Engineering Division,* ASCE, Vol. 101(7), pp. 633-649.

Reese, L. C., and Van Impe, W. F. (2001). *Single Piles and Pile Group under Lateral Loading*. A. A. Balkema, Rotterdam, pp. 463

Reese, L. C., Wang, S. T., Isenhower, W. M., and Arrellaga, J. A., and Hendrix, J. (2004). *Computer Program LPILE Plus Version 5.0 Technical Manual*, Ensoft, Inc., Austin, Texas.

Robertson, P. K., Davies, M. P., and Campanella, R. G. (1989). "Design of laterally loaded driven piles using the flat dilatometer." *Geotechnical Testing Journal*, ASTM, Vol. 12(1), pp. 30-38.

Rollins, K. M., Johnson, S.R., Petersen, K.T., and Weaver, T.J. (2003a). "Static and dynamic lateral load behavior of pile groups based on full-scale testing." *13th International Conference on Offshore and Polar Drilling,* International Society for Offshore and Polar Engineering, paper 2003-SAK-02, pp. 8.

Rollins, K. M., Olsen, R.J., Egbett, J.J., Olsen, K.G., Jensen, D.H., and Garrett, B.H. (2003b). "Response, analysis, and design of pile groups subjected to static and dynamic lateral loads." Utah Department of Transportation

SAA piling code (1978). "Rules for the design and installation of piling." AS 2159-1978, Standards Association of Australia, Sydney.

Seed, R. B., and Harder, L. F. (1990). "SPT-based analysis of cyclic pore pressure generation on undrained residual strength." *Proc., H. Bolton Seed Memorial Symp*osium, University of California, Berkeley, California, 351-376

SDC, Caltrans (2006). *Seismic design of abutments for ordinary standard bridges.*

Snyder, J. L. (2004). "Full-scale lateral-load tests of a 3x5 pile group in soft clays and silts." M.S. thesis, Brigham Young University, Department of Civil and Environmental Engineering, Utah.

Sowers G. B., and Sowers, G. F. (1970). *Introductory Soil Mechanics and Foundations,* New York, Macmillan Publishing Company, Inc.

Spillers, W. R., and Stoll, R. D. (1964). ''Lateral response of piles.'' *Journal of Soil Mechanics and Foundation Division,* ASCE, Vol. 90(6), pp. 1–9.

Stevens, J. B., and Audibert, J. M. E. (1979). "Re-examination of p-y curve formulation." *Proc. Of the XI Annual Offshore Technology Conference*, Houston, Texas, OTC 3402, 397-403.

Stewart, D.P. (1999). “Reduction of undrained lateral pile capacity in clay due to an adjacent slope”, *Australian Geomechanics,* pp. 17-23.

Taylor, D. W. (1942). “Cylindrical compression research program on stress-deformation and strength characteristics of soils.” 9th Progress Rep. to U.S. Army Corps of Engineers, Waterways Experiment Station, Massachusetts Inst. Of Technology, Cambridge, Mass.

Terashi, M., Kitazume, M., Manuyama, A., and Yamamoto, Y. (1991). “Lateral resistance of a long pile in or near the slope.” *Proc., Centrifuge '91*. H.-Y. Ko. And F. Mclean, eds., Balkema, Rotterdam, The Netherlands, pp. 245-252.

Terzaghi, K. (1955). “Evaluation of coefficients of subgrade reaction.” *Geotechnique*, Vol. 5(4), pp. 297-326.

Terzaghi, K., and Peck, R. B., (1967). *Soil Mechanics in Engineering Practice*. A Wiley International Edition.

Thompson, G. R. (1977). “Application of the finite element method to the development of p-y curves for saturated clays,” M.S. thesis, Department of Civil Engineering, University of Texas at Austin, TX.

Ti, K. S., Bujang B. K. H. J. N. M. S. J. and Gue, S. E. (2009). ‘A review of basic constitutive models for geotechnical application.” Electronic Journal of Geotechnical Engineering. Vol. 14

University of Florida (1996). *User's Manual for FLORIDA-PIER Program*. Dept. of Civil Engineering, University of Florida, Gainesville.

Vesic, A. S. (1961). “Beam on elastic subgrade and the Winkler hypothesis.” *Proc. 5th Int. Conf. Soil Mechanics and Foundation Engineering*, Paris, Vol. 1, pp. 845-850.

Walsh, J. M. (2005). “Full scale lateral load test of a 3x5 pile group in sand.” M.S.thesis, Brigham Young University, Department of Civil and Environmental Engineering.

Wang, S. and Reese, L. C. (1993). “COM624P-Laterally loaded pile analysis program for the microcomputer, version 2.0.” *FHWA-SA-91-048*, U.S. DOT, Federal Highway Administration.

Wang, S. T. (1982). “Development of a Laboratory Test to Identify the Scour Potential of Soils at Piles Supporting Offshore Structures,” M.S. thesis, Department of Civil Engineering, University of Texas at Austin, TX.

Winkler, E. (1867). “Die lehre von elasticzitat and festigkeit (on elasticity and fixity).” *Prague*, pp. 182.

Yang, K., and Liang, R. (2007). “Methods for deriving *p-y* curves from instrumented lateral load tests.” *ASTM Geotechnical Testing Journal,* Vol. 30, pp 31-38.

Yegian, M. and Wright, S. G. (1973). "Lateral soil resistance – displacement relationships for pile foundations in soft clays." *Proc. 5th Annual Offshore Technology Conference*, OTC 1893, Offshore Technology Conference, Houston, Vol. 2, pp. 663.

Zhang, L., Francisco, S., and Ralph, G. (2005). "Ultimate lateral resistance to piles in pp. 78-83.

16. APPENDIX A

Table A-1. Summary of All Borings Conducted at GEFRS and at Caltrans Test Site

Date	Boring Name	Boring Description	Note
7/16/72	B-1	Exploratory Boring	Prior to 2008
7/16/72	B-2	"	
7/16/72	B-3	"	
1/18/96	B-4	"	
8/23/96	B-5	"	
10/6/97	B-6	"	
10/6/97	B-7	"	
10/11/97	CPT-1	CPT Boring	
10/11/97	CPT-2	CPT Boring	
Fall '97	DMT-1	DMT Boring	
Fall '97	DMT-2	DMT Boring	
4/7/00	CPT-3	CPT Boring	
4/7/00	CPT-4	CPT Boring	
10/2/01	B-8	Exploratory Boring	
10/2/01	B-9	Exploratory Boring	
10/12/01	CPT-5	CPT Boring	
10/18/01	DMT-3	DMT Boring	
10/2/08	B-10	Exploratory Boring	2008-Present
10/2/08	B-11	Exploratory Boring	
10/3/08	CPT-6	CPT Boring	
10/3/08	DMT-4	DMT Boring	
10/14/09	B-12	Exploratory Boring	
10/14/09	B-13	Exploratory Boring	
10/14/09	CPT-7	CPT Boring	
10/14/09	CPT-8	CPT Boring	
10/14/09	DMT-5	DMT Boring	

Table A-2. Summary of Water Contents, Atterberg Limits and Percent Fines from GEFRS Report

Sample Depth (ft)	Natural Water Content (%)	PL	LL	PI	USCS Classification	Percent Fines (%)
3.5	28	21	64	43	CH	
4						92
5	33	25	75	50	CH	
6.5	33	28	48	20	ML	93
6.5	36					72
8	36	28	37	9	ML	
8.5	38					
9	40	27	51	24	CH	62
10	46	37	55	18	MH	62
10	38					
15.5	30	22	39	17	CL	
25.5	58	52	90	38	MH	
26.5	68	57	81	24	MH	93
35	41					
36.5	37					
40	52	46	85	39	MH	
46.5	85					
48	48					
49	55					
49.5	53					

Note: Two additional samples from 13-18 ft were classified as MH

Table A-3. Summary of Water Contents, Atterberg Limits from Caltrans Site Samples

Sample Depth (ft)	Natural Water Content (%)	PL	LL	PI	USCS Classification	Percent Fines (%)
1	19.3	29	46	17	ML/MH	
2.5	25.0	29	69	40	CH	
3	25.8	29	70	41	CH	
3.5	28.7	34	61	28	MH	
4	32.6	30	70	40	CH	
6	34.9	33	68	35	MH/CH	
7	34.9	32	59	27	MH	
9	39.8	33	49	16	ML	

Table A-4. Corrected Blow Count Versus Depth from GEFRS Report.

Sample Depth (ft)	Corrected Blow Counts, N_1 (blows/ft)
3	24
3.5	16
6	7
6	9
6	12
7	6
7.5	22
8.5	4
10.5	75
17.5	21
17.5	25
18	56
20	40
20.5	41
21	42
25.5	26
26	16
31	15
31.5	19
35	15
35	22
42	17
42	18

Table A-5. Corrected Blow Count versus Depth from Caltrans Boring B-10 and B-11.

Sample Depth (ft)	Corrected Blow Counts, N_1 (blows/ft)
2	38
5.5	14
5.5	12
9	19
10.5	47
10	23
12	28
15	5
18	10
18	35
20	71
25	27
28	29

Table A-6. Summary of TXCU Tests from GEFRS Report

Sample No.	Shipton #1	Shipton #2	Shipton #3	#101	#102
Type of Test	CU	CU	CU	CU	CU
Date of Testing	09/96	11/96	11/96	10/01	10/01
Sample Depth (ft)	10	15	16	8	48
Sample Length (in)	7.44	7.25	7.75	-	-
Sample Width (in)	2.75	2.75	2.75	-	-
Consolidation Pressure (psi)	50	56	65	27.77	40
Sample Pressure (psi)	43	45	54	7.5	20
Induced OCR	1.2	1.2	1.2	3.7	2.0
Strain Rate (mm/min)	0.096	0.096	0.096	0.048	0.021
Wet unit weight (pcf)	126	130	123.4	113.9	103.7
Water Content (%)	38.5	44.3	42.6	42	55.4
B-Parameter	0.987	0.987	0.971	-	-
Initial Void Ratio, e_0	-	-	-	1.14	-
$\Delta_{dev,max}$ (psi) @ Fail. Criteria 1	23	22	28	16	29.5
ε_{Axial} (%) @ Fail. Criteria 1	2.5	2	4	9.7	11.3
$\Delta_{dev,max}$ (psi) @ Fail. Criteria 2	-	-	-	12.25	26.8
ε_{Axial} (%) @ Fail. Criteria 2	-	-	-	5.2	10.2

Note: Failure criteria 1 - condition at which maximum deviator stress occurs

Failure criteria 2 - condition at which maximum principle stress ratio (σ'_1/σ'_3) occurs

Table A-7. Summary of TXCU Tests from Reser Stadium Expansion Project

Sample No.	SH-2-3 (No. 1)	SH-2-3 (No. 2)	SH-2-3 (No. 3)	SH-5-6 (No. 1)	SH-5-5 (No. 2)	SH-5-5 (No. 3)	B-4-3 (No. 1)
Type of Test	CU	CU	CU	CU	CU	CU	CU
Date of Testing	10/03	10/03	10/03	11/03	11/03	11/03	04/02
Sample Depth (ft)	7.5-9	7.5-9	7.5-9	12.5-14.5	12.5-14.5	12.5-14.5	8.5
Sample Length (in)	5.56	5.72	5.56	5.69	5.7	5.65	6
Sample Width (in)	2.84	2.86	2.84	2.86	2.86	2.86	2.87
Cell Pressure (psi)	36	30	42	42	36	48	-
Sample Pressure (psi)	30	25	35	35	30	40	-
Induced OCR	1.2	1.2	1.2	1.2	1.2	1.2	
Strain Rate (mm/min)	0.02	0.02	0.02	0.01	0.01	0.01	0.03
Dry Unit Weight (pcf)	82.2	81.3	82.2	83.8	84.8	83.8	79.6
Water Content (%)	38.9	38.9	38.9	35.9	35.9	35.9	40.6
Initial Void Ratio, e_0	1.05	1.04	1.05	0.97	0.97	0.97	1.12
% Saturation	99.9	99.5	99.9	97.8	99	97.8	97.9
$\Delta_{dev,max}$ (psi) @ Fail.	14.7	11.5	21.8	17.9	15.5	26.8	12.5
ε_{Axial} (%) @ Fail.	5	6.2	2	4.6	5.25	3.75	1.8
c (total stress) , psi	1.97	1.97	1.97	2.84	2.84	2.84	-
ϕ (total stress) , psi	20	20	20	21.7	21.7	21.7	-

Note: Failure criteria 1 - condition at which maximum deviator stress occurs
Only Sample No. B-4-3 from Kelly Engineering Center expansion project

Table A-8. Summary of UUTX Tests from Caltrans Boring (B-12 and B-13)

Sample No. (Boring No.)	SH 1-15 (B-12)	SH-2-6 (B-13)	SH-2-5 (B-13)	SH-1-3* (B-12)	SH-1-5* (B-12)	SH-1-1 (B-12)	SH-1-1a (B-12)	SH-1-5a (B-12)
Type of Test	UU	UU	UU	UU	UU	UU	UU	UU
Date of Testing	1/21/10	1/26/10	1/28/10	2/2/10	2/4/10	2/9/10	2/9/10	2/11/10
Sample Depth (ft)	26-26.5	8.5-9	6.5-7	3.5-4	7.5-8	0-0.5	1-1.5	8-8.5
Sample Length (in)	6.02	6.11	6.07	5.69	6.01	6.67	5.93	6.05
Sample Width (in)	2.85	2.88	2.70	2.85	2.86	2.86	2.82	2.88
Cell Pressure (psi)	14.6	7.1	6.2	3.0	6.8	-	-	7.2
Strain Rate (%/min)	1	1	1	1	1	1	1	1
Unit Weight (pcf)	94	114	123	108	117	103	99	117
Water Content (%)	68	37	34	25	43	13	19	34
$q_{,max}$ (psi)	34.5	8.2	17	(4.91)	(1.8)	15.3	6.3	7.9
ε_{Axial} @ q_{max}	5.5	5.6	5.9	(9.2)	(8.6)	1.6	2.0	1.5
ε_{50}	2.3	1.4	1.9	(0.55)	(0.11)	0.7	1	0.5

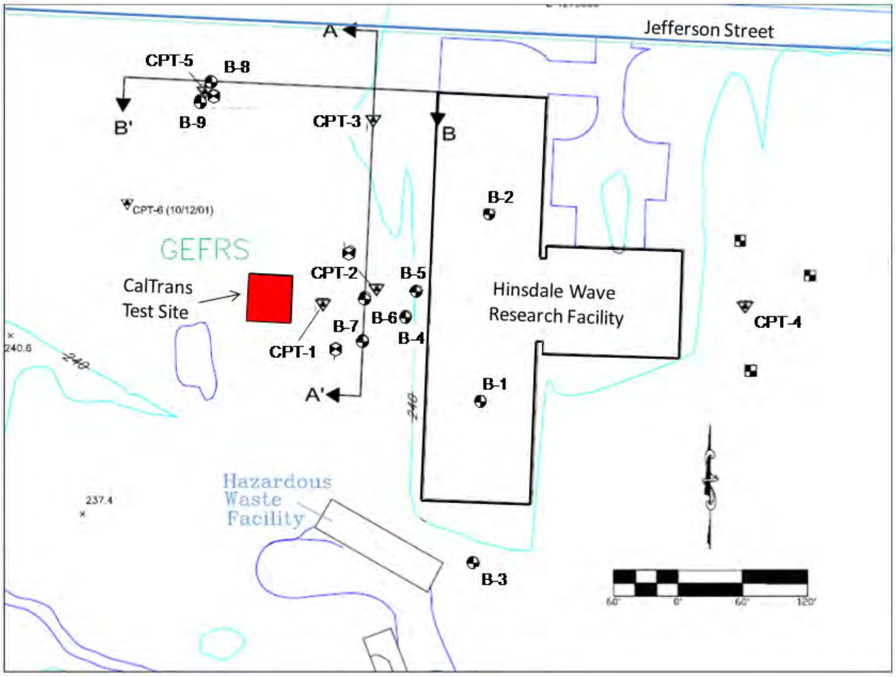

Figure A-1. Location of Caltrans Test Site and GEFRS Site Plan and Existing Boring Locations (modified from Dickenson, 2006)

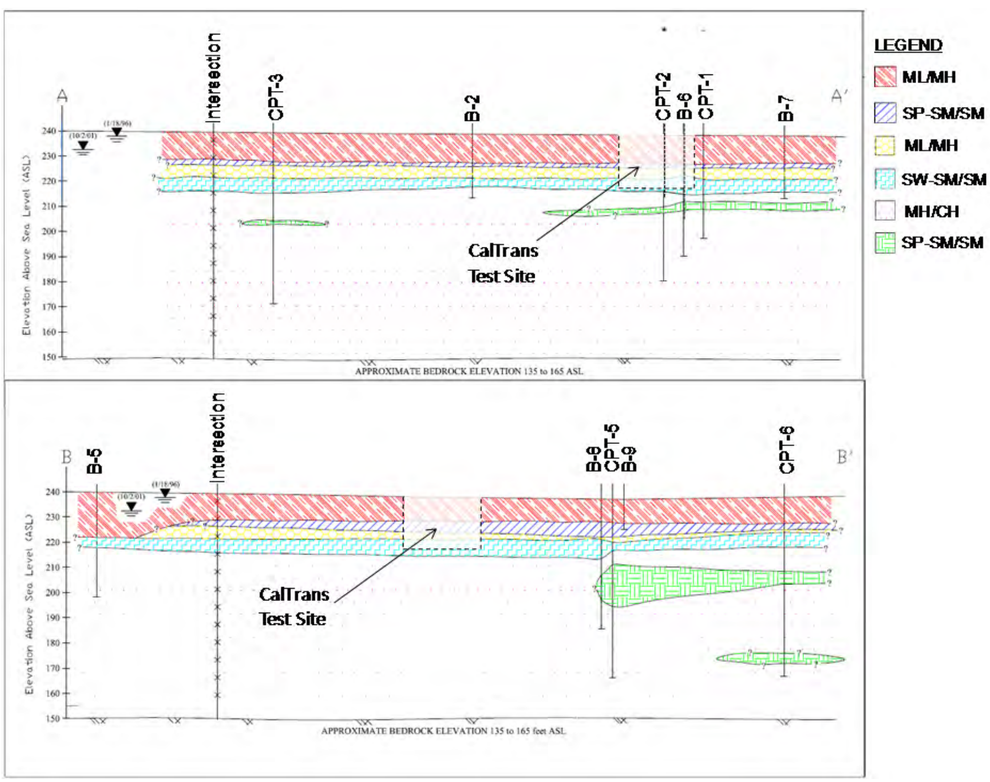

Figure A-2. Location of Caltrans Section Projected onto Cross Section A-A' and B-B' (modified from Dickenson, 2006)

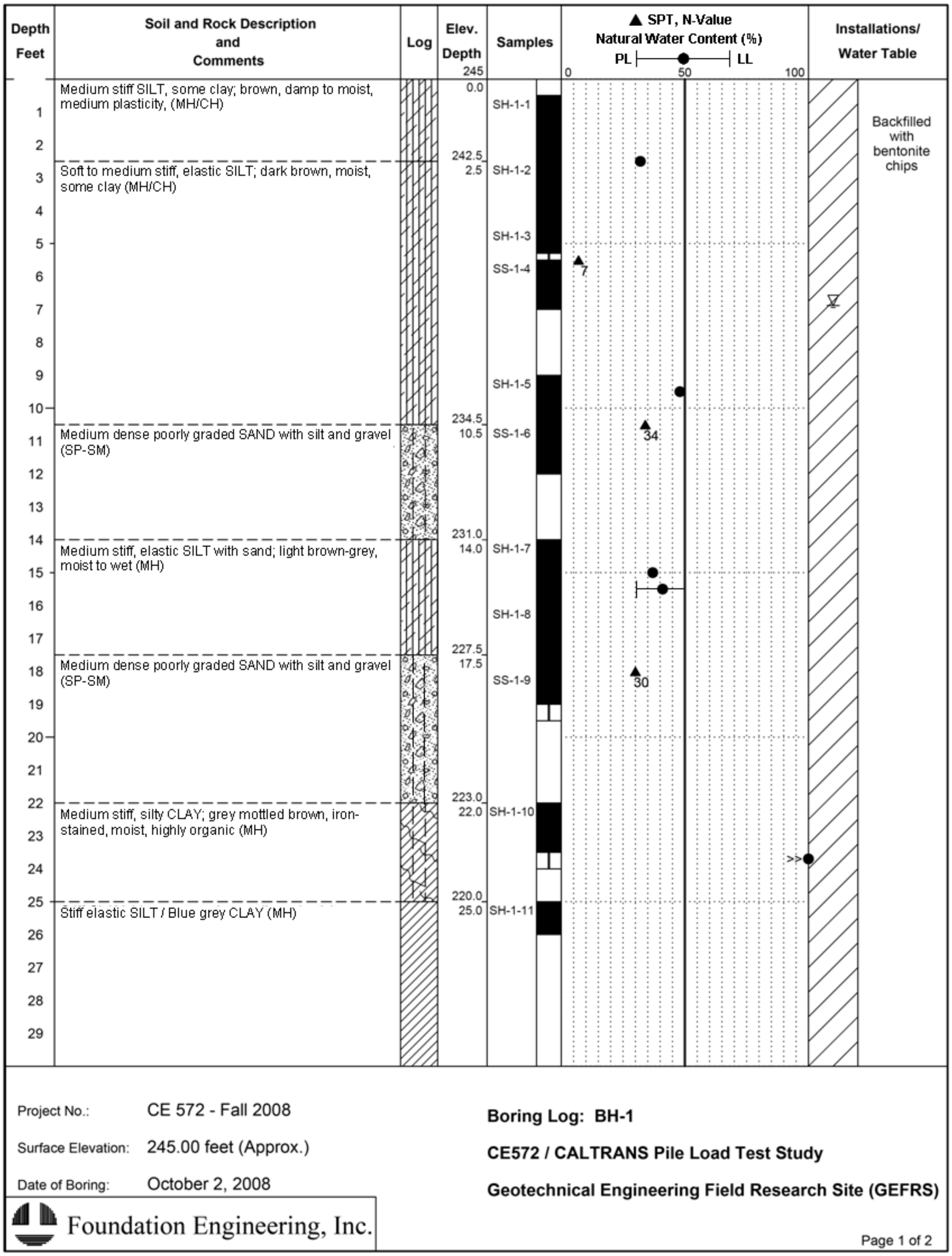

Figure A-3. Soil Boring Log, B-10

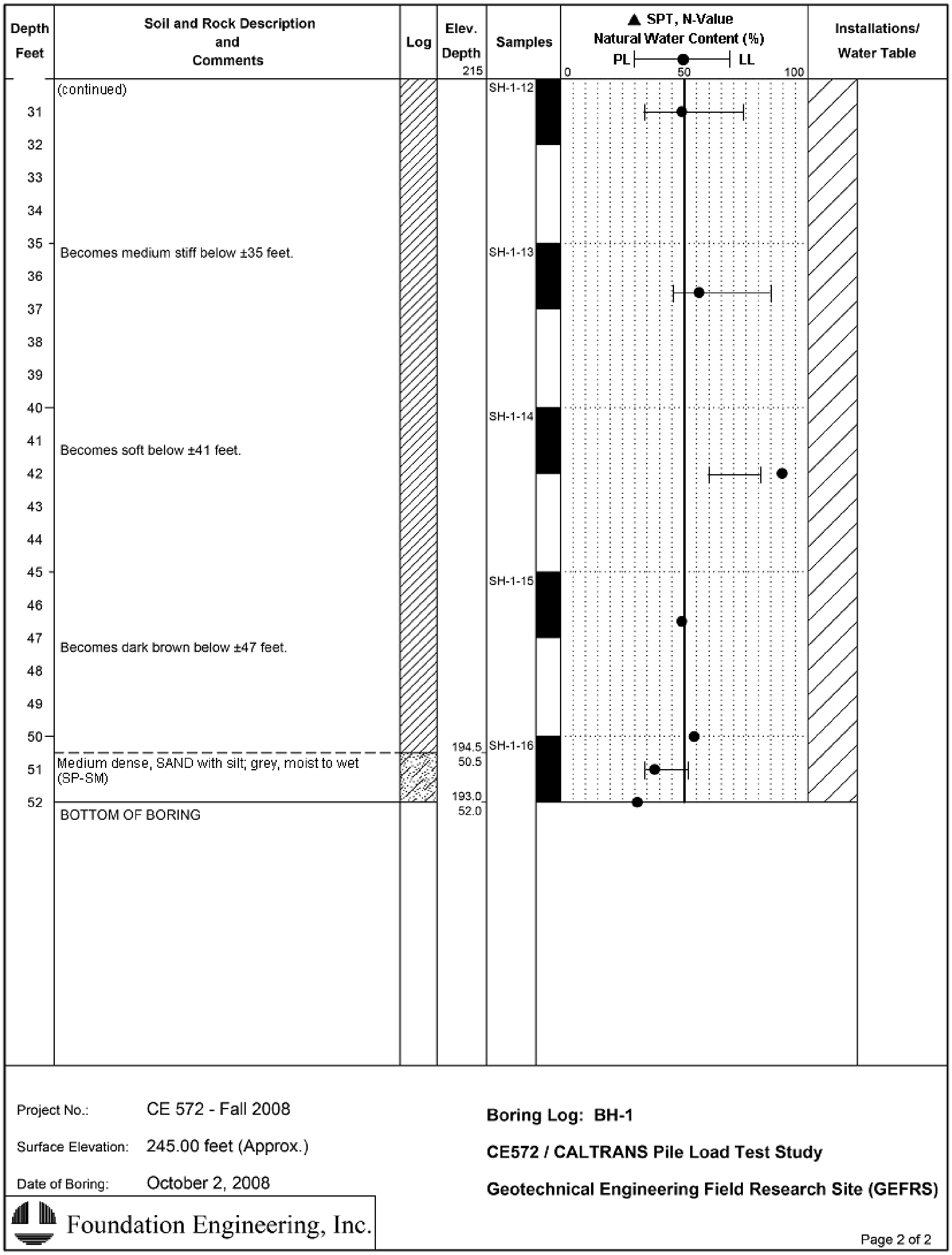

Figure A-3. Soil Boring Log, B-10 (continued)

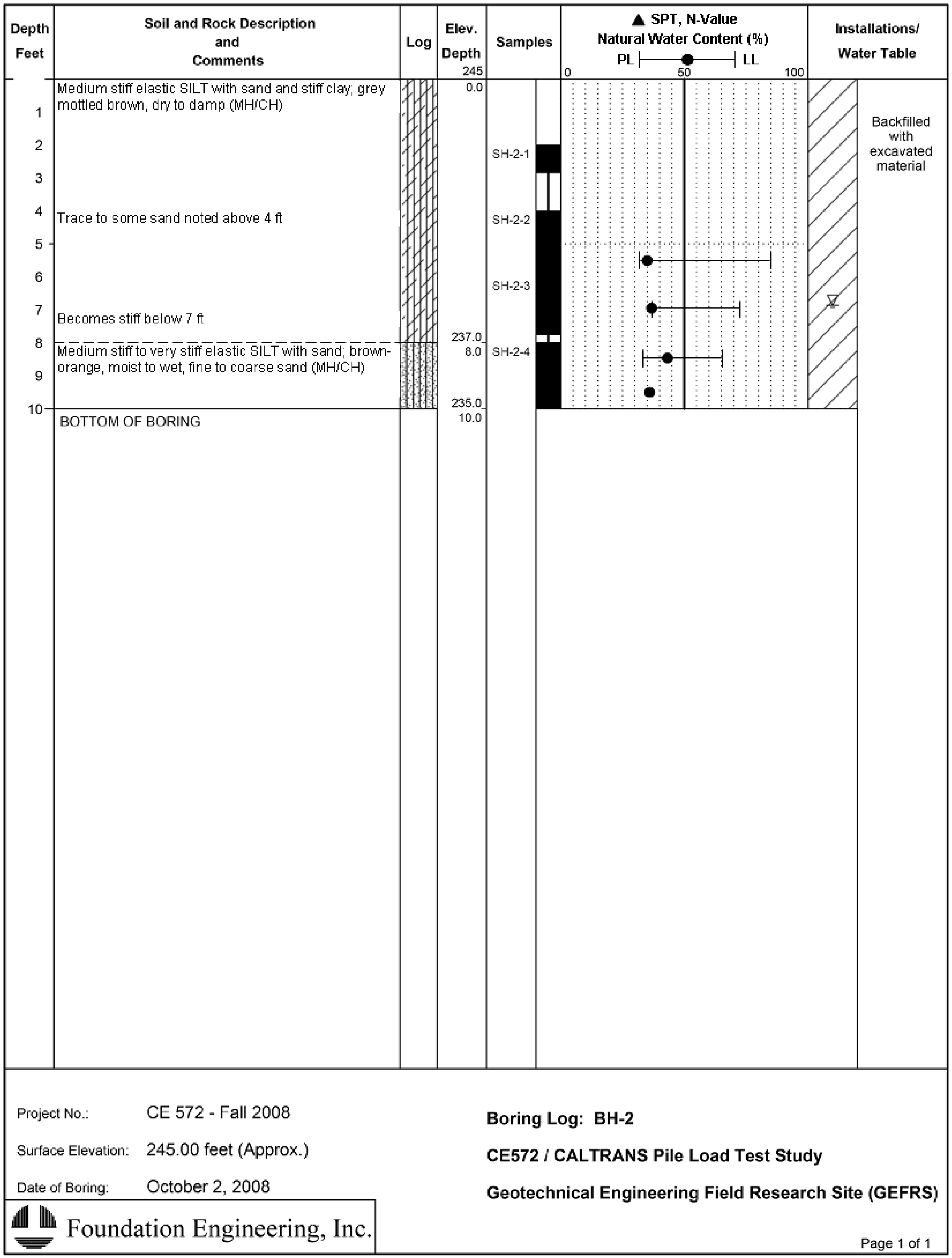

Figure A-4. Soil Boring, Log B-11

17. APPENDIX B

Table B-1. Reported Yield Strength for Steel Pipe Piles

Pile No.	Heat Number	f_y (psi)
I-1	M87651A	83.8
I-2	US0151A	70.6
I-3	US0152A	71.8
I-4	US0151A	75.4
I-5	US0152A	71.4
I-6	US0115	71.8
I-7	M87660A	80.7
I-8	M87657A	81.3
Calibration	L711042	51.6

14000 San Bernardino Ave.
Fontana, California 92335

TUBULAR PRODUCTS CERTIFIED TEST REPORT

CUSTOMER KELLY PIPE COMPANY
DIV. SHAPCO, INC.
P.O. BOX 2827
SANTA FE SPRINGS CA 90670

SHIP TO NATIONAL PIPE & PILING
WILL CALL
WILL CALL CA

TALLY NUMBER

SHIPPING DATE

CAR NUMBER

MO. NUMBER 96-4749-01

CUSTOMER ORDER 1098347

PRODUCT ERW PIPE - STOCK

END USE JOBBER STOCK

SPEC ASTM-A-252-98-GR.2/GR.3-500 PSI

SIZE 12-3/4OD x .375 x 49.61#

FT

US

CS

CHEMICAL COMPOSITION %

HEAT LOT	TYPE	C	Mn	P	S	Si	Cu	Ni	Cr	Mo	Al	V	Cb	Ti	CA	B	CEQ (1)	SEW (2)
M87651 A	H	.06	1.47	.010	.001	.200	.00	.00	.01	.00	.028	.021	.049	.000	.0032	.0000	.00	.000
	P	.07	1.43	.012	.001	.216	.00	.01	.01	.00	.036	.021	.054	.002	.0011	.0000	.00	.000
	B	.07	1.43	.012	.001	.219	.00	.01	.01	.00	.037	.021	.054	.002	.0011	.0000	.00	.000

I CERTIFY THAT THE MATERIAL HEREIN DESCRIBED HAS BEEN MANUFACTURED IN ACCORDANCE WITH THE ORDERED SPECIFICATION, AND THAT THIS TEST INFORMATION IS CORRECT AS CONTAINED IN THE RECORDS OF THE COMPANY

Sr. Chemist - Laboratory Services

MANUFACTURED IN U.S.A.

(1)

(2)

TENSILE STRENGTH							LONGITUDINAL IMPACT TEST										TRANSVERSE IMPACT TEST									
TYPE	LOC	DIR	YIELD STRENGTH KSI	TENSILE STRENGTH KSI	% ELONG. 2"	Y/T	LOT	TYPE	ENERGY FT-LB SPEC 1	SPEC 2	SPEC 3	AVG	% SHEAR APPEARANCE SPEC 1	SPEC 2	SPEC 3	AVG	LOT	TYPE	ENERGY FT-LB SPEC 1	SPEC 2	SPEC 3	AVG	% SHEAR APPEARANCE SPEC 1	SPEC 2	SPEC 3	AVG
P	B	T	83.8	90.4	25	.92																				
P	W			89.0																						

Gauss in pipe =< 20.

CONFORMS TO
NACE MRO 175
FOR HARDNESS ONLY

SPECIMEN TYPE STRIP MILL WIDTH 1 ½" NOM

TYPE I

ISSP

DEFINITIONS OF CODES FOUND IN TYPE, LOCATION AND DIRECTION COLUMNS 12/08/08 8:35:40

B-BODY
C-CHECK ANALYSIS

H-HEAT ANALYSIS
L-LONGITUDINAL

M-MILL CONTROL
N-NOTCHED WELD

P-PIPE
R-RECHECK

T-TRANSVERSE

Figure B-1. Material Properties for Steel Pile I-1

14000 SanBernardino Ave.
Fontana, California 92335

TUBULAR PRODUCTS CERTIFIED TEST REPORT

CUSTOMER KELLY PIPE COMPANY
DIV. SHAPCO, INC.
P.O. BOX 2827
SANTA FE SPRINGS CA 90670

SHIP TO NATIONAL PIPE & PILING
WILL CALL
WILL CALL CA

TALLY NUMBER
SHIPPING DATE
CAR NUMBER
MO. NUMBER 96-4749-01
CUSTOMER ORDER 1098347

PRODUCT ERW PIPE - STOCK

END USE JOBBER STOCK

SPEC ASTM-A-252-98-GR.2/GR.3-500 PSI

SIZE 12-3/4OD x .375 x 49.61#

FT | BS | CS

CHEMICAL COMPOSITION %

HEAT LOT	TYPE	C	Mn	P	S	Si	Cu	Ni	Cr	Mo	Al	V	Cb	Ti	CA	B	CEQ (1)	SPM (2)
US0151 A	H	.07	1.23	.008	.003	.257	.03	.01	.03	.00	.036	.001	.039	.002	.0020	.0001	.00	.000
	P	.07	1.25	.008	.003	.270	.03	.02	.02	.00	.034	.000	.043	.002	.0021	.0001	.00	.000
	P	.07	1.24	.008	.003	.263	.03	.02	.03	.00	.033	.000	.042	.002	.0021	.0001	.00	.000

I CERTIFY THAT THE MATERIAL HEREIN DESCRIBED HAS BEEN MANUFACTURED IN ACCORDANCE WITH THE ORDERED SPECIFICATIONS, AND THAT THIS TEST INFORMATION IS CORRECT AS CONTAINED IN THE RECORDS OF THE COMPANY

Sr. Chemist - Laboratory Services

MANUFACTURED IN U.S.A.

(1) (2)

TENSILE STRENGTH

TYPE	LOC	DIR	YIELD STRENGTH KSI	TENSILE STRENGTH KSI	% ELONG. 2"	Y/T
P	B	T	70.6	79.4	35	.88
P	W			82.6		

LONGITUDINAL IMPACT TEST

LOT	TYPE	ENERGY FT-LB SPEC 1	SPEC 2	SPEC 3	AVG	% SHEAR APPEARANCE SPEC 1	SPEC 2	SPEC 3	AVG

TRANSVERSE IMPACT TEST

LOT	TYPE	ENERGY FT-LB SPEC 1	SPEC 2	SPEC 3	AVG	% SHEAR APPEARANCE SPEC 1	SPEC 2	SPEC 3	AVG

Gauss in pipe =< 20.

CONFORMS TO
NACE MRO 175
FOR HARDNESS ONLY

MINED AND MELTED IN USA

SPECIMEN TYPE STRIP FULL WIDTH 1.5" NOM

T/R | INSP

DEFINITIONS OF CODES FOUND IN TYPE, LOCATION AND DIRECTION COLUMNS 12/08/08 8:35:40

B-BODY C-CHECK ANALYSIS | H-HEAT ANALYSIS L-LONGITUDINAL | M-MILL CONTROL N-NOTCHED WELD | P-PIPE R-RECHECK RETEST | T-TRANSVERSE W-WELD

Figure B-2. Material Properties for Steel Pile I-2

TUBULAR PRODUCTS CERTIFIED TEST REPORT

14000 San Bernardino Ave.
Fontana, California 92335

CUSTOMER KELLY PIPE COMPANY
DIV. SHAPCO, INC.
P.O. BOX 2827
SANTA FE SPRINGS CA 90670

SHIP TO NATIONAL PIPE & PILING
WILL CALL
WILL CALL CA

TALLY NUMBER
SHIPPING DATE
CAR NUMBER
MO. NUMBER 96-4749-01
CUSTOMER ORDER 1098347

PRODUCT ERW PIPE - STOCK

END USE JOBBER STOCK

SPEC ASTM-A-252-98-GR.2/GR.3-500 PSI

SIZE 12-3/4OD x .375 x 49.61#

F T | L B S | F C S

CHEMICAL COMPOSITION %

HEAT LOT	TYPE	C	Mn	P	S	Si	Cu	Ni	Cr	Mo	Al	V	Cb	Ti	CA	B	CEQ (1)	SUM (2)
US0152 A	H	.06	1.26	.009	.004	.250	.02	.02	.04	.00	.032	.001	.043	.002	.0020	.0001	.00	.000
	P	.07	1.29	.008	.003	.260	.02	.02	.03	.00	.034	.000	.046	.002	.0018	.0000	.00	.000
	P	.06	1.29	.008	.003	.262	.02	.02	.03	.00	.033	.000	.046	.002	.0015	.0003	.00	.000

I CERTIFY THAT THE MATERIAL HEREIN DESCRIBED HAS BEEN MANUFACTURED IN ACCORDANCE WITH THE ORDERED SPECIFICATION AND THAT THIS TEST INFORMATION IS CORRECT AS CONTAINED IN THE RECORDS OF THE COMPANY

Sr. Chemist - Laboratory Services

MANUFACTURED IN U.S.A.

(1) (2)

TENSILE STRENGTH

TYPE	LOC	DIR	YIELD STRENGTH KSI	TENSILE STRENGTH KSI	% ELONG. 2"	Y/T
P	B	T	71.4	80.8	35	.88
P	W			82.5		

LONGITUDINAL IMPACT TEST

LOT	TYPE	ENERGY FT-LB SPEC 1	SPEC 2	SPEC 3	AVG	% SHEAR APPEARANCE SPEC 1	SPEC 2	SPEC 3	AVG

TRANSVERSE IMPACT TEST

LOT	TYPE	ENERGY FT-LB SPEC 1	SPEC 2	SPEC 3	AVG	% SHEAR APPEARANCE SPEC 1	SPEC 2	SPEC 3	AVG

Gauss in pipe =< 20.

CONFORMS TO
NACE MR0175
FOR HARDNESS ONLY

MINED AND MELTED IN USA

SPECIMEN TYPE: STRIP 1 FULL WIDTH: 1 1/2 NOM.

T/R INSP

DEFINITIONS OF CODES FOUND IN TYPE, LOCATION AND DIRECTION COLUMNS 12/08/08 8:35:40

B-BODY
C-CHECK ANALYSIS
H-HEAT ANALYSIS
L-LONGITUDINAL
M-MILL CONTROL
N-NOTCHED WELD
P-PIPE
R-RECHECK TEST
T-TRANSVERSE
W-WELD

Figure B-3. Material Properties for Steel Pile I-3 and I-5

14000 SanBernardino Ave.
Fontana, California 92335

TUBULAR PRODUCTS CERTIFIED TEST REPORT

CUSTOMER KELLY PIPE COMPANY DIV. SHAPCO, INC. P.O. BOX 2827 SANTA FE SPRINGS CA 90670	SHIP TO NATIONAL PIPE & PILING WILL CALL WILL CALL CA	TALLY NUMBER SHIPPING DATE CAR NUMBER
		MO. NUMBER 96-4749-01
PRODUCT ERW PIPE - STOCK		CUSTOMER ORDER 1098347
END USE JOBBER STOCK		

SPEC: ASTM-A-252-98-GR.2/GR.3-500 PSI

SIZE: 12-3/4OD x .375 x 49.61# FT BS CS

CHEMICAL COMPOSITION %

HEAT LOT	TYPE	C	Mn	P	S	Si	Cu	Ni	Cr	Mo	Al	V	Cb	Ti	CA	B	CEQ (1)	SUM (2)
US0151	H	.07	1.23	.008	.003	.257	.03	.01	.03	.00	.036	.001	.039	.002	.0020	.0001	.00	.000
	P	.05	1.26	.007	.003	.264	.04	.02	.03	.00	.035	.000	.043	.002	.0024	.0000	.00	.000
	P	.07	1.26	.008	.003	.267	.03	.02	.02	.00	.034	.000	.043	.002	.0027	.0001	.00	.000

I CERTIFY THAT THE MATERIAL HEREIN DESCRIBED HAS BEEN MANUFACTURED IN ACCORDANCE WITH THE ORDERED SPECIFICATION, AND THAT THIS TEST INFORMATION IS CORRECT AS CONTAINED IN THE RECORDS OF THE COMPANY

Sr. Chemist - Laboratory Services

MANUFACTURED IN U.S.A.

(1) (2)

TENSILE STRENGTH

TYPE	LOC.	DIR	YIELD STRENGTH KSI	TENSILE STRENGTH KSI	% ELONG. 2"	Y/T
P	B	T	75.4	84.6	34	.89
P	W			84.3		

LONGITUDINAL IMPACT TEST

LOT	TYPE	ENERGY FT - LB SPEC 1	SPEC 2	SPEC 3	AVG	% SHEAR APPEARANCE SPEC 1	SPEC 2	SPEC 3	AVG

TRANSVERSE IMPACT TEST

LOT	TYPE	ENERGY FT - LB SPEC 1	SPEC 2	SPEC 3	AVG	% SHEAR APPEARANCE SPEC 1	SPEC 2	SPEC 3	AVG

Gauss in pipe =< 20.

CONFORMS TO
NACE MR0 175
FOR HARDNESS ONLY

MINED AND MELTED IN USA

SPECIMEN TYPE: STRIP WIDTH: 1 1/2 NOM.

T/J/R INSP

DEFINITIONS OF CODES FOUND IN TYPE, LOCATION AND DIRECTION COLUMNS 12/08/08 8:35:40

B-BODY C-CHECK ANALYSIS H-HEAT ANALYSIS L-LONGITUDINAL M-MILL CONTROL N-NOTCHED WELD P-PIPE R-RECHECK TEST T-TRANSVERSE W-WELD

Figure B-4. Material Properties for Steel 2D pile (I-4)

14900 San Bernardino Ave.
Fontana, California 92335

TUBULAR PRODUCTS CERTIFIED TEST REPORT

CUSTOMER KELLY PIPE COMPANY DIV. SHAPCO, INC. P.O. BOX 2827 SANTA FE SPRINGS CA 90670	SHIP TO NATIONAL PIPE & PILING WILL CALL WILL CALL CA	TALLY NUMBER SHIPPING DATE CAR NUMBER
PRODUCT ERW PIPE - STOCK		MO. NUMBER 96-4749-01
END USE JOBBER STOCK		CUSTOMER ORDER 1098347

SPEC: ASTM-A-252-98-GR.2/GR.3-500 PSI

SIZ: 12-3/4OD x .375 x 49.61#

F Y | L B S | P C S

CHEMICAL COMPOSITION %

HEAT LOT	TYPE	C	Mn	P	S	Si	Cu	Ni	Cr	Mo	Al	V	Cb	Ti	CA	B	CEQ (1)	SUM (2)
US0115	H	.07	1.24	.008	.004	.264	.03	.02	.03	.00	.031	.002	.038	.002	.0020	.0001	.00	.000
	P	.06	1.24	.007	.003	.257	.03	.02	.03	.00	.028	.000	.040	.002	.0023	.0000	.00	.000
	P	.07	1.25	.007	.004	.260	.03	.02	.03	.00	.030	.000	.041	.002	.0025	.0000	.00	.000

I CERTIFY THAT THE MATERIAL HEREIN DESCRIBED HAS BEEN MANUFACTURED IN ACCORDANCE WITH THE ORDERED SPECIFICATION, AND THAT THIS TEST INFORMATION IS CORRECT AS CONTAINED IN THE RECORDS OF THE COMPANY

Sr. Chemist - Laboratory Services

MANUFACTURED IN U.S.A.

(1) (2)

TENSILE STRENGTH							
TYPE	LOC	DIR	YIELD STRENGTH KSI	TENSILE STRENGTH KSI	% ELONG. 2"	Y/T
P	B	T	71.8	81.5	33	.88
P	W			85.5		

SPECIMEN TYPE: STRIP 1 WIDTH 1 1/2" NOM.

LONGITUDINAL IMPACT TEST: LOT | TYPE | ENERGY FT-LB: SPEC 1 | SPEC 2 | SPEC 3 | AVG | % SHEAR APPEARANCE: SPEC 1 | SPEC 2 | SPEC 3 | AVG

TRANSVERSE IMPACT TEST: LOT | TYPE | ENERGY FT-LB: SPEC 1 | SPEC 2 | SPEC 3 | AVG | % SHEAR APPEARANCE: SPEC 1 | SPEC 2 | SPEC 3 | AVG

Gauss in pipe =< 20.

CONFORMS TO
NACE MRO 175
FOR HARDNESS ONLY

MINED AND MELTED IN USA

T/R | MILL | INSP

DEFINITIONS OF CODES FOUND IN TYPE, LOCATION AND DIRECTION COLUMNS 12/08/08 8:39:40

B-BODY C-CHECK ANALYSIS H-HEAT ANALYSIS L-LONGITUDINAL M-MILL CONTROL N-NOTCHED WELD P-PIPE R-RECHECK/RETEST T-TRANSVERSE W-WELD

Figure B-5. Material Properties for Steel 8D pile (I-6)

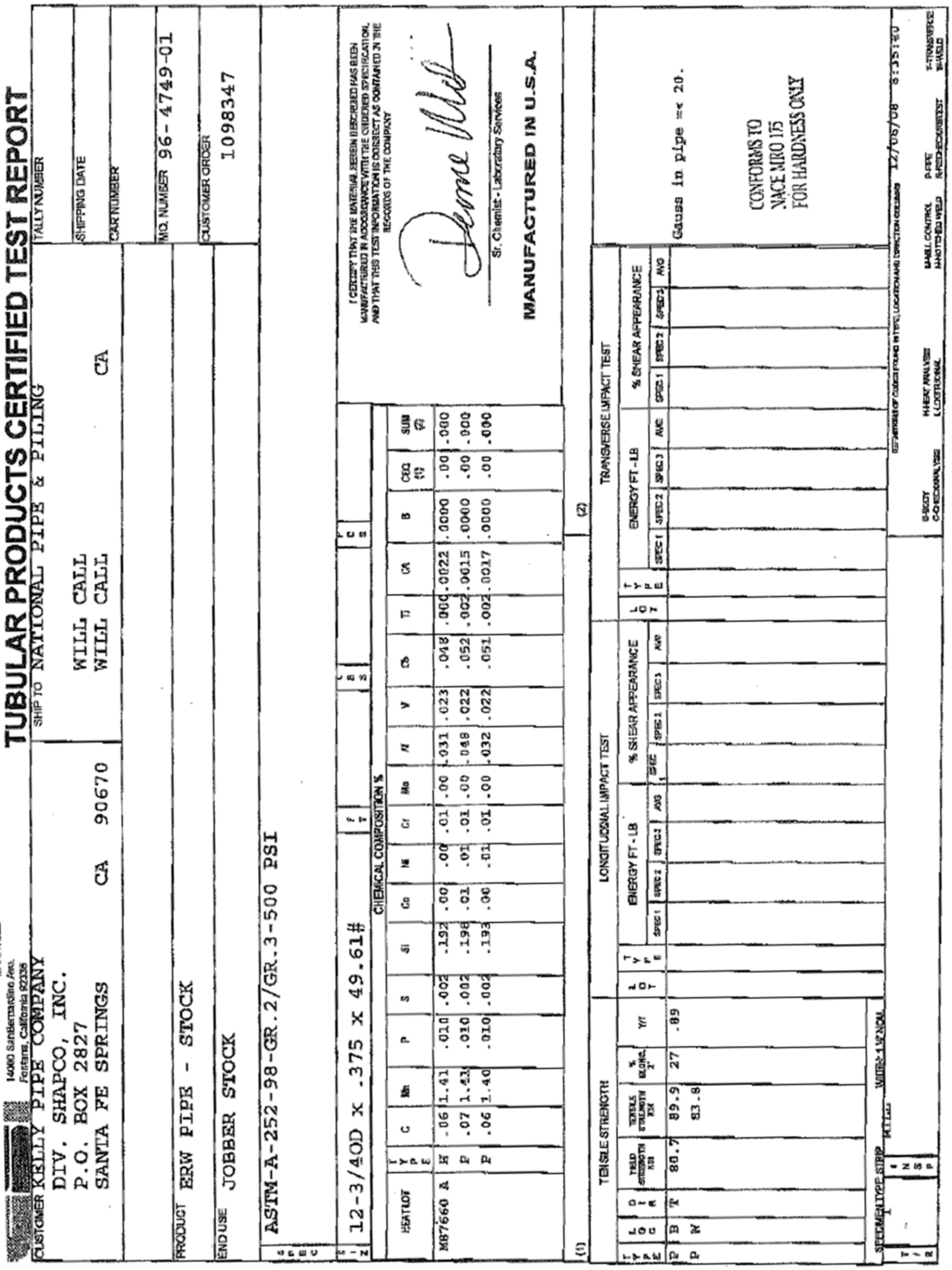

14000 San Bernardino Ave.
Fontana, California 92336

TUBULAR PRODUCTS CERTIFIED TEST REPORT

CUSTOMER: KELLY PIPE COMPANY
DIV. SHAPCO, INC.
P.O. BOX 2827
SANTA FE SPRINGS CA 90670

SHIP TO: NATIONAL PIPE & PILING
WILL CALL
WILL CALL CA

TALLY NUMBER
SHIPPING DATE
CAR NUMBER
MO. NUMBER 96-4749-01
CUSTOMER ORDER 1098347

PRODUCT: ERW PIPE - STOCK

END USE: JOBBER STOCK

SPEC: ASTM-A-252-98-GR.2/GR.3-500 PSI

SIZE: 12-3/4OD x .375 x 49.61#

CHEMICAL COMPOSITION %

HEAT/LOT	TYPE	C	Mn	P	S	Si	Cu	Ni	Cr	Mo	Al	V	Cb	Ti	CA	B	CEQ (1)	SUM (2)
M87660 A	H	.06	1.41	.010	.002	.192	.00	.00	.01	.00	.031	.023	.048	.000	.0022	.0000	.00	.080
	P	.07	1.43	.010	.002	.198	.01	.01	.01	.00	.048	.022	.052	.002	.0015	.0000	.00	.000
	P	.06	1.40	.010	.002	.193	.00	.01	.01	.00	.032	.022	.051	.002	.0017	.0000	.00	.000

I CERTIFY THAT THE MATERIAL HEREIN DESCRIBED HAS BEEN MANUFACTURED IN ACCORDANCE WITH THE ORDERED SPECIFICATION, AND THAT THIS TEST INFORMATION IS CORRECT AS CONTAINED IN THE RECORDS OF THE COMPANY

Sr. Chemist - Laboratory Services

MANUFACTURED IN U.S.A.

(1) (2)

TENSILE STRENGTH

TYPE	LOC	DIR	YIELD STRENGTH KSI	TENSILE STRENGTH KSI	% ELONG. 2"	Y/T
P	B	T	80.7	89.9	27	.89
P	W			83.8		

LONGITUDINAL IMPACT TEST: LOT, TYPE, ENERGY FT-LB (SPEC 1, SPEC 2, SPEC 3, AVG), % SHEAR APPEARANCE (SPEC 1, SPEC 2, SPEC 3, AVG)

TRANSVERSE IMPACT TEST: LOT, TYPE, ENERGY FT-LB (SPEC 1, SPEC 2, SPEC 3, AVG), % SHEAR APPEARANCE (SPEC 1, SPEC 2, SPEC 3, AVG)

Gauss in pipe =< 20.

CONFORMS TO
NACE MRO 175
FOR HARDNESS ONLY

SPECIMEN TYPE STRIP 1 WIDTH 1 1/2" NOM.

T/R, INSP

DEFINITIONS OF CODES FOUND IN TYPE, LOCATION AND DIRECTION COLUMNS 12/06/08 8:35:20

B-BODY, C-CHECK ANALYSIS, H-HEAT ANALYSIS, L-LONGITUDINAL, M-MILL CONTROL, N-NOTCHED WELD, P-PIPE, R-RECHECK/RETEST, T-TRANSVERSE, W-WELD

Figure B-6. Material Properties for Steel 0D pile (I-7)

14000 San Bernardino Ave.
Fontana, California 92335

TUBULAR PRODUCTS CERTIFIED TEST REPORT

CUSTOMER KELLY PIPE COMPANY DIV. SHAPCO, INC. P.O. BOX 2827 SANTA FE SPRINGS CA 90670	SHIP TO NATIONAL PIPE & PILING WILL CALL WILL CALL CA	TALLY NUMBER SHIPPING DATE CAR NUMBER
		MO. NUMBER 96-4749-01
PRODUCT ERW PIPE - STOCK		CUSTOMER ORDER
END USE JOBBER STOCK		1098347

SPEC: ASTM-A-252-98-GR.2/GR.3-500 PSI

SIZE: 12-3/4OD x .375 x 49.61#

CHEMICAL COMPOSITION %

HEAT LOT	TYPE	C	Mn	P	S	Si	Cu	Ni	Cr	Mo	N	V	Cb	Ti	CA	B	CEQ (1)	SUM (2)
M87657 A	H	.08	1.44	.012	.001	.241	.00	.00	.01	.00	.030	.023	.052	.000	.0022	.0000	.00	.000
	P	.06	1.42	.012	.001	.236	.00	.01	.01	.00	.030	.022	.054	.002	.0009	.0000	.00	.000
	P	.08	1.43	.013	.002	.237	.00	.01	.01	.00	.032	.022	.054	.002	.0018	.0000	.00	.000

I CERTIFY THAT THE MATERIAL HEREIN DESCRIBED HAS BEEN MANUFACTURED IN ACCORDANCE WITH THE ORDERED SPECIFICATION, AND THAT THIS TEST INFORMATION IS CORRECT AS CONTAINED IN THE RECORDS OF THE COMPANY

Sr. Chemist - Laboratory Services

MANUFACTURED IN U.S.A.

(1) (2)

TENSILE STRENGTH

TYPE	LOC	DIR	YIELD STRENGTH KSI	TENSILE STRENGTH KSI	% ELONG. 2"	Y/T
P	B	T	81.3	90.2	28	.90
P	W			92.7		

SPECIMEN TYPE: STRIP WIDTH: 1 ½" NOM

LONGITUDINAL IMPACT TEST

LOT	TYPE	ENERGY FT-LB SPEC 1	SPEC 2	SPEC 3	AVG	% SHEAR APPEARANCE SPEC 1	SPEC 2	SPEC 3	AVG

TRANSVERSE IMPACT TEST

LOT	TYPE	ENERGY FT-LB SPEC 1	SPEC 2	SPEC 3	AVG	% SHEAR APPEARANCE SPEC 1	SPEC 2	SPEC 3	AVG

Gauss in pipe =< 20.

CONFORMS TO
NACE MRO 175
FOR HARDNESS ONLY

Y/R I MILL INSP

DEFINITIONS OF CODES FOUND IN TYPE, LOCATION AND DIRECTION COLUMNS 12/08/06

B-BODY C-CHECK ANALYSIS H-HEAT ANALYSIS L-LONGITUDINAL M-MILL CONTROL N-NOTCHED WELD P-PIPE R-RECHECK/RETEST T-TRANSVERSE W-WELD

Figure B-7. Material Properties for Steel Pile I-8

质证书编号/Certificate NO.： 2007070601
订货单位/ Customer:R&R Trading Co.,Ltd.
到站/Receive：加拿大温哥华/VANCOUVER B.C.,CANADA

® 浙江金洲管道工业有限公司
Zhejiang Kingland Pipe Industry Co., Ltd.

Inspection Certificate

名称/ Description：螺旋埋弧焊钢管/ Spiral SAW Pipe 执行标准/ Spec.：ASTM A252 钢 级/Grade：ASTM A252 GR.3
规格/ Size：12.75"(323.85mm) O.D×0.375"(9.53mm)WT×40'(12.19m)L Pieces (pcs):222pcs 总重/Total Weight :199.900吨/MT

序号 NO.	管号Pipe No.	炉批号 Heat No	母材化学成分/ Base Metal Chemical Analysis（%）															母材物理性能 BaseMetalMechanicalProperties				焊接接头物理性能 Weld Joint Mechanical Properties			静水压试验 Hydro-test Mpa	冲击试验 Impact Test(-1℃)								落锤试验 DWTT SA (%) 0℃	无损检测NDT	
			C	Mn	Si	S	P	Nb	V	Ti	Ni	Cr	Cu	Mo	Al	Ceq	Pcm	屈服强度 Yield Strength Mpa	抗拉强度 Tensile Strength Mpa	屈强比σ0.5/σb Yield Ratio %	延伸率 Elonga-tion %	抗拉强度 Tensile Strength Mpa	正弯180° Face Bend	反弯180° Root Bend		母材Base Metal J				母材剪切面积 Base Metal					10%UT	RT
			X100			X1000										X100										1	2	3	平均 Avg	1	2	3	平均 Avg			
1	5-8081-4302	L711042	14	146	39	21	15											356	479	74	40	489	ok	ok											ok	
2																																				
3																																				
4																																				
5																																				
6																																				
7																																				
8																																				
9																																				
10																																				
11																																				
12																																				
13																																				
14																																				
15																																				
16																																				
备注Note: 1																																				
2																																				
3																																				
4																																				

兹证明此质保单中所描述的产品的生产，取样和试验都符合相关技术规范和材质要求。
We certify that the products described herein were manufactured,sampled, and tested in accordance with the specifications and grade mentioned.
检验员/Inspector: 林恒金. 负责人/QA manager: 徐泽旋 日期/Date: 2007/7/6

Figure B-8. Material Properties for Steel Pile used for Calibration Test

LUDWIG & ASSOCIATES LTD.

LABORATORY ACCREDITATION BUREAU
ISO/IEC 17025 ACCREDITED
Certificate Number L2857

LABORATORY TEST REPORT

CUSTOMER:	**Dominion Pipe & Piling** 2400 - 61st Avenue S.E. Calgary, Alberta T2C 2L7	**Laboratory Test No.:**	C06-1665.1
		Date:	November 23, 2006
Attention:	Ken Darling		

Material: Carbon Steel Pipe

Size: 762 mm (30.0 in.) O.D. x 14.3 mm (0.562 in.) w.t.

TENSILE TEST

SPECIMEN NUMBER	T1	
WIDTH mm (in.)	37.9	(1.49)
THICKNESS mm (in.)	14.2	(0.559)
AREA sq. mm (sq. in.)	538	(0.834)
GAUGE LENGTH mm (in.)	50.8	(2.00)
YIELD STRENGTH METHOD	0.2% Offset	
LOAD AT YIELD N (lbs)	304 400	(68,400)
YIELD STRENGTH MPa (psi)	566	(82,000) ✓
ULTIMATE LOAD N (lbs)	345 200	(77,600)
ULTIMATE STRESS MPa (psi)	641	(93,000) ✓
% ELONGATION	36	
TYPE OF FRACTURE	Partial Cup & Cone	

We certify the test results in this report and that the specimen(s) were prepared and tested in accordance with the requirements of ASTM A370 – 06. *The information regarding material identification (i.e. size, thickness, heat number, etc.) has been provided by the customer whose name appears on this report.*

Laboratory Test Conducted By: Inderjit Rai / Steve Rieberger, C.E.T.

6227 - 14 Street S.E., CALGARY, ALBERTA T2C 3K6 PHONE: (403) 262-7072 FAX: (403) 266-3169
7925 Davies Road, EDMONTON, ALBERTA T6E 4N1 PHONE: (780) 468-3030 FAX: (780) 468-3032

Page 1 of 1

Figure B-9. Example Reported Tensile Test for Steel Pile

18. APPENDIX C

Table C-1 Reported Yield Strength for Steel Pipe Piles

Pile No.	Heat Number	f_y (psi)
P-2	US5151A	70.6
P-3	US0152A	71.4
P-4	US151	75.4
P-5	US0152A	71.4
P-6	US0125	71.6
P-7	US0115	75.4
P-8	M87657A	81.3

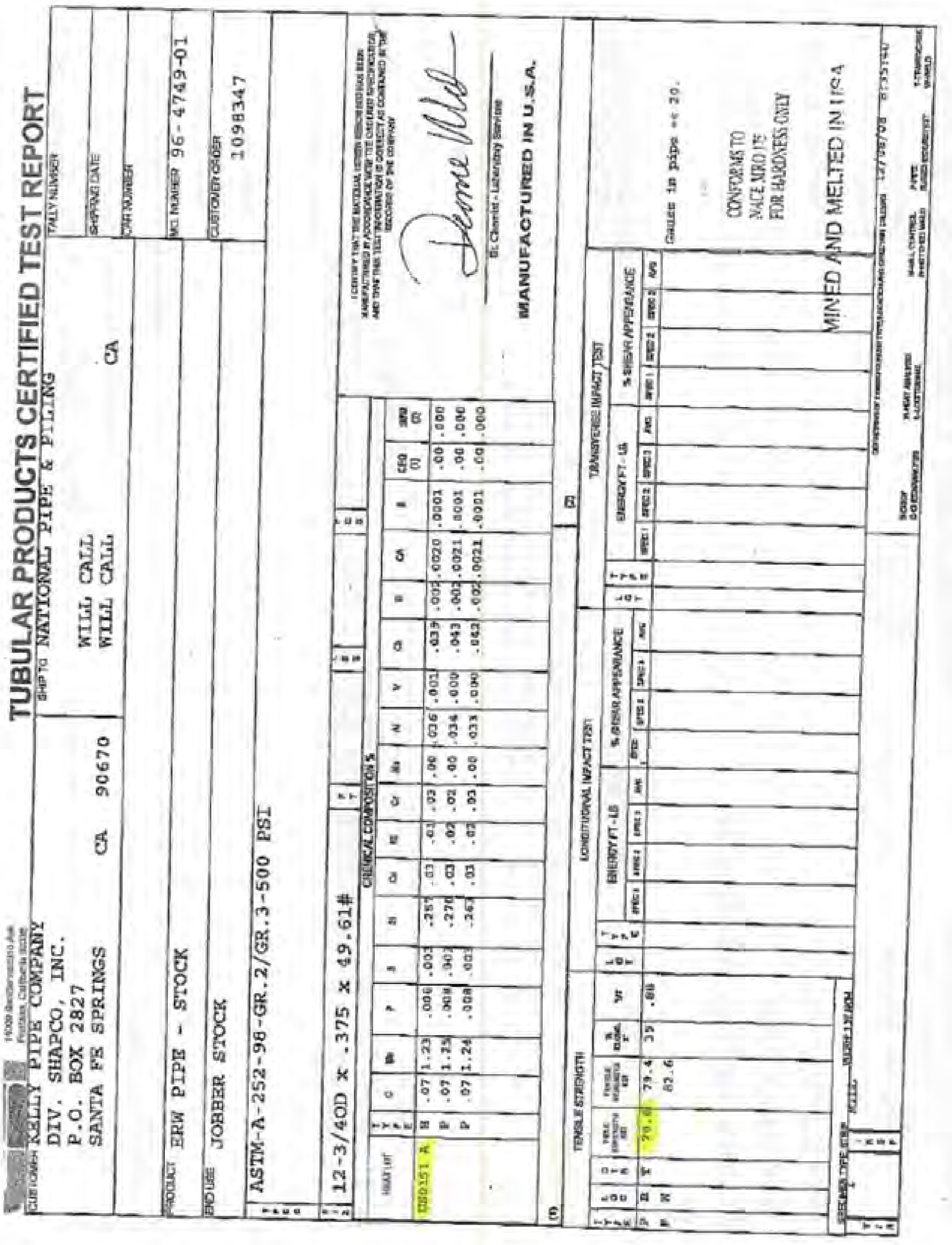

TUBULAR PRODUCTS CERTIFIED TEST REPORT

CUSTOMER KELLY PIPE COMPANY
DIV. SHAPCO, INC.
P.O. BOX 2827
SANTA FE SPRINGS CA 90670

SHIP TO NATIONAL PIPE & PILING
WILL CALL
WILL CALL CA

TALLY NUMBER

SHIPPING DATE

CAR NUMBER

MO. NUMBER 96-4749-01

CUSTOMER ORDER 1098347

PRODUCT ERW PIPE - STOCK

END USE JOBBER STOCK

ASTM-A-252-98-GR.2/GR.3-500 PSI

12-3/4OD x .375 x 49.61#

CHEMICAL COMPOSITION %

HEAT LOT	TYPE	C	Mn	P	S	Si	Cu	Ni	Cr	Mo	Al	V	Cb	B	CA	N	CEQ (1)	SPM (2)
U80151 A	H	.07	1.23	.006	.003	.257	.03	.01	.03	.00	.036	.001	.039	.002	.0020	.0001	.00	.000
	P	.07	1.25	.008	.002	.270	.03	.02	.02	.00	.034	.000	.043	.002	.0021	.0001	.00	.000
	P	.07	1.24	.008	.003	.263	.03	.02	.03	.00	.033	.000	.042	.002	.0021	.0001	.00	.000

I CERTIFY THAT THE MATERIAL HEREIN DESCRIBED HAS BEEN MANUFACTURED IN ACCORDANCE WITH THE ORDERED SPECIFICATION AND THAT THIS TEST INFORMATION IS CORRECT AS CONTAINED IN THE RECORDS OF THE COMPANY

St. Clair - Laboratory Services

MANUFACTURED IN U.S.A.

TENSILE STRENGTH

TYPE	LOC	DIR	YIELD STRENGTH KSI	TENSILE STRENGTH KSI	% ELONG. 2"	Y/T
P	B	T	78.6	79.4	35	.88
P	W			82.6		

LONGITUDINAL IMPACT TEST — ENERGY FT-LB — % SHEAR APPEARANCE

TRANSVERSE IMPACT TEST — ENERGY FT-LB — % SHEAR APPEARANCE

Gauss in pipe <= 20.

CONFORMS TO
NACE MR0175
FOR HARDNESS ONLY

MINED AND MELTED IN USA

SPECIMEN TYPE STRIP FULL

12/08/08

Figure C-1 Material Properties for Steel Test Pile

TUBULAR PRODUCTS CERTIFIED TEST REPORT

14000 ... Ave.
Fontana, California 92335

CUSTOMER KELLY PIPE COMPANY
DIV. SHAPCO, INC.
P.O. BOX 2827
SANTA FE SPRINGS CA 90670

SHIP TO NATIONAL PIPE & PILING
WILL CALL
WILL CALL CA

TALLY NUMBER
SHIPPING DATE
CAR NUMBER
SO NUMBER 96-4749-01
CUSTOMER ORDER 1098347

PRODUCT BRW PIPE - STOCK
END USE JOBBER STOCK
SPEC ASTM-A-252-98-GR.2/GR.3-500 PSI
SIZE 12-3/4OD x .375 x 49.61#

CHEMICAL COMPOSITION %

HEAT LOT	TYPE	C	Mn	P	S	Si	Cu	Ni	Cr	Mo	Al	V	Cb	Ti	CA	B	CEQ (1)	SUB (2)
080115	H	.07	1.24	.008	.004	.264	.03	.02	.03	.00	.031	.002	.038	.002	.0020	.0001	.00	.000
	P	.06	1.24	.007	.003	.257	.03	.02	.03	.09	.028	.000	.040	.002	.0023	.0000	.00	.000
	P	.07	1.25	.007	.004	.260	.03	.02	.03	.06	.030	.000	.041	.002	.0025	.0000	.09	.006

(1)

(2)

TENSILE STRENGTH

TYPE	LOC	DIR	YIELD STRENGTH KSI	TENSILE STRENGTH KSI	% ELONG. 2"	Y/T
P	B	T	71.6	81.5	33	.88
P	W			85.5		

LONGITUDINAL IMPACT TEST: LOT, TYPE, ENERGY FT-LB (SPEC 1, SPEC 2, SPEC 3, AVG), % SHEAR APPEARANCE (SPEC 1, SPEC 2, SPEC 3, AVG)

TRANSVERSE IMPACT TEST: LOT, TYPE, ENERGY FT-LB (SPEC 1, SPEC 2, SPEC 3, AVG), % SHEAR APPEARANCE (SPEC 1, SPEC 2, SPEC 3, AVG)

SPECIMEN TYPE SIZE T FULL
TEMP
TEST LOCATION

I CERTIFY THAT THE MATERIAL HEREIN DESCRIBED HAS BEEN MANUFACTURED IN ACCORDANCE WITH THE SPECIFIED SPECIFICATIONS, AND THAT THIS TEST INFORMATION IS CORRECT AS CONTAINED IN THE RECORDS OF THE COMPANY

Deone Wil

S. Chemist - Laboratory Services

MANUFACTURED IN U.S.A.

Gauss in pipe =< 20.

CONFORMS TO
NACE MR0175
FOR HARDNESS ONLY

MINED AND MELTED IN USA

12/07/98

SHEET CHEMISTRY · SHEET ANALYSIS LONGITUDINAL · WELD CONTROL WHETHER WELD · PIPE MECHANICAL TEST · T-TRANSVERSE W-WELD

Figure C-2 Material Properties for Steel Test Pile

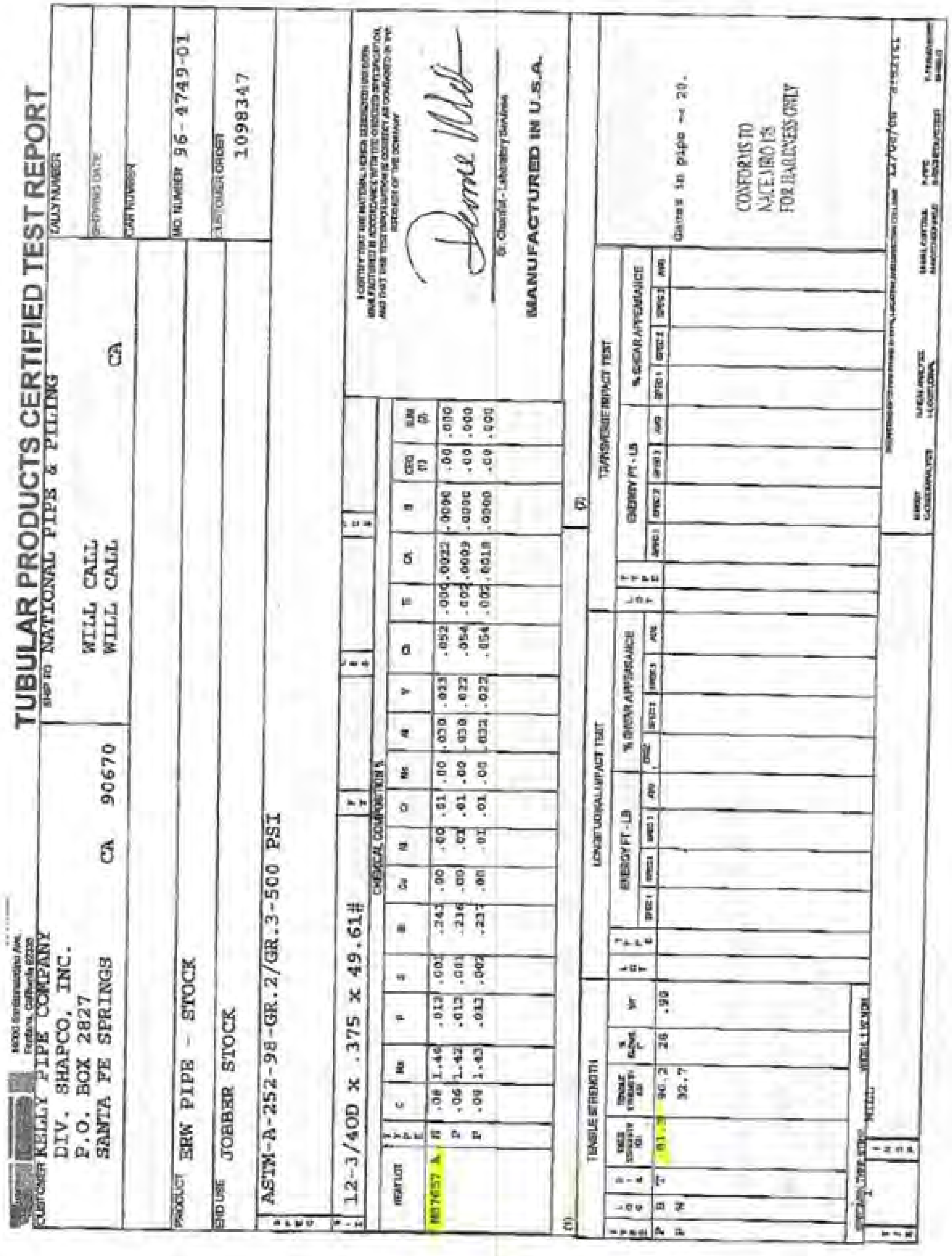

TUBULAR PRODUCTS CERTIFIED TEST REPORT

CUSTOMER KELLY PIPE COMPANY
DIV. SHAPCO, INC.
P.O. BOX 2827
SANTA FE SPRINGS CA 90670

SHIP TO NATIONAL PIPE & PILING
WILL CALL
WILL CALL CA

TALLY NUMBER
SHIPPING DATE
CAR NUMBER
MO. NUMBER 96-4749-01
CUSTOMER ORDER 1098347

PRODUCT ERW PIPE - STOCK
END USE JOBBER STOCK
SPEC ASTM-A-252-98-GR.2/GR.3-500 PSI
12-3/4OD x .375 x 49.61#

CHEMICAL COMPOSITION %

HEAT LOT	TYPE	C	Mn	P	S	Si	Cu	Ni	Cr	Mo	Al	V	Cb	Ti	CA	B	CEQ (1)	SUM (2)
M87657 A	R	.08	1.46	.012	.002	.242	.00	.00	.01	.00	.030	.033	.052	.000	.0022	.0000	.00	.030
	P	.06	1.42	.013	.001	.216	.00	.01	.01	.00	.030	.032	.054	.002	.0009	.0000	.00	.000
	P	.08	1.43	.013	.002	.237	.00	.01	.01	.00	.032	.022	.054	.002	.0018	.0000	.00	.000

I CERTIFY THAT THE MATERIAL HEREIN DESCRIBED HAS BEEN MANUFACTURED IN ACCORDANCE WITH THE ORDERED SPECIFICATION, AND THAT THE TEST INFORMATION IS CORRECT AS CONTAINED IN THE RECORDS OF THE COMPANY

Sr. Chemist - Laboratory Services

MANUFACTURED IN U.S.A.

TENSILE STRENGTH

TYPE	LOC	DIR	YIELD STRENGTH (KSI)	TENSILE STRENGTH (KSI)	% ELONG. 2"	Y/T
P	B	T	81.3	96.2	26	.99
P	N			32.7		

LONGITUDINAL IMPACT TEST
TRANSVERSE IMPACT TEST

Gates in pipe -- 20.

CONFORMS TO
NACE MR0175
FOR HARDNESS ONLY

Figure C-3 Material Properties for Steel Test Pile

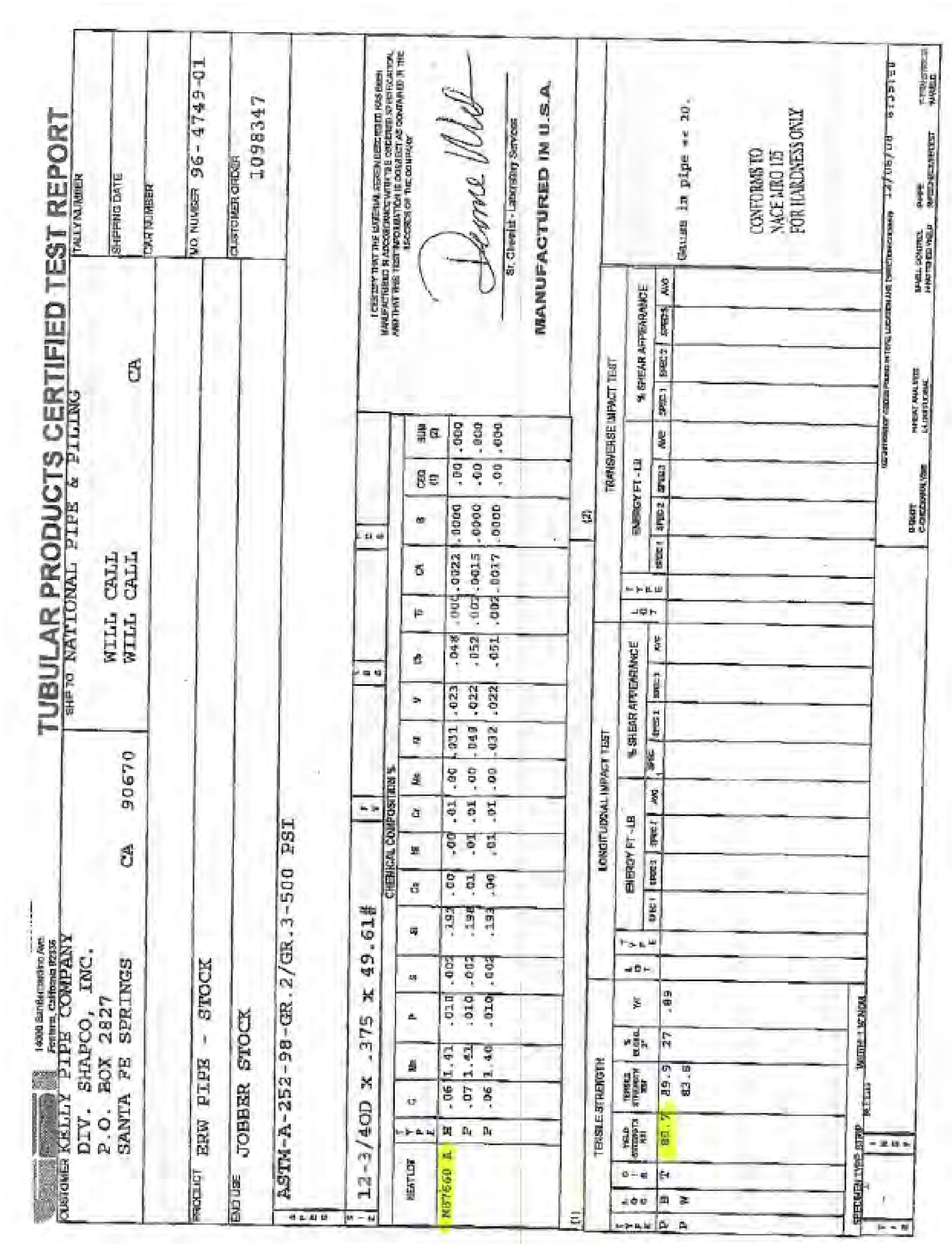

TUBULAR PRODUCTS CERTIFIED TEST REPORT

14000 San Bernardino Ave. Fontana, California 92335

CUSTOMER KELLY PIPE COMPANY
DIV. SHAPCO, INC.
P.O. BOX 2827
SANTA FE SPRINGS CA 90670

SHIP TO NATIONAL PIPE & PILING
WILL CALL
WILL CALL CA

TALLY NUMBER
SHIPPING DATE
CAR NUMBER
W.O. NUMBER 96-4749-01
CUSTOMER ORDER 1098347

PRODUCT ERW PIPE - STOCK
END USE JOBBER STOCK
SPEC ASTM-A-252-98-GR.2/GR.3-500 PSI
SIZE 12-3/4OD x .375 x 49.61#

CHEMICAL COMPOSITION %

HEAT LOT	TYPE	C	Mn	P	S	Si	Cu	Ni	Cr	Mo	Al	V	Cb	Ti	CA	B	CEQ (1)	SUM (2)
N87660 A	H	.06	1.41	.010	.002	.192	.00	.00	.01	.00	.031	.023	.048	.000	.0022	.0000	.00	.000
	P	.07	1.41	.010	.002	.198	.01	.01	.01	.00	.049	.022	.052	.002	.0015	.0000	.00	.000
	P	.06	1.40	.010	.002	.193	.00	.01	.01	.00	.032	.022	.051	.002	.0017	.0000	.00	.000

I CERTIFY THAT THE MATERIAL HEREIN DESCRIBED HAS BEEN MANUFACTURED IN ACCORDANCE WITH THE ORDERED SPECIFICATION, AND THAT THIS TEST INFORMATION IS CORRECT AS CONTAINED IN THE RECORDS OF THE COMPANY

Sr. Chemist - Laboratory Services

MANUFACTURED IN U.S.A.

TENSILE STRENGTH

TYPE	LOC	DIR	YIELD STRENGTH KSI	TENSILE STRENGTH KSI	% ELONG. 2"	Y/T
P	B	T	80.7	89.9	27	.89
P	W			83.6		

LONGITUDINAL IMPACT TEST — ENERGY FT-LB / % SHEAR APPEARANCE

TRANSVERSE IMPACT TEST — ENERGY FT-LB / % SHEAR APPEARANCE

Gauss in pipe <= 20.

CONFORMS TO
NACE MR0 175
FOR HARDNESS ONLY

12/06/08

Figure C-4 Material Properties for Steel Test Pile

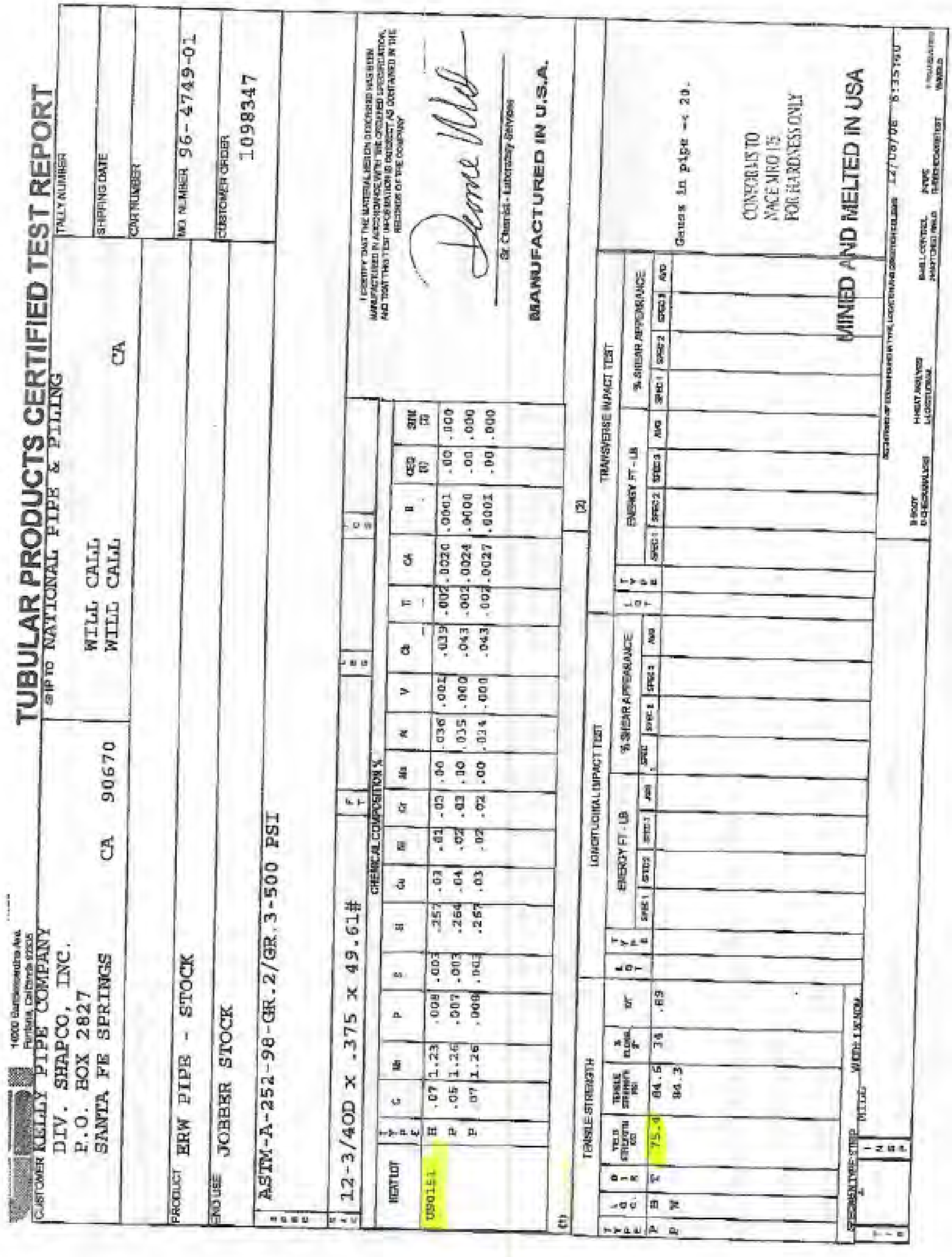

14000 Santa Ana Ave.
Fontana, California

TUBULAR PRODUCTS CERTIFIED TEST REPORT

CUSTOMER KELLY PIPE COMPANY
DIV. SHAPCO, INC.
P.O. BOX 2827
SANTA FE SPRINGS CA 90670

SHIP TO NATIONAL PIPE & PILING
WILL CALL
WILL CALL CA

TALLY NUMBER
SHIPPING DATE
CAR NUMBER
MO. NUMBER 96-4749-01
CUSTOMER ORDER 1098347

PRODUCT ERW PIPE - STOCK
END USE JOBBER STOCK

ASTM-A-252-98-GR.2/GR.3-500 PSI

12-3/4OD x .375 x 49.61#

CHEMICAL COMPOSITION %

HEAT LOT	TYPE	C	Mn	P	S	Si	Cu	Ni	Cr	Mo	N	V	Cb	Ti	CA	B	CEQ (1)	SINI (2)
U90151	H	.07	1.23	.008	.003	.257	.03	.01	.03	.00	.036	.001	.039	.002	.0020	.0001	.00	.000
	P	.05	1.26	.007	.003	.264	.04	.02	.03	.10	.035	.000	.043	.002	.0024	.0000	.00	.000
	P	.07	1.26	.008	.003	.267	.03	.02	.02	.00	.034	.000	.043	.002	.0027	.0001	.00	.000

I CERTIFY THAT THE MATERIAL HEREIN DESCRIBED HAS BEEN MANUFACTURED IN ACCORDANCE WITH THE ORDERED SPECIFICATION, AND THAT THIS TEST INFORMATION IS CORRECT AS CONTAINED IN THE RECORDS OF THE COMPANY

Sr. Chemist - Laboratory Services

MANUFACTURED IN U.S.A.

TENSILE STRENGTH

TYPE	LOC.	DIR	YIELD STRENGTH KSI	TENSILE STRENGTH KSI	% ELONG. 2"	Y/T
P	B	T	75.4	84.5	34	.89
P	W			84.3		

LONGITUDINAL IMPACT TEST — ENERGY FT - LB; % SHEAR APPEARANCE

TRANSVERSE IMPACT TEST — ENERGY FT - LB; % SHEAR APPEARANCE

Gauss in pipe =< 20.

CONFORMS TO
NACE MRO 175
FOR HARDNESS ONLY

MINED AND MELTED IN USA

12/08/06 8:35:50

Figure C-5 Material Properties for Steel Test Pile

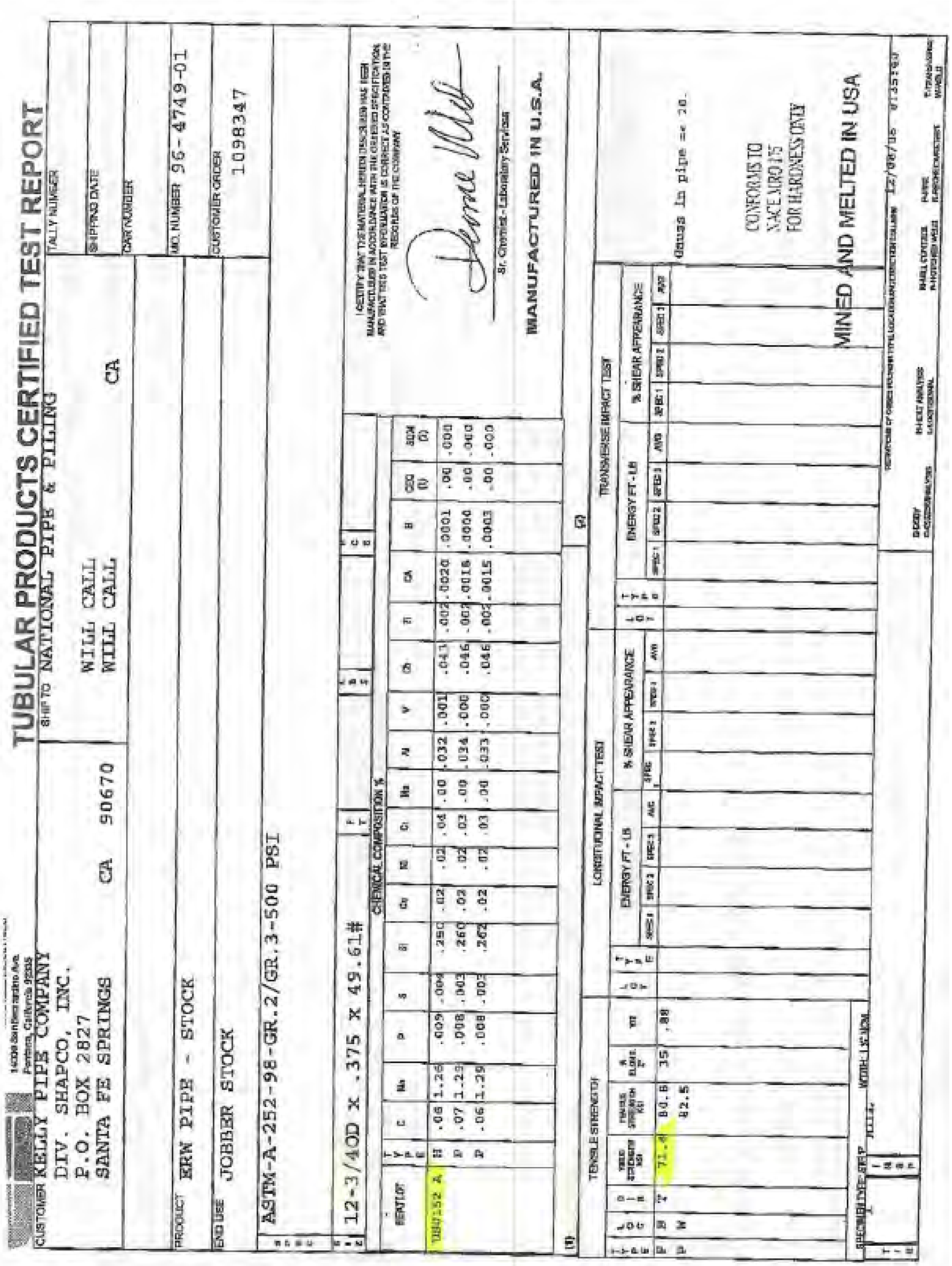

TUBULAR PRODUCTS CERTIFIED TEST REPORT

14000 San Bernardino Ave.
Fontana, California 92335

CUSTOMER KELLY PIPE COMPANY
DIV. SHAPCO, INC.
P.O. BOX 2827
SANTA FE SPRINGS CA 90670

SHIP TO NATIONAL PIPE & PILING
WILL CALL
WILL CALL CA

TALLY NUMBER
SHIPPING DATE
CAR NUMBER
MO. NUMBER 96-4749-01
CUSTOMER ORDER 1098347

PRODUCT ERW PIPE - STOCK
END USE JOBBER STOCK

SPEC ASTM-A-252-98-GR.2/GR.3-500 PSI

SIZE 12-3/4OD x .375 x 49.61#

CHEMICAL COMPOSITION %

HEAT LOT	TYPE	C	Mn	P	S	Si	Cu	Ni	Cr	Mo	Al	V	Cb	Ti	CA	B	CEQ (1)	SCM (2)
U80152 A	H	.06	1.26	.009	.004	.250	.02	.02	.04	.00	.032	.001	.041	.002	.0020	.0001	.00	.000
	P	.07	1.29	.008	.003	.260	.02	.02	.03	.00	.034	.000	.046	.002	.0016	.0000	.00	.000
	P	.06	1.29	.008	.003	.262	.02	.02	.03	.00	.033	.000	.046	.002	.0015	.0003	.00	.000

I CERTIFY THAT THE MATERIAL HEREIN DESCRIBED HAS BEEN MANUFACTURED IN ACCORDANCE WITH THE ORDERED SPECIFICATION AND THAT THIS TEST INFORMATION IS CORRECT AS CONTAINED IN THE RECORDS OF THE COMPANY

Sr. Chemist - Laboratory Services

MANUFACTURED IN U.S.A.

TENSILE STRENGTH

TYPE	LOC	DIR	YIELD STRENGTH KSI	TENSILE STRENGTH KSI	% ELONG. 2"	Y/T
P	B	T	71.4	80.8	35	.88
P	W			82.5		

LONGITUDINAL IMPACT TEST — ENERGY FT-LB — % SHEAR APPEARANCE

TRANSVERSE IMPACT TEST — ENERGY FT-LB — % SHEAR APPEARANCE

Gauss in pipe =< 20.

CONFORMS TO
NACE MR0175
FOR HARDNESS ONLY

MINED AND MELTED IN USA

SPECIMEN TYPE: STRIP FULL WIDTH: 1.5" NOM.

12/08/06

Figure C-6 Material Properties for Steel Test Pile

STATE OF CALIFORNIA DEPARTMENT OF TRANSPORTATION

RELATIVE COMPACTION TEST

TL-297 (REV 10/2005)

Job Stamp	Location STOCKPILE	Test No. 1
	Material SAND	From .
	Impact by BOB NIXA	Sand Vol. By
	Date TESTED 5-18-11	Date SAMPLED 5-12-11

Remarks: TESTED BY
AC&S MATERIALS TESTING SERVICES
2495 PROGRESS DRIVE, SUITE A
REDDING, CA 96001

SAND VOLUME DATA

A	Initial Wt. of Sand (g)	
B	Wt. of Residue (g)	
C	Wt. of Sand Used (A-B)	
D	Cone Correction (g)	
E	Wt. of Sand in Hole (C-D)	
F	Sand Density (g/cc)	
G	Volume of Hole (E/F)	
H	Wet Density (g/cc) (L/G)	

IMPACT TEST DATA

I	Initial Wet Weight of Test Specimen (g)				
	Increment	1	2	3	4
	Water Adjustment (g)	+100	+150	+200	
J	Tamper Reading	11.6	11.2	11.4	
K	Adjusted Wet Density (g/cc)	2.04	2.12	2.08	

ROCK CORRECTION

L	Total Sample Weight	(g)	22,756.5
M	+ 3/4-Inch Weight in Air	(g)	0
N	+3/4-inch Weight in Water	(g)	
O	+3/4-inch Volume	(M - N)	
P	% +3/4-inch	100 * (M / L)	0
Q	% -3/4-inch	100 - P	
R	Density of +3/4-inch	(M / O)	
S	(%+3/4-inch) / Density of +3/4-inch	(P / RY)	
T	(%-3/4-inch) / Density of -3/4-inch	(Q / K)	
U	Sum of S and T	(S + T)	
V	Average Adjusted Wet Density	(100 / U)	2.12

Percent Relative Compaction*	Spec	Failed	or less
		Passed	

*(H / K) for 10% or less +3/4-inch; (H / V) for > 10% +3/4-inch

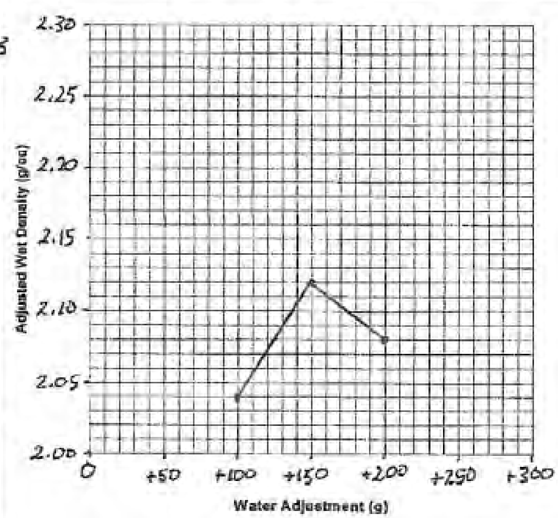

MOISTURE ADJUSTMENT FOR AGGREGATE BASE PAY QUANTITY

a	In-place Wet wt.		e	Test Spec. Wet Wt. (opt.)	
b	In-place Dry wt.		f	Test Spec. Dry Wt.	
c	In-place Water (a - b)		g	Test Spec. Water (e - f)	
d	In-place % Water (c / b)		h	Test Spec. % Water (g / f)	

Moisture Corr. (h + 1%) - d =

Moisture Corr. in excess of Opt. + 1% | % Moisture by CTM 226

+ 3/4-Inch Aggregate Adjustment (Y)

% + 3/4-inch (P)	Adjustment
20 or less	1.00
21-25	0.99
26-30	0.98
31-35	0.97
36-40	0.96
41-45	0.95
46-50	0.94

ATTACHMENT 2

Figure C-7 Relative Compaction Test Data Sheet (Caltrans Test 216)

Carlson Testing, Inc.

Bend Office	(541) 330-9155
Geotechnical Office	(503) 601-8250
Eugene Office	(541) 345-0289
Salem Office	(503) 589-1252
Tigard Office	(503) 684-3460

Report Of In-Place Density Tests

Client: Knife River (Corporate Operations) Date: May 20th, 23rd and 24th, 2011

Project: OSU Hinsdale Wave Research Lab CTI Job No. S1106470

Job Address: 3550 SW Jefferson Way – Corvallis, Oregon Permit No.: n/a

Material Description: Cohesionless Soil from Knife River

Method of Test: Cal Trans 216

Maximum Wet Density 2.12 g./cc. Optimum Moisture: n/a % Required Compaction: 95 %

Source of Value Lab log # 11-3309 Source of Value Dated 5-18-11 ☑ Project Specific ☐ Current Fill Source Proctor

☐ Supplied By: AC & S Material Tests

Gauge Serial #: 39525 Standard Counts – Density: 2660 Moisture: 741 Calibration Date: 2/2011

Date of Test	Test No.	Test Location	Density Count	Moist. Count	Mode	Depth	Elev. Ft.	% Field Moist.	In-Place Density (lbs/cu.ft.) Wet	Dry	% Comp.
5-20-11	1	CENTERLINE; 25' FROM WEST	2345		DT	6"	-9 ½'	9.6	2.065		97.4
5-20-11	2	50' FROM SOUTH, 36' FROM EAST	2699		DT	6"	-9 ½'		2.035		96.0
5-20-11	3	EAST – CENTERLINE, 9' FROM TOE	1579	122	DT	8"	-9'	6.3	2.038	1.918	96.1
5-20-11	4	NORTH – CENTERLINE, 12' FROM TOE	1686	92	DT	8"	-9'	4.5	2.007	1.917	95
5-20-11	5	SOUTH – CENTERLINE, 6' FROM TOE	1495	160	DT	8"	-9'	8.6	2.072	1.908	97.7
5-20-11	6	WEST – CENTERLINE, 15' FROM TOE	1671	138	DT	8"	-9'	6.9	2.009	1.862	95
5-20-11	7	SW CORNER	1634	162	DT	8"	-8 ½'	9.0	2.014	1.848	95.0
5-20-11	8	SE CORNER	1563	167	8"	-8 ½'	9.1	2.042	1.871	96.3	96.3
5-20-11	9	NE CORNER	1548	169	8"	-8 ½'	9.2	2.048	187.5	96.6	96.6

Asterisked (*) percent compaction test results did not meet listed acceptance criteria.

Remarks:
Bold / Circled – Failing Shots

Inspector: Gordon Cooper Reviewed by: [signature] Date: 5/25/11

Figure C-8 In-Place Density Test (Nuclear Density Gauge) for Cohesionless Embankment

Carlson Testing, Inc.

Bend Office	(541) 330-9155
Geotechnical Office	(503) 601-8250
Eugene Office	(541) 345-0289
Salem Office	(503) 589-1252
Tigard Office	(503) 684-3460

Report Of In-Place Density Tests

Client: Knife River (Corporate Operations)   Date: May 20th, 23rd and 24th, 2011

Project: OSU Hinsdale Wave Research Lab   CTI Job No. S1106470

Job Address: 3550 SW Jefferson Way – Corvallis, Oregon   Permit No.: n/a

Material Description: Cohesionless Soil from Knife River

Method of Test: Cal Trans 216

Maximum Wet Density 2.12 g./cc.   Optimum Moisture: n/a %   Required Compaction: 95 %

Source of Value Lab log # 11-3309   Source of Value Dated 5-18-11   ☑ Project Specific   ☐ Current Fill Source Proctor

☐ Supplied By: AC & S Material Tests

Gauge Serial #: 39525   Standard Counts – Density: 2660   Moisture: 741   Calibration Date: 2/2011

Date of Test	Test No.	Test Location	Density Count	Moist. Count	Mode	Depth	Elev. Ft.	% Field Moist.	In-Place Density (lbs/cu.ft.) Wet	Dry	% Comp.
5-20-11	10	NW CORNER	1574	157	DT	8"	-8 ½'	8.4	2.036	1.878	96.0
5-23-11	11	EAST, CENTERLINE	1659	116	DT	8"	-6'	6.0	2.016	1.887	95.1
5-23-11	12	SOUTH, CENTERLINE	1615	130	DT	8"	-6'	6.9	2.018	1.888	95.2
5-23-11	13	WEST, CENTERLINE	1542	155	DT	8"	-6'	8.4	2.047	1.888	96.6
5-23-11	14	NORTH, CENTERLINE	1647	128	DT	8"	-6'	6.8	2.015	1.878	95.0
5-23-11	15	SE CORNER	1402	161	DT	8"	-5'	8.5	2.108	1.943	99.4
5-23-11	16	SW CORNER	1562	153	DT	8"	-5'	8.3	2.038	1.882	96.1
5-23-11	17	NE CORNER	1661	108	DT	8"	-5'	6.5	2.016	1.893	95.1
5-23-11	18	NW CORNER	1521	162	DT	8"	-5'	8.6	2.091	1.925	98.6

Asterisked (*) percent compaction test results did not meet listed acceptance criteria.

Remarks:
Bold / Circled – Failing Shots

Inspector: Gordon Cooper   Reviewed by: Date: 5/25/11

Figure C-9 In-Place Density Test (Nuclear Density Gauge) for Cohesionless Embankment

Carlson Testing, Inc.

Bend Office	**(541) 330-9155**
Geotechnical Office	**(503) 601-8250**
Eugene Office	**(541) 345-0289**
Salem Office	**(503) 589-1252**
Tigard Office	**(503) 684-3460**

Report Of In-Place Density Tests

Client: Knife River (Corporate Operations)   Date: May 20th, 23rd and 24th, 2011

Project: OSU Hinsdale Wave Research Lab   CTI Job No. S1106470

Job Address: 3550 SW Jefferson Way – Corvallis, Oregon   Permit No.: n/a

Material Description: Cohesionless Soil from Knife River

Method of Test: Cal Trans 216

Maximum Wet Density 2.12 g./cc.   Optimum Moisture: n/a %   Required Compaction: 95 %

Source of Value Lab log # 11-3309   Source of Value Dated 5-18-11   ☑ Project Specific   ☐ Current Fill Source Proctor

☐ Supplied By: AC & S Material Tests

Gauge Serial #: 39525   Standard Counts – Density: 2660   Moisture: 741   Calibration Date: 2/2011

Date of Test	Test No.	Test Location	Density Count	Moist. Count	Mode	Depth	Elev. Ft.	% Field Moist.	In-Place Density (lbs/cu.ft.) Wet	Dry	% Comp.
5-23-11	19	WEST, CENTERLINE	1670	123	DT	8"	-4'	6.6	2.019	1.894	95.2
5-23-11	20	SOUTH, CENTERLINE	1554	131	DT	8"	-4'	6.9	2.043	1.912	96.4
5-23-11	21	EAST, CENTERLINE	1540	167	DT	8"	-4'	9.2	2.047	1.875	96.6
5-23-11	22	NORTH, CENTERLINE	1664	127	DT	8"	-4'	6.8	2.017	1.889	95.1
5-23-11	23	WEST, CENTERLINE	1595	132	DT	8"	-3'	7.0	2.036	1.903	96.0
5-23-11	24	NORTH CENTERLINE	1634	127	DT	8"	-3'	6.8	2.020	1.891	95.3
5-23-11	25	SOUTH, CENTERLINE	1638	140	DT	8"	-3'	7.6	2.008	1.867	95
5-23-11	26	EAST, CENTERLINE	1436	160	DT	8"	-3'	8.5	2.093	1.929	98.7
5-24-11	27	SE CORNER	1620	137	DT	8"	-1'	7.4	2.010	1.872	95.0

Asterisked (*) percent compaction test results did not meet listed acceptance criteria.

Remarks:
Bold / Circled – Failing Shots

Inspector: Gordon Cooper   Reviewed by: Date: 5/25/11

Figure C-10 In-Place Density Test (Nuclear Density Gauge) for Cohesionless Embankment

Carlson Testing, Inc.

Bend Office	(541) 330-9155
Geotechnical Office	(503) 601-8250
Eugene Office	(541) 345-0289
Salem Office	(503) 589-1252
Tigard Office	(503) 684-3460

Report Of In-Place Density Tests

Client: Knife River (Corporate Operations) Date: May 20th, 23rd and 24th, 2011

Project: OSU Hinsdale Wave Research Lab CTI Job No. S1106470

Job Address: 3550 SW Jefferson Way – Corvallis, Oregon Permit No.: n/a

Material Description: Cohesionless Soil from Knife River

Method of Test: Cal Trans 216

Maximum Wet Density 2.12 g./cc. Optimum Moisture: n/a % Required Compaction: 95 %

Source of Value Lab log # 11-3309 Source of Value Dated 5-18-11 ☑ Project Specific ☐ Current Fill Source Proctor

☐ Supplied By: AC & S Material Tests

Gauge Serial #: 39525 Standard Counts – Density: 2660 Moisture: 741 Calibration Date: 2/2011

Date of Test	Test No.	Test Location	Density Count	Moist. Count	Mode	Depth	Elev. Ft.	% Field Moist.	In-Place Density (lbs/cu.ft.) Wet	Dry	% Comp.
5-24-11	28	NE CORNER	1336	1663	DT	8"	-1'	8.6	2.140	1.971	100.9
5-24-11	29	NW CORNER	1610	110	DT	8"	-1'	6.0	2.016	1.902	95.1
5-24-11	30	SW CORNER	1485	172	DT	8"	-1'	9.5	2.071	1.891	97.7
5-24-11	31	EAST, CENTERLINE	1502	157	DT	8"	0'	8.5	2.065	1.902	97.4
5-24-11	32	WEST, CENTERLINE	1625	138	DT	8"	0'	7.5	2.014	1.874	95.0
5-24-11	33	SOUTH, CENTERLINE	1623	151	DT	8"	0'	8.4	2.015	1.859	95.0
5-24-11	34	NORTH, CENTERLINE	1523	171	DT	8"	0'	9.5	2.055	1.876	96.9

Asterisked (*) percent compaction test results did not meet listed acceptance criteria.

Remarks:
Bold / Circled – Failing Shots

Inspector: Gordon Cooper Reviewed by: Date:

Figure C-11 In-Place Density Test (Nuclear Density Gauge) for Cohesionless Embankment